Magmatism in southern Uruguay and the early rifting of the South Atlantic

Thesis

Magmatism in southern Uruguay and the early rifting of the South Atlantic.

A thesis presented for the degree of
Doctor of Philosophy

by

Linda A. Kirstein
BSc. (Hons) N.U.I. (*Cork*) 1993

Department of Earth Science,
The Open University

August, 1997

Abstract

A suite of early Cretaceous volcanic rocks (Puerto Gómez and Arequita Fms.) are preserved within the N60° E trending Santa Lucía Basin, southern Uruguay which lies at the southern margin of the Paranà - Etendeka continental flood basalt province. New Ar-Ar ages of the basalts range from 134 to 130 Ma while ages from the rhyolites range from 130 to 124 Ma. This magamtism was contemporaneous with the main flood basalt event, although rhyolite activity continued after rifting (127 - 126 Ma). The province therefore contains unique information about melting conditions at the periphery of the influence of the Tristan da Cunha plume.

The volcanic rocks of southern Uruguay are bimodal in silica, and the majority of basalts of the Puerto Gómez Fm., herein termed the Treinte Y Trés magma type, have major-, trace- element and initial isotope ratios similar to the low -Ti/Y Gramado -Tafelberg magma types of the Paranà - Etendeka. There are also a number of unique basalt samples termed the Santa Lucía magma type, which have low La/Nb, and are considered to have been generated by mixing between lithosphere - and asthenosphere - derived melts. These magmas represent the first sampling of true plume material in this CFB province. The rhyolites of the Arequita Fm. are relatively evolved with variably sized euhedral to anhedral quartz phenocrysts, and ignimbritic textures that are the first described from this province. The rhyolites have lower magmatic temperatures (850 - 950 °C) than those of the Paranà - Etendeka, and are divided into two geochemical series, the Lascano Series and the Aigüa Series. The rhyolites of the Lascano and Aigüa Series are not related to the Puerto Gómez Fm. basalts, but rather they originated from separate sources in the mid to lower crust, where melting was facilitated by mid-crustal level intrusions of basaltic material as recognised from a large gravity anomaly. Melt production rates in southern Uruguay were low (0.01 $km^3\ yr^{-1}$) similar to the rates calculated for the waning stages of magmatism on the Serra Geral escarpment, southern Brazil. These rates are consistent with the notion that by this time the principal melt production was located in the newly forming ocean with Uruguay at the margins of the influence of the plume.

Acknowledgements

The Milton Keynes experience is one that I am unlikely to forget quickly for all its thrills and spills! First there was Uruguay, an amazing place with the incredible ability to feel like Donegal in the cold and wet on first arrival. My introduction to cachaca and capirinhas led perhaps to slightly less samples but no doubt improved my alcohol tolerance many fold. Field work would not have been possible or gone so smoothly (?) without the expertise of Marta Mantovani and the Uruguayan survey to whom I am very grateful. Brazil, the near death road experiences, and Sao Paulo made me appreciate life so much more!

Back at the O.U. my supervisors Chris Hawkesworth and Simon Turner require praise indeed for finding enthusiasm and endless suggestions in the light of strange interpretations and dreadful misunderstandings. Chris' special supply of red ink and illegible scrawl will scar my dreams for a very long time but I like to think that it was all worth while! Special thanks also to Dave Peate and his amazing enthusiasm for the Paraná and related magmatism. Helpful hints and discussions with Steve Blake and Nick Rogers are also appreciated. Janet you are a dream, what more can I say.

Thanks to Kay, Andy T and all the folks downstairs for their tolerance of me and my desire to have everything at the drop of a hat. Also many thanks to Mabs and Peter for their insight into mass specs., isotopes, lab parties and incredible amounts of chocolate. In the argon lab Simon Kelley and Jo require a special mention for their ability to share an understanding of stable isotopes, PCs and running a commercial sample or two to enable my second field trip to take place! Rita, Anita, Andy L and John T special thanks for everything ....

The Etendeka ..... now there is a place not to be missed and certainly not to be done without the able guidance of Simon Milner and Roger Swart. Thanks also to Shell for paying all the field expenses and not complaining about all the igneous outcrops they were accidently brought to. Simon and Debs must have been mad for sharing their anniversary weekend in Etosha but I shall certainly treasure the memory. Chris Harris, Anton le Roex, Dave Reid and everyone else at Cape Town are also acknowledged for their hospitality and for a spontaneous trip around the Cape for dyke samples.

Enough of work. I am in awe of the task of trying to acknowledge and appreciate all the friends I have made while at the OU. My body will never be the same following my womens rugby encounter - thanks Treez for the opportunity but next time warn me about the ten tonne women that want to flatten little wingers for breakfast. Sporting experiences including hockey/ squash/ tennis were all the more enjoyable because of the people involved and a special thanks to Fran for playing all games at my level! Jane, Paul, Fran, Ben, Phil, Butts, Dr. E, Ayse, Derek and all the other fun loving foodies are all forever welcome to come and party unexpectedly. Phil requires a special mention for his amazing approach to my lack of confidence and for calling a spade a spade, his insights have and always will bring a very big smile to my face. Thanks also to Lizzie for being a remarkably similar Virgo; Mike, Russ, Yvette, Laurie, Trevor, Johnny, Beto and H for cups of tea and tips on good housekeeping and Lou for a never ending supply of treats. My family deserve a big thank you for their encouragement and support and hopefully realise how much I appreciate them. Thanks also to Tim for stepping in at the end and making sure it all happened .....

Table of Contents.

Chapter 1

Chapter 2

Chapter 3

Appendix C

Appendix D

List of Figure Captions

Chapter 1

Chapter 2

Chapter 3

Chapter 4.

Chapter 5

Appendix D

List of Tables.

Chapter 1

Chapter 2

Chapter 3

Chapter 4

Chapter 5

Appendix A

Appendix B

Appendix D

List of Plates.

Appendix C

Chapter 1.

Introduction to Concepts & Regions.

1.1 Thesis Outline.

The early Cretaceous volcanic rocks of southern Uruguay are considered to be linked to tectonic processes related to the fragmentation of Gondwana, and the opening of the South Atlantic. The relationship of these Uruguayan rocks to the main Paraná - Etendeka Continental Flood Basalt (CFB) province of South America and Africa is investigated in this work, with petrogenetic, geochemical and geochronological evidence applied to certain models to provide greater insight into the processes of rifting and magmatism.

The thesis is comprised of five chapters, commencing with a basic introduction to some of the concepts and theories necessary to gain insight into magmatism and rifting (Chapter 1). More specifically, this first chapter introduces the mechanisms of rifting; the definition of lithosphere and asthenosphere; and the characteristics, models of origin and potential sources of continental flood basalts. In addition, the history of the Gondwana supercontinent and particularly the background geology and details of the volcanics of the Paraná - Etendeka province are discussed. Finally the Uruguayan province is introduced with an account of its geological setting and fieldwork undertaken there.

Chapter 2 consists of a detailed account of the petrology, geochemistry and petrogenesis of the basalts, andesites, dacites and rhyolites of the Uruguayan province. Contemporaneous alkaline magmatism, particularly a Uruguayan syenite is also briefly considered. Chapter 3 considers thermometry and its applicability to Mesozoic rocks, together with a mode of origin for the Uruguay rhyolites. Chapter 4 is a geochronology

chapter, which reviews all previous dates for the Paraná-Etendeka province, it introduces and presents the new data produced in the course of this project. These Ar-Ar dates are then used to constrain the timing of rifting in relation to magmatism in the South Atlantic, with the aid of dyke data. Finally Chapter 5 summarises all previous chapters and concludes with a model for constraining the rate and direction of rifting in this region.

1.2 General Introduction.

The concept of continental drift has been controversial ever since its description by Wegener in 1912. Palaeomagnetic studies of the ocean floor by Vine & Matthews (1963) were virtually a corollary of the theory of ocean floor spreading and magnetic reversals. Blocks of normal and reversely magnetized crust drifting away from the ridge axis, that Vine & Matthews speculated to be associated with sea floor spreading, are accepted as such today. Yet, the mechanics and driving forces that underlie plate movements and culminate in the break-up of continents remain a subject of debate (cf. William Smith Lecture to the Geol. Soc. Lond., 1992 given by P. Ziegler).

Particularly relevant in the context of this work is the break-up of the Gondwana supercontinent which once included Africa, South America, India, Antarctica, Australia and Madagascar (Fig. 1.1), and more specifically the rifting of South America from Africa and the opening of the South Atlantic Ocean. The relationship between one of the world's largest preserved Continental Flood Basalt (CFB) province, located on the South American and African continents, the Paraná - Etendeka, and the rifting process remains controversial. The relationship of the Paraná - Etendeka CFB to the southern Uruguay volcanics remains unresolved. The processes of rifting and magmatism are undoubtedly linked, but the question as to how remains, and is central to this thesis.

In the next three sections the driving mechanisms that result in plate fragmentation and reorganisations will be discussed and summarised. A brief

description of the forces involved is followed by a more detailed look at the two main models for rifting in Section 1.3.3.

Fig. 1. 1 Reconstruction of Gondwana (after Smith, 1992).

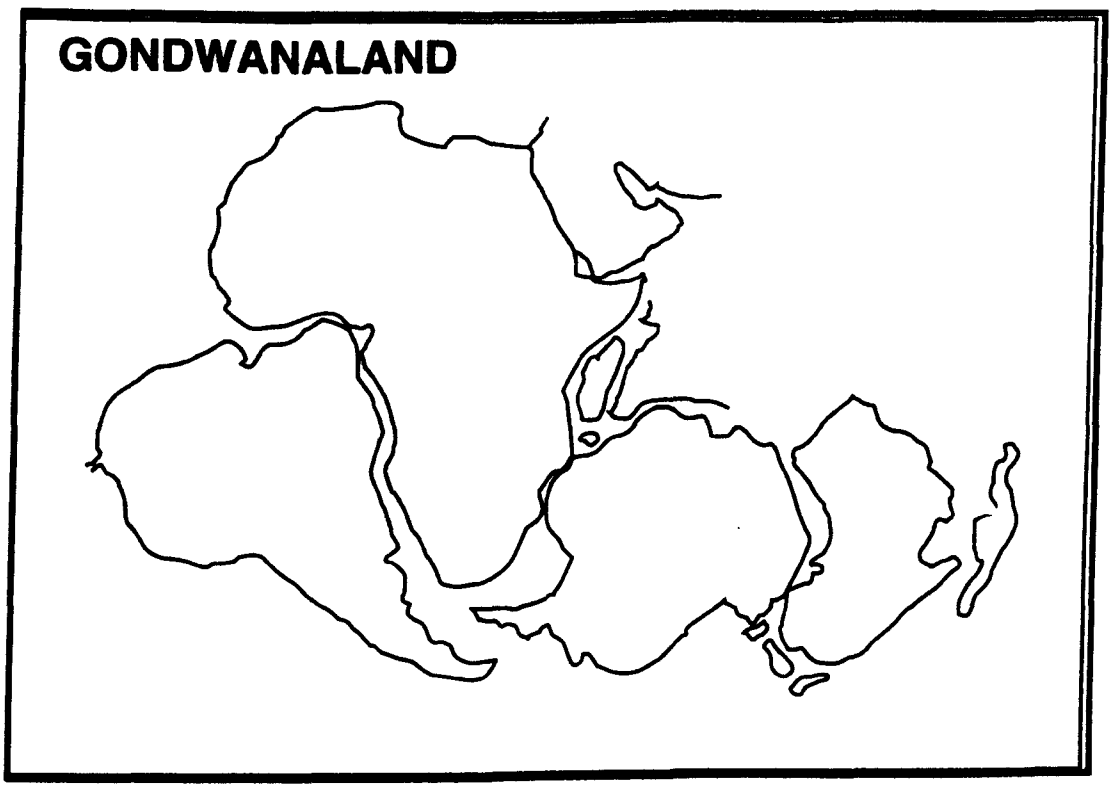

1.3 Dispersal of Continents.

The continents are thought to be dispersed by a number of different forces including ridge push (F_{RP}), slab pull (F_{SP}) and continental drag (F_{CD}) (Fig. 1.2). Lateral variations in potential energy distribution across the plate may also have a role. According to some authors the principle driving forces are edge forces such as ridge push and subduction pull (Jurdy & Stefanick, 1991; Bott, 1993). Others have favoured frictional drag forces caused by convection in the mantle (Ziegler, 1993), or argued that the forces of ridge push and slab pull and/or frictional drag are not sufficient, or always present, to divide continents (Sandiford & Coblentz, 1994; Richards *et al.*, 1991). Alternatively, Sandiford & Coblentz (1994) and Richards *et al.*, (1991) have invoked lateral variations in potential energy, contributing to deviatoric stresses in the

lithosphere, and active upwelling of mantle material in the form of plumes or hot spots, respectively (Fig. 1.2).

1.3.1 Origin of Forces.

The principal driving mechanisms resulting in plate re-ordering are briefly described as follows:

Ridge Push (F_{RP}):

The presence of hot, low density upwelling asthenosphere and consequently warmed lithosphere results in elevation of the ridge relative to the cold ocean floor. The resultant stresses include local tensional stress regimes within the ridge due to buoyant loading (Bott, 1993). However, the main stresses in young oceanic crust are focused in the zone of weakness directly beneath the ridge, where the plates divide, and as this region cannot support deviatoric stresses the consequent intraplate stresses result in a ridge push force.

Slab Pull (F_{SP}) & Trench Suction (F_{TS}):

Oceanic lithosphere thickens with age, becomes cooler and more dense, and eventually it reaches a state of negative buoyancy and descends back into the asthenosphere at destructive plate boundaries (Condie, 1989). At subduction zones (e.g. Peru-Chile Trench), a different stress regime to that at mid ocean ridges is operable. The dynamics of subduction forces include local compression in the trench-arc region from the downward motion of the slab and its surface flexure; with local tension in the back arc region perhaps produced by low density mantle material and, in the arc due to crustal thickening (Whittaker *et al.*, 1992). The subduction process gives rise to the slab pull force due to negative buoyancy with only the leading edge of the overriding plate being a site of compressional tectonics, (Fig. 1.2 F_{SP}), which may be coupled with the trench suction force to pull the subducting plate toward the subduction zone.

Fig. 1.2. Forces acting on lithospheric plates, including driving and resistive forces, which result in plate dispersal (after Forsyth & Uyeda, 1975).

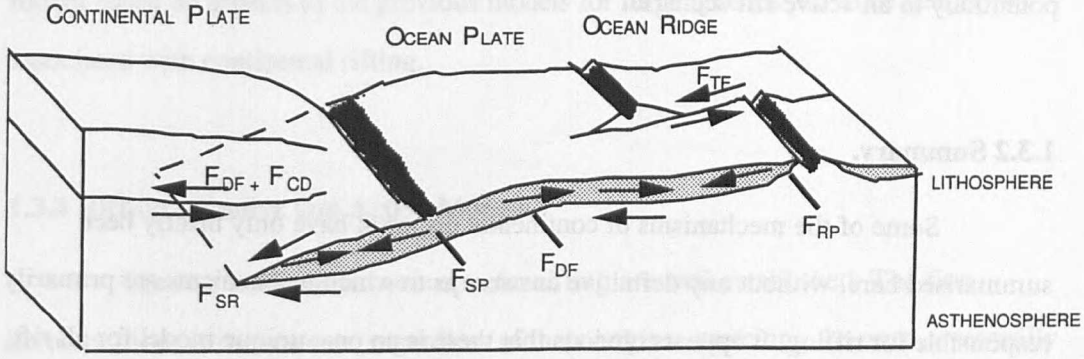

KEY:	
Drag Force F_{DF}	Slab Resistance F_{SR}
Continental Drag F_{CD}	Slab Pull F_{SP}
Ridge Push F_{RP}	Transform Fault F_{TF}

Drag Forces, Potential Energy Variations & Plumes:

Drag forces exerted on the base of the lithosphere by the convecting mantle, in addition to plate boundary forces, govern the motion of lithospheric plates according to Ziegler (1993). In fact the shear-traction exerted by the convecting mantle may be a dominant factor in the movement and rifting of plates, as in the past subduction zones have migrated at the trailing edge of drifting continents and are therefore not responsible for plate motion (Ziegler, 1993). Similar arguments regarding the absence of subduction zones have been used by Sandiford & Coblentz (1994) in suggesting that growth and ageing of oceanic lithosphere alters the potential energy across individual plates. A build up in potential energy and consequently the intraplate stress fields contributes to deviatoric stresses in the lithosphere and helps to fragment continents and more importantly in the case of Gondwana supercontinents.

Richards *et al.*, (1989) consider a model whereby active impingement of a mantle plume on the base of the crust may in certain circumstances initiate rifting, following thermal doming, and so is independent of the result that the forces already

described. Melting at the base of the lithosphere occurs due to the excess temperature of the hot mantle diapir, and this accelerates thinning and possibly destabilisation leading potentially to an active rift scenario.

1.3.2 Summary.

Some of the mechanisms of continental dispersal have only briefly been summarised here, without any definitive answers as to which mechanisms are primarily responsible for rifting. It appears obvious that there is no one, unique model for all rift scenarios but it is the intention of this project to develop a consistent model for break-up and the formation of the South Atlantic and the generation of the associated magmatism in the Paraná - Etendeka CFB province, taking into account as many variables as possible.

Rifting as a process is recognised world wide, and is important in the development and positioning of the continents as they are observed. Magmatism can be, but is not always, associated with the processes whereby continental lithosphere is thinned and fractured. The origin of this magmatism, where it is observed, tends to fascinate geochemists and geophysicists alike. Where does the magma originate? In the asthenosphere or in the lithosphere? The large volume of magma, generally associated with CFB provinces, implies the presence of a mantle plume. If so, how does this affect rifting models?

Magma that originated in the asthenosphere has distinctive geochemical and isotopic signatures akin to Ocean Island Basalts (OIB) or Mid Ocean Ridge Basalts (MORB). If, however this is not the case, then an origin in the lithosphere of some if not all of the characteristics is surmised. One solution is to mobilise small degree melts from the lithosphere for mixing models, so that the volume of magma is generated in the asthenosphere, but the trace element and isotopic characteristics are lithospheric in origin. Alternatively it has been suggested that the lithosphere melts, which evokes numerous questions as to how vast quantities of magma are generated in the rigid outer layer of the Earth, and whether or not it is possible to melt such large amounts of the lithosphere.

These are some of the multitude of questions that this project hopes to address, but first it is important that the main arguments are introduced prior to developing a model based on aspects of the previous models for large igneous province generation associated with continental rifting.

1.3.3 Rifting - Passive and Active Models.

The two fundamental concepts for rifting are well established. The first involves tectonic movements, regardless of their origins, stretching the crust, eventually fracturing it and allowing the underlying mantle to rise diapirically to the surface (Fig. 1.3(a)). In such models, tensional failure is typically concentrated along pre-existing stresses in the lithosphere. In the second model (Fig. 1.3(b)), rift zones are produced by asthenospheric upwelling, doming and splitting the continent along pre weakened zones. The former is referred to as the 'passive' model, the latter the 'active' model (Sengör & Burke, 1978; Keen, 1985). Leading exponents of passive models have included Profs. White and McKenzie. In Scientific American (1989), they modelled magma generation at rifts and argued that the vast quantities of magma generated at oceanic and continental rifts were generated passively, because 'extensive melting does not begin until the mantle has upwelled above the base of unrifted lithosphere'. However, in many cases, the initiation of a mantle plume may be a deciding factor in initiating rifting by doming and increasing the driving forces by adding gravitational forces. The presence of a plume is necessary for the generation of the vast quantities of magma observed in flood basalt provinces.

In principle, it should be possible to distinguish between these two mechanisms on the basis of the timing of rifting and volcanism; the active case being doming - volcanism - rifting, while the sequence for the passive case is rifting - doming - volcanism (Keen, 1985; Wilson, 1989). However, nature is rarely so simple, and discriminating between the two processes is often not easy (Table 1.1).

Fig. 1.3. Simplistic overview of models for passive and active rifting (after Keen, 1985; Wilson, 1989).

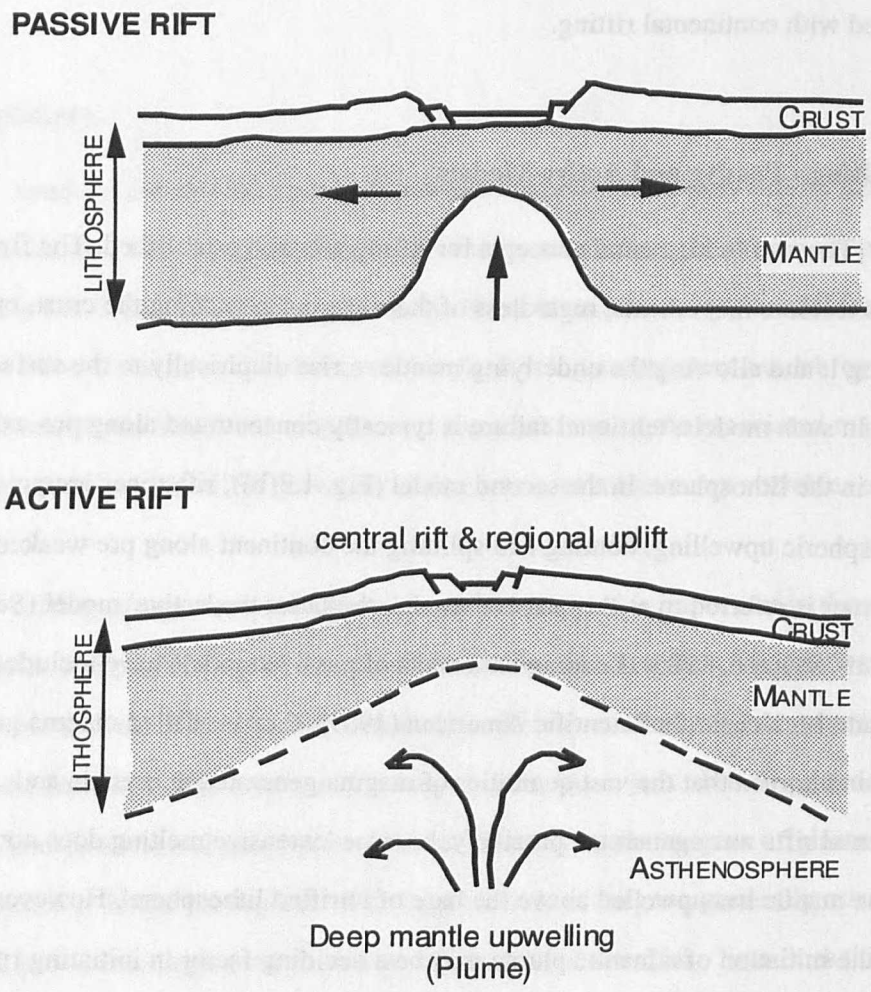

Having examined the basic models of rifting and the consequent potential for melt generation via decompression of asthenosphere, the characteristic features of continental flood basalts are described. Furthermore the models to explain the origin and potential sources of CFB are introduced in the following sub-sections.

Table 1.1. Arguments for and against the model for the generation of CFB by the decompression of anomalously hot asthenosphere as a passive response to continental stretching and rifting.

Arguments For:	Arguments Against
(i) Stretching of continents results in crustal subsidence and the formation of sedimentary basins (e.g. The North Sea (White & McKenzie, 1989));	(i) Not all CFB are associated with rifting events (e.g. Columbia River Basalts (Carlson *et al.*, 1981; Hooper, 1982);
(ii) Significant underplating beneath the continental margins is observed to occur (e.g. Hatton Bank);	(ii) Dyke swarms associated with Deccan and Karoo are randomly oriented and distributed over broad cratonic areas (Eales *et al.*, 1984; Richards *et al.*, 1989);
	(iii) In many cases rifting was preceded by the main flood basalt eruptive period (e.g. Paraná (Piccirillo *et al.*, 1989; Stewart *et al.*, 1996);

1.4 Characteristic Features of Continental Flood Basalt Provinces

Continental Flood Basalt (CFB) provinces consist of massive subaerial sheet flows which erupted episodically, with variable eruption timescales, but ultimately in great volumes onto the continental crust. Individual flows are thick (10 - 15 m on average for the Columbia River) and can sometimes be traced for tens (e.g. Deccan; Etendeka) to hundreds (e.g. Columbia River) of kilometers, although exposure is rarely

good. Extrusion rates are thought to have been rapid, in that, for example ~10^6 km^3 of Deccan basalt was erupted in less than 4 Ma (Courtillot *et al.*, 1986). However, the Paraná - Etendeka is thought to have been active for up to 10 Ma (Turner *et al.*, 1994), and so its average eruption rate is comparatively low.

Lavas with basaltic compositions dominate the sequences, although rhyolites, picrites and nephelinites occur locally in some provinces (Cox, 1980). The basalts are relatively evolved (SiO_2 ~ 49-55 wt%, with relatively low magnesium-iron ratios (Mg#) (45-60) in comparison to primitive magmas (Mg# = 70-75)). Phenocrysts are rare in most units (< 10%). Typical phases are clinopyroxene and plagioclase, while olivine and orthopyroxene are less common. Abundances of incompatible elements and Sr, Nd and Pb isotopes vary widely, from being similar to oceanic basalts, to highly enriched similar to that of for example, lamproites (Foley, 1991).

Another feature of CFB, and particularly those associated with the fragmentation of Gondwana, is that subgroups of magma types can be mapped out over large areas on the basis of Ti/Y ratios. Etendeka CFB, for example, is divided into a Northern Etendeka Province and a Southern Etendeka Province on the basis of variation in Ti contents (a detailed description of the chemistry of the Paraná-Etendeka CFB is given in Section 1.13). Characteristically the majority of CFB are relatively enriched relative to primitive mantle in all incompatible elements, except for Nb and Ta (the Deccan CFB excepted, with negligible Nb-Ta anomalies), while isotopic compositions are also distinctive.

1.4.1 Models for the origin of Continental Flood Basalts.

The sheer volume of magma in Continental Flood Basalt (CFB) provinces and the rate at which this magma is erupted requires anomalously hot temperatures in the mantle (White, 1989; White &McKenzie, 1995). Moreover, many Mesozoic CFB appear to be linked to hot spot traces on the adjacent ocean floor (Richards *et al.*, 1989; Leeman *et al.*, 1994). However, the nature of the association between CFB and mantle plumes continues to be a matter of great debate. The situation is complicated by variation of the chemical signatures of the magmas with time, linked by some to

changes in source region from lithospheric to asthenospheric (or vice versa) (Antarctica - Storey & Alabaster, 1991; Siberia - Lightfoot *et al.*, 1993; Paraná - Peate & Hawkesworth, 1996). Individual CFB also have variable major-, trace-element and isotopic signatures and are considered to contain significant contributions from different sources. The conclusion drawn by several authors is that magmas in different CFB provinces may have been triggered by different processes (Peate *et al.*, 1990; Turner *et al.*, 1995).

In order to gain an understanding of CFB provinces two fundamental problems require attention: (i) the processes which have potentially altered the magmas (crystallisation, melting, contamination), and (ii) the nature and source characteristics of the magmas. Mid-ocean ridges are the primary sites of magma generation today. Here diapiric upwelling of upper mantle material induces partial melting by adiabatic decompression to form basaltic magma - MORB (Mid Ocean Ridge Basalt). MORB are compositionally fairly uniform, although heterogeneities do occur (le Roex, 1987). Normal ocean ridge is characterised by N-type MORB and anomalous ocean ridge by E-type MORB. The different types of MORB are distinguished on the basis of incompatible trace and rare earth elements, particularly Zr, Nb, Y and La (Fig. 1.4). The trace element and isotopic geochemistry of MORB is distinctive also, with the source of MORB considered to be in a depleted layer of the upper mantle.

In contrast, Ocean Island Basalts (OIB) exhibit wide ranging compositional diversity from tholeiitic to potassic - alkalic, and most are directly associated with hot spots/plume magmatism (Morgan, 1983; Sleep, 1990). The source reservoir of OIB, which varies for different OIB, is considered to be isolated from the MORB source reservoir, and potentially consists of primordial mantle with subducted components (e.g. Cohen & O'Nions, 1982). Chondrite normalised Rare Earth Element (REE) patterns of OIB are distinct from MORB in that the light-REE tend to be enriched relative to the heavy-REE (Fig. 1.4).

Fig. 1.4. Chondrite normalised Rare Earth Element patterns of average OIB and MORB (data and normalising values from Sun & McDonough, 1989). E-type MORB - enriched mantle by compared with normal (N-type) MORB .

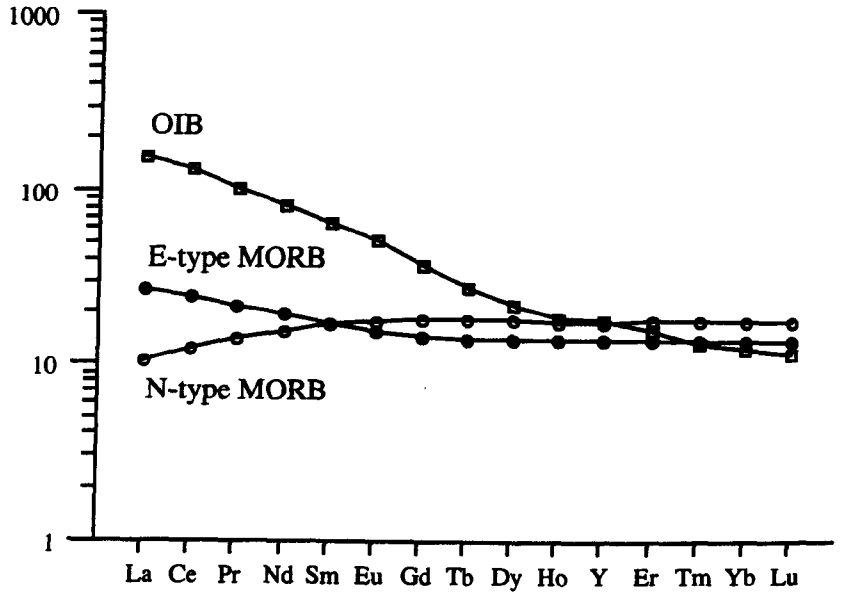

1.4.2 Source compositions.

In principle, isotopic compositions of melts are inherited directly from the source, although they may have been subsequently modified by other components, as during crustal contamination. The concentrations of trace elements are affected by the source composition, the conditions under which melting occurs i.e. water present or absent, and the degree of partial melting in addition to subsequent fractional crystallisation processes. Major elements depend on bulk composition, temperature, pressure and the types and abundances of volatile phases at the site of melting.

A wide range of potential source components have been invoked for CFB, and these may usefully be subdivided into primary sources and contaminants. Primary sources include: (i) mantle plumes; magma derived from a mantle plume is likely to be compositionally similar to plume-derived rocks in oceanic settings (cf. Iceland); and (ii) continental mantle lithosphere; kimberlite composition or basalt-borne mantle xenoliths, also lherzolites and harzburgites are characteristic. Contamination of magmas may then

occur with material from (i) upper continental crust - estimated from samples of granitoids and sediments (Cohen & O'Nions, 1982; Taylor and McLennan, 1985); and (ii) lower crust - from high-pressure granulite terrains and xenoliths (see Rudnick and Presper, 1990). There may be complications, in that sediment subduction at destructive plate margins for example, is considered by some (Cohen & O'Nions, 1982; White & Hofmann, 1982) to enrich locally the mantle in incompatible elements. One consequence is that magmas derived from such sources may have some geochemical features of crustal rocks, even though they have not experienced crustal contamination on route to the surface.

In detail, a number of models have been developed to account for the individual geochemical characteristics of different CFB, i.e. Nb-Ta anomalies. The main models are as follows:

(i) Plumes from the core-mantle boundary with minimal involvement of lithospheric mantle or the crust - (Richards *et al.*, 1989; Campbell & Griffiths, 1990 and Sharma *et al.*, 1991; 1992).

(ii) Melting in the lithospheric mantle - arguments for Karoo, Paraná, Ferrar and the Siberian Traps - (Hergt *et al.*, 1989; Gallagher & Hawkesworth, 1994).

(iii) Contamination of plume derived melts (either active or passive) by small-degree melts from enriched sub-lithospheric shallow mantle (Ellam & Cox, 1988; Arndt & Christensen, 1992; Kerr, 1994).

(iv) Contamination of mantle derived magma with material from the continental crust (Carlson *et al*, 1981).

Large volumes of magma and high Mg picrites imply anomalously hot sources, and hence the presence of mantle plumes. However, as noted by Hawkesworth & Gallagher (1993) this does not require that melt generation was confined to within the plume. Conversely, the presence of OIB-like magmas (considered to have originated in the asthenospheric mantle) is not necessarily evidence for a mantle plume, as it might simply reflect small degrees of melting in the asthenospheric upper mantle (Hawkesworth & Gallagher, 1993). Melting of the lithosphere and contamination of

asthenospheric melts were surmised as potential alternatives that would result in the observed, 'non OIB-like' geochemical compositions.

In summary each model appears to be incomplete in that it cannot account for certain specific CFB characteristics, for example in the Richards *et al* (1989) model it is difficult to generate the distinctive minor and trace element compositions of some CFB. It is here accepted that no one model will be suitable to all CFB provinces, however a model most appropriate to the Paraná - Etendeka province will be discussed later, after a brief discussion on lithosphere and asthenosphere terminology and a more indepth review of source models and controls on melt generation.

1.5 Terminology.

Prior to entering into a discussion of the relative merits of each of the main source models, it is important to define what is meant by the lithosphere, as it is viewed differently in various fields of the Earth Sciences. The asthenosphere is also briefly described.

1.5.1. The Lithosphere.

The lithosphere is, in general terms, the rigid outer layer of the Earth that moves around as tectonic plates, and it includes both the Earth's crust and some material in the underlying mantle. For geochemists, it is the layer of shallow level material that has retained its identity for long periods of time in order to develop distinctive radiogenic isotopes. The term lithosphere, as used by Hawkesworth and Gallagher (1993) and others, is linked to strength and, due to the thermal dependence of mantle rheology it is also linked to temperature. In the lithosphere, heat is transferred by conduction, unlike in the asthenosphere where heat is transferred primarily by convection.

Fig. 1.5. Idealised sketch of the lithosphere and the asthenosphere on the basis of geophysical and thermodynamic constraints. The curved solid line is the horizontally averaged thermal structure of old oceanic lithosphere over normal temperature asthenosphere (Potential temperature (T_P) = 1280°C). The dotted line is the adiabatic upwelling curve in the absence of melting (after White, 1988; Jordan, 1988). CBL - continental boundary layer; MBL - mechanical boundary layer; TBL - thermal boundary layer.

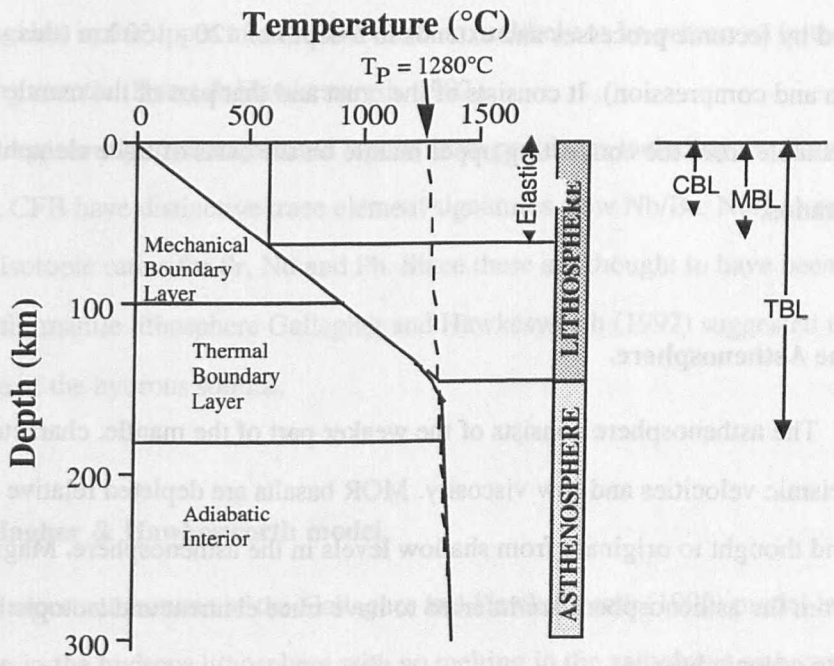

The lithosphere is taken to consist of the Mechanical Boundary Layer (MBL) and the upper part of the Thermal Boundary Layer (TBL). The MBL is the rigid, non-convecting, upper layer which consists of the crust, mantle probably depleted by melt extraction, and mantle which has simply cooled conductively without changing its composition from that of the underlying convecting upper mantle (Hergt & Hawkesworth, 1992). The TBL is the transition zone between the lithosphere and the asthenosphere. The upper TBL although it lacks long term strength, is usually included in the lithosphere. Mantle flows readily at temperatures above 650 °C (White, 1988) and, although the base of the lithosphere is usually taken to have temperatures of ~1280 °C. Anderson (1994) goes further and argues that only mantle colder than 600 °C qualifies as elastic lithosphere in the rheological sense, with material above 650 °C regarded as the transient part of the plate. However, in general the lithosphere is

considered to be 120-150 km thick, although within cratonic provinces the thickness may vary (Jordan, 1988), but the fact remains that temperatures at such depths are considerably higher, in the order of 1000 °C (McKenzie & Bickle, 1988). Magmas from the lithosphere are often inferred to have trace-element characteristics distinct from MORB or OIB.

In summary, the lithosphere is here considered to be that part of the Earth that is affected by tectonic processes and extends to a depth of 120 - 150 km (this varies with extension and compression). It consists of the crust and that part of the mantle that is distinguishable from the convecting upper mantle on the basis of trace element and isotopic ratios.

1.5.2 The Asthenosphere.

The asthenosphere consists of the weaker part of the mantle, characterised by lower seismic velocities and low viscosity. MOR basalts are depleted relative to bulk earth, and thought to originate from shallow levels in the asthenosphere. Magmatic suites from the asthenosphere are inferred to have trace element and isotopic signatures similar to oceanic basalts.

1.6. Lithospheric Source Regions.

Melt generation at the anhydrous peridotite solidus, cannot take place within the continental mantle lithosphere according to most geophysical models (Arndt & Christensen, 1992). However if the lithosphere is hydrous and the underlying asthenosphere is anhydrous then significant amounts of melt can be produced in the lithosphere before any melt is produced in the asthenosphere (Gallagher & Hawkesworth, 1992). This occurs with only modest increases in the temperature of the lower lithosphere and in the absence of significant extension.

Chemical observations for many CFB are consistent with an origin in the sub-continental lithospheric mantle. These include the fact that the distinctive trace element and isotopic signatures of such CFB are restricted to the continents, and if the source

region is in the convecting upper mantle basalts with similar compositions should be erupted in oceanic settings. Also the major-element compositions of at least some CFB suggest that the source is both depleted in major elements and relatively shallow, consistent with the basalt-depleted nature of the sub-continental lithospheric mantle (Erlank *et al.*, 1984; Hergt *et al*, 1991; Lightfoot *et al.*, 1993; Peate & Hawkesworth, 1996). Furthermore, the isotopic ratios observed suggest old, trace-element-enriched source regions in the upper mantle, and these are unlikely to be preserved in the convecting mantle (Hergt & Hawkesworth, 1992).

Apparently uncontaminated basalts from provinces including the Paraná - Etendeka CFB have distinctive trace element signatures (low Nb/Ba; Nb/La) and enriched isotopic ratios for Sr, Nd and Pb. Since these are thought to have been derived from within mantle lithosphere Gallagher and Hawkesworth (1992) suggested melting took place at the hydrous solidus.

1.6.1 Gallagher & Hawkesworth model.

Important features of the Gallagher and Hawkesworth (1992) model include:
(i) Melting in the hydrous lithosphere with no melting in the anhydrous asthenosphere is favoured at low degrees of extension, and a thicker MBL. Melting in the asthenosphere with no melting in the lithosphere occurs when the MBL is thinner, or at low values of the mantle potential temperature provided the stretching factor (β) is high.
(ii) Where partial melting occurs in both the lithosphere and asthenosphere, the lithosphere will melt at lower values of β.
(iii) For a given MBL thickness, lower values of the mantle potential temperature (T_p) require more extension to initiate melting in the asthenosphere, as do greater thicknesses of the MBL at a particular T_p.
(iv) Partial melting in the absence of extension requires higher T_p or a thinner MBL.

A number of arguments against a volatile-bearing lithosphere have been put forward including those of Arndt & Christensen (1992). Objections include (i) hydrous, metasomatized peridotites are rare in xenolith suites from kimberlites and alkali basalts. (ii) Melting of a hydrous source produces water-rich magmas. However, CFB have low

water contents, hydrous minerals are virtually absent and explosive volcanism is rare; (iii) Certain mismatches occur between the likely compositions of partial melts of hydrous lithosphere and those of CFB. It seems unlikely that hydrous melts would have highly magnesian compositions similar to the picrites found in many flood volcanic sequences (Ellam & Cox, 1991), but such compositions are not found in the Paraná. Hydrous metasomatized lithospheric peridotites also appear to lack the negative Nb-Ta anomalies characteristic of most CFB.

The conclusion by many, therefore, is that the continental lithosphere is too cold and too dry and does not have an appropriate trace element signature to be a major source for CFB. Nonetheless, some interaction between plume derived magmas and the continental lithosphere probably occurs as the magma moves from the asthenosphere through the lithosphere to the surface. The level and nature of this interaction is uncertain.

1.7 Asthenospheric Sources.

Models that propose asthenospheric sources for CFB, and in particular the arrival of a mantle plume to generate large volumes of magma and initiate rifting include those of Richards *et al.* (1989) and Campbell & Griffiths (1990). Melting occurs in response to decompression within the mantle plume, and in some circumstances mantle plumes may be responsible for crustal extension. The magmas are generated in the plume and so they should be similar to plume related OIB. A plume initiation model provides a plausible explanation for the high eruption rates for flood basalts compared to those for the associated hotspot tracks. In such models, flood basalts represent plume heads, while hotspots represent continuing magmatism from plume tails, and in the model of Richards *et al.* (1989) a thin conduit connects the head to the source. An intrinsic assumption is that the plume has much lower viscosity than the surrounding material, with the temperature of plume material being several hundred degrees hotter. The size of the flood basalt province is then a function of the feed rate, and the instability initially originates at the core-mantle boundary.

Plume impaction models such as Kent *et al.* (1992) and Campbell & Griffiths (1990) try to explain the different styles of intraplate volcanism. Campbell and Griffiths (1990) suggest voluminous magmatism will occur quickly but ~10Ma after the plume head impinges on the base of the lithosphere. The mantle plume has a central tail or conduit made up of material derived directly from the plume source, and a large head, comprising a mixture of source material and entrained upper mantle. The lithosphere is thinned rapidly by small-scale secondary convection in the plume head. A longer time scale is suggested by the Kent *et al.* (1992) model in which the plume can incubate beneath thick (150km) lithosphere for up to 150Ma before the lithosphere thins enough to allow voluminous basalt production.

An alternative to the theme of a primary asthenospheric source for CFB, is that melts from the asthenosphere mix with small degree melts (lamproites) from the lithosphere (Ellam & Cox, 1991). In this model the distinctive trace element and isotopic signatures are derived from the lithosphere, but the main mass of magma is from the underlying hotter asthenosphere. The problem is that the plume-derived melts would need to have very low trace-element contents of Ti in particular in order to generate the eruptive composition of CFB, and yet plume-derived oceanic basalts tend to have relatively high Ti. Arndt & Christensen (1992) suggest that plumes are the source of > 95 % of the CFB, but they interact with the mantle lithosphere where phases such as amphibole and oxides scavenge elements - Nb and Ti, for example, out of the melt to explain their low abundances. The resultant melt may then assimilate continental crust to attain other more extreme chemical and isotopic signatures.

1.8 Controls on melt generation.

The composition of liquids produced by decompression melting of mantle peridotite are controlled primarily by the bulk composition, the degree of partial melting, and the nature and composition of the starting and residual minerals. The latter depend on the temperature of the source and pressure/depth at which melting occurs. Pressure has a direct control on melt composition, and with increasing pressure the

aluminous phase changes from plagioclase to spinel to garnet. Also the stability fields of olivine and pyroxene change with pressure, and so with decreasing pressure the melt becomes increasingly olivine rich (Cox, 1980).

The volume of melt produced by upwelling of mantle material depends on the thickness of the MBL and the temperature of the upwelling mantle material and on the volatile content (McKenzie & Bickle, 1988; Gallagher & Hawkesworth, 1994). Typical asthenospheric temperatures are of the order of 1280 °C; relatively high temperatures of 1480 °C represent plume conditions.

The compositions of CFB are controlled by lithospheric thickness, which influences the depth and degree of mantle melting of a mantle plume. Partial melting of peridotite at sub-lithospheric depths results in highly magnesian (20 - 25 wt% MgO) liquids with variable trace element contents. Thick lithosphere implies that the source melts at high pressure, garnet is a residual phase at least at small degrees of melting. Such melts would be depleted in Y and HREE, and have high incompatible-trace-element contents. If the lithosphere is thin, the plume ascends to shallower levels, the degree of melting is greater for the same potential T, trace element concentrations are lower and there is more likely to be residual spinel rather than garnet in the source. Melting at shallower depths as a result of lithospheric thinning by erosion of the base and/or melting of hotter upwelling mantle will, in general, result in more extensive degrees of melting.

Hot mantle plumes ascending from depth are hotter than the ambient mantle as discussed before, and so they will intersect the solidus at greater depths, and they also require less extension to produce large volumes of melt (McKenzie and Bickle, 1988). The amount of extension will greatly affect the thickness of the lithosphere, and consequently the greater the β (stretching) factor the greater the proportion of melt from the asthenosphere (McKenzie & Bickle, 1988; Kerr, 1994), although this will depend on the initial thickness of the lithosphere (Gallagher & Hawkesworth, 1992).

The compositions of CFB also depend on the processing of magmas in crustal level chambers that are periodically replenished and tapped, while continuously fractionating and assimilating the wall rocks. The composition thus becomes far

removed from the inferred parental picritic magmas. Major elements in CFB reflect olivine, pyroxene and plagioclase fractional crystallization, which places the chambers at relatively low pressures within the crust (Cox, 1980; Wilson, 1989).

Fig. 1.6. Mantle-normalised diagram of incompatible elements showing anomalous Nb - Ti values associated with some CFB (Gramado - Paraná); also shown are a small degree mafic potassic melt and bulk continental crust (Data from McCulloch & Bennett, 1994; Gibson *et al.*, 1995 and Peate & Hawkesworth, 1996) and the asthenosphere derived Deccan CFB (Mahoney, 1988). Normalised to primitive mantle using data from Sun & McDonough (1990).

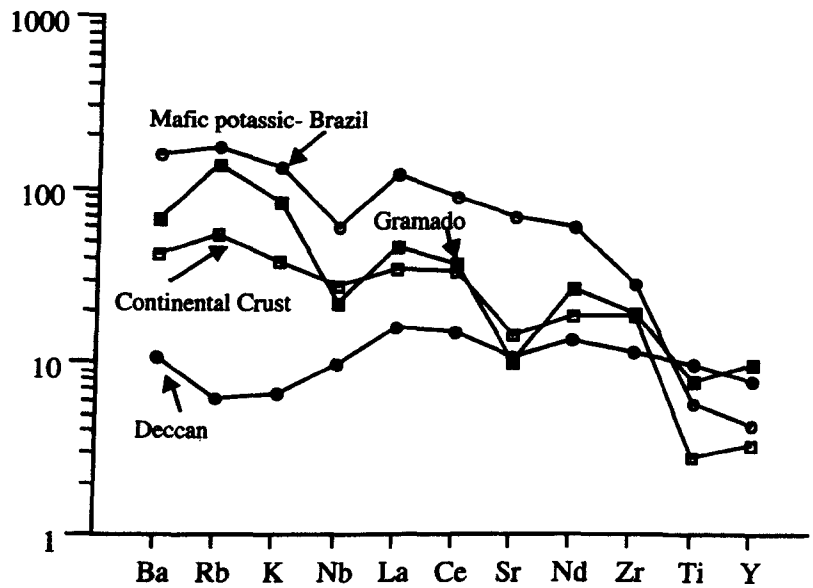

1.9 Small degree melts.

Lamproites are small degree melts from the lithospheric mantle that have high incompatible-trace-element concentrations, higher than those in the continental crust. They are ultrapotassic, magnesian rocks with $K_2O/Na_2O > 5$ (Bergman, 1987). Lamproites occur close to cratonic margins, commonly as dykes and flows. Their minor- and trace-element signatures are also very different to oceanic basalts. In many cases they have enriched isotopic ratios which imply the source regions were relatively enriched in trace elements for long periods of time. High εNd values and low Sm/Nd ratios suggest old sub-continental mantle which has been preserved in the non-conducting part of the upper mantle for a billion or so years. Unlike lamproites,

however, CFB have trace element abundances that are low enough to be influenced by crustal contamination and thus will be examined next (Fig. 1.6).

1.10. Continental Crust & Contamination

The trace-element and isotopic compositions of some continental basalts are similar to those compositions of granitoids and sedimentary rocks. Therefore, in some cases it is possible to conclude that the magmas were derived from the asthenospheric upper mantle, but that they were subsequently contaminated by crustal rocks. Continental crust has higher SiO_2 and K_2O contents, higher Rb/Sr and lower Sm/Nd than melts from the asthenosphere. Old continental crust tends to have high $^{87}Sr/^{86}Sr$ ratios, radiogenic Pb isotopic compositions and low εNd values. The lower crust may have low εNd values and combined with unradiogenic Sr and Pb isotopic compositions.

Negative Nb-Ta anomalies (low Nb/La ratios) are found in almost all rocks of the continental crust, and peridotite xenoliths from the continental mantle lithosphere and most rocks from oceanic regions have Nb/La ratios similar to or greater than chondritic ratios (Arndt & Christensen, 1992). Comparison of the chemical and isotopic compositions of continental flood basalts with those of likely mantle and crustal reservoirs has therefore been used to suggest that the continental crust is the source of the distinctive chemical features observed in some CFB such as low Nb/La ratios (Carlson *et al.*, 1981; Hawkesworth *et al.*, 1984; Arndt *et al.*, 1993).

Objections to crustal contamination models tend to be centred around the difficulty of generating the compositions and chemical variations of CFB by simple assimilation and fractional crystallisation models. Even if highly magnesian parental magmas are invoked, as suggested by partial melting at sub-lithospheric depths it has proved difficult to reconcile the negative Nb-Ta anomalies in particular with simple AFC models (Turner & Hawkesworth, 1995; Turner *et al.*, 1996). Thus this feature is often attributed to processes in the lithospheric mantle which may then either be the bulk source of CFB, or a contaminant into asthenosphere-derived melts. The amount of crustal contamination required to produce the trace-element signatures observed in some

CFB may be as much as 25 - 30 %, however it would be difficult to retain a basaltic composition in the resultant lavas.

1.11 Summary.

It appears therefore that unlike the model of White & McKenzie (1989) which aptly describes the situation at mid-ocean ridges, no one model consistently describes the origin and source of **all** continental flood basalts. In this thesis it is hoped to develop a suitable model to describe fully the dynamics that lead to the formation of the Uruguayan volcanics and to expand this model in relation to the evolution of the South Atlantic rift system. First however the tectonic history of the Gondwana supercontinent is addressed in order to understand the kinematic regimes active in the region pre-, syn-, and post-rifting. Following this discussion will be a brief introduction to the Paraná - Etendeka CFB with the main geochemical features of the province summarised in order to provide the basis for a detailed comparison with the Uruguayan volcanics in Chapter 2.

1.12. Case of Gondwana.

In the case of the disintegration of Gondwana, according to Storey (1995), plumes are not the ultimate driving force for break-up; instead break-up can be linked to changes in plate boundary forces and the tectonic regime (the kinematics operating in the area of the South Atlantic at this time are briefly described in a following subsection). Nonetheless, hotspot activity is known to have occurred in the region as a number of current hotspots can be retraced to their positions in the Jurassic/Cretaceous periods. These include Tristan da Cunha and St. Hélena in the South Atlantic.

The timing and direction of rifting once initiated, and the temporal relationship between rifting and the products of volcanic activity need also to be understood. In the South Atlantic, seafloor spreading appears to have begun in the south and propagated northwards (Uchupi, 1989). Magnetic anomaly M10 (> 133 Ma) has been described by Martin (1987) at a triple junction near the tip of the Falkland plateau, which is close to

the age of the main CFB. First oceanic crust was recognised in the vicinity of the Tristan da Cunha plume at M4 (127 - 126 Ma, Kent & Gradstein, 1985), almost 10 Ma after the main magmatic event. The timing and duration of magmatism in this region remains a subject of debate with some published data suggesting that the entire province was erupted in 1 - 2 my (Renne *et al*, 1992), while others including Turner *et al.* (1994) suggest that magmatism occurred between 137 - 128 Ma, with the main eruptive phase at ~ 133 Ma. It is with these thoughts of trying to add to the understanding of the tectonic processes that operated in the South Atlantic pre-, syn- and post- rifting and to add constructively to the debate regarding timing of magmatism that this project was undertaken.

1.12.1 History of Gondwana prior to break-up in the Cretaceous.

Gondwana was assembled during the latest Precambrian and earliest Cambrian Pan African orogenic cycle (Fig. 1.7a). The formation of the megacontinent Laurussia (from Laurentia-Greenland & Fennoscandia-Baltica) was accompanied by rifting along the northern margin of Gondwana and the successive detachment from it of different continental terranes (Ziegler, 1992). The 'SWEAT' hypothesis of Moores (1991) suggests the juxtaposition of the southwest United States and East Antarctica (SWEAT) prior to the opening of the Pacific during the Neoproterzoic (1000 – 540 Ma; Dalziel, 1997). The SWEAT hypothesis questions traditional geographic reconstructions in the latest Proterozoic, with rapid motion of Laurentia to equatorial latitudes occurring during the Cambrian (Dalziel, 1997). In Ordovician and Silurian times Gondwana drifted over the South Pole in a sinistral, rotational fashion (Fig. 1.7b), and a number of basins were formed including the Paraná (Unternehr *et al.*, 1988).

In the Late Silurian - Early Devonian, reorganization of the plates occurred and Gondwana began to converge with Laurussia through clockwise rotation. The beginning of the Hercynian orogenic cycle was marked by the collision of Gondwana with Laurussia, coupled by their joint clockwise rotation and northward drift (Ziegler, 1992). The results ranged from the formation of a fold belt to shear systems; lithospheric thickening and intraplate compressional deformation and new arc-trench

systems in one segment of the globe. While elsewhere, orogenic activity ceased and rifting phases commenced.

In the late Carboniferous and Early Permian the long standing subduction systems were abandoned (Ziegler, 1993). Activity, however, increased along the subduction system at the Pacific margin of the newly accreted Pangea supercontinent (Fig. 1.7c). In the Late Permian and Triassic, 40° counterclockwise rotation of Pangea occurred around a pivot in the Gulf of Mexico (Ziegler, 1992) (Fig. 1.7d), and northward drift of Pangea commenced in the early Jurassic. Meanwhile, rifts propagated both in the north-east resulting in the separation of Cimmeria, and also southward into areas between Africa & Madagascar and India & Australia. In southern Africa, in particular, numerous dyke swarms trend in a variety of directions. Furthermore, the basalts and dolerites of the Southern Africa (Karoo) and Antarctica, Australia & New Zealand (Ferrar Dolerites and Kirkpatrick Basalts) were erupted as a precursor to the separation of Africa from Antarctica and the formation of the Indian Ocean (Cox, 1978). Magmatism is also evident in Argentina related to subduction along the Pacific margin and the development of the Chon-Aike, Tobífera and Marifil formations (Pankhurst & Rapela, 1995).

The interior of Pangea was further dismantled by westward and southward propagating rift systems to form the Tethys and Norwegian-Greenland Sea respectively. In the Late Triassic and Early Jurassic, crustal distension in the Gulf of Mexico - Central Atlantic - Tethys Rift zone, accompanied by extrusion of basalts in the Central Atlantic domain, culminated in a discrete divergent/transform plate boundary between Laurussia and Gondwana (Ziegler, 1992). This reorganization resulted in a new kinematic regime which influenced further break-up of Gondwana and the newly assembled Laurasia megacontinent until crustal separation of these two megacontinents took place in the Late Jurassic.

Fig. 1.7 a & b Continent configurations and subduction zone locations during the early Proterozoic (a) Cambrian & (b) Silurian (after Ziegler, 1992).

Fig.1.7a.

LATE CAMBRIAN

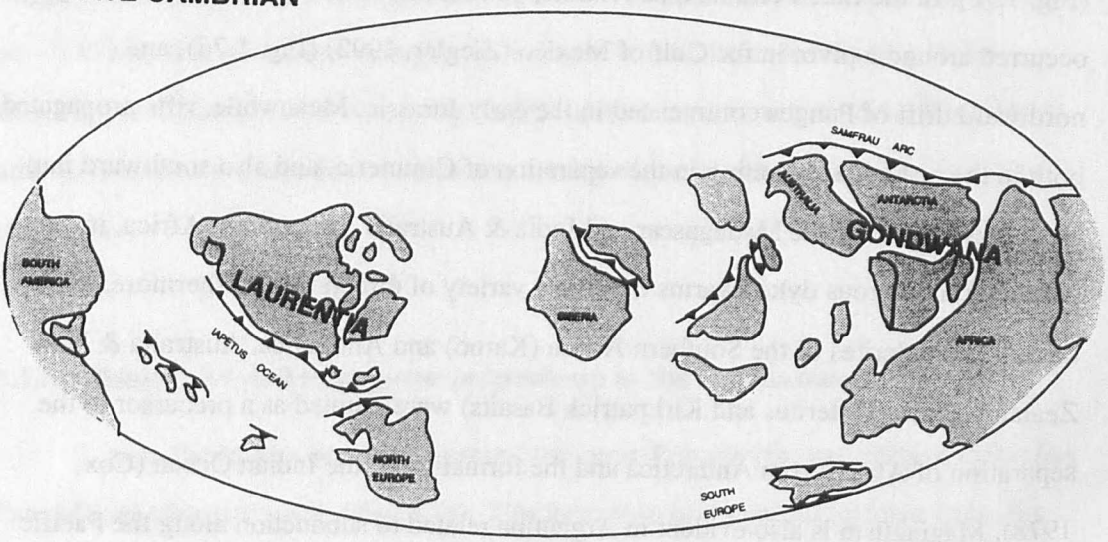

Fig. 1.7b

MIDDLE SILURIAN

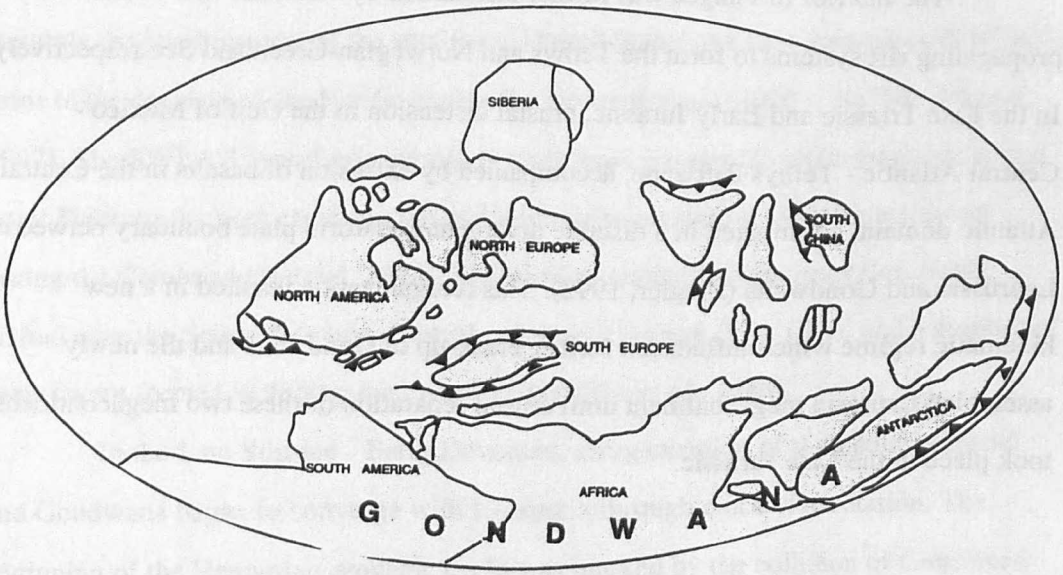

Fig. 1.7c & d. Configuration of newly accreted Pangea supercontinent during the Carboniferous and its migration thereafter through the Permian.

Fig. 1.7c

LATE CARBONIFEROUS

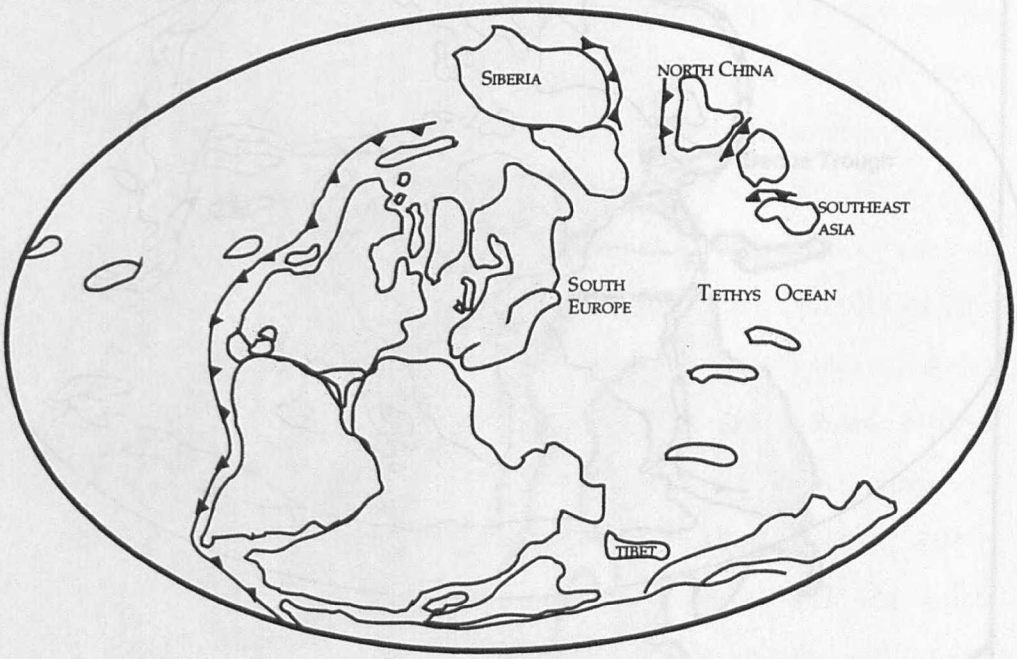

Fig. 1.7d

TRIASSIC

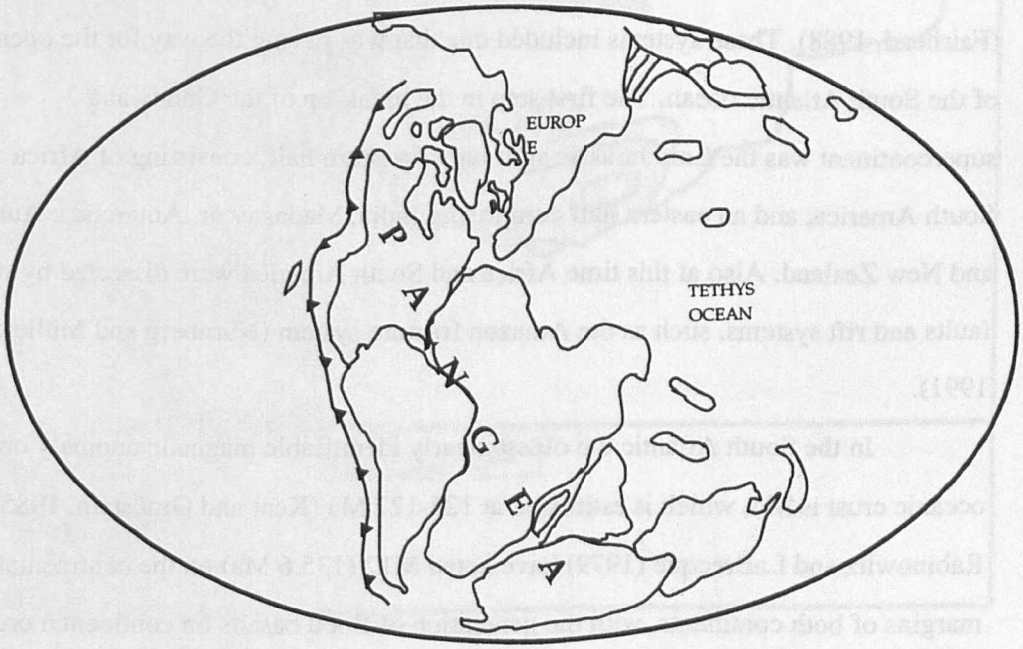

Fig. 1.8 Positioning of the major continents following fragmentation of Pangea during the Jurassic and Cretaceous.

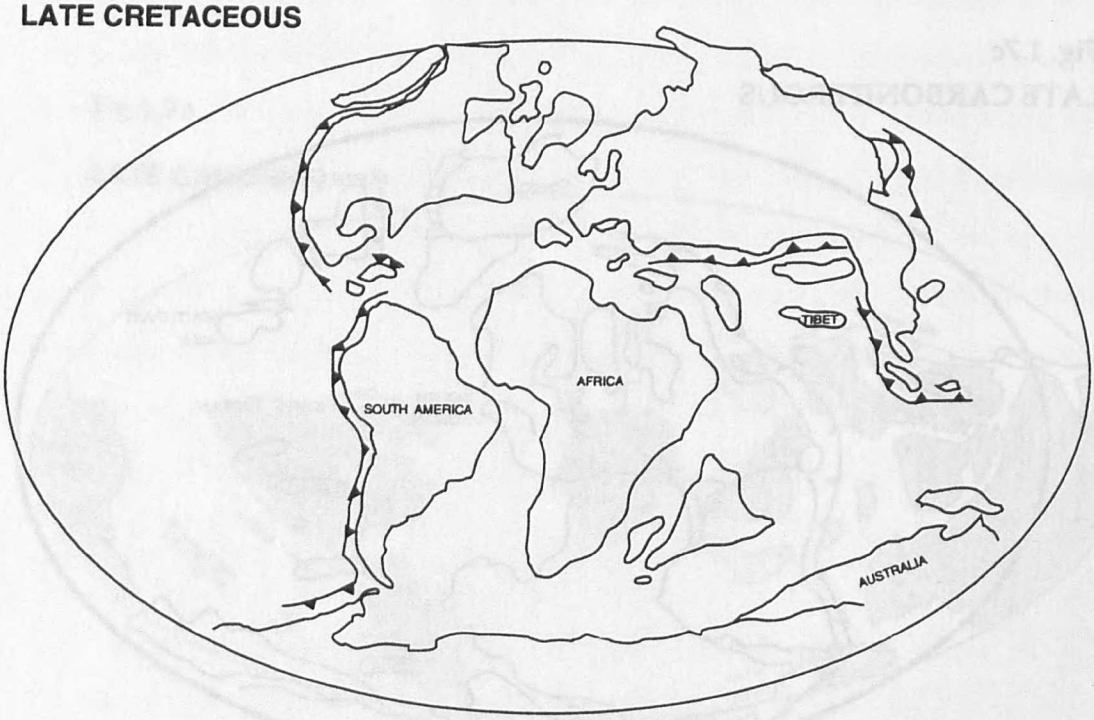

During the Late Jurassic and Early Cretaceous Gondwana remained more or less stationary but it was deformed internally by rift systems and extensional tectonics (Fairhead, 1988). These systems included one that was paving the way for the opening of the South Atlantic ocean. The first step in the break-up of the Gondwana supercontinent was the Late Jurassic split into a western half, consisting of Africa and South America, and an eastern half comprising India, Madagascar, Antarctica, Australia and New Zealand. Also at this time Africa and South America were dissected by wrench faults and rift systems, such as the Amazon fracture system (Nürnberg and Müller, 1991).

In the South Atlantic the oldest clearly identifiable magnetic anomaly on the oceanic crust is M4, which is estimated at 126-127 Ma (Kent and Gradstein, 1985). Rabinowitz and LaBrecque (1979) have noted M12 (135.6 Ma) on the continental margins of both continents, with the generation of flood basalts on continental crust prior to onset of rifting.

Fig. 1.9. Structure of the South American & African continents prior to and during break-up in the Cretaceous showing basins, including the Paraná - Etendeka CFB province.

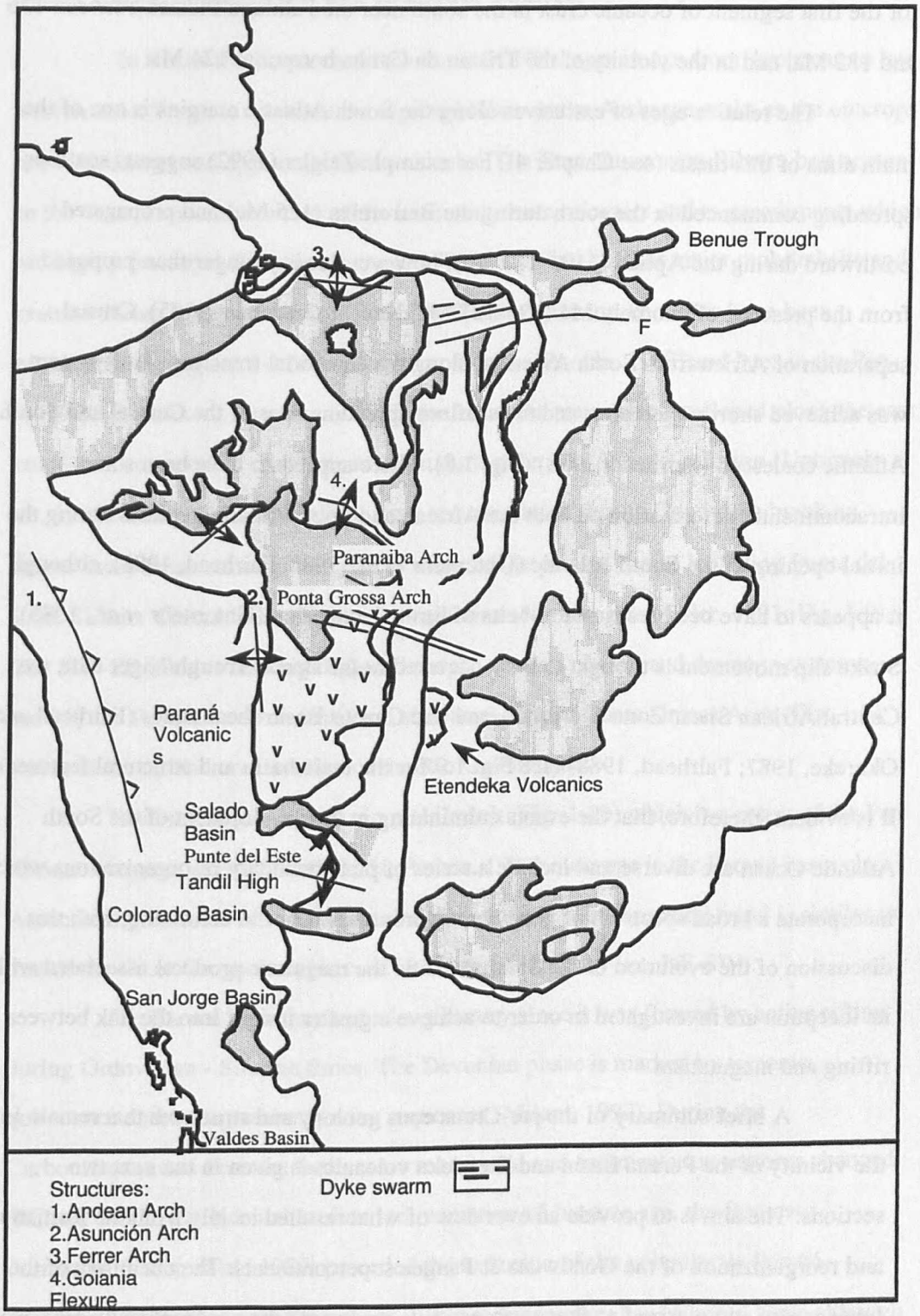

Seafloor spreading is therefore thought to have commenced in mid Lower Cretaceous and to have propagated northwards thereafter (Nürnberg & Müller, 1991) with evidence for the first segment of oceanic crust in the south near the Falkland Plateau between 136 and 132 Ma, and in the vicinity of the Tristan da Cunha hotspot at 124 Ma.

The relative ages of extrusives along the South Atlantic margins is one of the main aims of this thesis (see Chapter 4). For example Zeigler (1992) suggests seafloor spreading commenced in the south during the Barremian (125 Ma) and propagated northward during the Aptian (119 - 113 Ma), however this is younger than proposed from the presence of anomaly M4 (126-127 Ma, Kent & Gradstein, 1985). Crustal separation of Africa from South America, along the equatorial transform fault system was achieved shortly thereafter and the seafloor spreading axes of the Central and South Atlantic coalesced (Fairhead, 1988) (Fig. 1.8). There appears to have been some intracontinental deformation on both the African and South American plates during the initial opening of the South Atlantic (Unternehr *et al.*, 1988; Fairhead, 1988), although it appears to have been restricted to belts of limited extension (Unternehr *et al.*, 1988). Strike slip movement is thought to have occurred in the Benue Trough/Niger Rift, the Central African Shear Zone and the Paraná and Chacos Basin shear zones (Fairhead and Okereke, 1987; Fairhead, 1988) (see Fig. 1.9 for the main basin and structural features). It is evident, therefore, that the events culminating in the development of the South Atlantic Ocean are diverse and include a series of plate boundary re-organizations which incorporate a broad spectrum of geodynamic processes. Prior to continuing with this discussion of the evolution of the South Atlantic the magmatic products associated with its inception are investigated in order to achieve a greater insight into the link between rifting and magmatism.

A brief summary of the pre-Cretaceous geology and structures that remain in the vicinity of the Paraná Basin and Etendeka volcanics is given in the next two sections. The aim is to provide an overview of what resulted locally from the formation and reorganization of the Gondwana & Pangea supercontinents. The chemistry of the lavas is also summarized so that a comparative study with the geographically proximal Uruguayan volcanics may be undertaken in Chapter 2.

1.13. The Paraná Basin.

1.13.1 Background geology and structural features.

In Brazil the basement to the Paraná CFB ranges in age from Archaean to late Proterozoic. There is no dominant regional fabric in the Archaean rocks as the outcrops are fragmented and appear as discrete blocks. The Transamazonian Ribeira belt occurs in the central and eastern part of the basin with metavolcanics and metasediments which are highly fractured (Mantovani *et al.*, 1991) (See Fig. 1.10 for major mobile belts and cratons during the Proterozoic). The NW-SE structures are known to have been reactivated during a 1.1-1.0 Ga orogenic collision (Porada, 1989) and later in the Pan African (Brasiliano) orogeny. NW-SE dextral shear zones also developed along the east coast to accommodate intraplate rotation during the Pan African collision (Unternehr *et al.*, 1988). Extension is thought to have occurred later, during Gondwana break up, across these shear zones giving rise to many of the present basins including Punte del Este, Salado, Colorado and Valdes in Argentina (Nürnberg & Müller, 1991; Fig. 1.9). The NW-SE trend is also highlighted by dyke swarms, faults, and drainage systems, namely the Paranaiba Arch (antiform structure) and the Ponta Grossa Arch (Fig. 1.9), which is the onland continuation of the Rio Grande Rise.

The Proterozoic Brasiliano mobile belt (Fig. 1.10) which is a result of the Pan African orogenic event (750-500 Ma, Porada, 1989) outcrops in the Paraná basin also. Associated granitoids intrude regional metasediments. The structural trend is similar to that of the Ciclo Orogenico observed in Southern Uruguay (i.e. NE-SW).

The Paraná basin has had a long history since it was formed by active rifting during Ordovician - Silurian times. The Devonian phase is marked by tectonic quiescence and transgressive marine sequences (Milani, 1992). During the Carboniferous and Permian faults were reactivated and sedimentation patterns changed (Milani, 1992). Continental aeolian sedimentation of Jurassic age, the Botucatu Formation (Zalan *et al.*, 1987) preceded the extrusion of the voluminous Paraná - Etendeka CFB in the early Cretaceous. Little sedimentation has occurred since although minor aeolian sands are preserved in the northern part of the basin overlying some

basalts. The three dimensional structure of the basin is well known from oil exploration boreholes and detailed mapping. In the north in the deepest part of the basin between 1.5 and 1.7 km of basaltic rocks are preserved (Peate *et al.*, 1992), but the better exposures are along the Serra Geral escarpment and they have been the subject of many of the more detailed studies. Contemporaneous alkaline magmatism, including carbonatites, syenites, phonolites and granites, is noted around the margins of the basin (Ulbrich & Gomes, 1981; Milner *et al.*, 1995). Mention of alkaline complexes will be given greater attention in Chapter 2 when the Uruguayan syenite is described.

1.13.2 The Paraná - Etendeka CFB Province.

The areal and volumetric distribution of the Paraná- Etendeka CFB is highly asymmetric, with most of the outcrop preserved on the South American continent (Fig. 1.9). The province is here described in two geographical sections, the Paraná Province in South America, and the Etendeka Province in southern Africa, both for convenience and because they have often been described separately in the literature. The Paraná CFB is a sequence of ~790,000 km^3 (Bellieni *et al.*, 1986), occurring principally in southern Brazil and extending into northern Uruguay, Paraguay and Argentina, predominantly within the Paraná sedimentary basin. Paraná magmatism is dominated (~ 90 %) by tholeiitic basalts and basaltic andesites, with volumetrically less significant rhyolites overlying the basalts at the top of the sequence, particularly in SE Brazil. The sequence is bimodal in silica, with rocks of intermediate composition rare. The preserved thickness of the basaltic sequence is variable with 1723 m recorded in a borehole in the north of the basin (Peate, 1989).

1.13.3 Paraná Basalts.

As with many CFB the basaltic rocks of the Paraná are virtually aphyric to subaphyric with phenocrysts and microphenocrysts of pyroxene and plagioclase feldspar, and some scarce Mg - Olivine. The pyroxenes are principally augite and pigeonite, with pigeonite dominating the pyroxene compositions in the south of the province while augite is more common in the north (Comin-Chiaramonti *et al.*, 1988). Ti-magnetite and ilmenite are ubiquitous.

Fig. 1.10. Structural outline of South America and Africa during the Proterozoic.

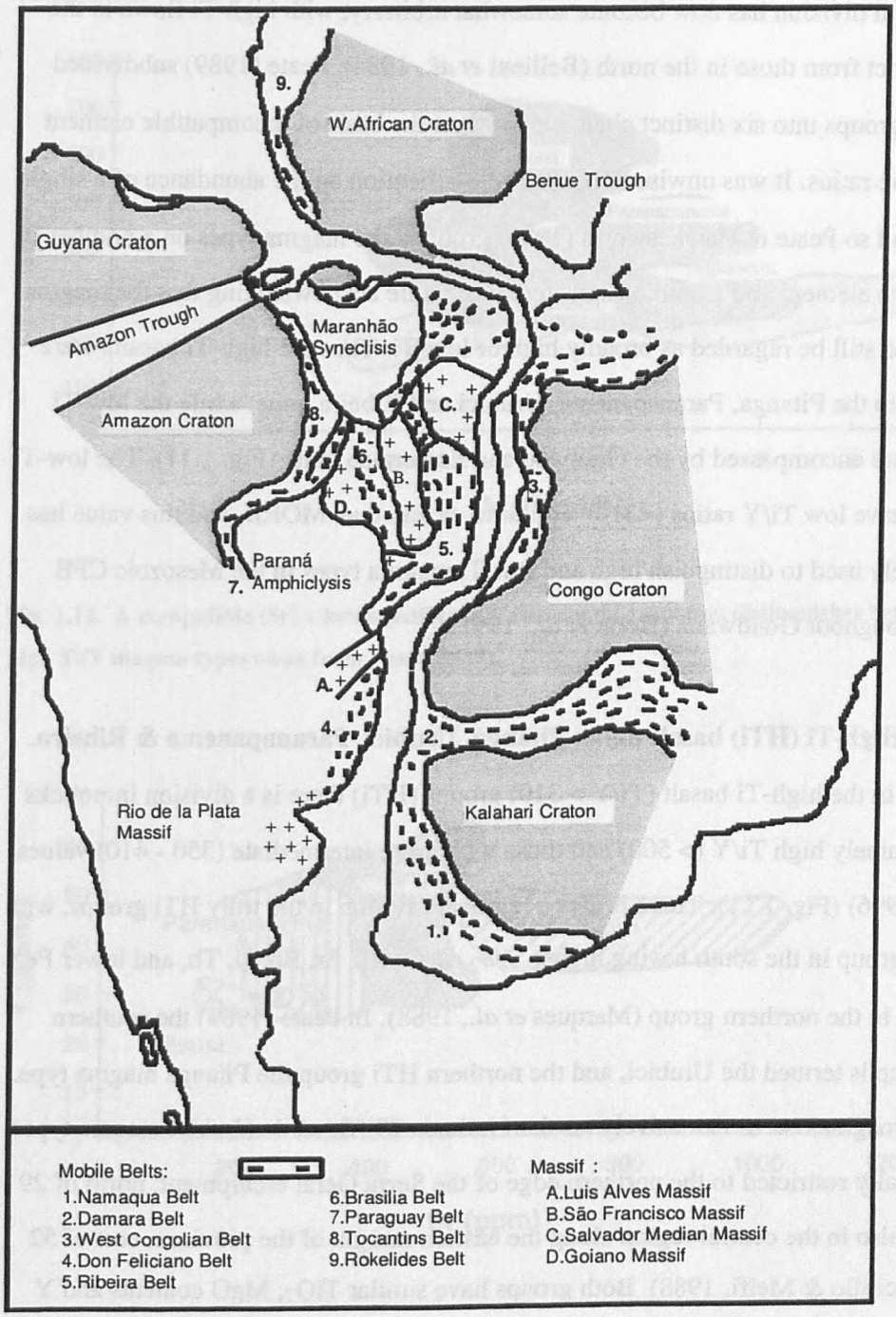

Studies of the chemistry of the Paraná CFB initially allowed Bellieni *et al.*, (1984) and Mantovani *et al.*, (1985) to subdivide the basalts into two distinct groups on the basis of Ti abundances. The groups are also distinct geographically with the high-Ti magma types (> 2 wt% TiO_2) occurring principally in the north of the basin, and Low

Ti magma types (< 2 wt% TiO_2) in the south. The north-south/highTi-lowTi geographical division has now become somewhat arbitrary, with high-Ti flows in the south distinct from those in the north (Bellieni *et al.*, 1984). Peate (1989) subdivided the basalt groups into six distinct chemical units on the basis of incompatible element and isotopic ratios. It was unwise to base the classification on the abundance of a single element and so Peate & Hawkesworth (1996) grouped the magma types on a number of major, trace element and isotopic characteristics, while acknowledging that the magma types could still be regarded as broadly high or low-Ti. Thus the high-Ti basalts were divided into the Pitanga, Paranapanema, Urubici and Ribeira units, while the low-Ti basalts were encompassed by the Gramado and Esmeralda units (Fig. 1.11). The low-Ti magmas have low Ti/Y ratios (<310) similar to or less than MORB, and this value has been widely used to distinguish high and low Ti magma types in the Mesozoic CFB found throughout Gondwana (Hergt *et al.*, 1991).

1.13.3.1 High-Ti (HTi) basalt units: Pitanga, Urubici, Paranapanema & Ribeira.

In the high-Ti basalt (Ti/Y > 310) groups (HTi) there is a division into rocks with genuinely high Ti/Y (> 500) and those with more intermediate (350 - 410) values (Peate, 1996) (Fig. 1.11). There is also a regional division in the truly HTi groups, with the HTi group in the south having higher SiO_2, K_2O, Rb, Sr, Ba, U, Th, and lower Fe than that in the northern group (Marques *et al.*, 1988). In Peate (1989) the southern HTi group is termed the Urubici, and the northern HTi group the Pitanga magma type. Pitanga magmas occur extensively north of latitude 27 °S, while Urubici magma types are spatially restricted to the northern edge of the Serra Geral escarpment, north of 29 °S, and also in the central region along the eastern margin of the province, east of 52 °W (Piccirillo & Melfi, 1988). Both groups have similar TiO_2, MgO contents and Y and Yb abundances. However, Sr is lower (< 600 ppm) in the Pitanga magma type and so it is used to distinguish these two magma types, as is the relative enrichment of some incompatible elements in the Urubici magma type over the Pitanga magma type (Peate, 1989) (Fig. 1.12).

Fig. 1.11. Magma types of the Paraná CFB illustrated on a diagram of Ti/Y - MgO (Data from Peate, 1989).

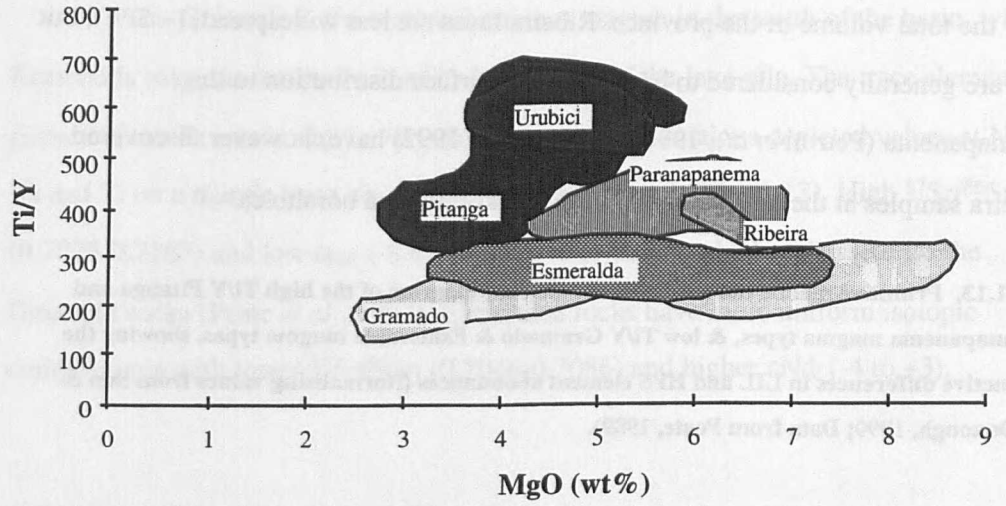

Fig. 1.12. A compatible (Sr) v incompatible (Zr) element diagram that distinguishes between the high Ti/Y magma types (data from Peate, 1989).

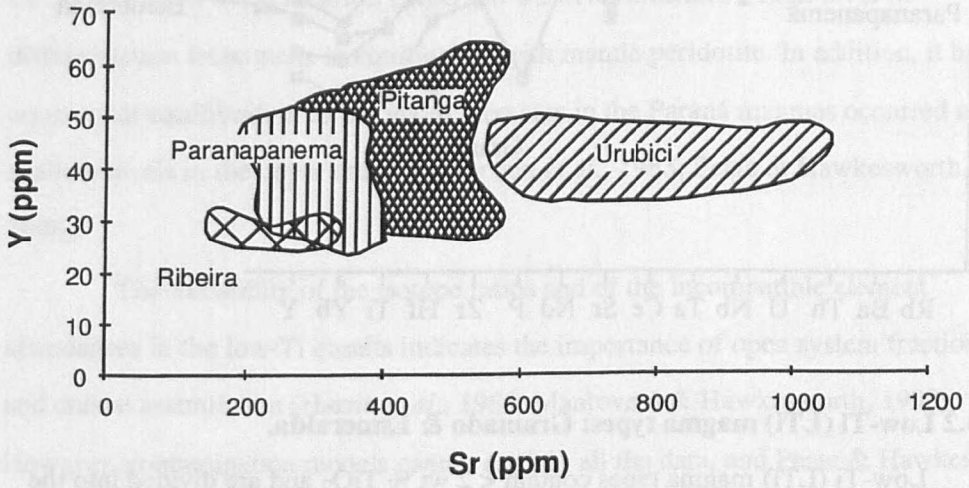

The Paranapanema and Ribeira magma types have similar LILE concentrations to the Pitanga magma type shown in Fig. 1.13. Isotopic abundances cannot be used to discriminate between these magma types as the range in values is restricted relative to other Paraná magma types (Peate, 1989). Exposures of the Paranapanema occur in the west in Paraguay and this magma type forms the upper

most stratigraphic unit of the lavas in the north of the basin (Bellieni *et al.*, 1986). Thus the Paranapanema lavas tend to overlie Pitanga lavas and together they constitute ~ 20 % of the total volume of the province. Ribeira lavas are less widespread, (~ 5 %), but they are generally considered to have a similar surface distribution to the Paranapanema (Petrini *et al.*, 1987). Peate *et al.*, (1992) have, however discovered Ribeira samples at the bottom of one of the central Paraná boreholes.

Fig. 1.13. Primitive mantle normalised trace element diagram of the high Ti/Y Pitanga and Paranapanema magma types, & low Ti/Y Gramado & Esmeralda magma types, showing the distinctive differences in LIL and HFS element abundances (Normalising values from Sun & McDonough, 1990; Data from Peate, 1989).

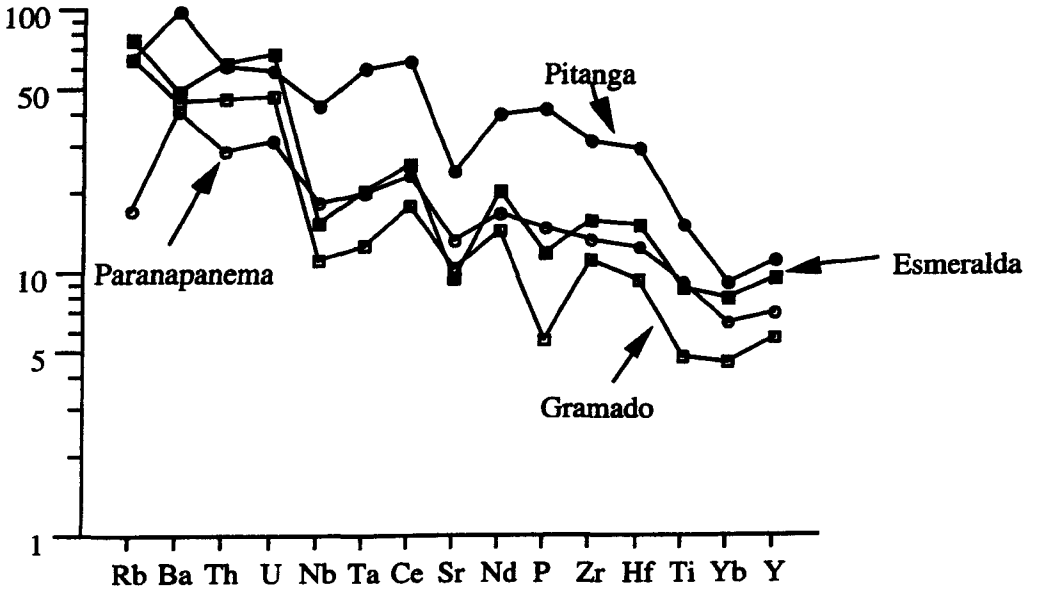

1.13.3.2 Low-Ti (LTi) magma types: Gramado & Esmeralda.

Low-Ti (LTi) magma types contain < 2 wt % TiO_2 and are divided into the Gramado & Esmeralda units (Fig. 1.11). These magma types are concentrated principally in the south of the Paraná basin and they have been distinguished on the basis of Fe, Ti/Zr & Ba (Fodor *et al.*, 1985). The Esmeralda magma type has lower SiO_2 and Al_2O_3, and higher TiO_2 and Fe_2O_3(t), than the Gramado magma type (Peate *et al.*, 1992). The incompatible elements Zr, Nb & Ba are lower in the Esmeralda unit, while Y is slightly enriched and Ti/Zr is higher than in the Gramado type. The

Esmeralda magma type also displays a range in certain incompatible element ratios (i.e. Sm/Nd), ratios that remain virtually constant for all other magma types in the Paraná.

The Gramado is the most voluminous magma in the south of the basin, while Esmeralda magmas tend to be confined to the top of the lava pile. The trace element pattern of the Gramado unit is very distinctive with anomalous depleted values at Nb, Ta and Ti on a mantle trace element normalised diagram (Fig. 1.13). High $^{87}Sr/^{86}Sr_i$ (0.7075-0.7167) and low ε_{Ndi} (-8 to -3) relative to bulk earth also characterise the Gramado rocks (Peate *et al.*, 1992). Esmeralda rocks have more uniform isotopic compositions with lower $^{87}Sr/^{86}Sr_i$ (0.7046-0.7086) and higher εNd_i (-4 to +3).

1.13.4 Potential sources for the Paraná basalts.

Geochemical evidence suggests that the different Paraná magma types cannot be related to one another by simple fractionation and assimilation processes (Mantovani *et al.*, 1985; Peate *et al.*, 1992; Peate & Hawkesworth, 1996). The evolved nature of the majority of Paraná magmas (MgO 3.0-6.5wt%) indicates a high level of differentiation from melts in equilibrium with mantle peridotite. In addition, it has been argued that equilibration of the major elements in the Paraná magmas occurred at shallow levels in the upper crust (Thompson *et al.*, 1983; Peate & Hawkesworth, 1996).

The variability of the isotope ratios and of the incompatible element abundances in the low-Ti basalts indicates the importance of open system fractionation and crustal assimilation (Harris *et al.*, 1989; Mantovani & Hawkesworth, 1990). However, contamination models cannot explain all the data, and Peate & Hawkesworth (1996), for example, have argued that the variation between the two low-Ti magma types, Gramado and Esmeralda, is not simply due to variations in crustal input as previously thought (Petrini *et al.*, 1987). Instead two distinct parental magmas are required, with the Gramado magma type dominated by crustal assimilation and fractional crystallisation, but with a parental magma derived from the continental mantle lithosphere. The Esmeralda magma type, in contrast, appears to reflect mixing

between an asthenospheric melt and a Gramado-type magma (Peate & Hawkesworth, 1996).

Thus in the debate over the sources of the different Paraná-Etendeka CFB magma types there is a possible shift from lithospheric to asthenospheric with time in the evolution of the province (Peate & Hawkesworth, 1996). The presence of a plume is considered essential to generate such large volumes of magma (Morgan, 1981; Turner *et al.*, 1994) and the Tristan da Cunha hotspot is known to have been in the region during the Cretaceous. The late stage Esmeralda basalts contain the only asthenospheric component recognised in the surface flows, and are volumetrically extremely small (Peate & Hawkesworth, 1996).

Overall the lithosphere is generally agreed to play an important role in the variability of chemical signatures observed in CFB (Ellam & Cox, 1991; Gallagher & Hawkesworth, 1992; Arndt *et al.*, 1993). As discussed previously the lithosphere is potentially a source (Section 1.6) (Gallagher & Hawkesworth, 1992; Turner *et al.*, 1996), with lithospheric thickness having an important control on melt composition (Section 1.8) (Arndt *et al.*, 1993). In the case of the Paraná both the high Ti/Y Pitanga, Paranapanema & Ribeira and the low Ti/Y Gramado magma types are considered to have a source within the continental mantle lithosphere (Hergt *et al.*, 1991; Turner & Hawkesworth, 1995; Garland *et al.*, 1996).

1.13.5 Paraná Rhyolites.

The Paraná rhyolites top the basalt sequences particularly in the SE of the Paraná province and overall cover an area of ~ 17,000 km^2. They were subdivided chemically into the Chapecó rhyolite group and the Palmas rhyolite group on the basis of Ti concentration (Mantovani *et al.*, 1985; Bellieni *et al.*, 1986). These rhyolite groups also show a provinciality with the high-Ti Chapecó rhyolites occurring in the centre and north of the basin, and the low-Ti Palmas rhyolites outcropping in the south. Peate *et al.*, (1992) and Garland *et al.*, (1995) further subdivided the rhyolite groups into three low Ti and two high Ti subgroups based on trace and rare-earth-element

chemistry and $^{87}Sr/^{86}Sr_i$ ratios (Table 1.2). These subgroups were also found to be distinct in the field.

Table 1.2. Subdivision of Paraná Rhyolites from the classifications of Piccirillo *et al.*, (1988); Peate *et al.*, (1992) & Garland *et al.*, (1995).

Piccirillo *et al.*, (1988)	Peate *et al.*, (1992)	Garland *et al.*, (1995)
low Ti: Palmas (PAV)	low Ti: Caxias do Sul; Santa Maria;	low Ti: Caxias do Sul Santa Maria; Anita Garibaldi
high Ti: Chapecó (CAV)	high Ti: Guarapuava; Ourinhos;	high Ti: Guarapuava; Ourinhos;

Many of the present-day outcrops of the rhyolites are preserved on the continental margins, with rhyolites also outcropping extensively in the Etendeka province. Peate (1997) suggested that this implied that the generation of the rhyolites was in some way closely linked to the rifting of the South Atlantic.

1.13.5.1 High-Ti Chapecó Rhyolites.

The Chapecó rhyolites of the northern Paraná are volumetrically less significant than the Palmas rhyolites forming 0.6 % vol. of the total outcrop of the Paraná CFB (Piccirillo *et al.*, 1988). The maximum thickness observed is 200 m, and there are local intercalations with tholeiitic basalts (Bellieni *et al.*, 1985). Petrographically the group is more phenocryst rich (10-15 % phenocrysts) than the Palmas, with phenocrysts predominantly of plagioclase, pyroxene and magnetite (Bellieni *et al.*, 1986b). The group is enriched in incompatible elements relative to the Palmas group (Bellieni *et al.*, 1986), with consistently higher abundances of high field strength elements (HFSE) such as Zr, Nb, P, Ti Ta & Hf. Temperatures obtained for the Chapecó rhyolites from pyroxene thermometry are in the range of 1000 - 1100 °C (Whittingham, 1991; Garland, 1994).

The Chapecó rhyolites may be subdivided into the Guarapuava and the Ourinhos subgroups. The Ourinhos is the most northerly rhyolite outcrop, and it has higher silica and large-ion-lithophile (LIL) elements then the Guarapuava subgroup. Fresh hand specimens yield plagioclase phenocrysts, unlike the Guarapuava in which alteration is more common and pyroxene phenocrysts are abundant.

The outcrop of the Guarapuava subgroup is more extensive, being mainly in the centre of the basin but with isolated outcrops in the north and occasional acid dykes intruding the basement to the east (Regelous, 1993). Guarapuava flows tend to overlie Gramado basalts in the south, whereas the isolated outcrops in the north are surrounded by Pitanga & Paranapanema basalt units (Piccirillo *et al.*, 1987; Garland, 1994). Overall the subdivision of the Chapecó rhyolites is best seen on a diagram of LILE vs. HFSE such as Rb vs. Zr (Fig. 1.14), simply because the Ourinhos subgroup has higher SiO_2, LIL and lower HFS than the Guarapuava (Peate *et al.*, 1992).

1.13.5.2 Low-Ti Palmas Rhyolites.

As noted in Table 1.2 the low Ti Palmas rhyolite group was subdivided most recently by Garland *et al.* (1995) into three units, namely the Caxias do Sul, the Santa Maria and the Anita Garibaldi. Volumetrically the Palmas rhyolites are much more significant than the Chapecó rhyolites and they are characteristically aphyric, < 5 % phenocrysts of plagioclase, pyroxene & titanomagnetite, and lower incompatible element concentrations (Peate *et al.*, 1992). Palmas rhyolite pyroxene temperatures are in the range 950 - 1050 °C, slightly lower than the Chapecó rhyolites (Garland *et al.*, 1995).

The Caxias do Sul subgroup is the more dominant Palmas-type rhyolite. It is stratigraphically the lowest unit and outcrops principally in the SE corner of the Paraná basin (Garland, 1994). It is characterised by having 3 - 5 % phenocrysts, with plagioclase dominant over pyroxene, and an occasional speckled appearance in hand specimen indicative of a devitrified matrix.

Fig. 1.14. Subdivision of the Paraná rhyolites on the basis of Large-Ion-Lithophile v High-Field-Strength element abundances (Data from Peate, 1989; Garland, 1994).

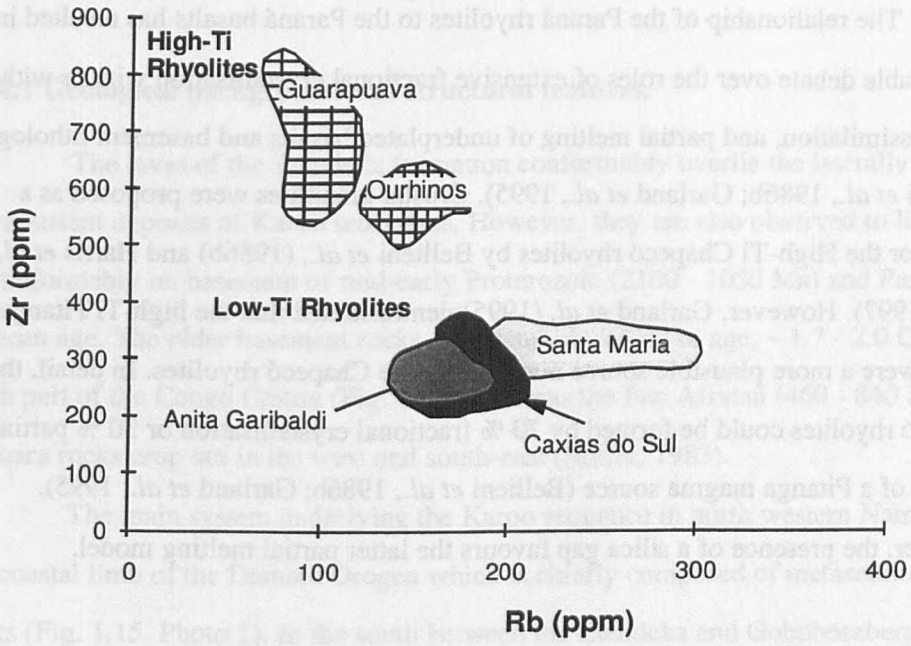

The Anita Garibaldi subgroup occurs in a distinct geographic region to the north of the main Palmas rhyolites and they are characterised by their glassy, vesiculated appearance in the field.

The Santa Maria rhyolites outcrop stratigraphically above the Caxias do Sul, separated by a thin basalt flow (Garland, 1994). They are characterised by a sugary texture in hand specimen and a virtual lack of phenocrysts. Chemically they have higher radiogenic $^{87}Sr/^{86}Sr_i$ (0.723-0.728) than the Caxias do Sul, $^{87}Sr/^{86}Sr_i$ (0.718-0.722).

1.13.6 Origin of the rhyolites.

High-Ti rhyolites- Chapecó.

Garland *et al.* (1995) argued that the Chapecó rhyolites could not be related to the Palmas by low-pressure fractionation of the observed fractionating assemblage. The Fe-Ti oxide abundances in the fractionating assemblage would have to be unrealistically

high to achieve a petrogenetic link, for example, between the Guarapuava subgroup and the Santa Maria. Independent parental magmas are inferred because of the much higher abundances of for example Zr and Nb in the Chapecó relative to the Palmas (Garland *et al.*, 1995).

The relationship of the Paraná rhyolites to the Paraná basalts has resulted in considerable debate over the roles of extensive fractional crystallisation with or without crustal assimilation, and partial melting of underplated basalts and basement lithologies (Bellieni *et al.*, 1986b; Garland *et al.*, 1995). Crustal granulites were proposed as a source for the High-Ti Chapecó rhyolites by Bellieni *et al.*, (1986b) and Harris *et al.*, (1990; 1997). However, Garland *et al.* (1995) demonstrated that the high-Ti Pitanga basalts were a more plausible source material for the Chapecó rhyolites. In detail, the Chapecó rhyolites could be formed by 70 % fractional crystallisation or 30 % partial melting of a Pitanga magma source (Bellieni *et al.*, 1986b; Garland *et al.*, 1995). However, the presence of a silica gap favours the latter partial melting model.

Low-Ti rhyolites - Palmas.

In contrast to the Chapecó, the Palmas rhyolites are considered not to be crustal melts primarily because of the fact that the Paraná basement has lower Nd isotope ratios than the rhyolites (May, 1990; Garland *et al.*, 1995). In addition the upper crustal sources implied by Sr & Pb isotopic values would appear to be in conflict with the high eruption temperatures and major-element compositions which indicate that these magmas were derived from lower crustal sources (Bellieni *et al.*, 1986b; Garland *et al.*, 1995). Variation diagrams such as Rb vs. MgO; Y vs. Zr are consistent with liquid lines of descent from the associated Gramado basaltic magma type suggesting a role for fractional crystallisation (Bellieni *et al.*, 1986b), and Garland *et al.* (1995) obtained good fits for open system fractionation of low-Ti Gramado magma with assimilation of upper crustal material. The silica gap between the two magma types was attributed to the onset of magnetite fractionation as it rapidly increases the SiO_2 content of a melt with a small degree of fractionation (Garland *et al.*, 1995). Compositional

differences between the Palmas subgroups were accounted for by regional variations in the extent and nature of assimilation, and the fractionating crystal assemblage.

1.14 South west Africa - Etendeka province.

1.14.1 Geological background and structural features.

The lavas of the Etendeka formation conformably overlie the laterally impersistent deposits of Karoo sediments. However, they are also observed to lie unconformably on basement of mid-early Proterozoic (2100 - 1050 Ma) and Pan African age. The older basement rocks are Transamazonian in age, ~ 1.7 - 2.0 Ga and form part of the Congo Craton (Fig. 1.10), whereas the Pan African (460 - 840 Ma) Damara rocks crop out in the west and south-east (Miller, 1983).

The main system underlying the Karoo sequence in north western Namibia is the coastal limb of the Damara Orogen which is chiefly composed of metasedimentary rocks (Fig. 1.15, Photo 1). In the south between the Etendeka and Goboboseberge lava fields, at least two phases of deformation are evident with the first giving rise to north-south trending isoclinal folds. Syn- and post- tectonic granites occur principally in the south although scattered intrusions are evident in the Kaoko Belt to the north. The Karoo sedimentary sequence consists of a number of formations including the Etjo; Gai-as; Prince Albert and Dwyka Formations. The sediments of the Gai-as Formation are Carboniferous to Jurassic in age and are currently preserved close to rivers as sedimentation was strongly influenced by the Pre-Karoo glacial topography (Milner, 1988). The older Permian sediments of the Dwyka Formation, (a tillite, only locally preserved) and the Prince Albert Formation (carbonaceous muds, siltstones and sandstones) form the base of much of the sequence (de Beer, 1992). Aeolian deposits of the Etjo Formation form the uppermost unit, and can be seen to overstep the older sediments to lie directly on basement. This sandstone can also be seen to be interbedded with the Cretaceous lavas of the Etendeka, and in some areas lavas are preserved flowing around massive dune structures (Fig. 1.15, Photo 2).

Fig. 1.15. Photo 1. **Metasediments deformed by the Damara orogen.**

Fig. 1.15. Photo 2. **The association of lavas and dune structures in the Etendeka. Exposed, rubble material in the foreground forms part of a 5m high dune structure, with Interbedded basalts and quartz latites are exposed in the upper 20m.**

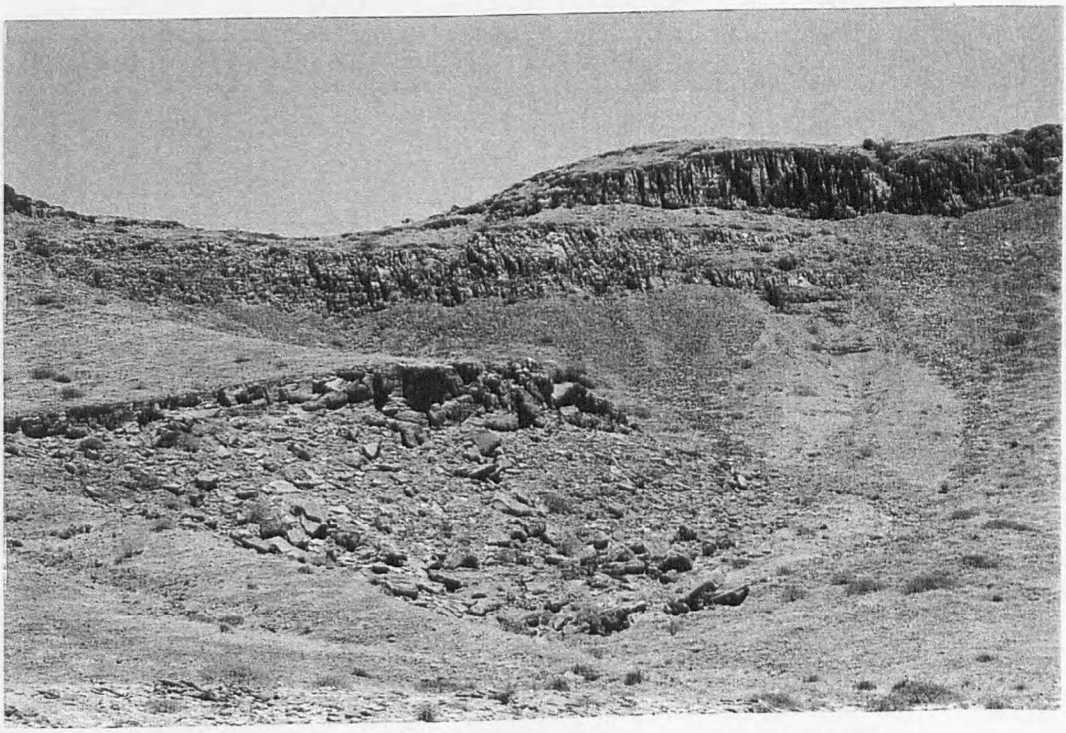

Thus similar rock types are found in the basement on both continents, indicating potentially similar environments of deposition and possibly tectonic stresses and strains prior to the fragmentation of Gondwana and more specifically Pangea. The intercalation of dune sands with the basal Paraná - Etendeka lavas on both continents is also important for later discussions on the timing of magmatism and rates of eruption.

1.14.2 The Etendeka CFB province.

The Etendeka CFB outcrops in Namibia, Angola and S. Africa. It was once thought to be the youngest part of the Karoo CFB (Eales *et al.*, 1984), but since then the Etendeka Formation has been promoted to Group status by Milner *et al.* (1994). It is now known to be intrinsically linked to the Paraná province on the basis of chemistry, geochronology and plate reconstruction. Most plate tectonic reconstructions place the Etendeka province adjacent to the south-east corner of the Paraná during the Early Cretaceous (de Wit *et al.*, 1988) (Fig. 1.9).

Remnants of the Etendeka occur within an area of 78,000 km^2 , the main outcrop is between Cape Cross and Cape Fria (Fig. 1.16), and the main lava field spans an area of 12,000 km^2 (Milner, 1988). Individual flow thicknesses vary from < 10 cm to > 1.5 m, and the maximum observed thickness of lavas is ~ 900 to 1000 m at the coast. The Etendeka forms only ~ 6 % of the volume of the entire Paraná - Etendeka CFB, and within it two distinct provinces are recognised, the Northern Etendeka Province and the Southern Etendeka Province, with remnants outside the Etendeka region at Erongo. These provinces are primarily recognised on the basis of chemistry, as in the north the basalts & quartz latites have high TiO_2 and Zr, while in the south the lavas have lower concentrations.

Overall the Etendeka CFB consists of basic to intermediate lavas (51-59 % SiO_2) interbedded with more acid quartz latite (QL) units (66 - 69 % SiO_2). In marked contrast to the Paraná the QL units comprise more than 50 % of the preserved outcrop thickness in some areas (Milner *et al.*, 1995). Dykes and sills associated with the sequence are seen to intrude the Damara granites (Erlank *et al.*, 1984). The basalts are tholeiitic, and tend to be aphyric to subaphyric with phenocrysts of plagioclase, clinopyroxene or more rarely pseudomorphosed olivine. The quartz latite term was

initially introduced by Erlank *et al.* (1984) and is compositionally equivalent to dacite, trachydacite and rhyolite on a TAS diagram (Le Maitre *et al.*, 1989; Milner *et al.*, 1992). Locally preserved pyroclastic textures has led to the quartz latites being termed rheomorphic ignimbrites by Milner *et al.*, (1992).

The basic to intermediate rocks are subdivided on the basis of incompatible element abundances, mainly Ti and Zr, and in the next two sub-sections they are compared with the Paraná magma types.

Fig. 1.16. Map of the distribution of the Etendeka volcanics, showing the type areas for different stratigraphic sections (after Milner, 1988; 1994). The Ambrosius Berg Fault Zone (ABFZ) divides the main lava field into two sections with >1000 m of volcanics preserved in the coastal succession. Brandberg and Messum intrusive complexes also included. Messum complex is the proposed eruption centre for the Awahab Fm. rhyolites.

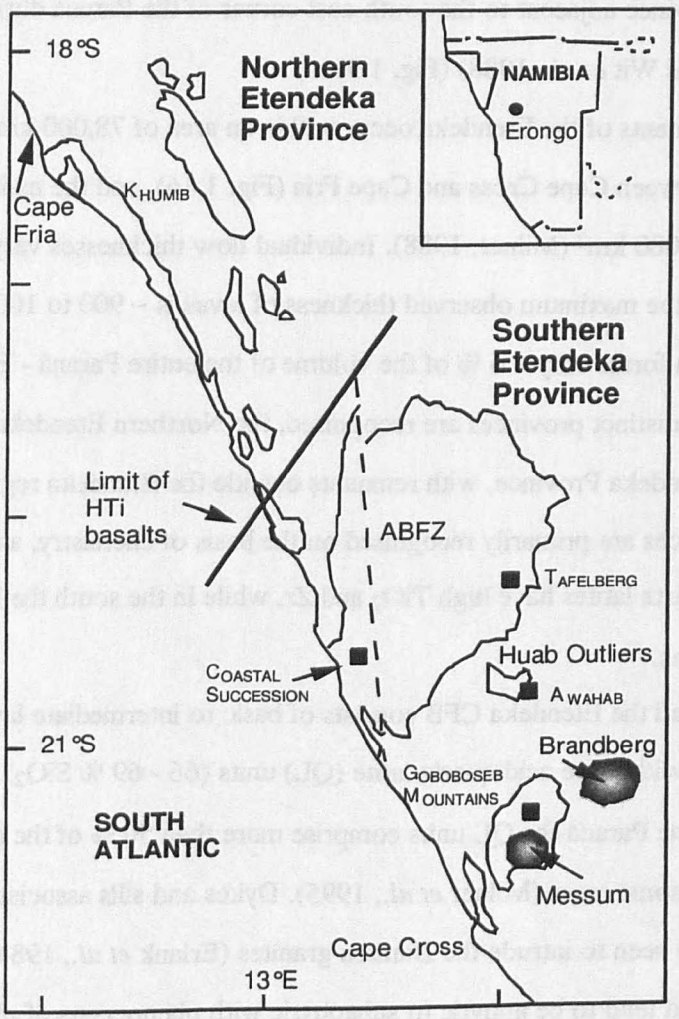

1.14.3 High-Ti basalts: Khumib.

The division into northern and southern provinces is based on geochemistry, with high TiO_2 (> 2.5 wt %), Zr (> 250 ppm) and P mafic lavas occurring in the north. These northern lavas are generally enriched in high field strength elements (HFSE), and were termed the HTZ (high Ti & Zr) basalts by Duncan *et al.*, (1990). Similar values of Sr, Fe and Ti imply close links with the Paraná, high-Ti Urubici magma type (Fig. 1.8) (Peate *et al.*, 1992). There are both aphyric and sparsely porphyritic samples, with phenocrysts of plagioclase, pyroxene, magnetite and occasionally olivine. LTZ Tafelberg lavas are interbedded with the HTZ Khumib lavas in the northern part of the main lava field but thin out and disappear to the south. The Khumib remnant is found outcropping north of latitude 19°30' S and, on closing the South Atlantic, the Khumib and Urubici magma types are geographically adjacent to each other. However together they form < 5 % of the total volume of lava erupted in the Paraná-Etendeka province (Peate, 1996).

Fig. 1.17. The high and Low Ti magma types of the Etendeka CFB (data from Milner & Duncan, 1987).

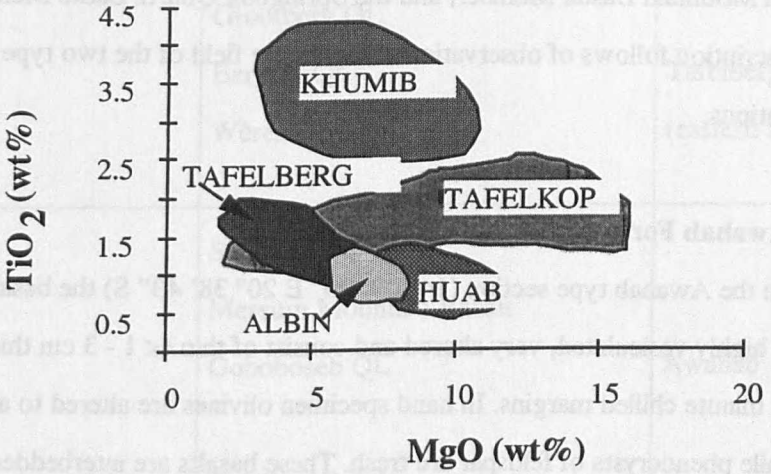

By comparison with those in the north the lavas in the south of Namibia are much more voluminous and have lower concentrations of Ti, Zr and P, and are termed the LTZ basalts, or low-Ti basalts (Fig. 1.17). These lavas together with the associated QL were investigated in a field trip to the Huab Basin, between the Huab and the Ugab rivers, and also to the Messum Complex in February 1996 (Fig. 1.16). These are

described in the next sub-section, with slightly more detail than given for the Paraná equivalents.

1.14.4 Low Ti (LTZ) basalts & associated quartz latites.

The Southern Etendeka Province is divided asymmetrically into two by the Ambrosius Berg Fault Zone (ABFZ) (Fig. 1.16). West of the ABFZ the Coastal succession outcrops in tilted fault blocks in which up to 1000 m of basalts and quartz latites are preserved. Using the recently published stratigraphic framework of Milner *et al.* (1994) this succession is included in the Tafelberg Formation as a lateral facies variant. In the eastern part of the lava field the Tafelberg Formation consists of, from the base to the top of the sequence, the Wêreldsend Member, the Grootberg Member and the Beacon Member.

The Tafelberg Formation disconformably overlies the Awahab Formation which includes the Tafelkop basalts at the base, the Goboboseb Quartz Latite Member, the Messum Mountain Basalt Member, and the Springbok Quartz Latite Member. A detailed description follows of observations made in the field of the two type sections of these formations.

Awahab Formation.

In the Awahab type section (14° 09' 20" E 20° 38' 43" S) the basal Tafelkop basalts are highly vesiculated, very altered and consist of thin (< 1 - 3 cm thick) multiple flows with minute chilled margins. In hand specimen olivines are altered to an orange colour, while phenocrysts of feldspar are fresh. These basalts are interbedded with sandstones of the Etjo Formation with which they have a close temporal relationship, i.e. the sand dunes are considered to have been unconsolidated when the lavas flowed over them. The eruption of the lavas in a desert environment has implications for the timing and duration of magmatism. Climatic conditions appear to have remained remarkably constant from Lower to Upper Cretaceous with tropical to subtropical flora preserved (Riccardi, 1988), and aeolian sands are preserved both at the beginning and end of the

the beginning and end of the sequence. The lack of palaeosols and entablature are also attributed to this arid environment.

Table 1.3. Nomenclature of the Southern Etendeka Province (after Milner *et al.*, 1994)

Southern Etendeka Province		
Succession	Member	Formation
(Interbedded) Coastal	Upper: Middle: Lower: Gemini QL Wêreldsend QL	Tafelberg (western area)
Tafelberg	Beacon QL Grootberg QL Bergsig QL Wêreldsend QL	Tafelberg (eastern area)
Springbok	Springbok QL Messum Mountain Basalt Goboboseb QL Tafelkop Basalt	Awahab

Fig. 1.18. Photo 3. Migration of sand down through cooling fractures, Etendeka.

Fig.1.18. Photo 4. Shards from pyroclastic explosion of rhyolites, Uruguay.

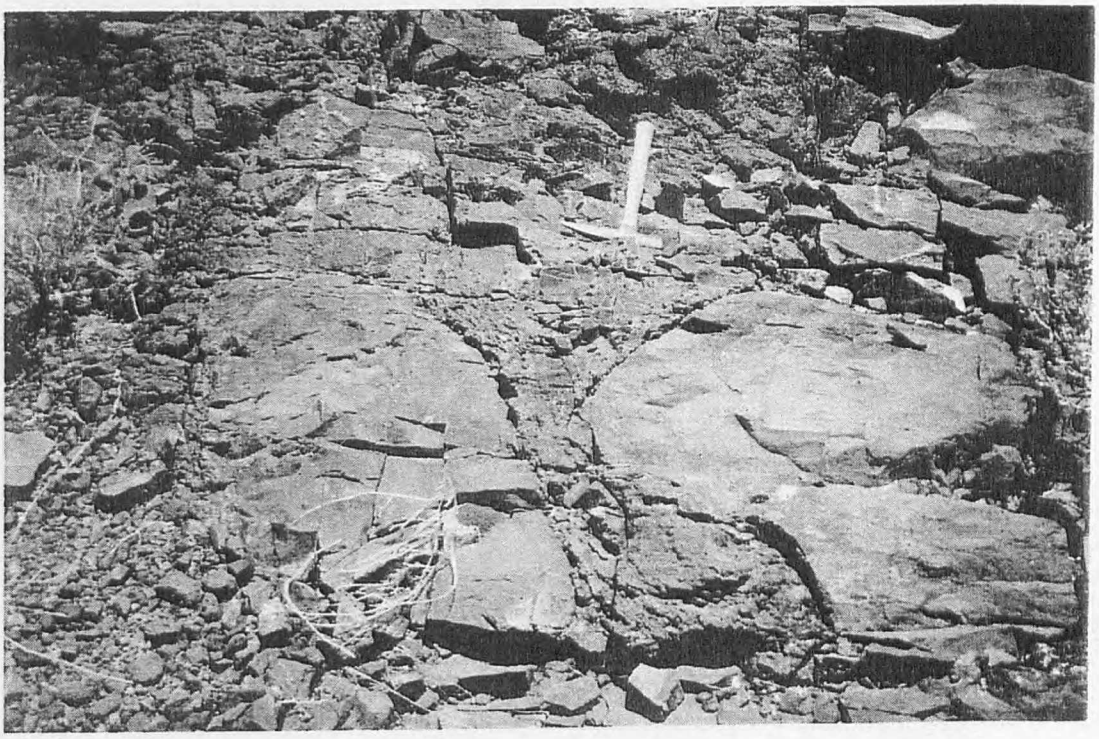

These basal basalts have previously been omitted from descriptions of the basaltic successions, as their relationship to the main lava had not been studied. Sand is seen to have migrated down between fractures and cracks in the basalts and forms lenses 10 cm thick (Fig. 1.18, Photo 3). The tops of the basalt flows are often brecciated with angular lava fragments encompassed by sand. Finely laminated dune structures 1 - 1.5 m high are evident between lava flow sequences. The overall thickness of this member at Krone Farm is 130 m, and this estimate does not include all the basal lavas due to the quantity of sediment involved.

Overlying this interbedded sandstone and basalt unit is the Goboboseb QL Member which consists of pitchstones and quartz latites. Dark black glassy pitchstone lenses are 50 cm thick, with thin lamellar devitrified quartz latite units. The lamellar banding is seen to be contorted close to the base. The pitchstones vary up to 2 m thick in this section and are vaguely amygdaloidal. A brecciated quartz latite (QL) unit follows in which variably sized pumice-like angular clasts of QL are encompassed in a QL matrix (Photo 4), this unit is only 1.5 m thick. This QL is followed by a 10 m thick basalt unit, which in turn is overlain by a pitchstone unit, ~2 m, which passes upwards into a thick 5 m QL of the Springbok Member. The upper part of the Springbok Member, which forms the cliff faces in this area, consists of massive, columnar jointed QL with no particular textural variability.

The stratigraphic disconformity between the Springbok Member of the Awahab Fm. and the Wêreldsend Member of the Tafelberg Formation is traversed in a stream section 6 km west of Fonteine Farm (13° 57' 00"E 20° 16' 00"S). The Springbok Member at this locality consists of large angular, well jointed pitchstone blocks with highly vesiculated very altered QL infilling the spaces between the blocks. The overlying basalt unit displays characteristic spheroidal weathering and is dark green - grey in colour. Calcite veining is common in the basalt. The entire unit is about 30m thick. Between the basalt and the next obvious QL unit is a zone of colluvial breccia with blocks of QL surrounded by vesicular basalt, which marks the top surface of the Springbok Member. 10m along section QL blocks are set in a fine grained red coloured matrix of sedimentary material. There is no clear contact with the overlying

QL, which forms a massive, jointed unit 60 - 70 m thick; this is the base of the Wêreldsend Member.

Vesicles and amygdales within the Springbok QL Member vary in size from 1cm at the base to > 50 cm at the top, while the frequency of amygdale occurrence also increases up through the unit. Amygdales vary from agate to quartz to zeolites to calcite, and the shapes also vary from roughly circular to ovoid. The very top of the unit is brecciated with blocks and fragments of QL, and bright red material in the spaces, similar to the lower brecciated unit described from the base of the section. Overlying this QL is a thick basalt unit 75 m thick, which is jointed and has a slightly coarser texture than the basalt lower down the sequence, but the contact is poorly exposed.

Tafelberg Formation.

Apart from the Wêreldsend quartz latites at Krone Farm the main Tafelberg Formation is best described from the Coastal Succession which was not examined on the February 1996 field trip. Three other low Ti or LTZ basaltic lava types, in addition to the basal Tafelkop basalts, were identified on the basis of geochemistry and/or petrology by Erlank *et al* (1984). These are the Albin, Tafelberg and Huab magma types, which include those lavas with up to 58 wt% SiO_2.

The Albin magma type occurs in the lowermost part of the volcanic sequence in the coastal region and is seen to be interbedded with the Tafelberg magma type. Erlank *et al.*, (1984) describe the Albin basic lavas as fine to medium grained porphyritic rocks, that are volumetrically minor by comparison with the aphyric Tafelberg. Plagioclase is the dominant phenocryst phase and it occurs as glomerophyric intergrowths up to 7 mm in length. This has lead to speculation that they are enriched variations of the less evolved Tafelberg group (Peate, 1989). Clinopyroxene occurs as augite with pigeonite cores. In the groundmass subhedral plagioclase, pyroxene, Ti-magnetite and glass phases coexist. Alteration is common. Chemically the Albin and Tafelberg basalt types are similar, with the Albin plotting at the high end of the negative correlations of Al_2O_3 and MgO with SiO_2 (Milner & Duncan, 1987). The

Albin group also plots at lower levels of TiO_2, Fe_2O_3, K_2O and P_2O_5 when plotted against SiO_2 than most of the rocks in the Tafelberg field (Fig. 1.19).

The Tafelberg lavas are the most extensive basalt unit forming the main part of the Etendeka lava field. They have variable mineralogy but uniform textures. Most are fine grained equigranular samples, with very sparse phenocrysts of plagioclase, pseudomorphed olivine and clinopyroxene; Ti-magnetite is also present. Euhedral plagioclase laths form an interlocking framework with granular pyroxene. For a more detailed description see Erlank *et al.*, (1984). The presence of phenocrysts appears to be a function of where in the stratigraphic succession the lavas are located. In the stratigraphically higher Springbok basalts lower MgO abundances are observed. Tafelberg compositions range between 48.9 wt % and 57.8 wt % SiO_2 with initial $^{87}Sr/^{86}Sr$ ratios of 0.7078 - 0.7135 (Erlank *et al.*, 1984).

The Huab basalts are considered to be a more basic variant of the Tafelberg type but they have, for example, higher ε_{Nd} values (Milner *et al.*, 1990). They are volumetrically minor, with fine grained intergranular textures, but they have not been extensively described in the literature.

Following on from the descriptions of the principle magma types and their origins in the Paraná-Etendeka CFB province, southern Uruguay is now examined in a similar context. By characterising the chemistry and petrogenesis of the Uruguayan magma types, and undertaking a detailed dating program, it was hoped to obtain greater insight into the possible relationships between age, volume and percentage melting with distance across a plume. A detailed comparison therefore between different aspects of the magmas from all regions will occur in the following chapters, but first an introduction to Uruguay, its geological background and volcanic province.

Fig. 1.19. Etendeka low-Ti magma types. The basal Tafelkop basalts of the Awahab type section are seen to span the entire compositional range. The Albin and Tafelberg magma types appear genetically related with the Albin possibly being less fractionated and plotting at lower SiO_2 levels (data courtesy of Milner & Duncan).

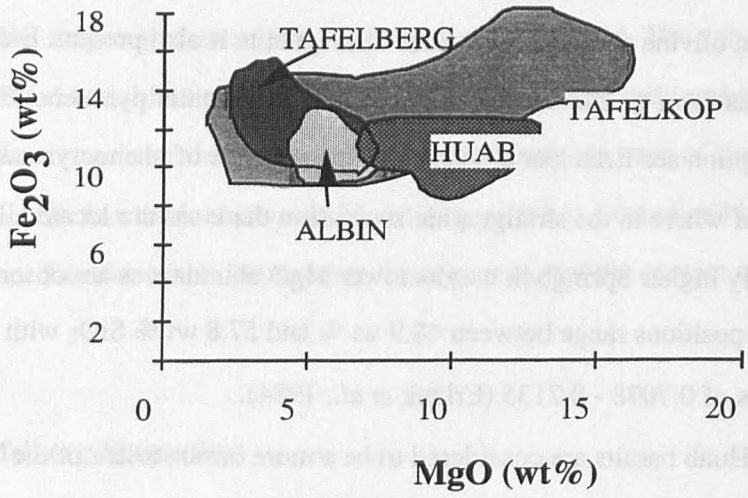

1.15. Introduction to the Geology of Uruguay.

Northern Uruguay is located at the southern edge of the present day asymmetric province of Paraná - Etendeka CFB (Fig. 1.20). The geology further south in Uruguay is comparatively less well described, and it is here at the periphery of the inferred thermal influence of the Tristan da Cunha plume that further information is being sought regarding the relationship of magmatism and rifting during the Cretaceous.

On the "Carta Geologica del Uruguay" the extrusive and intrusive rocks of interest in this study are shown to have Jurassic to Cretaceous ages, and unconformably overlie late Precambrian to early Cambrian rocks. As the geology of Uruguay is little known outside South America a brief introduction to the lithologies and structures of importance follows.

Fig. 1.20. **The location of the Uruguayan volcanic province associated with the opening of the South Atlantic and its relation to the Paraná-Etendeka Province. The inferred position of the Tristan da Cunha plume at 130 Ma is also shown (after Garland, 1994).**

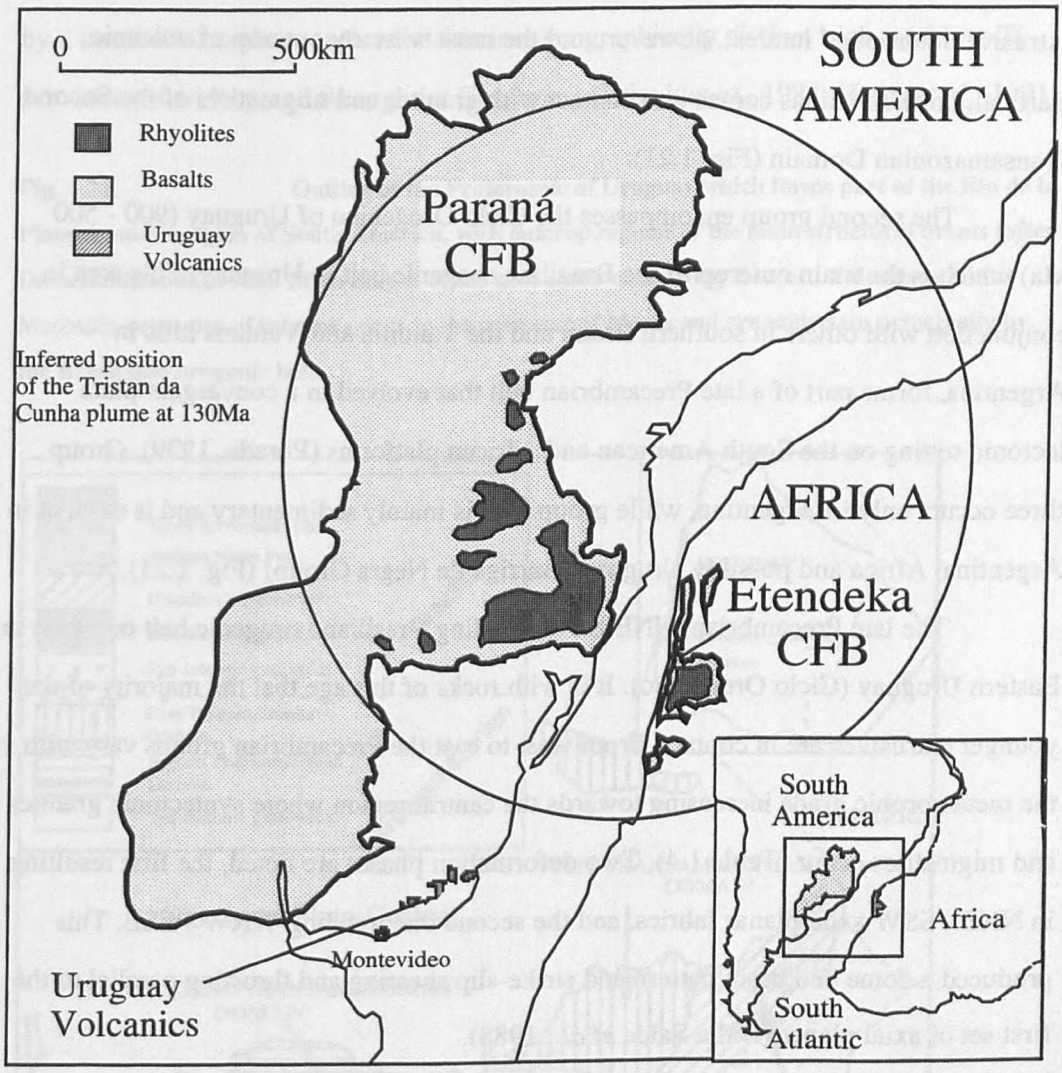

1.15.1 Background geology and basement structures.

The Proterozoic of Uruguay divides the country structurally with the Transamazonian domain in the west and Brazilian orogenic belt in the east (Fig. 1.21). According to Dalla Salda *et al.* (1988) the Precambrian and some of the lower Palaeozoic units of south-western Gondwana comprise four main lithological groups. The first occurs in the Rio de la Plata craton which encompasses much of southern

Uruguay. The craton is divided into two domains by an east-west trending fault that runs from Fray Bentos to Valentines (inset Fig. 1.21). Each of the domains is characterized by different lithologies with an ENE-WSW regional schistose fabric well developed in the Second Transamazonian Domain. This area occurs west of the main extrusive outcrops of interest, however, and the most westerly outcrop of volcanic material, north of Minas comes into contact with granites and migmatites of the Second Transamazonian Domain (Fig. 1.21).

The second group encompasses the Ciclo Orogenico of Uruguay (900 - 500 Ma) which is the main outcrop of the Brazilian orogenic belt in Uruguay. This area in conjunction with others in southern Brazil and the Tandilia and Ventana hills in Argentina, forms part of a late Precambrian belt that evolved in a convergent plate tectonic setting on the South American and African platforms (Porada, 1979). Group three occurs only in Argentina, while group four is mainly sedimentary and is evident in Argentina, Africa and possibly Uruguay (Barriga de Negra Group) (Fig. 1.21).

The late Precambrian, NNE-SSW trending Brasiliano orogenic belt outcrops in Eastern Uruguay (Ciclo Orogenico). It is with rocks of this age that the majority of the younger extrusives are in contact. From west to east the Precambrian groups vary with the metamorphic grade increasing towards the central region where syntectonic granites and migmatites occur (Table 1.4). Two deformation phases are noted, the first resulting in NNE - SSW axial planar fabrics, and the second one trending WNW - ESE. This produced a dome and basin pattern and strike-slip shearing and thrusting parallel to the first set of axial planes (Dalla Salda *et al.*, 1988).

The basement rocks are not only important structurally but also chemically in providing possible contaminants to alter the trace element and isotopic compositions of mantle derived melts. Basement that was once part of a mobile belt and has been thinned will potentially allow more melt generation for similar mantle temperatures than thickened crust, and so may be an important control in the evolution of the magmatic province. Provinciality of basement has, for example, also been invoked by Gibson *et al.* (1995) to explain the provinciality of, and difference between high and low-Ti mafic Mesozoic potassic magmas in Brazil. The geographical provinciality of the high- and

low- Ti basalts has been considered to result from variable degrees of melting beneath the province (Fodor, 1987), also spatial heterogeneities within the lithosphere (Arndt *et al.*, 1993). Both such models are contentious as incompatible element variations are not explained. A major compositional discontinuity in the lithospheric mantle is favoured by a number of authors as the division into geographically distinct high- and low-Ti provinces is widespread throughout Gondwana (Erlank *et al.*, 1984; Hergt *et al.*, 1991).

Fig. 1.21. Outline of the Proterozoic of Uruguay which forms part of the Rio de la Plata cratonic region of South America, with outcrop regions of the main structural events (after Dalla Salda *et al.*, 1988). Main map is of the area south of the Fray Bentos - Valentines fault. Mesozoic volcanics of interest occur in the area east of Minas and are underlain principally by the Brasiliano orogenic belt.

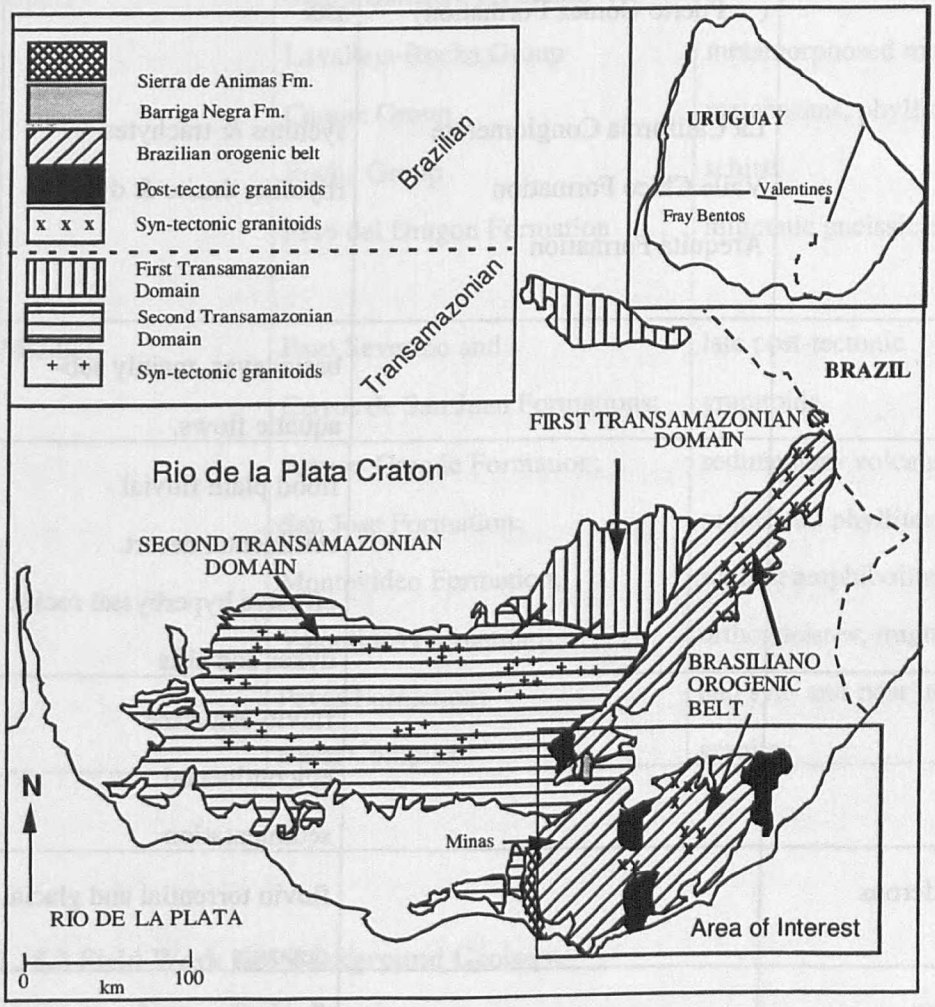

Table 1.4. Detailed division of the Precambrian/Cambrian and Cretaceous rock types of Uruguay, with the rock types of the interim ages also briefly described, after Preciozzi *et al*, 1988; Dalla Salda *et al.*, 1988).

Age:	Formation:	Rock types
Cretaceous-Upper	Migues Formation	continental sediments
	Guichon Formation	arid sedimentation
	Mercedes Formation	fluvio-continental sed.
	Ascencio Formation	arid sedimentation.
Cretaceous-Lower	Arapey Formation	tholeiitic lavas & aeolian
	(= Puerto Gómez Formation)	ssts.
	La California Conglomerate	syenites & trachytes
	Valle Chico Formation	rhyolite, dacite & dykes
	Arequita Formation	
Jurassic		basic lavas, mainly sub-aquatic flows.
Triassic		flood plain fluvial - continental desert. effusive hyperbyssal rocks; dykes and sills
Permian		fluvio-estuarine epicontinental sedimentation
Carboniferous		fluvio torrential and glacial deposits
Devonian		fluviatile - marine sedimentation

Table 1.4. cont.

Silurian		
Ordovician		sandstones; quartzites; conglomerates and limestones
Cambrian		syenites; rhyolites; trachytes
Cambrian-PreCambrian,	Barriga de Negra Group	sedimentary sequence post tectonic granites, leucogranites
Upper	Sierra Ballfna Formation:	
	Lavalleja-Rocha Group	metamorphosed marble
	Carape Group	metabasites, phyllites & schists
	Rocha Group	
	Paso del Dragon Formation	migmatic gneissic complex
Middle:	Paso Severino and Cerros de San Juan Formations;	late post-tectonic granitoids.
	Arroyo Grande Formation;	sedimentary volcanic sequence : phyllites; schists; amphibolites; orthogneisses; migmatites and syn- and post- tectonic granites
	San Jose Formation;	
	Montevideo Formation;	
	Valentines Formation;	
	Pavas Formation;	
	Basal Complex	

1.15.2 Field Work and Background Geology.

Trending parallel to the present coastline, from Piriapolis to Cbo Polonia, the volcanic rocks under study in this project outcrop in isolated areas from Minas to 18 de

Julio, a distance of over 175 km, and as far north as Treinte Y Trés (Fig. 1.22). Exposure is discontinuous and rather sparse in areas with outcrops separated by Precambrian and Cambrian basement west of Aigüa, while to the east Pliocene and Pleistocene sediments dominate the landscape with the volcanics forming outliers.

The areas sampled were chosen from the Uruguayan Geological Survey (UGS) 1: 500,000 geological map and from observations made while in the field. There has been no obvious post-extrusional deformation although some units appear tilted. Heights are rarely in excess of 300 m today, implying minimal uplift post extrusion or latter stage subsidence. Weathering of the region has been extensive although no constraints can be placed on the volume of erosion that has occurred. The result being that the best exposures are located adjacent to roads, as it was only in the vicinity of such road cuttings that the soil cover was removed and fresh rock exposed. Much of the sampling was done along routes 8, 13, 14, 15, & 19 (Fig. 1.23), and adjacent tracks.

The outcrops from which samples were collected are concentrated into five principal regions on the UGS geology map (Figs. 1.22, 1.23). From the south-west to the north these are:

(i) Arequita, 6km north north-west of Minas, is a steep-sided, flat-topped mesa of rhyolitic material, covering an area of 12.5 km x 4.5 km and reaching a maximum height of 100m with identifiable flow units 1 - 2 m thick;

(ii) 15 km east north east of Minas town, between the Arroyo Juan José and Route 8 (Fig. 1.23), lies a region of fragmental, angular brecciated, material, together with highly vesiculated basaltic outcrops. The upper reaches of the hillside have a thin rhyolitic cover, with evidence of flow. Layering of the rhyolitic material tends to be steep and is thought to be syn- rather than post- extrusive as it is characteristic of this upper layer only. The stratigraphic relationship between the basalts and the rhyolites appears undisturbed.

(iii) at Puente de Marmarajá Route 13 branches off from Route 8 and marks the beginning of a large area of volcanic and plutonic rocks. 15 km eastwards along Route 13 is the town of Aigua which is at the southern margin of a faulted volcanic region which stretches east for 25 km into the Paso de los Talas region. Samples

collected were principally rhyolitic and appear oxidised, with individual flow thicknesses of ~1m, and aligned feldspar phenocrysts. Off the road in the Parque Municipal de Salamanca and between the Cerro de las Cuentas and Cerro de Cabrera Hills there is good exposure of rhyolitic material.

At the edge of the Paso de los Talas region is the margin of a syenite intrusion which covers an area of over 200 km^2 from north-east of Mariscala to Cerro Partido and to Alférez. Syenite outcrop is limited as it is weathered into a flat lying scarp with no obvious structural or emplacement features. Dykes of a felsic nature and up to 2 m wide intrude the syenite at Alférez, close to Rincón de Mariscala, and trend in a NW-SE direction. The adjacent rocks are volcanic and highly weathered.

2 km north of Mariscala along Route 8 is the Cerro Partido region where the unconformable contact between the Cambrian granites and the volcanics can be observed. The contact is distinct and undulating, tilting by 10 degrees to the north. The volcanic material is well weathered and oxidised, predominantly in the form of dykes 2 - 3 m wide. Texturally the dykes vary from saccroidal to phenocrystic. These dykes, unlike those seen to intrude the syenite, trend in an east-west direction. 18 km further north along Route 8 is Piraraja, where dark grey, basaltic material with no obvious phenocrysts outcrops.

(iv) Lascano is a region at the same latitude as Piraraja but 35 km to the east on Route 15. The outcrop has an unusual Y shape appearance and is 20 km long by 6 km wide at most. There are also a number of much smaller outliers adjacent to the main one. The outcrop is predominantly rhyolitic flows, which display ignimbritic flow textures with flattened pumice fragments. However there is also basaltic material that is spheroidally weathered and is feldspar phyric. There is no clear contact between the basalts and the rhyolites. Some of the rhyolites are fragmented with pumice fragments incorporated in a rhyolitic matrix, and there is some interaction between the lavas and syn-depositional sediments.

In addition some flow textures in the lavas is seen as it forms curves in the apparent bedding pattern. Scattered rhyolitic outcrops span the distance between

Lascano and 18 de Julio at the coast. The rhyolite is quartz rich and very similar to that observed at Lascano.

Fig. 1.22. Major locations of volcanic outcrops in southern Uruguay.

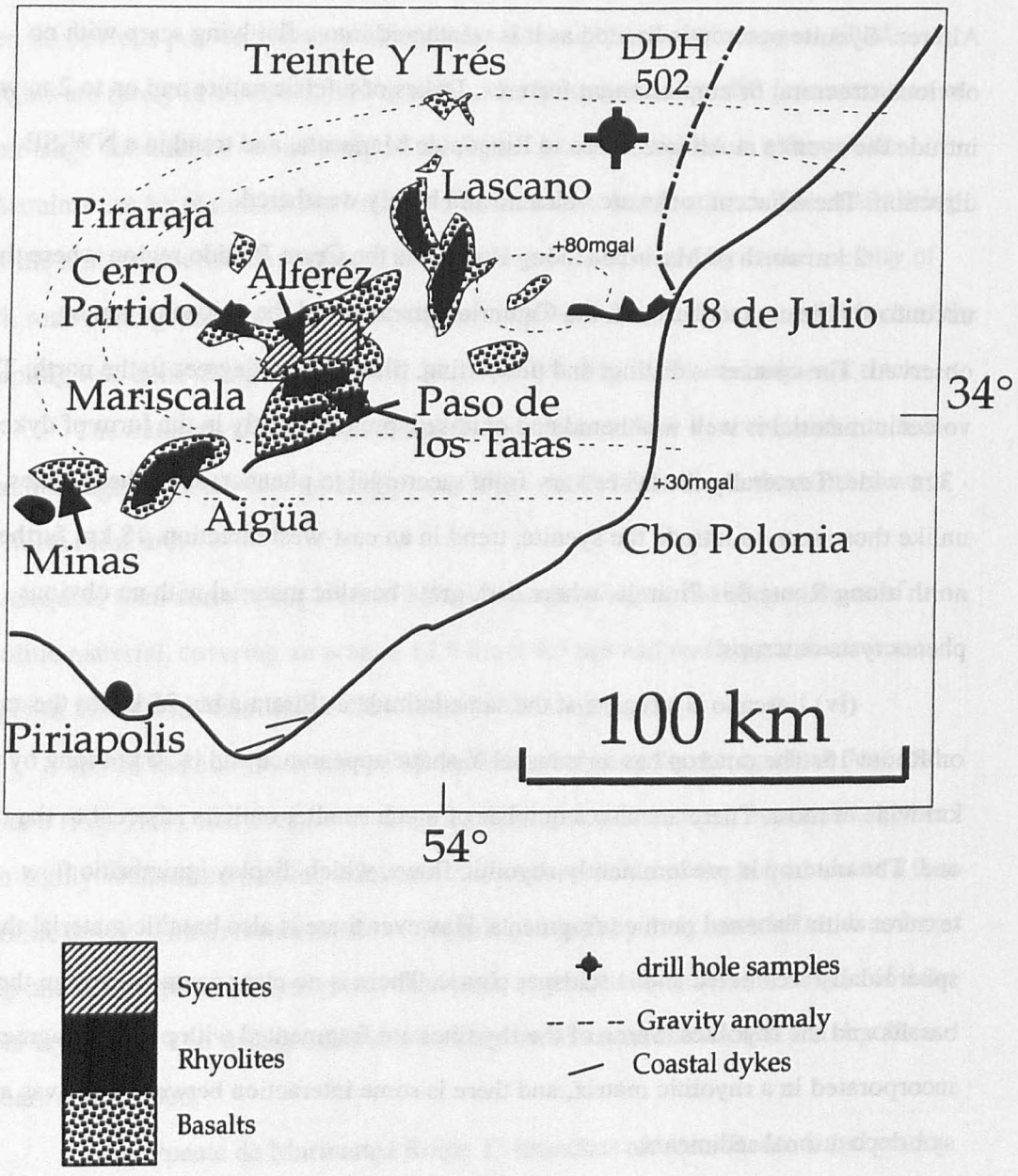

Fig. 1.23. Location map with major infrastucture, drainage and regions.

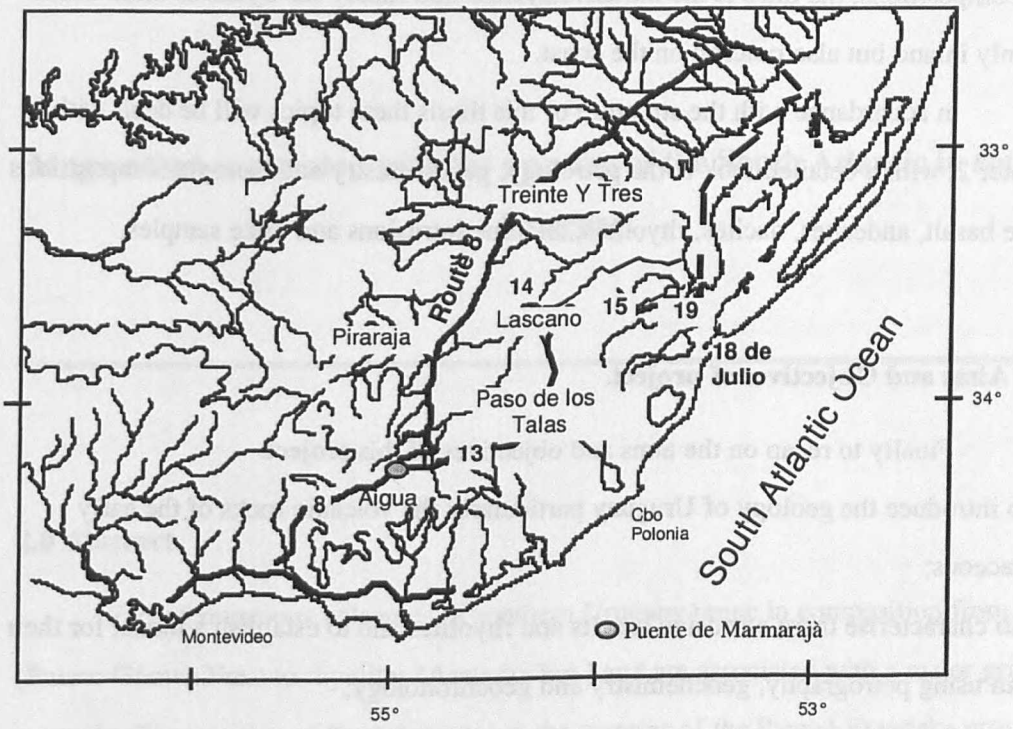

(v) The most northern outcrop of volcanic material sampled was at Treinte Y Trés. Here, basaltic material occurs without any rhyolite covering. The samples tend to be vesiculated and have calcite amygdales, or are phenocryst rich, all are quite weathered.

From field evidence it appears that the rhyolites stratigraphically overlie the basalts which rest unconformably on Cambrian and Precambrian basement, commonly granite. The rhyolites form the topographic highs of the region. Drill core from the UGS provides an important vertical section through the basalt - rhyolite sequence to a depth of 1002 m, and is consistent with field observations. This borehole (DDH 502) is located in eastern Uruguay at approx. 053.5/033.3 (Fig. 1.22). The timing of the intrusion of the syenite member, which itself is intruded by numerous extrusive dykes, is mapped by the Uruguayan Geological Survey (UGS) as being younger than the surrounding basalts, although possibly not the rhyolites, but this is not certain.

In conclusion therefore it is considered that there are at least four separate stratigraphic groupings, which may ultimately be linked by a common thread. The first

is the stratigraphically lowest basic to andesitic outcrops, the second is the more evolved acid compositions, the third is the intrusive syenite and finally the dykes as these occur not only inland but also outcrop on the coast.

In accordance with the structure of this thesis these topics will be dealt with in Chapter 2, with a detailed look at the petrology, geochemistry and isotopic compositions of the basalt, andesites, dacites, rhyolites, alkaline intrusions and dyke samples.

1.16 Aims and Objectives of project.

Finally to recap on the aims and objectives of this project:

(i) to introduce the geology of Uruguay particularly the volcanic rocks of the early Cretaceous;

(ii) to characterise these extrusive basalts and rhyolites and to establish a model for their origin using petrography, geochemistry and geochronology;

(iii) to date precisely the extrusive volcanics and evaluate the relationship between the Uruguayan rocks and those of a similar age and composition in the Paraná CFB;

(iv) to provide greater insight into the processes of rifting and magmatism in a continental setting by understanding the petrogenesis of the rocks at the surface;

(v) to add to the understanding of the tectonic processes that operated in the South Atlantic region pre-, syn- and post- rifting by obtaining absolute ages for the coastal dykes on both sides of the present day ocean and estimating the amounts of extension at particular times leading up to the opening of the South Atlantic.

Chapter 2.

Magmatism associated with the opening of the South Atlantic in southern Uruguay.

2.0 Abstract.

Early Cretaceous volcanics of southern Uruguay range in composition from basalts (Puerto Gómez Fm.) to rhyolites (Arequita Fm.) and are associated with a major gravity anomaly. The position of these outcrops at the margins of the Paraná-Etendeka province, one of the most voluminous continental flood basalt (CFB) provinces preserved today, provides an opportunity to investigate possible lateral variations across an area of plume related magmatism.

The mafic lavas of the Puerto Gómez Formation have been divided geochemically into two distinctive magma types; the more voluminous Treinte Y Trés magma types, which have similar Ti/Y and Nb/La ratios to the low Ti/Y Gramado magma type of the Paraná province, and the Santa Lucía magma type, a distinct and rare basalt type with a predominantly asthenospheric signature.

The overlying rhyolites of the Arequita Formation are also examined, both mineralogically and chemically. Unlike the main Paraná - Etendeka rhyolites they are occasionally alkali feldspar and quartz phyric, and are considered to be unrelated to the basaltic lavas. These rhyolites are further characterised by distinctly low $^{143}Nd/^{144}Nd_i$ and variable $^{87}Sr/^{86}Sr_i$, very different to the low-Ti and high-Ti rhyolites of the Paraná - Etendeka. The rhyolites were generated by melting mafic lower crust, and variously contaminated by an upper crustal component, with high $\delta^{18}O$ values similar to those observed in the rhyolites.

2.1 General Introduction.

Mesozoic magmatism associated with the break-up of the Gondwana supercontinent is widespread throughout South America, southern and equatorial Africa, and Antarctica. Associated magmatic events range in age from the early Jurassic to late Cretaceous/Tertiary. Early Jurassic flood basalt sequences include the Ferrar magmatic province and the Karoo igneous province. The Ferrar tholeiitic basalts and dolerites extend from the Transantarctic Mountains to New Zealand (Elliot, 1992), while Karoo volcanism occurs in southern Africa (Erlank, 1984; Cox, 1992). Extrusion of the extensive Paraná lava field in South America, and the less voluminous Etendeka lavas of Namibia, which together once formed a single continental flood basalt (CFB) province prior to opening of the South Atlantic (Erlank *et al.*, 1984; Bellieni *et al.*, 1986), occurred during the early Cretaceous. This large igneous province is linked to the Tristan mantle plume via the Rio Grande Rise and the Walvis Ridge (O'Connor & Duncan, 1990) (Fig. 2.1). Small volume late Cretaceous alkalic provinces are also common in Brazil, Paraguay, Angola and Namibia.

Volumetrically less significant tholeiitic magmatism is also evident in southern Uruguay, and these volcanics are now known to be broadly contemporaneous with the main Paraná - Etendeka province (Stewart *et al.*, 1996; Chapter 4). This magmatic province of southern Uruguay is situated at the edge of the extensive Paraná-Etendeka CFB province, and it is therefore of considerable interest in attempts to establish the lateral variations in source compositions and degrees of partial melting across an area of plume-related magmatism.

The Mesozoic volcanic rocks of southern Uruguay extend from the Santa Luciá tectonic basin to the Laguna Merín basin (Fig. 2.1). The Santa Luciá tectonic basin (Ricardi, 1988; also known as the Canelones Basin, Urien & Zambrano, 1973) lies in a system of faulted basement blocks in southern Uruguay trending approximately N60°E. This basin together with the similarly oriented Laguna Merín Basin, and the ESE trending Salado and Colorado Basins of Argentina were successively infilled with volcanic and sedimentary sequences during the Late Jurassic and Early Cretaceous (Riccardi, 1988) (Fig. 2.1). The Santa Lucía and Laguna Merín regions are underlain by a gravity anomaly of +90 mGal, with a mass excess which has been calculated by Hallinan (unpublished data) as M_E = $7\pm2 \times 10^{15}$ kg, given a density contrast of 200 kg/m^3 with a volume of 35,000 km^3

interpreted as a large mafic body. The shape is a crude oblong 100 km long and, assuming the density contrast is effective over 15 km of crustal thickness, the width (extension) is ~23 km (Fig. 1.22). It is orientated in a rough E-W direction similar to many of the other structural features related to the internal deformation of the South American plate during the Jurassic (Nürnberg and Müller, 1991).

Fig. 2.1. Cretaceous basins of South America, including the Santa Luciá tectonic graben and the Laguna Merín Basin of southern Uruguay. Inset figure shows the present day relationship between the Paraná - Etendeka province, the fossil plume trace of the Rio Grande Rise and the Walvis Ridge, and the Tristan da Cunha plume.

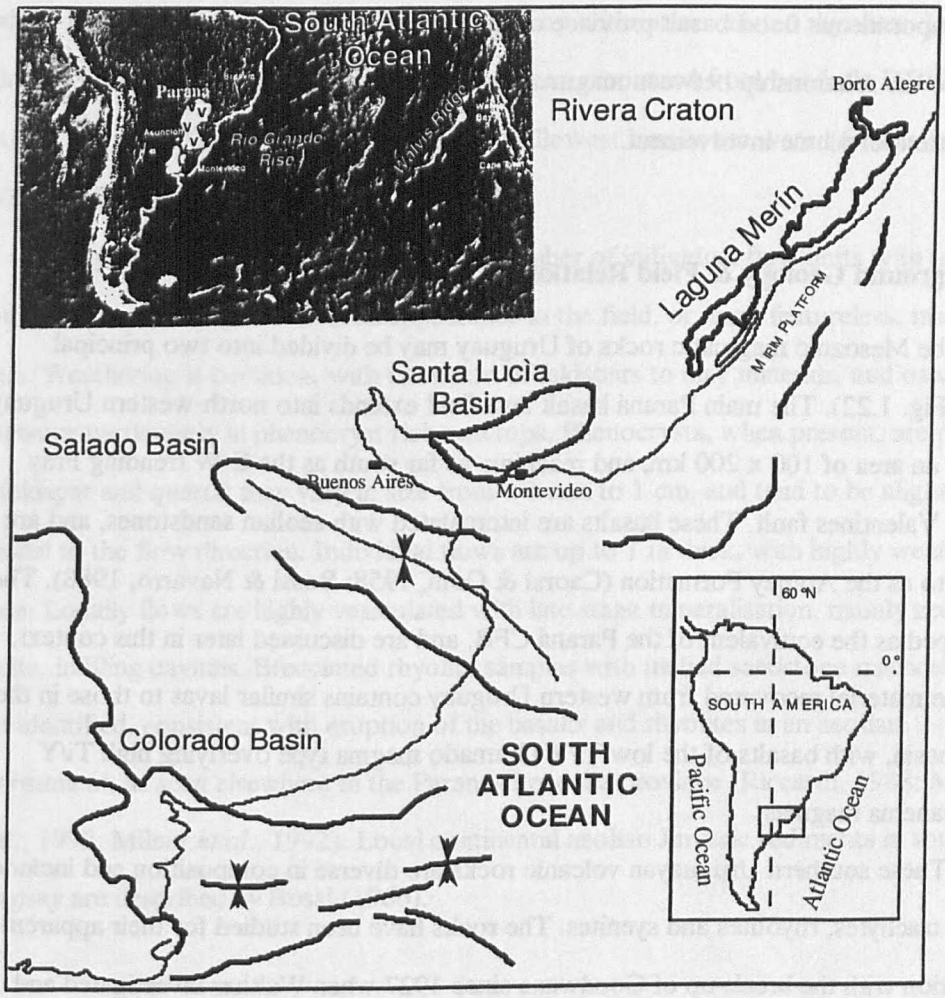

This chapter is concerned with describing the basalts and rhyolites of southern Uruguay and determining the relationship between these basalts and rhyolites. Comparisons are made with the different rock types of the main Paraná - Etendeka CFB province in order to determine possible petrogenetic links between these geographically adjacent magmatic provinces. Thus constraints are established on the lateral extent of similar magma types, and consequently the degrees of melting at the margins of a plume. Information regarding discrete source regions in the area is also presented. It is proposed to extend the Paraná - Etendeka province by a further 20,000 km^2 in southern Uruguay implying even greater volumes of magma erupted in this province during the Cretaceous. The aim of this chapter is therefore to compare this Early Cretaceous magmatic province of southern Uruguay with the contemporaneous flood basalt province of the Paraná-Etendeka, in order to gain further insight into the relationship between magmatic products on both sides of the South Atlantic and the extent of plume involvement.

2.2 Background Geology & Field Relations.

The Mesozoic magmatic rocks of Uruguay may be divided into two principal regions (Fig. 1.22). The main Paraná basalt lava field extends into north-western Uruguay, covering an area of 100 x 200 km, and reaching as far south as the E-W trending Fray Bentos - Valentines fault. These basalts are intercalated with aeolian sandstones, and are referred to as the Arapey Formation (Caorsi & Goñi, 1958; Bossi & Navarro, 1988). They are mapped as the equivalent of the Paraná CFB, and are discussed later in this context. Drill hole material recovered from western Uruguay contains similar lavas to those in the Paraná basin, with basalts of the low Ti/Y Gramado magma type overlying high Ti/Y Paranapanema magmas.

These southern Uruguayan volcanic rocks are diverse in composition and include basalts, trachytes, rhyolites and syenites. The rocks have been studied for their apparent association with the break-up of Gondwana since 1927 when Walther investigated and subdivided the rhyolites, trachytes and syenites into the Aigüa and Lascano series. Table 2.1 contains a summary of the previous nomenclature and that applied in this study. Formations

are mappable units, in accordance with the definition of Whittaker *et al.*, (1991), while magma types are identified on the basis of geochemical differences.

Most of the samples collected are rhyodacite - rhyolite, perhaps because of the poor preservation potential of the basaltic rocks in this area. Thus, it is likely that the surface expression of the basalts was originally more extensive, similar to the area underlain by the large positive Bouguer gravity anomaly. Stratigraphically the rhyolites overlie the basalts, consistent with the age data (basalts - 134 to 130 Ma; rhyolites - 132 to 124 Ma), or overstep them to lie directly on basement. Rhyolite exposures dominate the landscape, forming topographic highs from Arequita in the far south to Lascano (Fig. 1.22). Nowhere in the region is there a clear contact between the mafic and acidic rock types, and only at Treinte Y Trés in the north do mafic lavas outcrop without associated rhyolites. In addition, a 1 km long intersection of mafic material has been recovered from borehole DDH 502 in eastern Uruguay (GR053.5 033.3), with the shallowest basalts recovered from a depth of 267 m below the surface.

Rhyolite outcrops consist either of a number of individual flow units with ignimbritic flow textures, which give a layered appearance in the field, or more featureless, massive units. Weathering is common, with alteration of feldspars to clay minerals, and oxidation is extensive particularly in phenocryst rich outcrops. Phenocrysts, when present, are primarily of feldspar and quartz; they vary in size from < 1 mm to 1 cm, and tend to be aligned parallel to the flow direction. Individual flows are up to 1 m thick, with highly weathered bases. Locally flows are highly vesiculated with late stage mineralisation, mainly zeolite and calcite, infilling cavities. Brecciated rhyolite samples with melted sandstone matrices were also identified, consistent with eruption of the basalts and rhyolites in an aeolian environment, as seen elsewhere in the Paraná-Etendeka province (Riccardi, 1988; Mizusaki *et al.*, 1992; Milner *et al.*, 1992). Local continental aeolian Jurassic sediments in southern Uruguay are described by Bossi (1966).

Fig. 2.2. **Mesozoic magmatic provinces of southern Uruguay, showing the close geographic relationship of this region to the main Paranà Continental Flood Basalt Province.**

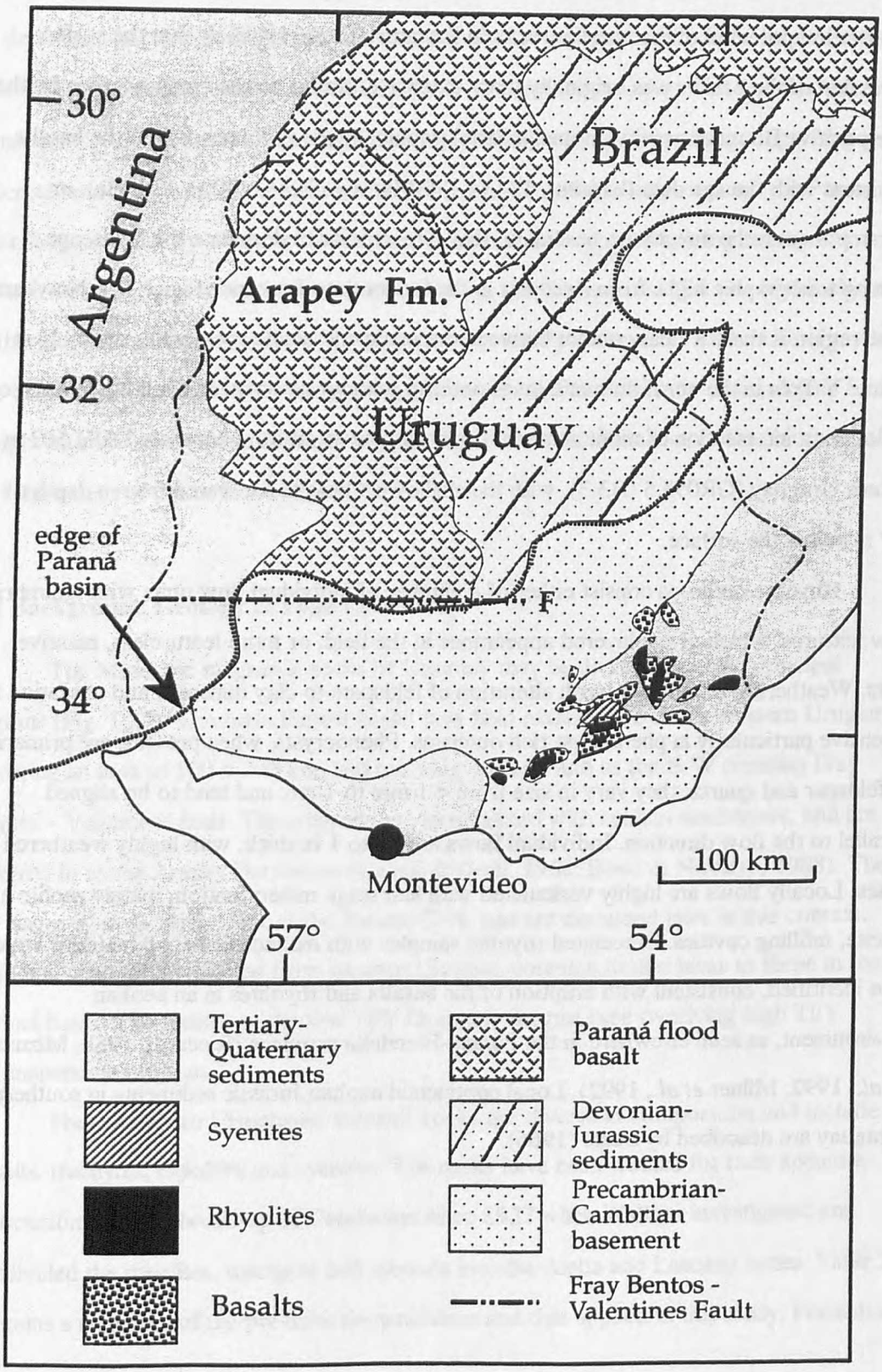

Two characteristic rhyolite sequences are recognised in the field principally in the Lavalleja and Maldonado Départmentos on the basis of mineralogy and texture. The first type consists of some of the less evolved samples and flow features are common with oriented feldspar. Feldspar is the dominant mineral phase, forming ~ 60 % of the rock. Rhyolites of this type occur principally in the Minas, Aigüa, Cerro Partido and Paso de los Talas regions (Fig. 1.22). These are referred to as Type 1. The second type, Type 2, are recognised primarily on the presence of variably sized, euhedral to anhedral quartz phenocrysts. Ignimbritic textures are common but not ubiquitous. The two types also share a number of features, particularly at Aigüa where the rhyolites tend to be layered and vesiculated.

In the field the type locality for Type 1 is in the Parque Municipal de Salamanca, in Paso de los Talas (Fig. 1.22), where a 10 m thick sequence of rhyolite is exposed. Thin lamellae flows at the base, ~1 m thick, are overlain by more massive units which have a tendency to pinch out whilst others flow undisturbed to infill the spaces. At the top of this unit is an undulating surface with brittle lamellae of fragile material overlain by a massive distinctly layered unit. The regional dip of the rhyolites is 20° to the south-west. The size of phenocrysts evident in hand specimen varies between units in certain individual sequences. For example in some sequences, the phenocrysts are 1 - 2 mm at the base of the exposure, and much more variable from 2 mm to 1 cm in the next 10 m, and then uniformly 5 mm at the top of the sequence. There is also evidence of effusive rhyolite flow in the area, with flow folds identified in some outcrops and silicic dyke intrusions.

The type locality for the Type 2 rhyolites is at Aigüa (Fig. 1.22) in the Maldonado region, where phenocryst-rich rhyolite flows with eutaxitic textures overlie vent material in which angular volcanic fragments (< 5 cm in size) are encompassed in a rhyolitic flow and highly vesiculated basalts. The regional dip of the outcrops is 20° which is considered to be post-extrusive. At Lascano (Fig. 1.22), there are ignimbrites with numerous quartz phenocrysts, up to 6 mm in size. The size and frequency of these quartz phenocrysts varies throughout the area, with very splintery, glassy, phenocryst free rhyolites also occurring. Again brecciated material is identified with large angular pumice and sandstone fragments incorporated by a siliceous flow which suggests a local source for these rhyolites. Rhyolites

of both types are encountered in all the main exposures throughout the region, and so they do not appear to represent mappable units confined to particular areas.

Table 2.1. Summary of nomenclature applied to the southern Uruguay Cretaceous volcanics. Exposure of rhyolites is not continuous therefore the stratigraphical relationship between Type 1 and Type 2 cannot be determined.

Literature Source	Basalts & Andesites	Rhyolites, Dacites & Syenites
Walther (1927)		Aigüa & Lascano Series
Jones (1956)	Treinte Y Très & Canelones Fm.	
Caorsi & Goñi (1958)	Puerto Gómez Fm.	Aigüa & Lascano Series
Bossi (1966)	Puerto Gómez Fm.	Arequita Fm.
Ferrando & Fernández (1971)		Valle Chico Fm.
Preciozzi *et al.* (1980; 1985)	Puerto Gómez Fm.	Arequita Fm.
This study (1997)	Puerto Gómez Fm. -Santa Lucía magma type -Treinte Y Trés magma type	Arequita Fm. - Lascano Series - Aigüa Series Valle Chico Fm. -Alferez syenite

An intrusive syenite plug and ring dyke complex forms the Valle Chico Fm. and span the regions of Cerro Partido, Alferez, Paso de los Talas and Mariscala. Representative samples were collected from southern Alférez and in northern Paso de los Talas and Mariscala (Fig. 1.22). The syenite outcrops are extensively weathered, with the result that exposures are featureless flat scarp areas with no obvious structures. Similar alkalic complexes, broadly contemporaneous with the main flood basalt event, occur both in South America and in Africa (Toyoda *et al.*, 1994; Milner *et al.*, 1995). In Brazil these include the Jacupiranga and Anitapolis carbonatites (132 Ma and 131 Ma respectively, Renne *et al.*, 1993). In Africa, the complexes are predominantly concentrated along a north-east trending broad belt in the Damaraland province, and include Messum, Okenyenya and Cape Cross (Milner *et al.*, 1995). The Valle Chico syenite has been dated at 132 ± 2 Ma (Chapter 4).

2.3 Petrology.

2.3.1 Syenite Petrography.

In hand specimen the Alférez syenite of the Valle Chico Fm. contains large glassy quartz and feldspar phenocrysts up to 1cm, together with interstitial platy biotite and granular hornblende. Leucocratic minerals form ~65% of the bulk rock, and alteration gives an overall green tinge to some samples.

In thin section the mineralogy is alkali feldspar, quartz, plagioclase, hornblende, biotite, pyroxene, apatite and alteration products of chlorite, sericite and iron oxides. The mineral proportions and the degree of pseudomorphism vary between samples. Texturally the rocks are inequigranular with mafic minerals occurring interstitially or poikilitically enclosed by the much larger felsic minerals. Intergrowths of quartz and alkali feldspar give rise to granophyric textures. Alkali feldspar dominates the mineralogy and occasionally solution rims and consertal textures are evident. Alteration of the larger phenocrysts is common, undulose extinction patterns are noted in some quartz phenocrysts, and the alkali feldspars are zoned. Pyroxene phenocrysts are characterised by herring bone textures reflecting exsolution from pigeonite, and indicating an inversion temperature in the region of ~ 900 °C. Apatite needles are the principal accessory phase.

The chemistry of the Alférez syenite is not considered further in this paper, but its contemporaneous occurrence with the Paraná - Etendeka intrusive complexes, principally the syenites, granites and granodiorites of the mobile Damara belt in Namibia is noted. The Awahab Formation and the lower flows of the Tafelberg succession of the Etendeka have been centred at the Messum volcanic complex (Milner *et al.*, 1992; 1995), which is a large alkalic complex with intrusive nepheline syenites; gabbros and granodiorites. The occurrence of an intrusive syenite together with evidence of vent material in the Alférez region potentially suggests that the source of the Uruguay rhyolites was close at hand.

2.3.2 Basalt petrography.

The main basalt outcrops occur in the north at Treinte Y Trés and Piraraja, although there are limited exposures at Aigüa, Lascano and Paso de los Talas (Fig. 1.22). In keeping with previous nomenclature these lavas are termed the Puerto Gómez Formation. In the field basalt outcrops are limited, but a number of individual, massive flows are evident.

Most of the fresh samples are from relatively isolated outcrops and so the field relationships between the basalts and rhyolites are not clear. However, the rhyolites form the topographic highs of the region and since there is no obvious post extrusion deformation, the basalts are presumed to be older, confirmed by Ar - Ar dating. At Treinte Y Trés, the basaltic samples are dark grey, feldspar phyric, and are often vesiculated with zeolites and calcite amygdale infilling. The percentage of feldspar phenocrysts is variable (5 - 30 %), as is the size of the phenocrysts which may be up to 1 cm long. Samples in which pumice fragments are incorporated in a basaltic matrix, suggest explosive eruption, although these are relatively rare. The fragments are angular, highly vesiculated and variable in size, but no vent was recognised in the field. Such features have not previously been recognised in the Paraná where there is no evidence of an eruption center for the basalts preserved.

The basaltic samples have an anhydrous mineralogy of clinopyroxene and plagioclase feldspar together with iron oxides ± olivine and with phenocrysts forming up to 40 % of the section. Most of the samples are porphyritic, and contain variably scaled intergrowths of lamellar twinned plagioclase (1 - 3 mm), with pyroxene phenocrysts. Samples from the DDH502 borehole are broadly similar in appearance, being highly vesiculated with calcite amygdales, and plagioclase phyric. Extensive veining and oxidation are also common. Simple twinning is evident in the pyroxene phenocrysts, and common textures include glomerophyric intergrowths of feldspar and pyroxene, sub-ophitic enclosure of feldspar by pyroxene, and vice versa, and trachytic alignment of plagioclase phenocrysts. The occurrence of such a high proportion of phenocrysts in most samples suggests large scale cooling either in a higher level magma chamber or on the way to the surface prior to eruption. The large scale positive gravity anomaly underlying this region, which has been modelled at depths of up to 15 km, is potentially the site of much of this crystallisation.

2.3.3 Basalt Mineral Compositions.

Pyroxene, feldspar and iron oxide compositions were analysed by microprobe for major elements, and the trace elements Cr, Ba, Ni, V & Zn where appropriate for seven basaltic samples (Table 2.2). In each section a number of phenocrysts were probed to ascertain any compositional variability, and in zoned phenocrysts a number of analyses were taken across the crystal face. Only analyses that total 100 ± 0.5 wt% were used. (See Appendix B for running conditions.)

Fig. 2.3. Or-Ab-An ternary diagram for basalt and rhyolite feldspars. There is an apparent geographical control on the distribution of the plagioclase in the Lascano Series rhyolites with more sodic plagioclase occurring in the Paso de los Talas region.

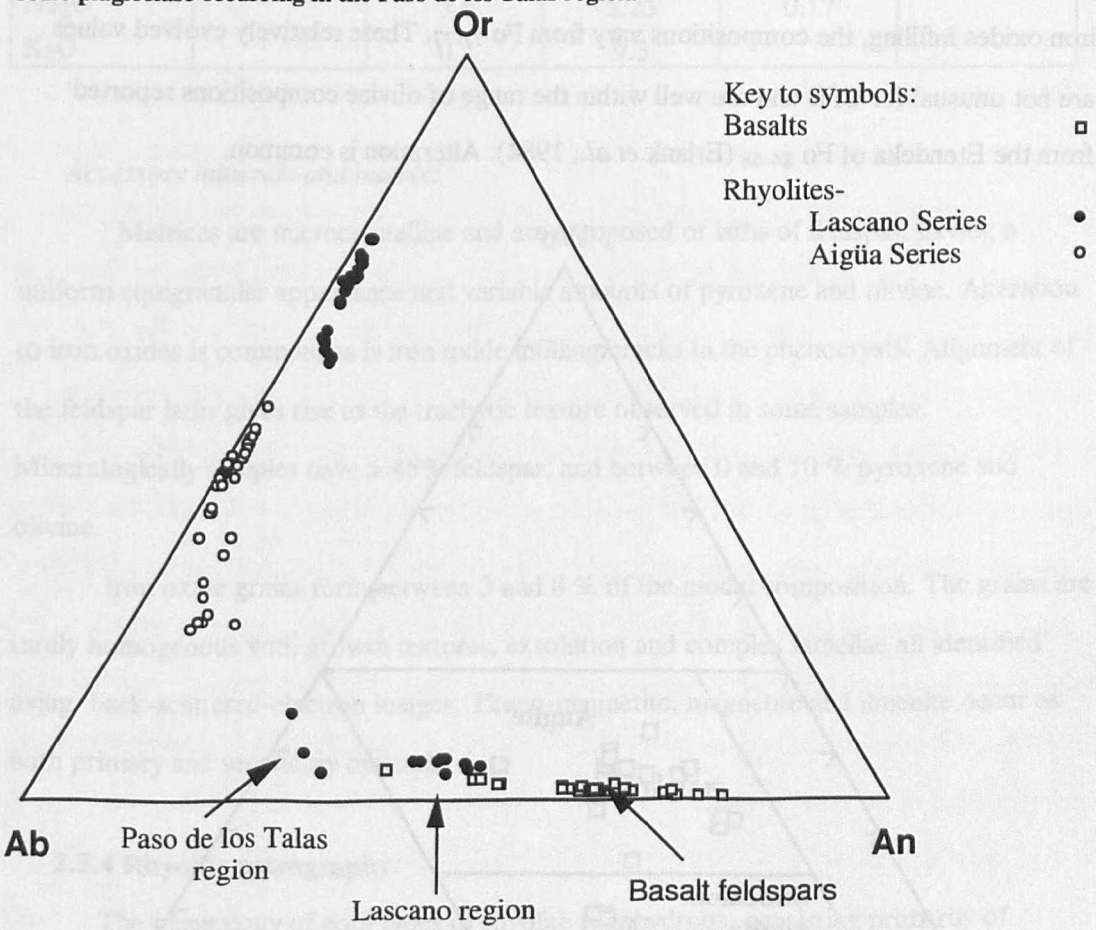

Feldspar:

Euhedral feldspar phenocrysts contrast with the more subhedral, smaller phenocrysts (0.2 - 0.8 mm) of pyroxene. The anorthite content of the majority of mafic plagioclase

phenocrysts analysed varies from An_{50}-An_{82} (labradorite/bytownite), while andesine (An_{30}-An_{50}) is common in the more evolved andesitic lithologies (Fig. 2.3).

Pyroxene:

Pyroxene microprobe analyses generally gave rise to both low and high totals due to varying amounts of alteration with the result that relatively few analyses were usable. The compositions are principally augite which vary from ferroan to sub calcic (Fig. 2.4).

Olivine:

Fresh olivine is evident in the more primitive samples. Generally highly cracked with iron oxides infilling, the compositions vary from Fo $_{71\text{-}77}$. These relatively evolved values are not unusual for CFB and are well within the range of olivine compositions reported from the Etendeka of Fo $_{84\text{-}48}$ (Erlank *et al.*, 1984). Alteration is common.

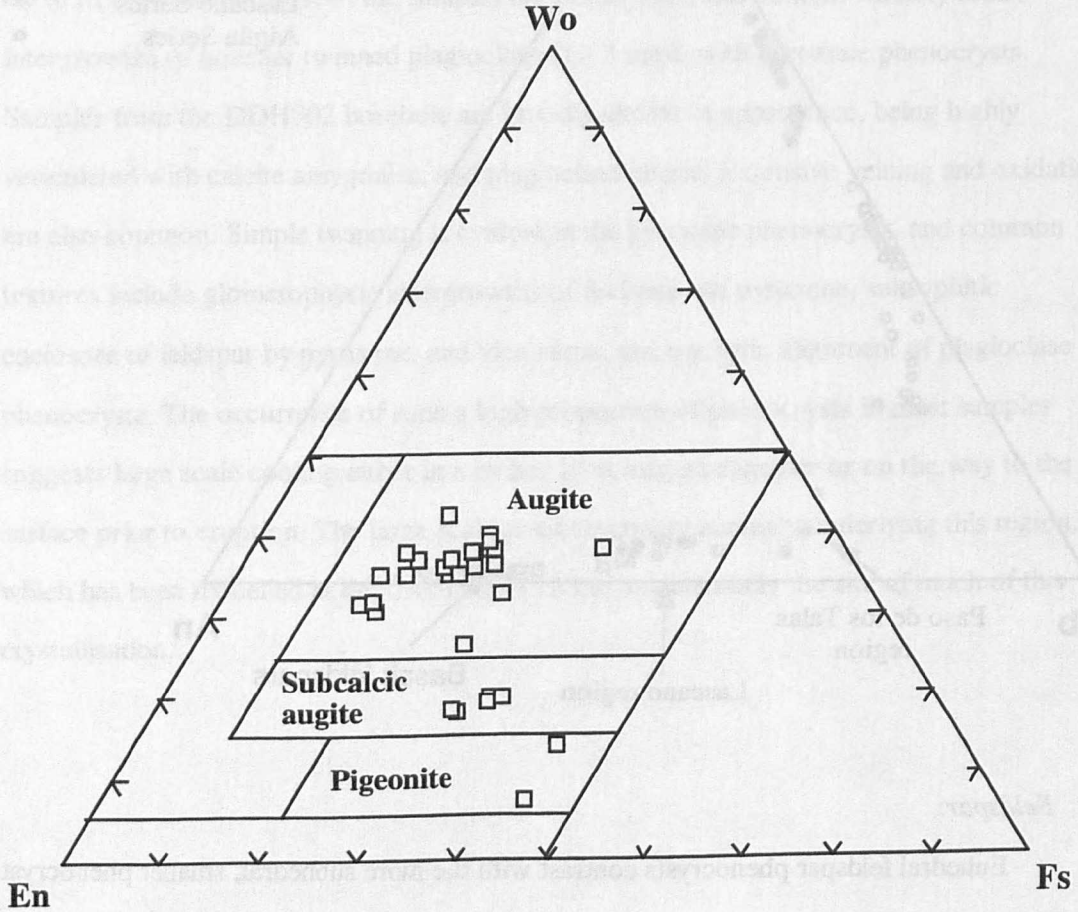

Fig. 2.4. **Ca-Mg-Fe* (molecular %) plot of pyroxene compositions of the basaltic samples.**

Table 2.2. Selected microprobe data from basaltic and rhyolitic samples which are used to constrain the proportions of fractionating phases.

Oxide / Sample	Olivine 92U12	Plagioclase 92U12	K-feldspar 93L36	Clino-px. 93L93	Magnetite 93L53
SiO_2	38.0	51.0	66.7	52.4	0.2
TiO_2	0.03	0.06	0	0.5	14.9
Al_2O_3	0.03	30.4	18.7	1.6	2.2
FeO	25.5	0.5	0.1	11.1	67.8
MnO	0.4			0.25	0.5
MgO	36.3	0.1		16.9	0.7
CaO	0.3	13.9	0.16	17.0	0.02
Na_2O		3.6	5.25	0.17	
K_2O		0.2	9.3		

Accessory minerals and matrix:

Matrices are microcrystalline and are composed of laths of feldspar, having a uniform equigranular appearance and variable amounts of pyroxene and olivine. Alteration to iron oxides is common, as is iron oxide infilling cracks in the phenocrysts. Alignment of the feldspar laths gives rise to the trachytic texture observed in some samples. Mineralogically samples have > 45% feldspar, and between 0 and 10 % pyroxene and olivine.

Iron oxide grains form between 3 and 8 % of the modal composition. The grains are rarely homogenous with growth textures, exsolution and complex lamellae all identified using back-scattered-electron images. Titano-magnetite, magnetite and ilmenite occur as both primary and secondary minerals.

2.3.4 Rhyolite petrography.

The mineralogy of both types of rhyolite is anhydrous, consisting primarily of plagioclase, alkali feldspar, pyroxene and iron oxide, with quartz present primarily in the evolved high silica rhyolites. Accessory minerals include zircon and apatite, while glass is evident, in varying proportions, but usually less than 5 %. Disequilibrium in the feldspars is marked by sieve and skeletal textures. Phenocrysts are mainly discrete (up to 15 %) but some intergrowths of plagioclase and alkali feldspar occur. Devitrification has resulted in a

cryptocrystalline matrix for most samples, with occasional granophyric intergrowths of quartz and alkali feldspar (see Appendix C for selected photomicrographs of some of these textures).

Rhyolites of the second type described in the field, Type 2, are readily distinguished in thin section as (a) they commonly contain pristine, quartz phenocrysts, up to 5 mm in size, which are euhedral to anhedral and, occasionally embayed; (b) the amount of plagioclase is less than that of alkali feldspar, and (c) matrix flow and wrap-around textures are common (Appendix C).

True ignimbritic textures have only occasionally been recognised in the rhyolitic outcrops of the Paraná - Etendeka province (Milner *et al.*, 1992; Garland, 1994). This has been attributed primarily to the high temperatures of eruption involved, with the result that the Paraná - Etendeka rhyolites are often interpreted as rheoignimbrites (Milner *et al.*, 1992). Some of the rocks of Type 2 are unusual in that they do preserve ignimbritic textures (Appendix C). Flattened pumice fragments and glass shards are evident, as are phenocrysts of quartz and alkali feldspar set in a fine matrix, within which a regular alignment of flattened fragments gives rise to a eutaxitic texture. Fiammé are stretched and illustrate secondary mass flowage of the tuff, termed rheomorphism. Phenocrysts are predominantly subhedral although embayments are common. Quartz phenocrysts are of two principal types: (i) small, euhedral to subhedral with small hairline type fractures. The bipyramidal shape of these phenocrysts suggests that these are low pressure, high temperature β-form quartz. (ii) Larger embayed phenocrysts with rounded edges, slightly strained extinction and a greater degree of fracturing, although this is not extensive. Apparent rotation due to mass flowage is evident particularly in some of the smaller phenocrysts, while pressure fractures are relative rare (Appendix C).

2.3.5 Rhyolite Mineral Compositions.

The Uruguayan rhyolites were initially subdivided into two types on the basis of petrography, and primarily on the presence or absence of variably sized and rounded to β-form quartz phenocrysts. These divisions are however not characterised by different major and trace element compositions, except that the more quartz rich samples tend to be more evolved. Instead the rhyolite data from southern Uruguay are used to define two

geochemical series, the Lascano Series and the Aigüa Series which are not equivalent to the previously defined rhyolite types from petrography. Any differences that are evident in the mineral compositions of either series are noted. The use of the term series in the key to Figure 2.4 therefore refers to the divisions realised from chemical investigations as described in Section 2.11 rather than petrological Types 1 and 2.

Plagioclase:

Plagioclase is common both as larger phenocrysts (megacrysts) (1 cm) and smaller phenocrysts (0.5 - 2 mm) particularly in the low SiO_2 rhyolites of both rhyolite series (Fig. 2.3). Euhedral tabular/lath forms give way to more rounded phenocrysts, with sieve and skeletal textures implying disequilibrium (Barker, 1989). Twinning in the plagioclase is lamellar and asymmetric. Plagioclase compositions vary between labradorite, andesine and oligoclase (An_{30} - An_{60}) and show a slight provinciality in the Lascano Series with sodic plagioclase phenocrysts being primarily from the Paso de los Talas region and more calcic plagioclases being concentrated in the Lascano region (Fig. 2.3).

Alkali feldspar:

In general the abundance of alkali feldspar increases with increasing silica content and it is therefore one of the prime modal components in the more evolved high-silica rhyolites. Phenocrysts of alkali feldspar, up to 5 mm in size, occur both discretely and intergrown with plagioclase, and range in composition from anorthoclase to sanidine in the low silica rhyolites. The alkali feldspar compositions of the high-silica rhyolites tend towards sanidine with in general higher potassium abundances, and tend to be discrete or form glomerophyric intergrowths with quartz. There is a regional variation in the alkali feldspar composition of some of the rhyolite, with alkali feldspars from the Aigüa Series being more sodic, and those from the Lascano Series (Fig. 4). Similar disequilibrium textures to those shown by plagioclase in both series are noted. In addition to perthitic textures, there are also granophyric intergrowths of groundmass quartz and K-feldspar in both rhyolite series. Such textures have previously been recognised in old (>100 Ma) devitrified glassy rocks where the quartz and feldspar have re-crystallised (Cas & Wright, 1988). Evidence of dissolution includes rims around some feldspar phenocrysts.

Pyroxene:

Clinopyroxenes of augite composition are present in the less evolved trachydacite rock types of both series, and there are also rare pigeonitic orthopyroxenes. In general the pyroxenes are altered and replaced predominantly by iron oxides. Some zoning and twinning are noted, as is the herring bone structure of pigeonite. Locally the pyroxene is poikilitically encompassed by feldspar.

Oxides & Accessory phases:

Iron oxides are ubiquitous, both as a primary phase and also as secondary phases as replacement minerals after pyroxene. The compositions range between magnetite and titanomagnetite with rare ilmenite occurrences. Similar disequilibrium textures to those noted in the basalts are evident. Zircon and apatite are the main accessory phases.

Matrix:

The matrix varies from microcrystalline to cryptocrystalline. Where distinguishable, it is composed of feldspar, quartz, iron oxides and devitrified glass. Trachytic alignment of groundmass feldspars is noted in some samples, paralleled by larger phenocrysts, but more often the matrix is aphanitic, spherulitic and devitrified.

It is useful to compare the petrology of the southern Uruguay rhyolites with that of the Paraná - Etendeka province in order to constrain possible similarities. The rhyolites from the Paraná province, are divided into two compositional groups, the low-Ti Palmas group from the south and the high-Ti Chapecó group in the north, and these are also distinct petrographically. The Palmas rhyolite group are virtually aphyric (< 5 % phenocrysts), in contrast to the plagioclase - rich Chapecó rhyolites (< 25 % phenocrysts) (Garland *et al.*, 1995). The quartz latites of the Etendeka are sparsely porphyritic (< 10 % phenocrysts) with a basic mineralogy of plagioclase, pyroxene and iron oxides, primarily titanomagnetite and more rarely ilmenite (Milner *et al.*, 1992). The Paraná rhyolites have a similar anhydrous mineralogy. Units of the Palmas rhyolite group of the southern Paraná are equivalent to the low-Ti Etendeka rhyolites (Milner *et al*, 1995), and they both lack the

main components of the more evolved Uruguayan rhyolites, namely alkali feldspar and quartz. In the Paraná-Etendeka province true ignimbritic textures, such as those described from Uruguay are very rarely seen. However, there is local preservation of pyroclastic textures, possibly of ignimbritic origin, particularly in the Etendeka and so the quartz latites have been considered as high temperature, low viscosity welded ignimbrites (Milner *et al.*, 1992).

2.4 Geochemistry.

Major and trace element abundances were determined by X-ray Fluorescence (XRF) analysis, and rare earth and other trace element concentrations by Instrument Neutron Activation Analysis (INAA) (Details in Appendix B). Given the petrographic evidence for alteration, screening was required in order to remove any bias that might be due to alteration processes. Milner & Duncan (1987) using adjacent pitchstone and crystalline samples remarked on the relationship between K_2O and Loss On Ignition (LOI) in samples from the Etendeka and concluded that H_2O^+ was the principal exchange component for K^+ in glass in the more evolved compositions, and that this resulted in a reduction in K_2O in the pitchstone samples. Low temperature, post-extrusion interaction of available groundwater with the lavas is considered to have been important in rocks with relatively high LOI values. Samples with an LOI of > 3 % were therefore discarded, and the compositions of the remaining samples were recalculated on a volatile-free basis (Selected analyses are presented in Table 2.3). The mobility of certain trace elements, such as Rb and Ba within the Large Ion Lithophile Elements (LILE) was also monitored.

The bulk rock compositions are illustrated on a total alkalis - silica diagram in Figure 2.6. The most salient feature is that although there is no clear silica gap in the samples analysed, they do plot in two distinct fields on the total alkalis - silica diagram. The more mafic rocks vary from basalt to andesite and include a few trachybasalts and basaltic trachyandesites using the classification scheme of Le Maitre *et al.*, (1989). Following other studies in the Paraná (Bellieni *et al.*, 1986; Peate *et al.*, 1992) it is still convenient to subdivide the Uruguay rocks into 'basalts' with < 60 wt% SiO_2, and 'rhyolites' with > 60 wt% SiO_2.

Fig. 2.5. Total alkalis versus silica classification diagram of Le Maitre *et al.*, (1989). Open squares are mafic samples; Filled circles are rhyolites from Uruguay. Grey fields in the background are for the basalts and rhyolites of the Paraná CFB province, data from Peate, (1989) and Garland, (1995).

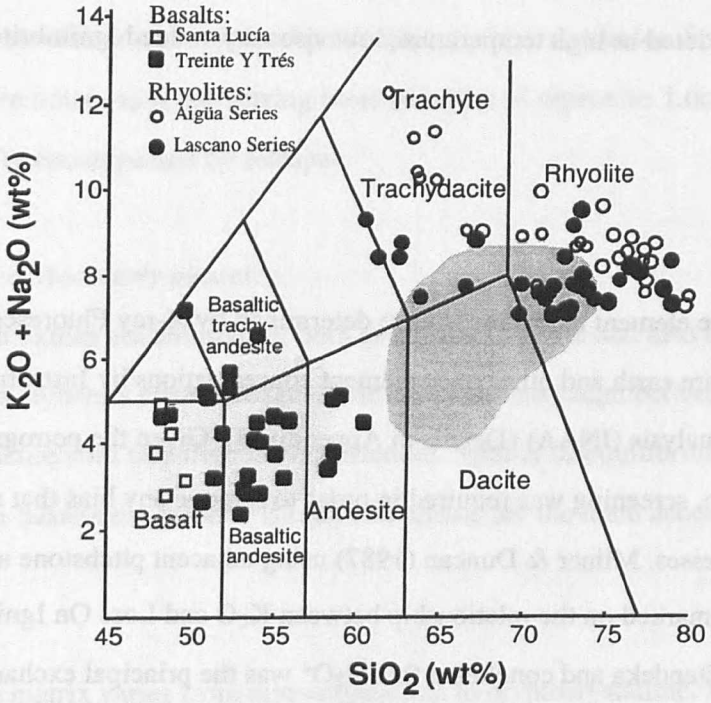

The rhyolitic rocks plot as trachytes or trachydacites and rhyolites in Figure 6. A few of the less evolved samples are trachytic (on the basis of CIPW normative calculations with Q > 20 %), but most are trachydacites (Q < 20 %). The subdivision of volcanic rocks into alkaline and subalkaline series using the boundary lines of either Kuno (1966) or Irvine & Barager (1971) place the majority of the Uruguay basic rocks in the subalkaline/tholeiitic field, although a few plot clearly in the alkaline series. The bimodal nature of the mafic lavas and rhyolites primarily on the basis of total alkalis (basalts < 61 wt% SiO_2 and $K_2O + Na_2O$ <7%; rhyolites > 61 wt% SiO_2 and > 7 wt% $K_2O + Na_2O$) is unique to this area, as elsewhere in the Paraná-Etendeka province the lavas are bimodal in silica abundances with a gap at 60 - 64 wt% SiO_2 , but overlap in total alkalis (Fig. 2.5) (Piccirillo *et al.*, 1988; Peate *et al.*, 1992). An important implication therefore is that the petrogenetic relations between the basalts and rhyolites may be different in Uruguay.

Ti/Y ratios have been widely used to characterise CFB (e.g. Hergt *et al*, 1991 - Ferrar magmatic province; Peate *et al.*, 1992 - Paraná; Erlank *et al.*, 1984; Milner *et al.*, 1992 - Etendeka) and a plot of Ti/Y v SiO_2 also shows the gap between the basalt and rhyolite rock types from Uruguay (Fig. 2.6). The mafic rocks appear to plot in two groups (Treinte Y Trés and Santa Lucía magma types), both of which have lower Ti/Y than the high Ti/Y magmas of the northern Paraná, and are more closely associated chemically as well as geographically with the low Ti/Y Gramado and Esmeralda magma types of the southern Paraná. The volumetrically minor Santa Lucía magma type, plots at lower SiO_2 and higher TiO_2 and Fe_2O_3 than the Treinte Y Trés magma type, the main group of basalts (Table 2.3). Nb & Ni may both be used to distinguish between the Treinte Y Trés and Santa Lucía basalts, since the Treinte Y Trés basalts tend to have lower Nb and Ni abundances at low SiO_2 and Zr contents (Fig. 2.7). The two basaltic magma types may also be distinguished on the basis of initial isotopic ratios in that the Santa Lucía basalts have lower $^{87}Sr/^{86}Sr_i$ (0.7046 to 0.7085) and higher $^{143}Nd/^{144}Nd_i$ (0.5124 to 0.5122) than the Treinte Y Trés rocks (0.7089 - 0.7201 and 0.5122 to 0.5119).

Fig. 2.6. Incompatible trace element ratio of Ti/Y v SiO_2 comparing the main Paraná mafic and silicic magma types with the volcanics of southern Uruguay. Data from Peate, 1989; Garland, *et al.* (1995) and current study. Low Ti/Y is less than 310, high Ti/Y is above this value.

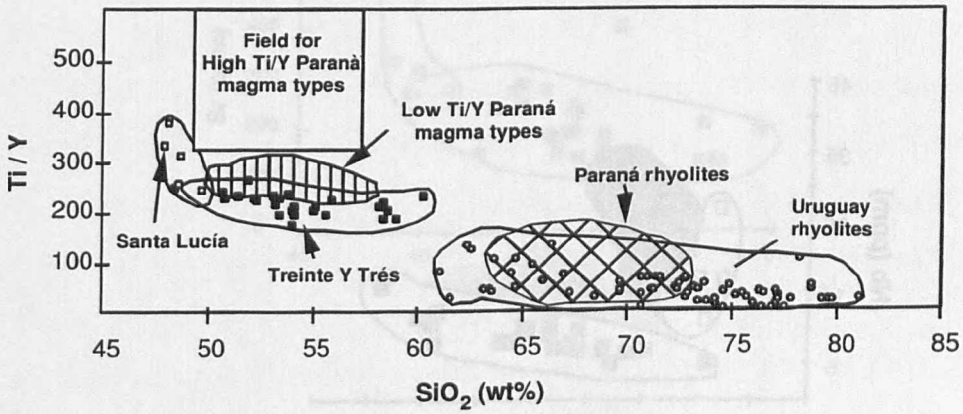

Fig. 2.7. Major and trace element variation diagrams distinguishing between the Treinte Y Trés and Santa Lucía basalts and the different high and low Ti/Y magma types of the Paraná . Data from Peate (1989); Garland (1995) and this study. Open symbols for the Santa Lucía magma type, closed for the Treinte Y Trés.

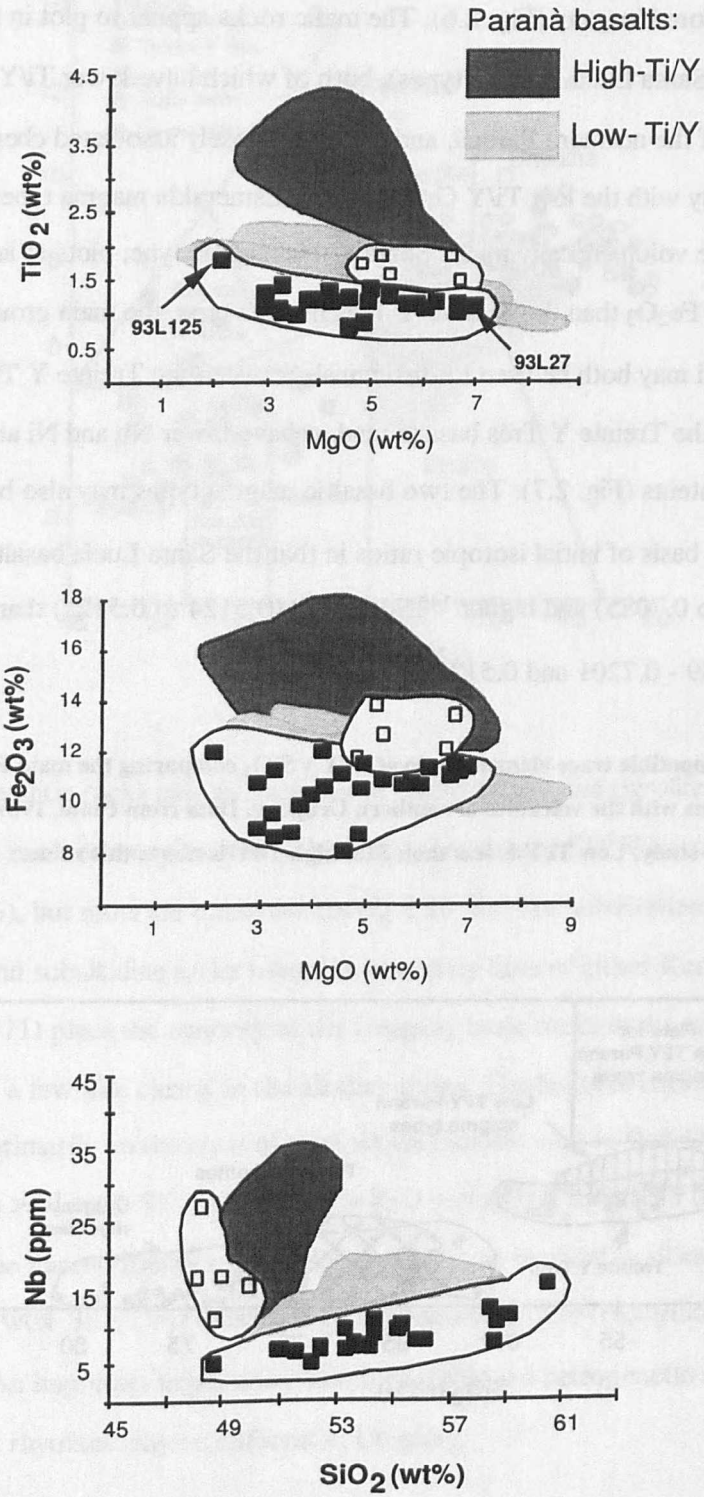

Fig. 2.7. cont.

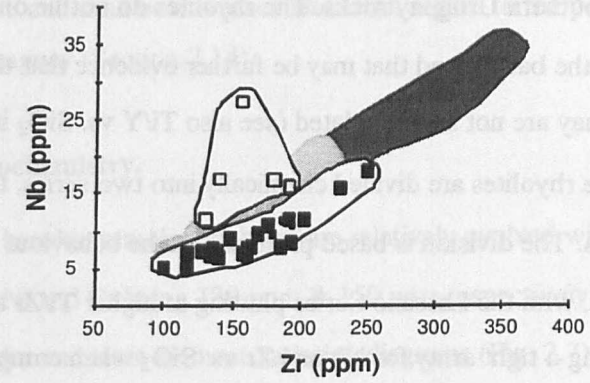

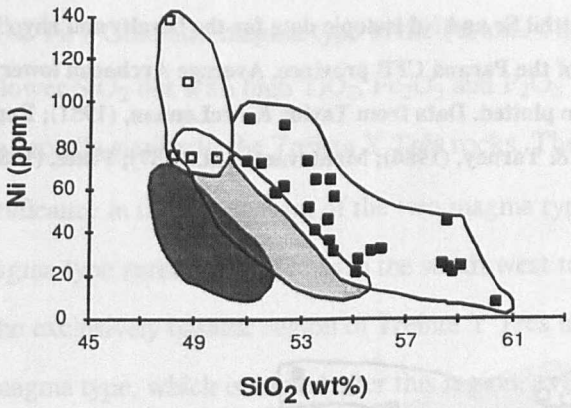

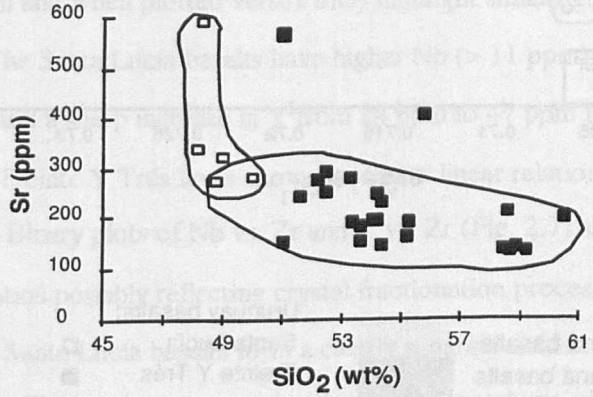

Sr and Nd isotopic data further highlight the relationships between the basalts and rhyolites of southern Uruguay and those of the Paraná province (Fig. 2.8). All the initial Sr

and Nd isotopic ratios are calculated back to 130 Ma, and Figure 2.9 illustrates a number of important features of the southern Uruguay rocks. The rhyolites do not lie on a continuous Nd - Sr isotope trend with the basalts and that may be further evidence that the basalts and rhyolites in southern Uruguay are not simply related (see also Ti/Y vs. SiO_2 in Fig. 2.6). As discussed previously the rhyolites are divided chemically into two series, the Lascano Series and the Aigüa Series. The division is based primarily on the behaviour of the trace elements Nb, Zr, Ti and Sr, with the Lascano Series plotting at higher Ti/Zr and Sr vs. SiO_2, and in general forming a tight array for Nb and Zr vs. SiO_2 when compared with the Aigüa Series (Figs. 2.18, 2.19).

Fig. 2.8. Variation in initial Sr and Nd isotopic data for the basalts and rhyolites of southern Uruguay compared with those of the Paraná CFB province. Average Archaean lower crust and Proterozoic upper crust are also plotted. Data from Taylor & McLennan, (1981); Rogers & Hawkesworth, (1982); Weaver & Tarney, (1984); Mantovani et al.(1987); Peate, (1989); Garland, (1994).

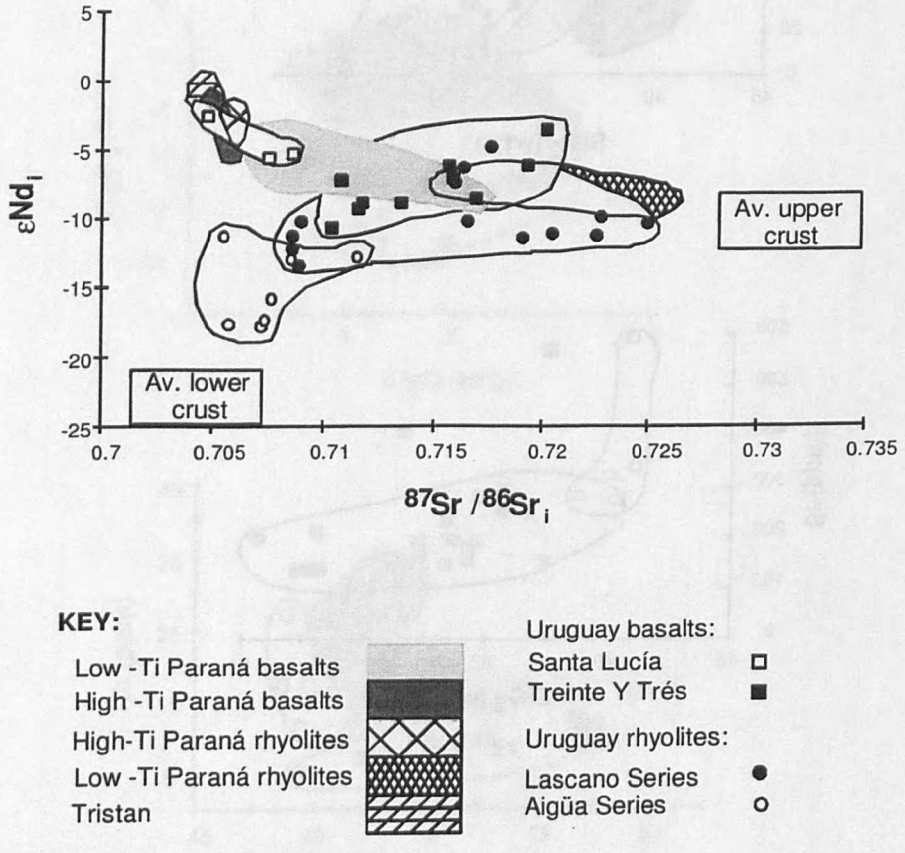

The Lascano Series range in $^{87}Sr/^{86}Sr_i$ from 0.7084 to 0.7248 and in εNd_i from -13.3 to -4.7, while the Aigüa series forms a much tighter array at low $^{87}Sr/^{86}Sr_i$ and very low εNd_i

(Fig. 2.8). The variations particularly in εNd_i of the rhyolites are distinct in relation to the Paraná province and shall be discussed later with regard to the petrogenesis of the rhyolites of southern Uruguay (Section 2.14).

2.5 Basalt Geochemistry.

All the basaltic samples analysed are relatively evolved with MgO varying from > 2 to 7 wt%, and Ni and Cr being 139 ppm & 150 ppm respectively in the most primitive sample. On major and trace element variation diagrams (Fig. 2.7), two distinct magma types emerge as previously described for Figures 2.7 and 2.9. The main magma type, herein termed the Treinte Y Trés magma type includes the majority of the lavas, and it is broadly similar to the low Ti/Y Gramado magma type in the Paraná. The Santa Lucía magma type tends towards lower SiO_2 but with high TiO_2, Fe_2O_3 and P_2O_5 while MgO, Al_2O_3, CaO & K_2O ranges are broadly similar to the Treinte Y Trés rocks. There is no apparent geographic significance in the distribution of the two magma types, with samples from the Santa Lucía magma type spread from Minas in the south-west to Lascano (Fig. 1.22). All samples from the exclusively basaltic region of Treinte Y Trés in the north are stereotypical of the second magma type, which is named after this region, even though the magma type is widespread throughout southern Uruguay.

The High Field Strength (HFS) elements (Zr, Y, Ti and Nb) are relatively immobile during alteration and when plotted versus SiO_2 highlight similar groups to those of the major oxides. The Santa Lucía basalts have higher Nb (> 11 ppm) and Ti at SiO_2 values of 47 to 50 wt%, and a sharp increase in Y from 28 ppm to 47 ppm for a similar range in SiO_2 (Fig. 2.7). The Treinte Y Trés lavas show a constant linear relationship between Nb, Y and Zr versus SiO_2. Binary plots of Nb vs. Zr and Y vs. Zr (Fig. 2.7) show broadly constant trace element ratios possibly reflecting crystal fractionation processes within the Treinte Y Trés lavas. The Santa Lucía basalts form a clearly separate field in for example diagrams of Nb - Zr and Nb - SiO_2 and appear unrelated to the main volume of lavas. Using more mobile elements such as Sr, Ba & Rb and plotting them against SiO_2 the general trends are maintained although they are more scattered (Fig. 2.7), due in part to plagioclase accumulation (in the case of Sr) and alteration.

Table 2.3. Selected chemical analyses of the Uruguay mafic and acid volcanics, subgroup names are as described in the text.

Magma type:	Santa Lucía			Treinte Y Trés			
Sample:	93L47	92-U12	93L106	93L27	93L96	502-936	93L124
(wt%)							
SiO_2	47.99	48.19	49.81	48.52	51.44	52.33	53.93
TiO_2	1.63	1.88	1.91	1.20	1.23	1.20	1.32
Al_2O_3	17.86	16.99	15.7	17.75	16.77	14.35	15.48
Fe_2O_3	12.8	12.3	14.03	11.77	10.89	11.51	11.28
MnO	0.14	0.18	0.15	0.22	0.17	0.36	0.17
MgO	5.27	6.44	5.13	6.57	5.6	6.86	4.45
CaO	10.27	8.57	9.84	10.97	10.58	7.61	9.14
Na_2O	2.84	3.78	2.25	2.4	2.29	3.86	2.46
K_2O	0.92	1.14	0.87	0.43	0.9	1.81	1.62
P_2O_5	0.28	0.52	0.32	0.17	0.14	0.13	0.16
LOI	1.86	0.86	1.52	2.00	1.46	2.15	0.41
Rb	18	22	22	6	22	70	55
Sr	344	596	285	281	248	257	202
Y	29.7	30	47	29	32	32	37
Zr	138	154	190	97	138	137	158
Nb	17	28	16	6	7	7.9	8
Ba	392	551	401	309	257	608	381
Ni	139	76	75	27	72	89	46
Cu	92	66	71	70	88	158	98
La	16.4	27.3		10.4	15.4	17.2	
Ce	34.7	57.7		23.5	34.5	34.8	
Nd	20.1	27.2		14.9	18.8	17.6	
Sm	4.22	6.2		3.4	4.45	4.61	
Eu	1.57	2.07		1.24	1.35	1.16	
Tb	0.78	0.93		0.72	0.91	0.88	
Yb	2.85	2.5		2.64	3.21	2.85	
Lu	0.43	0.37		0.43	0.47	0.44	
$^{87}Sr/^{86}Sr_m$	0.70636	0.70480			0.71111	0.71705	
$^{143}Nd/^{144}Nd_m$		0.51247		0.51207	0.51223	0.51229	
$^{87}Sr/^{86}Sr_i$	0.70608	0.70460			0.71063	0.71559	
εNd_i		-2.4		-10.1	-7.1	-3.4	

Table 3: *continued.*

Magma type:	**Treinte Y Trés**			**Lascano**			
Sample:	92-U17	502-306	93L125	93L78	93L64	93L76	93L115
SiO_2	54.22	58.31	60.39	61.19	66.50	73.74	69.78
TiO_2	1.25	1.49	1.88	1.52	1.15	0.48	0.64
Al_2O_3	15.68	13.9	12.66	14.77	13.22	12.66	12.45
Fe_2O_3	10.74	11.46	12.14	9.35	7.54	3.41	6.44
MnO	0.15	0.19	0.18	0.15	0.13	0.05	0.18
MgO	4.82	3.16	2.02	0.78	1.07	0.20	0.38
CaO	10.18	7.92	6.07	3.26	2.30	0.73	2.24
Na_2O	1.71	2.56	2.53	3.87	4.3	2.97	2.71
K_2O	1.10	0.81	1.93	4.48	3.39	5.65	5.06
P_2O_5	0.15	0.20	0.21	0.64	0.39	0.10	0.12
LOI	0.58	1.92	1.82	1.10	2.22	1.17	2.06
Rb	27	88	107	122	95	209	176
Sr	238	144	205	313	168	113	134
Y	36	43	49	112	52	54	105
Zr	146	207	227	491	373	492	367
Nb	10	13	16.2	53.2	43	54	29
Ba	409	361	509	2776	1172	805	1192
Ni	57	26	7	7	3	4	14
Cu	66	77	94	9	12	13	9
La		27.3	30.7	142	57.4		85.9
Ce		56.9	65	211	120		138
Nd		28.2	33.3	115	52.2		73.9
Sm		6.71	7.73	20.5	9.81		15.1
Eu		1.49	1.87	5.44	2.66		3.45
Tb		1.12	1.38	3.01	1.41		2.65
Yb		3.76	4.65	8.84	4.88		8.21
Lu		0.6	0.69	1.38	0.72		1.19
$^{87}Sr/^{86}Sr_m$		0.72254	0.71965	0.71101	0.71179		0.72330
$^{143}Nd/^{144}Nd_m$		0.51229	0.51216	0.51204	0.51189		0.51226
$^{87}Sr/^{86}Sr_i$		0.71922	0.71685	0.70892	0.70878		0.71628
εNd_i		-6.0	-8.5	-10.1	-13.3		-6.2

Table 3: *continued.*

Magma type:	**Lascano**						
Sample:	92-U15	93L127	93L102	93L128	93L109	93L99	92-U14
SiO_2	71.27	71.62	72.90	72.57	73.48	76.30	76.54
TiO_2	0.66	0.60	0.57	0.59	0.43	0.33	0.31
Al_2O_3	12.77	12.27	11.59	12.46	12.50	11.63	11.58
Fe_2O_3	6.22	5.65	5.35	5.70	4.42	3.10	2.72
MnO	0.16	0.12	0.07	0.07	0.05	0.02	0.02
MgO	0.20	0.66	0.39	0.36	0.18	0.11	0.08
CaO	1.15	1.92	1.30	1.09	0.84	0.27	0.50
Na_2O	2.79	2.69	1.87	1.97	2.12	1.66	1.63
K_2O	4.65	4.36	5.84	5.09	5.85	6.51	6.56
P_2O_5	0.12	0.11	0.12	0.12	0.12	0.06	0.06
LOI	1.39	1.13	1.43	2.07	1.28	1.59	0.92
Rb	168	172	148	185	200	212	209
Sr	134	125	94	122	118	61	72
Y	99	57	53	65	63	55	62
Zr	365	354	333	469	389	327	304
Nb	28	28	25	27	23	20	21
Ba	1285	754	827	1218	1527	1226	1270
Ni	8	5	3	6	6	4	5
Cu	13	14	14	11	8	7	7
La		47.7		64.9	71.7	66.2	65.7
Ce		102		148	154	132	138
Nd		46.4		65.3	68.8	57.6	60.6
Sm		9.55		12.7	12.9	10.9	11.6
Eu		1.99		2.30	2.30	1.64	1.6
Tb		1.52		1.88	1.89	1.54	1.65
Yb		5.48		6.28	5.79	5.38	5.77
Lu		0.8		0.92	0.83	0.79	0.82
$^{87}Sr/^{86}Sr_m$				0.72710	0.72947	0.74110	0.73828
$^{143}Nd/^{144}Nd_m$				0.51199	0.51201	0.51199	0.51206
$^{87}Sr/^{86}Sr_i$				0.71898	0.72039	0.72241	0.72262
εNd_i				-11.3	-11.0	-11.1	-9.9

Table 3: *continued:*

Magma type:		**Aigüa**					
Sample:	93L126	93L86	93L18	93L48	93L46	93L22	93L36
SiO_2	78.88	61.74	64.76	67.37	73.00	77.15	76.46
TiO_2	0.33	0.43	0.70	0.55	0.30	0.19	0.10
Al_2O_3	9.80	17.1	15.61	14.51	13.05	12.09	12.36
Fe_2O_3	3.10	7.15	5.70	6.46	4.10	1.56	2.04
MnO	0.06	0.21	0.13	0.08	0.07	0.01	0.02
MgO	0.29	0.29	0.63	0.32	0.14	0.05	0.05
CaO	0.22	0.7	2.2	1.54	0.65	0.34	0.10
Na_2O	0.70	5.79	3.93	3.04	2.74	3.05	3.44
K_2O	6.56	6.45	6.25	6.00	5.88	5.52	5.41
P_2O_5	0.05	0.10	0.13	0.14	0.05	0.04	0.03
LOI	1.75	1.06	6.41	1.39	1.37	0.82	0.71
Rb	164	188	164	145	174	164	584
Sr	35	16	264	197	59	25	324
Y	42	95	87	94	58	31	7
Zr	285	1008	955	1047	620	391	136
Nb	17	191	136	40	51	33	333
Ba	776	162	935	2291	705	262	167
Ni	1	4	3	4	3	3	4
Cu	4	9	6	12	10	10	5
La	44.5	133	110	91.8	95.2	48.5	79.6
Ce	91.9	245	214	170	196	92.2	172
Nd	40.4	98.8	86.5	88.8	86.6	43.5	60.7
Sm	7.9	17.2	15.2	16.5	13.6	7.74	14.4
Eu	1.34	2.01	2.21	4.46	2.35	0.7	0.24
Tb	1.17	2.59	2.29	2.34	1.64	0.9	3.24
Yb	3.89	10.9	9.27	8.11	6.43	4.42	12.8
Lu	0.57	1.59	1.34	1.25	0.94	0.64	1.73
$^{87}Sr/^{86}Sr_m$	0.74128		0.71471	0.71238			
$^{143}Nd/^{144}Nd_m$	0.51206	0.51215	0.51191	0.51191		0.5117	0.51184
$^{87}Sr/^{86}Sr_i$	0.71650		0.71138	0.70846			
εNd_i	-10.1	-8.0	-12.6	-12.8		-17.6	-14.8

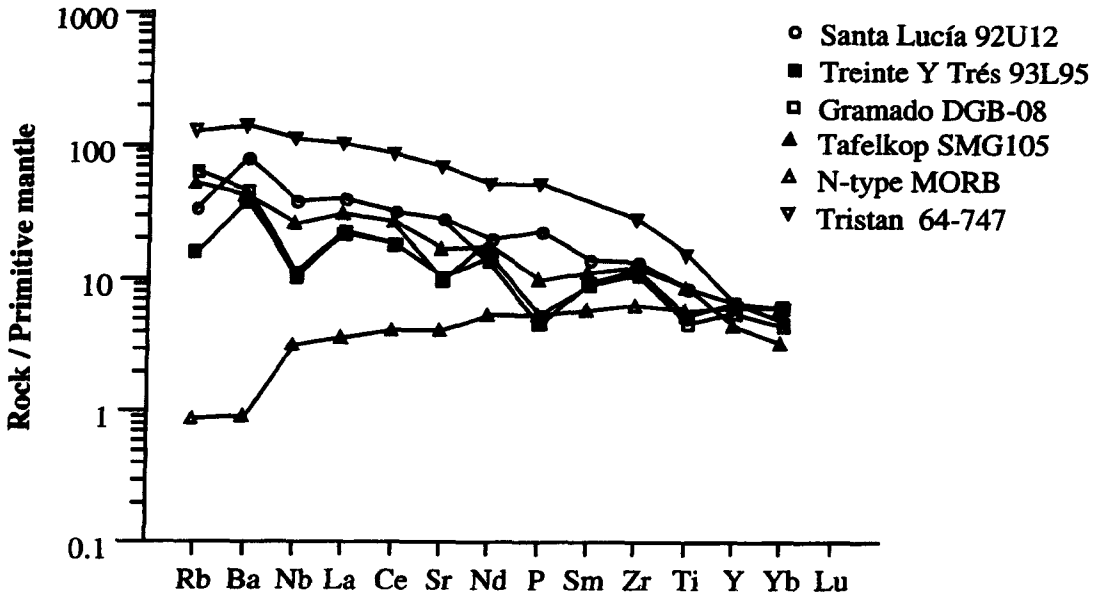

Fig. 2.9. Mantle normalised incompatible element diagram comparing the Treinte Y Trés and Santa Lucía magma types. The Treinte Y Trés samples are distinguished by low Nb/La. These samples are also compared with samples considered to be derived from the asthenosphere including the Tafelkop magma type of the Etendeka. Data from le Roex *et al.*, (1989); Peate, (1989); Sun & McDonough, (1989); Ewart *et al.*, (1997).

The differences between the Treinte Y Trés and Santa Lucía lavas are most striking on a mantle-normalised incompatible element diagram (Fig. 2.9). The Santa Lucía basalts are characterised by relatively smooth incompatible element signatures, similar to those of asthenosphere-derived ocean island basalt (OIB). This is unusual for any basalts associated with the Paraná province, although Milner & le Roex (1996) recently reported basalts in the Etendeka with incompatible trace element and isotopic compositions similar to recent basalts associated with the Tristan plume (Fig. 2.9). Prior to break-up the Etendeka province would have been spatially close to Uruguay and these Tafelkop basalts have Ti/Y ratios > 500 and Nb/La ~ 1, broadly similar to the Santa Lucía rocks albeit at lower concentrations. The Treinte Y Trés lavas have very different mantle-normalised patterns with distinctive negative anomalies at Nb, P and Ti in particular, and at least in tholeiites these are generally thought to be unrelated to the degree of melting (e.g. Hawkesworth *et al.*, 1988). On mantle-normalised plots, magmas derived by partial melting of asthenospheric upper mantle should define more or less smooth profiles, with the degree of

compatibility of these elements in the melt increasing from Ba through to Yb. The observed pattern for the Treinte Y Trés lavas is more akin to the main volume of lava in the south of the Paraná basin, the low Ti/Y Gramado magma type which is also characterised by low Nb/La ratios.

Both Uruguay basalt magma types are LREE enriched relative to HREE, with the LREE abundances being slightly lower in the Treinte Y Trés rocks. Negative Eu anomalies develop with increasing SiO_2 and are associated with increasing plagioclase fractionation.

Sr & Nd isotopes:

The Treinte Y Trés and Santa Lucía magma types have different Sr and Nd isotopic ratios (Fig. 2.8), with the Treinte Y Trés magma type having a much wider range in εNd_i from -3.4 to -10.6. These extend to lower values than those reported from the Gramado rocks of -1.3 to -8.7 (Bellieni et *al.*, 1986; Peate *et al.*, 1992; Peate & Hawkesworth, 1996). The range of εNd_i for the Santa Lucía basalts varies from -2.4 to -5.4. Initial Nd isotopic ratios for Tristan da Cunha, Walvis Ridge and Inaccessible Island are -3.3 to -0.9, -4.5 to 1.5 and -1.9 to 0.2 respectively (Humphris & Thompson, 1982; le Roex *et al.*, 1990; Cliff *et al.*, 1991). Therefore the Santa Lucía data may indicate a degree of mixing between an asthenospheric component, as indicated by the smooth incompatible element diagram (Fig. 2.9), and an older presumably lithospheric component which results in a shift to lower εNd_i values. On a plot of $^{87}Sr/^{86}Sr_i$ vs. SiO_2 the Treinte Y Trés magma type ranges from 0.7089 to 0.7210 as SiO_2 increases from 52 to 60 wt% (Fig. 2.10), while in the Santa Lucía basalts $^{87}Sr/^{86}Sr_i = 0.7046$ to 0.7085 at lower SiO_2 contents. The range in initial Sr isotope ratios is broadly similar to that described for the Gramado rocks of the Paraná in which $^{87}Sr/^{86}Sr_i = 0.706$-$0.715$ (Bellieni *et al.*, 1986; Piccirillo *et al.*, 1988; Peate and Hawkesworth, 1996). These variations in Sr and Nd isotope compositions and also in highly incompatible element ratios indicate the importance of open system behaviour particularly with regard to the evolution of the Treinte Y Trés magma type. The increase in $^{87}Sr/^{86}Sr_i$ with increasing SiO_2 is consistent with an Assimilation and Fractional Crystallisation (AFC) style of crustal contamination where the assimilant has higher SiO_2 and high $^{87}Sr/^{86}Sr_i$ than the parental basalts (Fig. 2.10).

Fig. 2.10. Variation in initial Sr isotope ratios with SiO_2 for the different types of Uruguay basalts and rhyolites, as compared with certain Paraná magma types. Vectors refer to open system fractionation (AFC), and closed system fractionation (FC).

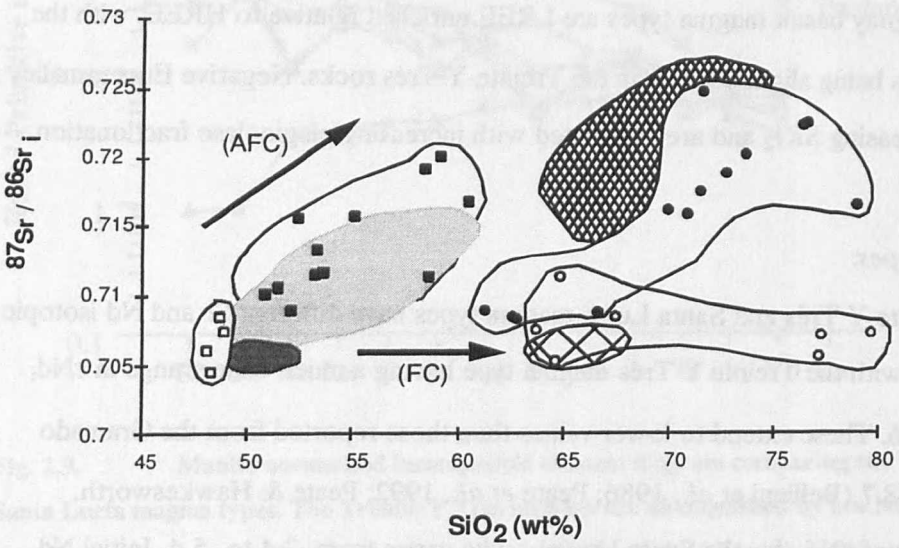

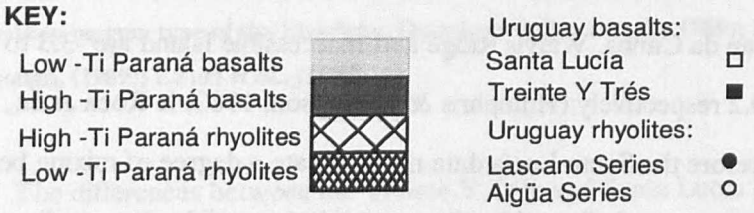

There are a number of obvious affinities between the Treinte Y Trés and the Gramado magma types in terms of major, trace-element and isotope compositions, whereas the distinctive Santa Lucía basalts are relatively rare. The petrogenetic histories of the Uruguayan magmas have been modelled using major, trace, REE and isotope data and further compared with the low Ti/Y Gramado magma type of the Paraná in particular.

2.6 Fractional Crystallisation & Assimilation.

Neither the Santa Lucía nor the Treinte Y Trés lavas represent primary mantle melts as indicated by the minor modal percentage of olivine, and the low magnesian numbers (Mg# = 24 to 54) and Ni (7 to 139 ppm) concentrations. In general the Mg# is insensitive to the degree of partial melting, but it is highly sensitive to the amount of fractional crystallisation, particularly of olivine. In the Treinte Y Trés samples there is strong evidence

for open system behaviour, as in the marked increase in $^{87}Sr/^{86}Sr_i$ with increasing SiO_2 (Fig. 2.10). This next section is concerned with resolving the effects of different high level magma chamber processes such as fractional crystallisation, magma mixing and crustal contamination in the petrogenesis of these rocks from southern Uruguay.

The porphyritic nature of the samples in thin section suggests at least some crystal-liquid fractionation, possibly by a mechanism of simple gravitational crystal removal, prior to extrusion. Major element trends indicate that gabbroic fractionation (olivine, clinopyroxene and plagioclase) had a major control on the evolution of the system (Fig. 2.11). Using Pearce element ratio plots the mineral assemblages are recognised by the slope of the trends, since the slopes of the trends are sensitive to the stoichiometry of the crystallising and segregating phases (Russell & Nicholls, 1988). These ratio plots (Fig. 2.11) show primary control by both olivine and clinopyroxene on the Fe and Mg abundances, while plagioclase fractionation affects the Na, Ca and Al abundances. Gabbroic fractionation should buffer SiO_2 with decreasing MgO contents (Cox, 1980), however SiO_2 (wt%) ranges from 47 to 60 and that may in part be due to assimilation of crustal material.

Least squares analyses were initially undertaken to assess qualitatively the proportions of the different phases involved in fractional crystallisation and the fraction of melt remaining at the end of each fractionation increment (F value). There is concern however about the possible effects of crustal contamination being reflected in the results of such least squares modelling with the result that the proportions of high SiO_2 minerals such as feldspar calculated may be too high. Least squares modelling clearly provides only an estimate of the phases involved with the relationship between parent and daughter assemblages assumed to be closed system, and so the affects of any assimilation was not taken into account.

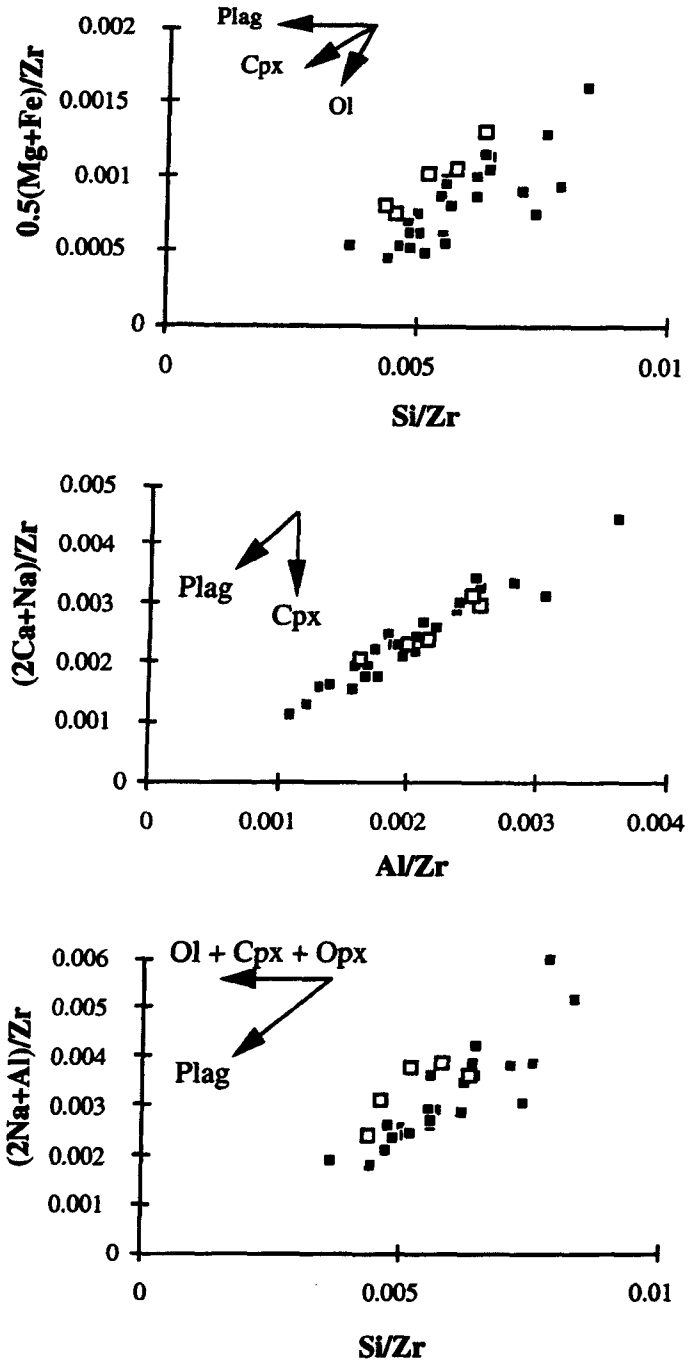

Fig. 2.11. **Pearce element ratio plots for Uruguay data. The plots are used in order to indicate the phases that are fractionating. Plot (i) distinguishes between plagioclase/clinopyroxene and olivine, plot (ii) plagioclase and clinopyroxene and plot (iii) compares ferromagnesian minerals and plagioclase. Vectors are after Nicholls (1988) and Russell & Nicholls (1988).**

The phases were constrained both from the mineralogy observed in thin section, and from other studies of tholeiitic magmas (Cox, 1980). The presence of normative diopside, olivine, hypersthene and quartz suggest that these rocks last equilibrated relatively shallow at low pressures of ~ 1 atm (Thompson *et al.*, 1983). Table 4 summarises the proportions

of the mineral phases used in the least squares calculations. The results for the Treinte Y Trés magma type are broadly similar to the ratios of the phenocryst phases observed in thin section, but with more olivine predicted than observed. Decreases in MgO accompanied by increases in Fe_2O_3 and Na_2O, and decreases in CaO and Al_2O_3 are consistent with gabbroic fractionation involving olivine-plagioclase-clinopyroxene-magnetite extraction (Cox, 1980), in the proportions of approximately 15 : 55 : 25 : 5. F is the amount of crystal fractionation and it is calculated from the amount of liquid remaining after the best fit of the data has been achieved and as can be seen in Table 4 is variable from 60 to 80 %. Contamination is however an important factor in the petrogenesis of the Treinte Y Trés basalts in particular (Fig. 2.10) and so the results of the least squares modelling are only used as a qualitative guide to the fractionating assemblage. Nonetheless as MgO decreases from 6.57 to 2.02 wt% the amount of fractional crystallisation, F is calculated to be approximately 80 %.

The phase proportions as calculated from least squares analyses were used to calculate the bulk distribution coefficients for different trace elements, and the values of F from the major element modelling were used initially to constrain F for the models of the trace element variations in both closed and open systems. Contamination is known to play an important role in the evolution of the system (e.g. Fig. 2.10) and it is seen to exert a major control on the variation of more mobile elements including Rb and Sr.

Table 2.4. Fractionating assemblages generated using the Mix 'n' Mac 2.6L program (D.R.Mason, 1987) for the mafic Treinte Y Trés suite of lavas. Phase compositions and abbreviated as follows: Olivine - Ol; Plagioclase - Plag; Clinopyroxene - Cpx and Magnetite - Mt. Σr^2 indicates how good the fit is for the fractionation model with values < 1 considered valid. F (%), the amount of fractional crystallisation = (1 - liquid) *100.

Parent	Daughter	F (%)	Ol (%)	Plag (%)	Cpx (%)	Mt (%)	Σr^2
93L27	502-936	66.8	4	41.7	16.8	5.2	0.32
93L27	92U17	60.4	7.8	37.4	10.5	4.4	0.20
93L27	93L98	74.9	8.7	44.4	14.7	6.7	0.18
93L27	93L125	81.4	8.6	49.3	17.6	6.1	0.09

Table 2.5. Partition coefficients for basaltic melts.

Element	Olivine	Clino-pyx.	Plagioclase	Magnetite
Rb	0.001	0.03	0.07	
Nb	0.01	0.005	0.01	0.4
Sr	0.014	0.06	1.8-3.3	
Nd	0.0066	0.3	0.085	2.0
Zr	0.012	0.1	0.048	0.1
Ti	0.02	0.4	0.04	7.5
Y	0.01	0.9	0.03	0.2
Yb	0.02	0.6	0.06	1.5
Ba	0.009	0.026	0.23	

The bulk D values were calculated according to the proportion of phases calculated from the major elements, and reported partition coefficients between liquid and crystals (Table 2.5). The mineral partition coefficients were taken from a variety of sources including Pearce & Norry (1979), McKenzie & O'Nions (1991), Thirlwall *et al.* (1994) and Rollinson (1993), and while there is considerable variation in the quoted distribution coefficients for each element, the K_D values used were for rocks of between 48 and 60 wt% SiO_2. The results reflect crude groupings of the parameters likely to affect trace element partitioning, such as temperature, pressure and bulk composition (Blundy & Wood, 1991).

Particular attention was given to the behaviour of Sr partitioning into plagioclase feldspar, as the D_{Sr} (& D_{Ba}) in plagioclase feldspar has been shown to be controlled by crystal chemistry (Blundy & Wood, 1991). Over a range of temperatures there is a relationship between D_{Sr} (& D_{Ba}) and the mole fraction (X_{An}), and plots of $\ln D_{Sr}$ versus X_{An} yield linear arrays with negative slopes. Microprobe data on feldspar composition was used to determine X_{An} and hence to calculate the D_{Sr} for the Treinte Y Trés lavas according to the model of Blundy & Wood (1991). The calculated D_{Sr} values for the Treinte Y Trés samples varied from 3.3 in Labradorite at T = 1333 °K and X_{An} = 0.5, to 1.95 in Labradorite at T = 1460 °K and X_{An} = 0.7. Furthermore using the Blundy & Wood (1991) equations, Sr is inferred to be almost 3 to 4 times more compatible in Albite (X_{An} = 0) than in labradorite (X_{An} = 0.5) due largely to the inferred differences in temperature, and this clearly has a considerable effect on any potential modelling involving Sr. A number of

different partition coefficients for Sr were evaluated for the Treinte Y Trés data and an average value of $D_{Sr} = 2.4$ was used for modelling. This implies that in terms of the Blundy & Wood (1991) model the plagioclase is primarily labradorite ($X_{An} \sim 0.6$) with an estimated temperature constraint in the order of 1450 °K (1177 °C). This temperature is slightly lower than the experimental temperature assumed for labradorite crystals in perfect equilibrium with the melt of 1285 °C however the content of water in the system might lower the temperature (Deer, Howie & Zussman, 1966).

Fig. 2.12a. Evolution of the Treinte Y Trés (filled squares) and Santa Lucía (open squares) magma types, modelled for both closed and open system fractionation. See text for details. Gramado data from Peate, (1989), is represented by field of vertical lines.

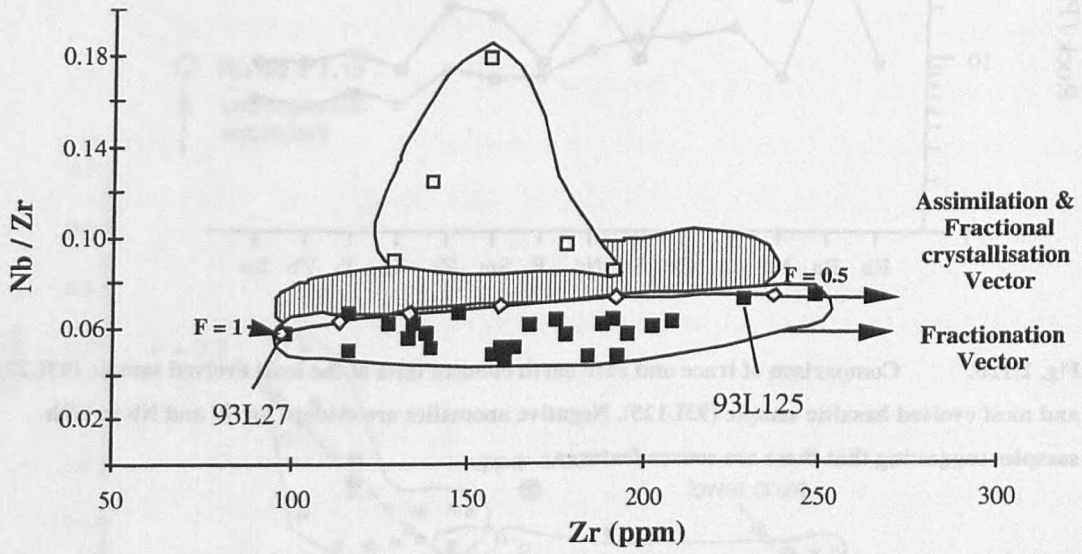

The trace element variations in the Treinte Y Trés and Santa Lucía basalts were initially modelled by closed system fractionation involving olivine, clinopyroxene, plagioclase and magnetite in the proportions ol: cpx: plag: mag = 15: 25: 55: 5. This assemblage is the same as that suggested from the major element modelling. The most primitive samples in the Treinte Y Trés and Santa Lucía magma types, 93L27 and 93L47 respectively, were chosen as C_o. The results of the modelling show that the differences in Nb/Zr between the two magma types (0.04 to 0.18) is not due to fractional crystallisation. The variation in Zr data in the Treinte Y Trés magmas particularly between samples 93L27 and 93L125 can be modelled by 60% fractionation using the calculated bulk D_{Zr} of 0.06

(Fig. 2.12b), which is significantly less than that inferred from the major element modelling (80 %, Table 2.4). 25% fractionation is required to model the variation in Zr within the Santa Lucía rocks (Fig. 2.12a). Zr increases with increasing $^{87}Sr/^{86}Sr_i$ suggesting that assimilation or mixing was an important process in the evolution of the Santa Lucía basalt system.

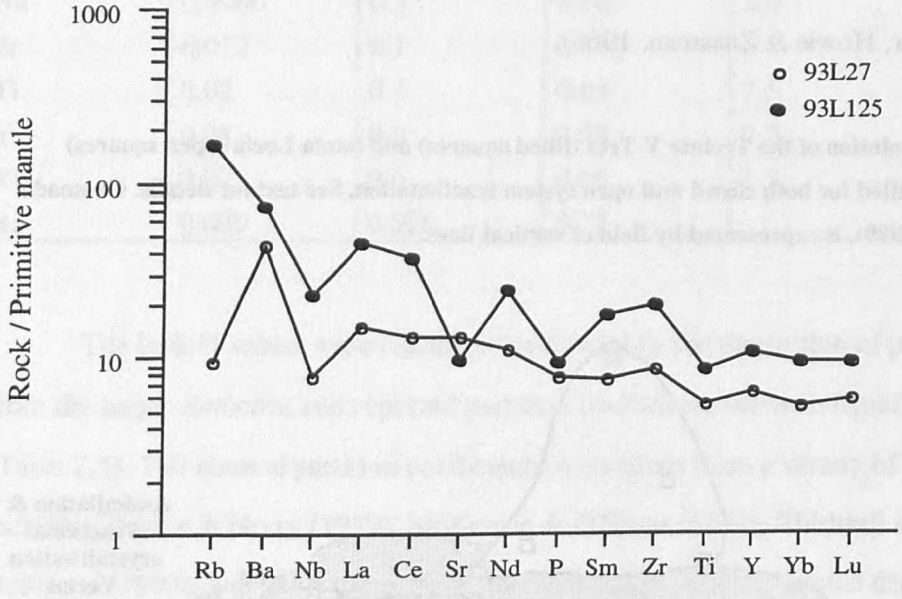

Fig. 2.12b. Comparison of trace and rare earth element data of the least evolved sample (93L27) and most evolved basaltic sample (93L125). Negative anomalies are evident for Ti and Nb in both samples suggesting that these are source features.

Open system fractional crystallisation and assimilation (AFC) was modelled for the Treinte Y Trés basalts using the equations of De Paolo (1981). One of the more primitive Treinte Y Trés lavas was again used as the starting composition (93L27) (C_o), with olivine, clinopyroxene, plagioclase and magnetite involved in the fractionating assemblage in the same proportions as above. The ratio of the rate of assimilation to the rate of fractional crystallisation, r, was fixed at 0.25 for the vector shown in Figure 2.13a, although this value was varied slightly to give a better fit to the data set. The choice of assimilant was constrained from the compositions of the basalts to have low TiO_2 at high SiO_2 and $^{87}Sr/^{86}Sr_i$, and 11 ppm Nb and Zr = 60 ppm. These concentrations are similar to those described for foliated granites and leucogranites from Brazil (May, 1990). Another distinctive feature of the inferred contaminant is that it has Rb/Ba (2.8) much higher than

estimates of the average lower and upper continental crust (0.16 and 0.046 respectively, Taylor & McLennan, (1985)). The assimilant is therefore considered to have been derived from the upper crust, but as a partial melt in order to have the high Rb/Ba ratios, since fractionation of Rb from Ba only occurs during partial melting of crust by incongruent melting of micas (Harris & Inger, 1991; Garland *et al.*, 1995). A Brazilian leucogranite (RSM2B) was chosen to represent the crustal component from data compiled by May (1990) (Fig. 2.13).

Fig. 2.13. AFC trend for the variation in the Treinte Y Trés and Santa Lucía basalts illustrated on a diagram of Sr versus Rb/Ba. The modelled assimilant is a Brazilian leucogranite (RSM2B) May (1990). Upper continental crust from Taylor & McLennan (1981); lower crust from Weaver & Tarney (1984).

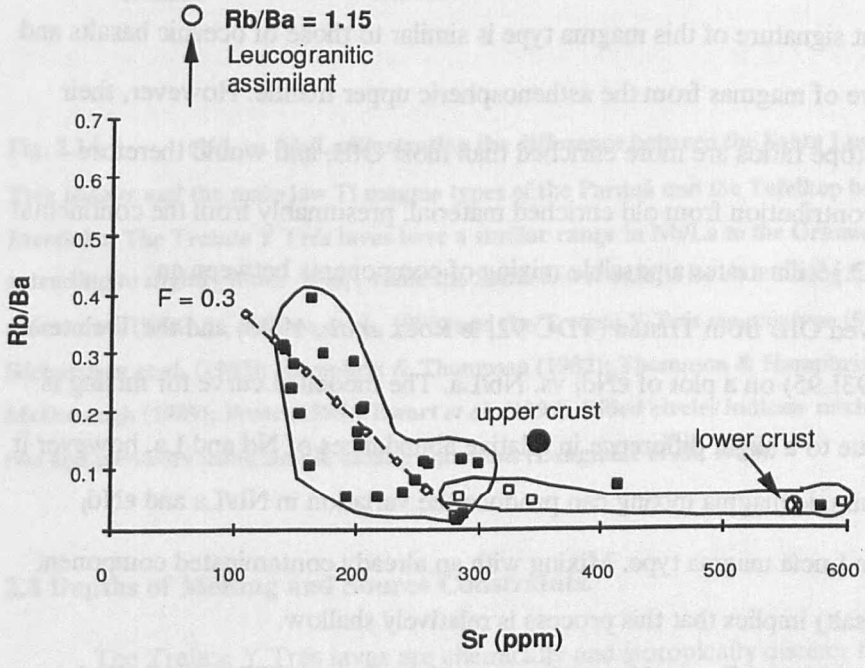

In summary Nb & Zr are both highly incompatible in basaltic melts with Nb slightly more so than Zr, therefore the ratio is relatively unaffected by fractionation and by partial melting, except when the amounts of melting are small. As long as F>>D the incompatible element ratio Nb/Zr should not change. Plotting Nb/Zr v Zr (Fig. 2.12) the overall trend of the Treinte Y Trés magma type can be explained by varying degrees of fractionation and assimilation from the least evolved sample, although this composition is also removed from that of a primary basaltic liquid. The ratio of Rb/Ba is sensitive to contamination and so the

effects of AFC are well illustrated on a diagram of Sr vs. Rb/Ba (Fig. 2.13). Assuming a constant rate of assimilation of 35 % of an upper crustal leucogranitic component (RSM2B) the amount of fractional crystallisation required to explain the variation in the data set is ~50 % (Fig. 2.13). AFC processes are therefore considered to control the evolution of the Treinte Y Trés lavas, however the amount of assimilation appears to be quite high. The differences between the Treinte Y Trés and the Santa Lucía lavas are addressed further when the depths of melting and source constraints are examined.

2.7 Mixing.

The Santa Lucía magma type contains some of the most primitive rocks associated with the Paraná CFB province. In addition, the smooth primitive mantle-normalised incompatible element signature of this magma type is similar to those of oceanic basalts and is therefore indicative of magmas from the asthenospheric upper mantle. However, their initial Sr and Nd isotope ratios are more enriched than most OIB, and would therefore appear to reflect a contribution from old enriched material, presumably from the continental lithosphere. Figure 2.15 illustrates a possible mixing of components between an asthenosphere-derived OIB from Tristan (TDC-92, le Roex *et al.*, 1990) and the Treinte Y Trés magma type (93L95) on a plot of εNd_i vs. Nb/La. The modelled curve for mixing is not exactly linear due to a slight difference in relative abundances of Nd and La, however it demonstrates that simple magma mixing can produce the variation in Nb/La and εNd_i evident in the Santa Lucía magma type. Mixing with an already contaminated component (Treinte Y Trés basalt) implies that this process is relatively shallow.

Variations within the Esmeralda magma type of the Paraná CFB were similarly modelled by mixing of an asthenospheric melt and the Gramado magma type by Peate and Hawkesworth (1996). In this case though, the asthenospheric component was characterised by a relatively depleted incompatible element signature similar to MORB. As can be seen in Figure 2.15 such a component would not be suitable for the Santa Lucía magma type which might suggest that these lavas in southern Uruguay were erupted prior to the Esmeralda magma type while the plume still had a major influence prior to the movement of South America away from the site of the hotspot.

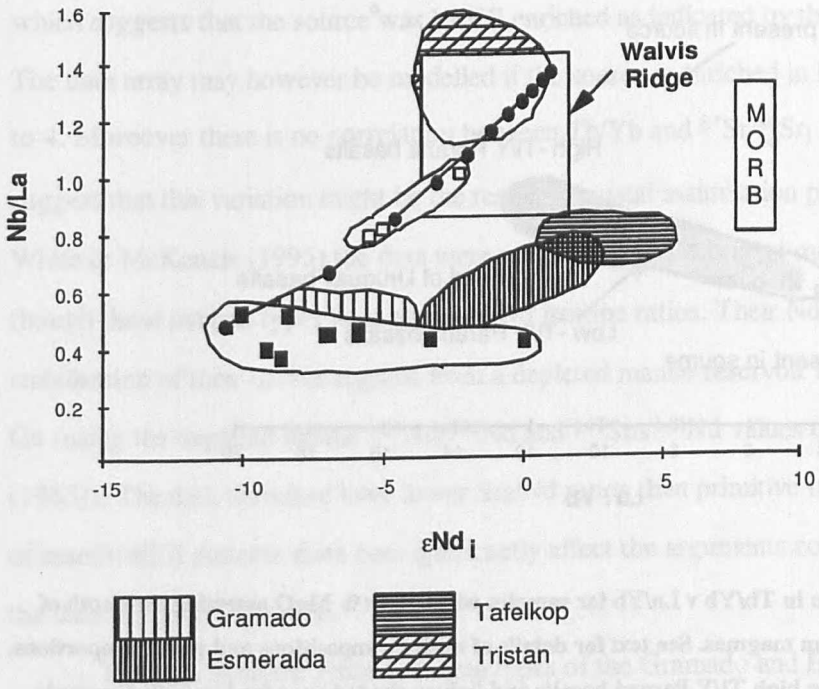

Fig. 2.14. **εNd_i vs. Nb/La illustrating the difference between the Santa Lucía and Treinte Y Trés basalts and the main low Ti magma types of the Paraná and the Tafelkop basalt from the Etendeka. The Treinte Y Trés lavas have a similar range in Nb/La to the Gramado magma type extending to slightly lower εNd_i, while the Santa Lucía basalts lie on a mixing line between Tristan plume data (TDC-91, le Roex *et al.*, 1990) and the Treinte Y Trés magma type (502-936). Data from Richardson *et al.* (1982); Humphris & Thompson (1982); Thompson & Humphris (1982); Sun & McDonough (1989); Peate (1989); Ewart *et al.* (1997). Filled circles indicate mixing trend between the two end members using simple mixing equations (Langmuir *et al.*, 1978).**

2.8 Depths of Melting and Source Constraints.

The Treinte Y Trés lavas are chemically and isotopically distinct from the Santa Lucía basalts and show an affinity with the low Ti/Y Paraná basalts. The evolution of the Treinte Y Trés basalts has been shown to be dominated by shallow level processes, but the question of the nature of the source for these and the Santa Lucía basalts remains. In this section mantle melting and in particular the depth at which melting occurred is addressed primarily through the use of rare earth element data in order to evaluate whether the differences between the two magma types in southern Uruguay are primary (source related) or secondary (process related).

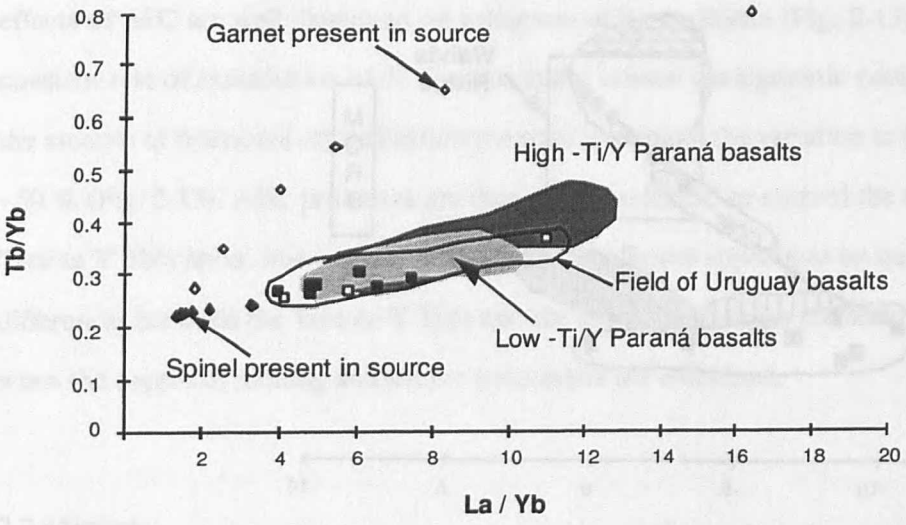

Fig. 2.15. Variation in Tb/Yb v La/Yb for samples with > 5 wt% MgO assessing the depth of melting for the Uruguayan magmas. See text for details of modal compositions and phase proportions. Dark grey shaded area for high Ti/Y Paraná basalts and lighter shaded area for low Ti/Y Gramado field, data from Peate (1989). Filled squares = Treinte Y Trés magma type; Open squares = Santa Lucía magma type.

Both modal and non-modal melting models have been explored. The modal compositions and the phase proportion entering the melt (ol: opx: cpx: sp - 20: 20: 55: 5 and ol: opx: cpx: gnt - 20: 20: 30: 30) are taken from Ellam (1992) for both spinel and garnet lherzolite. Using these data and a primitive mantle source from Sun and McDonough (1989) an assessment of the residual mineralogy was made on the basis of Tb/Yb vs. La/Yb (Fig. 2.15). Only the more primitive samples (> 5 wt% MgO) were used in order to minimise fractionation and crustal assimilation effects. The plot of Tb/Yb vs. La/Yb follows Thirlwall *et al.*, (1994) who pointed out that such a figure readily distinguished melts from garnet and spinel peridotite and mixtures between them. Strong fractionation of REE occurs in the presence of residual garnet, since Yb is highly compatible into garnet and Tb has a K_D in garnet of between 0.7 and 1 (Irving & Frey, 1978). La is highly incompatible during melting in both the garnet and spinel stability fields, and so melting in the garnet and spinel peridotite zones may be distinguished by the fractionation of Tb/Yb relative to La/Yb. There is relatively little variation between the Tb/Yb and La/Yb ratios in both the Treinte Y Trés and Santa Lucía magma types, and they plot close to but just above the curve for melting in the spinel stability field. The data plot to the right of the spinel curve

which suggests that the source was LREE enriched as indicated by the low Nd initial ratios. The data array may however be modelled if the source is enriched in La/Yb by between 3.5 to 4. Moreover there is no correlation between Tb/Yb and $^{87}Sr/^{86}Sr_i$ in these rocks to suggest that this variation might be the result of crustal assimilation processes. Following White & McKenzie (1995) the data were modelled using primitive mantle values, even though these magma types have enriched Nd isotope ratios. Their Nd model ages suggests stabilisation of their source regions from a depleted mantle reservoir between 1.8 and 1.1 Ga (using the depleted mantle $^{143}Nd/^{144}Nd$ and $^{147}Sm/^{144}Nd$ values of Allegre *et al.*, (1983)). The data therefore have lower Sm/Nd ratios than primitive mantle, but the choice of mantle REE patterns does bot significantly affect the arguments concerning the slope of the data arrays in Figure 16.

The data from the Paraná magma types of the Gramado and Esmeralda were also plotted to evaluate any variation in the inferred source ratios and depths of melting. However the Gramado and Esmeralda data plot very close to the fields for both the Treinte Y Trés and Santa Lucía magma types suggesting similar depths and degrees of melting in the spinel stability field. This magmatism in southern Uruguay occurs over an area of > 20,000 km^2 from the edge of the Paraná basin, in which > 200,000 km^3 of low Ti/Y basalt was erupted (Stewart *et al.*, 1996).

2.8.1 Major Element Regression.

Klein & Langmuir (1987) evaluated variations in MORB extrapolated back to 8 wt% MgO and interpreted the results in terms of depths and degrees of partial melting. Certain major elements including Si_8 and Fe_8 (subscript 8 denotes extrapolation back to 8 wt% MgO) are pressure dependent (Hirose & Kushiro, 1993), and there is a negative correlation between Fe_8 and Na_8 in MORB which Klein & Langmuir (1987) attributed to differences in the pressures and degrees of melting. Higher degrees of melting at higher pressures are indicated by low Na_8 and high Fe_8, and lower degrees of partial melting at lower pressures are indicated by low Fe_8 and high Na_8. Na is incompatible except at high pressures and temperatures, and so it reflects the degrees of partial melting with high abundances in small degree melts, and lower abundances as the degree of melting increases. In addition, source fertility and water contents may be reflected in both Fe_8 and Si_8, in that

a source that has undergone previous melt extraction events will be depleted in elements such as Fe, Na and Ti (Turner & Hawkesworth, 1995), while melts of hydrous peridotite will tend to have higher Si and lower Fe due to incongruent melting of orthopyroxene (Kushiro, 1968). Ti abundances may also reflect previous melt extraction events, since it is highly incompatible in basaltic melts (Garland *et al.*, 1996). As noted by Hergt *et al.* (1991) low Ti Gondwana CFB in general are displaced to lower Fe_8 and Na_8 than the MORB array of Klein & Langmuir (1987) which has a broad negative slope. Turner & Hawkesworth (1995) noted that the low Ti Gondwana CFB tend to form sub-horizontal arrays on plots of Na_8 vs. Fe^*_8, Ti_8 v Si_8 and $Mg\#_8$ v Si_8.

Kinzler and Grove (1993) derived equations in terms of Fe_8 and Na_8 for calculating the pressures and hence the depths of melting for the generation of MORB, and these have since been applied to extrapolated Paraná data to constrain the depths of melting for the different magma types (Garland *et al.*, 1996). These equations are also utilised at the end of this section to estimate the depths of melting for the Treinte Y Trés and Santa Lucía magma types.

The Treinte Y Trés magma type is characterised by low Nb/La and εNd_i and high $^{87}Sr/^{86}Sr_i$ with relatively high SiO_2 but low TiO_2, CaO/Al_2O_3, Fe_2O_3 and Na_2O. The Santa Lucía basalts in contrast have higher Nb/La, and tend to have lower $^{87}Sr/^{86}Sr_i$, SiO_2 and higher εNd_i, TiO_2 and Fe_2O_3. As previously discussed the chemical variations within the Treinte Y Trés basalts are primarily controlled by AFC processes. The combined effects of gabbroic fractionation and crustal assimilation may be at least partially corrected for by extrapolation of the major elements back to 8 wt% MgO (Klein & Langmuir, 1987, 1989; Turner & Hawkesworth, 1995). Samples with < 56 wt% SiO_2 and > 5 wt% MgO were regressed by initially calculating the slope of the best-fit line and then correcting the individual analyses back to 8 % MgO. The compositions at 8 % MgO have lower SiO_2, higher Fe_2O_3 and higher Mg# than the erupted lavas, and they are plotted on Figure 2.17. Separate regressions were performed for the Treinte Y trees and Santa Lucía datasets as the data form two subparallel arrays particularly for TiO_2 and Fe_2O_3 vs. MgO (Fig. 2.7) suggesting there is no common liquid line of descent for the two groups.

High Fe_8 combined with low Si_8 is characteristic of melts produced at higher pressures, while low Fe_8 and high Si_8 are characteristic of low pressure melts (Hirose &

Kushiro, 1993). There is little difference between the two magma types with Si_8 in the Treinte Y Trés magma type varying from 45.6 to 50.8 wt% and in the Santa Lucía magma type from 46 to 47.5 wt%, while the variation in Fe_8 and Na_8 between the two magma types is also not significant (Fig. 2.16). The data set tends to define a horizontal array for Fe_8 vs. Si_8 similar to that described for other low-Ti CFB by Turner and Hawkesworth (1995). Na_8 vs. Fe_8 plot at the end of the MORB array with a similar range in Na_8 (Fig. 2.16).

In addition the Si_8 - Fe_8 data for the Uruguayan rocks, Fig. 2.16 also shows similarly corrected results for the Ambenali lavas of the Deccan igneous province, which are considered to originate in the asthenosphere (Mahoney, 1988), and the low-Ti Paraná basaltic rocks. The Treinte Y Trés and Santa Lucía samples and the low-Ti Paraná are displaced to lower Fe^*_8 relative to the Deccan basalts. As indicated above, low Fe^*_8 reflects either lower pressures or a source that has been depleted in a previous melt extraction event.

A plot of Na_8 vs. Fe^*_8 shows that the Uruguay data overlap with the high Fe_8 and low Na_8 end of the MORB array and are displaced to lower Na_8 than Tristan data (Fig. 2.16b). The relatively depleted Fe^*_8 contents of the Treinte Y Trés and Santa Lucía basalts are similar to that described from the low-Ti Paraná Gramado magma type (Turner & Hawkesworth, 1995), while the Ferrar CFB data of Hergt *et al.*, (1991) are displaced further from the MORB array to low Fe_8 of ~ 9.01 and low Na_8 of ~ 1.7. The Fe_8 and Na_8 contents of the Treinte Y Trés magma type overlap the recent South Atlantic MORB data but it is unlikely that they were generated at similar pressures due to the thick lithosphere through which the CFB were erupted. Thus, the low Fe^*_8 observed is interpreted as a source feature. Both Hergt *et al.* (1991) and Turner & Hawkesworth (1995) concluded that the magmas were generated from a source depleted in Fe from previous melt extraction events which they argue to be in the continental lithospheric mantle.

Lower crustal assimilation would result in the increases in Si_8 observed, while Fe_8 would vary little. However the low Ti_8 and CaO/Al_2O_3 trends for the Treinte Y Trés basalts are not easily explained by AFC processes or mixing between asthenospheric OIB-like material and crustal components. The Uruguay magmas are therefore considered to be derived from a similar source in the sub-continental lithospheric mantle to other low Ti CFB on the basis of their Fe_8, Si_8 and Na_8 data.

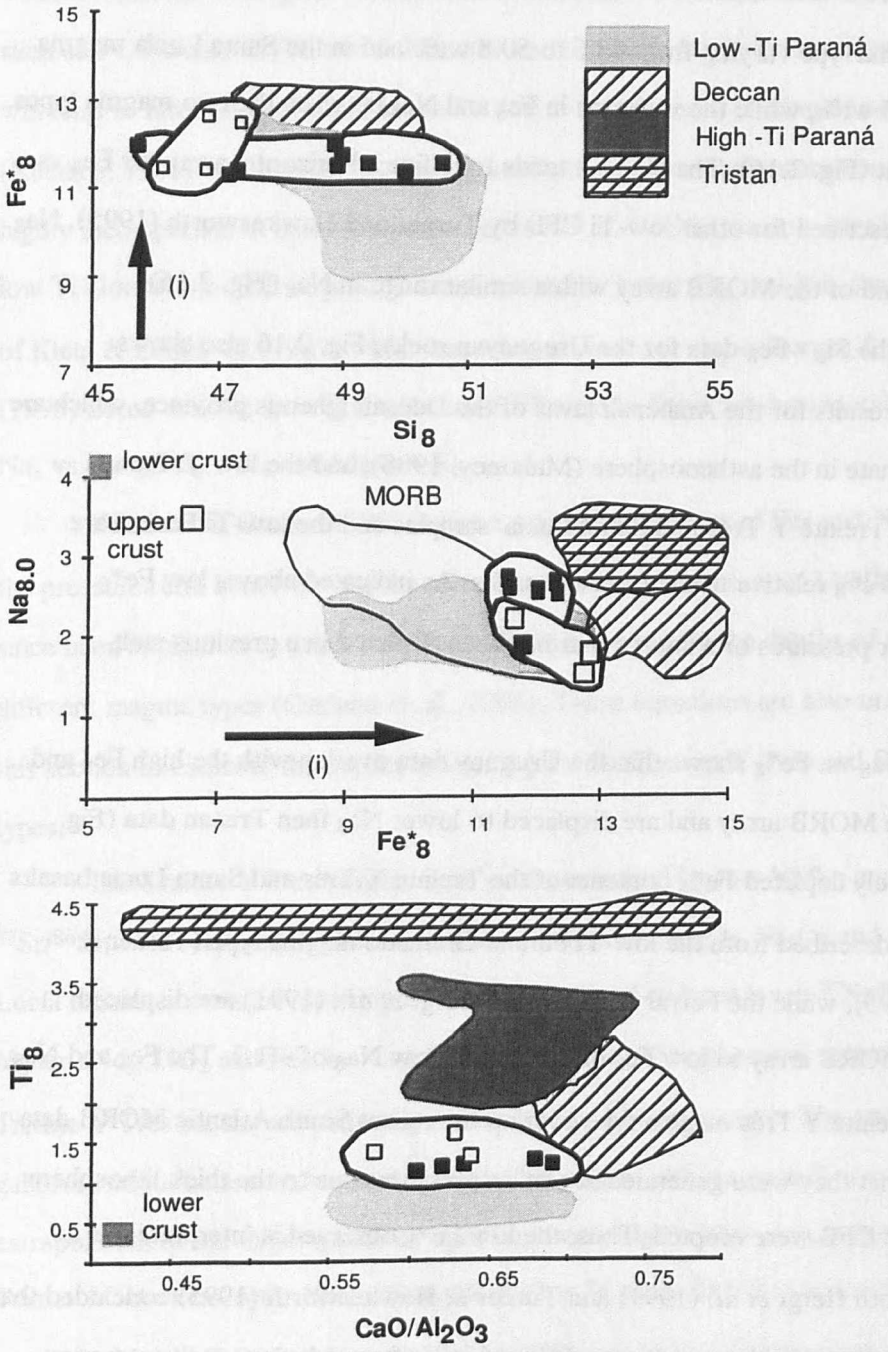

Fig. 2.16. **Major element data corrected to 8 wt% MgO. Vector indicates the effect of increasing pressure on (i) Fe_8 after Klein & Langmuir (1987); Turner & Hawkesworth (1995); Garland *et al.*, (1996); Tristan data from Weaver *et al.* (1987); Deccan data are from the Ambenali Formation (Mahoney, 1988). Lower crust from Weaver & Tarney (1981), upper crust is reproduced from Turner & Hawkesworth (1996).**

The average pressures and hence depths of melting were estimated from the Fe_8 and Na_8 values using the equations of Kinzler & Grove (1993). For the Treinte Y Trés lavas these yield relatively low pressures of 12-18 kbar and depths of 35 to 58 km. Such depths are too shallow to be realistic in continental areas, but the calculations do assume normal Fe contents in the mantle source regions. We suggest that the Uruguayan rocks were actually generated at deeper levels in relatively Fe-poor mantle within the mantle lithosphere. These results are akin to those described by Garland *et al.* (1996) for the low Ti/Y Gramado magma type of the Paraná province where magma generation was also considered to have taken place within the lithospheric mantle.

2.9 Origin of the Uruguay basaltic magmas.

A number of chemical and isotopic differences have been highlighted between the two basaltic magma types identified in southern Uruguay, and between these and oceanic basalts. Differences in trace-element compositions are best seen on mantle normalised trace element diagrams (Fig. 2.9). The smooth pattern of the Santa Lucía basalts is similar to the smooth signatures of asthenosphere derived magmas including MORB and OIB, while the Treinte Y Trés lavas are distinguished by their negative Nb and Ti anomalies. On a diagram of Nb/La v εNd_i (Fig. 2.14) the Santa Lucía basalts have high Nb/La ratios (0.8 - 1.1) similar to primitive mantle values of ~1 (Sun & McDonough, 1989). These Nb/La ratios are also similar to those described for the Tafelkop basalts in Namibia (0.65 to 0.88) (Milner & le Roex, 1996; Ewart *et al.*, 1997) and the low Ti/Y Esmeralda magma type of the Paraná (0.5 - 0.96) (Marques *et al.*, 1989; Peate *et al.*, 1992). This latter magma type has been modelled by Peate & Hawkesworth (1996) as a mixture of the low Ti/Y Gramado magma type and an asthenospheric component with incompatible element and isotopic characteristics similar to MORB. The overall trace element characteristics of the Esmeralda are however very different from those of the Santa Lucía basalts.

The εNd_i values in the Santa Lucía basalts are much lower than MORB, and they therefore plot closer to the Tristan field in Figure 14 since that has a range in initial Nd isotope values of -3.3 to -0.9 (le Roex *et al.*, 1990). However the Santa Lucía basalts extend to lower εNd_i values of -5.5 which is closer to the values reported for the Walvis

Ridge of -4.5 to 1.5 (Richardson *et al.*, 1982). These values are much lower than average values reported for typical OIB of +8 (Sun & McDonough, 1989), and for example the Hawaiian islands have values in the region of +6.1 (White & Hofmann, 1982). N-type MORB have higher εNd_i values of +13 (Sun & McDonough, 1989) which is broadly similar to the values for the Mid Atlantic Ridge of +12.3 (White & Hofmann, 1982). The range in Nb/La and εNd_i in the Santa Lucía basalts is therefore considered indicative of varying degrees of mixing between an asthenosphere derived melt such as described from Tristan TDC-91 (le Roex *et al.*, 1990) with a magma characterised by low Nb/La and εNd_i such as the Treinte Y Trés basalts (Fig. 2.14). As seen in Fig. 2.14 both MORB and OIB (Tristan) have similar Nb/La ratios, but MORB are characterised by less radiogenic Nd. Mixing between MORB and a lithospheric component has been proposed for the low Ti/Y Esmeralda magma type of the Paraná (Peate & Hawkesworth, 1996). As is evident in Fig. 2.14 for the Esmeralda data array there is a positive correlation between Nb/La and εNd_i in the direction of the MORB end member. The Santa Lucía data however trend towards an enriched mantle source (Tristan) which is characterised by more radiogenic initial Nd.

The Santa Lucía basalts have unusual major, trace element and isotopic compositions compared to the other magma types previously described in the Paraná province, apart from the Tafelkop. The Treinte Y Trés lavas have much lower Nb/La ratios of between 0.4 and 0.5, similar to the lower end of the data range for the Gramado rocks, and extending to lower εNd_i values. The slight variation in trace elements and the isotopic differences between the Gramado magma type and the Treinte Y Trés magmas appear to be regionally significant and potentially related to slight differences in their lithospheric source regions.

In summary, two distinct compositional magma types are recognised within the Puerto Gómez Formation of southern Uruguay. These magmas are termed the Santa Lucía and Treinte Y Trés magma types. It is argued that the Treinte Y Trés magmas were derived from source regions in the sub-continental lithospheric mantle primarily because they have trace element and isotopic compositions that are difficult to model by simple AFC processes contaminating asthenosphere-derived melts. The Santa Lucía basalts are however, unique compositionally when compared with the main volume of magma, the Treinte Y Trés magma type. The Santa Lucía basalts are considered to originate in the asthenosphere on

the basis of trace-element geochemistry and their similarity with OIB, particularly the Walvis Ridge and Tristan basalts. In detail, mixing of an asthenosphere derived melt with a magma characterised by low Nb/La and εNd_i such as the Treinte Y Trés, is required in order to explain the differences between the Santa Lucía basalts and the Walvis Ridge and Tristan plume data fields.

2.10 Rhyolite Chemistry.

The Uruguayan rhyolites have been divided into two geochemical series, the Lascano Series and the Aigüa Series on the basis of different major and trace element trends, and these are different to the rhyolite types recognised on the basis of petrography. As noted previously the division into two series is based primarily on differences between the trace elements Nb, Zr, Ti and Sr, with the Lascano Series having higher Ti/Zr and Sr vs. SiO_2, and in general forming a tight array for Nb and Zr when compared with the Aigüa Series (Figs. 2.18, 2.19a & b). The Lascano Series have a wider range in $^{87}Sr/^{86}Sr_i$ and in εNd_i, while the Aigüa Series forms a much tighter array at low $^{87}Sr/^{86}Sr_i$ and particularly low εNd_i (Fig. 2.8).

On major element variation diagrams the rhyolites show general decreases in CaO, Na_2O, Al_2O_3, P_2O_5, TiO_2, & Fe_2O_3 with increasing SiO_2, used here as an index of fractionation, while K_2O is more scattered (Fig. 2.17). These trends are broadly consistent with fractionation of an assemblage consisting of plagioclase, alkali feldspar, pyroxene and iron oxide ± quartz. The Lascano and Aigüa Series have broadly similar ranges of SiO_2 concentrations, ranging from 61 to 78 wt% and 61 to 81 wt% respectively (Fig. 2.17). The Lascano Series extends to higher TiO_2, CaO, Fe_2O_3 and lower Al_2O_3 and Na_2O than the Aigüa Series, in addition to having lower Nb, Zr and Rb and higher Sr and Ti (Fig. 2.17). Therefore these two series may be further characterised on the basis of such trace elements as Sr, Rb, Nb, Zr and Y. Two broad trends are outlined on a plot of Sr v SiO_2 with a clear negative correlation between Sr and SiO_2 in the Lascano Series while the Aigüa Series extends to lower Sr concentrations at high SiO_2 (Fig. 2.18a). Such very low Sr contents can only be obtained by extensive fractionation of a feldspar dominated assemblage, irrespective of whether the parental magma was a basalt or a crustal melt.

Fig. 2.17. Variation in major and trace element chemistry of the Uruguay rhyolites resulting in their division into two series, the Lascano Series and the Aigüa Series. Paraná data from Garland (1994), change in symbol for low –Ti rhyolites is for clarity of illustration.

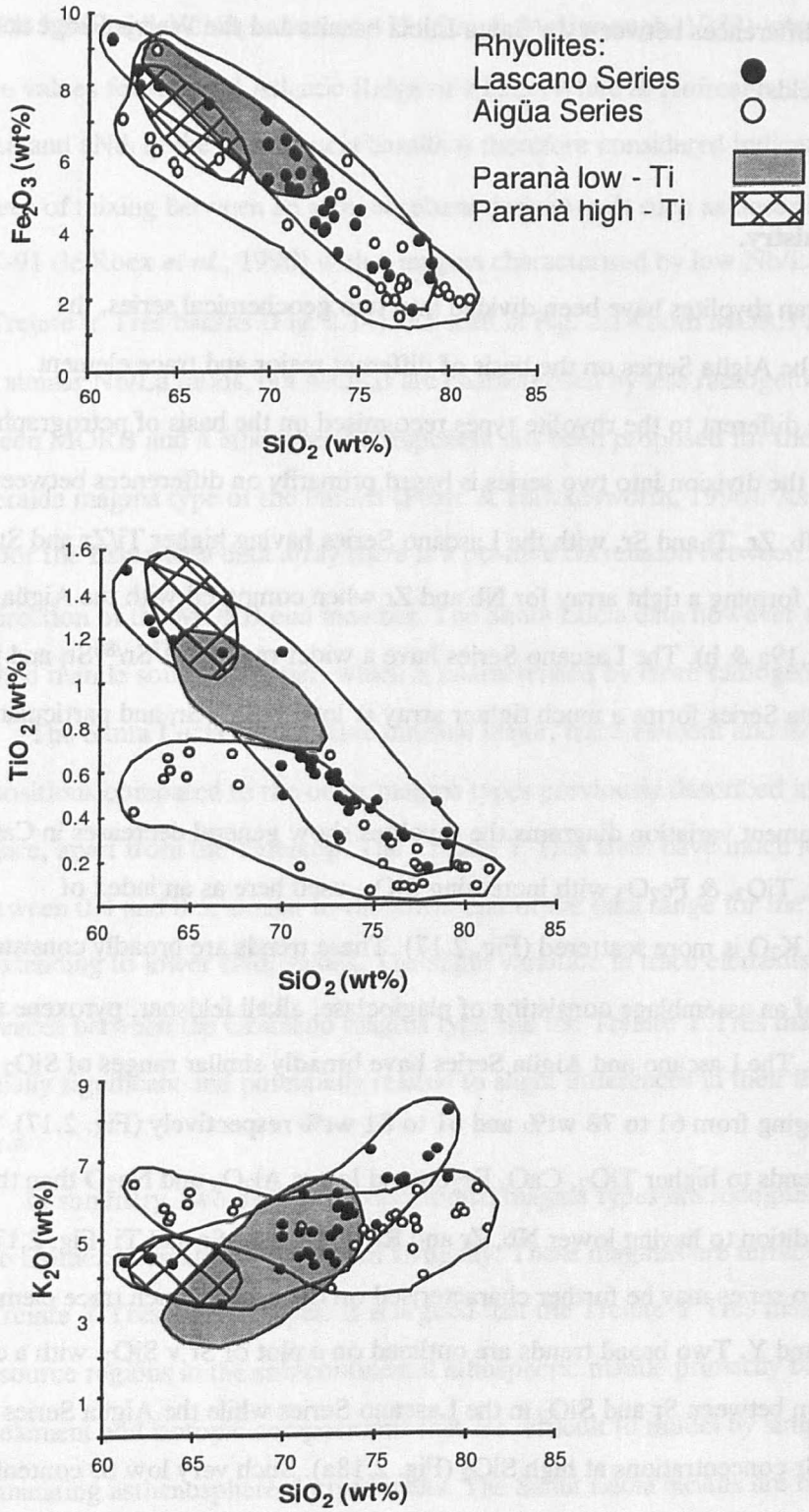

Fig. 2.17 cont.

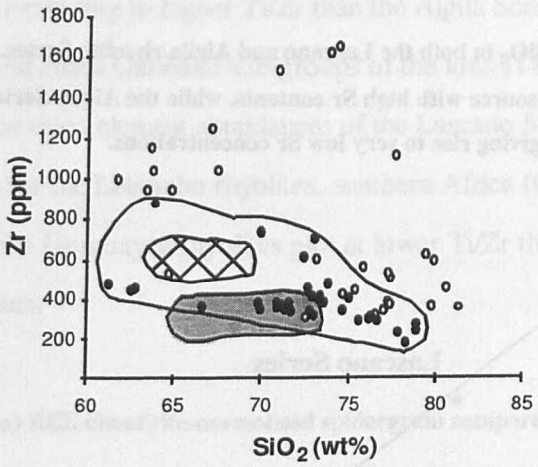

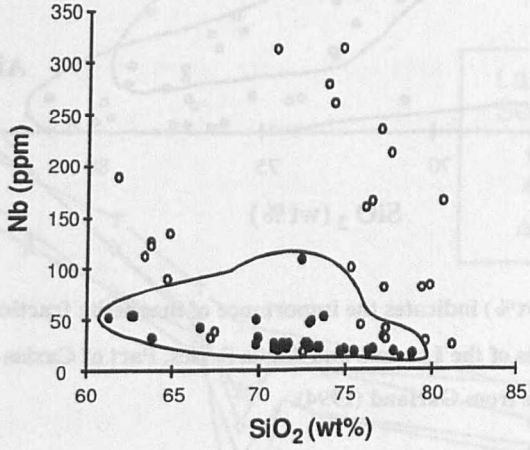

The high-silica rhyolites (76.8 - 77.9 wt% SiO_2) of Glass Mountain, California the precursor lavas to the Bishop Tuff, have Sr concentrations as low as 1ppm, with associated high Rb/Sr ratios which have been modelled by extensive fractional crystallisation (e.g. Christensen & Halliday, 1996). Since the lowest Sr concentrations are coincident with the highest SiO_2 values observed in these rhyolites the high SiO_2 values observed are deemed to be the result of fractionation in both series of rhyolite. SiO_2 concentrations of > 78 wt% are highly unusual in igneous rocks with the most evolved rhyolites previously described from, for example, Glass Mountain containing 77.6 wt% SiO_2 while granitic compositions are more typically less than 76 wt% SiO_2 (Cox, Bell & Pankhurst, 1979). Therefore the very high silica concentrations measured in some of the most evolved Uruguay rhyolites presumably reflect accumulation of quartz phenocrysts in the final stages of their

petrogenetic history. Three samples from the Aigüa Series have relatively high Sr which may be due to xenocrysts of feldspar entrained on the way to the surface.

Fig. 2.18a. Variation in Sr v SiO_2 in both the Lascano and Aigüa rhyolite Series. Lascano Series are considered to originate from a source with high Sr contents, while the Aigüa Series is characterised by residual feldspar giving rise to very low Sr concentrations.

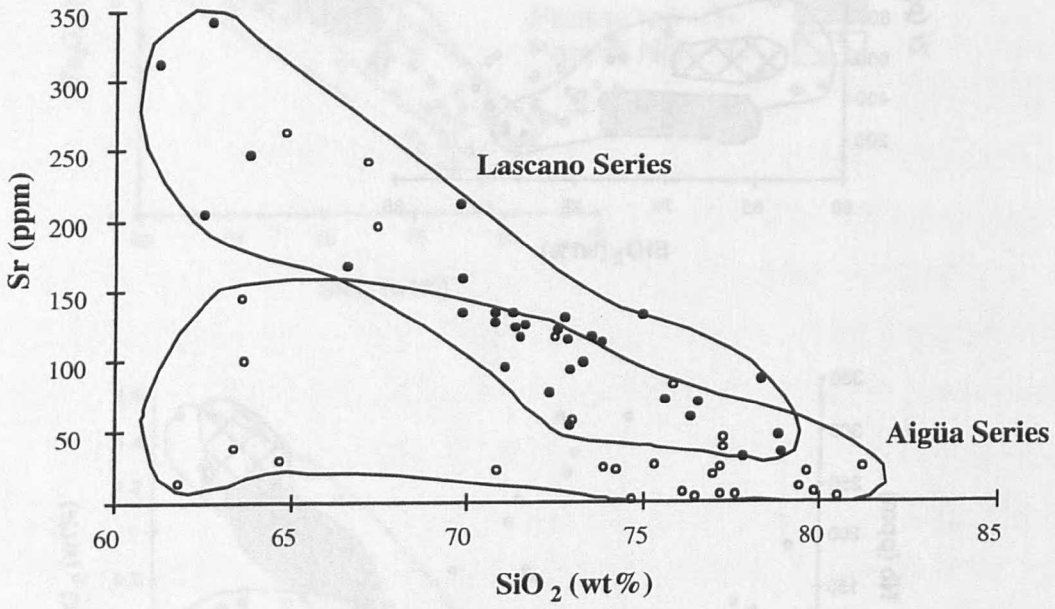

Fig. 2.18b. Ti/Zr vs. SiO_2 (wt%) indicates the importance of magnetite fractionation and clearly distinguishes between the rhyolites of the Lascano and Aigüa Series. Part of Caxias do Sul & Anita Garibaldi fields plotted only, data from Garland (1994).

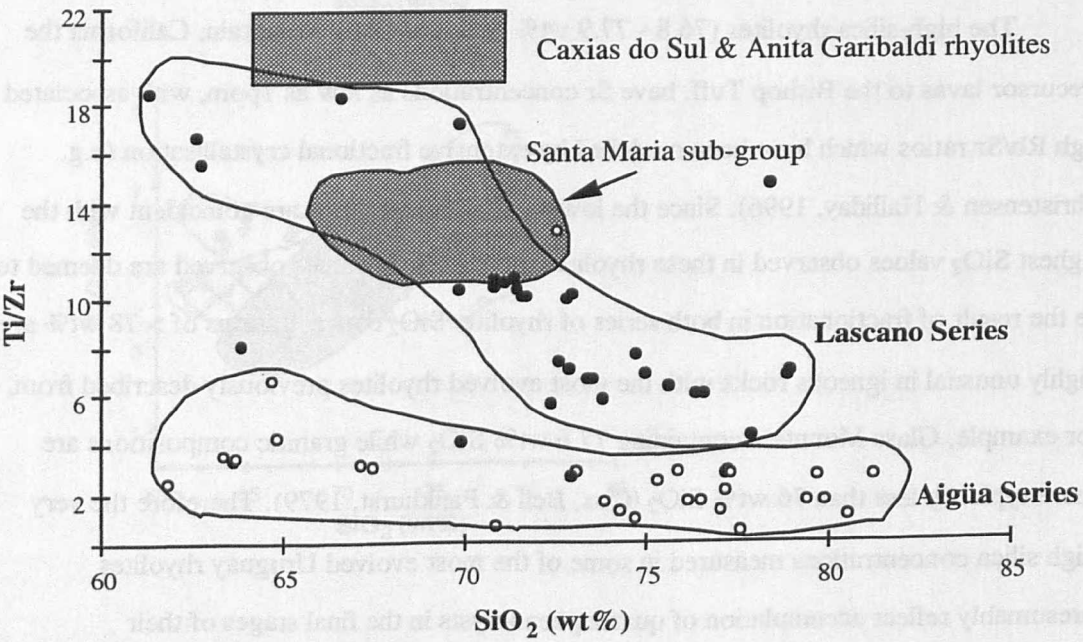

The two series are also clearly distinguished on a plot of Ti/Zr vs. SiO_2 with the Lascano Series extending to higher Ti/Zr than the Aigüa Series, broadly similar to the Caxias do Sul and Anita Garibaldi sub-groups of the low-Ti Palmas rhyolites of the Paraná (Fig. 2.18b). The trace-element abundances of the Lascano Series are broadly similar to those described for the Lebombo rhyolites, southern Africa (Cleverly *et al.*, 1984), while the majority of the Uruguayan rhyolites plot at lower Ti/Zr than either the Paraná or Etendeka rhyolites.

Fig. 2.19 a & b. (a) REE chondrite-normalised spidergram comparing the rare earth element behaviour between the two rhyolite series. (b) Variation in Ce vs. Zr suggesting a close correlation between accessory phase and REE behaviour.

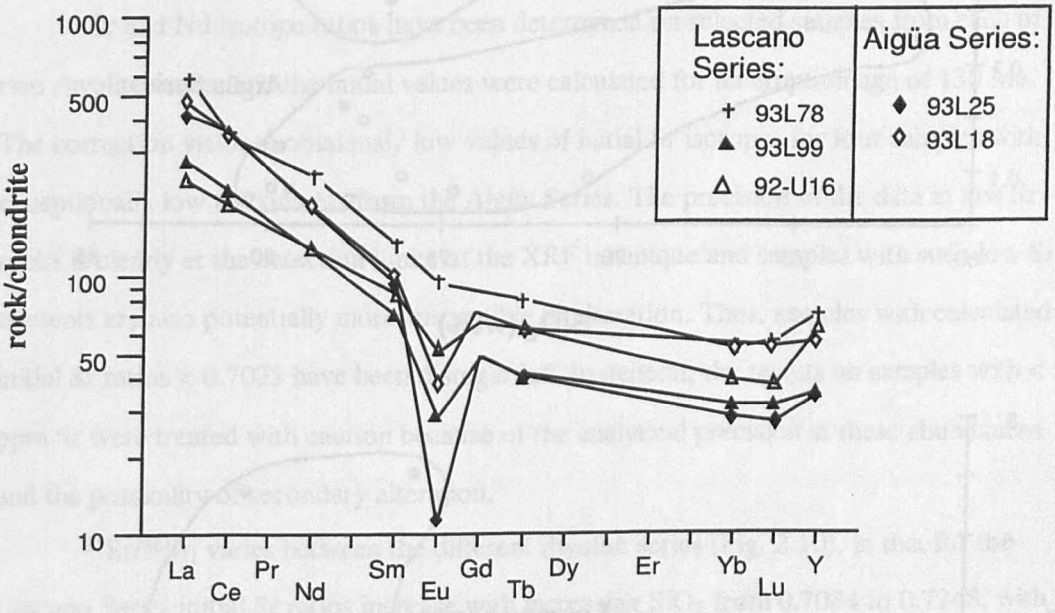

2.11 Rare Earth Elements.

The rare-earth-element abundances are highly variable (Table 2.3) and appear to have been affected by fractionation of accessory minerals such as monazite, zircon and apatite. The behaviour of the LREE is erratic in a number of samples, but overall both rhyolite series are enriched in LREE relative to HREE (Fig. 2.19a). In general the REE have a constant valency of three, although Eu and Ce occur in the 2+ state in natural

reducing systems (Henderson, 1984). The REE are also relatively immobile during hydration processes (Cameron & Cameron, 1986) however Eu anomalies in igneous rocks and minerals arise when Eu^{3+} is partly reduced to Eu^{2+}, similarly for Ce. On plotting Ce vs. Zr, although the data are highly scattered there appears to be a positive correlation between the behaviour of LREE (Ce) and zirconium (Zr) (Fig. 2.19b).

Fig. 2.20. Variation in Eu/Eu* vs. SiO_2 and vs. Sr/Eu* indicating the effects of both fractionation and oxygen fugacity on the evolution of the rhyolite series.

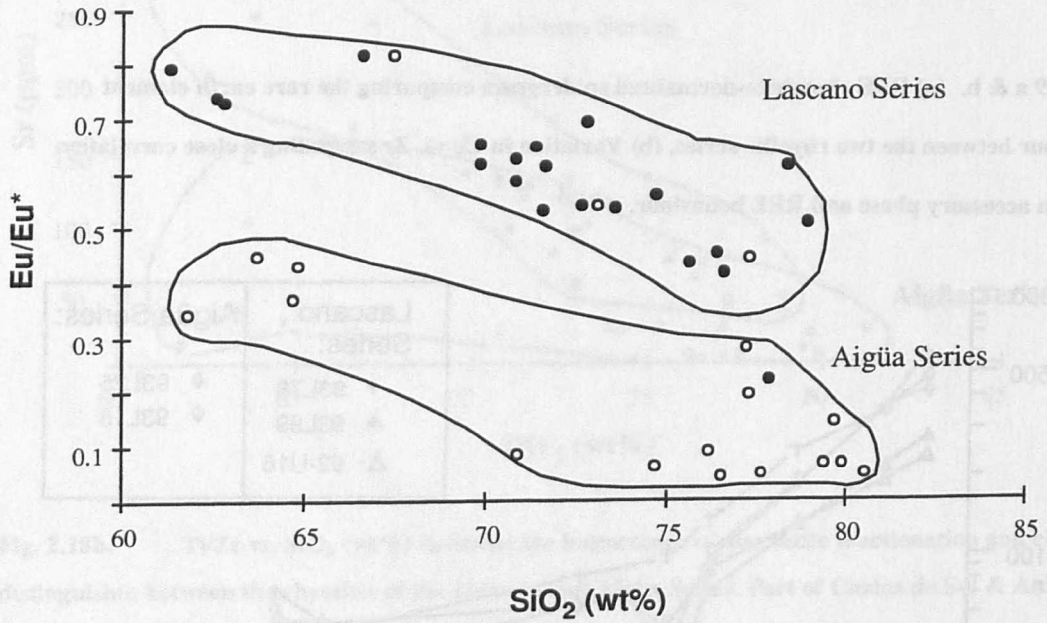

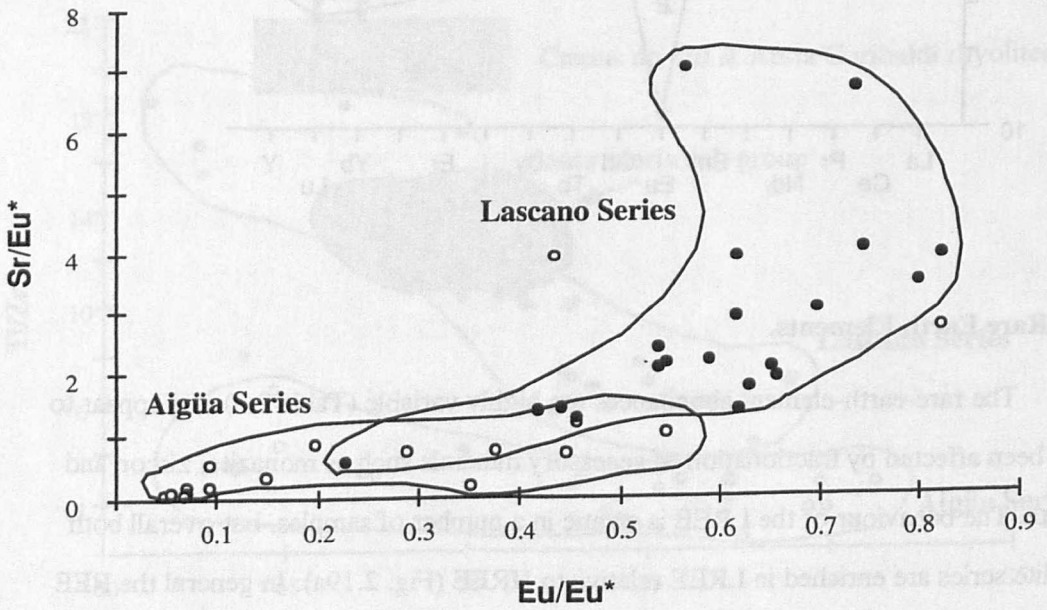

Eu anomalies are highlighted on a chondrite-normalised REE diagram (Fig. 2.19a) with negative Eu anomalies evident for many samples particularly from the Aigüa Series. Feldspar, clinopyroxene, garnet and amphibole fractionation can all contribute to produce negative anomalies particularly in felsic melts, as can partial melting of a source containing residual feldspar (Ragland, 1989). However, Eu anomalies are not evident in all of the samples from the Lascano Series which might reflect feldspar accumulation, alternatively this may be related to oxygen fugacity which can affect the size of an Eu anomaly (Cameron & Cameron, 1986). Plotting Eu/Eu* vs. SiO_2 (Fig. 2.20a) the Aigüa Series rhyolites are displaced to lower Eu/Eu* ratios than the Lascano Series.

2.12 Isotope data.

Sr & Nd isotopes

Sr and Nd isotope ratios have been determined on selected samples from each of the two rhyolite series, and the initial values were calculated for an eruption age of 130 Ma. The correction yields anomalously low values of initial Sr isotopes for four samples with exceptionally low Sr contents from the Aigüa Series. The precision of the data in low Sr rocks is clearly at the detection limits of the XRF technique and samples with such low Sr contents are also potentially more susceptible to alteration. Thus, samples with calculated initial Sr ratios < 0.7025 have been disregarded. In general, the results on samples with < 50 ppm Sr were treated with caution because of the analytical precision at these abundances and the possibility of secondary alteration.

$^{87}Sr/^{86}Sr_i$ varies between the different rhyolite series (Fig. 2.10), in that for the Lascano Series initial Sr ratios increase with increasing SiO_2 from 0.7084 to 0.7248, with one sample 93L122 (not shown) having an $^{87}Sr/^{86}Sr_i = 0.7545$ at 74.6 wt% SiO_2. In the Aigüa Series there is much less variation with the majority of samples having $^{87}Sr/^{86}Sr_i$ ranging from 0.7054 to 0.7084, and although one sample plots at 0.7114, the increase in $^{87}Sr/^{86}Sr_i$ is not simply related to increasing SiO_2 abundances. There is also considerable variation in initial Nd isotope ratios between the two series with the Lascano Series ranging in εNd_i from -13.3 to -4.7, and the Aigüa Series from -17.7 to -11.2 (Fig. 2.8).

Oxygen isotopes

Oxygen isotope ratios have been measured on quartz phenocrysts from both the Lascano and Aigüa Series by Chris Harris at the University of Cape Town using conventional fluorination techniques (see Harris & Erlank, 1992; Harris, 1995). NBS28 was run with each batch of 8 samples and used to correct the sample analyses to the SMOW scale, assuming a value of 9.64 for NBS28. Repeated analyses of NBS28 varied by < 0.15 ‰. All samples were duplicated with the variation in result indicated in brackets except where stated in Table 2.6, and for sample 93L51, two different mineral separates were analysed, labelled i and ii. Mineral separates were better than 95% pure, and the results are presented in Table 2.6 along with some average results for both Paraná and Etendeka silicic volcanics from Harris *et al.*, (1990).

Table 2.6. Isotopic compositions of silicic volcanic rocks together with a mafic sample from Uruguay and a local basement sample.

Sample	Rock type	δO_{18} (‰)	Separate	Location
92U12	Basalt (SL)	7.2 (0.10)	Plagioclase	Uruguay
93L20	Basement	10.0 (0.08)	Quartz	Uruguay
92U14*	Rhyolite (L)	10.8	Quartz	Uruguay
93L123*	Rhyolite (L)	10.6	Quartz	Uruguay
93L28	Rhyolite (A)	9.1 (0.05)	Quartz	Uruguay
93L49	Rhyolite (A)	10.0 (0.01)	Quartz	Uruguay
93L51 (i)	Rhyolite (A)	9.6 (0.11)	Quartz	Uruguay
93L51 (ii)		9.7 (0.05)		
SF1	Rhyolite	10.0	Pyroxene	S. Paraná
SM164	Rhyolite	9.0	Pyroxene	S. Etendeka
P20	Rhyolite	6.3	Pyroxene	N. Paraná
SM115	Rhyolite	6.6	Pyroxene	N. Etendeka

* Samples not duplicated. L = Lascano Series rhyolites; A = Aigüa Series.

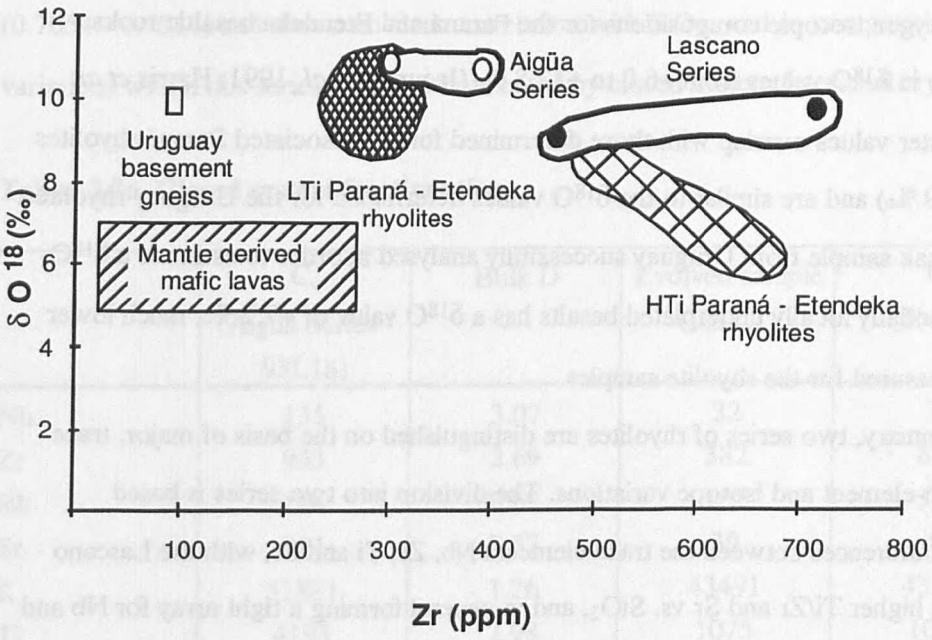

Fig. 2.21. Rhyolite variation in oxygen isotope analyses with Paraná fields for comparison. Oxygen isotope data on quartz phyric rhyolites from Uruguay.

Magma $\delta^{18}O$ values are considered to have been about 1 per mil lighter than the quartz values, as quartz tends to concentrate ^{18}O. The fractionation factor between mineral and melt ($\Delta_{mineral\text{-}melt}$), was taken to be -0.2 and +1.0 for $\Delta_{plag\text{-}melt}$ and $\Delta_{quartz\text{-}melt}$ respectively. Variations in $\delta^{18}O$ values can be attributed to three principal factors; (i) different sources, (ii) contamination by continental crust and (iii) alteration since eruption. This latter effect has been examined extensively in the Paraná and Etendeka mafic and silicic volcanics, and many of the bulk rock $\delta^{18}O$ values are higher than those of the separated minerals. This has been attributed to secondary post-eruptive hydrothermal exchange processes resulting in bulk rock $\delta^{18}O$ values of +15 to +19 ‰ (Harris *et al.*, 1989; Iacumin *et al.*, 1991). The use of quartz phenocryst separates however limits this effect as quartz can be effectively cleaned and it is immune from exchange with fluids at temperatures less than 300 °C (Hildreth *et al.*, 1991; Harris, 1995). $\delta^{18}O$ values of ~ +10 ‰ have been measured on quartz separates from a representative basement rock from southern Uruguay. This $\delta^{18}O$ value is broadly similar to some of the measured values particularly for the Lascano Series, suggesting a significant crustal contribution was involved in the generation of these rhyolites. An alternative source for the rhyolites is melting of altered underplated

basalt, with oxygen isotopic compositions for the Paraná and Etendeka basaltic rocks having a range in $\delta^{18}O$ values from +6.0 to +12.8 ‰ (Iacumin *et al.* 1991; Harris *et al.* 1989). The latter values overlap with those determined for the associated Paraná rhyolites (+9.8 to +17.9 ‰) and are similar to the $\delta^{18}O$ values determined for the Uruguay rhyolites. The single basalt sample from Uruguay successfully analysed in order to estimate a $\delta^{18}O$ value for potentially locally underplated basalts has a $\delta^{18}O$ value of +7.2 ‰, much lower than those measured for the rhyolite samples.

In summary, two series of rhyolites are distinguished on the basis of major, trace and rare-earth-element and isotope variations. The division into two series is based primarily on differences between the trace elements Nb, Zr, Ti and Sr, with the Lascano Series having higher Ti/Zr and Sr vs. SiO_2, and in general forming a tight array for Nb and Zr when compared with the Aigüa Series. The Lascano Series have a wider range in $^{87}Sr/^{86}Sr_i$ and in εNd_i, while the Aigüa Series forms a much tighter array at low $^{87}Sr/^{86}Sr_i$ and unusually low εNd_i, there is also ~ 1 ‰ difference in $\delta^{18}O$ values between the two series. The within series variations are considered to be related to high level processes including fractional crystallisation and assimilation, while the differences between the series particularly at low SiO_2 concentrations potentially reflect source heterogeneities and/or different conditions of partial melting. These variations are investigated in the next section where the petrogenesis of the series are evaluated.

2.13 Petrogenesis.

There are two main points which need to be addressed regarding the petrogenesis of the Uruguay rhyolites (i) the intra suite variations and the extent to which they may be modelled by closed/open system fractionation from the least evolved samples, and (ii) the generation of the least evolved magmas with regard to (a) potential links with the basalts of the Puerto Gómez Fm. and (b) partial melting of particular crustal rocks.

As illustrated in Figure 2.18 the major and trace element variations in the two rhyolite series are qualitatively consistent with fractional crystallisation of the observed phases. However, in the Lascano Series $^{87}Sr/^{86}Sr_i$ increases from 0.7084 to 0.7248 with increasing SiO_2, and this is inferred to reflect the effects of combined assimilation and fractional crystallisation (AFC). In the Aigüa Series $^{87}Sr/^{86}Sr_i$ varies over a smaller range

(0.7054 - 0.7084) and shows no clear correlation with SiO_2, and so compositional variations within this series are more dominated by closed system fractional crystallisation.

Table. 2.7a. Closed system fractionation.

	C_o (Aigüa Series - 93L18)	Bulk D	Evolved sample (93L21)	C_L (F= 0.5)
Nb	135	3.07	32	32
Zr	955	2.69	382	827
Rb	124	0.69	155	153
Sr	264	3.57	39	44
K	51881	1.26	43491	43315
Ti	4193	2.98	1075	1060
Ba	935	2.47	329	337
Ce	214	0.34	176	338
Eu	2.21	2.74	0.6	0.6
Yb	9.27	1.37	7.2	7.2
$^{87}Sr/^{86}Sr$			0.70715	

* Calculated assuming a fractionating assemblage of clinopyroxene : plagioclase : alkali feldspar : titanomagnetite : quartz: apatite : zircon of 5 : 44 : 35 : 15 : 1 : 0.5 : 0.1.

Table. 2.7b. Assimilation and Fractional crystallisation.

	C_o (Lascano Series -93L78)	Bulk D	Evolved sample (93L99)	Contaminant (RSM 2B)	C_L (F= 0.6; r = 0.25)
Nb	53	2.32	20	29	21
Zr	491	1.41	327	64	323
Rb	122	0.31	212	252	215
Sr	313	3.10	61	72	69
K	40509	0.56	54026	39264	53129
Ti	9113	3.06	1999	1738	2038
Ba	2776	1.92	1226	219	1268
Ce	211	0.34	132	86	294
Eu	5.4	2.57	1.6	0.9	1.6
Yb	8.8	1.47	5.4	1.3	5.5
$^{87}Sr/^{86}Sr$	0.70892		0.72241	0.85233	0.72246

* Calculated assuming a fractionating assemblage of clinopyroxene : plagioclase : alkali feldspar : titanomagnetite : quartz: apatite : zircon of 5 : 48 : 29 : 15 : 2 : 0.5 : 0.1.

Aigüa Series Closed System Fractionation:

The amount of fractionation within each series can be illustrated in terms of a number of elements including Rb, Sr, Ti, Nb, Zr and Eu (Figs. 18 - 21; Table 7). One of the most primitive samples in the series, 93L18 (SiO_2 = 64.7 wt %) was chosen as C_o, the minerals in the fractionating assemblage were constrained from least-squares modelling of the major-element variations. Most of the mineral partition coefficients used to calculate the bulk distribution coefficients (Table 7) were taken from Rollinson (1993) and references therein for rhyolitic magmas. However certain assumptions were had to be made regarding the behaviour of Zr in zircon, Ti and Nb in titanomagnetite and K in alkali feldspar. Zirconium is an essential structural constituent in zircon (Sun and Hanson, 1975) and therefore its behaviour is not simply governed by Rayleigh fractionation. In order to calculate an effective D value certain assumptions were made. The amount of zirconium in zircon = 484,430 ppm (Watson and Harrison, 1983), with $[ZrO_2]_{melt}$ assumed proportional to the dissolved zirconium concentration. If we assume the initial magma had a Zr concentration of 400 ppm and that the temperature remained constant at between 850 and 950 °C (Chapter 3), the D_{Zr} was calculated as approximately 1000, which is the value assigned for this modelling. The behaviour of Zr is markedly different between the two series. Zr initially increases in the Aigüa Series until the point of saturation, this occurs between 72 and 75 wt % SiO_2 and then decreases as zircon crystallises. In the Lascano Series Zr decreases with increasing SiO_2 which suggests that the melt has been saturated in zirconium and so the Zr abundance decreases systematically. However it is difficult to explain the continuous crystallisation of Zr in the Lascano Series which is either a function of temperature or the addition of the upper crustal material with high SiO_2 and low Zr (< 60 ppm).

Assumptions were also made regarding the distribution coefficients of Nb and Ti in the iron oxides. Microprobe data demonstrated that the most of the iron oxides are titanomagnetite with some ilmenite. The analyses showed that both minerals contain between 20 and 50 % more Ti than the magnetite in Deer, Howie and Zussman, (1966), and so the distribution coefficients used are higher than found elsewhere at $D_{Ti} = 20$; $D_{Nb} = 10$ for titanomagnetite. Finally potassium was assigned a K_D in alkali feldspar of 1.5.

The liquid composition (C_L) after 50 % fractionation is shown in Table 2.7a where it is compared with one of the more evolved samples in the Aigüa Series, 93L21. In general there is reasonable agreement between the calculated composition and sample 93L21 which suggests that closed system fractionation is the primary control on the within suite variation in the Aigüa Series. However Zr abundances have not been modelled successfully as fractionation of zircon would result in a rapid decrease in Zr and would not reflect the trend observed. Ce has been modelled with a bulk distribution coefficient of 0.34, which suggests it is incompatible in all phases and therefore Ce increases in the model. Ce decreases in abundance between samples 93L18 and 93L21 indicating control by an accessory phase not included in the modelling possibly monazite, which is Ce selective (Rapp and Watson, 1986).

Lascano Series Open System Fractionation.

The effects of open system fractionation were modelled for the Lascano Series as assimilation of a high SiO_2, high $^{87}Sr/^{86}Sr_i$ component is indicated by the within suite variations, for example Fig. 2.10. A similar fractionation assemblage of clinopyroxene, plagioclase, alkali feldspar, titanomagnetite, quartz, apatite and zircon was predicted from major element modelling but with a higher proportion of plagioclase to alkali feldspar. Clinopyroxene : plagioclase : alkali feldspar : titanomagnetite : quartz : apatite : zircon of 5 : 48 : 29 : 15 : 2 : 0.5 : 0.1. The least evolved sample in the Lascano Series, 93L78, was chosen as C_o and a similar array of trace elements including Rb, Ba, Sr, Ti and Nb was modelled. The assimilant used was an upper crustal leucogranite from the Pelotas Batholith, southern Brazil (RSM2B; May, 1990). The same mineral partition coefficients were used as for the Aigüa Series, although as noted previously the behaviour of Zr is different between the two series. Overall the within-suite trace-element variation in the Lascano Series data array can be modelled by 40% fractionation and 25% assimilation of upper crustal material (Table 2.7b).

The variation of $^{87}Sr/^{86}Sr_i$ and $^{143}Nd/^{144}Nd_i$ evident within the Lascano Series is also consistent with fractionation and assimilation of crustal material with high $^{87}Sr/^{86}Sr_i$ and $^{143}Nd/^{144}Nd_i$ (Fig. 2.22). The proposed AFC curve is for the ratio of the rate of crystallisation / rate of assimilation (r) of 0.25. In this model between 40 and 45%

fractionation and contamination is required from a starting composition of 93L78 in order to fit much of the data however, three samples plot at higher $^{143}Nd/^{144}Nd_i$ which are not easily modelled via AFC equations. All three samples are from the same geographical area and so the variation is potentially due to localised differences in the contaminant.

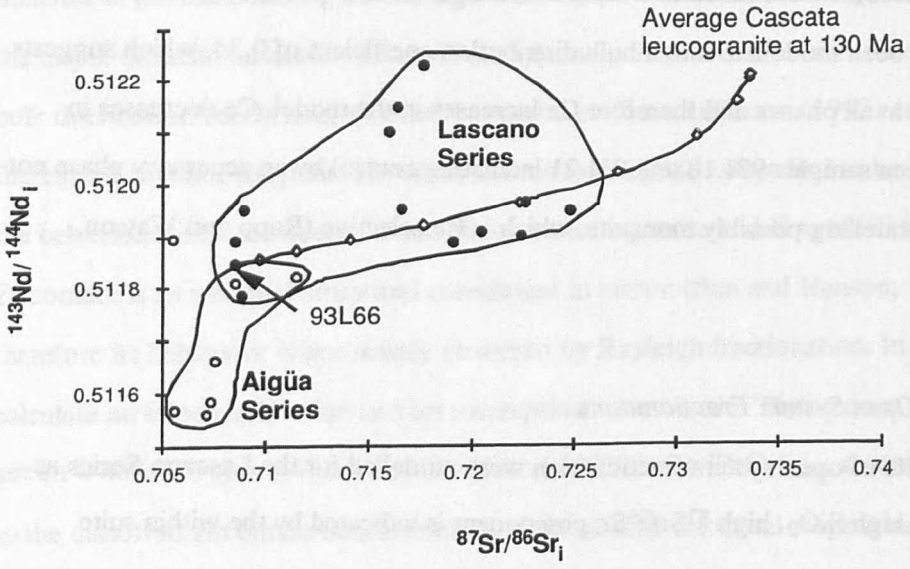

Fig. 2.22. AFC modelled for the Lascano Series assuming an r value = 0.3. The assimilant is an upper crustal average Cascata leucogranite from Brazil (May, 1990). Aigüa Series show no upper crustal signature.

Generation of the least evolved rhyolitic magmas.

The least evolved magmas in each of the series are very different particularly with regard to Ti/Zr, Sr and Eu/Eu* implying separate parental magmas which are now addressed in the following sections.

Relationship between Puerto Gómez Fm. and the Arequita Fm.

A number of interesting points emerge from a plot of $^{87}Sr/^{86}Sr_i$ versus SiO_2 which help to constrain the relations between basaltic and rhyolitic rocks in Uruguayan (Fig. 2.10). Firstly the Uruguayan mafic and acid volcanics share a similar range in initial Sr isotope ratios over a range in SiO_2 values. This appears to strengthen the argument for a genetic link between the basalts and rhyolites of the Puerto Gómez Formation and the Arequita

Formation. The initial Sr isotope data appear to support either closed system fractionation across a gap in SiO_2 in order to maintain similar ratios at different degrees of fractionation (SiO_2 contents) or remelting of underplated basalt. Closed system fractionation across a gap in silica is feasible (Bonnefoi *et al.*, 1995), and it is also possible that there was a sampling bias in the field which lead to possible intermediate compositions not being recognised. However when the initial Nd isotopic ratios of the basalts and rhyolites are compared both rhyolite series contain samples which plot at significantly lower $^{143}Nd/^{144}Nd_i$ than the basalts. The Lascano Series rhyolites overlap the basalt range with $^{143}Nd/^{144}Nd_i = 0.5117$ to 0.5122, and the Aigüa Series have $^{143}Nd/^{144}Nd_i = 0.5115$ to 0.5118 (Fig. 2.22). Thus, it is concluded that neither the Lascano Series nor the Aigüa Series rhyolites were generated either by fractional crystallisation from the associated basaltic magmas, nor by remelting of underplated Mesozoic basalts.

Different Sources.

Different sources and/or different melting conditions may also be inferred from the behaviour of Ti/Zr, Eu/Eu* and Eu/Sr in the two series. The Lascano Series is characterised by high Ti/Zr and the Aigüa Series by low Ti/Zr at SiO_2 contents of between 62 to 65 wt % (Fig. 2.18). The difference between Eu/Eu* in the two series suggests a different bulk D for Eu which might be related to different amounts of plagioclase in the source of the parental magmas and/or to different redox conditions and therefore different Eu^{3+}/Eu^{2+}. Sr/Eu* vs. Eu/Eu* clearly indicates that the low Eu/Eu* calculated ratio for the Aigüa Series and the higher Eu/Eu* of the Lascano Series (Fig. 2.20b) may be linked to residual feldspar in the source of the parental magma to the Aigüa Series which results in low Sr/Eu*.

The difference in isotope ratios between the two series ($\varepsilon Nd_i = -15$ in the Aigüa Series and $\varepsilon Nd_i = -12$ in the Lascano Series at low SiO_2 and similar $^{87}Sr/^{86}Sr_i$, Fig. 2.8) also implies different source regions.

Production of the least evolved rhyolitic melts.

Melting models were used in order to constrain the generation of the least evolved rhyolites in each of the series with a proposed source from the lower crust illustrated in Figure 2.24. Partial melting is considered to have occurred in the mid to lower crust under

fluid absent conditions and at temperatures between 850 and 950 °C (Chapter 3). Such temperatures are lower than those determined for the Paraná - Etendeka rhyolites (950 - 1100 °C. Bellieni *et al.*, 1986; Whittingham, 1991; Garland *et al.*, 1995) which have been taken for evidence for fractionation from basaltic magmas (Garland *et al.*, 1995). The lower temperatures determined for the southern Uruguay rhyolites therefore probably preclude an origin by direct fractionation from basaltic magmas. However they are well within the experimental fields for partial melting of amphibolites, pelites and tonalites (Rushmer, 1991; Skjerlie *et al.*, 1993). In addition the parent/daughter element ratios were constrained by the inferred source age and the initial Sr and Nd isotope ratios. The composition and petrogenesis of the lower crust has been investigated by Rudnick and Taylor (1987). Using the major-element compositions of lower crustal xenoliths of Rudnick and Taylor (1987), phase proportions were estimated from the normative mineralogies of possible source rocks. Bulk D values were calculated assuming 55 % plagioclase + 30 % orthopyroxene + 10 % Clinopyroxene + 5 % titanomagnetite in the source residue with mineral melt partition coefficients taken from Rollinson (1993). Modelling was performed in order to determine the approximate composition of a source (C_o) assuming the least evolved sample in each of the series (C_L) was produced by ~ 30 % partial melting which is that required for a granitic melt to separate from its source (McKenzie, 1985). The results of the modelling are illustrated on a primitive mantle normalised incompatible element diagram (Fig. 2.23) on which a lower crustal mafic xenolith (85-120, Rudnick and Taylor, 1987) is also plotted for comparison.

There is broad agreement between the trace element abundances calculated for a source C_o which produced sample 93L18 (C_L) after 20 % partial melting and the mafic xenolith (85-120) (Fig. 2.23). Rb, Sr and Ti are however markedly different. The Aigüa Series because of their higher average incompatible trace element concentrations could reflect lower degrees of partial melting than the Lascano Series. A source for the Lascano Series, similar in composition to that described by Rudnick and Taylor (1987) for mafic lower crust, was modelled by 30 % partial melting (Fig. 2.23). Rb, Sr and Ti were again very different and suggest that residual biotite, plagioclase and titanomagnetite may be important.

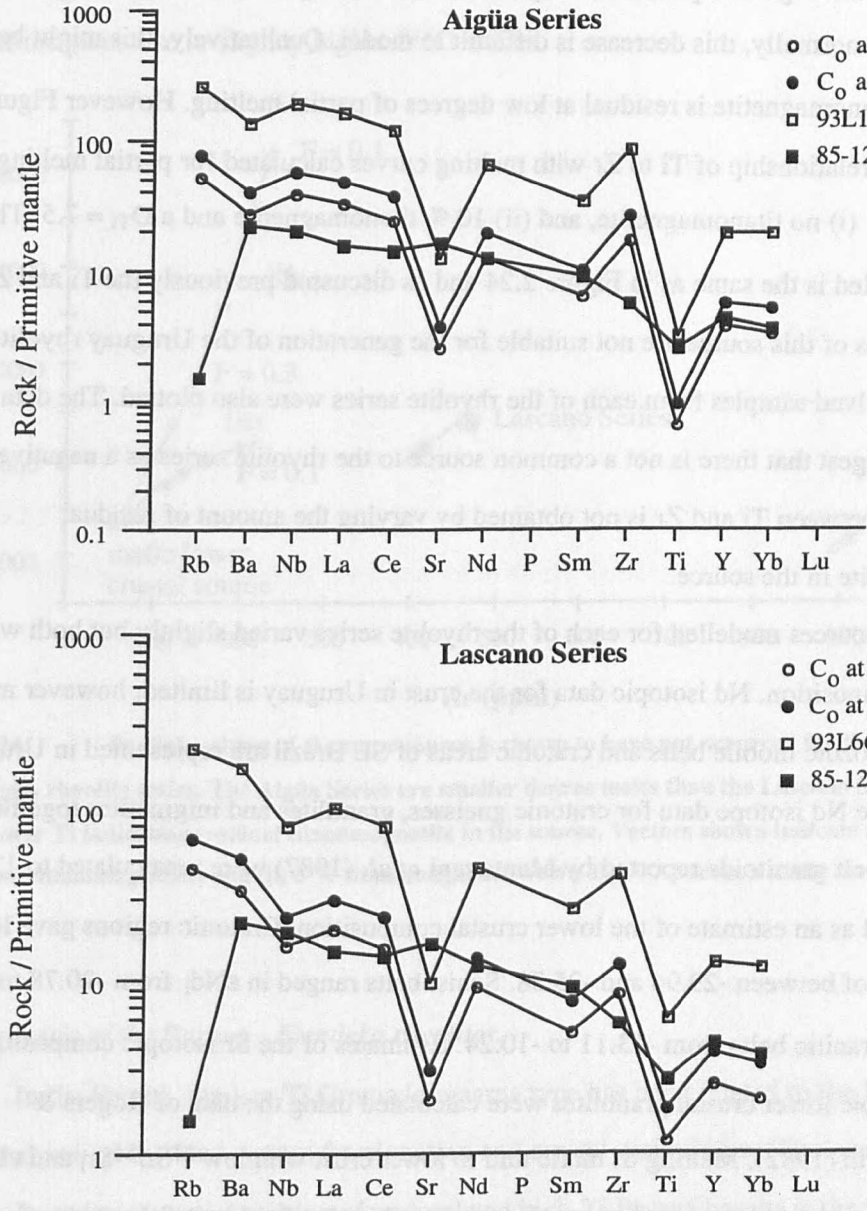

Fig. 2.23. Partial melting models for the generation of the least-evolved rhyolites in both series. The Lascano Series is considered to be generated from a larger degree of melting than the Aigüa Series. Modelling was performed by assuming the least-evolved sample as C_L with F varied between 0.1 and 0.4 as suggested by partial melting experiments. C_o was then calculated from the results and compared with a mafic melt composition, 85-120 from Rudnick and Taylor (1987).

The Aigüa Series have been modelled as smaller degree melts than the Lascano Series however they have lower Sr and Ti/Zr (Fig. 2.18) which cannot be related to differences in the degree of melting. Thus, if the parental magmas to the two rhyolites series simply reflect different degrees of partial melting Ti concentrations would have to

decrease with the degree of partial melting. Since both Ti and Zr tend to be incompatible and $D_{Ti} > D_{Zr}$ normally, this decrease is difficult to model. Qualitatively, this might be resolved if titanomagnetite is residual at low degrees of partial melting. However Figure 25 shows the relationship of Ti to Zr with melting curves calculated for partial melting of a source with (i) no titanomagnetite, and (ii) 10 % titanomagnetite and a $D_{Ti} = 7.5$. The source modelled is the same as in Figure 2.24 and as discussed previously the Ti and Zr concentrations of this source are not suitable for the generation of the Uruguay rhyolites. The least-evolved samples from each of the rhyolite series were also plotted. The data appear to suggest that there is not a common source to the rhyolite series as a negative relationship between Ti and Zr is not obtained by varying the amount of residual titanomagnetite in the source.

The sources modelled for each of the rhyolite series varied slightly but both were mafic in composition. Nd isotopic data for the crust in Uruguay is limited, however many of the Proterozoic mobile belts and cratonic areas of SE Brazil are represented in Uruguay. Therefore the Nd isotope data for cratonic gneisses, granulites and migmatites together with schist belt granitoids reported by Mantovani *et al.* (1987) were recalculated to 130 Ma and used as an estimate of the lower crustal composition. Cratonic regions gave low εNd_i values of between -29.94 and -25.38. Schist belts ranged in εNd_i from -20.78 to -11.85 and granitic belts from -13.11 to -10.24. Estimates of the Sr isotopic compositions of Proterozoic lower crustal granulites were calculated using the data of Rogers & Hawkesworth (1982). Melting of mafic mid to lower crust with low $^{87}Sr/^{86}Sr_i$ and εNd_i is proposed in order to generate the low εNd_i observed in the rhyolites of the Aigüa Series.

Typical Damaran basement $\delta^{18}O$ values range from 6.5 ‰ to 15.2 ‰ with the majority > 10 ‰, the Damara S-type granite averages at 11.4 ‰ (Haack *et al.*, 1983), while lower crust have $\delta^{18}O$ values of 10 - 12 ‰ (Feeley and Sharp, 1995). The geographical positioning of the Damara crystalline basement adjacent to the Uruguay province during the Mesozoic suggests the potential for melting of and/or contamination by such material. The quartz-bearing rhyolites of both series have similar $\delta^{18}O$ values to both the low-Ti rhyolites of the Paraná and the Etendeka (Fig. 2.21). The difference between the Lascano Series and the Aigüa Series is approximately 1‰, which can be accounted for by different degrees of assimilation of upper crust in the Lascano Series,

while the generation of the Aigüa Series from direct melting of mid to lower crustal granulites gives rise to slightly higher $\delta^{18}O$ values.

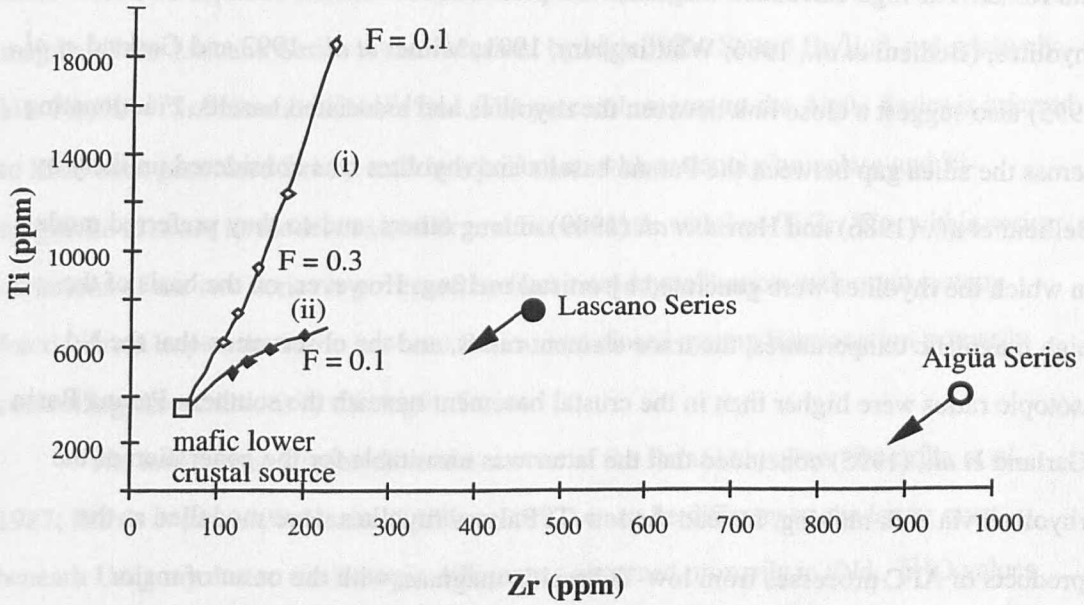

Fig. 2.24. Partial melting of the same source is shown to have not occurred for the Lascano and Aigüa rhyolite series. The Aigüa Series are smaller degree melts than the Lascano Series yet they have lower Ti indicating residual titanomagnetite in the source. Vectors shown indicate melting paths for (i) no titanomagnetite, and (ii) 5 % titanomagnetite with a D_{Ti} = 7.5 from a mafic lower crustal source.

Petrogenesis of the Paraná - Etendeka rhyolites.

In the Paraná, the low Ti Gramado magma type has been related to the low-Ti Palmas rhyolites by open system fractionation and crustal assimilation (Garland *et al.*, 1995). In contrast, partial melting of underplated high-Ti Paraná basalts is the widely accepted origin of the high-Ti Chapecó rhyolites (Piccirillo *et al.*, 1987; Garland *et al.*, 1995; Harris & Milner, 1997). Similarly in the Etendeka the high-Ti Sarusas rhyolites, which have slightly higher $\delta^{18}O$ values than the corresponding high-Ti rhyolites of the Paraná, are considered to have been derived by partial melting of underplated basalts which had undergone as much as 35% assimilation (Harris *et al.*, 1989). The origin of the more voluminous low-Ti Palmas rhyolites remains more controversial (Garland *et al.*, 1995, 1997; Harris & Milner, 1997).

Garland *et al.* (1995; 1997) invoked fractional crystallization from low-Ti Paraná basalt magmas, combined with assimilation, to explain some key observations in the low-

Ti Palmas rhyolites. These include similar incompatible element ratios in the basalts and rhyolites, and the upper crustal characteristics of some trace element ratios such as Rb/Ba and Rb/Zr. The high calculated magmatic temperatures of 950 °C - 1100 °C for the rhyolites, (Bellieni *et al.*, 1986; Whittingham, 1991; Milner *et al.*, 1992 and Garland *et al.*, 1995) also suggest a close link between the rhyolites and associated basalts. Fractionating across the silica gap between the Paraná basalts and rhyolites was considered unlikely by Bellieni *et al.*, (1986) and Harris *et al.* (1989) among others, and so they preferred models in which the rhyolites were generated by crustal melting. However, on the basis of the high magmatic temperatures, the trace-element ratios, and the observation that the Nd isotopic ratios were higher than in the crustal basement beneath the southern Paraná Basin Garland *et al.*, (1995) concluded that the latter was unsuitable for the generation of the rhyolites via bulk melting. Instead the low-Ti Palmas rhyolites were modelled as the products of AFC processes from low-Ti basaltic magmas, with the onset of major magnetite fractionation coincident with the start of the silica gap at ~ 56 wt % SiO_2. In such models the silica gap therefore reflects a rapid change in the liquid line of descent in response to a change in the composition of the fractionating assemblage.

Alternative models invoke partial melting of underplated basalt or granulite (Piccirillo *et al.*, 1987; Harris *et al.*, 1990). Melting of pre-Mesozoic middle to lower crust with similar isotopic compositions to the basement beneath the Etendeka rhyolites was proposed by Harris and Milner (1997), with the caveat that the source had been previously affected by a dehydration episode to explain the anhydrous nature of the rhyolites. The southern Etendeka rhyolites have high $\delta^{18}O$ values and so they are thought to have been derived from a source of mafic to intermediate composition, possibly similar to that of the Damara granites, or the restite phase thereafter (Milner, 1988; Harris *et al.*, 1989) (Fig. 2.21). Oxygen isotopic data and in particular high $\delta^{18}O$ values are important factors for the crustal melting models (Harris *et al.*, 1990; Harris & Milner, 1997). Whilst there may be no explicit line of evidence for or against either model for the Palmas rhyolites, the rhyolites of southern Uruguay are chemically distinct from those of the Paraná - Etendeka rhyolites and therefore shed additional light on the origins of rhyolitic magmas in this CFB province.

Comparison of the Uruguay rhyolites with those of the Paraná - Etendeka.

The variations between and within the two Uruguay rhyolite series suggest that there were two separate parental magmas for the Aigüa and Lascano Series. The parental magma of the Lascano Series is characterised by high Ti/Zr, Sr and Eu/Eu* and relatively low Nb, Zr, $^{87}Sr/^{86}Sr$ and $^{143}Nd/^{144}Nd$. The parental magma to the Aigüa Series is inferred to have been generated from a melt in equilibrium with residual plagioclase and Ti-magnetite in order to model the low Sr and Eu contents with low Ti/Zr. The within series variations of the two series is governed by fractional crystallisation with open system fractionation important in the Lascano Series, and closed system fractionation primarily controlling the variations in the Aigüa Series.

The lower crust suggested as the source of the Paraná rhyolites (Piccirillo *et al.*, 1987; Harris *et al.*, 1990; Harris & Milner, 1997) must be different to the lower crust beneath Uruguay due to the isotopic differences observed primarily in εNd_i, $\delta^{18}O$ values and $^{87}Sr/^{86}Sr_i$. The rhyolites in southern Uruguay show the first unambiguous evidence of crustal melting associated with the Paraná - Etendeka province and are considered to have formed at relatively shallow depths in the continental crust.

2.14 Conclusions - Basalts & Rhyolites.

Basalts:

Two distinct magma types are recognised within the Puerto Gómez Formation of southern Uruguay. These magma types named the Santa Lucía basalts and Treinte Y Trés lavas are distinguished both from elements and isotopes. The magmas were erupted contemporaneously with the main volume of the Paraná-Etendeka CFB province and there are distinct similarities between the low Ti/Y Gramado magma type, which is chemically linked to the Tafelberg member of the Etendeka, and the Treinte Y Trés magma type of southern Uruguay. A common source is proposed for the Gramado and Treinte Y Trés in the sub-continental lithospheric mantle due to trace element and isotopic ratios that are difficult to explain by simple AFC processes contaminating an asthenospheric melt.

The Santa Lucía basalts are however, unique and bear little resemblance to any previously described magma types in the province. They are considered to originate in the asthenosphere on the basis of trace-element geochemistry and their close links with OIB

fields on discriminant diagrams in particular that of Tristan. Mixing however of the Santa Lucía basalts with a magma characterised by low Nb/La and εNd_i such as the Treinte Y Trés, is required in order to explain the differences between these basalts and those of the Walvis Ridge (Tristan-like) and Tristan. This is the first documented occurrence of similar basalts to Tristan contemporaneous with the main flood basalt event. The Santa Lucía basalts are derived from the asthenosphere and in particular highlight the involvement of the Tristan da Cunha hotspot in the generation of this part of the CFB province.

Lateral variations in source compositions and degrees of partial melting across an area of plume related magmatism were highlighted in the introduction to this chapter. The occurrence of asthenosphere derived OIB-like magmas in southern Uruguay suggests greater amounts of decompression melting of the asthenosphere at this latitude. These basalts are contemporaneous with the low-Ti Esmeralda magma type of the Paraná which have been modelled as mixing between MORB and lithospheric mantle melts (Peate & Hawkesworth, 1996) which suggests that the plume may have been beneath southern Uruguay at this time (~133 Ma) instead of its previously considered position. Alternatively the lithosphere may be thinner in southern Uruguay thereby allowing for rapid decompression melting.

Rhyolites:

There is no apparent genetic relationship between the mafic lavas of the Puerto Gómez Fm. and the more voluminous acid flows of the Arequita Formation. The Arequita Fm. is subdivided into two types on the basis of petrography. Type 1 consists of some of the less evolved samples, while flow features are common with oriented feldspar. Feldspar is the dominant mineral phase, forming ~ 60 % of the rock. Type 2 is the most voluminous, these rhyolites are recognised primarily on the presence of variably sized, euhedral to anhedral quartz phenocrysts. Ignimbritic textures, although common are not ubiquitous. Such ignimbritic textures are unusual when compared with the rest of the Paraná-Etendeka province.

The types are not distinguished by the geochemical data and so they have been divided into two series, the Lascano Series and the Aigüa Series. These series are primarily recognised on the basis of trace element (Zr, Nb, Sr and Ti) and isotopic

behaviour but are both considered to have originated via melting of two different mid to lower crustal sources. The Lascano Series is considered to have originated from a parental magma characterised by high Ti/Zr and Sr. The petrogenesis of these rhyolites is controlled by open system AFC processes, and the assimilant is considered to be leucogranitic in composition. The parental magma of the Aigüa Series of rhyolites is characterised by low Ti/Zr and very low Sr which is thought to reflect residual plagioclase and titanomagnetite. Closed system fractionation is important in the evolution of the Aigüa Series rhyolites.

Uruguayan rhyolites as a whole are distinct from the rhyolites of the Paraná-Etendeka on the basis of petrology and chemistry. In addition the Uruguay rhyolites range in age from 132 to 124 Ma and are therefore later than the Paraná rhyolites (Chapter 4). The differences between the two rhyolite provinces are potentially related to changes in stretching factors allowing the ponding of basalts in the mid crust and consequently melting. The lower temperatures observed (850 - 950 °C) in the two rhyolite series (Chapter 3) are consistent with this model.

Chapter 3.

Basalt & rhyolite temperatures related to changing thermal & tectonic regimes.

3.1 Introduction.

Early Cretaceous volcanic rocks of the Paraná Basin (South America), and the Etendeka province (Namibia) have been previously linked with extension across the Tristan da Cunha mantle plume (Hawkesworth *et al.*, 1992; Milner *et al.*, 1995). The close spatial and temporal relationship of the Puerto Gómez Formation (Fm.) and the Arequita Fm. (southern Uruguay), with the Paraná - Etendeka Continental Flood Basalt (CFB) province may potentially give insight into changing mantle potential temperatures during rifting of the South Atlantic.

High basalt magma temperatures are not necessarily indicative of plume involvement (Ceuleneer *et al.*, 1993) in a province however, high rhyolite temperatures are of considerable interest. The occurrence of high temperature rhyolites in the Paraná - Etendeka province is well documented (Bellieni *et al.*, 1986; Garland *et al.*, 1995). The calculated temperatures are in the order of 950 – 1100°C, and potentially provide information regarding the origin of the rhyolites which is highly contentious (Garland *et al.*, 1995, 1997; Harris & Milner, 1997).

The rhyolites of southern Uruguay are distinct in appearance and in chemistry from those of the Paraná - Etendeka CFB province with unique textures and a more evolved phenocryst assemblage (Chapter 2, Appendix C). The difference in appearance is potentially due to different modes of origin and localised variations in mantle temperatures such as might be related to plume involvement. Both rhyolite exposures are considered to be linked to the opening of the South Atlantic.

3.2 Background Geology.

The Paraná - Etendeka CFB are strongly bimodal with a clear compositional division between basalts and rhyolites. The flood basalts show wide chemical diversity and were subdivided on the basis of chemistry, namely Ti/Y and $^{87}Sr/^{86}Sr$ initial ratios into a number of groups (Bellieni *et al.*, 1984; Mantovani *et al.*, 1985; Peate *et al.*, 1992). The division into high and low Ti/Y groups which are broadly geographical remains valid although the number of groups has been expanded, see Peate & Hawkesworth (1996) for most recent subdivisions. Division into high and low Ti/Y magma types (>310 • MORB < 310 respectively) has been used extensively to distinguish compositionally distinct magmas associated with the break-up of the Gondwana supercontinent during the Mesozoic (Hergt *et al.*, 1991; Peate *et al.*, 1992).

The mineralogy of the Paraná basalt groups is essentially anhydrous, consisting of augite, plagioclase, pigeonite and iron oxides, both Ti - magnetite and ilmenite, and rare Mg - olivine microphenocrysts. The basalts range from aphyric to porphyritic; the hypocrystalline groundmass consists of the same phenocryst phases, although quartz may also be present. Bellieni *et al.*, 1988 calculated magmatic temperatures (°C) of 1100 to 1250 from the compositions of early crystallised pyroxene and plagioclase for the basalts and are considered to be quenching temperatures. Furthermore crystallisation occurred at low pressures in water undersaturated conditions (Bellieni *et al.*, 1988). The presence of plagioclase in the phenocryst assemblage implies crustal depths and pressures of < 10 kbar.

The basalts of southern Uruguay, Puerto Gómez Fm. are Early Cretaceous in age (Chapter 4) and are considered to be part of the main melting event that resulted in the formation of the Paraná - Etendeka province (Chapter 2).

These basalts have been subdivided into two groups, the Treinte Y Trés and the Santa Lucía magma types on the basis of geochemistry, each with a distinct source. The voluminous Treinte Y Trés magmas have been shown to be chemically similar to the low-Ti Gramado magma type of the Paraná, and consequentially the Etendeka equivalent, the Tafelberg magma type (Chapter 2). The mineralogy of the two southern Uruguay magma types is anhydrous, with olivine, pyroxene, plagioclase and iron oxides present. Olivine is preferentially preserved in the rare Santa Lucía magmas.

A similar division into high and low-Ti groups is also applied to the acid volcanics of the Paraná, namely the low-Ti Palmas magma type and the high-Ti Chapecó (Piccirillo *et al.*, 1988). These groups have been further subdivided on the basis of their chemistry (Garland *et al.*, 1995). Palmas acid volcanics occur principally in the south of the Paraná basin and are closely associated with the low Ti/Y basalts. Chapecó type acid volcanics occur in the north of the basin, where they are closely associated with the high Ti/Y basalt magma types. The acid volcanics also have an anhydrous mineralogy consisting of plagioclase, augite, opaques and pigeonite phenocrysts with apatite as a common accessory in the high-Ti rhyolites (Comin-Chiarmonti *et al.*, 1988). The high-Ti Chapecó rhyolites of the Paraná are comparatively phenocryst rich (10 - 15 %) with plagioclase dominating over pyroxene and iron oxides. The low-Ti Palmas rhyolites of the Paraná are predominantly hyaline, with the majority containing < 5 % phenocrysts. Phenocrysts where evident tend to be discrete and consist of plagioclase, augite, orthopyroxene, opaques. Apatite is rare, and pigeonite is mainly confined to the matrix. The matrix ranges from glassy to crystalline; devitrification is common. Detailed work on the rhyolite petrography and chemistry has been used to subdivide the high- and low-Ti rhyolite groups further and to correlate the Paraná and Etendeka silicic volcanics (Whittingham, 1991; Milner *et al.*, 1995; Garland *et al.*, 1995).

A number of authors have calculated high temperatures of crystallisation (950 °C - 1100 °C), from pyroxene, feldspar and iron oxide geothermometry, and these are considered representative of magmatic conditions (Bellieni *et al.*, 1986; Whittingham, 1991; Milner *et al.*, 1992 & Garland *et al.*, 1995). The origin of the Paraná rhyolites remains contentious due to a number of reasons. Partial melting of underplated high Ti/Y Paraná basalts is the widely accepted origin of the high-Ti Chapecó rhyolites and the temperatures obtained for the eruption of these rhyolites are slightly higher than those for the Palmas rhyolites (Bellieni *et al.*, 1986; Garland *et al.*, 1995; Harris & Milner, 1997).

The origin of the more voluminous low-Ti Palmas rhyolites is more debatable (Garland *et al.*, 1995, 1997; Harris & Milner, 1997). Garland *et al.* (1995; 1997) propose fractional crystallization from low Ti/Y Paraná basalts, combined with assimilation, to explain some key observations in the low-Ti Palmas rhyolites including the similar incompatible element ratios of the basalts and rhyolites and the upper crustal

characteristics such as high Rb/Ba and Rb/Zr. The high calculated magmatic temperatures are also an intrinsic part of this argument. Partial melting of underplated basalt or granulite has also been proposed as an origin for the Palmas rhyolites (Bellieni *et al.*, 1986; Harris *et al.*, 1990). Melting of pre-Mesozoic middle to lower crust with similar isotopic compositions to the basement beneath the Etendeka rhyolites is proposed by Harris and Milner (1997) with the source affected by a previous dehydration episode to explain the anhydrous nature of the rhyolites. Whilst there may be no explicit line of evidence for or against either of the above models for the Palmas rhyolites, the rhyolites of southern Uruguay are chemically distinct and are considered to have undergone a separate petrogenesis (Chapter 2).

The Paraná - Etendeka rhyolites, although contemporaneous with the Uruguay rhyolites, are distinct in terms of petrology and chemistry. The origin of the Uruguay rhyolites is thought to be linked to changing thermal regimes and principal tectonic stress regimes. The southern Uruguay rhyolites have been divided into two main types, Type 1 and Type 2 on the basis of petrology. However these types were not distinguished on the basis of chemistry with the result that the rhyolites were instead divided into two series, the Lascano Series and the Aigüa Series (Chapter 2). Rhyolites of the Type 2 petrological type contain variably sized, euhedral to anhedral quartz phenocrysts. Ignimbritic textures, although common are not ubiquitous.

True ignimbritic textures have previously been little recognised in rhyolitic outcrops associated with the Paraná - Etendeka province. This was considered to be primarily due to the high temperatures of eruption involved, with the result that the Paraná - Etendeka rhyolites are often referred to as rheoignimbrites (Milner *et al.*, 1992). Type 2 rhyolites as discussed in Chapter 2, are often characterised by ignimbritic textures (Fig. 3.1). Flattened pumice fragments containing euhedral quartz phenocrysts and glass shards are evident, as are phenocrysts of quartz and alkali feldspar around which a fine matrix flows, this regular alignment of flattened fragments gives rise to a eutaxitic texture (Appendix C - Photomicrographs). Fiammé are stretched and illustrate secondary mass flowage of the tuff, indicative of elevated temperatures and/or low viscosities. Phenocrysts are predominantly subhedral although embayments are common. Quartz phenocrysts are of two principal types: (i) small, angular to sub-rounded with small

hairline type fractures, the bipyramidal shape of these phenocrysts suggests that they are low pressure, high temperature β-form quartz; and (ii) larger embayed phenocrysts with rounded edges, slightly strained extinction and a greater degree of fracturing, although this is not extensive.

The rhyolite mineralogy tends to be anhydrous, consisting primarily of plagioclase, alkali feldspar, pyroxene and iron oxide, with quartz indicating the more evolved lithologies. Accessory minerals include zircon and apatite. Original glass is evident, but is mainly devitrified.

3.3 Equilibrium or Disequilibrium in southern Uruguay volcanics?

Evidence of equilibrium between co-existing phenocrysts and between phenocryst phases and the melt is a prerequisite in the use of geothermometers. Phenocrysts of plagioclase, pyroxene, alkali feldspar and iron oxides were examined for textural evidence of equilibrium, both with other phenocrysts and with the melt. The choice of phenocrysts described is primarily a function of the thermometers already in use in determining temperatures of the Paraná - Etendeka province (Bellieni *et al.*, 1986; Whittingham, 1991; Garland *et al.*, 1995). Phenocryst appearance is broadly similar between the basalts and rhyolites and so they are discussed together in the following section. Compositionally the basalts are characterised by Ca-rich plagioclase and more magnesian pyroxene phenocrysts, iron oxide is primarily titanomagnetite while alkali feldspar and quartz are not present in basalt thin sections. Microprobe analyses were made either on a Cambridge Instruments Microscan 9 or on a Cameca SX100 wavelength dispersive electron microprobe. Running conditions involved an accelerating voltage of 20kV and variably focused 20nA beam with 0 to 20μm spot size depending on phenocryst size (Appendix B).

Fig. 3.1. Ignimbritic texture in rhyolite of petrological Type 2.

Plagioclase:

Plagioclase is common both as megacrysts (1cm) and smaller phenocrysts (0.5-2mm). Plagioclase ranges from An_{50} to An_{82} in the basalts, and from An_{28} to An_{55} in the rhyolites (Table 3.1). Euhedral tabular/lath forms give way to more rounded phenocrysts, with sieve and skeletal textures. Twinning in the plagioclase is lamellar and asymmetric. The majority of rhyolitic samples are porphyritic with glomerophyric intergrowths of plagioclase ± pyroxene ± alkali feldspar common. Trachytoid textures are evident in the intermediate rocks. Ophitic and sub-ophitic enclosure of olivine and pyroxene in plagioclase, and plagioclase in pyroxene is noted in the more primitive basaltic samples.

Pyroxene:

Clinopyroxene, namely augite occurs in both the basaltic and the less evolved silicic volcanic, mainly the trachydacites (Table 3.2). Clinopyroxene is virtually absent in the more evolved rhyolites. Pigeonite is rarely present, while orthopyroxene is absent. In general the pyroxenes are altered and pseudomorphed, predominantly by iron oxides. Some zoning and twinning is noted, as is the herring bone structure of pigeonite (Appendix C). Pyroxene may be poikilitically encompassed by feldspar. Phenocrysts are euhedral to anhedral often with chloritized rims. Pyroxene is a common groundmass constituent in the basalts. The Mg# test for phenocryst-melt equilibrium was applied to the pyroxene analyses to check if the phenocrysts are in equilibrium with the groundmass. The experimental Fe-Mg exchange distribution coefficient was taken to be 0.23 after Grove & Bryan (1983). The calculated $Mg\#_{liquid}$ with which the pyroxenes were in equilibrium with was found to be consistently lower than the $Mg\#_{Augite}$. This suggests that these are partially inherited pyroxenes that crystallised at an earlier, more mafic stage in the liquid line of descent of these magmas and that they have not fully equilibrated with the melt.

Alkali feldspar:

Alkali feldspar is more abundant than plagioclase in the high silica samples. Phenocrysts of alkali feldspar, up to 5mm, occur both discretely and intergrown with plagioclase. Composition ranges from anorthoclase to K-rich sanidine. Perthitic textures

formed by the intergrowth of Na- and K- feldspar occur, particularly in the samples from Mariscala (93L48; 93L81- Aigüa Series) (Fig. 1.22) (Table 3.1). In addition granophyric intergrowths of groundmass quartz and K-feldspar are also evident in some samples. Such textures have previously been recognised in old devitrified glassy rocks where the quartz and feldspar have intergrown either during devitrifcation or slow cooling. Evidence of dissolution includes rims around some feldspar phenocrysts preventing interaction with the matrix. Embayed alkali feldspars phenocrysts occur together with euhedral phenocryst and sieve and skeletal textures are also recognised (Appendix C).

Iron oxides:

Iron oxides are ubiquitous in both the mafic and felsic rocks. Both primary and secondary iron oxides are identified, the latter being the primary alteration mineral for pyroxene. Compositions are similar for both the basalts and rhyolites with magnetite and titanomagnetite dominating, ilmenite is least common and only found in the rhyolite assemblages (Table 3.3). The complexity of textures of iron oxides within the basalt and rhyolite suites could be the subject of a separate study of oxidation exsolution. Both coarse and fine lamellae of ilmenite are seen to be in sharp contact with titanomagnetite hosts (Fig. 3.2; Appendix C). Such characteristics are noted in several iron oxides using a scanning electron microprobe (SEM).

Matrix:

The matrix in basalts and rhyolites varies from microcrystalline to cryptocrystalline. The principal constituents vary from olivine, pyroxene, plagioclase and iron oxide microphenocrysts in the mafic rocks to feldspar, quartz, iron oxides and devitrified glass complete with accessory minerals including zircon and apatite in the evolved rhyolites. The matrix of the mafic assemblages is basically a much finer grained equivalent of the principal phenocrysts evident. Trachytic alignment of groundmass feldspars is noted in some samples, paralleled by larger phenocrysts, but more often the matrix is aphanitic, spherulitic and devitrified for rhyolitic samples. Many of the spherulites consist of a dense mass of very fine intergrown needles of quartz and alkali

feldspar radiating from a central nucleus. Euhedral zircon and apatite crystals are evident both as inclusions and as groundmass phenocrysts in the evolved rhyolite lithologies.

Table 3.1. Feldspar compositions for both the basalts and rhyolites.

Sample	92U12 - Santa Lucía	92U12 - Santa Lucía	93L27 - Treinte Y Trés	93L125 - Treinte Y Trés	93L78 - Lascano	93L83 - Aigüa	93L111 - Lascano
Magma type	**Labradorite**	**Labradorite**	**Labradorite**	**Labradorite**	**Sanidine**	**Anorthoclase**	**Labradorite**
Feldspar comp.							
SiO_2	51.01	55.34	51.40	53.06	59.68	65.31	57.87
TiO_2	0.06	0.14	0.07			0.05	0.03
Al_2O_3	30.31	27.60	30.12	28.53	24.47	20.48	25.93
MgO	0.11	0.12	0.20				0.01
CaO	13.96	10.46	13.49	12.65	6.63	1.65	8.71
MnO		0.01	0.001				0.002
FeO	0.53	0.76	0.88	0.87	0.46	0.19	0.48
BaO	0.03	0.04			0.32	0.12	0.11
Na_2O	3.63	5.37	3.87	4.40	7.24	7.60	5.98
K_2O	0.2	0.50		0.34	1.10	4.18	0.94
Total	99.86	100.34	100.12	99.85	99.90	99.59	100.06

Table 3.1. *Continued.*

Sample Magma type	93L105 - Lascano	93L105 - Lascano	93L44 - Aigüa	93L44 - Aigüa	93L28 - Aigüa	93L99 - Lascano	93L112 - Lascano
Feldspar comp.	**Andesine**	**Orthoclase**	**Orthoclase**	**Andesine**	**Sanidine**	**Orthoclase**	**Orthoclase**
SiO_2	56.01	64.36	64.12	62.14	66.91	64.84	64.31
TiO_2	0.03	0.03	0.04	0.01		0.05	0.04
Al_2O_3	27.14	18.98	19.64	23.10	18.68	18.66	18.99
MgO	0.01		0.001				
CaO	10.23	0.35	1.12	5.23	0.07	0.26	0.36
MnO	0.01	0.01	0.001		0.001		0.002
FeO	0.27	0.11	0.16	0.30	0.17	0.09	0.08
BaO	0.11	1.99	1.05	0.02	0.03	1.64	2.32
Na_2O	5.09	2.78	3.86	7.32	6.32	2.43	2.97
K_2O	0.80	11.44	9.96	2.07	7.80	12.19	11.20
Total	99.71	100.03	99.95	100.19	99.97	100.16	100.26

Table 3.2. Selected pyroxene analyses from mafic assemblages.

Sample	92 U12-	93L53 -	93L104 -	93L93 -	93L97 -	93L125 -	93L125 -
Magma type	Santa Lucía	Santa Lucía	Santa Lucía	Treinte Y Trés	Treinte Y Trés	Treinte Y Trés	Treinte Y Trés
Pyx. comp.	**Augite**	**Augite**	**Augite**	**Augite**	**Pigeonite**	**Augite**	**Pigeonite**
SiO_2	49.9	49.73	51.62	52.34	54.76	48.99	49.94
TiO_2	0.82	1.57	0.61	0.48	0.19	1.14	0.45
Al_2O_3	5.91	2.52	1.58	1.56	1.62	3.70	0.84
Cr_2O_3		0.04	0.12		0.33		0.02
MgO	14.76	12.77	16.20	16.96	29.22	10.79	16.46
CaO	19.19	20.38	18.80	16.93	2.0	10.60	5.29
MnO	0.21	0.28	0.28	0.25	0.27	0.52	0.58
FeO	8.40	12.48	9.85	11.03	11.97	23.74	25.28
BaO		0.01	0.01	0.01		0.04	0.01
Na_2O	0.60	0.37	0.19	0.18	0.02	0.53	0.03
K_2O				0.01	0.01	0.09	0.00
Total	99.82	100.15	99.27	99.74	100.38	100.12	98.90

Table 3.3. Selected iron oxide analyses.

Sample Magma type	92U12 - Santa Lucía	93L104 - Santa Lucía	93L125 - Treinte Y Trés	93L105 - Lascano	93L107 - Lascano	93L107 - Lascano	93L99 - Lascano
Iron oxide	**Magnetite**	**Magnetite**	**Titano - magnetite**	**Titano - magnetite**	**Titano - magnetite**	**Titano - magnetite**	**Titano - magnetite**
SiO_2	0.17	0.50	0.98	0.06	0.05	7.56	0.05
TiO_2	26.48	19.96	27.42	53.16	59.94	37.90	59.63
Al_2O_3	1.40	0.86	2.40	0.05	0.11	4.63	0.04
V_2O_3				0.28	0.30	0.16	0.37
Cr_2O_3	0.34	0.12	0.25	0.01	0.001	0.02	0.03
MgO	1.04	0.40	0.06	0.06	0.09	0.96	0.01
CaO	0.19	0.12	0.05			0.19	
MnO	0.69	0.35	0.91	0.81	0.48	0.53	0.27
FeO	65.30	74.37	58.4	44.26	36.03	43.59	35.78
NiO	0.002		0.32	0.02		0.001	
ZnO	0.1		0.06	0.05		0.07	0.01
Na_2O	0.002		0.03		0.03	0.59	
Total	95.73	96.68	90.89	98.76	97.04	96.41	96.18

Fig. 3.2. **Lamellae in iron oxides due to exsolution.**

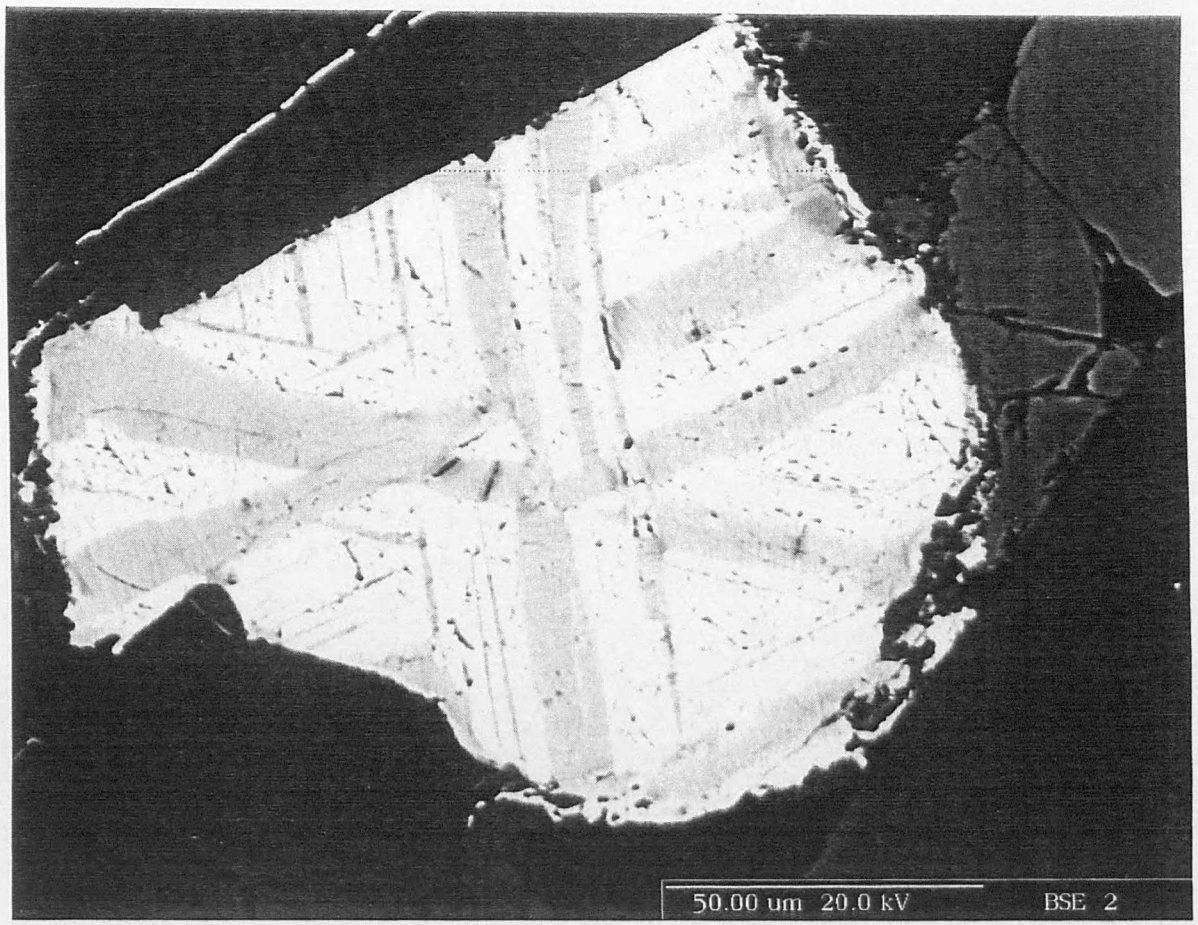
50.00 um 20.0 kV
BSE 2

Fig. 3.3. Brecciated silicic volcanics indicating explosive origins for rhyolites.

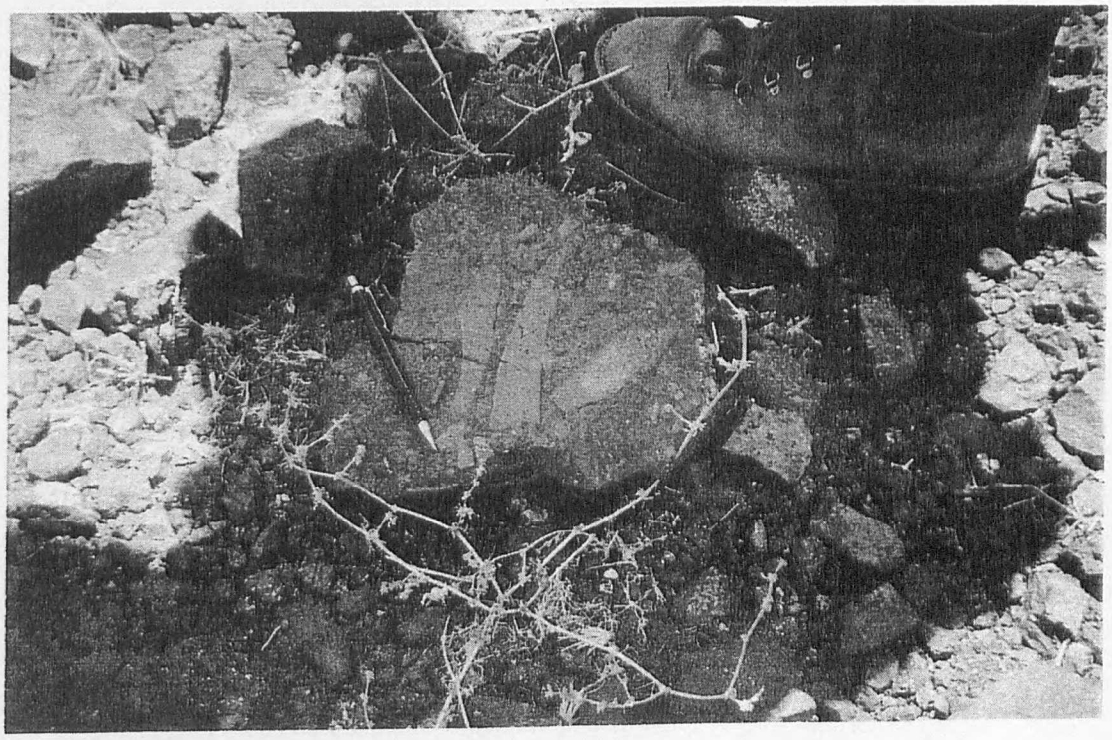

3.4 Origin of rhyolite textures.

The intratelluric phenocryst assemblage consists of plagioclase, olivine and pyroxene for the mafic assemblages, while that of the silicic suite is of plagioclase, alkali feldspar ± pyroxene ± quartz. Textural evidence suggests that at least some of the phenocrysts were in equilibrium as they have maintained euhedral forms and are found in glomerophyric intergrowths. Embayments such as those evident in some alkali feldspar and quartz phenocrysts are interpreted as resorption features, although they may also be due to rapidly growing crystals enclosing the groundmass. Quenching textures such as the skeletal growth of phenocrysts and the presence of glass in the rhyolites suggest rapid eruption and cooling. Careful selection was therefore required in choosing samples for thermometry, this was initially done via petrological evidence and the Mg# test for pyroxenes, and as shall be seen for iron-oxide thermometry the samples were checked via Mg - Mn partitioning in co-existing magnetites and ilmenites.

Outcrops containing sharp irregular fragments together with ignimbritic textures suggest an explosive origin for many of the rhyolites (Fig. 3.3), consistent with eruption from a vent. The welded nature of the ignimbrites suggests little loss of heat on eruption and hence low collapse heights, this in turn is indicative of low gas contents and low gas velocity (Cas & Wright, 1988). However no caldera structure has been recognised in the region. Not all the rhyolites have these distinctive textures and the origin of some of the more featureless rhyolites is debatable, with a lack of pyroclastic textures suggesting a passive mode of effusion from dyke-like fissures. A few E-W trending acid dykes were noted in the Cerro Partido region.

The style of eruption of the rhyolites of southern Uruguay appears to be unusual with regards to the main Paraná province and is discussed in greater detail later when better constraints can be placed on the temperatures, viscosity and water contents at the time of eruption. The eruption of the Etendeka province is also distinct with each unit divided into an basal, main and upper zone, with the basal and upper parts characterized by flow banding, pitchstone lenses and breccia with rare pyroclastic textures (Milner *et al.*, 1992). The large lateral extent of the Etendeka silicic rocks and the local preservation of pyroclastic textures including fiammé and eutaxitic textures resulted in classification of

these rocks as rheoignimbrites, high temperature ignimbrites that have undergone secondary mass flowage (Milner *et al.*, 1992).

3.5 Thermometry.

The Uruguay rhyolites are either peraluminous or sub-aluminous rocks based on Ca + Al ± Na ± K according to the classification system of Carmichael *et al.* (1967), with normative quartz (q), orthoclase (or), albite (ab), anorthite (an) and corundum (c). The applicability of certain thermometers to rocks of this age and composition is dealt with in the next section and the reliance of accessory phase thermometers is discussed. The limited assemblage of minerals within the rhyolites did not lend them to many geothermometers.

Pyroxene, feldspar and iron oxide thermometers have previously been applied to the Paraná - Etendeka province (Bellieni *et al.*, 1986; Whittingham, 1991; Garland *et al.*, 1995). The more commonly used thermometers including the pyroxene quadrilateral (Kretz, 1982; Lindsley, 1983) and ternary feldspars (Ghiorso, 1984; Price, 1985; & Fuhrman & Lindsley, 1988) were therefore initially investigated. Pyroxene thermometry was primarily used to place a temperature constraint on the basalts, while feldspar thermometry was applied to the rhyolites. Iron-titanium oxide thermometry (Buddington & Lindsley (1964); Powell & Powell (1977) & Ghiorso & Sack (1991)) was also attempted as both titanomagnetite and ilmenite coexist in some the rhyolites. Finally accessory-phase thermometry including the apatite solubility thermometers of Watson & Harrison (1984) and Pichavant *et al.*, (1992), the zircon thermometer of Watson & Harrison (1983) and the monazite thermometers of Rapp & Watson (1986) and Montel (1993) were applied. The presence of only one pyroxene in most samples and two feldspars in the rhyolites required use of different thermometers to those applied to Paraná samples, some of the main thermometers are reviewed initially for comparison purposes.

3.6 Pyroxene thermometry.

The use of pyroxene thermometry is predominantly precluded by the absence of two coexisting pyroxenes. The thermometers of Kretz (1981) and Lindsley (1983) are based on mutual solution between Ca-rich clinopyroxenes and orthopyroxene or pigeonite. Microprobe analyses of Ca- rich augite phenocrysts have been used to determine minimum temperature estimates (Fig. 3.4). One-pyroxene thermometers based on the Ca content of augite give minimum temperature estimates. Temperatures of between 950 °C and 1250 °C are estimated for the more mafic assemblages with an average crystallisation temperature in the order of 1150 °C, this temperature range is comparable with those described for the Paraná basalts (Picirrillo *et al.*, 1988). In the more evolved lithologies, there are Ca - rich pyroxenes but poor totals on the microprobe analyses indicate that they are too altered to be reliable.

Although commonly used to estimate temperatures the one pyroxene thermometers or two-pyroxene solvus thermometers may be considered relatively inaccurate in this instance due to a lack of quality data. This is due in part to the use of electron microprobes in determining the Fe content of minerals and having to calculate Fe^{2+}/Fe^{3+} ratios based on stoichiometry. Comparison of resultant temperatures with non-ferric iron dependent thermometers was therefore undertaken to substantiate results.

3.7 Feldspar thermometry.

The thermometers of Kudo & Weill (1970) and Mathez (1973) which were applied to the Paraná rhyolites (Bellieni *et al.*, 1986; Whittingham, 1991), are based on equilibria between plagioclase and hydrous silicate melts and are not applicable to the rhyolite exposures of southern Uruguay. Therefore ternary feldspar thermometry was applied due to the co-existence of plagioclase and alkali feldspar. In the ternary feldspar system, ($NaAlSi_3O_8$ - $KAlSi_3O_8$ - $CaAl_2Si_2O_8$), at high temperatures and low pressures there is complete solid solution on the Ab - Or and Ab - An binaries, but limited solid solution between Or - An. Ternary feldspar thermometry is based on the partitioning of the albite component between plagioclase and alkali feldspar, although similar equations can be written for Or and An components in two co-existing feldspars (Ghiorso, 1984;

Fuhrman & Lindsley, 1988). The compositions of co-existing feldspars and in particular the effects of cation ordering are strongly influenced by temperature, pressure, melt composition and water content (Ghiorso, 1984; Carpenter & Ferry, 1984; Marsh *et al.*, 1990; Housh & Luhr, 1991).

Fig. 3.4. **The pyroxene quadrilateral, showing isotherms (°C) on the Ca pyroxene slope of the solvus surface, after Kretz (1982). Basalt data are plotted and show temperatures in the range of 1100 and 1200°C.**

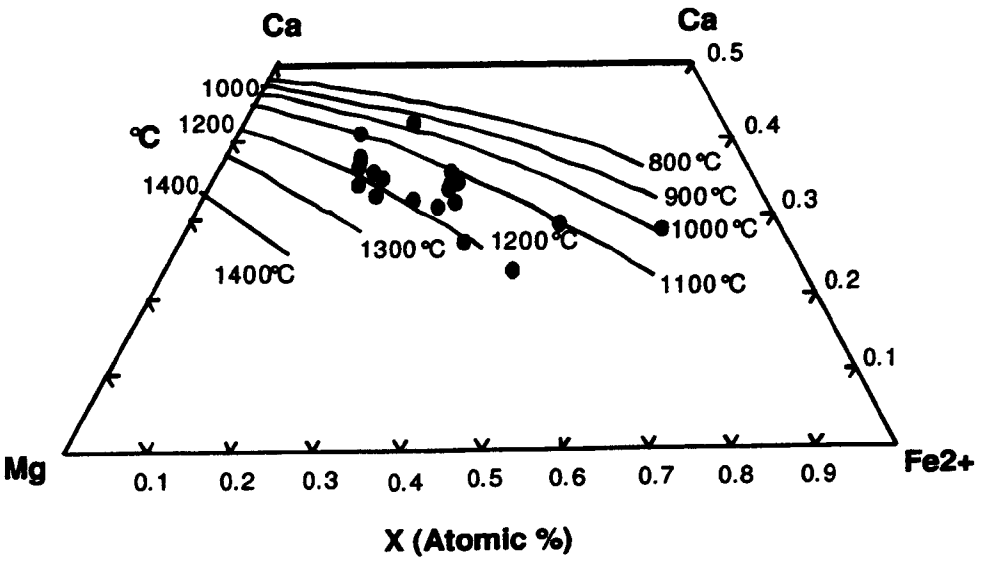

Table 3.4. Feldspar crystallisation temperatures for Uruguay rhyolites calculated from the thermometer as indicated. Temperatures are in degrees Celsius.

Thermometer **Rhyolite series:**	**93L44** **Aigüa** **Series**	**93L105 (i)** **Lascano** **Series**	**93L105 (ii)**
Stormer	774	788	772
Powell & Powell	710	701	712
Whitney & Stormer	944	888	865
Haselton *et al.*	888	845	861
Price	764	652	723

Temperatures from co-existing feldspar pairs are considered by Ghiorso (1984) to be minimum estimates of phenocryst crystallization in the rhyolites as a result of overestimation of feldspar miscibility in the original experiments of Seck (1971). Equilibrium between the feldspar pairs is critical, as for any of the feldspar thermometers the calculated temperatures are reliant on this thermodynamic state being achieved. A number of disequilibrium textures have already been described for Uruguay rhyolite samples and so relatively few feldspar temperatures are available.

Using the solution models proposed by Ghiorso (1984) temperature estimates in the order of 700 °C to 900 °C were calculated for the majority of the rhyolites (Fig. 3.5). Such values are semi-qualitative because of the sparsity of suitable data and other methods of geothermometry are investigated in order to constrain the temperatures further. Using the thermometers of Stormer (1975); Powell & Powell (1977); Whitney & Stormer (1977); Haselton *et al.* (1983) and Price (1985) with data for two specific samples with coexisting plagioclase and alkali feldspar, a range in temperatures was calculated (Table 3.4) suggesting that care must be applied in making comparisons between temperatures. The difference in temperature estimates is potentially due to preferences in the developmental procedure. For example the early thermometers such as that of Stormer (1975) do not take into account the effects of K- substitution in high temperature plagioclase.

The within-sample differences evident for sample 93L105 are potentially due to a lack of precision in analyses and for most of the thermometers the variation is 10 - 15 °C, except the Price (1985) thermometer which differs by over 70 °C. This is potentially due to multicomponent solid solutions, such as substitution by Ba in alkali feldspar or the inclusion of H_2O in the system. During the course of calculating temperatures from feldspar thermometry pressure was assumed to be 1 kbar and 1 wt % H_2O was included in the system.

Fig. 3.5. Proposed compositional sections through the solvus as a function of temperature after the theoretical calculations of Ghiorso (1984). Uruguay rhyolite data plot between the 500 and 1000°C contours.

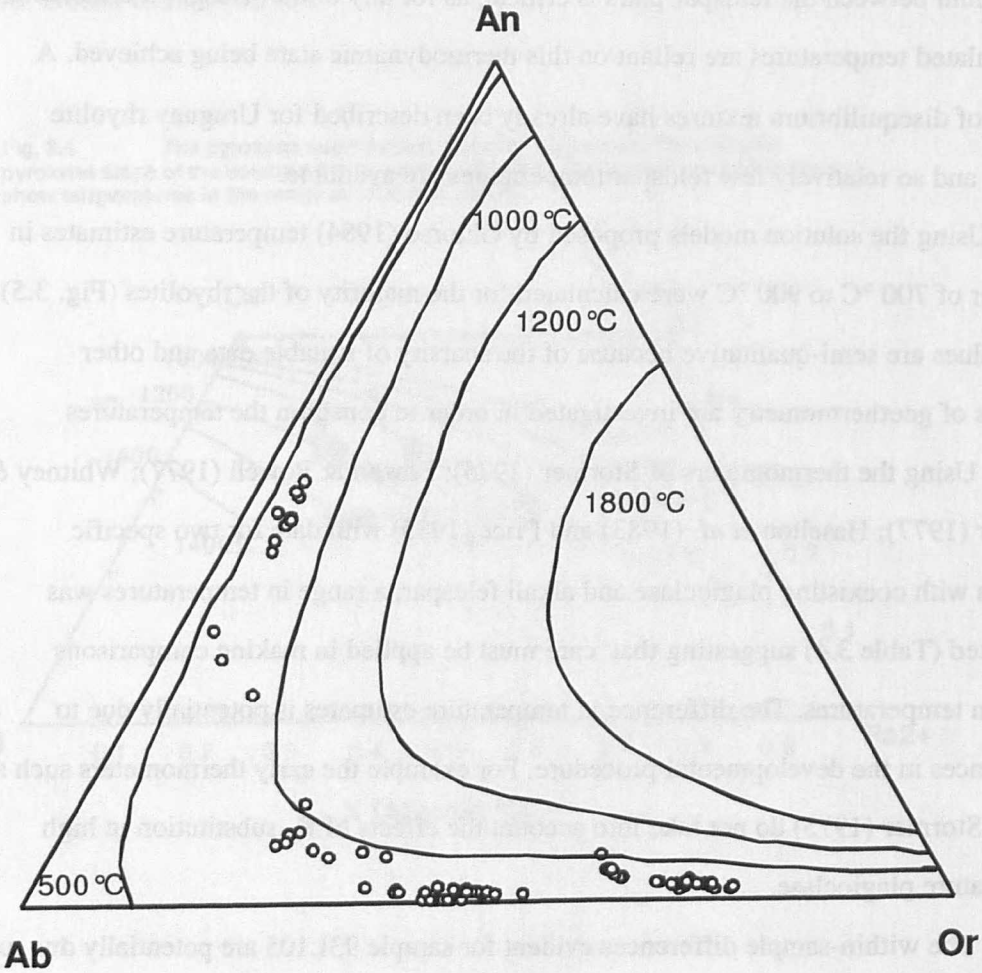

3.8 Fe-Ti oxide thermometry.

Buddington & Lindsley (1964) first proposed a thermometer for the FeO - Fe_2O_3 - TiO_2 system. The formation of co-existing pairs of titanomagnetite and ilmenite can also be used to determine oxygen fugacities. Ilmenite - magnetite trellis intergrowths such as those seen in the rhyolites from southern Uruguay are considered the result of subsolidus oxidation (Fig. 3.2). Only ilmenite-titanomagnetite pairs that appeared to be in equilibrium were used. These data were then further tested for equilibrium using the equations of Bacon & Hirschmann (1988) for the partitioning of Mg and Mn between co-existing phases. The partitioning of these elements is considered to be independent of bulk composition, temperature or pressure and is therefore independent of the major unknown

variables. The test is valid for fresh volcanics but in the case of the Uruguay rhyolites few of the analyses are close to equilibrium when plotted on a log $(Mg/Mn)_{mt}$ v log $(Mg/Mn)_{il}$ diagram (Fig. 3.6). This may be due to the highly oxidised nature of the rhyolites or it is discriminating between multiple populations of oxides. Pairs that survived the selection process however still gave rise to widely varying temperatures using the thermometer of Ghiorso & Seck (1991), ranging from 900 to 650 °C in one sample alone. The calculated temperatures are potentially magmatic but they are only useful in the context of the other methods applied.

Fig. 3.6. Establishing equilibrium conditions between co-existing magnetite and ilmenite using the criteria of Bacon and Hirschmann (1988). Slope of solid line equals equilibrium conditions, dashed line shows partitioning devised by Lindsley at 1100 °C.

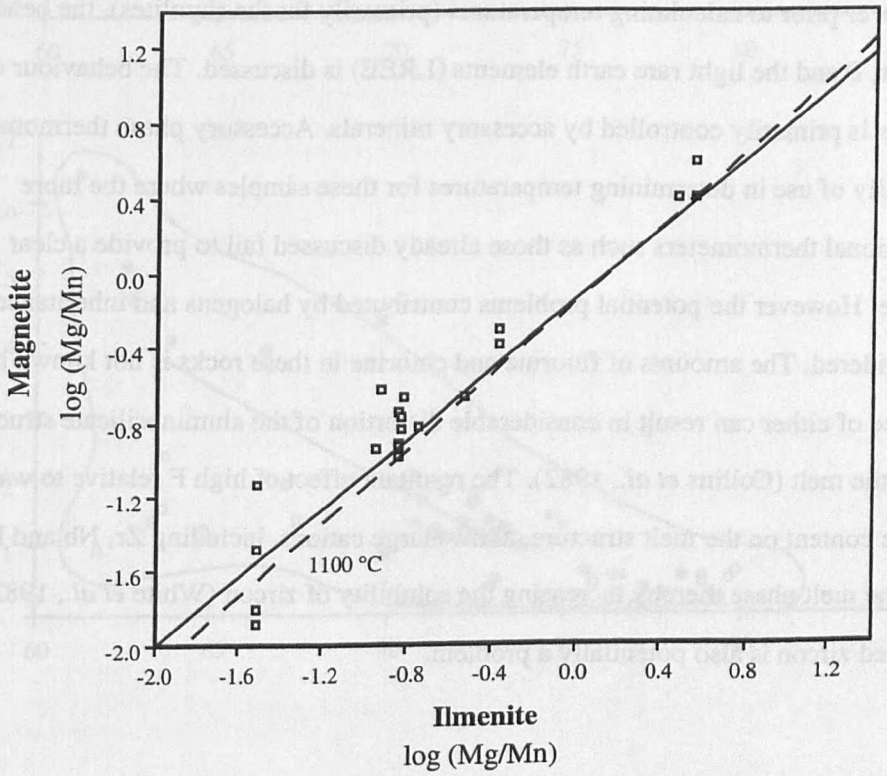

As with the pyroxene thermometry questions are also raised regarding the calculation of the ferric iron content from the measured ferrous ratio. The measured analyses have to be recalculated and this in itself could potentially produce a large error prior to temperature estimation, a magmatic $FeO/Fe_2O_3 = 0.85$ is assumed throughout these recalculations. Furthermore the measuring of the vanadium content of the oxides is

also prone to error due to the overlap of the V and Ti peaks on a wavelength dispersive spectrometer. In this case the overlap is considered to be up to 50 % on the V peak.

In summary, these thermometers are considered to give approximate temperatures for the eruption of the basalts and rhyolites, however the results are not conclusive in distinguishing within the rhyolite series temperature variations due to the paucity of appropriate data. The average basalt temperature is 1150 °C, while the rhyolites are range in temperature from 700 to 900 °C. These latter temperatures are consistent with the preservation of the textures described but further constraints are considered important in order to contribute to previous geochemical arguments for the origin of these rhyolites. Therefore accessory phase thermometry, which is widely applied to the intrusive equivalents of these rhyolites, was investigated.

3.9 Chemical evidence for accessory phase saturation.

The chemistry of the Uruguay basalts and rhyolites has been discussed in Chapter 2. However prior to calculating temperatures (primarily for the rhyolites), the behaviour of the Zr, P and the light rare earth elements (LREE) is discussed. The behaviour of these elements is primarily controlled by accessory minerals. Accessory phase thermometry is potentially of use in determining temperatures for these samples where the more conventional thermometers such as those already discussed fail to provide a clear estimate. However the potential problems contributed by halogens and inheritance must be considered. The amounts of fluorine and chlorine in these rocks is not known but the presence of either can result in considerable distortion of the aluminosilicate structure within the melt (Collins *et al.*, 1982). The resultant effect of high F relative to water in the volatile content on the melt structure, allows large cations, including Zr, Nb and REE, to enter the melt phase thereby increasing the solubility of zircon (White *et al.*, 1982). Inherited zircon is also potentially a problem.

Fig. 3.7 a, b & c. Essential structural constituents (ESC) behaviour , Zr - zircon; P_2O_5 - apatite; LREE - monazite. Open circles represent Aigüa Series rhyolites; Filled circles the Lascano rhyolite Series.

(a) and (b).

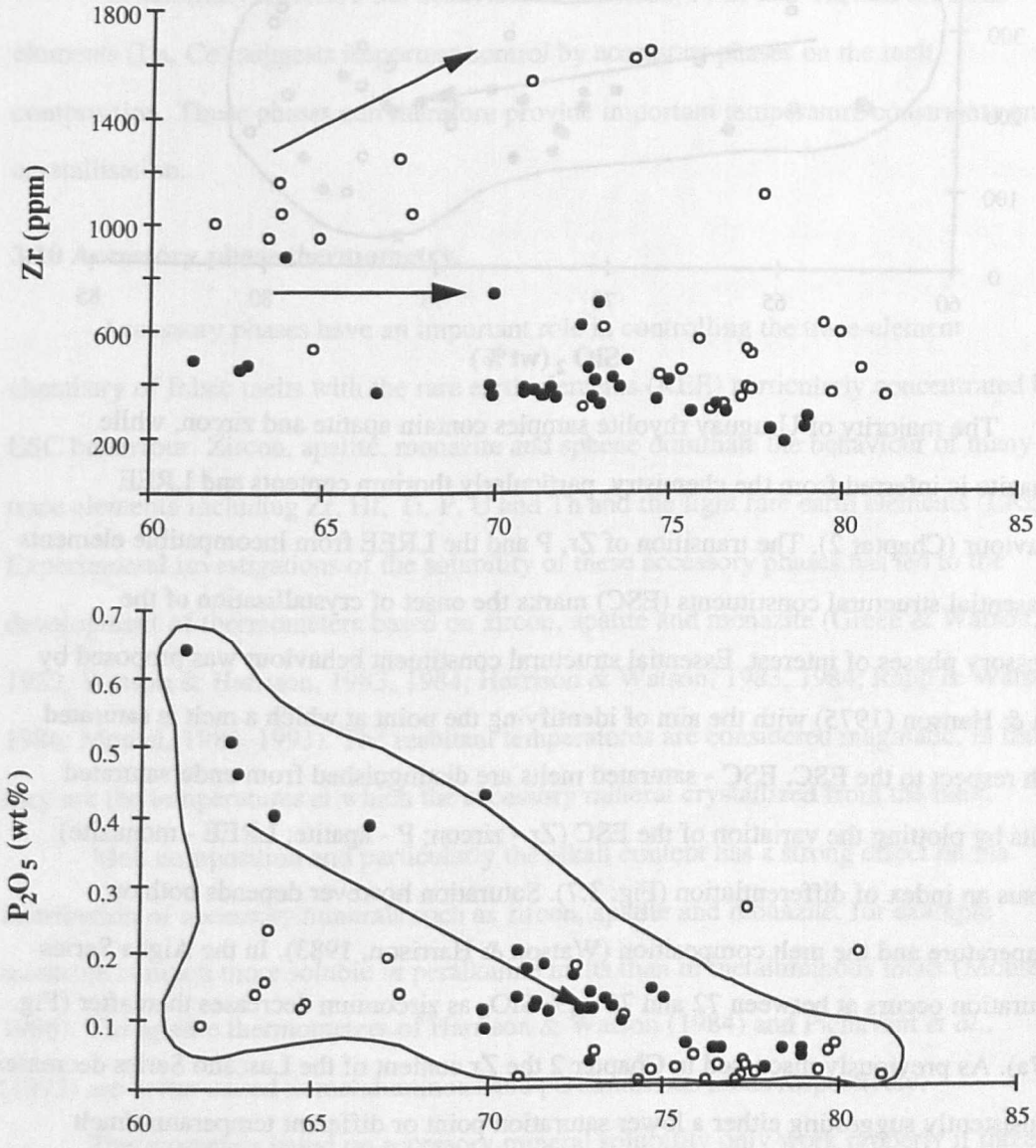

(c).

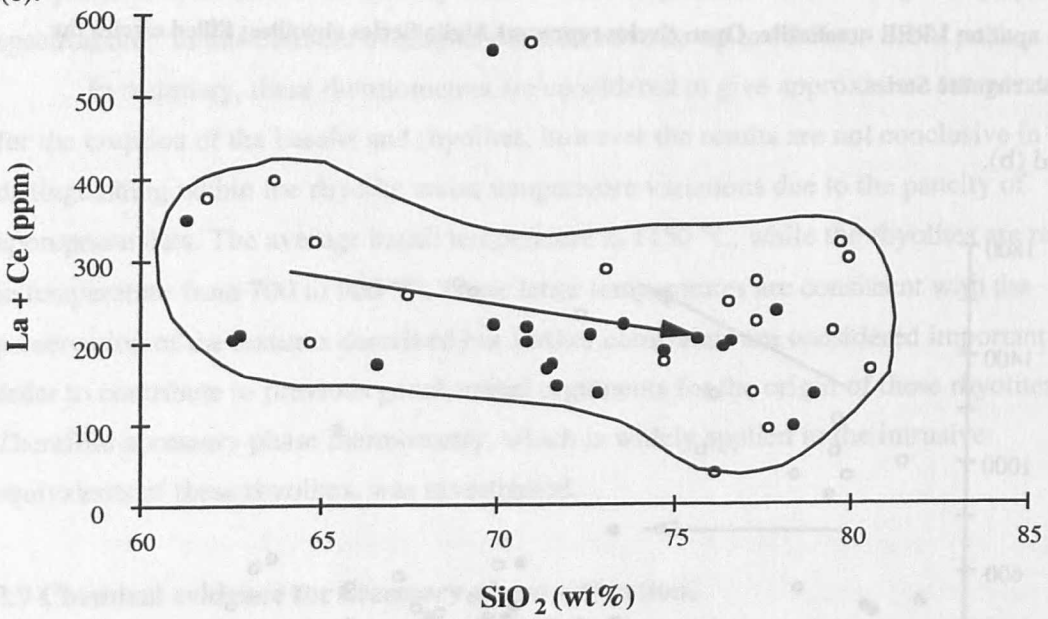

The majority of Uruguay rhyolite samples contain apatite and zircon, while monazite is inferred from the chemistry, particularly thorium contents and LREE behaviour (Chapter 2). The transition of Zr, P and the LREE from incompatible elements to essential structural constituents (ESC) marks the onset of crystallisation of the accessory phases of interest. Essential structural constituent behaviour was proposed by Sun & Hanson (1975) with the aim of identifying the point at which a melt is saturated with respect to the ESC. ESC - saturated melts are distinguished from undersaturated melts by plotting the variation of the ESC (Zr - zircon; P - apatite; LREE - monazite) versus an index of differentiation (Fig. 3.7). Saturation however depends both on temperature and the melt composition (Watson & Harrison, 1983). In the Aigüa Series saturation occurs at between 72 and 75 wt% SiO_2 as zirconium decreases thereafter (Fig. 3.7a). As previously discussed in Chapter 2 the Zr content of the Lascano Series decreases consistently suggesting either a lower saturation point or different temperature/melt composition of the parental magma. P_2O_5 depletion is considered to reflect apatite fractionation (Chapter 2).

All rhyolite samples are light rare-earth-element enriched relative to heavy REE, with just a couple of notable exceptions, namely 93L29, 93L39 and 93L87 of the Aigüa Series. Europium forms negative anomalies on chondrite normalised REE plots (Fig. 3.8), with the effects of plagioclase fractionation also being mirrored in the behaviour of Sr (Fig. 3.8). The affect is less extreme in quartz phyric samples from the Lascano Series

than from the Aigüa Series which was considered a source feature from previous discussion in Chapter 2. The behaviour of the LREE and Th in both rhyolite series appears to suggest control by monazite fractionation, however phenocrysts of monazite have not been recognised petrographically (Fig. 3.7c).

In summary therefore the behaviour of the trace, P, Zr and Th, and the LRE elements (La, Ce) suggests important control by accessory phases on the melt composition. These phases can therefore provide important temperature constraints on crystallisation.

3.10 Accessory phase thermometry.

Accessory phases have an important role in controlling the trace-element chemistry of felsic melts with the rare earth elements (REE) particularly concentrated by ESC behaviour. Zircon, apatite, monazite and sphene dominate the behaviour of many trace elements including Zr, Hf, Ti, P, U and Th and the light rare earth elements (LREE). Experimental investigations of the solubility of these accessory phases has led to the development of thermometers based on zircon, apatite and monazite (Green & Watson, 1982; Watson & Harrison, 1983, 1984; Harrison & Watson, 1983, 1984; Rapp & Watson, 1986; Montel, 1986, 1993). The resultant temperatures are considered magmatic, in that they are the temperatures at which the accessory mineral crystallized from the melt.

Melt composition and particularly the alkali content has a strong effect on the distribution of accessory minerals such as zircon, apatite and monazite, for example monazite is much more soluble in peralkaline melts than in metaluminous melts (Montel, 1986). The apatite thermometers of Harrison & Watson (1984) and Pichavant *et al.*, (1992) are better suited to metaluminous and peraluminous melts respectively.

Thermometers based on accessory mineral solubility only work properly if three main criteria are satisfied: (i) chemical equilibrium prevailed during crystallisation; (ii) the accessory mineral controls the behaviour of the element concerned; and (iii) the whole rock analyses represents a liquid composition (Montel, 1993). Bearing these difficulties in mind temperatures were calculated and compared with previous temperature determinations.

Fig. 3.8. Trace-element and rare-earth-element behaviour of selected Uruguay rhyolites indicating series variations. Normalising values for primitive mantle from Sun & McDonough (1989) and for REE of chondrites from Sun (1981).

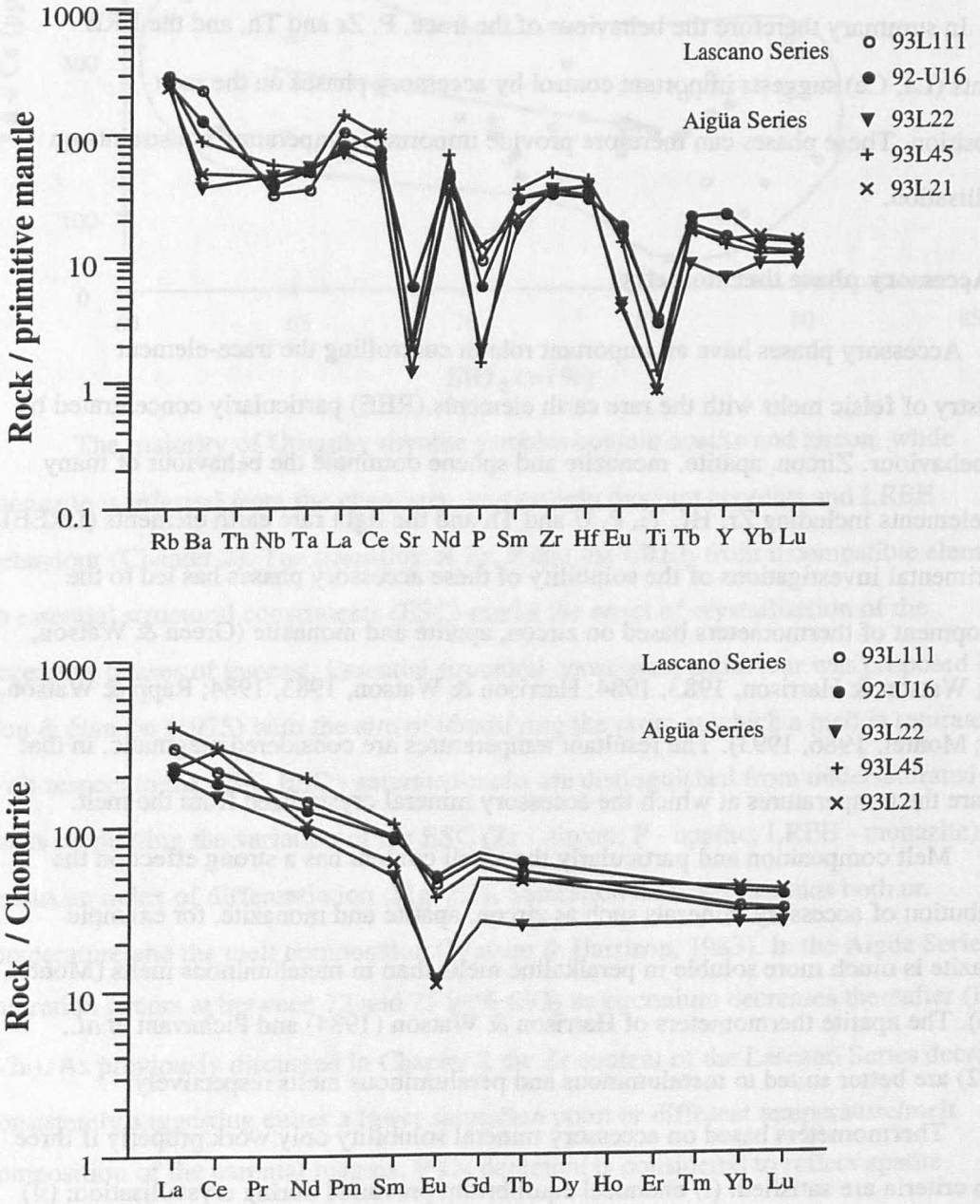

Zircon:

Zircon is a ubiquitous accessory phase in the high-silica rhyolites of southern Uruguay. Zircon saturation temperatures have therefore been calculated for the Uruguay rhyolite series. This thermometer is based on the investigations of Watson (1979, 1980);

Watson & Harrison (1983, 1984) and Harrison & Watson (1983, 1984) into zircon saturation, the kinetics of zircon dissolution and zirconium diffusion. The thermometer is valid for peraluminous and metaluminous melts and shows a strong dependence on magma alkalinity as estimated from the Na + K + 2Ca/(Si * Al) cation ratio (M factor in the equations of Harrison & Watson, 1983; Watson & Harrison, 1984). Zr is considered to act as an 'essential structural constituent' (ESC) for zircon as defined by Sun & Hanson (1975).

The temperature estimates obtained (Table 3.5) assume that the melts are saturated in zircon, which is of magmatic rather than restitic origin. The Uruguay samples have therefore been carefully selected and the results from those samples with Zr > 600 ppm in the Aigüa Series should be treated with caution. The experiments of Watson & Harrison (1983) on peraluminous and metaluminous glasses (SiO_2 59 to 76 wt%) were run at temperatures between 720 and 1020 °C and at pressures of 1.2 - 6.0 kbar which encompass the likely conditions of crystallisation of the Uruguay rhyolites. Low water contents (= 2 wt%) have important effects on the temperature estimates from this thermometer (Tucker Barrie, 1995), and so care is needed in the interpretation of results. The effect of residual zircon on the calculated T_{Zr}°C is discussed in the next section.

Table 3.5. Results of zircon thermometry. Classification system is as outlined in Chapter 2.

Classification	Sample	Classification	SiO_2 (wt%)	T (°C)	Zr (ppm)
Lascano Series	93L78	Metaluminous	61.2	829	491
Lascano Series	93L66	Metaluminous	62.5	825	459
Lascano Series	93L114	Peraluminous	70.7	861	372
Lascano Series	92U16	Peraluminous	71.3	854	362
Lascano Series	92U14	Peraluminous	76.5	854	304
Lascano Series	93L99	Peraluminous	76.3	865	327
Aigüa Series	93L86	Metaluminous	61.7	921	1008
Aigüa Series	93L70	Peraluminous	64.6	875	536
Aigüa Series	93L48	Peraluminous	67.4	956	1047
Aigüa Series	93L46	Peraluminous	73	920	620

The temperature variation evident from zircon saturation thermometry is within the range calculated from feldspar thermometry. This implies that the Zr concentrations primarily reflect magmatic zircon crystallisation. Results suggest however, that inherited zircon must be considered to have an affect particularly in samples from the Aigüa Series which tend to have elevated Zr concentrations, occasionally in excess of 1000 ppm. The affect of halogens and of water contents are also potentially important as noted above.

When the same zircon saturation thermometer of Watson & Harrison (1983) was applied to rhyolites of the Paraná province much lower temperatures of between 800 and 890 °C are calculated over a range in SiO_2 and Zr concentrations than from pyroxene and feldspar thermometers (Bellieni *et al.*, 1986; Garland *et al.*, 1995). This is considered to be possibly a function of halogen involvement where Zr is increased and Zr crystallisation has not occurred. The lower concentrations of Zr in the Paraná rhyolites as compared with the Uruguay rhyolites is also possibly related to varying concentrations of alkalis. Alkali excess favours the development of alkali-zircono-silicate complexes, increasing the Zr concentration in the melt (Collins *et al.*, 1982) but inhibiting the precipitation of zircon. In order to assess these results further apatite thermometry is examined as apatite is known to occur as an accessory mineral both in the Paraná rhyolites and in the rhyolites of southern Uruguay.

Apatite:

Uruguayan rhyolites are silica over-saturated and in terms of the parallel concept of alumina saturation may be considered peraluminous or metaluminous. This division is important specifically in terms of apatite thermometry. The solubility and dissolution kinetics of apatite in metaluminous and peralkaline felsic melts has been investigated by Harrison & Watson (1984). More recently Pichavant *et al.* (1992) looked at apatite solubility in peraluminous liquids. Combining the results of these two experiments, apatite saturation in felsic melts is shown to be dependent on temperature, SiO_2 content and on the ratio of Al/(Na+K+2Ca+Li) (A/CNK, molar). Pressure and water content of the melt are independent variables (Watson & Harrison, 1984; Pichavant *et al.*, 1992). The apatite thermometers are considered valid for rocks between 45 wt% and 75 wt% SiO_2, 0 - 10 % water and for a range of crustal pressures. Apatite phenocrysts are all

considered to be magmatic as for apatite to be restitic and hence xenocrystic the concentration of P_2O_5 in the melt should be greater than 1 wt% (Pichavant *et al.*, 1992).

A number of the low-SiO_2 rhyolites from both the Lascano and Aigüa Series are metaluminous (Table 3.5), and contain high concentrations of P_2O_5 (= 0.5 wt%), much higher than those considered by the Watson & Harrison (1984) thermometer. Therefore, in drawing any conclusions regarding temperature variation caution must be applied with particular attention to both the mineralogy and chemistry. Apatite dissolution experiments were used by Harrison & Watson (1984) to resolve the temperature dependence of apatite solubility and dissolution rate. The ability to calculate temperatures is an extension of that work. Apatite saturation is dependent on the amount of dissolved P_2O_5 in the melt that is in equilibrium with apatite, with the level of dissolved P_2O_5 for apatite saturation dependent on temperature and silica content of the melt (Harrison & Watson, 1984; Pichavant *et al.*, 1992). 42% of apatite is considered to be P_2O_5. P_2O_5* is therefore the P_2O_5 (wt%) concentration in the magma that is in equilibrium with apatite and is calculated assuming temperature constraints, therefore there is a inbuilt assumption in the temperature calculations.

The equations of both Watson & Harrison (1984) and Pichavant *et al.*, (1992) were used to calculate apatite saturation temperatures ($T(AP)^{HW}$ - Harrison & Watson; and $T(AP)^{PMR}$ - Pichavant *et al.* (Table 3.6)). Pressures are considered to be in the order of 1 to 2 kbar, while for the calculated P_2O_5 * a temperature of between 850 and 1000 °C was assumed for all Uruguay and Paraná samples. Variations in pressure expected in the crust are considered not to have significant affects on the results, while temperatures of crystallisation can range from 850 to 1500 °C (Harrison & Watson, 1984).

Paraná rhyolites contain apatite as an accessory phase in both the low-Ti Palmas group and in the high-Ti - Chapecó group. Apatite is more abundant in the high-Ti Chapecó group (Garland *et al.*, 1995). When data from both rhyolite groups were analysed using the two apatite thermometers discussed above the temperatures obtained using the Harrison & Watson (1984) thermometer were consistently similar to previously published temperatures using pyroxene and feldspar thermometers, ranging from 972 to 1010 °C. The thermometer of Pichavant *et al.* (1992) gave consistently lower and widely varying temperatures. The evidence from both studies therefore suggests that water

content could have an important effect on zircon temperatures, however as apatite solubility is insensitive to variations in water content, apatite thermometers are potentially more reliable.

Table 3.6. Apatite and monazite thermometry for the same samples as in Table 3.2.

Sample	*A/CNK	P_2O_5 (wt%)	$T(AP)^{HW}$ (°C)	$T(AP)^{PMR}$ (°C)	$T(M)^{RW}$ (°C)
93L78	0.64	0.64	1037	600	806
93L66	0.64	0.5	1018	576	761
93L86	0.89	0.95	807	518	852
93L70	0.98	0.12	865	805	829
93L114	0.93	0.13	942	658	
92U16	0.87	0.13	944	565	837
93L48	0.85	0.14	913	546	862
93L46	0.99	0.52	873	773	905
92U14	1.0	0.06	914	1736	880
93L99	1.08	0.06	913		887

*A/CNK = Al/(Na+K+2Ca) molar, $T(AP)^{HW}$, $T(AP)^{PMR}$, $T(M)^{RW}$ are the temperatures calculated using the formula of Harrison & Watson (1983); Pichavant *et al.*, (1992) and Montel (1993) respectively. Montel (1993) is based on monazite saturation, while Harrison & Watson (1983) and Pichavant *et al.*, (1992) are based on apatite solubility.

Monazite:

Monazite is a rare-earth phosphate that incorporates Ce in its crystal structure, and also variable amounts of Th (2 - 30 %) and U (Rapp & Watson, 1986). Crystallisation of monazite is proposed as a possible cause of the LREE variation seen within the Uruguay rhyolites. The solubility of monazite is most affected by water content, temperature and as mentioned previously the melt composition; pressure has little effect (Rapp & Watson, 1986; Montel, 1993). Equation (1) of Montel (1993), was used to calculate the temperatures in Table 6, X_{REEPO_4} the sum of the mole fractions of REE phosphates is assigned the value of 0.83, an average for peraluminous granites. Calibration of this thermometer is considered valid for both peraluminous and peralkaline melts, provided that the compositions are Ca -, Fe - and Mg - poor. Ca is known to destabilise monazite to allanite, thus Ca-rich assemblages are considered to have > 1.8 wt% CaO, and Ca-poor

assemblages <0.7 wt% CaO (Rapp & Watson, 1986). CaO (wt%) varies within the rhyolite series with only the quartz-bearing assemblages of the Lascano and Aigüa Series considered Ca - poor, ranging from 0.03 to 1.5 wt%.

The monazite thermometer also utilises the concept of ESCs which for monazite are the LREE as a group and P. The other common associated elements, Th, Ca, Si, are either in abundance or are not essential for monazite to be present. Monazite temperatures were calculated using the Rapp & Watson (1986) thermometer and show a similar variation in temperature from 800 to 950 °C, as does the zircon saturation thermometer of Watson & Harrison (1983). These temperatures are similar to those calculated from apatite thermometry, although the apatite thermometer is more applicable to a greater number of samples at which extreme temperatures in the region of 1000 °C are calculated.

3.11 H_2O content and viscosity.

The presence of water in a melt system has a direct effect on the crystallisation sequence, water also tends to depress liquidus temperatures. A drop in pressure as a water-saturated acid magma approaches the surface results in devolatisation and crystallisation, hence constraining the amount of water in the system, can aid the understanding of the crystallisation history of the system. Water is also a primary control on the solubility of a number of silicates including zircon. The eruption mechanism of rhyolitic magmas is also strongly controlled by the water content and viscosity of the melt with welding of hot pumice fragments to form an ignimbrite controlled by glass viscosity in addition to the lithostatic load (Cas & Wright, 1988).

The phenocryst assemblage is anhydrous in the basalts suggesting low volatile contents, and this is further supported via the presence of olivine, which is suppressed in water-present conditions in favour of orthopyroxene (McCarthy & Patiço, 1997). However up to 3-4 wt% H_2O can be accommodated in a melt before amphibole forms (Green & Ringwood, 1967; Sturn & Wyllie, 1978).

The lack of primary hydrous phases in the Uruguay rhyolites suggests a low water content, < 4 wt% for the rhyolitic magma. The presence of quartz in the more evolved lithologies constrains the water content to between 2 and 4 wt% according to the

experiments of Clemens *et al.*, (1986). Further estimates of water content were made using the equations of Housh & Luhr (1991), which are based on the exchange of Ca and Na between plagioclase and the melt. Using plagioclase compositions from microprobe analyses and assuming a temperature of 900 °C, values of ~ 3 wt% were calculated.

Water solubility decreases with pressure at P = 3 kbar (Holtz *et al.*, 1996). Temperature and composition have important effects on the pressure at which water solubility is constant. This pressure is 5 kbar for Ab melts, close to 2 kbar for Or melts and between 1.5 and 2.5 kbar for pure silica melts (Paillet *et al.*, 1992; Holtz *et al.*, 1996). Normative calculations for Q, Ab and Or components of the high silica Uruguay rhyolites suggest that they formed at low pressures. Water content also has a direct effect on viscosity with an increase in water content resulting in a decrease in viscosity (Carmichael *et al.*, 1974; Clemens, 1984).

The viscosity of the melt was estimated from Holtz *et al.*, (1996) with values of log η (poise) of between 6 and 7, using Shaw (1972) curves, and between 6.5 and 7.5 using Scaillet *et al.*, (1996), assuming a water content of 3 wt% and a temperature of between 800 °C and 900 °C. Rhyolites and ignimbrites commonly have viscosities between 10 and 1000 poise (Sparks, 1976; Cas & Wright, 1988). Using the iron oxide geothermometer / geobarometer of Ghiorso & Seck (1991) the oxygen fugacity of the system was estimated. Results suggest the log $f\ O_2$ is between -15 and -13. This is consistent with a range in temperature of 800 °C - to 950 °C between the quartz - magnetite - fayalite (Q.M.F) and hematite - magnetite (H-M) buffers.

3.12 Discussion.

3.12.1 Temperature Results.

Calculation of accurate temperatures for the Uruguay rhyolites has proved to be a difficult task due to the evidence for disequilibrium between co-existing phenocrysts and between phenocrysts and the melt. Accessory phase thermometers including the apatite thermometers of Harrison & Watson (1984) and Pichavant *et al.* (1992) give widely varying results with up to 300 °C difference in the temperatures obtained for the same

sample using these two thermometers. The thermometer of Pichavant *et al.* (1992) gives consistently lower values for the peraluminous rocks for which it was calibrated. This may reflect late stage P-rich fluids as the thermometer is very sensitive to water contents.

Monazite temperatures are remarkably similar (± 35 °C) to those calculated from zircon thermometry, apart from those samples with excess zirconium. Temperatures calculated from zircon-saturation thermometry are considered sensitive to water contents however, and potentially underestimate the true temperature as appears to be the case with the Paraná rhyolites, where temperatures are up to 200 °C cooler than estimated from other thermometers including pyroxene, feldspar and apatite (Bellieni *et al.*, 1986; Garland *et al.*, 1995).

Table 3.7. Summary of intensive parameters determined for each of the main rock types. Rhyolite subgroups are largely indistinguishable from each other on the basis of temperatures obtained. Paraná temperatures from Bellieni *et al.* (1986); Whittingham (1991) and Garland *et al* (1995); water contents from Garland *et al* (1995).

Rock type	**Basalts**	**Lascano Series**		**Aigüa Series**		**Chapecó**	**Palmas**
Sub-group		**Trachy-dacite**	**Rhyolite**	**Trachy-dacite**	**Rhyolite**	**Rhyolite**	
Temp. (°C)	1150-1250	900 - 1000	850 - 950	850 - 950	800 - 900	1000 - 1100	950 - 1050
P (kbar)	< 10	1 - 3	1 - 3	1 - 3	1 - 3		
H_2O (wt%)	0 - 0.04	2 - 4	2 - 4	2 - 4	2 - 4	2 - 3	2

Temperatures from southern Uruguay are in general lower than those calculated for the Paraná rhyolites independent of most thermometers apart from zircon thermometry which results in similar temperatures. These lower temperatures from zircon thermometry as discussed above are considered to be affected by water contents and possibly halogens and are not true magmatic temperatures. Trachydacites of the Lascano Series yield the highest temperatures from apatite thermometry while the rhyolites are indistinguishable from the Aigüa Series on all thermometers, with temperatures in the region of 850 ± 100

°C. Elevated temperatures within the Aigüa Series on the use of zircon saturation thermometry were attributed to the affects of the inheritance of zircon.

Fig. 3.9. Eruption models for Uruguay rhyolites. (a) Classic ignimbrite forming eruption with relatively small column length. (b) Cartoon of events leading to the formation of the Uruguay rhyolites.

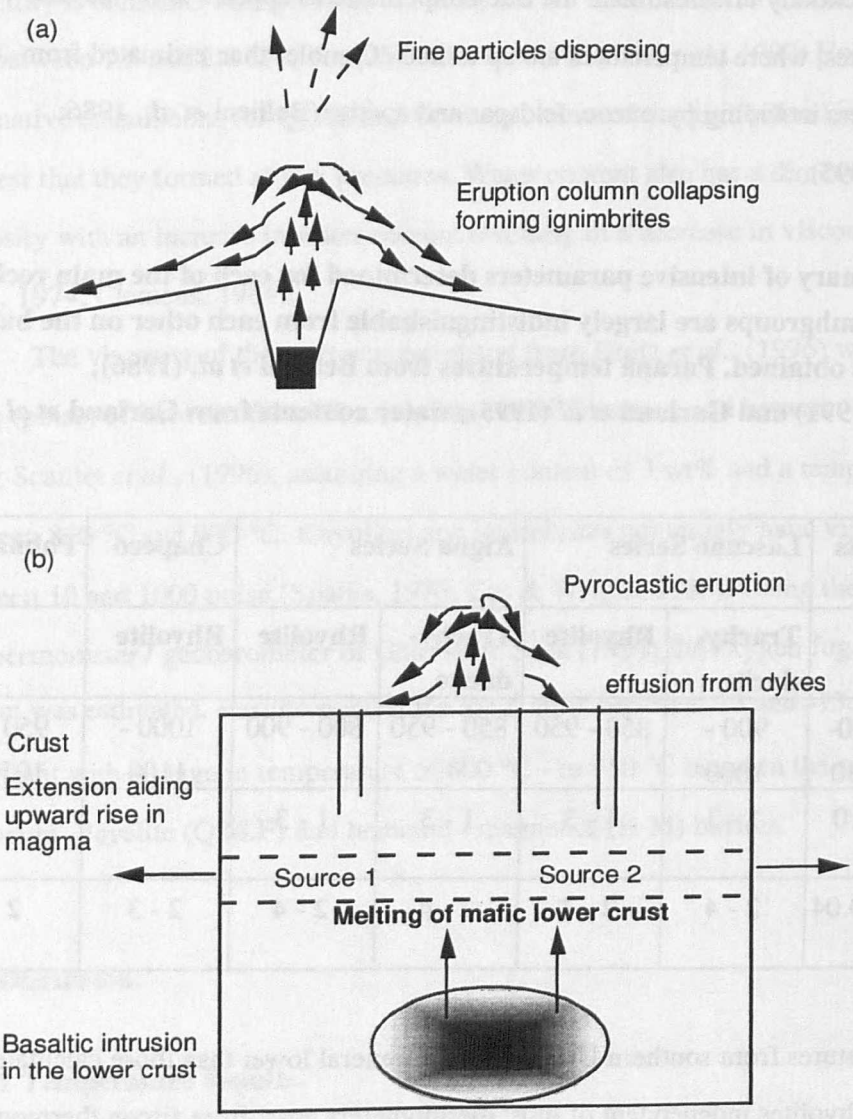

The temperatures calculated for both the Lascano Series and Aigüa Series rhyolites are consistent with the model proposed for the origin of these rhyolites of melting of mafic lower crust in Chapter 2. The temperature range for partial melting of mafic amphibolites in the deep crust under fluid-absent conditions is between 850 and

1000 °C (Rushmer, 1991). The amount of hydrate present in the rock, the feldspar/quartz ratio and the melt water content are the dominant controls on the amount of melt produced, with compositions of high silica and/or alkali contents melt at lower temperatures (Rushmer, 1991).

3.12.2 Mode of Eruption.

Temperature estimates from a number of different geothermometers appear to indicate that the Uruguay rhyolites were erupted at lower temperatures than the geographically adjacent rhyolites of the Paraná - Etendeka (Table 3.7). An extensive trans-Atlantic comparison of the eruptive sequences of the Paraná - Etendeka rhyolites was described by Milner *et al.* (1995). The Etendeka province has been divided into high and low-Ti/Zr units similar to the divisions in the Paraná, the high-Ti/Zr units are termed the Sarusas quartz latites and are mainly located north of the main Etendeka lava field. The low-Ti/Zr group is subdivided into a number of successions including the Tafelberg, Springbok, Coastal and Goboboseb. The Tafelberg Formation disconformably overlies the Awahab Formation, which is considered to have been erupted from the Messum complex (Milner & Ewart, 1989). The site of eruption of the Tafelberg Formation is not known. The Etendeka rhyolites are high temperature (1000 - 1100 °C) rheoignimbrites, with localised development of pyroclastic textures (Milner *et al.*, 1992). The basal Awahab Formation which includes the Goboboseb and Springbok members was compared favourably with the lower most units of the Palmas rhyolites of the southern Paraná using a variety of geochemical and petrological critera, including rare occurrences of pyroclastic textures at the margins of flows which in general tend to be rewelded due to very high eruption temperatures (Milner *et al.*, 1995). The upper Palmas flows were also correlated with part of the Tafelberg Formation in the Etendeka.

The mode of eruption and emplacement of such high-temperature rhyolites as these is controversial particularly when associated with continental hotspot tracks (Honjo *et al.*, 1992; Manley, 1995). The possibility of emplacement by effusion with sufficiently low viscosities, as potentially lowered by halides and/or water content (Holtz & Johannes, 1994), is considered a viable alternative in sourcing some of the large silicic lavas such as those of the Paraná, instead of the more traditional interpretation of secondary viscous

flow as rheomorphism (Garland *et al.*, 1995). The lack of caldera structures, the high eruption temperatures and sparsity of textural evidence reinforces this idea, particularly for the high-Ti Chapecó rhyolites which show scant evidence of being fully vitrified and have clear, well preserved, unfractured phenocrysts implying little explosive activity (Garland *et al.*, 1995). Acid dykes of Chapecó composition have also been recognised from the Ponta Grossa region (Regelous, 1993). Similar arguments were proposed for the Owyhee Plateau in south-western Idaho by Manley (1995) with low water contents cited as an important factor in preventing a large pyroclastic eruption.

The development of the ignimbritic textures previously described from the Uruguay rhyolites suggests that at least some of these rhyolites are associated with pyroclastic activity. No caldera structure has however been recognised in the region, and due to the distinctive chemistry of these rhyolites when compared with those of the Paraná - Etendeka province it is unlikely that they were sourced in the Messum complex. The source has therefore not yet been identified due perhaps to Mesozoic/Cenozoic erosion combined with the present day sedimentary cover, or was located closer to the final rift and is now located off-shore.

Those rhyolites that lack eutaxitic textures are considered to be silicic lavas, due to a number of features typical of felsic lavas including trachytic alignment, flow banding and flow folding. Passive effusion of silicic lava via acid dykes is considered to have occurred contemporaneously with the main explosive event as all the rhyolites are considered to have been erupted in a similar timespan (Chapter 4). Figure 3.10 is a cartoon model of proposed eruptive history of the Uruguay rhyolites, beginning with the intrusion of a large volume of hot mafic material in the lower crust. The resultant lower crustal melt has an andesitic composition and is characterised by low εNd_i and $^{87}Sr/^{86}Sr_i$ values.

The Lascano Series and the Aigüa Series rhyolites are considered to originate from separate sources, with the parental magma to the Lascano Series distinguished by low Ti/Zr, lower Nb and Zr and higher Sr and Eu/Eu* from that of the Aigüa Series. The andesitic magma generated by melting the source of the Lascano rhyolites undergoes fractionation and assimilates upper crustal material (e.g. Cascata leucogranite of the Pelotas batholith (May, 1990), Chapter 2) en route to the surface, with the ultimate

extrusion of this magma aided by increased extensional forces associated with the incipient opening of the South Atlantic (Chapter 4). The Aigüa Series is considered to originate from a slightly different source in the lower crust possibly more reducing (Chapter 2) which is similarly fractionated to the Lascano Series (~ 50%) but there is no evident of upper crust having been assimilated. The extensional forces invoked would also allow for the passive effusion of felsic lavas from dykes, which trend parallel to the main rift and, for drop in pressure and rapid release of volatiles associated with pyroclastic eruptions.

3.13 Conclusions.

The best temperature estimates are from the accessory phases particularly the apatite thermometer Harrison & Watson (1984). Zircon saturation thermometry (Watson and Harrison, 1983) and monazite saturation thermometry (Rapp and Watson, 1986) are in good agreement with each other however the low results calculated for the Paraná rhyolites appears to indicate that these thermometers are highly sensitive to water contents. Therefore using an overall average temperature calculated for each sample the apparent magmatic temperatures are between 800 °C and 950 °C, at least 100 °C cooler than the temperatures calculated for the Paraná - Etendeka (Bellieni *et al.*, 1986; Milner *et al.*, 1992; Garland *et al.*, 1995). Distinction of temperature control of the individual series was however impossible due a lack of suitable data. The overall data do however suggest that some of the rhyolites were erupted as lava flows with high gas contents, as indicated by the vesiculated nature of some samples and are not simply rheoignimbrites. Average water contents of between 2 and 4 wt% were calculated however there is no constraint on CO_2 or other gaseous contents of the magmas. The water solubility model for felsic magmas (Burnham, 1979) suggests that vapour saturation would occur at crustal depths of 1 - 4 km if unimpeded during ascent. The temperatures are consistent with an origin for the rhyolites in melting mafic lower crust as proposed Chapter 2, with the presence of the Tristan da Cunha plume initially generating the temperatures required for melting within

the lower crust following advection of heat from the emplacement of a large volume of mafic material.

The presence of a large positive gravity anomaly underlying the region of interest which defines a crude oblong shape 100 km long and assuming a density contrast of 200 kg/m^3 effective over 15 km of crustal thickness with a width of 23 km. Advection of heat by magma responsible for such a body of material would be a sufficient source to melt the lower crust. Extension leading to the opening of the South Atlantic is considered to have aided the upward migration and ultimate explosive eruption of the magma by decreasing pressures and allowing expansion of the volatiles. In addition this relationship to the opening of the South Atlantic is reinforced as shall be evident in Chapter 4 by the timing of eruption of the Uruguay rhyolites which is synchronous with increased stretching in this region.

Chapter 4.

Early Rifting of the South Atlantic, Paraná - Etendeka magmatism and sediment interactions.

4.1 Introduction.

Continental Flood Basalts (CFB) contribute significantly to the generation of new continental crust and are often linked with continental rifting and break-up (White & McKenzie, 1989). Links between CFB magmatism and rifting are both variable and difficult to ascertain. Nonetheless, information regarding the timing and duration of magmatism in the Paraná - Etendeka CFB province, and of the dyke intrusions along the margins of the African and South American continents provides useful constraints on the amount and orientation of extension with time. This extension, which ultimately resulted in the opening of the South Atlantic and the separation of Africa and South America, was responsible for the formation of hydrocarbon-bearing sedimentary basins and the generation of the associated magmatic rocks. In principle, melt generation rates inferred from estimated eruption rates and amounts of extension can be used to evaluate the role of the mantle plume, and hence the likely effect on the thermal gradients through sedimentary basins. In extreme cases rapid eruption rates and short durations of magmatism can only be accounted for by rapid decompression of a mantle plume. Slower rates of eruption allow for the possibility of melt generation in the sub-continental lithospheric mantle in response to the conduction of heat from a mantle plume.

This chapter presents new Ar-Ar ages on Paraná - Etendeka basalts and rhyolites from a section in southern Uruguay, and on selected dykes from southern Africa. These are combined with published ages on the lavas and dykes associated with the opening of the South Atlantic in a review of the timing, erupted volumes and dyke orientations in both South America and southern Africa. Other data which are considered include

palaeomagnetic results on the Paraná - Etendeka lavas which further constrain the duration of magmatism, and the relationship between sediment deposition, magmatism and rifting. Finally the changing tectonic stress regimes, as indicated by dyke swarms of different orientations, are discussed and related to the 3-D chemical stratigraphy of the Paraná lavas that is available through the use of borehole material and surface mapping.

Age constraints.

Age determinations for CFB provinces have become progressively more accurate and precise with the development of $^{40}Ar/^{39}Ar$ dating techniques, and a number of studies have been undertaken on the Paraná - Etendeka (Hawkesworth *et al.*, 1992; Renne *et al.*, 1992; 1996b; Turner *et al.*, 1994; Stewart *et al.*, 1996). Nonetheless, different approaches have been applied and in particular the age range of the Paraná - Etendeka CFB province remains contentious. A review of previous K-Ar and $^{40}Ar/^{39}Ar$ dates is given prior to introducing new age dates for mafic and silicic lavas in Southern Uruguay, and along the South Atlantic margin. The lavas in Southern Uruguay have close genetic and evolutionary ties with the main Paraná - Etendeka CFB and the main volume of mafic lava, Treinte Y Trés magma type in southern Uruguay is chemically similar to the low-Ti Gramado magma type of southern Brazil (Chapter 2). The rhyolites of Southern Uruguay are however, mineralogically and chemically different from those of the Paraná - Etendeka, and they also appear to differ in age.

The calculated eruption rates of continental flood basalt (CFB) provinces are highly variable with magmatic activity spanning from one to a 10's of millions of years. CFB such as those in the Deccan province are thought to have been erupted rapidly, with ~10^6 km^3 of basalt erupted in less than 4 Ma, and the principal activity lasting 1 to 2 Ma (Courtillot *et al.*, 1986; Duncan & Pyle, 1988). The average eruption rate for the Deccan Traps is therefore 1.5 km^3/year (Richards *et al.*, 1989), and this is similar to the rates proposed for oceanic plateau such as Ontong Java and Kerguelen (Heimann *et al.*, 1994). The age range in the Paraná - Etendeka CFB is more controversial and there is some evidence that magmatism persisted for longer than in the Deccan (Bellieni *et al.*, 1984; Renne *et al.*, 1992; 1996; 1996b; Turner *et al.*, 1994; Stewart *et al.*, 1996). The debate centres around the duration of magmatism before and after the principal eruptive phase

which is dated at between 130 and 134 Ma. Renne *et al.*, (1992) proposed that eruption of the entire province occurred in 1-2 my, but there are data from other studies which suggest that magmatism lasted for up to 10 my and that the rate of magmatism increased with time and the proximity of the South Atlantic rift system (Turner *et al.*, 1994; Stewart *et al.*, 1996).

The rate of magma production was calculated from estimates of the erupted volumes of lavas of different ages using both surface and borehole data in the Paraná province by Stewart *et al.* (1996). The volume of each of the different magma types of the Paraná was combined with the duration of each magma type estimated from the range of $^{40}Ar/^{39}Ar$ ages and the resultant eruption rates were in the range of 0.03 $km^3\ yr^{-1}$ from 138 to 135 Ma, they increased to 0.21 $km^3\ yr^{-1}$ from 133 to 131 Ma, and then decreased from 131 Ma until the point of generation of ocean crust at ~127 Ma.

Mantle plumes.

The association of large igneous provinces with present day hot spots together with their anomalous occurrence and large volumes has been used to invoke plume involvement in the generation of CFB (Morgan, 1983; Richards *et al.*, 1989). Melting occurs in response to the emplacement of the mantle plume, but in some models it is envisaged that the mantle plumes are responsible for regional uplift and extension (Hill, 1990; Sleep, 1990), while in other models (White & McKenzie, 1989) CFB are generated in response to extension over areas of anomalously high mantle temperatures. The nature of the association between CFB and mantle plumes is therefore a matter of debate, both over whether melting is triggered by extension or the emplacement of a mantle plume, and whether melt generation necessarily occurs within the mantle plume (*e.g.* Hawkesworth & Gallagher, 1993). Melting in the sub-continental lithospheric mantle has been one of the more controversial proposals (DePaolo & Wasserburg, 1979) which has been invoked in order to explain the variation in the chemical signature of the CFB, the thermal feasibility of which has been modelled by Gallagher & Hawkesworth (1992). The model requires a relatively long period of incubation (~10 - 15 Ma) in order to generate the large quantities of basalt involved in CFB provinces (Turner *et al.*, 1996).

Mantle plumes ascending from depth are hotter than the ambient mantle. They will therefore intersect the solidus at greater depths, and so more melt is generated for a given amount of extension (McKenzie & Bickle, 1988). The amount of extension affects the thickness of the lithosphere, and so the greater the β (stretching) factor the thinner the lithosphere and the greater the amount of melt which will be derived from the asthenosphere (McKenzie & Bickle, 1988). In principle the amount and orientation of the extension direction can be estimated from the numerous dyke swarms. Thus constraints can be placed on the value of β at different times leading up to continental separation, and once the first magnetic lineament is developed on the ocean floor, β is inferred to be infinite.

In the case of Gondwana it is often difficult to establish the roles of mantle plumes in continental break-up, but in practice changes in plate boundary forces are often invoked as the prime reasons for rifting (e.g. Storey, 1995). Nonetheless, hotspot activity is known to have occurred in the area of the South Atlantic as a number of current hotspots can be retraced to positions in the Jurassic and Cretaceous, and these include those presently beneath Tristan da Cunha and St. Hélena. A link between the two models for continental break-up and melt generation rates might potentially provide the key to understanding the dynamics of the evolution of the South Atlantic.

Sediments & Magmatism.

The interaction of rift related sediments with large scale CFB magmatism has implications for the thermal history and possible maturation of hydrocarbon source rocks. The affect of magmatism on sediments may be considered both locally and regionally. Regionally, the extensional processes may generate basins within which sediments accumulate, or they may fracture pre-existing reservoirs. Hydrocarbon generation and migration may be affected by the impingement of a mantle plume both in terms of regional uplift altering the sedimentation record and thermally with increased geothermal gradients perhaps over distances of > 1000 km. The effect of underplating, which is assumed to be at least equal to the surface expression of the lavas (Cox, 1993), on the local sedimentary sequence is also briefly assessed. Locally, the advection of heat from rising magmas within the rift basins, the extrusion of these lavas on the surface and the high level intrusion of

dykes and sills will modify the primary characteristics of the sediments and possibly the hydrocarbon potential.

In summary, this chapter briefly introduces the magmas of the Paraná - Etendeka province and links the chemistry of these lavas to the main intrusive dyke swarms. The orientations of these dykes, which act as feeder systems to the main CFB, are then used to assess the amount and orientation of extension during the generation of different magma types, which also have different erupted volumes. The timing and duration of magmatism is then assessed through detailed Ar-Ar dating of the lavas and dykes in order to evaluate the timing and amounts of extension leading up to continental separation.

4.2. The Paraná - Etendeka Province.

The Paraná - Etendeka province is linked to the Tristan da Cunha plume via the hot spot traces of the Rio Grande Rise and the Walvis Ridge respectively. The Paraná basin was formed during active rifting in the Ordovician to Silurian (Zalan *et al.*, 1987) with progressive sedimentation from the Devonian to the Jurassic. The voluminous extrusion of the Paraná - Etendeka CFB province during the Early Cretaceous occurred directly on continental aeolian sandstones and locally on to the underlying basement.

The areal and volumetric extent of the province is highly asymmetric with most of the outcrop preserved in the Paraná basin, on the South American continent. The Paraná CFB is a sequence of 790,000 km^3 of primarily mafic material that outcrops principally in Brazil but also extends into northern Uruguay, Paraguay and Argentina. Paraná magmatism is dominated by tholeiitic basalts and basaltic andesites with volumetrically less significant rhyolites (~ 5 %) at the top of the sequence particularly close to the coast in SE Brazil. The preserved thickness of the basaltic sequence is variable with a maximum of 1723 m recorded in a borehole in the north of the basin. The basalts were initially divided into high- and low-Ti provinces (Bellieni *et al.*, 1984; Mantovani *et al.*, 1985) similar to those subsequently described by Hergt *et al.* (1991) using Ti/Y ratios for the classification of other Gondwana flood basalts. Peate *et al.* (1990; 1992) expanded the initial classification of the Paraná basalts into six basaltic magma types. The four high-Ti/Y magma types of the Pitanga, Paranapanema, Urubici and Ribeira outcrop in the

north and central parts of the basin, while the two low-Ti/Y (< 310) Gramado and Esmeralda magma types occur in the south of the basin. These magma types have been used to investigate the internal structure of the Paraná lava pile by Peate *et al.* (1992).

The Etendeka province stretches from Angola into Namibia covering an area of 78,000 km^2. Rhyolites (locally known as quartz latites) form over 50% of the preserved outcrop, in sharp contrast to the Paraná. The rhyolites of the Awahab and lowest Tafelberg units of the Etendeka have been correlated with the Palmas rhyolites of the Paraná, and it has been argued that they were all erupted from the Messum volcanic centre in Namibia (Milner & Ewart, 1989; Milner *et al.*, 1995).

4.3. Dykes and dyke orientations.

Intrusive activity associated with the main Paraná - Etendeka CFB province includes extensive dyke and sill provinces both in South America and Africa (Fig. 4.1). Sills varying in thickness from 2 to 200 m have been described interleaved with Palaeozoic sediments from the Paraná basin, and in the northern part of the basin these sills have a combined thickness of over 1000 m (Bellieni *et al.*, 1984). Such dykes and sills are chemically similar to, and are therefore inferred to have acted as feeders to the lavas of the Paraná - Etendeka CFB province (Bellieni *et al.*, 1984; Peate *et al.*, 1992; Regelous, 1993). North of 26 °S the compositions are similar to the Pitanga and Paranapanema magma types, whereas further south the dykes and sills have a different orientation and are similar to the Gramado magma type (Peate *et al.*, 1992).

There are two main dyke orientations associated with Paraná - Etendeka magmatism. The first is coast perpendicular, mainly NW-SE trending, in the Ponta Grossa dyke swarm in Paraná State, northeastern Brazil and in Eastern Paraguay (Fig. 4.1). This dyke swarm is associated with the Ponta Grossa Arch and represents limited extension (10 %) along zones of crustal arching (Sial *et al.*, 1985). The dykes typically dip vertically and are seen to intrude Precambrian crystalline basement, Palaeozoic sediments and locally the overlying volcanics (Comin - Chiarmonti *et al.*, 1983). Their compositions are similar to the more northerly magma types of the Pitanga and the Paranapanema, and so the age range of those magma types is taken to reflect the duration of the extensional regime responsible for the NW-SE trending dykes (Regelous, 1993).

Fig. 4.1(a) Paraná province with two distinct dyke orientations after Riccardi, (1988); Peate *et al.*, (1992); Regelous (1993).

Dykes of a different orientation which roughly parallel the coast line and also the regional structural lineaments in the underlying basement occur along the Serra do Mar between Florianopolis and at Rio de Janeiro (Fig. 4.1a). Moreover, this was the principal dyke orientation in Namibia associated with the Etendeka CFB, where dykes are more readily visible because of the thin soils and sparse vegetation (Fig. 4.1b). These dykes are subvertical to vertical, are of variable size and they intrude the local basement, the Karoo sedimentary sequence and the overlying basalts. In detail, coastal dyke swarms are well preserved along the north Namibia coast in pre-Karoo basement from the Kuiseb River north to the Huab River, and further south in the Cape Peninsula (Marsh *et al.*, 1991; Reid & Rex, 1994). Figure 4.1c illustrates a particular area of the Cape Province, near Cape Town, South Africa from where two dykes of the False Bay dolerite dyke swarm were dated.

In a recent study Lord *et al.* (1996) compiled a dyke lineament map of the Central Zone of the Damara Orogen in Namibia from Landsat imagery. 413 linear dykes were identified with a dominant NNE-SSW trend (Fig. 4.1d), roughly parallel to the plate margin during the Early Cretaceous.

(b)

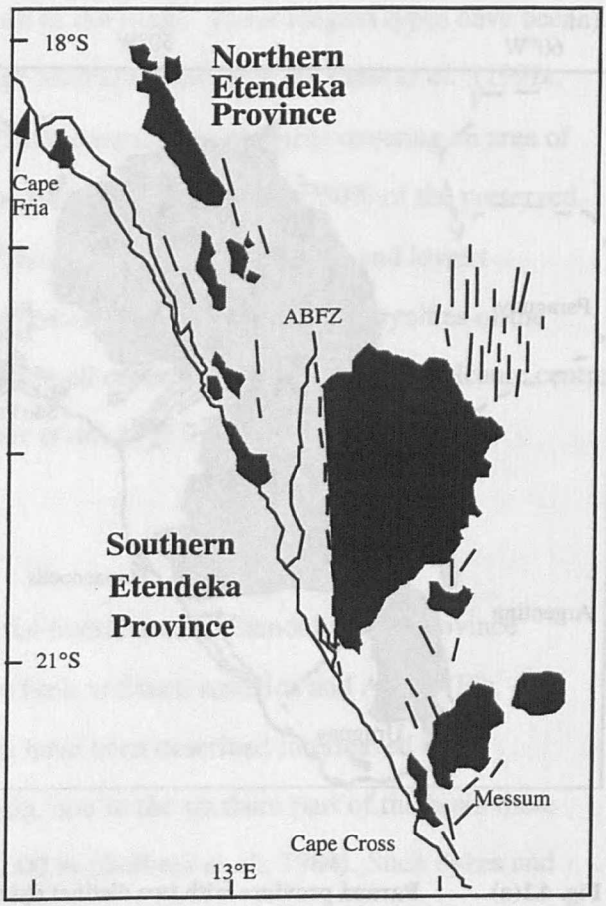

Fig. 4.1(b) Etendeka province with coast parallel dyke swarms after Milner *et al.*, (1992).

Chemically, the coast parallel dykes in Brazil and Namibia typically have compositions similar to the low-Ti/Y magma types of the Gramado and the Tafelberg respectively (Erlank *et al.*, 1984; Bellieni *et al.*, 1984; Milner & Duncan, 1987; Peate *et al.*, 1990; Regelous, 1993). Thus, it is again inferred that the range in the ages of both the intrusive and erupted rocks of those magma types reflects the timing of the extension responsible for the coast-parallel dykes. In addition, there is also a group of MORB-like, Horingbaai dykes which intrude basement rocks and the overlying Etendeka lavas in the coastal region from Cape Cross to the Huab River, and these are compositionally distinct from the known Etendeka lavas (Erlank *et al.*, 1984; Duncan *et al.*, 1990). The Huab sill complex which underlies the southern part of the main Etendeka lava pile consists of another three magma types geochemically distinct from the Tafelberg-type basalts (Duncan *et al.*, 1989).

Fig. 4.1(c). Cape Province and False Bay dykes associated with the opening of the South Atlantic (after Lord et al., 1996).

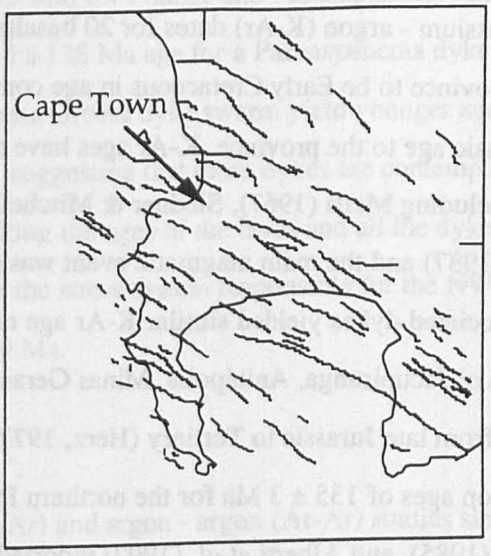

In southern Uruguay the dominant fault direction and dyke orientation is approximately coast parallel, but the principal NE strike direction of the faults appears to be basement controlled (Gierloff-Emden *et al.*, 1984). Dyke samples were collected from a number of localities on the coast stretching from Piriapolis, east of Montevideo (Fig. 4.1a) and these also strike NNE to ENE. Compositionally the mafic dykes are similar to the Santa Lucía magma type of southern Uruguay (Appendix A) with high Nb (18 - 25 ppm) and Ti/Y (262 - 296). The acidic dykes range in SiO_2 from 66 to 74 wt% and are chemically similar to the Aigüa series rhyolites with high Zr and Nb and low-Ti (Appendix A). The age of these dykes is however controversial as they are mapped by the U.G.S. as Cambrian.

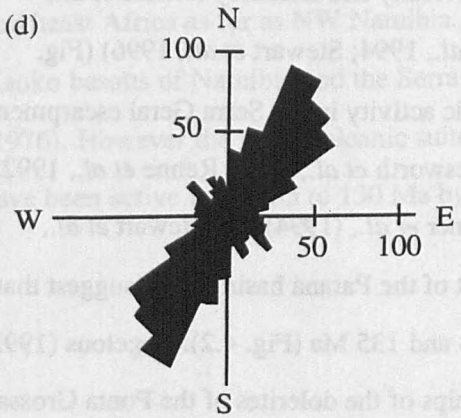

Fig. 4.1(d) Rose diagram of 413 dykes in Namibia showing the predominant NE-SW orientation after Lord *et al.*, (1996).

4.4. Geochronology: Previous studies.

(i) Paraná:

Dating of the Paraná province began in earnest in the 1960s with Amaral *et al.* (1966) reporting potassium - argon (K-Ar) dates for 20 basalts from southern Paraná. The results showed the province to be Early Cretaceous in age contrary to the previous assignment of a Jurassic age to the province. K-Ar ages have since been reported by a number of authors including Melfi (1967), Siedner & Mitchell (1976), Fodor *et al.* (1983) and Piccirillo *et al.* (1987) and the main magmatic event was constrained to have occurred at 130 ± 10 Ma. Associated dykes yielded similar K-Ar age ranges of 125 - 138 Ma, but the alkalic provinces of Jacupiranga, Anitápolis, Minas Gerais, Goias and São Sebastião yield ages that vary from late Jurassic to Tertiary (Herz, 1977; Ulbrich & Gomes, 1981).

Rb-Sr isochron ages of 135 ± 3 Ma for the northern Paraná rhyolites were reported by Mantovani *et al.* (1985), and Alberti *et al.* (1992) reported similar ages for the Giraul volcanics in southern Angola, which are geochemically equivalent to the Chapecó rhyolites of northern Paraná. K-Ar data on plagioclase separates for similar rocks yield consistently younger ages, and so Piccirillo *et al.* (1987) were concerned in case K had been mobilised after eruption. More recently detailed ^{40}Ar - ^{39}Ar studies have been undertaken particularly by groups at the Open University and Berkeley (Renne *et al.*, 1992; 1996; Hawkesworth *et al.*, 1992; Turner *et al.*, 1994; Stewart *et al.*, 1996) (Fig. 4.2). The results all suggest that the peak magmatic activity in the Serra Geral escarpment region occurred between 134 and 130 Ma (Hawkesworth *et al.*, 1992; Renne *et al.*, 1992; Turner *et al.*, 1994; Stewart *et al.*, 1996), but Turner *et al.*, (1994) and Stewart *et al.*, (1996) also reported ages from the north and west of the Paraná basin which suggest that magmatic activity commenced there between 138 and 135 Ma (Fig. 4.2). Regelous (1993) studied the geochemical and Ar-Ar age relationships of the dolerites of the Ponta Grossa and Sao Paulo dyke swarms. The results of this study suggested that the Ponta Grossa dykes acted as the feeder system to the basalt lava flows of the north namely the Pitanga and Paranapanema magma types of Peate *et al.* (1992), while the dolerites of Sao Paulo State are unrelated to the CFB province by any simple petrogenetic processes. The dating of dykes related to both the Paranapanema and Pitanga magma types suggested that the

Pitanga magmas were older (134.1 ± 1.3 Ma) than the Paranapanema magma type (130.5 ± 2.9 - 133.9 ± 2.5 Ma) (Regelous, 1993). This is consistent with the chemical stratigraphy defined by Peate *et al.* (1992), but subsequent dating by Turner *et al.* (1994) yielded older ages (139 to 133 Ma) for Pitanga and Paranapanema samples from the north and west of the lava field, and a 138 Ma age for a Paranapanema dyke in Paraguay. Recent Ar-Ar ages for the Ponta Grossa dyke swarm yield younger ages of between 129 - 132 Ma (Renne *et al.*, 1996), suggesting that these dykes are contemporaneous with the main phase of volcanism. Taking the ages of the lavas and all the dykes of similar composition, the age span for the stress system responsible for the NW trending dykes would be from 138 Ma to 129 Ma.

(ii) Etendeka:

Potassium - argon (K-Ar) and argon - argon (Ar-Ar) studies similar to those of the Paraná province have also been undertaken for the Etendeka province northwestern Namibia, and for the dykes along the South Atlantic coast and particularly around Cape Town including the False Bay dolerite dykes (Fig. 4.1).

Some of the earliest reported ages range from 196 to 114 Ma (Siedner & Miller, 1968), reflecting in part the widespread affect of the older Karoo volcanism which extended from southeast Africa as far as NW Namibia. K-Ar ages of 121 Ma were reported for the Kaoko basalts of Namibia and the Serra Geral basalts of Brazil by Siedner and Mitchell (1976). However the main volcanic suite of the Etendeka formation was considered to have been active from 135 to 130 Ma by Erlank *et al.*, (1984).

Fig. 4.2. **Age Map.**

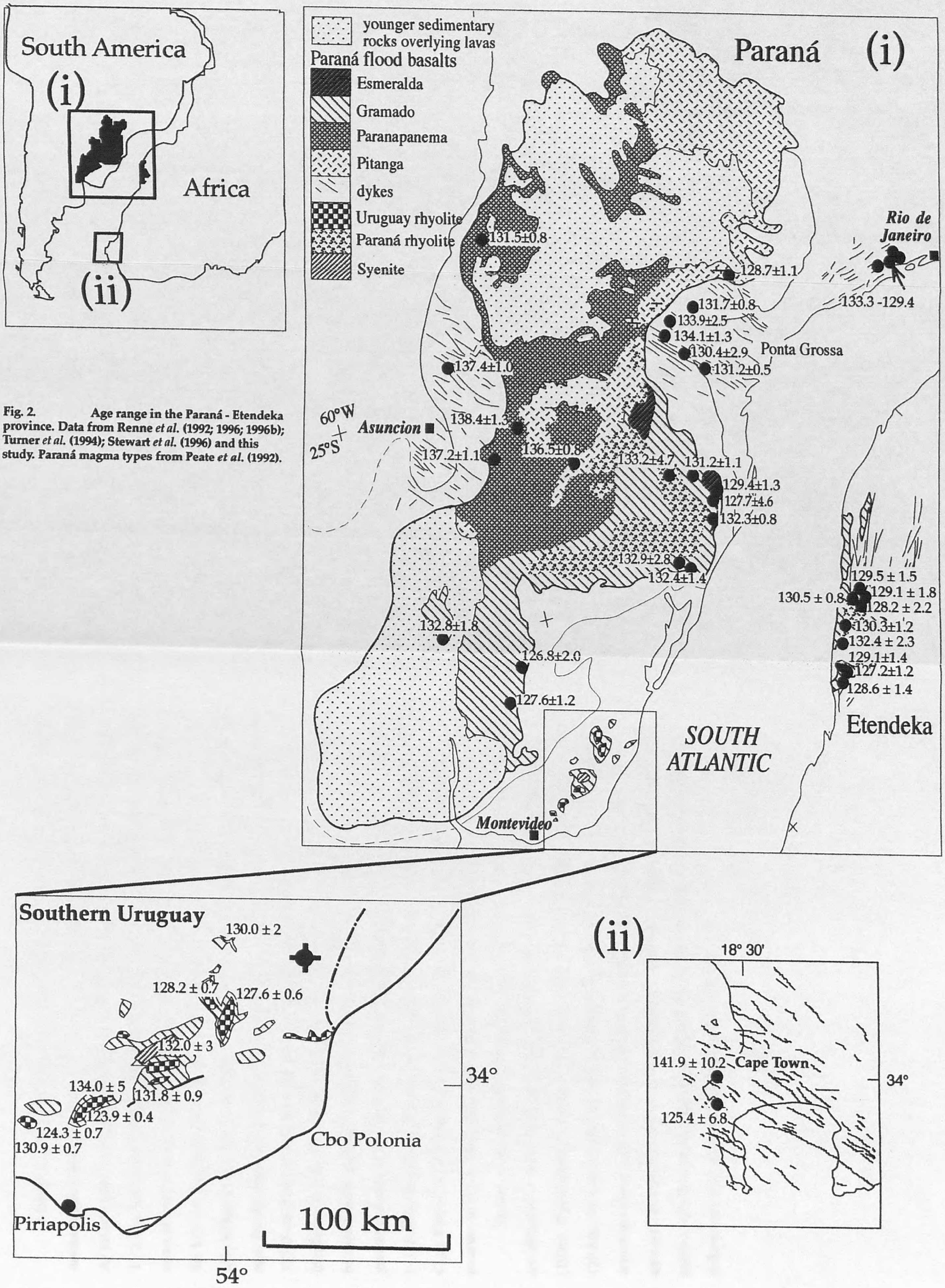

Fig. 2. Age range in the Paraná - Etendeka province. Data from Renne *et al.* (1992; 1996; 1996b); Turner *et al.* (1994); Stewart *et al.* (1996) and this study. Paraná magma types from Peate *et al.* (1992).

Milner *et al.* (1995) further constrained the timing of Mesozoic igneous activity in northwestern Namibia to between 137 and 124 Ma using Rb-Sr internal isochrons and Ar-Ar release spectrum ages. The main volume of magma is thought to have been erupted in 1 - 2 Ma, but activity among the Damaraland intrusive complexes continued until after the onset of seafloor spreading at ~ 129 Ma (Milner *et al.*, 1995); for example, Paresis (Rb-Sr: 132 ± 4 Ma; Manton & Siedner, 1967); Okenyenya (Rb-Sr: 128.6 ± 1 to 123.4 ± 1.4 Ma; Milner *et al.*, 1993); and Messum (Rb-Sr: 126.8±1.3 Ma; Milner *et al.*, 1993). Ar-Ar ages for the intrusive complexes of Damaraland have yielded a wider range in ages from 137.0 ± 0.7 Ma (comendite from Paresis, Milner *et al.*, 1995b) to 129.3 ± 0.7 Ma (nepheline syenite from Messum, Renne *et al.*, 1996b). These latter ages are considered to be closer to the true age range of the Damaraland intrusive complexes in view of the greater accuracy of the method. The MORB-like Horingbaai dykes appear to be younger (~125 Ma), than the main coast parallel dyke swarms such as the False Bay dolerites from Cape Town (132 ± 2 Ma; Reid *et al.*, 1991). K-Ar ages for coast parallel linear dyke swarms of 134 ± 5 Ma were also reported by Siedner & Mitchell (1976).

Recent Ar-Ar ages on Etendeka volcanics, dyke swarms and intrusive complexes are included in studies by Reid & Rex (1992), Renne *et al.*, (1996b) and Stewart *et al.*, (1996). Significantly, the ages reported are within error of each other, between 134 and 129 Ma, for both plagioclase and hornblende separates from the Etendeka rhyolites and associated dykes and the Messum intrusive complex. This suggests that differences in ages are not significant with regard to either the dating procedure or the phase analysed, and we note that similar ages are obtained when adjacent road sections are analysed by different techniques in the Paraná (Table 4.1, Fig. 4.3).

Table 4.1. Comparison of a selected number of published ages for two different Paraná magma types.

Magma type	Longitude	Latitude	RS	Age (Ma)	Author
Gramado	53.75	29.25	CJ	132.9 ± 0.6	Renne *et al.* (1992)
Gramado	51.02	29.47	MG	132.4 ± 1.4	Turner *et al.* (1994)
Gramado	52.71	26.38		133.1 ± 1.0	Stewart *et al.* (1996)
Urubici	49.83	28.45	GB	132.4 ± 0.7	Renne *et al.* (1992)
Urubici	49.46	28.12	SM	132.3 ± 0.8	Turner *et al.* (1994)

* RS = Road Section name from Serra Geral escarpment correlates with labels on Figure 3.

Combining the data from each of these studies the question remains as to the actual duration of magmatism in one of the worlds largest CFB provinces, the Paraná - Etendeka (Fig. 4.2). Was it all extruded within the space of a few million years as has been argued for similar sized CFB such as the Deccan (Courtillot *et al.*, 1986; Duncan & Pyle, 1988) and for this province by Renne *et al.* (1992; 1996b)? Or are there different controls operating which determine the rate of melting, as indicated by Stewart *et al.* (1996)? In order to add to the understanding of the relationship between the timing of magmatism and rifting a new dating programme was initiated on the volcanic rocks from southern Uruguay, Etendeka lavas, Namibia, and dyke exposures along the African margin as far east as Suurberg, eastern Cape Province (Fig. 4.1). Preliminary results were reported in Stewart *et al.* (1996), and those data are combined with new results in the next section.

Table 4.2. Correlation chart for the Lower Cretaceous rocks of the principal basins of concern in this study, after Riccardi (1988). Unconformities are indicated by dotted lines.

Epoch	Age	Salado Basin	Santa Lucía Basin	Paraná Basin
Lower Cretaceous	Albian	Serra Geral Formation	Migues Formation	Caiua Formation
	Aptian			
	Barremian		Castellanos Formation	
	Hauteri-vian			Serra Geral Formation
	Valangi-nian			
	Berriasian		Arequita & Puerto Gómez Formation	Serra Geral & Botocatu Formation

The position of the Tristan plume is highly debated (Duncan, 1989; Van Deccar, 1995) with Uruguay considered to lie at the periphery of the inferred influence of the Tristan da Cunha plume in the Early Cretaceous. However the occurrence of asthenosphere-derived magmas, Santa Lucía magma type in southern Uruguay, suggests a greater influence of the plume in this region. The mafic lavas of the Arapey Formation in northern Uruguay were contemporaneous with the widespread Serra Geral of the southern Paraná basin (Renne *et al.*, 1992). Moreover, the lavas of the Puerto Gómez Formation in the Santa Lucía basin of southern Uruguay have been shown to be similar both chemically and isotopically to those of the low-Ti Gramado magma type of the southern Paraná (Chapter 2). The eruption of these basalts in what may have been separate basins has led to different terms being proposed for what appear to be very similar rock units (Sprechmann *et al.*, 1981; Riccardi, 1988). Table 4.2 summarises

the correlation of formations between the main basins which contain significant amounts of Late Jurassic and Cretaceous volcanic rocks.

Fig. 4.3. Comparison of ages obtained along road sections in the Serra Geral escarpment. Names of road sections are from Peate *et al.* (1992), note SJ & SM of Renne *et al.* (1992). Ages in bold are from Turner *et al.* (1994) other age data are from Renne *et al.* (1992).

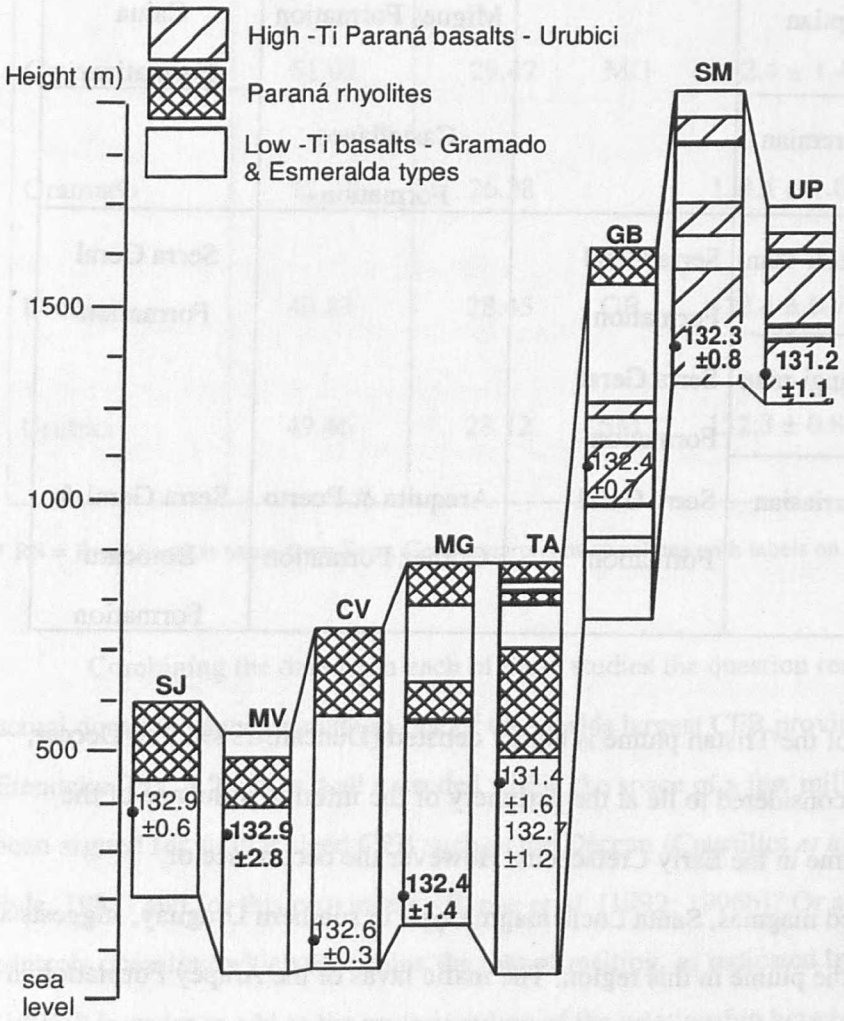

4.5. Argon Dating.

The ^{40}Ar-^{39}Ar dating technique is based on the decay of a naturally occurring isotope of potassium ^{40}K to an isotope of argon, ^{40}Ar. The calculated 'age' is the time since argon became trapped in the mineral or rock. This is termed 'closure' and in individual minerals it is controlled by composition, temperature, grain size and cooling

rate (Dodson, 1973). In volcanic rocks cooling is rapid and so for fresh rocks the measured age is taken to be that of eruption. The isotopic composition of argon in an igneous rock that has remained closed to argon since its crystallisation consists of two components, the initial trapped argon and the radiogenic component formed by the decay of ^{40}K and by the irradiation of ^{39}K. All Ar - Ar ages are calculated from the estimated $^{40}Ar^*/^{39}Ar$ ratio with the results presented either on isochron correlation plots of $^{36}Ar/^{40}Ar$ vs $^{39}Ar/^{40}Ar$, or as plateau ages described from plots of age vs cumulative ^{39}Ar release used particularly in the interpretation of stepped heating data.

For all the southern Uruguay volcanics and the other samples listed in Table 4.3 feldspar phenocrysts were separated, apart from sample 93L59 for which biotite separates were used. Samples were irradiated for either 60 hrs at the Ford reactor, Michigan, or 18 hrs. at Oregon State University (OSU). Tinto biotite (Rex & Guise, 1995) and 85G003 sanidine from the Taylor Creek rhyolite (Dalrymple & Duffield, 1988) were analysed as standards. The argon procedure operating at the Open University follows the technique detailed in Kelley (1995). Argon was extracted from individual grains by step laser heating using a Nd-doped yttrium aluminium garnet continuous wave laser. Step laser heating was preferred over spot analysis due to the use of a continuous wave laser system and because the mineral absorption coefficients of feldspar are low (Girard & Onstott, 1991). The laser power is absorbed in the top few tens of micrometers of the sample but temperature variations across single grains are negligible (Hall, 1990). The samples were heated in a number of 'steps' in order to release the maximum amount of Ar from the phenocrysts. During the course of analyses either a single grain, particularly of sanidine, or a number of grains (15 - 20 depending on their size and K contents) of plagioclase were heated. All the analyses were corrected for blank levels, ^{37}Ar decay and neutron interferences. The dimensionless parameter J used in age determinations was calculated from the standards (Tinto biotite and 85G003).

Isochron correlation plots of $^{36}Ar/^{40}Ar$ v $^{39}Ar/^{40}Ar$ were used to identify contributions from excess argon and to determine the intercept on the $^{39}Ar/^{40}Ar$ axis from which the ages are calculated (Fig. 4.4). The atmospheric ratio of $^{40}Ar/^{36}Ar$ is 295.5 and so data that intersect the y-axis either above this point indicate the presence of a non-

atmospheric component (excess ^{40}Ar) in the sample. Such effects can be corrected for and meaningful ages obtained.

Plateau ages are another way of interpreting stepped heating data and are described from plots of age v cumulative ^{39}Ar release. The ages obtained are defined by the weighted mean of the data and require three consecutive steps to contain more than 50% of the argon released and to be within a 2σ error of the weighted mean age of the plateau (Lanphere & Dalyrmple, 1978). Laser step-heating $^{40}Ar/^{39}Ar$ spectra are similar to age spectra derived from more traditional heating methods (Hall, 1990). The number of stages for each analysis was varied depending on the composition of the phenocrysts being ablated, with K-rich feldspar requiring a greater number of 'steps' than plagioclase. Sample 93L36, for example, was analysed using the laser step-heating technique in 24 stages on a single sanidine phenocryst. The temperature was increased by varying the current in incremental steps of 0.1 to 0.4 A from a starting current of 11.7A to total fusion at 15.7A. The resultant age spectrum yielded an age of 123.9 ± 0.8 Ma. This age is younger than anticipated as most of the Paraná - Etendeka rhyolites have apparent ages of ~ 132 Ma, but the data are considered to reflect the true crystallisation age of this sample. The isochron correlation and plateau age approaches were both used, and for most samples two ages are reported in Tables 4.3 and 4.4. Age ranges that were found to be internally consistent and with a MSWD between 1 and 2.5 were considered most reliable.

In all 13 samples were analysed from southern Uruguay, 6 mafic samples, 1 syenite and 6 rhyolites (Table 4.3). The results that are considered reliable are highlighted in Tables 3 and 4, the relatively large quoted errors on some samples tend to be due to samples clustering either at the atmospheric end of the array or at the radiogenic end with little mixing in between. Straight line mixing between radiogenic and atmospheric argon results in small errors on the ages obtained. The young age of sample 93L47 is considered a function of loss of radiogenic Ar with the small MSWD = 0.1018 implying a large underestimate of the error involved (Table 4.3). Similarly low MSWD were also seen in samples 93L97 and 93L125 again implying an underestimate in the error on the age (Table 4.3).

The intercept ages yielded from isochron correlation plots of $^{36}Ar/^{40}Ar$ vs $^{39}Ar/^{40}Ar$ were equally effected by excess argon in samples 93L53 and 93L93, and while

these samples yielded more reliable plateau ages the calculated errors remain large. Sample 93L42 gave the most precise age determination with over ten 'steps' analysed and both the intercept and plateau ages falling within error of each other (Table 4.3). Overall the basaltic samples yielded relatively imprecise ages, with the more reliable age range being from 130 ± 2 to 134 ± 5 Ma, which is effectively indistinguishable from the main phase of magmatism in the Paraná - Etendeka (Fig. 4.5, Renne *et al.*, 1992; 1996b; Turner *et al.*, 1994; Stewart *et al.*, 1996).

The biotite separate analysed from the Valle Chico Formation syenite of southern Uruguay yielded similar plateau and intercept ages which are well within error of each other at 132.0 ± 3 Ma and 132.3 ± 1.2 Ma respectively (Table 4.3). Six rhyolite samples from the Arequita Formation in southern Uruguay were also analysed. These ages were determined on multiple grains of alkali feldspar ablated at the same time, and because of the large amounts of argon gas released the ages were determined by step heating. Typically between 10 and 24 steps were required before total fusion occurred, and the resultant age spectra were consistently younger than those of rhyolites associated with the main Paraná - Etendeka event. However, there is no apparent relationship between the calculated age and radiogenic argon loss, except in sample 93L19, which yielded an exceptionally young age and has a low MSWD (Table 4.3).

Plateau ages are considered the best way of presenting the data in view of the number of steps involved in each analysis, although there is good agreement between plateau and intercept ages (Fig. 4.6a). The first step in all analyses was omitted from the final plateau age, principally as this step is most sensitive to any alteration not removed during the cleaning process (Fig. 4.6b). All the rhyolite ages are assumed to be true 'closure' ages although the range in age from 131.9 ± 0.5 to 123.9 ± 0.4 Ma is large and difficult to explain in relation to the timing of the opening of the South Atlantic.

Fourteen new samples were analysed from the lavas of the Etendeka province in northwestern Namibia and a number of dyke localities extending to Suurberg, South Africa. These samples were analysed with varying success and both excess argon and contamination by host rock feldspar are shown to have contributed to some of the ages obtained (Fig. 4.6c). Six samples including basalts, andesites and rhyolites yielded Early Cretaceous ages, and again those that are regarded as reliable are highlighted in Table 4.4,

internally consistent ages and a close correlation between both the intercept age and the plateau age together with reasonable MSWD were again the criteria used for acceptance of an age.

Fig. 4.4. **A plot of $^{36}Ar/^{40}Ar$ vs $^{39}Ar/^{40}Ar$ after Kelley (1995) used to distinguish excess argon. The plot illustrates the potential end member compositions: Radiogenic argon (intercept A on the $^{39}Ar/^{40}Ar$ axis; atmospheric argon (B on the $^{36}Ar/^{40}Ar$ axis) and excess argon (C, at the origin). Simple cases exhibit mixtures between atmospheric and radiogenic argon, yielding a precise age from the $^{39}Ar/^{40}Ar$ intercept. Mixtures of radiogenic argon and a component with $^{36}Ar/^{40}Ar$ ratios less than atmospheric (0.003384) reflect addition of ^{40}Ar.**

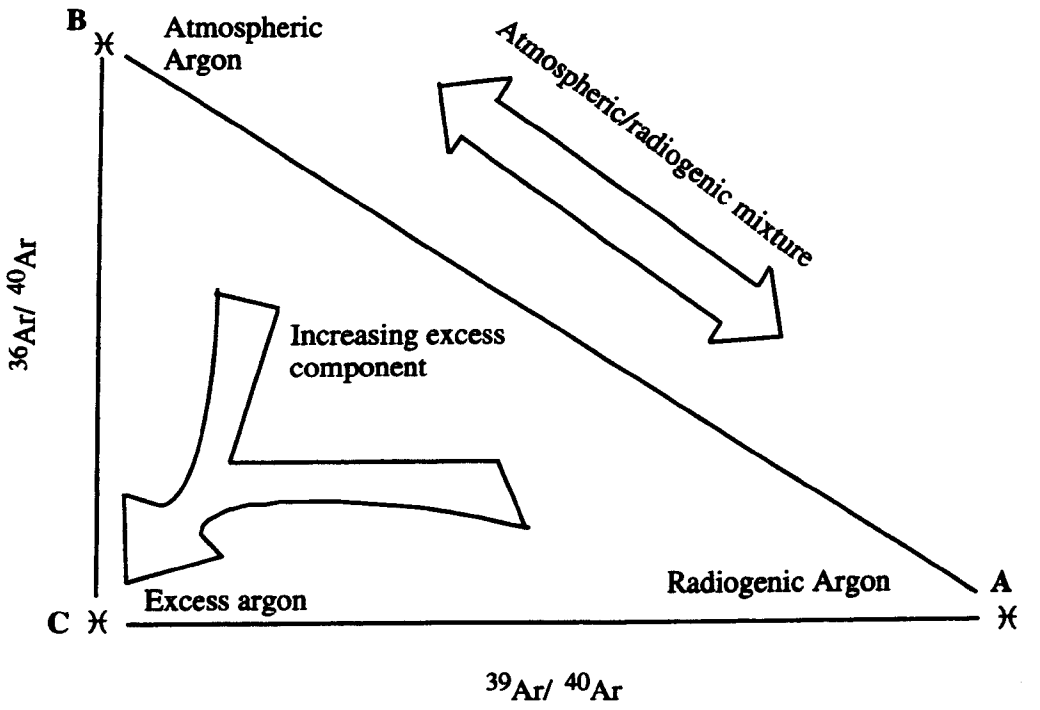

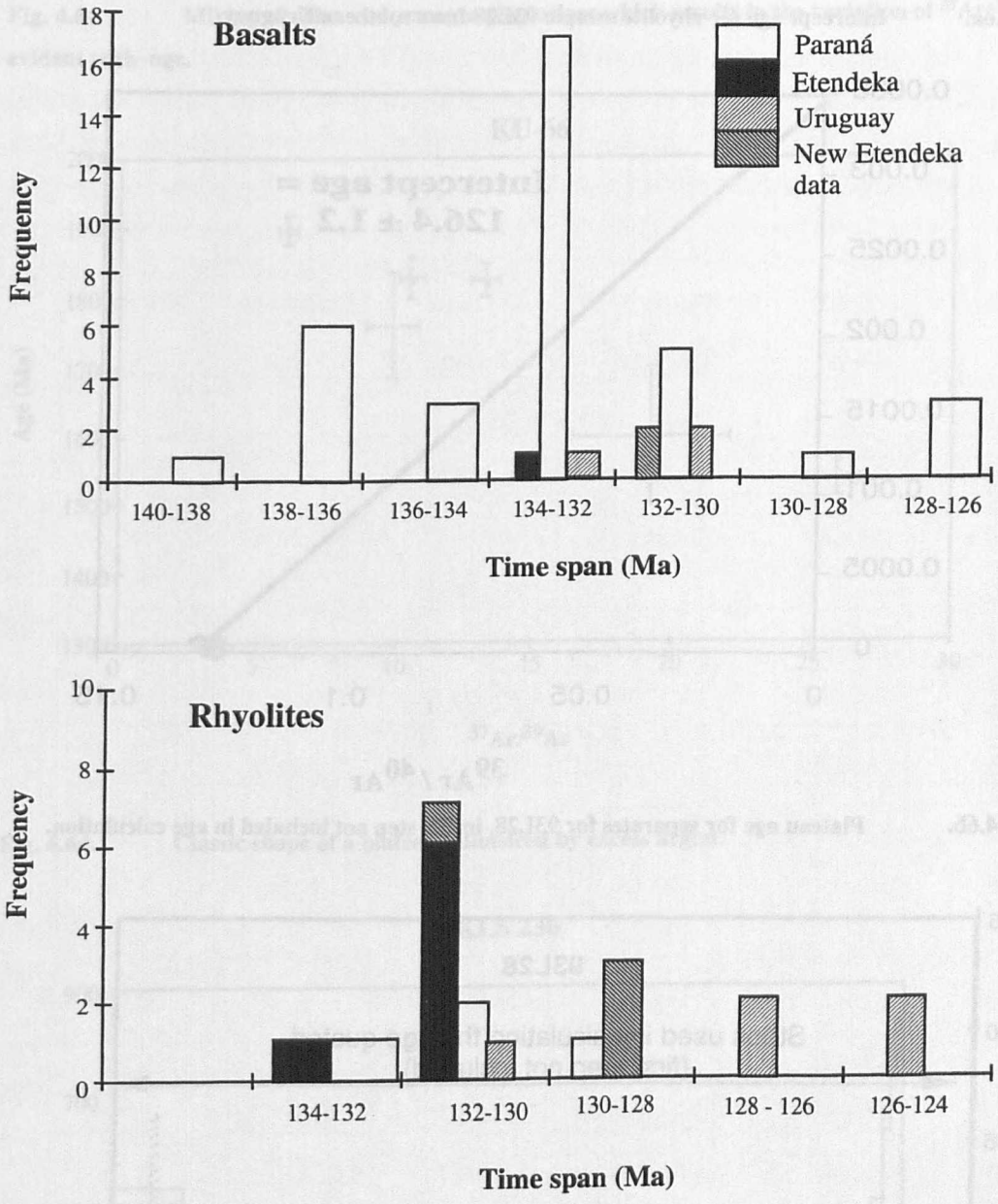

Fig. 4.5. **Frequency of published ages for the Paraná - Etendeka. Data from Turner *et al.*, (1994); Stewart *et al.*, (1996); Renne *et al.*, (1992;1996b). New age data from Uruguay and the Etendeka from present study also included for comparison.**

Fig. 4.6a. **Intercept age for rhyolite sample 93L28 from southern Uruguay.**

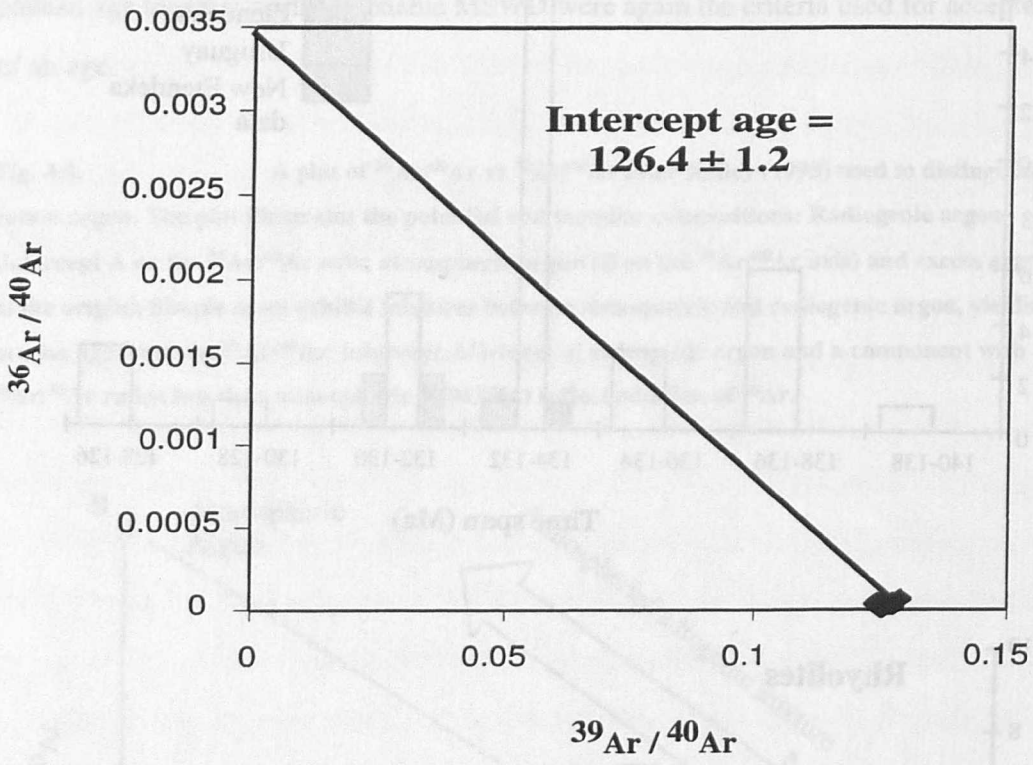

Fig. 4.6b. **Plateau age for separates for 93L28, initial step not included in age calculation.**

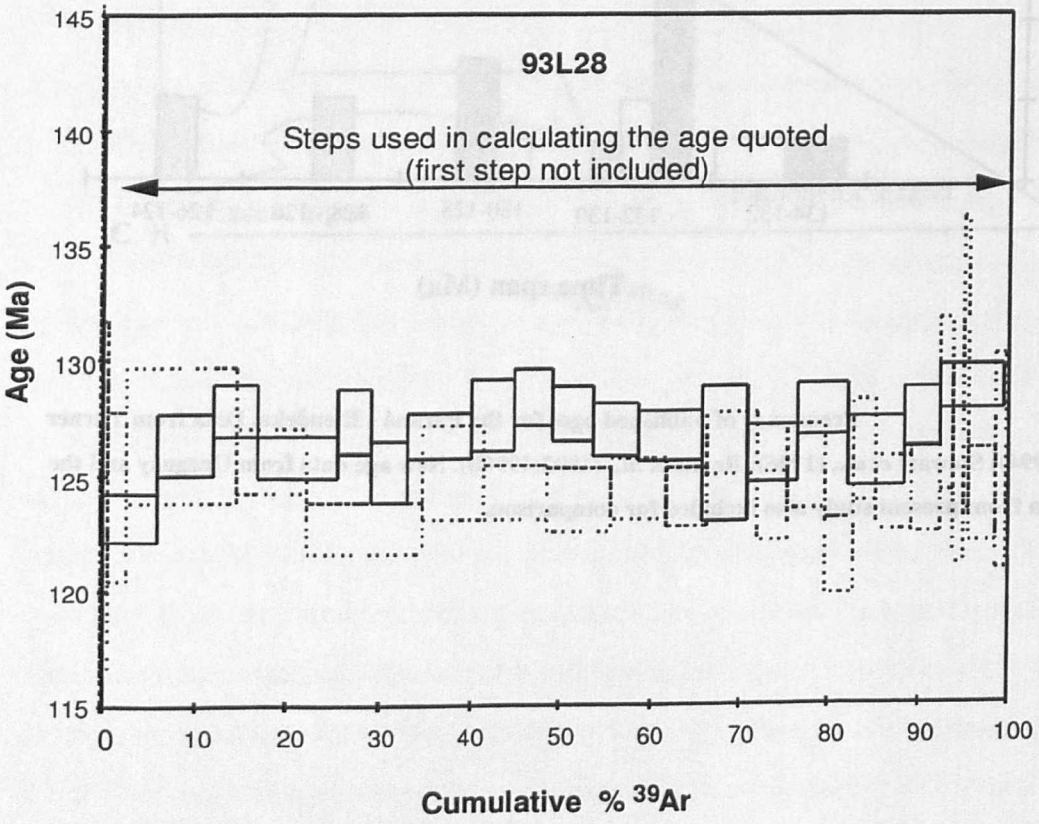

Fig. 4.6c. **Mixing of older and younger plagioclase which results in the variation of $^{37}Ar/^{39}Ar$ evident with age.**

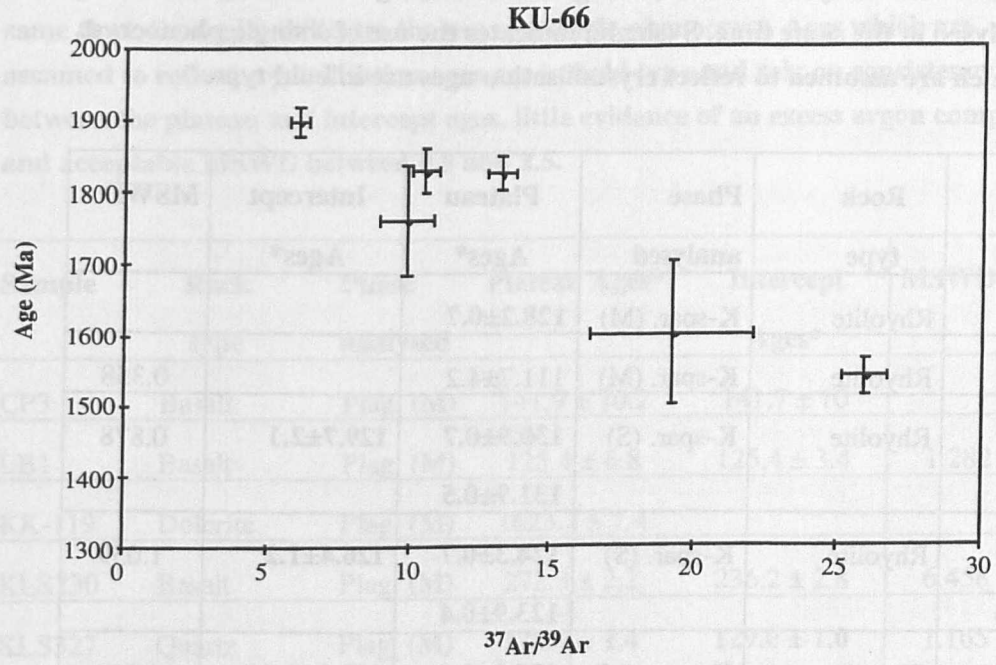

Fig. 4.6d. **Classic shape of a plateau influenced by excess argon.**

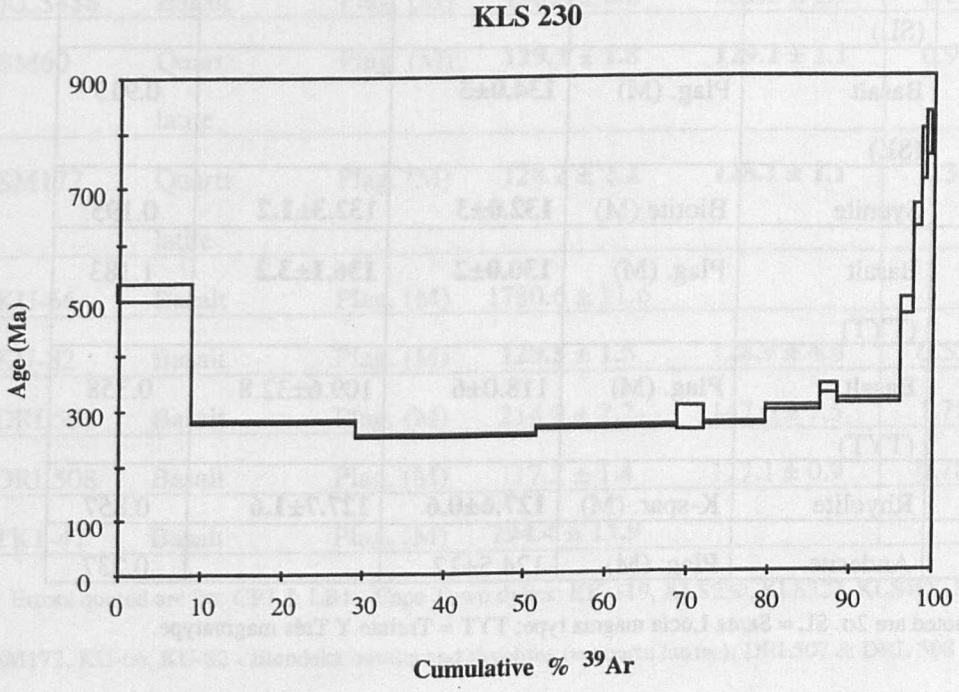

Table 4.3. Results of samples analysed from Uruguay. Both potassium feldspar and plagioclase were analysed with M (multigrain) indicating where more than one grain was analysed at the same time, S (single) indicates the use of a single phenocryst. Ages which are assumed to reflect crystallisation ages are in bold type.

Sample	Rock type	Phase analysed	Plateau Ages*	Intercept Ages*	MSWD
92U14	Rhyolite	K-spar. (M)	**128.2±0.7**		
93L19	Rhyolite	K-spar. (M)	111.7±4.2		0.358
93L22a 93L22b	Rhyolite	K-spar. (S)	**130.9±0.7** **131.9±0.5**	**129.7±2.1**	0.878
93L28a 93L28b	Rhyolite	K-spar. (S)	**124.3±0.7** **123.9±0.4**	**126.4±1.2**	1.059
93L36	Rhyolite	K-spar. (M)	**123.9±0.4**	**123.9±1.4**	1.083
93L42	Andesite	Plag. (M)	**131.8±0.9**	**132.9±0.9**	1.020
93L47	Basalt (SL)	Plag. (M)	128.0±3	125.8±5.1	0.101
93L53	Basalt (SL)	Plag. (M)	**134.0±5**		0.913
93L59	Syenite	Biotite (M)	**132.0±3**	**132.3±1.2**	0.195
93L93	Basalt (TYT)	Plag. (M)	**130.0±2**	**136.1±3.2**	1.183
93L97	Basalt (TYT)	Plag. (M)	118.0±6	109.6±32.8	0.358
93L107	Rhyolite	K-spar. (M)	**127.6±0.6**	**127.7±1.6**	0.857
93L125	Andesite	Plag. (M)	124.5±12		0.237

* Errors quoted are 2σ. SL = Santa Lucía magma type; TYT = Treinte Y Trés magmatype.

Table 4.4. Results of age dating from the Etendeka and related dykes in South Africa. M (multigrain) indicating where more than one grain was analysed at the same time, S (single) indicates the use of a single phenocryst. Ages which are assumed to reflect crystallisation ages are in bold type and rely on consistency between the plateau and intercept ages, little evidence of an excess argon component and acceptable MSWD between 0.8 and 2.5.

Sample	Rock type	Phase analysed	Plateau Ages*	Intercept Ages*	MSWD
CP3	Basalt	Plag. (M)	141.9 ± 10.2	141.7 ± 10	
LB1	Basalt	Plag. (M)	125.4 ± 6.8	125.4 ± 3.4	1.282
KK-119	Dolerite	Plag. (M)	1623.2 ± 7.4		
KLS230	Basalt	Plag. (M)	272.3 ± 2.2	236.2 ± 2.8	6.458
KLS327	Quartz latite	Plag. (M)	**128.6 ± 1.4**	**129.0 ± 1.0**	1.165
KLS348	Basalt	Plag. (M)	**132.4 ± 2.3**	**132.5 ± 2.4**	1.256
KLS488	Basalt	Plag. (M)	**130.5 ± 0.8**	**131.0 ± 1.9**	0.617
SM60	Quartz latite	Plag. (M)	**129.1 ± 1.8**	**129.1 ± 1.1**	0.923
SM172	Quartz latite	Plag. (M)	**128.2 ± 2.2**	**128.1 ± 1.1**	1.307
KU-66	Basalt	Plag. (M)	1780.6 ± 11.6		
KU-82	Basalt	Plag. (M)	**129.5 ± 1.5**	**128.9 ± 4.4**	0.524
DRL507	Basalt	Plag. (M)	214.9 ± 2.2	147.0 ± 7.5	1.758
DRL508	Basalt	Plag. (M)	117.2 ± 1.4	117.1 ± 0.9	0.784
TK1-47	Basalt	Plag. (M)	**194.4 ± 11.9**		

* Errors quoted are 2σ. CP3 & LB1 - Cape Town dykes; KK-119, KLS230, KLS327, KLS488, SM60, SM172, KU-66, KU-82 - Etendeka basalts and rhyolites (= quartz latites); DRL507 & DRL 508 - Mehlberg dyke; TK1-47 - Suurberg basalt.

The older Archaean/ Precambrian ages of samples KK-119 and KU-66 appear to reflect the presence of xenocrysts as these dykes intrude basement gneisses and granites of similar ages. Furthermore a plot of age versus $^{37}Ar/^{39}Ar$ preserves a mixing array between younger and older components, with older phenocrysts having lower Ca/K than the younger feldspars (Fig. 6c). The old age recorded by sample KLS230 is due to excess argon which results in a classic saddle shaped plateau age that is very unreliable (Fig. 6d). Excess argon in both the Cape Town dykes analysed resulted in poor ages, and the samples of the Mehlberg dyke gave widely varying results (Table 4) perhaps reflecting post-intrusion alteration processes. These samples intrude sandstone (DRL507) and granite (DRL508) which have very different K and Ca contents, and these may have influenced gain of K and/or loss of Ar (D. Reid, pers. com.) and therefore contributed to the range of ages obtained. Sample TK1-47 yielded a Jurassic age which is considered to be a true 'closure' age.

The two basalt samples (KLS 348, KLS 488) analysed give slightly older ages than the rhyolites (Table 4.4) consistent with their position at the base of the stratigraphic sequence. These ages are similar to those reported elsewhere for Etendeka basalts (e.g. Renne *et al*, 1996b). The rhyolites principally form tight clusters of data points close to the radiogenic axis on the isochron correlation diagram, apart from KLS327 which shows some mixing with atmospheric argon. All rhyolite ages are considered true 'closure' ages (Table 4.4). These ages are approximately a million years younger than many reported for the Etendeka province (Renne *et al.*, 1996b), but they define a much narrower age range for the province than the K-Ar dating technique.

The ages obtained therefore suggest that magmatism in southern Uruguay spanned 10 million years from 134 to 124 Ma. The Uruguay basalts range in age from 134 to 130 Ma which was contemporaneous with the main phase of Paraná - Etendeka flood volcanism (132 ± 2 Ma; Renne *et al.*, 1992; 1996b; Stewart *et al.*, 1996). The ages obtained for the Treinte Y Trés and Santa Lucía magma types are however not distinguishable from each other therefore it is difficult to determine a stratigraphical relationship. Nor can the timing of the increase of plume involvement in the province be therefore determined precisely. However since the magmatism is contemporaneous with

the main Paraná - Etendeka volcanism as implied from the age data, the position of the Tristan plume may be located further south than previously supposed.

The rhyolites from southern Uruguay range in age from 132 to 124 Ma. The majority of these ages are younger than those reported for the Paraná - Etendeka rhyolites which range from 132 to 129 Ma (Renne *et al.*, 1996b; Stewart *et al.*, 1996). The age range of the rhyolites is also younger than the ages reported for the southern Uruguay basalts suggesting bimodal activity. Furthermore activity in southern Uruguay continued after final continental separation which suggests a local source for the rhyolites as proposed in Chapter 3 from the presence of brecciated volcanics.

4.6. Palaeomagnetism.

The Early Cretaceous is known to be a period of high frequency reversals and short polarity intervals of less than a million years (Bellieni *et al.*, 1983; Kent & Gradstein, 1985), before the quiet period of no magnetic reversals from 124 to 83 Ma in the mid-Cretaceous (Larson & Olson, 1991; Larson & Kincaid, 1996). Thus, the number of reversals in a stratigraphic sequence from the Early Cretaceous can potentially provide important constraints on the timing of events. Reversals are however difficult to correlate from one area to another and so they can only be used with any confidence over relatively small areas. Palaeomagnetism is also used to investigate both crustal rotations and hence the responses to tectonic stress, and the duration of magmatic events (Cox & Hart, 1986).

Recent studies of the magnetostratigraphy of the Paraná - Etendeka province by Ernesto & Pacca, (1988), Milner *et al.* (1995) and Renne *et al.*, (1996b) indicate at least two reversals during the eruption of the main volume of magma, although up to seven reversals have been measured in flows from some areas suggesting longer periods of eruption (Peate *et al.*, 1992). Palaeomagnetic studies of the NW and NE trending Ponta Grossa dyke swarm by Raposa & Ernesto (1995) showed that the majority of dykes are of normal polarity and, although reversed polarity dykes do also occur, there is no link between polarity and dyke orientation. Coast-parallel dykes have not been studied in detail but some at least in the Awahab section of the Etendeka have reversed magnetic polarity, and two reversals have been recorded in three different sections of the Etendeka lavas (Renne *et al.*, 1996b). Although the Early Cretaceous was a period of high reversal

frequency, with 26 reversals recorded between 144 and 121 Ma (Gradstein *et al.*, 1994), the duration of each reversal period is highly variable. For example, there was only one reversal between 133 and 132 Ma, while three reversals have been recorded between 132 and 131 Ma (Gradstein *et al.*, 1994). Therefore, depending on exactly when in the Cretaceous the Paraná - Etendeka lavas were erupted the presence of three reversals might imply rapid extrusion of the province in 1 - 2 my. Palaeomagnetic variations in the Paraná - Etendeka have been taken to imply high rates of eruption (700 m in < 1 my), and to indicate the simultaneous eruption of mafic and acid lavas in different regions (Bellieni *et al.*, 1983; Ernesto & Pacca, 1988). However, such conclusions rely on the successful correlation of individual magnetic reversals over relatively large distances (> 1000 km). Therefore palaeomagnetic data appear to suggest short time scales for eruption in the Paraná - Etendeka of between 1 and 2 my, however the data require independent corroboration.

Interestingly a number of models exist which suggest a relationship between large scale plume-related basaltic magmatism and disruption of the magnetic reversal process (Larson & Olsen, 1991; Larson & Kincaid, 1996). There may be an inverse relationship between the frequency of magnetic reversals, heat removal due to plume formation and hence the rate of production of oceanic and continental flood basalts (Larson & Olsen, 1991). The removal of large quantities of basalt during the Mesozoic may have altered the stability of the D" layer at the core/mantle interface, and consequently lead to the magnetic quiet period later in the Cretaceous.

4.7. Rifting.

The fit of the continents around the South Atlantic was first modelled in detail by Bullard *et al.* (1965) with varying success for the degree of fit at particular points. The misfit of pre-drift reconstructions led to suggestions of intraplate deformation and plate rotations (Unternehr *et al.*, 1988; Fairhead, 1988; Müller *et al.*, 1993). The major sites of intraplate deformation are considered to be the Benue Trough, a sinistral wrench fault zone; the Central Africa shear zone, and the Paraná and Chaco basins in South America (Unternehr *et al.*, 1988; Fairhead, 1988). The Atlantic Mesozoic rift system consists of a number of different segments, such as the Equatorial Atlantic, between the Equatorial

Fracture zone and the Walvis Ridge, and the South Atlantic between the Walvis Ridge and the Agulhas Fracture zone (Uchupi, 1989) (Fig. 4.7). The opening of the Equatorial Atlantic occurred after the opening of the South Atlantic Ocean (Fairhead, 1988).

The large scale rifting which resulted in the first oceanic crust in the South Atlantic started during the Valanginian (137.5 – 133 Ma; Kent and Gradstein, 1985), with the ocean between Argentina and South Africa beginning to open about 130 Ma (Scotese *et al.*, 1988). North of 33 °S, rifting leading to the development of oceanic crust began in the late Hauterivian, and using the timescale of Kent and Gradstein (1985) that was around 127-126 Ma. North of the Walvis Ridge - Rio Grande Rise the first oceanic crust is late Aptian in age (~ 119 Ma, Mascle *et al.*, 1986).

Stretching of the Gondwana land mass resulted in the formation of a number of basins including the Pelotas, Campos and Santos basins of Brazil, the Santa Lucía and Punte Del Este basins of Uruguay, and the Salado and Colorado basins of Argentina during the Mesozoic (Fig. 4.7). The orientation of these basins is parallel to that of the early dyke swarms of the Ponta Grossa and eastern Paraguay, indicating that the principle extensional stresses were NE-SW. These basins contain rift related sediments and Cretaceous basalts similar to the onland Paraná magma types which have been described from several areas including the Campos, Santa Lucía and Salado basins.

Varying amounts of syntectonic sedimentation in extensional tectonic regimes occurred in basins throughout South America from the Middle Triassic to the Late Cretaceous (Uliana *et al.*, 1989), with some of the earliest rift related sedimentation in South America and Africa being Late Jurassic in age. Much of the early faulting follows the Palaeozoic structural grain in both Africa and South America (Cox, 1978), and there are typically three depositional sequences characterised by different facies and tectonic styles. These are best known from the East Brazilian rift system including the Campos basin along the eastern continental margin of Brazil (Chang *et al.* 1992) where syn-rift sediments have been described from three periods.

Fig. 4.7. Magnetic anomalies of the South Atlantic, after Austin & Uchupi (1982), with reinterpretation of the data of Rabinowitz & LaBrécque (1979).

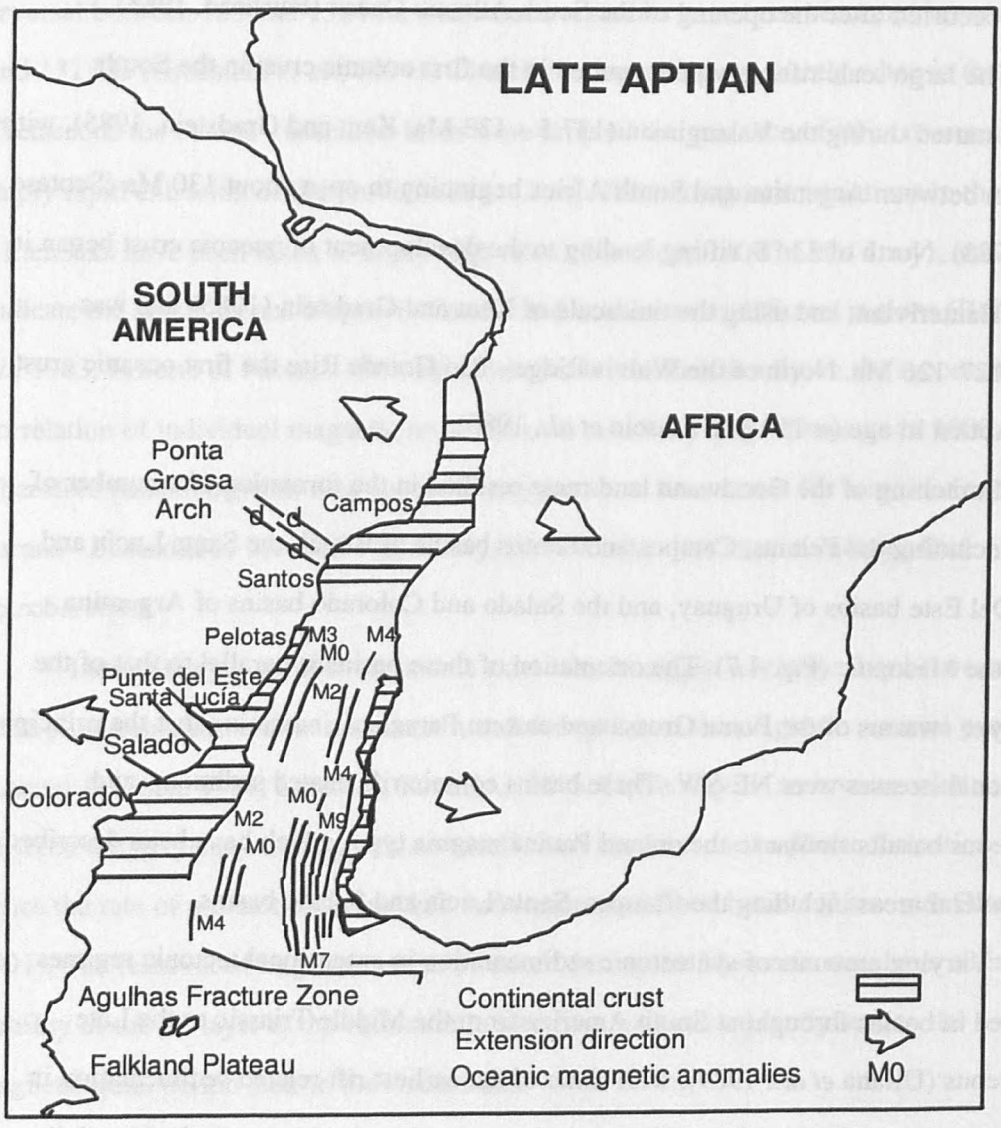

The oldest Syn-rift 1 sequence is Jurassic in age and it consists of coarse-grained fluvial and alluvial fan deposits with minor evaporites and aeolian sands, which are a feature of the African - Brazilian Depression. Late Jurassic extensional faulting has been described in many of these basins (Riccardi, 1988; Chang *et al.*, 1992). Syn-rift sequences II and III include Berriasian to Barremian sediments which are intercalated with volcanics in basins from the Campos, in eastern Brazil to the Colorado in Argentina (Riccardi, 1988). Rifting had commenced by the end of the Valanginian (133 Ma), with mature passive continental margins developed by Aptian times. This is marked in the sedimentary record by a transition from fluviatile to marine deposits (Dingle *et al.*, 1983). Transitional marine

sequences of Aptian age (121 - 113 Ma) overlie the rift sediments unconformably in many of these rift related basins indicating significant uplift and erosion at that time.

The Paraná - Etendeka rhyolites range in age from 132 to 128 Ma (Fig. 4.2; this study; Renne *et al.*, 1996b). Eruptive sequences within the province have been correlated on the basis of their bulk chemical compositions, phenocryst assemblages and mineral compositions by Milner *et al.* (1995). Specifically, silicic units of the Awahab Formation in the Etendeka which are centred in the Messum complex have been correlated with individual units in Brazil which implies that at least some of the units extended for distances of > 340 km from their source (Milner *et al.*, 1995). This has important implications for the timing of rifting in the South Atlantic since, if such correlations are correct, final separation presumably cannot have occurred until after the eruption of these magmatic units.

In Uruguay the Punte del Este basin forms a continuation of the northwest - southeast trending Salado basin (Fig. 4.7). Jurassic extension appears to have spawned the development of both these basins along pre-existing structures and they may reflect a different principal stress regime to that which eventually lead to continental separation. The Punte del Este basin is characterised by a three stage evolution process (Stoakes *et al.*, 1991). The initial rift sedimentation is preserved in asymmetric graben structures of Neocomian age (~ 144 to 127 Ma). These are overlain unconformably by Aptian to Maastrichtian continental and marine deposits, with varying amounts of basaltic material preserved which have been related to the main Paraná - Etendeka flood basalt sequence (Riccardi, 1988).

Table 4.5. Time - event chart for the development of the South Atlantic Ocean. The ages in millions of years are from Kent and Gradstein (1985). Summary of dates from text.

Aptian (121 - 113 Ma)		Mature passive continental margins, marine sedimentation. Oceanic crust in Equatorial Atlantic.
Barremian (127 - 121 Ma)	M4 ~ 127 Ma	First oceanic crust developed at latitude of the Paraná - Etendeka province.
Hauterivian (133 - 127 Ma)	127 Ma 133 – 127 Ma	Magmatism ceased. Continued Paraná-Etendeka CFB magmatism assoicated with both NW-SE trending and coast-parallel dykes (Figs. 4.2 and 4.5).
Valanginian (137.5 - 133 Ma)	134 Ma 136 Ma	Main phase of activity commenced. CFB Paraná magmatism, associated with the NW-SE trending dykes and coast parallel to lesser extent (Fig. 4.2). Seafloor spreading commenced at 36 °S.
Berriasian (144 - 137.5 Ma)	138.4 Ma	Oldest basalt from west of province (Fig. 4.2).
Tithonian (150 - 144 Ma)		Rift related sedimentation in South American basins including Campos, Salado & Colorado.

4.8. Magnetic anomalies - evidence from ocean floor.

The earliest evidence of seafloor spreading is provided by magnetic anomalies on the ocean floor, and correct identification of these anomalies provides important information regarding the timing and duration of rift propagation. However, there has been considerable uncertainty over the age of individual anomalies, as illustrated by the summary of the timescales used by different authors in Table 6, and so the absolute ages

of these anomalies have to treated with caution. In this study the timescale of Kent and Gradstein (1985) has been used since it is in good agreement with that of Harland *et al.* (1982) for the age of magnetic anomalies.

The opening of the South Atlantic has been described as an unzipping process with rifting commencing in the south and propagating northwards as far as the Rio Grande Rise - Walvis Ridge (Rabinowitz and LaBrécque, 1979; Nürnberg and Müller, 1991; Turner *et al.*, 1994). North of the Rio Grande Rise - Walvis Ridge system the age of the oldest magnetic anomalies decreases northwards, implying that rifting propagated northwards (Martin, 1987). Moreover, the oldest anomaly is M0 (118 to 121 Ma, Kent and Gradstein, 1985) and that is younger than the oldest anomaly identified further south. The oldest magnetic anomaly recognised south of Cape Town is M11 by Rabinowitz & LaBrécque (1979), which is ~ 133 Ma using the timescale of Kent & Gradstein (1985). However, in a seismic reflection study of the continental - oceanic transition off southwest Africa Austin & Uchupi (1982) argued that the critical older magnetic anomalies occur on thinned continental crust. Instead, they suggested that M9 was the oldest magnetic anomaly on true oceanic crust and that seafloor spreading therefore commenced at ~ 129 Ma, or 4 Ma after the Valanginian age previously ascribed using the timescale of Kent & Gradstein (1985). A sequence of northwest trending magnetic anomalies were described by Larson & Ladd (1973) from west of Cape Town, with the oldest lineations being M12 (which is equivalent to M4 of Kent & Gradstein, 1985). Magnetic anomaly M4 (~127) has also been identified further north in the vicinity of the Walvis Ridge and as far south as the Agulhas fracture zone (Cande *et al.*, 1989) (Fig. 4.7).

A number of questions remain unanswered even in the light of all the available palaeomagnetic data, including when exactly did the transition from continental to oceanic crust take place and how much did its timing vary with latitude along the South Atlantic. Anomaly M4 is recognised from the Walvis Ridge south to the Falkland plateau, indicating that seafloor spreading was well under way in the southern South Atlantic by 127 Ma. However, the presence of anomalies M9 and M7 off southern Africa suggests rifting started earlier in the south. Nonetheless, it remains difficult to tie down the age of these anomalies directly, and so there still appears to be a subjective element in the interpretation of the magnetic lineament data. Relative ages can be established, and

using the timescale of Kent and Gradstein (1985) adopted in this study the age of the oldest ocean floor rocks is taken to be 129 Ma off southern Africa and 127 Ma further north in the vicinity of the Walvis Ridge.

Table 4.6. Comparison of some magnetic anomalies with M12 highlighted in bold for clarity of comparison of the published corresponding ages.

Magnetic anomaly	Age (Ma)	Author
M25; **M12**; M9; M7; M4.	156.5-157.8; **135.5-136.6**; 129; 127.9 - 128.3; 126-127.	Kent & Gradstein, 1985
M25; M22; M21; **M12**; M11; M9; M4; M2.	160; 156; 153-145; **137**; 133; 130; 127; 123-114.	Harland *et al.*, 1982
M9; M4.	126; 123-117.	Austin & Uchupi, 1982 *after van Hinte (1976)*
M12; M4; M2.	**127**; 116; 112.	Larson & Ladd, 1973

4.9. Sediments and Magmatism.

The relationship between the extrusive volcanics and the sedimentary lithologies is of interest for a number of reasons not least of which is the hydrocarbon potential. In this section the possible interaction of rift related sediments and magmas is examined and the thermal implications are assessed briefly on both a regional and a local scale. The effects of magmatic underplating, high level intrusions and surface extrusion of large volumes of flood basalts on sediments are briefly addressed in view of the presence of volcanic material in many of the basins along the South American margin, e.g. the Campos, Punte del Este, Santa Lucía and Salado basins. Due to the large volume of both sediments and magma preserved in the Paraná basin it is an ideal locality to consider some of the interactions that occur both regionally and locally.

The Paraná basin contains over 5000 m of sediments and volcanics of Palaeozoic, Mesozoic and Cenozoic age and it is floored by Precambrian and Palaeozoic rocks (Zalan *et al.*, 1987; Riccardi, 1988). Sedimentation in the period leading up to eruption of the flood basalts and associated rhyolites is represented by continental aeolian deposits, and similar sediments have

been reported from other basins in the region including the Campos Basin (Chang *et al.*, 1992). These sandstones are referred to as the Botucatu Formation in the Paraná, which are correlated with the Etjo Sandstone Formation of Namibia, and they are considered to be Jurassic to Early Cretaceous in age (Amaral *et al.*, 1966; Riccardi, 1988). These aeolian sandstones are underlain by fluviatile or fluvio-lacustrine sediments and are intercalated with basaltic flows at the top of the sequence. The relationship between the sandstones and basalts is best preserved in the Etendeka where basalt flows wrap around well preserved dune structures (Fig. 4.8a, Photo 1), and sediments are seen infilling cooling fractures on the basalt surfaces (Fig. 4.8b, Photo 2). Similar interactions between sediments and magmatism are inferred for the marginal basins on a local scale.

Fig. 4.8a. **Photo 1. Relationship between the basalts and local dune deposits, Etendeka.**

Fig. 4.8b. **Photo 2. Sediments infilling cooling fractures indicating contemporaneous eruption and deposition.**

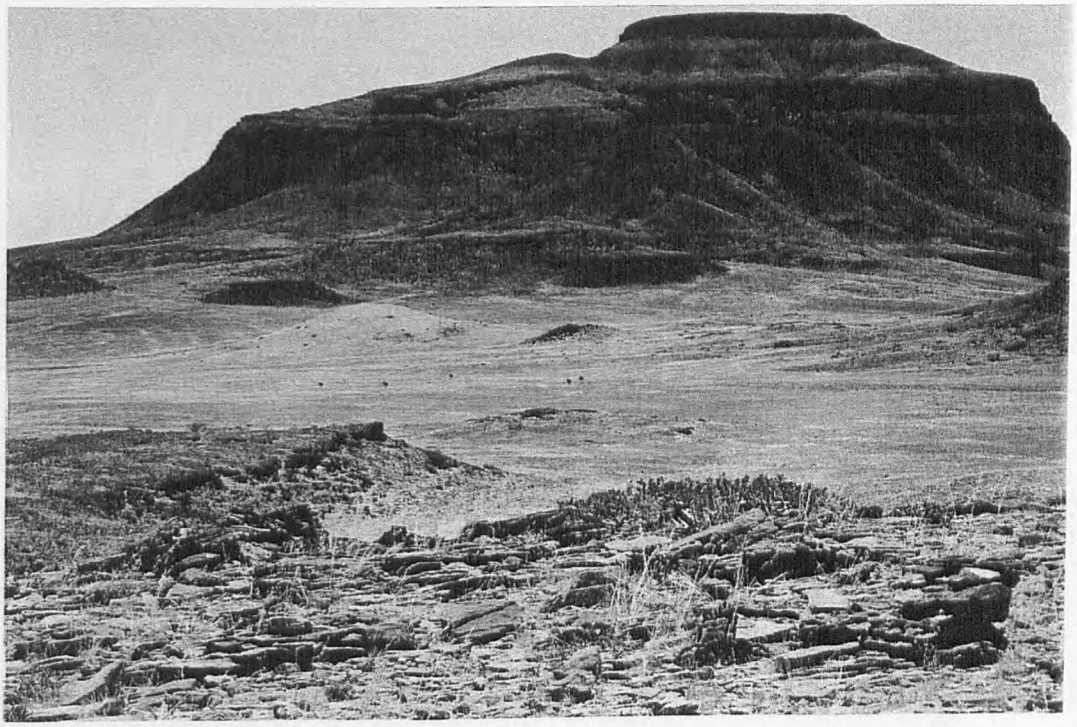

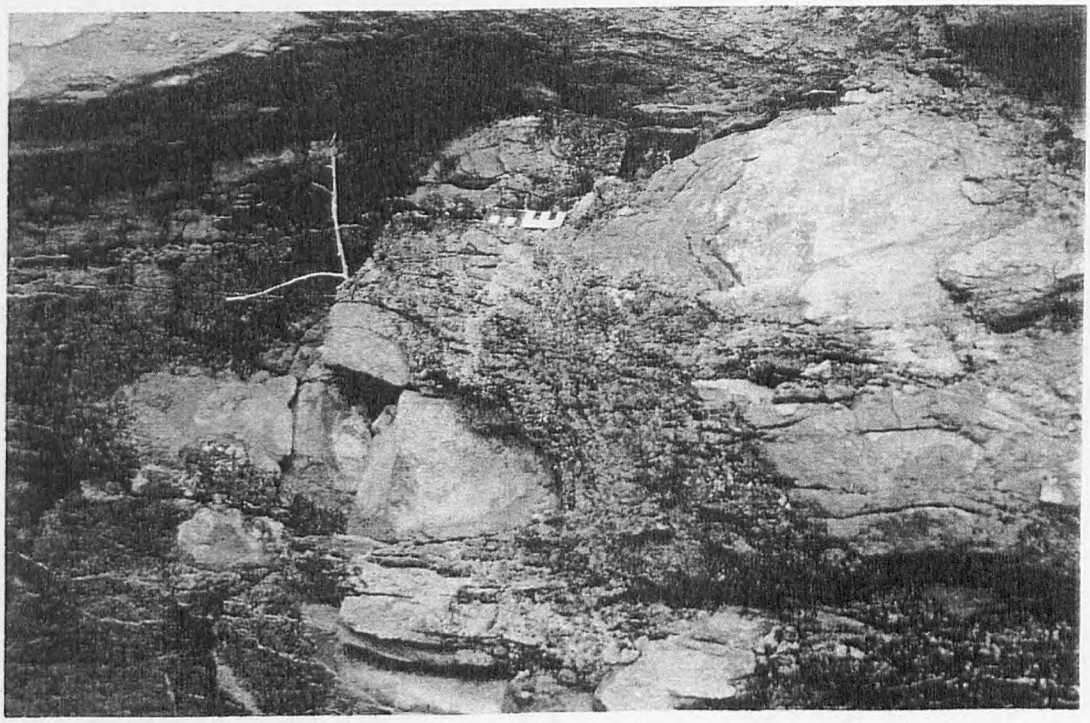

Fig. 4.9. Effect of magmatic underplating 10 km of basaltic material on the regional geothermal gradient , after Brown *et al.*, (1994).The model takes into account the conductive and advective transfer of heat within the lithosphere and also accommodates transient thermal anomalies. It is a numerical solution that assumes constant temperature boundary conditions at the surface and the base of the numerical grid and involves a heat production term (1 x 10^{-6} W m^{-3}) in order to obtain a near-surface steady state thermal gradient of 25 °C km^{-1}. Lower thermal boundary layer was kept at a constant temperature of 1350 °C. The lithosphere and crust have a combined thickness of 120 km (80 km and 40 km respectively). Density was assumed to be temperature dependent.

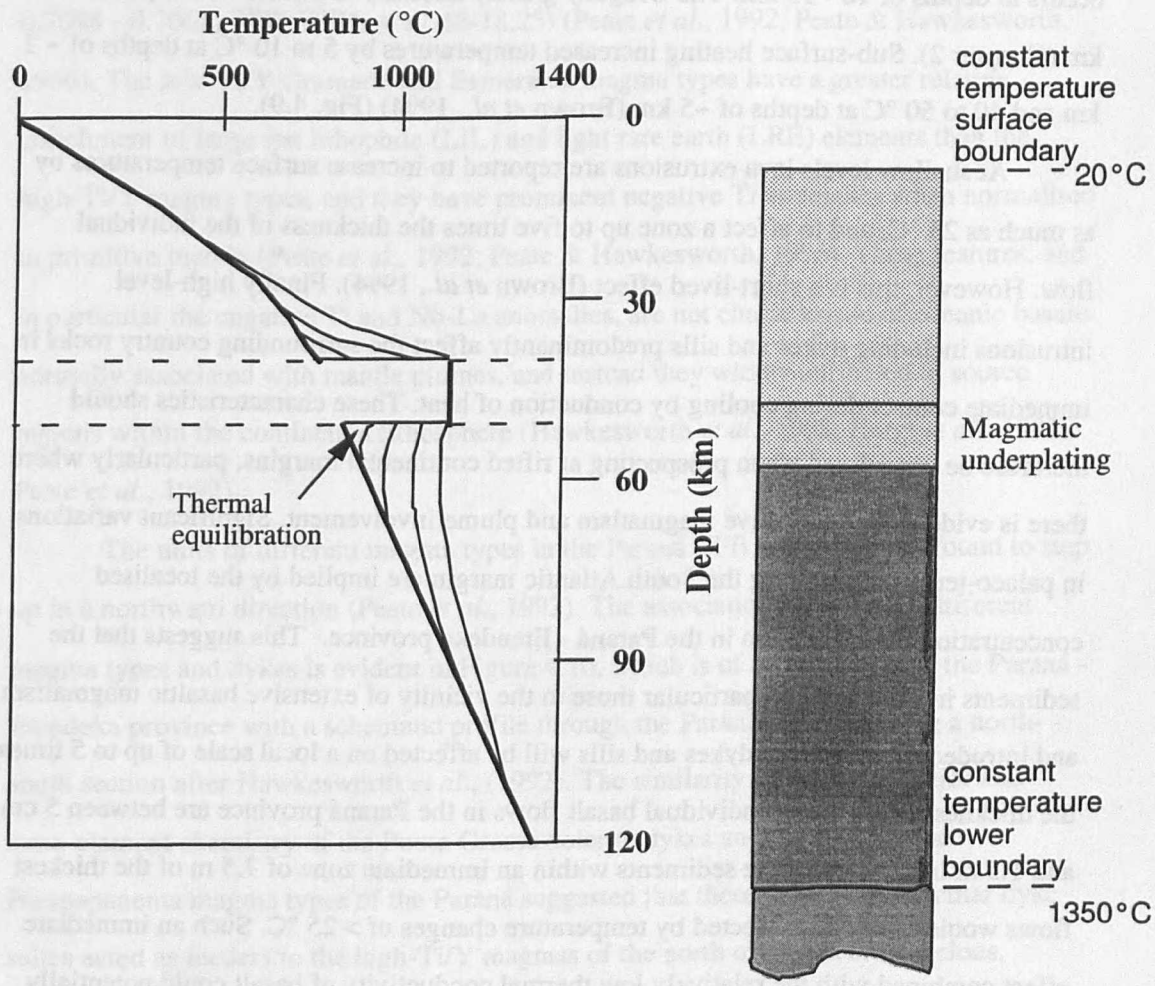

The sediments have undoubtedly been affected thermally both by the extrusion of the main Paraná - Etendeka CFB and associated lavas in the Early Cretaceous, and the associated magmatic underplating and high-level emplacement of dykes and sills. Such

thermal consequences of magmatic activity have previously been discussed by Brown *et al.* (1994) (Fig. 4.9), and although the details of their model are not repeated here, a number of their findings are important to this discussion. A simple shear extension model produced 100 km of extension over 10 my and this was shown not to elevate near surface temperatures significantly with a maximum sub-surface heating of ~ 10 °C at 4 to 5 km, but rather to concentrate excess heat at depths of between 60 and 100 km. Magmatic underplating, which at a minimum can be considered to be at least equal to the volume of material extruded at the surface (Cox, 1993), was shown to have a much greater effect than extension by altering the regional geothermal gradient particularly if underplating occurs at depths of 10 - 15 km. The Uruguay gravity anomaly is located at a depth of 15 km (Chapter 2). Sub-surface heating increased temperatures by 5 to 10 °C at depths of ~ 1 km and 40 to 50 °C at depths of ~5 km (Brown *et al.*, 1994) (Fig. 4.9).

At shallow levels lava extrusions are reported to increase surface temperatures by as much as 25 °C, and to affect a zone up to five times the thickness of the individual flow. However, this is a short-lived effect (Brown *et al.*, 1994). Finally high-level intrusions including dykes and sills predominantly affect the surrounding country rocks in immediate contact during cooling by conduction of heat. These characteristics should therefore be considered when prospecting at rifted continental margins, particularly where there is evidence for extensive magmatism and plume involvement. Significant variations in palaeo-temperature along the South Atlantic margin are implied by the localised concentration of magmatism in the Paraná - Etendeka province. This suggests that the sediments in this region in particular those in the vicinity of extensive basaltic magmatism and intruded by associated dykes and sills will be affected on a local scale of up to 5 times the thickness of the flow. Individual basalt flows in the Paraná province are between 5 cm and 1.5 m implying that the sediments within an immediate zone of 7.5 m of the thickest flows would have been affected by temperature changes of > 25 °C. Such an immediate effect combined with the relatively low thermal conductivity of basalt could potentially prolong the effect particularly if significant burial occurred with the result that hydrocarbon source rocks and reservoirs would be destroyed. The effects of magmatism on sediments is therefore immediate primarily within the top 2 km of the surface.

4.10. Lava Stratigraphy & its Relationship to dyke composition and orientation.

As discussed earlier, the relationship of the surface lavas and the dykes is of prime importance in understanding the relationship between rifting and magmatism in the South Atlantic, and the timing of the different extension episodes. A 3D stratigraphy of the different magma types in the Paraná lava pile is available through the use of borehole material and surface mapping (Peate *et al.* 1990, 1992). The high-Ti/Y magmas include the Pitanga, Paranapanema, Urubici and Ribeira magma types and are characterised chemically by negative Nb-Ta anomalies relative to the light rare earth (LRE) and large ion lithophile (LIL) elements, and a restricted range in isotope ratios ($^{87}Sr/^{86}Sr_{130}$ = 0.7048 - 0.7065; $^{206}Pb/^{204}Pb$ = 17.46-18.25) (Peate *et al.*, 1992; Peate & Hawkesworth, 1996). The low-Ti/Y Gramado and Esmeralda magma types have a greater relative enrichment of large ion lithophile (LIL) and light rare earth (LRE) elements than the high-Ti/Y magma types, and they have prominent negative Ti anomalies when normalised to primitive mantle (Peate *et al.*, 1992; Peate & Hawkesworth, 1996). These features, and in particular the negative Ti and Nb-La anomalies, are not characteristic of oceanic basalts normally associated with mantle plumes, and instead they widely attributed to source regions within the continental lithosphere (Hawkesworth *et al.*, 1988; Hergt *et al.*, 1991; Peate *et al.*, 1992).

The units of different magma types in the Paraná CFB province were found to step up in a northward direction (Peate *et al.*, 1992). The association between the different magma types and dykes is evident in Figure 4.10, which is of a sketch map of the Paraná - Etendeka province with a schematic profile through the Paraná lava pile along a north-south section after Hawkesworth *et al.*, (1992). The similarity between the major and trace-element chemistry of the Ponta Grossa dolerite dykes and the Pitanga and Paranapanema magma types of the Paraná suggested that these coast perpendicular dyke suites acted as feeders to the high-Ti/Y magmas of the north of the basin (Regelous, 1993). The dykes of the Ponta Grossa region trend NW - SE (Piccirillo *et al.*, 1990) (Fig. 4.10), and in recent studies by Regelous (1993) and Renne *et al.* (1996) were found to be of a similar age to some of the basalts. Dykes of both normal and reverse polarities have been recorded by Ernesto & Pacca (1988) therefore the dykes are considered to have been

intruded over a period of at least 0.8 Ma. The high-Ti/Y magmas and the associated dykes are therefore considered to have a bimodal age distribution with some of the lavas particularly those related to the eastern Paraguay dykes slightly older than the main phase of activity. The stretching factor (β) during this early magmatic stage has been measured as 1.1 (Oliveira, 1989).

The stretching factor (β) increased towards infinity as oceanic magmatism proceeded, with an average crustal β factor of 2.16 calculated on the Brazilian continental shelf by Chang *et al.* (1992) which increased almost linearly to $\beta = 5.8$ at the ocean - continent boundary (*ibid*). The coast-parallel dykes (Fig. 4.10) which are chemically similar to the more voluminous low Ti/Y magma types, indicate a change in the principal stress regime and an increase in β to ~ 1.4 at 133 Ma. The amount of crustal extension is constrained by the lateral extent of the rhyolites (calculated at between 240 and 500 km, Milner *et al.*, 1995) which succeded the eruption of the majority of the basalts. These rhyolites had to be erupted prior to major crustal extension otherwise the lateral extents would have to be the much greater than previously realised for similar extrusives. Therefore the main phase of extension parallel to the final rift commenced at 134 Ma when the orientation of the principle stress regime changed from NE - SW to roughly E - W, and this coincides with the eruption of the main volume of lava between 134 and 130 Ma.

Fig. 4.10. **(a) N-S section through the Paraná lava pile illustrating the internal stratigraphy based on the chemical divisions of Peate *et al.*, (1990; 1992). (b)Map of chemical association of dykes and lava flows as defined by Peate et al., (1992).**

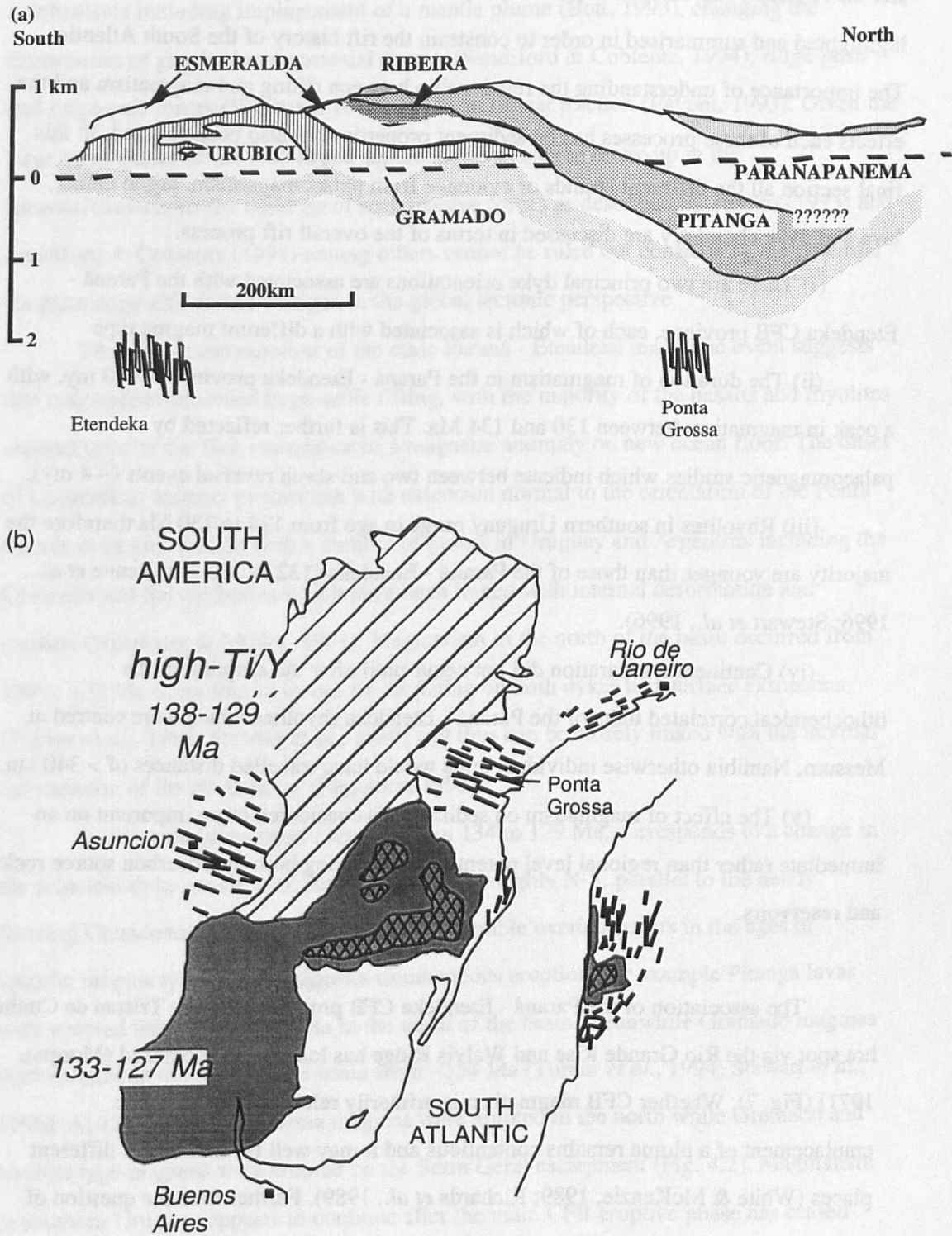

4.11. Discussion of Magmatism and Rifting.

During the course of this study new age data from southern Uruguay, the Etendeka and the African coast have been presented and a number of important features have been highlighted and summarised in order to constrain the rift history of the South Atlantic. The importance of understanding the relationship between rifting and magmatism and the effects each of these processes has on sediment properties has also been stressed. In this final section all the different strands of evidence from palaeomagnetism, argon dating, lava and dyke chemistry are discussed in terms of the overall rift process.

(i) There are two principal dyke orientations are associated with the Paraná - Etendeka CFB province, each of which is associated with a different magma type.

(ii) The duration of magmatism in the Paraná - Etendeka province is ~10 my, with a peak in magmatism between 130 and 134 Ma. This is further reflected by palaeomagnetic studies which indicate between two and seven reversal events (~ 4 my).

(iii) Rhyolites in southern Uruguay range in age from 124 to 130 Ma therefore the majority are younger than those of the Paraná - Etendeka (132 to 130 Ma; Renne *et al.*., 1996; Stewart *et al.*, 1996).

(iv) Continental separation did not occur until after the eruption of the lithochemical correlated units of the Paraná - Etendeka rhyolites which were centred at Messum, Namibia otherwise individual units would have travelled distances of > 340 km.

(v) The effect of magmatism on sediments is considered more important on an immediate rather than regional level potentially destroying both hydrocarbon source rocks and reservoirs.

The association of the Paraná - Etendeka CFB province with the Tristan da Cunha hot spot via the Rio Grande Rise and Walvis Ridge has long been recognised (Morgan, 1971) (Fig. 7). Whether CFB magmatism is primarily related to rifting or the emplacement of a plume remains contentious and it may well be different in different places (White & McKenzie, 1989; Richards *et al.*, 1989). Furthermore the question of whether magmatism is a response to the impingement of a mantle plume thinning the

lithosphere, and rising adiabatically, or whether magmatism is related to changes in the overall stress regime and absolute plate motions needs to be addressed.

Stretching of the lithosphere can occur via a variety of different active and passive mechanisms including impingement of a mantle plume (Bott, 1993), changing the distribution of gravitational potential energy (Sandiford & Coblentz, 1994), ridge-push and ridge-pull forces (Whittaker *et al.*, 1992) and shear traction (Pavoni, 1993). Given the large areal extent of the Gondwana supercontinent prior to break-up in the Jurassic/Cretaceous the build up of such passive forces as described by Pavoni (1993) and Sandiford & Coblentz (1994) among others cannot be ruled out considering the potential for plate edge effects and changes in the global tectonic perspective.

The timing and duration of the main Paraná - Etendeka magmatic event suggests that magmatism preceded large-scale rifting, with the majority of the basalts and rhyolites erupted prior to the first occurrence of a magnetic anomaly on new ocean floor. The onset of magmatism appears to correlate with extension normal to the orientation of the Ponta Grossa dyke swarm, and with a number of basins in Uruguay and Argentina including the Colorado and Salado basins which have been linked with internal deformation and rotation (Nürnberg & Müller, 1991). Magmatism in the north of the basin occurred from 138 to 132 Ma according to recent Ar-Ar dating on both dykes and surface extrusions (Turner *et al.*, 1994; Stewart *et al.*, 1996) and thus can be closely linked with the internal deformation of South America (Regelous, 1993).

An increase in magmatic activity from 134 to 129 Ma, corresponds to a change in the principal dyke orientation, from NW - SE to roughly N-S, parallel to the newly forming Cretaceous continental margin. Considerable overlap occurs in the ages of specific magma types which suggests simultaneous eruption, for example Pitanga lavas were erupted from 138 to 134 Ma in the north of the basin, meanwhile Gramado magmas were erupted in the south of the basin from ~134 Ma (Turner *et al.*, 1994; Stewart *et al.*, 1996). At 133 Ma Paranapanema magmas were erupted in the north while Gramado and Urubici type magmas were erupted on the Serra Geral escarpment (Fig. 4.2). Magmatism in southern Uruguay appears to continue after the main CFB eruptive phase has ceased with the eruption of silicic volcanics which have been dated in this study at between 130 and 123 Ma. Increased deviatoric stresses associated with final continental separation are

considered responsible for the arrival of these crustal melts at the surface by lowering the confining pressures.

Conclusions.

Firstly that there is no simple association between magmatism and rifting, but the duration of the magmatic event can place constraints on the origin of the magmas as rapid eruption rates are proposed to involve large scale decompression melting of a mantle plume. The age of the Paraná - Etendeka province has been constrained to within ten million years, the spread in this data from 138 to 127 Ma is important for any proposed interpretation on the association between rifting and magmatism. The main eruptive phase is centred between 134 and 130 Ma according to the frequency of ages obtained (Fig. 4.5).

Plume involvement in the province is recognised in order to generate such large volumes of magmas. The regional affect of such a plume on sedimentation is considered minimal. However high-level intrusions such as sills and dykes are considered to have an immediate affect on the local scale, and may be important when investigating the potential of offshore hydrocarbon resources in or close to a large volume igneous province.

Changes in the orientation of the regional stress field in the Paraná - Etendeka are linked with changes in the rate at which magma reaches the surface which suggests that increased regional extension factors are important in the generation of large-volume igneous provinces.

Chapter 5.

Summary: Melt production in Uruguay.

5.1. Introduction.

Basaltic and rhyolitic magmatism of Cretaceous age is found in southern Uruguay where it is associated with a major positive gravity anomaly (Fig. 1.22). Previous work on the southern Uruguay exposures is limited and this thesis presents the first major geochemical and geochronological study of the Puerto Gómez Formation basalts and the Arequita Formation rhyolites. In particular new geochemical and geochronological data provides new insights into the relationship of this magmatism to that of the Paraná - Etendeka flood basalt province and the Tristan plume, and to the opening of the South Atlantic.

The aim of this final chapter is to summarise the conclusions drawn from the previous chapters and to address the initial aims of this research which were outlined in Chapter 1. These aims were;

(a) to introduce the geology of Uruguay particularly the volcanic rocks of the Early Cretaceous;

(b) to characterise these extrusive basalts and rhyolites and to establish a model for their origin using petrography, geochemistry and geochronology;

(c) to date precisely the extrusive volcanics and to evaluate the relationship between the Uruguayan rocks and those of a similar age and composition in the Paraná - Etendeka;

(d) to provide greater insight into the processes of rifting and magmatism in a continental setting by understanding the petrogenesis of the rocks at the surface;

(e) to add to the understanding of the tectonic processes that operated in the South Atlantic region pre-, syn- and post-rifting by obtaining absolute ages for the coastal dykes on both

sides of the present day ocean and estimating the amounts of extension at particular times leading up to the opening of the South Atlantic.

5.2. Petrogenesis of the Puerto Gómez Formation.

The basalts and andesites of the Puerto Gómez Formation are tholeiitic and composed predominantly of clinopyroxene, plagioclase, iron oxides ± olivine ± pigeonite. The normative mineralogies of diopside, olivine, hypersthene and quartz suggest they were last in equilibrium at ~1 atm pressure in the plagioclase stability zone indicating differentiation at relatively shallow levels in the crust. Chemically and isotopically the Puerto Gómez Formation can be divided into two magma types, the more voluminous Treinte Y Trés magma type and the rare Santa Lucía magma type (Chapter 2).

The Treinte Y Trés magma type shares many chemical similarities with the low Ti Gramado magma type of the Paraná, and its compositional equivalent (Tafelberg member) in the Etendeka. Detailed chemical modelling indicates that the Treinte Y Trés and the Gramado magma types have a common source, inferred to be in the sub-continental lithospheric mantle. The parental magmas were subsequently affected by shallow level assimilation of upper crustal components and extensive fractional crystallisation, resulting in a wide range of evolved compositions (Mg #, 34 to 70) and Sr isotopic ratios (0.7089 - 0.7210).

The Santa Lucía magma type is unique and bears little resemblance to basalts previously described from the Paraná province. The Santa Lucía basalts are considered to be asthenospheric melts on the basis of their smooth primitive mantle-normalised incompatible element patterns and in having trace-element ratios similar to those of Tristan. Furthermore the Santa Lucía basalts have relatively unradiogenic $^{143}Nd/^{144}Nd_i$ values (0.5124 to 0.5122) and so mixing between a Tristan end member ($^{143}Nd/^{144}Nd$ = 0.5126 - 0.5124) and magma with more enriched isotope ratios has been proposed. In fact, simple magma mixing of a Treinte Y Trés basalt and a Tristan basalt reproduces the observed variation within the Santa Lucía magma type. This is the first documented occurrence of basalt similar to those on the Tristan hot-spot being contemporaneous with

the main Paraná flood basalt event and potentially marks the transition from lithospheric to asthenospheric-derived melts in the Paraná province.

5.3. Petrogenesis of the Arequita Formation.

The Arequita Formation consists of trachydacites and rhyolites with an anhydrous mineralogy of plagioclase, pyroxene, alkali feldspar, iron oxides ± quartz. The Arequita Formation rhyolites have been divided into two types on the basis of petrology. Type 1 contains the least evolved samples which are predominantly trachydacites with orientated feldspar phenocrysts. Type 2 is the more voluminous rhyolite type, and it is characterised by the presence of variably sized rounded to euhedral quartz phenocrysts and frequently preserved ignimbritic textures. The occurrence of such textures is highly unusual in rhyolites associated with the Paraná - Etendeka province even though a number of authors have inferred the rhyolites to be ignimbrites (Whittingham, 1991; Milner *et al.*, 1992; Milner *et al.*, 1995). The lack of well preserved pyroclastic textures elsewhere in the province has been attributed in part to the high temperatures associated with the Paraná - Etendeka rhyolites of between 950 and 1050 °C, which have resulted in rewelding of the original ignimbritic textures (Bellieni *et al.*, 1988; Milner *et al.*, 1992; Garland *et al.*, 1995).

The two rhyolite types recognised petrologically do not define distinct compositional groups based on major- and trace- element data, although the more quartz-rich rocks tend to be more evolved. Instead the rhyolite data from southern Uruguay have been divided chemically into two series, the Lascano Series and the Aigüa Series, which are not equivalent to the rhyolite types previously described on the basis of petrology. These series were identified on the basis of trace element and isotopic data with the Lascano Series characterised by high Sr, Ti/Zr, Eu/Eu* and lower Nb and Zr, and a wide range of initial Sr and Nd isotope ratios. The Aigüa parental magma is characterised by low Sr contents with low Ti/Zr, Eu/Eu*. Low εNd_i and $^{87}Sr/^{86}Sr_i$ ratios are also diagnostic of the Aigüa Series.

The source of the Lascano Series is also considered to be lower crustal but with notable high-level contamination by upper crustal components in order to generate the

wide variation in $^{87}Sr/^{86}Sr_i$ and Rb/Ba evident within the series. The Lascano source is characterised by higher Ti/Zr and Eu/Eu* than the Aigüa Series.

Uruguayan rhyolites as a whole are distinct from the rhyolites of the Paraná-Etendeka in terms of both petrology and composition. The differences are potentially temperature related, as suggested in Chapter 3 and summarised below. The timing of the rhyolitic magmatism (Chapter 4 and Stewart *et al.*, 1996) is seen to post-date much of the earlier basaltic volcanism and is more closely related to the formation of the first oceanic crust at M4 (126 - 127 Ma, Kent & Gradstein, 1985), suggesting that increased extension facilitated the melting and extrusion of these rhyolites.

5.4. Temperature variations and the Origin of the Rhyolites.

Calculation of accurate temperatures for the Uruguay rhyolites has proved to be difficult in view of the evidence for disequilibrium between co-existing phenocrysts and between phenocrysts and the melt. Temperatures from southern Uruguay are however consistently lower than those calculated for the Paraná rhyolites independent of the thermometer applied. Trachydacites of the Lascano Series yielded the highest temperatures from apatite thermometry (900 - 1037 °C) while the rhyolites of the Lascano Series are indistinguishable from those of the Aigüa Series on all thermometers, with temperatures in the region of 850 ± 100 °C.

An extensive trans-Atlantic comparison of the eruptive sequences of the Paraná - Etendeka rhyolites by Milner *et al.* (1995), suggested that the Awahab Formation low Ti rhyolites correlated with the lower most units of the Palmas group of the Paraná, and erupted from the Messum alkalic complex in the Etendeka (Milner & Ewart, 1989). The rhyolites of the Tafelberg member were correlated with some of the uppermost Palmas units and while the centre of eruption for these rhyolites has not been recognised it has been inferred from stratigraphy to be closer to Brazil (Milner *et al.*, 1995; Garland *et al.*, 1995).

Temperature estimates from a number of different geothermometers appear to indicate that the Uruguay rhyolites were erupted at lower temperatures than the geographically adjacent rhyolites of the Paraná - Etendeka. The Etendeka rhyolites are

high temperature (1000 - 1100°C) rheoignimbrites, with localised development of pyroclastic textures (Milner *et al.*, 1992). The development of the ignimbritic textures previously described from the Uruguay rhyolites suggests that at least some of these rhyolites are associated with pyroclastic activity. No caldera structure has however been recognised in the region, and in view of the distinctive chemistry of these rhyolites when compared with those of the Paraná - Etendeka province it is unlikely that they were sourced in either the Messum complex or from a similar complex to that proposed for the Upper Palmas units and Tafelberg rhyolites.

The rhyolites from southern Uruguay that lack eutaxitic textures are considered to be lavas, since they are characterised by a number of features typical of felsic lavas including trachytic alignment, flow banding and flow folding. Effusion of silicic lava via acid dykes is considered to have occurred contemporaneously with the main explosive events as the rhyolites of both petrologic types have been shown to be related via assimilation and/or fractional crystallisation processes within the two geochemically defined series.

5.5. Age of the Uruguay magmatic event.

The age of the volcanic rocks of southern Uruguay has been established by a detailed Ar - Ar dating study of 13 samples (6 basalts, 1 syenite and 6 rhyolites). The relatively phenocryst-rich nature of all the samples made them ideal for mineral separation with argon release from individual phenocrysts assuring minimum groundmass interference and hence a true 'closure' age for the sample. The stratigraphy of the lava pile suggested that the rhyolites were younger than the basalts and this was found to be the case with the basalts ranging in age from 134.0 ± 0.5 to 130.0 ± 2 Ma and the rhyolites from 130.9 ± 0.7 to 123.9 ± 0.4 Ma. The basalt age range is similar to that described for the lavas of the Serra Geral escarpment of the southern Paraná (Renne *et al.*, 1992, 1996; Turner *et al.*, 1994; Stewart *et al.*, 1996) which is mainly composed of the Gramado and Esmeralda magma types. This is therefore consistent with the conclusion from Chapter 2 that the main volume of basaltic lava in southern Uruguay was derived from similar

source regions to the Gramado magma type. The age range of the rhyolites is much larger than anticipated from the rhyolite activity in the Paraná - Etendeka (predominantly 132 to 130 Ma, Stewart *et al.*, 1996; Renne *et al.*, 1996b); but there is no evidence to suggest that the ages are unreliable particularly as the plateau age was averaged over 10 to 20 'steps' for many of the samples (Chapter 4).

An intrusive syenite of the Valle Chico Formation was dated by laser step heating of biotite separates at 132.0 ± 0.3 (plateau age). This is contemporaneous with similar intrusive complexes in the Damaraland province which have been dated between 137.0 ± 0.7 (Paresis, Milner *et al.*, 1995b) and 129.3 ± 0.7 Ma (Messum, Renne *et al.*, 1996b; Stewart *et al.*, 1996).

5.6. Duration of magmatism.

The dating of the Paraná - Etendeka province and hence the duration of magmatism has been the centre of much debate recently. In particular Renne *et al.* (1992) proposed that the entire Paraná - Etendeka volcanic province was erupted in less than one million years, while Turner *et al.*, (1994) and Stewart *et al.*, (1996) proposed a much longer time frame of between 10 to 12 my. More recently the duration of the extrusive and intrusive activity was inferred by Renne *et al*, (1996b) to be between 129 and 133 Ma with an overall 3 to 4 my duration, however this is still shorter than that proposed by Turner *et al.*, (1994) and Stewart *et al.*, (1996). These latter studies have published age ranges from the north-western part of the Paraná basin of between 138 and 132 Ma, with basalts and rhyolites further south ranging from 133 to 127 Ma. The protracted eruption time scale is thought to be supported by the intercalation of sand dunes and lavas at the base of the formation and by the recognition of at least one erosional surface (Milner *et al.*, 1995; Stewart *et al.* 1996).

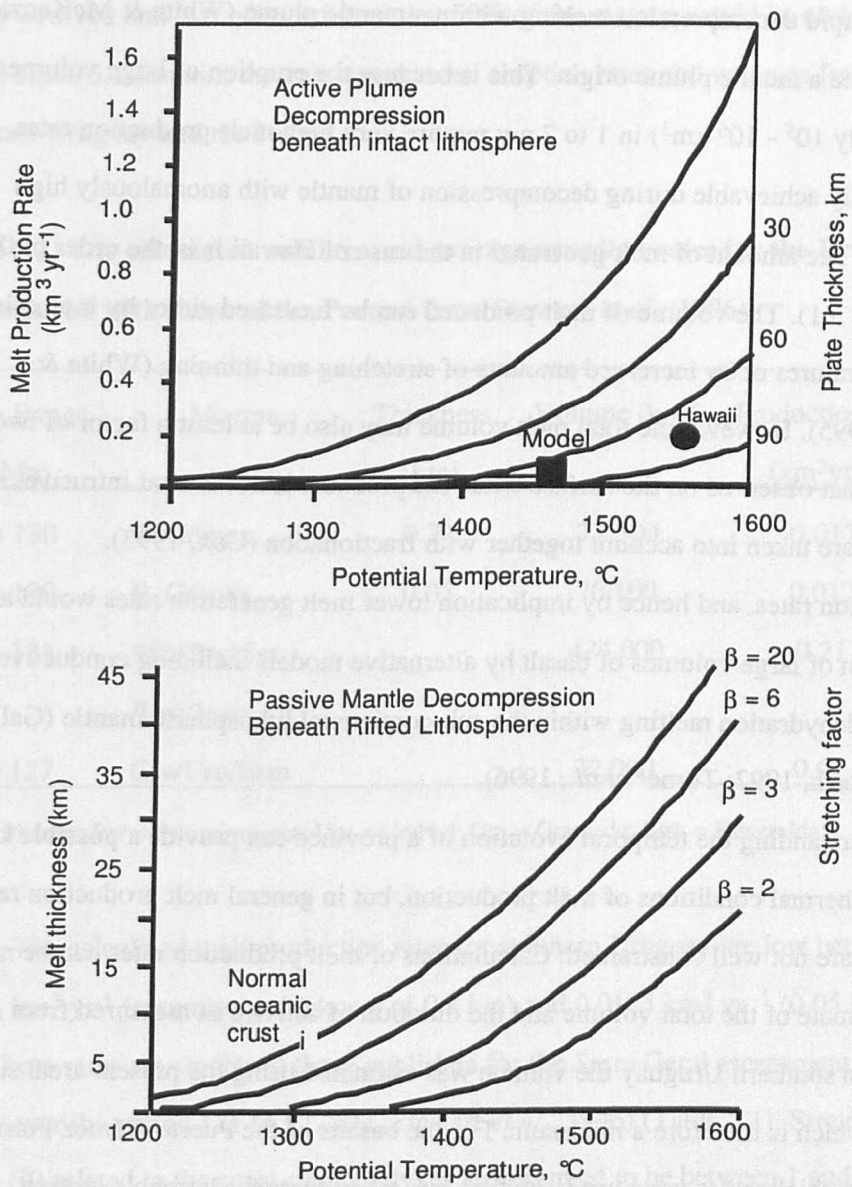

Fig. 5.1. Models of active plume decompression beneath intact lithosphere (a) and (b) Passive mantle decompression beneath rifted lithosphere after White &McKenzie (1995). Filled square represents the proposed temperature and melt-production rate assuming decompression melting as discussed in the text.

The debate over the duration of magmatism is important for a number of reasons. An implied mean eruption rate on the order of 1.5 km^3 yr^{-1} (Renne *et al.*, 1992) can be explained by rapid decompression melting within a mantle plume (White & McKenzie, 1995) and hence a mantle plume origin. This is because the eruption of large volumes of basalt (typically 10^5 - 10^6 km^3) in 1 to 2 my require very high melt-production rates, and these are readily achievable during decompression of mantle with anomalously high temperatures. The amount of melt generated in the case of Hawaii is in the order of 0.16 km^3 yr^{-1} (Fig. 5.1). The volume of melt produced can be increased either by increasing mantle temperatures or by increased amounts of stretching and thinning (White & McKenzie, 1995). However the total melt volume may also be at least a factor of two greater than that observed on the surface when the probable lower crustal intrusives and underplating are taken into account together with fractionation (Cox, 1993).
Slower eruption rates, and hence by implication lower melt generation rates would allow for generation of large volumes of basalt by alternative models including conductive heating and dehydration melting within the sub-continental lithospheric mantle (Gallagher & Hawkesworth, 1992; Turner *et al.*, 1996).

Understanding the temporal evolution of a province can provide a possible key to the tectono-thermal conditions of melt production, but in general melt production rates within CFB are not well constrained. Calculations of melt production rates can be made from an estimate of the total volume and the duration of activity as measured from Ar - Ar dating. In southern Uruguay the volume was estimated using the present areal surface exposures which is therefore a minimum. For the basalts of the Puerto Gómez Formation two different thicknesses were used, the first was taken from the borehole section (DDH502, Fig. 1.22) where the total thickness of mafic material encountered was 0.7 km, while the second is simply the basalt thickness at the surface (~ 5 m). To these values were added the volume estimated from the gravity anomaly (35,000 km^3) that underlies the surface exposures, which was doubled assuming 50% underplating (Cox, 1993). The total was divided by the duration of activity for the Uruguay basalts, which was inferred from Ar - Ar dating results to be 4 my. The thickness of the basalts has only a limited effect on the overall calculated eruption rate because the total volume is dominated by the

large volume of mafic material inferred to lie in the middle crust (Table 5.1). Melt production rates are assumed to be twice that of the eruption rate since the lavas are highly evolved and it is often inferred that 50% of the magma would be underplated (Cox, 1993. Table 5.1 contains the calculated areas, eruption rates and volumes for the basalts of southern Uruguay and the Paranà.

Table 5.1. The calculated volumes and average eruption rates for the Uruguay lavas as compared with those of the Paraná from Stewart *et al.* (1996).

Age Range (Ma)	Magma	Thickness (km)	Volume (km^3)	Production rate (km^3yr^{-1})
134 to 130	P. Gómez	0.77	71,300	0.017
134 to 130	P. Gómez	0.05	70,100	0.017
133 to 131	*Pit/Par/Gra /Uru/Esm		424,000	0.21
131 to 127	Gra/Uru/Esm		32,000	0.01

* Pit = Pitanga; Par = Paranapanema; Uru = Urubici; Gra = Gramado; Esm = Esmeralda;

The calculated melt production rates for southern Uruguay are low between 0.0178 $km^3\ yr^{-1}$ (assuming a thickness of 0.7 km) and 0.0175 $km^3\ yr^{-1}$ (0.05 km) (Table 5.1). These rates are similar to those published for the Serra Geral escarpment lavas in the Paraná over the period 131 to 127 Ma (Stewart *et al.*, 1996) (Table 5.1). Stretching factors (β) related to the coast-parallel dykes are assumed to be between 1 and 1.1 at the time of production of the thickest lava sequences (Oliveira, 1989). Extension increased towards infinity (•) at final rifting (126 - 127 Ma), and by 131 Ma it is assumed that $\beta \bullet 2$ assuming a linear relationship between stretching and time (Fig. 5.2). Therefore assuming an initial lithospheric thickness (z_{lo}) of 160 km the attenuated lithosphere would be 80 km (z_l) at 131 Ma. If the melt is produced from decompression melting in the asthenosphere and the mantle potential temperature (T_p) was 1480 °C as proposed by Gallagher & Hawkesworth (1994), the melt production rate for 80 km thick lithosphere would be •

0.001 $km^3\ yr^{-1}$ (Fig. 5.1) (White & McKenzie, 1994). It is therefore impossible to produce the volume of melt evident by decompression melting, without a large degree of attenuation at similar temperatures. Large scale extension was therefore clearly important in the generation of the flood basalts of the Paranà province.

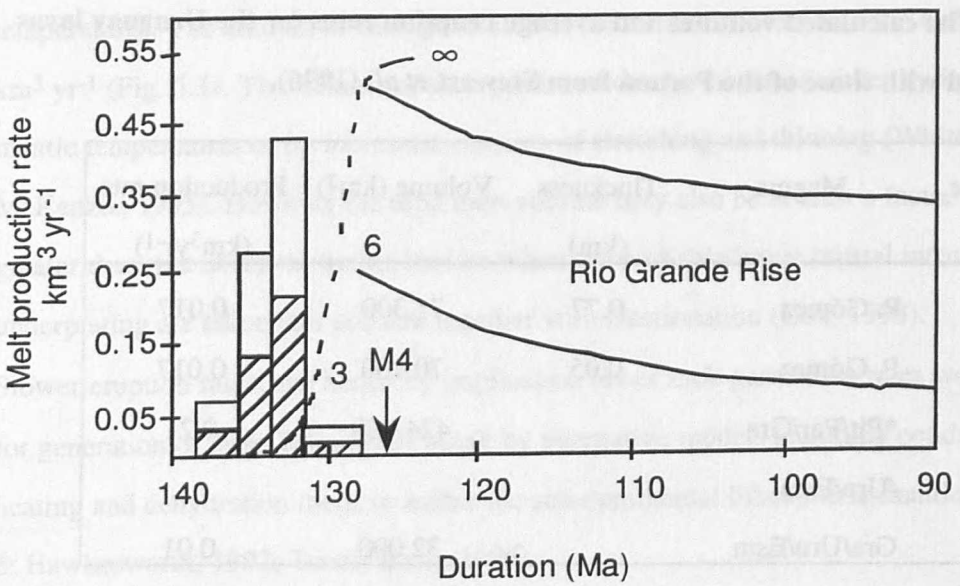

Fig. 5.2. Magma eruption/production rates versus time during the evolution of the Paraná province and the associated oceanic trace. M4 marks the age of the oldest magnetic anomaly found in the South Atlantic at the latitude of the Paraná (Nürnberg & Müller, 1991). The shaded area represents the calculated eruption rates and the open column is the amount assumed to be underplated (Cox, 1980). The dashed curve represents the melt production rates in the asthenosphere predicted by back tracking the plume (Tp = 1490 °C) beneath the continent and assuming the extension rate rapidly decreases both on moving onland and with increasing age. Diagram from Stewart *et al.*, (1996).

Evidence in support of melting eventually occurring by decompression of the asthenosphere instead of by conduction in the lithospheric mantle is best observed in southern Uruguay where for the first time there is evidence of mixing between an asthenosphere-derived Tristan magma type and a melt of lithospheric mantle (Chapter 2). This observation has important implications regarding the positioning of the associated plume during the early Cretaceous. Southern Uruguay, according to current models of the

plume position during the Early Cretaceous, lay at the periphery of the influence of the plume. However, the presence of asthenosphere-derived melts in southern Uruguay is therefore highly unusual as greater degrees of melting are expected where the plume is hottest, at the centre rather than on the margins.

5.7. Model for rifting in the South Atlantic.

Magmatism in the Paraná - Etendeka province is considered to be bimodal with the main volume of lava erupted between 131 and 133 Ma prior to the onset of seafloor spreading in the South Atlantic at 126 Ma. An earlier phase of magmatic activity between 138 and 135 Ma has been highlighted by the work of Turner *et al.* (1994) and Stewart *et al.* (1996). These older dates are primarily for samples of the Pitanga and Paranapanema magma types in the northwest of the Paraná province. These magma types have been chemically linked to the Ponta Grossa dyke swarm in the Paraná State, northeastern Brazil (Regelous, 1993) and the dyke swarm of eastern Paraguay. The Ponta Grossa dyke swarm and similarly orientated dykes in eastern Paraguay together with the Mesozoic Salado, Colorado, Santa Lucía and Punte del Este basins of Argentina and Uruguay have been linked to internal deformation and clockwise rotation of southern South America with a predominant NE - SW extensional direction (Martin, 1987; Nürnberg & Müller, 1991; Chang *et al.*, 1992).

An increase in magmatic activity from 134 to 129 Ma, corresponds to a change in the principal dyke orientation, from NW - SE to roughly N-S, parallel to the newly forming Cretaceous plate margin. Coast-parallel dykes, which are also parallel to the regional structural lineaments in the underlying basement, are seen in Brazil, in particular along the Serra do Mar between Florianopolis and Rio de Janeiro. NE-SW trending dykes are also evident in the Sao Paulo and Rio de Janeiro States (Fig. 5.3). Moreover, this was the principal dyke orientation in Namibia and South Africa prior to break-up, where there is dense intrusive activity of similar age to the main flood basalt event (Fig. 5.3). Chemically, the coast-parallel dykes are similar to the low-Ti/Y Tafelberg and Gramado magma types of the Etendeka-Paraná (Erlank *et al.*, 1984).

Considerable overlap occurs in the ages of specific magma types which suggests simultaneous eruption of different magma types, for example at 133 Ma Paranapanema magmas were erupted in the north while Gramado and Urubici type magmas were erupted on the Serra Geral escarpment (Turner *et al.*, 1994; Stewart *et al.*, 1996). Magmatism in southern Uruguay appears to coincide initially, but to continue after the main CFB eruptive phase has ceased with the eruption of silicic volcanics which have been dated in this study at between 130 and 124 Ma. Increased deviatoric stresses associated with final continental separation are considered responsible for the arrival of these crustal melts at the surface by lowering the confining pressures.

The recognition of magnetic anomalies M9 and M7 off the southern tip of Africa and nowhere else along the margin suggests that initial seafloor spreading occurred in this region first and paved the way for the final rift stretching from the Falkland plateau to the Rio Grande Rise - Walvis Ridge. However from the dating project undertaken in this study of Uruguay lavas, Etendeka lavas and coast-parallel dykes in southern Africa there is little evidence to support a correlation between magmatism and an unzipping model of rifting in the southern South Atlantic as the study failed to detect any variation in the age of dykes along the South Atlantic margin.

The stretching factor (β) increased towards infinity as oceanic magmatism proceeded, with an average crustal β factor of 2.16 calculated on the Brazilian continental shelf by Chang *et al.* (1992) which increased almost linearly to $\beta = 5.8$ at the ocean - continent boundary (*ibid*). The coast parallel dykes (Fig. 5.3) indicate a change in the principal stress regime, with β increasing to a value of ~ 1.4 at 133 Ma. The amount of crustal extension is constrained by the lateral extent of the rhyolites (calculated at between 240 and 500 km, Milner *et al.*, 1995) which succeded the eruption of the majority of the basalts. These rhyolites had to be erupted prior to major crustal extension otherwise their lateral extent would have to be much greater than previously realised for similar extrusives. The main phase of extension parallel to the final rift is herein considered to have commenced at 134 Ma, when the orientation of the principal stress regime changed from NE - SW to roughly E - W, and this coincides with the eruption of the main volume of lava between 134 and 130 Ma.

The opening of the South Atlantic during the Early Cretaceous is considered to be a rather complex process which occurred due to a combination of changing tectonic stress regimes and the presence of a mantle plume. Initial rifting occurred off the southern tip of Africa as indicated by the magnetic anomalies. There appears to be little evidence to support a model of incremental rifting north of this region, as far as the Walvis Ridge - Rio Grande Rise and so instantaneous collapse in this region is proposed. The propagation of the rift north of the Walvis Ridge - Rio Grande Rise is considered to have been affected by the thermal anomaly and voluminous magmatism associated with the presence of both the Tristan plume and later the Trinidade plume.

The relationship between rifting and magmatism and in particular the role of the Tristan plume in relation to the opening of the South Atlantic is speculative. However, it can be inferred from the presence and orientation of the basins, and the change in principle stress regimes as indicated from the associated dyke swarms that Gondwana was undergoing considerable internal deformation. This deformation was probably due to a number of factors including plate edge effects and lateral variations in potential energy combined with increased activity along subduction margins resulting in large scale plate rotations. Delamination by active upwelling plumes (including Tristan and Trinidade) may also have contributed to lithospheric fracturing and crustal failure, but this process is not considered to be important here. Furthermore from the dating project undertaken in this study of Uruguay lavas, Etendeka lavas and coast-parallel dykes in southern Africa there is little evidence to support a correlation between magmatism and an unzipping model of rifting in the southern South Atlantic as the study failed to detect any significant variation in the age of dykes along the South Atlantic margin.

The involvement of plumes in this region is irrefutable, however the role of the plume with regard to the rifting process is considered minimal, rather it may have hindered the northward progression of the rift. In balancing the evidence presented in this thesis the conclusions drawn regarding the rifting of the South Atlantic must be that the process was controlled by extension. This extension resulted in thinning of the lithosphere which paved the way for asthenospheric (plume) material to ultimately reach the surface.

Fig. 5.3. **Dyke orientations associated with magmatism of the Paraná - Etendeka province.**

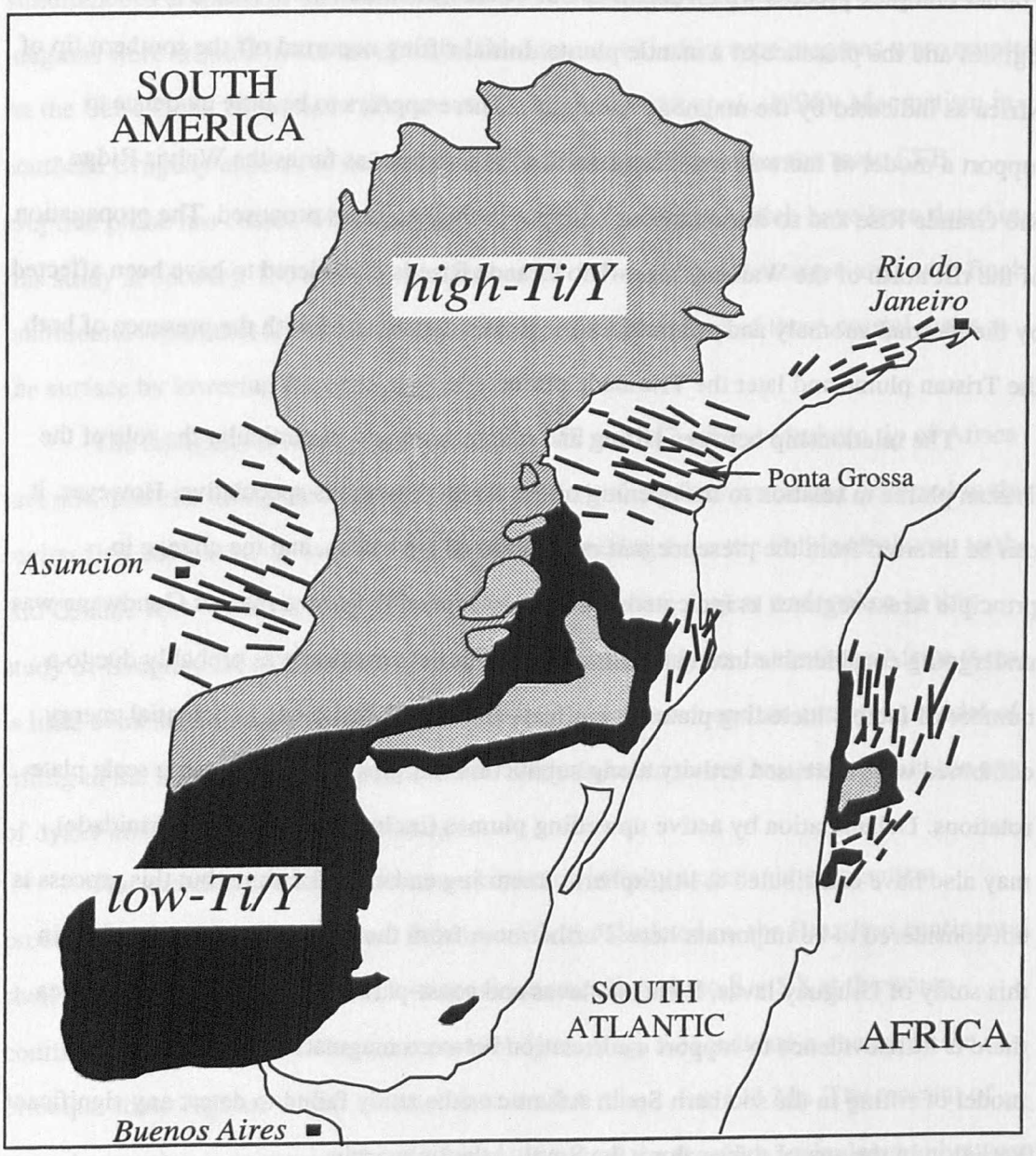

References

Alberti, A.; Piccirillo, E.M; Bellieni, G; Civetta, L; Comin-Chiarmonti, P; Morais, EA; (1992). *Mesozoic acid volcanics from southern Angola: petrology, Sr-Nd isotope characteristics and correlation with the acid stratoid volcanic suites of the Paraná Basin (south-eastern Brazil).* Eur. J. Mineral. **4**, 597-604.

Allegre, C.J; Hart, S.R & Minster, J.F (1983). *Chemical structure and evolution of the mantle and continents determined by inversion of Nd and Sr isotopic data, II, Numerical experiments and discussion.* Earth. Planet. Sci. Lett. **66**, 191-213.

Alric, V; Feraud, G; Bertrand,M; Haller,C; Labudia,C & Zubia,M. (1995). *$^{40}Ar/^{39}Ar$ dating of Patagonian Jurassic volcanism : new constraints on Gondwana break-up.* EUG8, Strasbourg, France, Blackwell Scientific Publications.

Amaral, G; Cordani, UG; Kawashita, K; Reynolds, JH (1966). *Potassium- argon dates of basaltic rocks from Southern Brazil.* Geochim. Cosmochim. Acta **30**, 159-189.

Anderson, D.L (1994). *The sublithospheric mantle as the source of continental flood basalts; the case against the continental lithosphere and plume head reservoirs.* Earth Planet. Sci. Lett. **123**, 269-280.

Arculus, R.J (1987). *The Significance of source versus process in the tectonic controls of magma genesis.* Jour. Volcan. Geothermal Res. **32**, 1-12.

Arndt, N.T & Christensen, U (1992). *The Role of Lithospheric Mantle in Continental Flood Volcanism: Thermal and Geochemical Constraints.* J. Geophys. Res. **97**, B7, 10,967-10,981.

Arndt, N.T; Czamanske, G.K; Wooden, J.L & Fedorenko, V.A (1993). *Mantle and crustal contributions to continental flood volcanism.* Tectonophysics **223**, 39-52.

Asmeron, Y; Jacobsen, S.B & Wernicke,B.P (1994). *Variations in magma source regions during large scale continental extension, Death Valley region, western United States.* Earth. Planet. Sci. Lett. **125**, 235-254.

Austin, J.A(Jr.) & Uchupi, E (1982). *Continental - Oceanic Crustal Transition Off Southwest Africa.* Am. Ass. Petroleum Geol. Bull. **66**, No.9, 1328-1347.

Bacon, C.R & Hirschmann, M.M (1988). *Mg/Mn partitioning as a test for equilibrium between coexisting Fe-Ti oxides.* American Mineralogist **73**, 57-61.

Baker, M.B; Hirschmann, M.M; Ghiorso,M.S & Stolper,E.M. (1995). *Compositions of near-solidus peridotite melts from experiments and thermodynamic calculations.* Nature **375**, 308-311.

Barbieri, M; Beccaluva, L; Brotzu,P; Conte,A; Garariño,C; Gomes,C.B; Loss,E.L; Macciotta,G; Morbidelli,L; Scheibe,L.F; Tamura,R.M & Traversa,G. (1987). *Petrological and Geochemical Studies of Alkaline Rocks from Continental Brasil. 1. Phonolite Suite from Piratini, RS.* Geochimica Brasiliensis **1**, 1, 109-138.

Barker, A.J. (1990). *Introduction to Metamorphic Textures and Microstructures* Glasgow and London, Blackie.

Barrie, CT (1995). *Zircon thermometry of high temperature rhyolites near volcanic - associated massive sulphide deposits, Abitibi subprovince, Canada.* Geology **23**, 2, 169-172.

Basu, A.R; Renne, P.R; Mertz, D & Poreda, R.J (1993). *Alkalic igneous complexes of the Deccan and Paraná; implications for the origin of continental flood basalts (CFB).* EOS **74**, 43, 552.

Bellieni, G; Brotzu, P; Comin Chiarmonti,P; Ernesto,M; Melfi,A; Pacca,I.G, Piccirillo,E.M &Stolfa,D (1983). *Petrological and Palaeomagnetic Data on the Plateau Basalt to Rhyolite Sequences of the Southern Paraná Basin (Brazil)* An. Acad. Brasil. Ciénc. **55**, 355-383.

Bellieni, G; Brotzu, P; Comin Chiarmonti,P; Ernesto,M; Melfi,A; Pacca,I.G & Piccirillo,E.M (1984). *Flood Basalt to Rhyolite Suites in the Southern Paraná Plateau (Brazil): Palaeomagnetism, Petrogenesis and Geodynamic Implications* Jour. Pet. **25**, 3, 579-618.

Bellieni, G; Comin Chiarmonti, P; Marques,L.S; Melfi,A; Piccirillo,E.M &Stolfa,D (1984b). *Low-Pressure Evolution of Basalt Sills from Bore-Holes in the Paraná Basin, Brazil* Tschermaks Mineralogische und Petrographische Milteilungen **33**, 24-47.

Bellieni, G; Comin-Chiaramonti, P; Marques,L.S; Melfi,A.J; Nardy,J.R; Papatrechas,C; Picirillo,E.M; Roisenberg,A & Stolfa,D. (1986). *Petrogenetic Aspects of Acid and Basaltic Lavas from the Parana Plateau (Brasil): Geological, Mineralogical and Petrochemical Relationships.* J. Petrol. **27**, Part 4, 915-944.

Bellieni, G; Comin Chiarmonti, P; Marques,L.S; Martinez,L.A; Melfi,A.J; Nardy,A.R.J; Picirillo,E.M; & Stolfa,D (1986b). *Continental flood basalts from the central- western regions of the Parana plateau (Paraguay and Argentina): petrology and petrogenetic aspects* Neues Jahrbuch Miner. Abh. **154**, 2, 111-139.

Bellieni, G; Piccirillo, E.M; Comin-Chiarmonti, P; Melfi, A.J & Da Roit, P (1988). *Mineral chemistry of stratoid volcanics and related intrusives from the Paraná Basin (Brasil).* In Piccirillo, E.M. & Melfi, A.J (eds) Mesozoic Flood Volcanism of the Paraná Basin: Petrogenetic and Geophysical Aspects. Sao Paulo, Inst. Astron. Geofis. 1-13.

Bergman, S.C (1987). *Lamproites and other K-rich igneous rocks a review of their occurrence, mineralogy and geochemistry* In Fitton, J.G. & Upton G.B.J. (eds) Alkaline Igneous Rocks. London, Geol. Soc. Spec. 103-190.

Binks, R.M & Fairhead, J.D. (1992). *A plate tectonic setting for Mesozoic rifts of West and Central Africa.* Tectonophysics **213**, 141-151.

Blundy, J & Wood, B (1991). *Crystal-chemical controls on the partitioning of Sr and Ba between plagioclase feldspar, silicate melts and hydrothermal solutions* Geochim. Cosmochim. Acta **55**, 193-209.

Bonnefoi, CC; Provost, A; Albarede, F; (1995). *The 'Daly gap' as a magmatic catastrophe.* Nature **378**, 270-272.

Bossi, J (1966). *Geología del Uruguay.* Montevideo, Uruguay, Universidad de la República.

Bossi, J & Navarro, R (1988). *Geologia del Uruguay* Inst. Geol. Urug.

Bossi, J; Civetta, L; Demarchi, G; Girardi, VAV; Mazzucchelli, M; Negrini, GR; Fragoso Cesar, ARS; Sinigoi, S; Teixeira, W; Piccirillo, EM; Molesini, M. (1993). *Early Proterozic dike swarms from western Uruguay: geochemistry, Sr-Nd isotopes and petrogenesis.* Chem. Geol. **106**, 263-277.

Bott, M.H.P (1992). *The stress regime associated with continental break-up.* In Storey,B.C; Alabaster,T & Pankhurst,R.J (eds) Magmatism and the Causes of Continental Break-up. London, Geol. Soc. Spec. Publn. 125-136.

Bott, M.H.P (1993). *Modelling the plate driving mechanism.* J. Geol. Soc. Lond. **150**, 941-951.

Bradshaw, T.K; Hawkesworth, C.J & Gallagher,K (1993). *Basaltic Volcanism in the Southern Basin and Range: no role for a mantle plume.*

Bristow, J.W (1988). *Flood basalts in new perspective.* International Journal of the AEC **No. 39**,

Brown, R; Gallagher, K & Duane, M (1994). *A quantitative assessment of the effects of magmatism on the thermal history of the Karoo sedimentary sequence.* Jour. Afr. Earth. Sci. **18**, 3, 227-243.

Buddington, A.F & Lindsley, D.H. (1964). *Iron-Titanium Oxide Minerals and Synthetic Equivalents.* Jour. Petrol. **5**, 2, 310-357.

Bullard, EC; Everett, JE; Smith, AG; (1965). *The Fit of the Continents around the Atlantic.* Phil. Trans. Royal. Soc. Lond. Series A Maths & Phys. Sciences **258**, 41-51.

Burke, K & Whiteman, A.J. (1973). *Uplift, Rifting and the Break-up of Africa.* London, London Academic Press.

Burke, K & Dewey, J.F (1974). *Two plates in Africa during the Cretaceous?* Nature **249**, 313-316.

Burnham, C.W (1979). *The importance of volatile constituents.* In Yoder, H. S. (ed) The Evolution of the Igneous Rocks: Fiftieth Anniversary Perspective. Princeton University Press. 439-482.

Cameron, M; Bagby, WC; Cameron, KL; (1980). *Petrogenesis of Voluminous Mid - Tertiary ignimbrites of the Sierra Occidental, Chihuahua, Mexico.* Contrib. Mineral. Petrol. **74**, 271-284.

Cameron, KL & Hanson, GN; (1982). *Rare earth element evidence concerning the origin of ignimbrites and related volcanic rocks, Sierra Occidental, Chihuahua, Mexico.* Geochim. Cosmochim. Acta **46**, 1489-1503.

Cameron, KL & Cameron, M; (1985). *Rare earth element, $^{87}Sr/^{86}Sr$ and $^{143}Nd/^{144}Nd$ compositions of Cenozoic orogenic dacites from Baja California, northwestern Mexico, and adjacent west Texas: evidence for the predominance of a subcrustal component.* Contrib. Mineral. Petrol. **91**, 1-11.

Cameron, KL & Cameron, M; (1986). *Whole rock / groundmass differentiation trends of rare earth elements in high silica rhyolites.* Geochim. Cosmochim. Acta **50**, 759-769.

Campbell, I.H. & Griffiths, R.W (1990). *Implications of mantle plume structure for evolution of flood basalts.* Earth. Planet. Sci. Lett. **99**, 79-93.

Cande, S.C; LaBreque, J.L; Larson, R.L; Pitman, W.C; Golovchenko, X & Haxby, W.F (1989). *Magnetic lineations of the world's ocean basins.* Tulsa, OK, Am. Assoc. Pet. Geol.

Caorsi, J.H & Goni, J.C (1958). *Geología Uruguaya.* Instituto Geológico Uruguay Boletín **37**, 9-73.

Carlson, R.W; Lugmair, G.W & MacDougall,J.D. (1981). *Columbia River volcanism: the question of mantle heterogeneity or crustal contamination.* Geochim. Cosmochim. Acta **45**, 2483-2499.

Carmichael, I.S.E (1967). *The iron-titanium oxides of salic rocks and their associated ferro-magnesian silicates.* Contrib. Mineral. Petrol. **14**, 36-64.

Carmichael, I.S.E; Turner, F.J & Verhoogen, J (1974). *Igneous Petrology* New York, McGraw-Hill.

Carpenter, M.A & Ferry, J.M (1984). *Constraints on the thermodynamic mixing properties of plagioclase feldspars.* Contrib. Mineral. Petrol. **87**, 138-148.

Cas, RAF & Wright, JV (1988). *Volcanic Successions - Modern and Ancient* Chapman & Hall.

Ceuleneer, G; Monnereau, M; Rabinowicz, M & Rosemberg, C (1993). *Thermal and petrological consequences of melt migration within mantle plumes.* Phil. Trans. Royal Soc. Lond. **342**, 53-64.

Chang, H.K; Kowsmann, R.O; Figueiredo,A.M.F & Bender,A.A. (1992). *Tectonics and stratigraphy of the East Brazil Rift system : an overview.* Tectonophysics **213**, 97-138.

Christensen, J.N & Halliday, A.N (1996). *Rb-Sr ages and Nd isotopic compositions of melt inclusions from the Bishop Tuff and the generation of silicic magma.* Earth. Planet. Sci. Lett. **144**, 3-4, 547-561.

Class, C; Altherr, R; Volker,F; Eberz,G & McCulloch,M.T (1994). *Geochemistry of Pliocene to Quaternary alkali basalts from the Huri Hills, northern Kenya* Chem. Geol. **113**, 1-22.

Clemens, JD (1984). *Water contents of silicic to intermediate magmas.* Lithos **17**, 273-287.

Clemens, JD; Holloway, JR; White, AJR; (1986). *Origin of A-type granite: Experimental constraints.* American Mineralogist **71**, 317-324.

Cleverly, R.W; Betton, P.J & Bristow, J.W (1984). *Geochemistry and Petrogenesis of the Lebombo Rhyolites.* In Erlank, A. J. (ed) Petrogenesis of the Volcanic Rocks of the Karoo Igneous Province. Johannesburg, Geol. Soc. South Africa. 171-194.

Cliff, R.A; Baker, P.E & Mateer, N.J (1991). *Geochemistry of Inaccessible Island volcanics.* Chem. Geol. **92**, 4, 251-260.

Coblentz, D.D & Sandiford, M (1994). *Tectonic stresses in the African plate: Constraints on the ambient lithospheric stress state.* Geology **22**, 831-834.

Coblentz, DD; Richardson, RM; Sandiford, M; (1994). *On the gravitational potential of the Earths lithosphere.* Tectonics **13**, 4, 929-945.

Cochran, J.R (1983). *Effects of finite rifting times on the development of sedimentary basins* Earth. Planet. Sci. Lett. **66**, 289-302.

Cohen, R.S. & O'Nions, R.K. (1982). *Identification of recycled continental material in the mantle from Sr, Nd and Pb isotope investigations* Earth Planet. Sci. Lett. **61**, 73-84.

Collins, WJ; Beams, SD; White, AJR; Chappell, BW. (1982). *Nature and Origin of A-type Granites with Particular reference to Southeastern Australia.* Contrib. Mineral. Petrol. **80**, 189-200.

Comin-Chiaramonti, P; Gomes, C.B ; Piccirillo, E.M & Rivalenti, G (1983). *High TiO_2 basaltic dikes in the coastline of Sao Paulo and Rio de Janeiro States (Brasil).* Neues Jahrbuch Miner. Abh. **146**, 133-150.

Comin-Chiarmonti, P; Bellieni, G; Piccirillo, E.M & Melfi, A.J (1988). *Classification and petrography of continental stratoid volcanics and related intrusives from the Paraná Basin (Brazil).* In Piccirillo, E.M & Melfi, A.J. (eds) Mesozoic Flood Volcanism of the Paraná Basin - petrogenetic and geophysical aspects. Sao Paulo University. 47-72.

Condie, K.C (1989). *Plate Tectonics & Crustal Evolution* Pergamon Press.

Cordani, U.G; Sartori, P.L.P & Kawashita,K (1980). *Geoquimica dos Isotopos de Estroncio e a Evolucao da Atividade Vulcanica na Bacia do Parana (Sul do Brasil) Durante o Cretaceo.* An. Acad. Brasil. Ciénc. **52**, 4,

Corner, B (1983). *An interpretation of the aeromagnetic data covering the western portion of the Damara orogen in south west Africa / Namibia.* Spec. Publ. Geol. Soc. S. Afr. **11**, 339-354.

Courtillot, V; Besse, J; Vandamme, D; Montigny, R; Jaeger, J.J & Cappetta, H (1986). *Deccan flood basalts at the Cretaceous/Tertiary boundary?* Earth. Planet. Sci. Lett. **80**, 361-374.

Cox, K.G (1978). *Flood basalts, subduction and the break-up of Gondwanaland.* Nature **274**, 47-49.

Cox, K; Bell; J.D & Pankhurst, R.J (1979). *Interpretation of Igneous Rocks* London, Allen and Unwin.

Cox, KG; (1980). *A Model for Flood Basalt Vulcanism.* Jour. Petrol. **21**, 4, 629-650.

Cox, K.G (1988). *Numerical Modelling of a Randomized RTF Magma Chamber: A Comparison with Continental Flood Basalt Sequences.* Jour. Petrol. **29**, 3, 681-697.

Cox, K.G (1992). *Karoo igneous activity, and the early stages of the break-up of Gondwanaland.* In Storey, B.C; Alabaster, T; Pankhurst, R. (eds) Magmatism and the causes of Continental Break-up. London, Geol. Soc. Spec. Publ. 137-148.

Cox, K.G (1993). *Continental Magmatic Underplating.* Phil. Trans. Royal Soc. Lond. **A342**, 155-166.

Creaser, RA; White, AJR; (1991). *Yardea Dacite - Large-volume, high temperature felsic volcanism from the Middle Proterozoic of South Australia.* Geology **19**, 48-51.

Creer, K.M; Miller, J.A & Gilbert Smith,A (1965). *Radiometric Age of the Serra Geral Formation.* Nature **20**, 282-283.

Dalla Salda, L; Bossi, J & Cingolani,C (1988). *The Rio de la Plata Cratonic Region of Southwestern Gondwanaland.* Episodes **11**, 4, 263-269.

Dalrymple, GB; Grommé, CS; White, RW; (1975). *Potassium - Argon age and Palaeomagnetism of Diabase Dikes in Liberia: Initiation of Central Atlantic Rifting.* Geol. Soc. Am. Bull. **86**, 399-411.

Dalrymple, G.B & Duffield, W.A (1988). *High precision $^{40}Ar/^{39}Ar$ dating of Oligocene rhyolites from the Mogollan - Datil volcanic field using a continuous laser system.* Geophys. Res. Letts. **15**, 463-466.

Dalrymple, G.B; Czamanske, G.K & Lamphere,M.A. (1991). *$^{40}Ar/^{39}Ar$ Ages of Samples From the Norilsk-Talnakh Ore Bearing Intrusions and the Siberian Flood Basalts, Siberia.* EOS **72**, 44, 570.

Dalziel, I.W.D. (1997). *Neoproterozoic-Paleozoic geography and tectonics: Review, hypothesis, environmental speculation.* G.S.A. Bulletin **109**, 1, 16-42.

Daux, V; Crovisier, JL; Hemond, C; Petit, JC; (1994). *Geochemical evolution of basaltic rocks subjected to weathering : Fate of the major elements, rare earth elements, and thorium.* Geochim. Cosmochim. Acta **58**, 22, 4941-4954.

Davies, GF; (1992). *On the emergence of plate tectonics.* Geology **20**, 963-966.

Davies, G.F (1994). *Thermomechanical erosion of the lithosphere by mantle plumes.* J. Geophys. Res **99**, B8, 15,709-15,722.

Davies, GF; (1994). *Thermomechanical erosion of the lithosphere by mantle plumes.* J. Geophys. Res. **99**, B8, 15,709-15,722.

Davis, J.M; Elston, W.E & Hawkesworth,C.J *Basic and Intermediate volcanism of the Mogollan Datil Volcanic Field; Implications for the mid-Tertiary tectonic and magmatic transitions in southwestern New Mexico, U.S.A.* Spec. Publ. Geol. Soc. Lond.

de Beer, CH; (1992). *Structural evolution of the Cape Fold Belt syntaxis and its influence on syntectonic sedimentation in the SW Karoo Basin.* In de Wit & Ransome (eds) Inversion Tectonics of the Cape Fold Belt, Karoo and Cretaceous Basins of Southern Africa. Rotterdam, Balkema. 197-206.

De Paolo, DJ (1981). *Trace element and isotopic effects of combined wallrock assimilation and fractional crystallisation.* Earth. Planet. Sci. Lett. **53**, 189-202.

de Wit, M; Jeffrey, M; Berg, H & Nicolaysen, L (1988). *Geological map of sectors of Gondwana reconstructed to their disposition at 130Ma.* Tulsa, Am. Ass. Petroleum Geol. & Uni. Witwatersrand.

Dingle, RV; Siesser, WG; Newton, AR; (1983). *Mesozoic and Tertiary Geology of Southern Africa* Rotterdam, Balkema.

Dodson, M.H (1973). *Closure temperature in cooling geochronological and petrological systems.* Contrib. Mineral. Petrol. **40**, 259-274.

Doglioni, C; (1993). *Geological evidence for a global tectonic polarity.* J. Geol. Soc. Lond. **150**, 991-1002.

Drake, M.J (1975). *The oxidation state of europium as an indicator of oxygen fugacity.* Geochim. Cosmochim. Acta **39**, 55-64.

Druecker, M.D & Gay, S.P(Jr.) (1985). *Mafic Dyke Swarms Associated with Mesozoic Rifting in Eastern Paraguay, South America.* In. Mafic Dyke Swarms. Halls,H.C & Fahrig,W.F (eds.). Geological Association of Canada Special Paper 34, 187-193.

Duncan, AR; (1987). *The Karoo Igneous Province - A problem area for inferring tectonic setting from basalt geochemistry.* Jour. Volcano. Geothermal. Res. **32**, 13-37.

Duncan, R.A & Pyle, D.G (1988). *Rapid eruption of the Deccan flood basalts at the Cretaceous/Tertiary boundary.* Nature **333**, 841-843.

Duncan, A.R; Newton, S.R; van den Berg,C & Reid,D.L (1989). *Geochemistry and petrology of dolerite sills in the Huab River Valley, Damaraland, northwestern Namibia.* Communs geol. Surv. Namibia **5**, 5-17.

Duncan, A.R; Armstrong, R.A; Erlank,A.J; Marsh,J.S & Watkins,R.T (1990). *MORB-related dolerites associated with the final phases of Karoo flood basalt volcanism in southern Africa.* In Parker; Rickwood & Tucker (eds) Mafic Dykes and Emplacement Mechanisms, 119-129.

Duncan, A.R; Marsh, J.S; Erlank,A.J & Milner,S.C (1990). *Geochemistry and Petrogenesis of the Basaltic rocks of the Etendeka Formation, Northwestern Namibia.* Geocongress, Cape Town

Eales, H.V; Marsh, J.S & Cox, K.G (1984). *The Karoo igneous province: an introduction.* Spec. Publ. Geol. Soc. S. Afr. **13**, 1-26.

Ellam, R.M. & Cox, K.G. (1989). *A proterozoic lithospheric source for karoo magmatism: evidence from the Nuanetsi picrites* Earth. Planet. Sci. Letts. **92**, 207-218.

Ellam, R & Cox, K (1991). *An interpretation of Karoo picrite basalts in terms of interaction between asthenospheric magmas and the mantle lithosphere.* Earth. Planet. Sci. Letts. **105**, 330 - 342.

Ellam, R.M (1992). *Lithospheric thickness as a control on basalt geochemistry.* Geology **20**, 2, 153-156.

Elliot, D.H (1992). *Jurassic magmatism and tectonism associated with Gondwanaland break-up: an Antarctic perspective.* In Storey, B.C; Alabaster, T & Pankhurst, R.J (eds) Magmatism and the Causes of Continental Break-up. London, Geol. Soc. Spec. Publ. 165-184.

Emery, K.O; Uchupi, E; Bowin,C.O; Phillips,J & Simpson,S.W. (1975). *Continental Margin off Western Africa: Cape St. Francis (South Africa) to Walvis Ridge (South-West Africa).* Am. Ass. Petroleum Geol. Bull. **59**, 1, 3-59.

Erlank, AJ, Ed. (1984). *Petrogenesis of the Volcanic Rocks of the Karoo Province,.* Geological Society of South Africa.

Erlank, AJ; Marsh, JS; Duncan, AR; Miller, RMcG; Hawkesworth, CJ; Betton, PJ; Rex, DC (1984). *Chemistry and Petrogenesis of the Etendeka volcanic rocks from SWA/Namibia.* In Erlank, A.J. (eds) Petrogenesis of the Volcanic Rocks of the Karoo Province. Spec. Publ. Geol. Soc. S. Afr. 195-245.

Erlank, A.J; le Roex, A.P; Harris,C; Miller,R.McG & McLachan,I (1990). *Preliminary note on the geochemistry of basalt samples from the Kudu boreholes.* Communs. Geol. Surv. Namibia **6**, 59-61.

Ernesto, M; Hiodo, F.Y & Pacca, I.G (1979). *Estudo Palaeomagnetico de Sequencia de Derrames Basalticos da Formacao Serra Gerral em Santa Catarina* An. Acad. Brasil. Ciénc. **51**, 2,

Ernesto, M & Pacca, I.G (1988). *Paleomagnetism of the Paraná Basin flood volcanics, southern Brazil.* In Piccirillo, E.M & Melfi, A.J (eds) The Mesozoic Flood Volcanism of the Paraná Basin : Petrogenetic and Geophysical Aspects. Sao Paulo, Univ. Sao Paulo. 229-255.

Evans, OC; Hanson, GN; (1993). *Accessory - mineral fractionation of rare- earth element (REE) abundances in granitoid rocks.* Chem. Geol. **110**, 69-93.

Fairhead, J.D (1988). *Mesozoic Plate teconic reconstructions of the Central South Atlantic Ocean: The role of the West and Central African rift system.* Tectonophysics **155**, 181-191.

Fairhead, J.D & Okereke, C.S (1988). *Depths to major density contrasts beneath the West African Rift System in Nigeria and Cameroon based on spectral analysis of gravity data.* J. Afr. Earth Sci. **7**, 769-777.

Feeley, T.C. & Sharp, Z.D. (1995*). (super 18) O/ (super 16) O isotope geochemistry of silicic lava flows erupted from Volcan Ollaguee, Andean central volcanic zone.* Earth. Planet. Sci. Lett. **133**; 3-4, 239-254.

Ferrando, L & Fernández, J (1971). *Esquema tectónico cronoestratigráfico del Pre-Devoniano en Uruguay.* XXV Congresso Brasileiro Geologia, Anais,

Fleitout, L (1991). *The sources of lithospheric tectonic stresses.* Phil. Trans. Royal Soc. Lond. A. **337**, 73-81.

Fodor, RV; McKee, EH; Asmus, HE; (1983-1984). *K-Ar ages and the opening of the South Atlantic ocean: Basaltic Rock from the Brazilian Margin.* Marine Geology **54**, M1-M8.

Fodor, R.V & Vetler, S.K (1984). *Rift zone magmatism : Petrology of basaltic rocks transitional from CFB to MORB, southeastern Brazil margin.* Contrib. Mineral Petrol. **88**, 307-321.

Fodor, R.V; Corwin, C & Roisenberg,A (1985). *Petrology of Serra Geral (Parana) continental flood basalts, southern Brazil: crustal contamination, source material, and South Atlantic magmatism.* Contrib. Mineral. Petrol. **91**, 54-65.

Fodor, RV; Corwin, C; Sial, AN; (1985). *Crustal signatures in the Serra Geral flood basalt province, southern Brazil: O- and Sr- isotope evidence.* Geology **13**, 763-765.

Fodor, RV; (1987). *Low- and high- TiO_2 flood basalts of southern Brazil: origin from picritic parentage and a common mantle source.* Earth. Planet. Sci. Lett. **84**, 423-430.

Foley, SF; (1991). *The Origin of Kimberlite and Lamproite in Veined Lithospheric Mantle.* 5th International Kimberlite Conference, Brazil.

Forsyth, D.W. & Uyeda, S. (1975). *On the Relative Importance of the Driving Forces of Plate Motion* Geophy. J. Royal. Ast. Soc. **43**, 1, 163-200.

Forsythe, L.M; Nielsen, R.L & Fisk,M.R (1994). *High-field-strength element partitioning between pyroxene and basaltic to dacitic magmas.* Chem. Geol. **117**, 107-125.

Fowler, AC; (1993). *Boundary Layer Theory and Subduction.* J. Geophys. Res. **21**, B12, 21,997-22,005.

Frost, B.R & Lindsley, D.H. (1992). *Equilibria among Fe-Ti oxides, pyroxenes, olivine, and quartz: Part II. Application* American Mineralogist **77**, 1004-1020.

Fuhrman, M.L & Lindsley, D.H (1988). *Ternary-felspar modeling and thermometry.* American Mineralogist **73**, 201-215.

Furnes, H; Kryza, R; Muszynski,A; Pin,C & Garmann,L.B (1994). *Geochemical evidence for progressive, rift related early Palaeozoic volcanism in the western Sudetes.* J. Geol. Soc. Lond. **151**, 91-109.

Gallagher, K; Hawkesworth, C; (1992). *Dehydration melting and the generation of continental flood basalts.* Nature **358**, 57-59.

Gallagher, K & Hawkesworth, C.J (1994). *Mantle plumes, continental magmatism and asymmetry in the South Atlantic.* Earth. Planet. Sci. Lett. **123**, 105-117.

Garland, F.E (1994) *The Parana Rhyolites, southern Brazil: their petrogenetic relationship to the associated flood basalts.* Doctor of Philosophy, The Open University.

Garland, F; Hawkesworth, CJ; Mantovani, MSM; (1995). *Description and Petrogenesis of the Paraná Rhyolites, Southern Brazil.* J. Petrol. **36**, 5, 1193-1227.

Garland, F; Turner, S & Hawkesworth,C.J (1996). *Shifts in the Source of the Parana Basalts through Time.* Lithos **37**, 223-243.

Garland, F; Hawkesworth, CJ & Mantovani, MSM (1997). *Reply to the Comment by Harris & Milner on the paper 'Description and Petrogenesis of the Paraná Rhyolites, Southern Brazil.'* J. Petrol. **38**, 2, 303-305.

Ghiorso, M.S (1984). *Activity/composition relations in the ternary feldspars.* Contrib. Mineral. Petrol. **87**, 282-296.

Ghiorso, M.S & Sack, R.O (1991). *Fe-Ti oxide geothermometry: thermodynamic formulation and the estimation of intensive variables in silicic magmas.* Contrib. Mineral. Petrol. **108**, 485-510.

Gibson, SA; Thompson, RN; Dickin, AP; Leonardos, OH; (1995). *High Ti and low Ti mafic potassic magmas: Key to plume-lithosphere interactions and continental flood - basalt genesis.* Earth. Planet. Sci. Lett. **136**, 149-165.

Girard, J.P & Onstott, T.C (1991). *Application of $^{40}Ar/^{39}Ar$ laser-probe and step-heating techniques to the dating of diagenetic K-feldspar overgrowths.* Geochim. Cosmochim. Acta **55**, 3777-3793.

Gradstein, F.M; Agterberg, F.P; Ogg,J.G; Hardenbol,J; van Veen,P; Thierry,J & Huang,Z. (1994). *A Mesozoic time scale.* J.G.R. **99**, B12, 24,051-24,074.

Green, T.H & Watson, E.B (1982). *Crystallisation of apatite in natural magmas under high pressure, hydrous conditions with particular reference to 'orogenic' rock series.* Contrib. Mineral. Petrol. **84**, 66-72.

Green , D.H & Ringwood, A.E (1967). *The genesis of basaltic magmas.* Contrib. Mineral. Petrol. **15**, 103-190.

Grove, TL & Bryan, WB (1983). *Fractionation of pyroxene-phyric MORB at low pressure: An experimental study.* Contrib. Mineral. Petrol. **84**, 293-309.

Grunder, AL; Mahood, GA; (1988). *Physical and Chemical Models of Zoned Silicic Magmas: The Loma Seca Tuff and Calabozos Caldera Southern Andes.* J. Petrol. **29**, 4, 831-867.

Guirand, R & Maurin, J.C (1992). *Early Cretaceous rifts of Western and Central Africa : an overview.* Tectonophysics **213**, 153-168.

Gust, D.A; Biddle, K.T; Phelps,D.W & Uliana M.A (1985). *Associated Middle to late Jurassic volcanism and extension in Southern south America.* Tectonophysics **116**, 223-253.

Haack, U; Hoefs, J; Gohn, E (1983). *Genesis of the Damaran granites in the Rb/Sr and* $\delta^{18}O$ *data.* In Martin, H & Eder, FW (eds) Intracontinental fold belts. Berlin, Springer. 847-872.

Hall, C.M (1990). *Calculation of Expected Thermal Gradients in Laser* $^{40}Ar/^{39}Ar$ *Step Heating Experiments.* EOS **71**, 653.

Hansen, V.L; Goodge, J.W; Keep,M & Oliver,D.H (1993). *Asymmetric rift interpretation of the western North American margin.* Geology **21**, 1067-1070.

Hanson, RE; Elliot, DH; (1996). *Rift related Jurassic basaltic phreatomagmatic volcanism in the central Transantarctic Mountains: precursory stage to flood-basalt effusion.* Bull. Volcanol. **58**, 327-347.

Harland, W.B; Cox, A.V; Llewellyn, P.G; Pickton, C.A.G; Smith, A.G & Walters, R (1982). *A Geological Time scale.* New York, Cambridge Unibversity Press.

Harris, C; Smith, H.S; Milner,S.C; Erlank,A.J; Duncan,A.R; Marsh,J.S & Ikin,N.P (1989). *Oxygen isotope geochemistry of the Mesozoic volcanics of the Etendeka Formation, Namibia.* Contrib. Mineral Petrol. **102**, 454-461.

Harris, C; Whittingham, A.M; Milner,S.C & Armstrong,R.A (1990). *Oxygen isotope geochemistry of the silicic volcanic rocks of the Etendeka - Parana province: Source constraints.* Geology **18**, 1119-1121.

Harris, N.B.W & Inger, S (1991). *Trace element modelling of pelite-derived granites.* Contrib. Mineral. Petrol. **110**, 46-56.

Harris, C & Erlank, AJ (1992). *The production of large volume low-$\delta^{18}O$ rhyolites during the rifting of Africa and Antarctica: the Lebombo Monocane.* Geochim. Cosmochim. Acta **56**, 3561-3570.

Harris, C (1995). *The oxygen isotope geochemistry of the Karoo and Etendeka volcanic provinces of Southern Africa.* South African Jour. Geol. **98**, 126-139.

Harris, C & Milner, S (1997). *Crustal origin for the Paraná rhyolites: Discussion of 'Description and Petrogenesis of the Paraná Rhyolites, southern Brazil' by Garland et al. (1995).* J. Petrol. **38**, 2, 299-302.

Harrison, TM; Watson, EB; (1983). *Kinetics of Zircon Dissolution and Zirconium Diffusion in Granitic Melts of Variable Water Content.* Contrib. Mineral. Petrol. **84**, 66-72.

Harrison, TM; Watson, EB; (1984). *The behaviour of apatite during crustal anatexis: Equilibrium and kinetic considerations.* Geochim. Cosmochim. Acta. **48**, 1467-1477.

Harry, D.L & Sawyer, D.S (1991). *Basaltic volcanism, mantle plumes and the mechanics of rifting : The Parana flood basalt province of South America.* Geology

Haselton, H.T; Hovis, G.L; Hemingway, B.S & Robie, R.A (1983). *Calorimetric investigation of the excess entrophy in analbite-sanidine solid solutions: lack of evidence for Na, K short order and implications for two feldspar thermometry.* American Mineralogist **68**, 398-413.

Hawkesworth, CJ; Powell, M; (1980). *Magma genesis in the Lesser Antilles Island Arc.* Earth. Planet. Sci. Lett. **51**, 297-308.

Hawkesworth, C.J; Erlank, A.J; Marsh,J.S; Menzies,M.A & van Calsteren,P (1983). *Evolution of the Continental Lithosphere : Evidence from Volcanics and Xenoliths in Southern Africa.* In Hawkesworth,C.J & Norry,M.J (eds) Continental Basalts and Mantle Xenoliths. 111-272.

Hawkesworth, C.J; Mantovani, M.S.M; Taylor,P.N & Palacz,Z (1986). *Evidence from the Parana of south Brasil for a continental contribution to Dupal basalts.* Nature **322**, 356-359.

Hawkesworth, C; Mantovani, M; Peate, D; (1988). *Lithosphere remobilization during Paraná CFB Magmatism.* J. Petrol. **Spec. Lithosphere Issue**, 205-223.

Hawkesworth, CJ; Kempton, PD; Rogers, NW; Ellam, RM; van Calsteren, PV; (1990). *Continental mantle lithosphere, and shallow level enrichment processes in the Earth's mantle.* Earth. Planet. Sci. Lett. **96**, 256-268.

Hawkesworth, C.J; Gallagher, K; Kelley,S; Mantovani,M.S.M; Peate,D.W; Regelous,M & Rogers,N.W (1992). *Paraná magmatism and the opening of the South Atlantic.* In Storey,B.C; Alabaster,T & Pankhurst,R.J (eds) Magmatism and the causes of Continental Breakup. Geol. Soc. Spec. Publ. 221-240.

Hawkesworth, C.J & Gallagher, K (1993). *Mantle plumes and regional tectonics as causes of intraplate magmatism.* Terra Nova **5**, 6, 552-559.

Heimann, A; Fleming, TH; Elliot, DH; Foland, KA; (1994). *A short interval of Jurassic continental flood basalt volcanism in Antarctica as demonstrated by $^{40}Ar/^{39}Ar$ geochronology.* Earth. Planet. Sci. Lett. **121**, 19-41.

Henderson, P (1984). *Rare Earth Element Geochemistry* Amsterdam, Elsevier.

Hergt, J; Chappell, B; McCulloch, T.M; McDougall, I & Chivas, A.R (1989). *Geochemical and isotopic constraints on the origin of the Jurassic dolerites of Tasmania.* J. Petrol. **30**, 341-383.

Hergt, J.M; Peate, D.W & Hawkesworth,C.J (1991). *The petrogenesis of Mesozoic Gondwana low Ti flood basalts.* Earth. Planet.Sci. Lett. **105**, 1-3, 134-148.

Hergt, J; Hawkesworth, CJ; (1992). *The Remobilisation of continental mantle lithosphere.* Sci. Progress, Oxford,

Herz, N (1977). *Timing of spreading in the South Atlantic : Information from Brazilian alkalic rocks.* Geol. Soc. Am. Bull. **88**, 101-112.

Herzberg, CT; (1993). *Lithosphere peridotites of the Kaapvaal craton.* Earth. Planet. Sci. Lett. **120**, 13-29.

Hildreth, W; Halliday, AN; Christiansen, RL (1991). *Isotopic and chemical evidence concerning the genesis and contamination of basaltic and rhyolitic magma beneath the Yellowstone Plateau Volcanic field.* J. Petrol. **32**, 63-138.

Hill, R.I (1990). *Starting plumes and continental break-up.* Earth. Planet. Sci. Lett. **104**, 398-416.

Hill, R.I; Campbell, I.H; Davies,G.F & Griffiths,R.W (1991). *Plume tectonics.* Cal.Tech Symposium

Hill, R.I; Campbell, I.H; Davies,G.F & Griffiths,R.W (1992). *Mantle Plumes and Continental Tectonics* Science **256**, 186-193.

Hirose, K & Kushiro, I (1993). *Partial melting of dry peridotites at high pressures; determination of compositions of melts from peridotite using aggregates of diamond.* Earth. Planet. Sci. Lett. **114**, 4, 477-489.

Hole, M.J; Kempton, P.D & Millar,I.L (1993). *Trace element and isotopic characteristics of small-degree melts of the asthenosphere : Evidence from the alkalic basalts of the Antartic Peninsula.* Chem. Geol. **109**, 51-68.

Holtz, F; Johannes, W; (1994). *Maximum and minumum water contents of granitic melts: implications for chemical and physical properties of ascending magmas.* Lithos **32**, 149-159.

Holtz, F; Scaillet, B; Behrens, F; Pichavant, M; (1996). *Water contents of felsic melts: application to the rheological properties of granitic magmas.* Trans. Royal. Soc. Edin. Earth. Sci. **87**, 57-64.

Honjo, N; Bonnichsen, B; Leeman, WP; Stormer, JC; (1992). *Mineralogy and geothermometry of high- temperature rhyolites from the central and western Snake River Plain.* Bull. Volcanol. **54**, 220-237.

Hooper, P.R (1982). *The Columbia River basalts.* Science **215**, 1463-1468.

Hooper, P.R & Hawkesworth, C.J (1993). *Isotopic and Geochemical Constraints on the Origin and Evolution of the Columbia River Basalt.* J. Petrol. **36**, Part 6, 1203-1246.

Houseman, G; England, P (1986). *A dynamical model of lithosphere extension and sedimentary basin formation.* J. Geophys. Res. **91**, B1, 719-729.

Housh, TB; Luhr, JF; (1991). *Plagioclase melt equilibria in hydrous systems.* American Mineralogist **76**, 477-492.

Humphris, S.E & Thompson, G (1982). *A geochemical study of rocks from the Walvis Ridge, South Atlantic.* Chem. Geol. **36**, 3-4, 253-274.

Iacumin, P; Piccirillo, EM; Longinelli, A; (1991). *Oxygen isotopic composition of Lower Cretaceous tholeiites and Precambrian basement rocks from the Paraná basin (Brazil): The role of water rock interaction.* Chem. Geol. **86**, 225-237.

Irvine, TN & Baragar, WRA (1971). *A guide to the chemical classification of the common volcanic rocks.* Can. J. Earth. Sci. **8**, 523-548.

Irving, AJ & Frey, FA (1978). *Distribution of trace elements between garnet megacrysts and host volcanic liquids of kimberlitic to rhyolitic composition.* Geochim. Cosmochim. Acta **42**, 771-787.

Jackson, M (1984). *Contributions to the Geology and Hydrology of Southeastern Uruguay Based on Visual Remote Sensing Interpretation.* Nelles-Verlag, München.

Janasi, V.A & Ulbrich, H.H.G.J (1991). *Late Proterozoic granitoid magmatism in the state of Sao Paulo, southeastern Brasil.* Precambrian Research **51**, 351-374.

Jones, G.H (1956). *Some deep Mesozoic Basins Recently Discovered in Southern Uruguay.* Congreso Geologico Internacional XX Sesion. Seccion II El Mesozoico del Hemisferio Occidental Y Sus Correlaciones Mundiales., Mexico,

Jones, G (1956). *Some deep Mesozoic basins recently discovered in southern Uruguay.* XX International Geological Congress II,

Jordan, T.H. (1988). *Structure and formation of the continetal tectosphere* In Cox, K.G & Menzies, M.A. (eds) Oceanic and continental lithosphere: similarities and differences. J. Petrol. 11-37.

Jurdy, D.M & Stefanick, M (1991). *The forces driving the plates : constraints from kinematics and stress observations.* In Whitmarsh,R.B; Bott,M.P.H; Fairhead,J.D & Kuznir,N.J. (eds) Tectonic Stress in the Lithosphere. London, Phil. Trans. Royal. Soc. Lond. A. 127-139.

Kay, R.W (1984). *Elemental abundances relevant to identification of magma sources.* Phil. Trans. Royal. Soc. Lond. **A310**, 535-547.

Keen, C.E (1985). *The dynamics of rifting: deformation of the lithosphere by active and passive driving forces.* Geophy. J. Royal.Ast. Soc. **80**, 95-120.

Kelemen, P.B; Shimizu, N & Dunn,T. (1993). *Relative depletion of niobium in some arc magmas and the continental crust: partitioning of K, Nb, La and Ce during melt/rock reaction in the upper mantle.* Earth. Planet. Sci. Lett. **120**, 111-134.

Kelley, S.P; Arnaud, N.O & Turner,S.P. (1994). *High Spatial resolution $^{40}Ar/^{39}Ar$ investigations using an ultra-violet laser probe extraction technique.* Geochim. Cosmochim. Acta **58**, 16, 3519-3525.

Kelley, S.P (1995). *Ar-Ar dating by laser microprobe.* In Potts, P.J; Bowles, J.F.W; Reed, S.J.B & Cave, M.R (eds) Microprobe Techniques in the Earth Sciences. London, Chapman & Hall. 327-356.

Kent, D.V & Gradstein, F.M (1985). *A Cretaceous and Jurassic Chronology.* Geol. Soc. Am. Bull. **96**, 1419-1427.

Kent, R.W; Storey, M & Saunders, A.D (1992). *Large igneous provinces: Sites of plume impact or plume incubation.* Geology **20**, 891-894.

Kerr, A.C (1994). *Lithospheric thinning during the evolution of continental large igneous provinces : A case study from the North Atlantic Tertiary province.* Geology **22**, 1027-1030.

Kincaid, C; Ito, G & Gable,C. (1995). *Laboratiry investigations of the interaction of off-axis mantle plumes and spreading centres.* Nature **376**, August, 758-761.

Kinzler, RJ & Grove, TL (1993). *Corrections and further discussion of Kinzler & Grove (1992).* J. Geophys. Res. **98**, 22,339-22,347.

Kinzler, R.J & Langmuir, C.H. (1995). *Minute mantle melts.* Nature **375**, May, 274-275.

Klein, EM; Langmuir, CH; (1987). *Global correlations of Ocean Ridge Basalt chemistry with axial depth and crustal thickness.* J. Geophys. Res. **92**, B8, 8,089-8,115.

Klein, EM; Langmuir, CH; (1989). *Local versus global variations in ocean ridge basalt compositions: A reply.* J. Geophys. Res. **94**, B4, 4,241-4,252.

Kress, VC; Carmichael, ISE; (1991). *The compressibility of silicate liquids containing Fe_2O_3 and the effect of composition, temperature, oxygen fugacity and pressure on their redox states.* Contrib. Mineral. Petrol. **108**, 82-92.

Kretz, R (1981). *Transfer and exchange equilibria in a portion of the pyroxene quadrilateral as deduced from natural and experimental data.* Geochim. Cosmochim. Acta **46**, 411-421.

Kudo, A.M & Weil, D.F (1970). *An Igneous Plagioclase Thermometer* Contrib. Mineral. Petrol. **25**, 52-65.

Kuno, H (1966). *Lateral variation of basalt magma types across continental margins and island arcs.* Bull. Volcanol. **29**, 195-222.

Kushiro, I (1968). *The system forsterite-diopside-silica with and without water at high pressures.* Am. J. Sci. **267**, 269-294.

Lambaise, J.J. (1989). *The Framework of African Rifting During the Phanerozoic.* J. Afr. Earth Sci. **8**, 2/3/4, 183-190.

Langmuir, C.H., Vocke, R.D., Hanson, G.N. & Hart, S.R. (1978). *A general mixing equation with applications to Icelandic basalts.* Earth. Planet. Sci. Lett. **37**, 3, 380-392.

Lanphere, M.A. & Dalrymple, G.B (1978). *Identification of excess ^{40}Ar in the evaluation of disturbed K-Ar systems.* U.S.Geological Survey Open-file Report **78-701**, 241-243.

Larson, RL; Ladd, JW; (1973). *Evidence for the opening of the South Atlantic in the Early Cretaceous.* Nature **246**, 209-213.

Larson, RL & Olson, P (1991). *Mantle plumes control magnetic reversal frequency.* Earth. Planet. Sci. Lett. **107**, 437-447.

Larson, RL; Kincaid, C; (1996). *Onset of mid-Cretaceous volcanism by elevation of the 670km thermal boundary layer.* Geology **24**, 6, 551-554.

Lassiter, J.C; DePaolo, D.J & Mahoney,J.J. (1995). *Geochemistry of the Wrangellia Flood Basalt Province : Implications for the Role of Continental and Oceanic Lithosphere in the Flood Basalt Genesis.* J. Petrol. **36**, 4, 983-1009.

Lawyer, L; Sclater, JG; Meinke, L; (1985). *Mesozoic and Cenozoic reconstructions of the South Atlantic.* Tectonophysics **114**, 233-254.

Le Fort, J.P. & Van Der Voo, R (1981). *A kinematic model for the collision and complete suturing between Gondwanaland and Laurussia in the Carboniferous* J. Geol. **89**, 5, 537-550.

Le Maitre, R.W (1969). *Kaersutite-bearing plutonic xenoliths from Tristan da Cunha, South Atlantic.* Mineralogical Magazine **37**, No. 286,

Le Maitre, RW; Bateman, P; Dudek, A; Keller, J; Lameyre Le Bas, MJ; Sabine, MA; Schmid, R; Sorensen, H; Streckeisen, A; Wooley, AR; Zanetlin, B. (1989). *A classification of igneous rocks and glossary of terms.* Oxford, Blackwell.

Le Pichon, X & Sibuet, J-C (1981). *Passive Margins: A Model of Formation* J. Geophys. Res. **86**, B5, 3708-3720.

le Roex, A.P (1985). *Geochemistry,Mineralogy and Magmatic Evolution of the Basaltic and Trachytic Lavas from Gough Island, South Atlantic.* J. Petrol. **26**, Part 1, 149-186.

le Roex, A.P; Cliff, R.A & Adair, B.J.I (1990). *Tristan da Cunha, South Atlantic: Geochemistry and petrogenesis of a basanite-phonolite lava series.* J. Petrol. **31**, 779-812.

Leeman, W.P; Gerlach, D.C; Garcia,M.O & West,H.B (1994). *Geochemical variations in lavas from Kahoolawe volcano, Hawaii : evidence for open system evolution of plume - derived magmas.* Contrib. Mineral Petrol. **116**, 62-77.

Leinz, V; Bartorelli, A & Isotta, C.A.L (1968). *Contribuicao ao Estudo do Magmatismo Basaltico Mesozoico da Bacia do Parana* An.Acad. Brasil. Cienc. **40**, Supplemento,

Leyden, R; Ludwig, WJ & Ewing, M (1971). *Structure of Continental Margin off Punte del Este, Uruguay, and Rio de Janeiro, Brazil.* Am. Ass. Petroleum. G. Bull. **55**, 12, 2161-2173.

Lightfoot, P.C; Hawkesworth, C.J; Hergt,J.M; Naldrett,A.J; Gorbachev,N.S; Fedorenko,V.A & Doherty,W (1993). *Remobilisation of the continental lithosphere by a mantle plume: major-, trace-element, and Sr-, Nd-, and Pb- isotope evidence from picritic and tholeiitic lavas of the Noril'sk District, Siberian Traps.* Contrib.Mineral.Petrol. **114**, 171-188.

Lindsley, DH; Grover, JE; (1980). *Fe-rich pigeonite : a geobarometer.* Geol. Soc. Am.,

Lindsley, D.H (1983). *Pyroxene Thermometry* American Mineralogist **63**, 477-493.

Lindsley, D.H. & Frost, B.R (1992). *Equilibria among Fe-Ti oxides, pyroxenes, olivine, and quartz: Part I. Theory* American Mineralogist **77**, 987-1003.

Lord, J; Oliver, GJH; Soulsby, JH; (1996). *Landsat MSS imagery of a Lower Cretaceous dyke swarm Damaraland, Namibia: a precursor to the splitting of Western Gondwana.* Int. Jour. Remote Sensing **17**, 15, 2,945-2,954.

Mahoney, JJ (1988). *Deccan Traps* In MacDougall, J. (eds) Continental Flood Basalts. Dordrecht, Netherlands, Kluwer Academic Publishers. 151-195.

Manley, C.R (1995). *How voluminous rhyolite lavas mimic rheomorphic ignimbrites: Eruptive style, emplacement conditions and formation of tuff like textures* Geology **23**, 4, 349-352.

Mantovani, M.S.M; Cordani, U.G & Roisenberg,A (1985a). *Geoquimica Isotopica em Vulcanicas Acidas da Bacia do Parana, e Implicacoes Geneticas Associadas.* Revista Brasileira de Geociencias **15**, 1, 61-65.

Mantovani, M.S.M; Marques, L.S; DeSousa,M.A; Civetta,L; Atalla,L & Innocenti,F (1985b). *Trace Element and Strontium Isotope Constraints on the Origin and Evolution of the Paraná Continental Flood Basalts of Santa Catarina State (Southern Brazil)* J. Petrol. **26**, 1, 187-209.

Mantovani, M.S.M; Hawkesworth, C.J & Basei, M.A.S (1987). *Nd and Pb isotope studies bearing on the crustal evolution of southeastern Brazil.* Revista Brasileira de Geociencias **17**, 263-268.

Mantovani, M.S.M & Hawkesworth, C.J (1990). *An inversion approach to assimilation and fractional crystallisation processes.* Contrib. Mineral. Petrol. **105**, 289-302.

Mantovani, M.S.M. ; Vasconelles A.C.B.C. & Shukowsky, W. (1991). *Brusque transect (SA20) from the Dom Feliciano belt to the Amazon craton: explanatory pamphlet.* Global Geoscience Transects Project

Marques, L.S; Piccirillo, E.M; Melfi, A.J; Comin-Chiarmonti, P & Bellieni, G (1989). *Distribution of rare earth and other trace elements in the basalts of the Paraná Basin, southern Brazil.* Geochimica Brasiliensis **3**, 1, 33-50.

Marsh, J.S. (1973). *Relationships between Transform Directions and Alkaline Igneous Rock Lineaments in Africa and South America.* Earth. Planet. Sci. Lett. **18**, 317-323.

Marsh, J.S; Lock, B.E & Fuchter,W.H (1979). *New Chemical Analyses of the Suurberg Volcanic Rocks and Their Significance in Relation to Mesozoic Volcanism in Southern Africa.* South African J. Sci. **75**, 227-229.

Marsh, J.S (1987). *Basalt geochemistry and tectonic discrimination within CFB provinces.* Jour. Volcano. Geothermal Res. **32**, 35-49.

Marsh, B.D; Fournelle, J; Myers,J.D & Chou,I.M (1990). *On plagioclase thermometry in island arc rocks: Experiments and theory.* In Spencer,R.J & Chou,I.M(eds) Fluid Mineral Interactions: A Tribute to H.P.Eugster. The Geochemical Society.

Marsh, J.S; Erlank, A.J & Duncan,A.R (1991). *Report : Preliminary geochemical data for dolerite dykes and sills of the southern part of the Etendeka Igneous Province.* Communs. geol. Surv. Namibia **7**, 71-73.

Martin, AK; Hartnady, CJH; Goodlad, SW; (1981). *A revised fit of South America and South Central Africa.* Earth Planet. Sci. Lett. **54**, 293-305.

Martin, AK; (1984). *Propagating rifts: Crustal extension during continental rifting.* Tectonics **3**, 6, 611-617.

Martin, A.K & Hartnady, C.J.H (1986). *Plate Tectonic Development of the South West Indian Ocean: A Revised Reconstruction of East Antartica and Africa* J. Geophys. Res. **91**, B5, 4767-4786.

Martin, A.K. (1987). *Plate reorganisations around Southern Africa, hot-spots and extinctions.* Tectonophysics **142**, 309-316.

Mascle, J; Marinho, M & Wannesson, J (1986). *The structure of the Guinean continental margin: implications for the connection between central and the South Atlantic Oceans.* Geol. Rundsch. **75**, 1, 57-70.

Mathez, E.A (1973). *Refinement of the Kudo-Weill plagioclase thermometer and its application top basaltic rocks.* Contrib. Mineral. Petrol. **41**, 61-72.

May, SE (1990) *Pan-African magmatism andregional tectonics of South Brazil.* PhD., Open.

McCarthy, T.C & Patino Douce, A.E (1997). *Experimental evidence for high temperature felsic melts formed during basaltic intrusion of the deep crust.* Geology **25**, 5, 463-466.

McCulloch, M.T & Bennett, V.C (1994). *Progressive growth of the Earth's continental crust and depleted mantle : Geochemical constraints.* Geochim. Cosmochim. Acta **58**, No.21, 4717-4738.

McKenzie, D (1978). *Some remarks on the development of sedimentary basins* Earth. Planet. Sci. Lett. **40**, 25-32.

McKenzie, D. (1985). *The extraction of magma from the crust and mantle.* Earth. Planet. Sci. Lett. **74**; 1, 81-91.

McKenzie, D & Bickle, M.J (1988). *The Volume and Composition of Melt Generated by Extension of the Lithosphere.* J. Petrol. **29**, Part 3, 625-679.

McKenzie, D; (1989). *Some remarks on the movement of small melt fractions in the mantle.* Earth Planet. Sci. Lett. **95**, 53-72.

McKenzie, D & O'Nions, RK (1991). *Partial Melt Distributions from Inversion of Rare Earth Element Concentrations.* J. Petrol. **32**, 5, 1021-1091.

Melfi, AJ; (1967). *Potassium - argon ages for core samples of basaltic rocks from Southern Brazil.* Geochim. Cosmochim. Acta **31**, 1,079-1,089.

Menzies, M; Rogers, N; Tindle, A; Hawkesworth, C; (1987). *8. Metasomatic and enrichment processes in lithospheric peridotites, an effect of asthenosphere - lithosphere interaction.* In Menzies, M & Hawkesworth, C; (eds) Mantle Metasomatism. London, Academic Press. 313-361.

Mercier, J.C.C (1976). *Single pyroxene geothermometry and geobarometry* American Mineralogist **61**, 603-615.

Milani, E.J. (1992). *Intraplate tectonics and the evolution of the Parana basin, SE Brazil.* In M. deWit & Ransome (eds) Inversion tectonics of the Cape Fold Belt, Karoo and Cretaceous Basins of Southern Africa. Rotterdam, Balkema. 101-108.

Miller, R Mc G (1983). *The Pan-African Damara Orogen of South west Africa/ Namibia.* Spec. Publ. Geol. Soc. S. Afr. **11**, 431-515.

Milner, S.C (1986). *The Geological and Volcanological Features of the Quartz Latites of the Etendeka Formation.* Communs. Geol. Surv. S.W Africa/Namibia **2**, 109-116.

Milner, Sc & Duncan, AR (1987). *Geochemical characterisation of quartz latite units in the Etendeka formation.* Communs. Geol. Surv. SW Africa/Namibia **3**, 83-90.

Milner, S.C. (1988) *The Geology and Geochemistry of the Etendeka Quartz Latites, Namibia.* Doctor of Philosophy, University of Cape Town.

Milner, S.C; Duncan, A.R; Marsh,J.S & Miller,R.McG (1988b). *Field Excursion Guide to the Etendeka Volcanics and Associated Intrusives, N.W.Namibia.*

Milner, S.C & Ewart, A (1989). *The geology of the Goboboseb Mountain volcanics and their relationship to the Messum Complex, Namibia* Geol. Surv. Namibia Communs. **5**, 31-40.

Milner, S.C; Duncan; A.R & Ewart, A (1992). *Quartz latite rheoignimbrite flows of the Etendeka Formation, north western Namibia.* Bull. Volcanol. **54**, 200-219.

Milner, S.C; LeRoex, A.P & Watkins,R.J (1993). *Rb-Sr age determinations of rocks from the Okenyenya igneous complex, northwestern Namibia.* Geol. Mag. **130**, 3, 335-343.

Milner, SC; Duncan, AR; Ewart, A; Marsh, JS (1994). *Promotion of the Etendeka Formation to Group status: A new integrated stratigraphy.* Communs. Geol. Surv. Namibia **9**, 5-11.

Milner, S.C; LeRoex, P & O'Connor,J.M (1995). *Age of Mesozoic igneous rocks in northwestern Namibia and their relationship to continental breakup.* J. Geol. Soc. Lond. **152**, 94-104.

Milner, S.C; Duncan, A.R; Whittingham,A.M & Ewart,A (1995b). *Trans-Atlantic correlation of eruptive sequences and individual silicic volcanic units within the Paraná-Etendeka igneous province.* J.Volcano.Geothermal Res. **69**, 137-157.

Milner, S.C & le Roex, A.P (1996). *Isotope characteristics of the Okenyenya igneous complex, northwestern Namibia: constraints on the composition of the early Tristan plume and the origin of the EM1 mantle component.* Earth. Planet. Sci. Lett. **141**, 277-291.

Mizusaki, A.M.P; Petrini, R; Bellieni,G; Comin-Chiarmonti,P; Dias,J; DeMin,A & Piccirillo,E.M (1992). *Basalt magmatism along the passive continental margin of SE Brasil (Campos Basin).* Contrib. Mineral. Petrol. **111**, 143-160.

Mohr, P. (1992). *Nature of the crust beneath magmatically active continental rifts.* Tectonophysics **213**, 269-284.

Mohriak, WU; Hobbs, R; Dewey, JF; (1990). *Basin - forming processes and the deep structure of the Campos Basin offshore Brazil.* Marine and Petroleum Geology **7**, 94-122.

Montel, J.M (1986). *Experimental determination of the solubility of Ce-monazite in SiO_2-Al_2O_3-K_2O-Na_2O melts at 800°C, 2kbar, under H_2O saturated conditions.* Geology **14**, 659-662.

Montel, JM; (1993). *A model for monazite/melt equilibrium and application to the generation of granitic magmas.* Chem. Geol. **110**, 127-146.

Montes-Lauar, C.R; Pacca, I.G; Melfi, A.J; Piccirillo,E.M; Bellieni,G; Petrini,R & Rizzieri,R (1994). *The Anari and Tapirapuã Jurassic formations western Brazil: paleomagnetism, geochemistry and geochronology* Earth Planet. Sci. Lett. **128**, 357-371.

Moore, A.E (1976). *Controls of Post-Gondwanaland Alkaline Volcanism in Southern Africa.* Earth. Planet. Sci. Lett. **31**, 291-296.

Morgan, WJ; (1983). *Hotspot tracks and the early rifting of the Atlantic.* Tectonophysics **94**, 123-139.

Morgan, N. (1991). *The Fires that cracked a continent.* New Scientist June, 42-45.

Mortimer, N & Parkinson, D (1996). *Hikurangi Plateau: A Cretaceous large igneous province in the southwest Pacific Ocean.* J. Geophys. Res. **101**, B1, 687-696.

Mussett, A.E & Taylor, G.K (1994). *^{40}Ar-^{39}Ar ages for dykes from the Falkland Islands with implications for the breakup of southern Gondwanaland.* J. Geol. Soc. Lond. **151**, 79-81.

Müller, RD; Royer, JY; Lawyer, LA (1993). *Revised plate motions relative to the hotspots from combined Atlantic and Indian Ocean hotspot tracks.* Geology **21**, 275-278.

Neill, W.M (1976). *Mesozoic epeirogeny at the South Atlantic margin and the Tristan hot spot* Geology **4**, 495-498.

Nicholls, J. (1988). *The statistics of Pearce element diagrams and the Chayes closure problem.* Contrib. Mineral. Petrol. **99**; 1, 11-24.

Nixon, PH; Rogers, NW; Gibson, IL; Grey, A; (1981). *Depleted and fertile mantle xenoliths from Southern African kimberlites.* Ann. Rev. Earth Planet. Sci. **9**, 285-309.

Norry, MJ; Fitton, JG; (1983). *Compositional differences between oceanic and continental basic lavas and their significance.* In Hawkesworth, C; Norry, MJ;(eds) Continental Basalts and Mantle Xenoliths. Shiva. 5-19.

Nürnberg, D & Müller, R.D (1991). *The tectonic evolution of the South Atlantic from late Jurassic to present.* Tectonophysics **191**, 27-53.

O'Connor, J.M & Duncan, R.A (1990). *Evolution of the Walvis Ridge - Rio Grande Rise Hot Spot System : Implications for African and South American Plate Motions over Plumes.* J. Geophys. Res. **95**, No. B11, 17475-17502.

O'Connor, J.M & LeRoex, A.P. (1992). *South Atlantic Hotspot-plume systems: 1.Distribution of volcanism in time and space.* Earth. Planet. Sci. Lett. **113**, 343-364.

O'Nions, R.K (1984). *Isotopic abundances relevant to the identification of magma sources.* Phil. Trans. Royal. Soc. Lond. **A310**, 591-603.

O'Nions, R.K & McKenzie, D.P (1988). *Melting and continent generation.* Earth. Planet. Sci. Lett. **90**, 449-456.

Oliveira, L.O.A (1989). *Aspectos de evoluçao termomecânica da Bacia do Paraná no Brasil* Rev. Bras. Geocienc. **19**, 330-342.

Pacca, I.G & Hiodo, F.Y (1976). *Paleomagnetic Analysis of Mesozoic Serra Geral Basaltic Lava Flows in Southern Brazil.* An. Acad. Bras. Cienc. **48**, Supplemento,

Pankhurst, R.J & Rapela, C.R. (1995). *Production of Jurassic rhyolite by anatexis of the lower crust of Patagonia.* Earth. Planet. Sci. Lett. **134**, 23-36.

Parsons, I (1981). *The Klokken Gabbro-Syenite Complex, South Greenland: Quantitative Interpretation of Mineral Chemistry* J. Petrol. **22**, 2, 233-260.

Pavoni, N (1993). *Pattern of mantle convection and Pangaea break-up as revealed by the evolution of the African plate.* J. Geol. Soc. Lond. **150**, 953-964.

Pearce, J.A & Cann, J.R (1973). *Tectonic Setting of Basic Volcanic Rocks Determined using Trace Element Analyses.* Earth. Planet. Sci. Lett. **19**, 290-300.

Pearce, JA & Norry, MJ (1979). *Petrogenetic implications of Ti, Zr, Y and Nb variations in volcanic rocks.* Contrib. Mineral. Petrol. **69**, 33-47.

Pearce, J.A (1982). *Trace element characteristics of lavas from destructive plate boundaries.* In Thorpe,R.S (ed). Andesites.

Peate, DW; Mantovani, M; Hawkesworth, C; (1988). *Geochemical stratigraphy of the Paraná continental flood basalts: borehole evidence.* Revista Brasileira de Geociências **18**, 2, 212-221.

Peate, D.W. (1989) *Stratigraphy and Petrogenesis of the Paraná Continental Flood Basalts, Southern Brazil.* Doctor of Philosophy, Open.

Peate, D.W; Hawkesworth, C.J; Mantovani,M.S.M & Shukowsky,W (1990). *Mantle plumes and flood basalt stratigraphy in the Parana, South America.* Geology **18**, 1223-1226.

Peate, D.W; Hawkesworth, C.J & Mantovani,M.S.M (1992). *Chemical stratigraphy of the Parana lavas (South America) : classification of magma types and their spatial distribution.* Bull. Volcanol. **55**, 119-139.

Peate, D.W & Hawkesworth, C.J. (1996). *Lithospheric to asthenospheric transition in Low-Ti flood basalts from southern Paraná, Brazil.* Chem. Geol. **127**, 1-24.

Pegram, WJ; (1990). *Development of continental lithospheric mantle as reflected in the chemistry of the Mesozoic Appalachian tholeiites, U.S.A.* Earth. Planet. Sci. Lett. **97**, 316-331.

Petrini, R; Civetta, L; Piccirillo,E.M; Bellieni,G; Comin Chiaramonti,P; Marques, L.S & Melfi,A.J (1987). *Mantle Heterogeneity and Crustal Contamination in the Genesis of Low-Ti Continental Flood Basalts from the Paraná Plateau (Brazil): Sr-Nd Isotope and Geochemical Evidence* J. Petrol. **28**, 4, 701-726.

Piccirillo, E.M; Raposa, M.I.B; Melfi,A.J; Comin-Chiaramonti,P; Bellieni,G; Cordani,U.G & Kawashita,K (1987). *Bimodal Fissural Volcanic Suites from the Parana Basin (Brazil): K-Ar Age, Sr Isotopes and Geochemistry.* Geochimica Brasiliensis **1**, 1, 53-69.

Piccirillo, EM; Comin-Chiarmonti, P; Melfi, AJ; Stolfa, D; Bellieni, G; Marques, LS; Giaretta, A; Nardy, AJR; Pinese, JPP; Raposa, MIB; Roisenberg, A. (1988). *Petrochemistry of continental flood basalt- rhyolite suites and related intrusives from the Paraná basin (Brazil).* In Piccirillo, EM & Melfi, AJ(eds) The Mesozoic flood volcanism of the Paraná Basin: Petrogenetic and geophysical aspects. Universidade de Sao Paulo. 94-106.

Piccirillo, E.M; Civetta, L; Petrini, R; Longinelli, A; Bellieni, G; Comin Chiarmonti, P; Marques, L.S. & Melfi, A.J (1989). *Regional variations within the Paraná flood basalts (Southern Brazil): Evidence for subcontinental mantle heterogeneity and crustal contamination.* Geology **75**, 103-122.

Piccirillo, E.M; Bellieni, G; Cavazzini,G; Comin-Chiaramonti,P; Petrini,R; Melfi,A.J; Pinese,J.P.P; Zantadeschi,P & DeMin,A (1990). *Lower Cretaceous tholeiitic dyke swarms from the Ponta Grossa Arch (southeast Brasil) : Petrology, Sr-Nd isotopes and genetic relationships with the Parana flood volcanics.* Chem. Geol. **89**, 19-48.

Pichavant, M; Montel, JM; Richard, L; (1992). *Apatite solubility in peraluminous liquids: Experimental data and an extension of the Harrison - Watson model.* Geochim. Cosmochim. Acta **56**, 3,855-3,861.

Potts, P.J; Webb, P.C; Watson, J.S; (1984). *Energy dispersive X-ray flourescence analysis of silicate rocks for major and trace elements.* X-ray Spectrom. **13**, 2-15.

Porada, H (1989). *Pan African Rifting and Orogenesis in Southern to Equatorial Africa and Eastern Brasil.* Precambrian Research **44**, 103-136.

Powell, R & Powell, M (1977). *Geothermometry and oxygen barometry using coexisting iron-titanium oxides: a reappraisal.* Min. Mag. **41**, 257-263.

Preciozzi, F; Spotumo, J; Heinzen, W; Rossi, P; (1985). *Memoria explicativa de la Carta Geologica del Uruguay a escala 1:500,000* Montevideo, Dir. Nac. Min. Geologia.

Price, J.G (1985). *Ideal site mixing in solid solutions, with an application to two-feldspar geothermometry.* American Mineralogist **70**, 696-701.

Rabinowitz, P.D & LaBreque, J (1979). *The Mesozoic South Atlantic Ocean and Evolution of Its Continental Margins.* J. Geophys. Res. **84**, B11,

Ragland, P.C (1989). *Basic Analytical Petrology* Oxford, Oxford University Press.

Ramos, VA; Kay, SM; (1992). *Southern Patagonia plateau basalts and deformations : backarc testimony of ridge collisions.* Tectonophysics **205**, 261-282.

Rampino, MR; (1987). *Impact cratering and flood basalt volcanism.* Nature **327**, 468.

Rampino, MR; Stothers, RB; (1988). *Flood basalt volcanism during the past 250 million years.* Science **241**, 663-668.

Raposo, MIB & Ernesto, M (1995). *An Early Cretaceous paleomagnetic pole from Ponta Grossa dikes (Brazil): Implications for the South American Mesozoic apparent polar wander path.* J. Geophys. Res. **100**, B10, 20,095-20,109.

Rapp, RP; Watson, EB; (1986). *Monazite solubility and dissolution kinetics: implications for the thorium and light rare earth chemistry of felsic magmas.* Contrib. Mineral. Petrol. **94**, 304-316.

Regelous, M. (1993) *Geochemistry of dolerites from the Parana flood basalt province, southern Brazil.* Doctor of Philosophy, The Open University.

Reid, D.L (1990). *The Cape Peninsula dolerite dyke swarm, South Africa.* In Parker, Rickwood & Tucker (eds) Mafic Dykes and Emplacement Mechanisms. 325-334.

Reid, D.L; Erlank, A.J & Rex,D.C (1991). *Age and correlation of the False Bay dolerite dyke swarm, south-western Cape, Cape Province.* S. Afr. J. Geol. **94**, 213, 155-158.

Reid, D.L & Rex, D.C. (1994). *Late Karoo Dolerite Dykes in the Richtersveld.* S.Afr.J.Geol. **97**, 2, 135-145.

Reid, D; Rex, DC; (1994b). *Cretaceous dykes associated with the opening of the South Atlantic : the Mehlberg dyke, northern Richtersveld.* S. Afr. Jour. Geol. **97**, 2, 135-145.

Renne, P.R; Ernesto, M; Pacca,I.G; Coe,R.S; Glen,J.M; Prevot,M & Perrin,M (1992). *The Age of Parana Flood Volcanism,Rifting of Gondwanaland, and the Jurassic-Cretaceous Boundary.* Science **258**, 975-979.

Renne, P.R; Deckart, K; Ernesto, M; Feraud, G & Piccirillo, E.M (1996). *Age of the Ponta Grossa dike swarm (Brazil), and implications to Paraná flood volcanism.* Earth. Planet. Sci. Lett. **144**, 1-2, 199-211.

Renne, PR; Glen, JM; Milner, SC; Duncan, AR (1996b). *Age of Etendeka flood volcanism and associated intrusions in southwestern Africa.* Geology **24**, 7, 659-662.

Rex, D.C & Guise, P.G (1986). *Age of the Tinti Felsite, Lanarkshire; a possible 39/40 Ar monitor.* Bulletin of Liaison and Informations, IGCP Project 196, Calibration of the Phanerozoic Time Scale. **6**, 8-10.

Riccardi, AC (1988). *The Cretaceous System of Southern South America.* Geol. Soc. Am. Memoir.

Richards, M.A; Duncan, R.A & Courtillot,V.E (1989). *Flood Basalts and Hot-Spot Tracks: Plume Heads and Tails.* Science **24**, 103-107.

Richards, M.A; Jones, D.L; Duncan,R.A & DePaolo,D.J. (1991). *A Mantle Plume Initiation Model for the Wrangellia Flood Basalt and Other Oceanic Plateaus.* Science **254**, 263-267.

Richardson, S.H; Erlank, A.J; Duncan, A.R & Reid, D.L (1982). *Correlated Nd, Sr and Pb isotope variation in Walvis Ridge basalts and implications for the evolution of their mantle source.* Earth. Planet. Sci. Lett. **59**, 2, 327-342.

Rogers, N & Hawkesworth, C (1982). *Proterozoic age and cumulate origin for granulite xenoliths, Lesotho* Nature **299**, 5882, 409-413.

Rollinson, H (1993). *Using geochemical data: evaluation, presentation, interpretation.* Essex, Longman Scientific & Technical.

Royer, JY; Gahagan, LM; Lawyer, LA; Mayes, CL; Nürnberg, D; Sandwell, DT; Scotese, CR; *A tectonic chart for the Southern Ocean derived from Geosat altimetry data.* In St. John, B; (eds) Antarctica as an exploration frontier, hydrocarbon potential, geology, and hazards. Tulsa, AAPG Studies in Geology. 89-99.

Rudnick, R.L & Taylor, S.R (1987). *The composition and petrogenesis of the lower crust: A xenolith study.* J. Geophys. Res. **92**, 13,981-14,005.

Rudnick, R.L & Presper, T (1990). *Geochemistry of Intermediate to High Pressure Granulites* In Vielzeuf, D & Vidal, P (eds) NATO ASI Series.

Rudnick, RL (1995). *Making continental crust.* Nature **378**, 571-578.

Rushmer, T. (1991). *Partial melting of two amphibolites; contrasting experimental results under fluid-absent conditions.* Contrib. Mineral. Petrol. **107**; 1, 41-59.

Russell, J.K. & Nicholls, J. (1988). *Analysis of petrologic hypotheses with Pearce element ratios.* Contrib. Mineral. Petrol. **99**; 1, 25-35.

Sadowski, GR (1987). *A possible relation between pulses of platform activation and plate kinematics.* Tectonophysics **143**, 43-57.

Sandiford, M; (1989). *Horizontal structures in granulite terrains. A record of mountain building or mountain collapse?* Geology **17**, 449-452.

Sandiford, M; Powell, R; (1990). *Some isostatic and thermal consequences of the vertical strain geometry in convergent orogens.* Earth. Planet. Sci. Lett. **98**, 154-165.

Sandiford, M; Coblentz, D; (1994). *Plate scale potential - energy distributions and the fragmentation of ageing plates.* Earth. Planet. Sci. Lett. **126**, 143-159.

Sandiford, M; Coblentz, DD; Richardson, RM; (1995). *Ridge torques and continental collision in the Indian - Australian plate.* Geology **23**, 7, 653-656.

Saunders, A.D; Storey, M; Kent,R.W & Norry,M.J (1992). *Consequences of plume-lithosphere interactions.* In Storey,B.C; Alabaster,T & Pankhurst,R.J (eds) From Magmatism and the Causes of Continental Break-up. Geol. Soc. Spec. Publ. 41-60.

Sawyer, E.W (1994). *Melt segregation in the continental crust.* Geology **22**, 1019-1022.

Scaillet, B; Holtz, F; Pichavant, M & Schmidt, M (1996). *Viscosity of Himalayan leucogranites; implications for granitic magma ascent.* J. Geophys. Res. **101**, 12, 27,691 - 27,699.

Scotese, C.R; Gahagan, L.M & Larson, R.L (1988). *Plate tectonic reconstructions of the Cretaceous and Cenozoic ocean basins.* In Scotese, C.R & Sager, W (eds) Mesozoic and Cenozoic plate reconstructions. Amsterdam, Elsevier. 27-48.

Seck, H.A (1971). *Der Einfluss des Drucks auf die Zusammensetzung keoxistierender Alkalifeldspate and plagioclase in system* $NaAlSiO_8$-$KAlSi_3O_8$-$CaAl_2Si_2O_8$-H_2O Contrib. Mineral. Petrol. **31**, 67-86.

Sengör, A.H.C & Burke, K (1978). *Relative timing of rifting and volcanism on earth and its tectonic implications.* Geophys. Res. Lett. **5**, 419-421.

Sharma, M; Basu, A.R & Nesterenko, G.V (1991). *Nd-Sr isotopes, petrochemistry, and origin of the Siberian flood basalts, USSR.* Geochim. Cosmochim. Acta **55**, 4, 1183-1192.

Sharma, M; Basu, A.R & Nesterenko, G.V (1992). *Temporal Sr, Nd and Pb-isotopic variations in the Siberian flood basalts: implications for plume source characteristics.* EOS **73**, 14, 329.

Shaw, H (1972). *Viscosities of magmatic silicate liquids: An empirical method of prediction.* Am. J. Sci. **272**, 870-893.

Shirley, S.B; Klewin, K.W; Berg,J.H & Carlson,R.W (1994). *Temporal changes in the sources of flood basalts: Isotopic and trace element evidence from the 1100Ma old Keweenawan Mamainse Point Formation, Ontario, Canada.* Geochim. Cosmochim. Acta **58**, 20, 4475-4490.

Sial, A.N; Oliveira, E.P & Choudhuri,A (1985). *Mafic Dyke Swarms of Brazil* In Halls,H.C & Fahrig,W.F (eds) From Mafic Dyke Swarms. Geol. Ass. Can. Spec. Paper. 467-481.

Siedner, G & Miller, J.A (1968). *K-Ar Age Determinations on Basaltic Rocks from South-west Africa and their bearing on Continental Drift.* Earth. Planet. Sci. Lett. **4**, 451-458.

Siedner, G & Mitchell, J.G (1976). *Episodic Mesozoic Volcanism in Namibia and Brazil: A K-Ar Isochron study bearing on the Opening of the South Atlantic.* Earth. Planet. Sci. Lett. **30**, 292-302.

Skjerlie, K.P., Patino-Douce, A.E. & Johnston, A.D. (1993). *Fluid absent melting of a layered crustal protolith; implications for the generation of anatectic granites.* Contrib. Mineral. Petrol. **114**; 3, 365-378.

Sleep, N.H (1990). *Hotspots and mantle plumes. Some phenomenology.* J. Geophys. Res. **95**, 6715-6736.

Sleep, N.H (1995). *A wayward plume?* Nature **378**, 19-20.

Smith, J.V. (1992). *Experimental Kinematic Analysis of en Echelon Structures in Relation to the Cobar Basin, Lachlan fold belt.* Tectonophysics **214**, 1-4, 269-276.

Smrekar, S.E & Parmentier, E.M (1996). *The interaction of mantle plumes with surface thermal and chemical boundary layers: Applications to hotspots on Venus.* J.Geophys.Res. **101**, B3, 5397-5410.

Somoza, R (1994). *South American reference pole for the Mid- Cretaceous: Further constraints in the interpretation of Andean paleomagnetic data.* Geology **22**, 933-936.

Sonder, LJ; England, PC; (1989). *Effects of a temperature - dependent rheology on large scale continental extension.* J. Geophys. Res. **94**, B6, 7,603-7,619.

Sparks, R.S.J (1976). *Grain size variations in ignimbrites and implications for the transport of pyroclastic flows.* Sedimentology **23**, 147-188.

Spencer, KJ; Lindsley, DH; (1981). *A solution model for coexisting iron - titanium oxides.* American Mineralogist **66**, 1,189-1,201.

Sprechmann, P; Bossi, J & Da Silva, J (1981). *Cuencas del Jurásico y Cretácico del Uruguay.* Cuencas Sedimentarias del Jurásico y Cretácico América del Sur. **1**, 239-270.

Steiger, R.H & Jäger, E (1977). *Subcommision on geochronology: convention on the use of decay constants in geo- and cosmochronology.* Earth. Planet. Sci. Lett. **36**, 359-362.

Stern, C.R & Wyllie, P.J (1978). *Phase compositions through crystallisation intervals in basalt-andesite-H_2O at 30kbar with implications for subduction zone magmas.* American Mineralogist **63**, 641-663.

Stewart, K; Turner, S; Kelley, S; Hawkesworth, C; Kirstein, L; Mantovani, M. (1996). *3D, ^{40}Ar-^{39}Ar geochronology in the Paraná continental flood basalt province.* Earth. Planet. Sci. Lett. **143**, 95-109.

Stoakes, F; Campbell, C & Cass,R (1990). *Seismic Stratigraphic Analysis of the Punta del Este Basin, Offshore Uruguay.* CSPG-Reservoir **17**, 6, 2-9.

Stoakes, F.A; Campbell, C.V; Cass,R & Ucha,N. (1991). *Seismic stratigraphic Analysis of the Punte del Este Basin, Offshore Uruguay, South America.* Am. Ass. Petroleum. Geol. Bull. **75**, 2, 219-240.

Storey, B.C & Alabaster, T (1991). *Tectonomagmatic controls on Gondwana break-up models: evidence from the proto-Pacific margin of Antarctica.* Tectonics **10**, 1274-1288.

Storey, B.C (1995). *The role of mantle plumes in continental breakup: case histories from Gondwanaland.* Nature **377**, 301-308.

Stormer, J.C (1975). *A Practical Two-feldspar Geothermometer* American Mineralogist **60**, 667-674.

Stormer, JC; (1983). *The effects of recalculation on estimates of temperature and oxygen fugacity from analyses of multicomponent iron - titanium oxides.* American Mineralogist **68**, 586-594.

Stormer, J.C & Whitney, J.A (1985). *Two feldspar and iron-titanium oxide equilibria in silicic magmas and the depth of origin of largs volume ash-flow tuffs.* American Mineralogist **70**, 52-64.

Sun, S.S & Hanson, G.N (1975). *Origin of Ross Island basanitoids and limitations on the hetrogeneity of mantle source for alkali basalts and nephelinites.* Contrib. Mineral. Petrol. **52**, 77-106.

Sun, S & McDonough, W.F (1989). *Chemical and isotopic systematics of oceanic basalts: Implications for mantle composition and processes.* In Saunders,A.D & Norry,M.J (eds) Magmatism in the Ocean Basins. Geol. Soc. Spec. Publ. 313-345.

Sweeney, R.J; Falloon, T.J; Green,D.H & Tatsumi,Y (1991). *The mantle origins of Karoo picrites.* Earth. Planet. Sci. Lett. **107**, 256-271.

Tarling, D.H & Tarling, M.P. (1977). *Continental Drift - A Study of the Earth's Moving Surface.* Pelican.

Taylor, S.R & McLennan, S.M (1981). *The rare earth element evidence in Precambrian sedimentary rocks: Implications for crustal evolution.* In Kroner, A. (eds) Precambrian Plate Tectonics. Amsterdam, Elsevier. 527-548.

Taylor, S.R & McLennan, S.M (1985). *The Continental Crust: its composition and evolution.* Blackwell Scientific Publications.

Thirlwall, MF; Upton, BGJ; Jenkins, C (1994). *Interaction between Continental Lithosphere and the Iceland Plume - Sr-Nd-Pb Isotope Geochemistry of Tertiary Basalts, NE Greenland.* J. Petrol. **35**, 3, 839-879.

Thompson, R.N; Morrison, M.A; Dickin, A.P. & Hendry, G.L (1983). *Continental flood basalts ..... arachnids rule OK?* In Hawkesworth, C.J & Norry, M.J (eds) Continental flood basalts and mantle xenoliths. Shiva Press. 158-185.

Thompson, R.N; Morrison, M.A; Hendry,G.L & Parry,S.J (1984). *An assessment of the relative roles of crust and mantle genesis: an elemental approach.* Phil. Trans. Royal. Soc. Lond. **A310**, 549-590.

Thompson, RN; Morrison, MA; (1988). *Asthenospheric and lower - lithospheric mantle contributions to continental extensional magmatism: An example from the British Tertiary Province.* Chem. Geol. **68**, 1-15.

Thompson, R.N & Gibson, S,A (1991). *Subcontinental mantle plumes, hotspots and pre-existing thinspots.* J. Geol. Soc. Lond. **148**, 973-977.

Thompson, RN; Gibson, SA; (1994). *Magmatic expression of lithospheric thinning across continental rifts.* Tectonophysics **233**, 41-68.

Tistl, M; Burgath, K.P; Hohndorf,A; Kreuzer,H; Munoz,R & Salinas,R (1994). *Origin and emplacement of Tertiary ultramafic complexes in northwest Colombia: Evidence from geochemistry and K-Ar, Sm-Nd and Rb-Sr isotopes.* Earth. Planet. Sci. Lett. **126**, 41-59.

Toyoda, K; Horiuchi, H & Tokonami,M (1994). *Dupal anomaly of Brazilian carbonatites: Geochemical correlations with hotspots in the South Atlantic and implications for the mantle source.* Earth. Planet. Sci. Lett. **126**, 315-331.

Turcotte, DL; (1983). *Mechanisms of crustal deformation.* J. Geol. Soc. Lond. **40**, 701-724.

Turcotte, DL & Emerman, SH (1983b). *Mechanisms of active and passive rifting.* Tectonophysics **94**, 39-50.

Turner, S; Hawkesworth, C; Liu,J; Rogers,N; Kelley,S & vanCalsteren,P (1993). *Timing of Tibetan uplift constrained by analysis of volcanic rocks.* Nature **364**,

Turner, S; Regelous, M; Kelley,S; Hawkesworth,C.J & Mantovani,M.S.M (1994). *Magmatism and continental breakup in the South Atlantic: High precision ^{40}Ar-^{39}Ar geochronology.* Earth. Planet. Sci. Lett. **121**, 333-348.

Turner, S & Hawkesworth, C (1995). *The nature of the sub-continental mantle: constraints from the major- element composition of continental flood basalts.* Chem. Geol. **120**, 295-314.

Turner, S; Hawkesworth, C; Gallagher,K; Stewart,K; Peate,D & Mantovani,M (1996). *Mantle plumes, flood basalts, and thermal models for melt generation beneath continents: Assessment of a conductive heating model and application to the Paraná.* J. Geophys. Res. **101**, B5, 11,503-11,518.

Turner, S.P; Hawkesworth, C.J; Gallagher,K; Stewart,K; Peate,D & Mantovani,M. (1996). *Flood basalts and flood basalts: the Parana case.* Earth. Planet. Sci. Lett.

Uchupi, E. (1989). *The tectonic style of the Atlantic Mesozoic rift system.* J. of Afr. Earth Sciences. **8**, 2/3/4, 143-164.

Ulbrich, H.H.G.J & Gomes, C.B (1981). *Alkaline Rocks from Continental Brazil.* Earth Science Reviews **17**, 135-154.

Uliana, M.A; Biddle, K.T & Cerdan,J. (1989). *Mesozoic Extension and the Formation of Argentine Sedimentary Basins.* In AJ.Tankard & HR.Balkwill (eds) Extensional Tectonics and Stratigraphy of the North Atlantic Margins. Am. Ass. Petroleum Geol.

Unternehr, P; Curie, D; Olivet,J.L; Goslin,J & Beuzart,P. (1988). *South Atlantic fits and intraplate boundaries in Africa and South America.* Tectonophysics **155**, 169-179.

Ures, C; Féraud, G; Bertrand, H; Bossi, J; (1997). *New age and geochemical constraints on the Paraná flood volcanism: Additional data on Uruguay extrusive and intrusive formations.* EUG 9, Strasbourg,

Urien, C.M & Zambrano, J.J (1973). *The Geology of the Basins of the Argentine Continental Margin and Malvinas Plateau.* In Nairn,A.E.M & Stehli,F.G (eds) The Ocean Basins and Margins. 135-169.

Urien, C.M; Martins, L.R & Zambrano,J.J. (1976). *The Geology and Tectonic Framework of Southern Brazil, Uruguay and Northern Argentina Continental Margin: Their Behaviour During the Southern Atlantic Opening.* An. Acad. Bras. Cienc. **48**, Supplemento,

Valencio, DA; Vila, JF; (1970). *Palaeomagnetism of some Middle Jurassic lavas from south-east Argentina.* Nature **225**, 262-264.

Van Deccar, J.C; James, D.E & Assumpção, M. (1995). *Seismic evidence for a fossil mantle plume beneath South America and implications for plate driving forces.* Nature **378**, 25-31.

Vierbuchen, R.C; George, R.P & Vail,P.R. *A Thermal-Mechanical Model of Rifting with Implications for Outer Highs on Passive Continental Margins.* In J. S. W. C.L.Drake (eds) Studies in Continental Margin Geology. AAPG.

Vine, F.J &Matthews, D.H (1963). *Magnetic Anomalies over Oceanic Ridges* Nature **199**, 947-949.

Walther, K (1927). *Contribucíon al conocimiento de las rocas 'basálticas' de la formación de Gondwana en la América del Sur.* Instituto Geología y Perforaciones Uruguay **Boletín 9**, 1-43.

Watson, EB; (1979). *Zircon saturation in felsic liquids: Experimental results and applications to trace element geochemistry.* Contrib. Mineral. Petrol. **70**, 407-419.

Watson, EB; (1980). *Some experimentally determined zircon / liquid partition coefficients for the rare earth elements.* Geochim. Cosmochim. Acta **44**, 895-897.

Watson, E.M & Harrison, T.M (1983). *Zircon saturation revisited: temperature and composition effects in a variety of crustal magma types.* Earth. Planet. Sci. Lett. **64**, 295-304.

Watson, EB; Harrison, TM; (1984). *Accessory minerals and the geochemical evolution of crustal magmatic systems: a summary and prospectus of experimental approaches.* Physics Earth Planet. Int. **35**, 19-30.

Watson, EB; (1996). *Dissolution, growth and survival of zircons during crustal fusion: kinetic principles, geological models and implications for isotopic inheritance.* Trans. Royal Soc. Edin. **87**, 43-56.

Weaver, B.L & Tarney, J (1984). *Empirical approach to estimating the composition of the continental crust.* Nature **310**, 575-577.

Wedepohl, K.H (1995). *The composition of the continental crust.* Geochim. Cosmochim. Acta **59**, 7, 1217-1232.

Wegener, A (1967). *The origin of continents and oceans* Methuen & Co.

Weiss, S & Troll, G (1989). *The Ballachulish Igneous Complex, Scotland. Petrography, Mineral Chemistry, and Order of Crystallization in the Monzodiorite-Quartz Diorite Suite and in the Granite* J. Petrol. **30**, 5, 1069-1115.

White, AJR; Collins, WJ; Chappell, BW. (1982). *Influence of the melt structure on the trace element composition of granites.* Geology of Granites and their Metallogenetic relations., Nanjing University, China,

White, W.M & Hofmann, A.W (1982). *Sr and Nd isotope geochemistry of oceanic basalts and mantle evolution.* Nature **296**, 821-825.

White, R.S. (1987). *When continents drift.* Nature **327**, May, 191.

White, R.S., Spence, G.D., Fowler, S.R., McKenzie, D.P., Westbrook, G.K & Bowen, A.N (1987). *Magmatism at rifted continental margins* Nature **330**, 439-444.

White, R.S (1988). *The Earth's Crust and Lithosphere* In Menzies,M.A & Cox,K.G (eds) Oceanic and Continental Lithosphere: Similarities and Differences. Oxford, J. of Petr., Oxford University Press. 445.

White, R.S (1989). *Asthenospheric control on magmatism in the ocean basins.* In Menzies,M.A & Cox,K.G (eds) Magmatism in the Ocean Basins. London, Geol. Soc. Spec. Publ. 17-27.

White, R.S & McKenzie, D.P (1989(a)). *Volcanism at Rifts.* Scientific American 44-55.

White, R.s & McKenzie, D.P (1989(b)). *Magmatism at rift zones: the generation of volcanic continental margins and flood basalts.* J. Geophys. Res. **94**, 7685-7729.

White, R.S (1992). *Magmatism during and after continental breakup.* In Storey,B.C; Alabaster,T & Pankhurst,R.J (eds) Magmatism and the causes of Continental Break-up. Geol. Soc. Spec. Publ. 1-16.

White, R.S; McBride, J.H; Henstock,T.J & Hobbs,R.W (1994). *Internal structure of a spreading segment of Mesozoic oceanic crust.* Geology **22**, 597-600.

White, R.S & McKenzie, D.P (1995). *Mantle plumes and flood basalts.* J.Geophys.Res. **100**, 17543-17585.

Whitney, J.A & Stormer, J.C (1976). *Geothermometry and geobarometry in epizonal granitic intrusions: a comparison of iron-titanium oxides and coexisting feldspars* American Mineralogist **61**, 751-761.

Whitney, JA; Dorais, MJ; Stormer, JC; Kline, SW; Matty, D; (1988). *Magmatic conditions and development of chemical zonation in the Carpenter Ridge Tuff, Central san Juan volcanic field, Colorado.* Am. J. Sci. **288-A**, 16-44.

Whittaker, A; Cope, J; Cowie, J; Gibbons, W; Hailwood, E.A; House, M.R; Jenkins, D.G; Rawson, P.F; Rushton, A.W.A.; Smith, D.G; Thomas, A.T & Wimbledon, W.A. (1991). *A guide to stratigraphical procedure* J. Geol. Soc. Lond. **148**, 5, 813-824.

Whittaker, A; Bott, M.H.P & Waghorn,G.D (1992). *Stresses and Plate Boundary Forces Associated With Subduction Plate Margins.* J. Geophys. Res. **97**, B8, 11933-11944.

Whittingham, A.M (1991) *Stratigraphy and petrogenesis of the volcanic formations associated with the opening of the South Atlantic, southern Brazil.* PhD., Oxford.

Whittington, A.G; Harris, N.B.W & Butler, R.W.H (1996). *Contrasting anatectic styles at Nanga Parbat, northern Pakistan.* 11th Himalaya-Karakorum-Tibet Workshop, Flagstaff, Arizona, Geol. Soc. Am. Spec. Publ.

Whittney, J.A & Stormer, J.C (1977). *The distribution of $NaAlSi_3O_8$ between coexisting microcline and plagioclase and its effect on geothermometric calculations.* American Mineralogist **62**, 687-691.

Wilson, M. (1989). *Igneous Petrogenesis : A Global Tectonic Approach.* Unwin Hyman Ltd.

Wilson, M (1992). *Magmatism and continental rifting during the opening of the South Atlantic Ocean : a consequence of Lower Cretaceous super-plume activity?* In Storey,B.C; Alabaster,T & Pankhurst,R.J (eds) Magmatism and the Causes of Continental Break-up. Geol. Soc. Spec. Publ. 241-255.

Wilson, M & Guirand, R. (1992). *Magmatism and rifting in Western and Central Africa, from Late Jurassic to Recent times.* Tectonophysics **213**, 203-225.

Wilson, M (1993). *Plate-moving mechanisms: constraints and controversies.* J. Geol.Soc.Lond. **150**, 923-926.

Wilson, M (1993). *Geochemical signatures of oceanic and continental basalts: a key to mantle dynamics.* J. Geol. Soc. Lond. **150**, 977-990.

Winchester, J.A & Floyd, P.A (1977). *Geochemical discrimination of different magma series and their differentiation products using immobile elements.* Chemical Geology **20**, 325-343.

Winters-Butler, L. (II) (1969) *Shallow Structure of the Continental Margin, Southern Brazil and Uruguay.* Doctor of Philosophy (part fulfillment), University of Illinois.

Wold, C.N (1990) *Fit and Initial Opening of the Continents around the Atlantic Ocean from Early Jurassic to Early Cretaceous.* MSc, University of Colorado.

Wood, D.A (1979). *A variably veined suboceanic upper mantle - Genetic significance for mid-ocean ridge basalts from geochemical evidence.* Geology **7**, 499-503.

Wood, B.J & Virgo, D (1989). *Upper mantle oxidation state: Ferric iron contents of lherzolite spinels by ^{57}Fe Mössbauer spectroscopy and resultant oxygen fugacities.* Geochim. Cosmochim. Acta **53**, 1277-1291.

Yoder, H.S (1988). *The Great Basaltic 'Floods'.* South African J. Geol. **91**, No.2,

Zalán, PV; Wolff, S; Conceicao, JCJ; Astolfi, MAM; Vieira Ines, S; Appi, VT; Zanotto, OA; Marques, A. (1987). *Tectonics and sedimentation of the Paraná Basin.* Anais do VII Symposium do Gondwana,

Zambrano, JJ & Urien, CM (1970). *Geological outline of the basins in Southern Argentina and their continuation off the Atlantic shore.* J. Geophys. Res. **75**, 8, 1363-1396.

Ziegler, P.A. (1992). *Plate tectonics, plate moving mechanisms and rifting.* Tectonophysics **215**, 9-34.

Ziegler, P.A (1993). *Plate-moving mechanisms: their relative importance.* J. Geol. Soc. Lond. **150**, 927-940.

APPENDIX A

GEOCHEMICAL DATA

The following pages contain all the new data generated during the course of this research into the chemistry of the volcanics of southern Uruguay. The samples are listed in the magma types/series that they are ascribed to in Chapter 2 with the abbreviations used in brackets:

Puerto Gómez Formation:

Santa Lucía (Santa L) magma type

Treinte Y Trés (TYT) magma type

Arequita Formation:

Aigüa Series

Lascano Series

Valle Chico Formation (Syenite).

All major element data are corrected for the individual loss on ignition values of each sample.

Name	*Santa L*	*Santa L*	*Santa L*	*Santa L*	*Santa L*	*TYT*
Sample #	**93L47**	**92-U12**	**93L104**	**93L53**	**93L106**	**93L27**
SiO_2	47.99	48.19	48.63	48.85	49.81	48.52
TiO_2	1.63	1.88	1.52	1.76	1.91	1.20
Al_2O_3	17.86	16.99	16.19	18.05	15.71	17.75
Fe_2O_3	12.80	12.31	13.59	11.93	14.03	11.77
MnO	0.14	0.18	0.16	0.14	0.15	0.22
MgO	5.27	6.44	6.61	4.77	5.13	6.57
CaO	10.27	8.57	10.31	9.98	9.84	10.97
Na_2O	2.84	3.78	2.23	3.05	2.25	2.40
K_2O	0.92	1.14	0.56	1.14	0.87	0.43
P_2O_5	0.28	0.52	0.21	0.32	0.31	0.17
LOI	1.86	0.86	2.00	1.89	1.52	2.00
Total	101.92	100.24	100.39	100.26	100.65	100.57
XRF						
Rb	18.10	21.90	10.00	28.70	21.70	6.10
Sr	344.10	596.80	280.40	326.30	285.00	280.90
Y	29.70	30.30	36.30	34.30	47.40	29.20
Zr	138.00	154.00	128.00	177.00	190.00	97.00
Nb	17.50	27.80	11.80	17.40	16.40	5.60
Ba	392.00	551.00	401.00	439.00	401.00	309.00
Pb	4.00	4.00	5.00	4.00	7.00	3.00
Th	3.00	3.00	4.00	4.00	5.00	2.00
U	3.00	2.00	0.00	0.00	0.00	0.00
Sc	33.00	30.00	43.00	26.00	39.00	42.00
V	222.00	236.00	295.00	235.00	298.00	208.00
Cr	150.00	107.00	137.00	197.00	44.00	317.00
Co	51.00	52.00	49.00	38.00	48.00	51.00
Ni	139.00	76.00	110.00	75.00	75.00	27.00
Cu	92.00	66.00	56.00	67.00	71.00	70.00
Zn	98.00	88.00	115.00	103.00	119.00	102.00
Ga	19.00	19.00	20.00	20.00	21.00	20.00
Mo	0.00		0.00	0.00	0.00	0.00
As	2.00		0.00	2.00	1.00	3.00
S	87.00		156.00	81.00	71.00	165.00
INAA						
La	16.40	27.30	14.30	21.60		10.40
Ce	34.70	57.70	27.70	39.10		23.50
Nd	20.10	27.20	16.90	22.00		14.90
Sm	4.22	6.20	4.20	5.05		3.40
Eu	1.57	2.07	1.38	1.73		1.24
Tb	0.78	0.93	0.90	0.91		0.72
Yb	2.85	2.50	3.48	3.07		2.64
Lu	0.43	0.37	0.52	0.51		0.43
Th	1.76	2.29	1.63	1.83		0.89
U	0.50	0.60		0.50		
Ta	1.19	1.56	0.77	1.15		0.37
Hf	3.30	3.44	3.31	4.10		2.47
Isotopes						
$^{87}Sr/^{86}Sr_i$	0.7061	0.7046	0.7085	0.7074		
$^{143}Nd/^{144}Nd_i$		0.5124	0.5122	0.5122		0.5120
delta O_{18}		7.20				

Name	*TYT*	*TYT*	*TYT*	*TYT*	*TYT*	*TYT*
Sample #	**93L95**	**502-875**	**93L96**	**93L94**	**502-992**	**502-936**
SiO_2	50.84	50.92	51.44	52.01	52.31	52.33
TiO_2	1.23	1.09	1.23	1.25	1.18	1.20
Al_2O_3	17.15	15.90	16.77	14.64	15.52	14.35
Fe_2O_3	10.97	11.19	10.89	11.53	11.38	11.51
MnO	0.17	0.21	0.17	0.18	0.21	0.36
MgO	5.76	6.51	5.60	6.11	6.65	6.86
CaO	11.13	8.89	10.58	9.91	7.29	7.61
Na_2O	2.20	3.84	2.29	2.43	4.00	3.86
K_2O	0.41	1.35	0.90	1.80	1.30	1.81
P_2O_5	0.15	0.12	0.14	0.14	0.16	0.13
LOI	3.82	2.67	1.46	1.35	2.60	2.15
Total	100.21	99.93	100.22	100.58	100.14	100.02
XRF						
Rb	9.80	78.30	22.10	40.80	50.50	70.10
Sr	576.70	160.80	247.70	283.90	298.70	256.80
Y	31.20	29.00	32.40	28.80	31.50	32.30
Zr	132.00	132.00	138.00	115.00	156.00	137.00
Nb	7.40	7.40	7.10	5.80	7.50	7.90
Ba	271.00	197.00	257.00	338.00	437.00	608.00
Pb	5.00	8.00	5.00	5.00	3.00	8.00
Th	4.00	4.00	3.00	4.00	4.00	4.00
U	2.00	1.00	2.00	1.00	1.00	0.00
Sc	40.00	40.00	35.00	46.00	41.00	45.00
V	248.00	263.00	257.00	299.00	264.00	295.00
Cr	185.00	167.00	180.00	280.00	172.00	298.00
Co	43.00	50.00	42.00	43.00	51.00	53.00
Ni	73.00	92.00	72.00	59.00	62.00	89.00
Cu	87.00	126.00	88.00	104.00	37.00	158.00
Zn	86.00	84.00	85.00	106.00	98.00	93.00
Ga	19.00	15.00	20.00	18.00	16.00	16.00
Mo	0.00		0.00	0.00		
As	1.00		1.00	0.00		
S	130.00		88.00	85.00		
INAA						
La	15.30		15.40	13.30		17.20
Ce	32.80		34.50	27.90		34.80
Nd	17.90		18.80	16.90		17.60
Sm	4.34		4.45	3.89		4.61
Eu	1.33		1.35	1.36		1.16
Tb	0.88		0.91	0.74		0.88
Yb	3.10		3.21	2.78		2.85
Lu	0.47		0.47	0.42		0.44
Th	3.34		3.50	2.03		5.11
U	0.50		0.70			0.65
Ta	0.41		0.44	0.27		0.40
Hf	3.53		3.59	2.99		3.35
Isotopes						
$^{87}Sr/^{86}Sr_i$	0.7102		0.7106	0.7089		0.7156
$^{143}Nd/^{144}Nd_i$	0.5120		0.5121			0.5121
delta O_{18}						

Name	*TYT*	*TYT*	*TYT*	*TYT*	*TYT*	*TYT*
Sample #	**93L93**	**93L97**	**502-732**	**502-1008**	**93L124**	**502-703**
SiO_2	53.17	53.24	53.49	53.52	53.93	54.05
TiO_2	1.22	1.35	0.93	1.17	1.32	0.87
Al_2O_3	14.92	15.80	17.99	15.61	15.48	17.84
Fe_2O_3	11.25	11.04	8.91	10.91	11.28	8.26
MnO	0.17	0.17	0.15	0.14	0.17	0.14
MgO	6.52	5.24	4.76	5.92	4.45	4.47
CaO	10.25	10.06	10.85	9.38	9.14	7.73
Na_2O	1.83	2.19	1.99	2.42	2.46	5.20
K_2O	0.51	0.74	0.82	0.78	1.62	1.34
P_2O_5	0.15	0.17	0.11	0.16	0.16	0.10
LOI	1.76	0.65	0.92	1.08	0.41	2.62
Total	100.95	100.10	100.35	100.15	99.32	100.67
XRF						
Rb	10.00	53.20	25.30	15.80	55.30	53.50
Sr	285.70	199.20	160.20	190.40	201.50	202.50
Y	31.80	37.90	29.00	31.20	33.60	25.70
Zr	159.00	177.00	126.00	162.00	158.00	115.00
Nb	7.40	10.10	7.90	8.40	8.20	7.70
Ba	330.00	317.00	227.00	276.00	381.00	260.00
Pb	6.00	6.00	10.00	8.00	7.00	5.00
Th	5.00	6.00	5.00	3.00	7.00	4.00
U	0.00	3.00	1.00	0.00	0.00	1.00
Sc	43.00	38.00	29.00	41.00	36.00	31.00
V	266.00	263.00	202.00	264.00	270.00	174.00
Cr	193.00	123.00	118.00	251.00	56.00	99.00
Co	43.00	44.00	37.00	49.00	41.00	33.00
Ni	73.00	52.00	41.00	64.00	46.00	36.00
Cu	47.00	65.00	40.00	71.00	98.00	40.00
Zn	96.00	93.00	71.00	93.00	90.00	66.00
Ga	20.00	20.00	19.00	18.00	20.00	15.00
Mo	0.00	0.00			1.00	
As	2.00	1.00			0.00	
S	114.00	207.00			61.00	
INAA						
La	19.40			19.60		
Ce	38.10			38.40		
Nd	21.10			19.60		
Sm	4.56			4.56		
Eu	1.40			1.27		
Tb	0.84			0.78		
Yb	2.99			2.65		
Lu	0.46			0.43		
Th	3.31			3.66		
U				0.73		
Ta	0.39			0.31		
Hf	3.92			3.72		
Isotopes						
$^{87}Sr/^{86}Sr_i$	0.7116	0.7134		0.7117		
$^{143}Nd/^{144}Nd_i$	0.5120	0.5120		0.5124		
delta O_{18}						

Name	*TYT*	*TYT*	*TYT*	*TYT*	*TYT*	*TYT*
Sample #	**93L103**	**92-U17**	**502-334**	**502-657**	**502-506**	**93L42**
SiO_2	54.08	54.22	54.23	55.04	55.16	55.65
TiO_2	1.42	1.25	1.41	1.06	1.29	1.26
Al_2O_3	15.27	15.68	15.65	17.39	16.65	15.42
Fe_2O_3	11.66	10.74	12.20	9.00	10.02	10.77
MnO	0.16	0.15	0.17	0.13	0.17	0.15
MgO	4.87	4.82	4.08	3.47	3.66	4.12
CaO	7.81	10.18	8.08	9.16	9.18	9.27
Na_2O	2.54	1.71	2.79	2.24	2.79	2.08
K_2O	1.93	1.10	1.22	2.36	0.91	1.10
P_2O_5	0.25	0.15	0.18	0.14	0.17	0.18
LOI	1.16	1.37	3.20	0.58	2.67	2.26
Total	100.21	99.94	98.87	100.21	100.08	99.56
XRF						
Rb	65.80	26.60	63.10	88.70	84.60	38.30
Sr	254.10	237.70	152.50	170.00	195.40	412.00
Y	48.70	35.50	44.20	32.00	37.10	39.00
Zr	247.00	146.00	187.00	166.00	194.00	191.00
Nb	18.40	9.70	11.50	10.10	11.00	8.90
Ba	557.00	409.00	319.00	293.00	293.00	519.00
Pb	8.00	7.00	13.00	11.00	15.00	13.00
Th	10.00	5.00	8.00	6.00	8.00	9.00
U	1.00	0.00	2.00	2.00	1.00	0.00
Sc	34.00	40.00	43.00	33.00	36.00	32.00
V	224.00	272.00	269.00	200.00	239.00	247.00
Cr	45.00	134.00	38.00	56.00	48.00	40.00
Co	40.00	43.00	51.00	35.00	40.00	36.00
Ni	64.00	57.00	31.00	22.00	28.00	31.00
Cu	53.00	66.00	57.00	39.00	52.00	69.00
Zn	109.00	83.00	116.00	87.00	91.00	89.00
Ga	18.00	18.00	25.00	19.00	19.00	20.00
Mo	0.00					0.00
As	0.00					0.00
S	58.00					68.00
INAA						
La				22.00		
Ce				45.50		
Nd				22.10		
Sm				5.14		
Eu				1.26		
Tb				0.87		
Yb				2.92		
Lu				0.45		
Th				6.91		
U				1.17		
Ta				0.47		
Hf				3.99		
Isotopes						
$^{87}Sr/^{86}Sr_i$				0.7156		
$^{143}Nd/^{144}Nd_i$				0.5121		
delta O_{18}						

Name	*TYT*	*TYT*	*TYT*	*TYT*	*TYT*	*TYT*
Sample #	**93L43**	**502-306**	**93L98**	**502-372**	**502-269**	**502-403**
SiO_2	56.02	58.31	58.46	58.53	58.71	59.07
TiO_2	1.29	1.49	1.16	1.11	1.37	1.18
Al_2O_3	15.50	13.90	15.04	15.66	14.34	15.27
Fe_2O_3	10.49	11.46	9.69	8.84	10.94	9.16
MnO	0.14	0.19	0.11	0.14	0.15	0.14
MgO	3.84	3.16	3.12	3.18	2.85	2.82
CaO	8.05	7.92	8.87	7.38	7.72	7.10
Na_2O	2.18	2.56	1.76	2.51	3.01	2.52
K_2O	2.33	0.81	1.64	2.50	0.73	2.58
P_2O_5	0.17	0.20	0.14	0.16	0.18	0.16
LOI	2.62	1.92	1.34	0.39	0.08	0.35
Total	100.05	100.62	99.96	100.35	98.96	99.83
XRF						
Rb	63.30	87.70	41.70	107.50	101.20	112.20
Sr	1084.00	144.30	217.40	138.90	146.70	140.50
Y	34.90	43.30	32.00	35.60	40.40	38.30
Zr	183.00	207.00	133.00	174.00	201.00	190.00
Nb	8.60	12.90	8.30	11.10	12.10	12.00
Ba	520.00	361.00	721.00	341.00	356.00	362.00
Pb	11.00	17.00	6.00	13.00	15.00	16.00
Th	8.00	8.00	5.00	8.00	9.00	9.00
U	1.00	2.00	1.00	2.00	2.00	3.00
Sc	36.00	37.00	37.00	34.00	33.00	34.00
V	231.00	264.00	233.00	210.00	231.00	203.00
Cr	32.00	37.00	121.00	48.00	27.00	45.00
Co	39.00	46.00	33.00	33.00	43.00	34.00
Ni	33.00	26.00	45.00	24.00	22.00	25.00
Cu	108.00	77.00	62.00	40.00	60.00	45.00
Zn	90.00	102.00	79.00	84.00	91.00	85.00
Ga	21.00	20.00	15.00	20.00	18.00	20.00
Mo	0.00		0.00			
As	6.00		3.00			
S	102.00		91.00			
INAA						
La		27.30	20.40			27.20
Ce		56.90	32.20			56.70
Nd		28.20	23.40			26.50
Sm		6.71	4.99			6.20
Eu		1.49	1.40			1.37
Tb		1.12	0.93			1.01
Yb		3.76	2.96			3.40
Lu		0.60	0.43			0.52
Th		8.42	3.55			8.44
U		2.34	0.50			1.73
Ta		0.73	0.47			0.68
Hf		5.02	3.55			4.68
Isotopes						
$^{87}Sr/^{86}Sr_i$		0.7192	0.7115			0.7201
$^{143}Nd/^{144}Nd_i$		0.5120	0.5120			0.5123
delta O_{18}						

Name	*TYT*	*Syenite*	*Syenite*	*Syenite*	*Lascano*	*Lascano*
Sample #	**93L125**	**93L62**	**93L59**	**93L67**	**93L78**	**93L66**
SiO_2	60.39	59.80	61.15	65.60	61.19	62.49
TiO_2	1.88	1.46	1.33	1.00	1.52	1.29
Al_2O_3	12.66	14.87	15.20	14.34	14.77	14.32
Fe_2O_3	12.14	8.93	7.94	6.49	9.35	8.47
MnO	0.18	0.17	0.15	0.13	0.15	0.16
MgO	2.02	1.77	1.41	1.06	0.78	1.34
CaO	6.07	4.04	3.47	2.22	3.26	3.07
Na_2O	2.53	4.42	4.31	3.81	3.87	3.77
K_2O	1.93	3.96	4.56	4.99	4.48	4.58
P_2O_5	0.21	0.58	0.49	0.36	0.64	0.51
LOI	1.82	0.27	0.33	1.44	1.10	2.12
Total	100.57	100.63	99.82	99.95	99.85	100.08
XRF						
Rb	107.10	101.40	126.90	160.90	122.40	143.30
Sr	204.70	339.40	295.80	279.90	313.30	206.20
Y	49.20	70.40	67.70	63.80	112.10	58.00
Zr	227.00	649.00	560.00	427.00	491.00	459.00
Nb	16.20	78.30	82.70	55.10	53.20	56.70
Ba	509.00	1312.00	1239.00	1363.00	2776.00	1198.00
Pb	13.00	12.00	18.00	19.00	14.00	16.00
Th	11.00	10.00	11.00	18.00	12.00	13.00
U	1.00	4.00	2.00	0.00	1.00	1.00
Sc	29.00	15.00	16.00	14.00	23.00	18.00
V	288.00	83.00	50.00	30.00	30.00	37.00
Cr	7.00	9.00	9.00	10.00	6.00	7.00
Co	30.00	15.00	13.00	9.00	9.00	12.00
Ni	7.00	6.00	5.00	5.00	7.00	3.00
Cu	94.00	16.00	19.00	13.00	9.00	11.00
Zn	107.00	113.00	115.00	99.00	129.00	119.00
Ga	19.00	24.00	23.00	21.00	22.00	22.00
Mo	0.00	4.00	3.00	1.00	2.00	1.00
As	3.00	4.00	3.00	1.00	3.00	0.00
S	71.00	145.00	55.00	50.00	300.00	107.00
INAA						
La	30.70	79.30	81.10	74.00	142.00	69.10
Ce	65.00	155.00	159.00	150.00	211.00	138.00
Nd	33.30	68.90	65.90	61.50	115.00	61.90
Sm	7.73	12.90	12.50	11.70	20.50	11.60
Eu	1.87	3.29	2.90	2.31	5.44	2.86
Tb	1.38	1.98	1.78	1.65	3.01	1.71
Yb	4.65	7.15	7.06	6.27	8.84	5.91
Lu	0.69	1.09	1.05	0.89	1.38	0.89
Th	9.84	8.68	11.00	14.68	9.65	11.60
U	1.70	2.80	2.20	2.20	1.70	2.30
Ta	1.16	5.06	5.24	3.74	3.51	3.77
Hf	5.96	15.80	13.50	10.69	10.90	10.70
Isotopes						
$^{87}Sr/^{86}Sr_i$	0.7169	0.7067	0.7065		0.7089	0.7085
$^{143}Nd/^{144}Nd_i$	0.5120	0.5118	0.5118		0.5119	0.5118
delta O_{18}						

Name	*Lascano*	*Lascano*	*Lascano*	*Lascano*	*Lascano*	*Lascano*
Sample #	**93L65**	**93L50**	**93L64**	**93L74**	**93L115**	**93L111**
SiO_2	62.69	63.77	66.50	69.73	69.78	70.76
TiO_2	1.24	1.20	1.15	1.15	0.64	0.69
Al_2O_3	14.39	14.62	13.22	12.17	12.45	13.11
Fe_2O_3	8.05	8.05	7.54	7.12	6.44	5.58
MnO	0.16	0.14	0.13	0.07	0.18	0.05
MgO	1.18	0.94	1.07	0.45	0.38	0.28
CaO	3.10	3.47	2.30	1.87	2.24	1.71
Na_2O	4.14	3.00	4.30	2.77	2.71	2.41
K_2O	4.58	4.40	3.39	4.24	5.06	5.19
P_2O_5	0.46	0.40	0.39	0.43	0.12	0.21
LOI	2.18	1.26	2.22	1.83	2.06	1.11
Total	99.70	100.25	100.08	100.18	99.31	100.24
XRF						
Rb	136.20	98.60	94.80	120.10	175.50	188.50
Sr	343.50	247.20	168.10	211.90	133.90	128.00
Y	58.60	68.00	51.50	123.70	104.70	66.50
Zr	475.00	883.00	373.00	398.00	367.00	393.00
Nb	56.10	33.20	43.20	51.30	28.70	23.30
Ba	1623.00	2169.00	1172.00	2809.00	1192.00	1567.00
Pb	13.00	19.00	15.00	12.00	23.00	26.00
Th	13.00	7.00	10.00	12.00	17.00	21.00
U	2.00	1.00	1.00	1.00	3.00	2.00
Sc	20.00	19.00	18.00	15.00	14.00	10.00
V	32.00	118.00	40.00	41.00	9.00	51.00
Cr	8.00	10.00	7.00	7.00	9.00	9.00
Co	9.00	13.00	8.00	9.00	7.00	4.00
Ni	5.00	9.00	3.00	8.00	14.00	6.00
Cu	14.00	21.00	12.00	10.00	9.00	9.00
Zn	112.00	131.00	102.00	76.00	128.00	70.00
Ga	19.00	20.00	17.00	17.00	18.00	17.00
Mo	1.00	3.00	1.00	1.00	1.00	1.00
As	5.00	0.00	0.00	2.00	6.00	6.00
S	81.00	64.00	52.00	382.00	99.00	163.00
INAA						
La	70.00		57.40	232.00	85.90	71.30
Ce	142.00		120.00	325.00	138.00	132.00
Nd	62.90		52.20	201.00	73.90	65.60
Sm	11.80		9.81	35.70	15.10	13.30
Eu	2.87		2.66	7.08	3.45	2.60
Tb	1.72		1.41	4.48	2.65	1.95
Yb	5.93		4.88	9.58	8.21	5.51
Lu	0.91		0.72	1.36	1.19	0.80
Th	12.10		9.00	9.98	15.03	17.08
U	2.00		1.70	2.30	3.70	1.89
Ta	3.81		2.71	3.44	2.06	1.47
Hf	11.00		8.36	9.67	9.30	9.41
Isotopes						
$^{87}Sr/^{86}Sr_i$	0.7085		0.7088		0.71628	
$^{143}Nd/^{144}Nd_i$	0.5119				0.51216	
delta O_{18}						

Name	*Lascano*	*Lascano*	*Lascano*	*Lascano*	*Lascano*	*Lascano*
Sample #	**93L114**	**93L119**	**92-U15**	**92-U16**	**93L116**	**93L127**
SiO_2	70.76	71.01	71.27	71.33	71.49	71.62
TiO_2	0.67	0.68	0.66	0.63	0.67	0.60
Al_2O_3	12.90	13.11	12.77	12.63	12.80	12.27
Fe_2O_3	6.53	5.23	6.22	6.15	5.16	5.65
MnO	0.07	0.05	0.16	0.10	0.04	0.12
MgO	0.21	0.23	0.20	0.20	0.26	0.66
CaO	1.04	0.62	1.15	1.31	1.70	1.92
Na_2O	3.09	2.74	2.79	2.91	2.48	2.69
K_2O	4.57	6.15	4.65	4.62	5.20	4.36
P_2O_5	0.13	0.18	0.12	0.13	0.18	0.11
LOI	1.76	1.52	1.39	1.03	1.42	1.13
Total	99.72	100.02	99.64	100.26	100.07	99.67
XRF						
Rb	173.80	216.90	167.50	168.30	178.50	171.80
Sr	134.00	95.80	134.10	123.30	116.80	125.10
Y	120.70	64.60	99.10	97.60	62.70	56.50
Zr	372.00	380.00	365.00	362.00	394.00	354.00
Nb	28.70	22.40	28.00	27.90	23.00	27.60
Ba	1499.00	1308.00	1285.00	889.00	998.00	754.00
Pb	21.00	25.00	24.00	23.00	23.00	19.00
Th	17.00	21.00	14.00	16.00	20.00	18.00
U	3.00	4.00	1.00	3.00	1.00	4.00
Sc	18.00	13.00	15.00	16.00	15.00	13.00
V	14.00	46.00	32.00	29.00	38.00	17.00
Cr	4.00	10.00	12.00	9.00	8.00	7.00
Co	6.00	9.00	19.00	14.00	5.00	1.00
Ni	4.00	13.00	8.00	7.00	6.00	5.00
Cu	11.00	15.00	13.00	12.00	16.00	14.00
Zn	104.00	101.00	94.00	91.00	84.00	81.00
Ga	18.00	16.00	19.00	19.00	17.00	18.00
Mo	1.00	1.00			1.00	1.00
As	7.00	6.00			8.00	4.00
S	161.00	164.00			58.00	60.00
INAA						
La	84.2			55.50	56.9	47.65
Ce	137			114.00	119	102.40
Nd	81.1			58.80	54.0	46.40
Sm	16.5			13.00	10.9	9.55
Eu	3.58			2.94	1.96	1.99
Tb	2.83			2.28	1.67	1.52
Yb	9.11			6.69	5.79	5.48
Lu	1.35			0.95	0.84	0.80
Th	15.4			15.00	17.5	14.90
U	2.5			2.16	2.4	3.10
Ta	2.09			2.07	1.51	1.91
Hf	9.54			9.10	9.67	8.53
Isotopes						
$^{87}Sr/^{86}Sr_i$	0.71589			0.71769	0.72481	
$^{143}Nd/^{144}Nd_i$	0.51211			0.51223	0.51195	
delta O_{18}						

Name	*Lascano*	*Lascano*	*Lascano*	*Lascano*	*Lascano*	*Lascano*
Sample #	**93L88**	**93L128**	**93L113**	**93L102**	**93L107**	**93L110**
SiO_2	72.36	72.57	72.74	72.90	72.83	73.29
TiO_2	0.59	0.58	0.60	0.57	0.50	0.48
Al_2O_3	13.30	12.46	12.13	11.59	12.95	12.41
Fe_2O_3	4.25	5.70	5.55	5.35	4.56	4.82
MnO	0.04	0.07	0.07	0.07	0.08	0.12
MgO	0.58	0.36	0.10	0.39	0.79	0.19
CaO	0.36	1.09	1.44	1.30	1.11	0.81
Na_2O	3.75	1.97	2.84	1.87	1.78	2.14
K_2O	4.61	5.09	4.41	5.84	5.27	5.60
P_2O_5	0.17	0.12	0.12	0.12	0.14	0.13
LOI	1.41	2.07	0.81	1.43	2.72	1.19
Total	100.10	100.35	100.15	99.75	99.35	100.07
XRF						
Rb	179.90	184.50	166.50	147.70	192.00	195.70
Sr	78.60	121.60	132.00	94.10	114.60	99.60
Y	83.10	64.60	60.80	53.00	52.00	66.30
Zr	625.00	469.00	359.00	333.00	421.00	431.00
Nb	109.50	27.00	28.40	24.90	23.70	23.80
Ba	812.00	1218.00	806.00	827.00	1250.00	1300.00
Pb	4.00	25.00	23.00	20.00	25.00	27.00
Th	28.00	21.00	16.00	16.00	20.00	19.00
U	4.00	2.00	0.00	3.00	2.00	1.00
Sc	4.00	14.00	14.00	13.00	13.00	8.00
V	70.00	39.00	28.00	13.00	12.00	37.00
Cr	8.00	7.00	9.00	10.00	10.00	9.00
Co	7.00	3.00	2.00	2.00	3.00	8.00
Ni	14.00	6.00	4.00	3.00	5.00	6.00
Cu	11.00	11.00	11.00	14.00	11.00	9.00
Zn	109.00	103.00	91.00	87.00	82.00	50.00
Ga	25.00	19.00	19.00	17.00	17.00	15.00
Mo	1.00	1.00	2.00	0.00	1.00	1.00
As	0.00	8.00	5.00	1.00	5.00	9.00
S	111.00	68.00	39.00	60.00	69.00	70.00
INAA						
La		64.9	47.4			
Ce		148	94.0			
Nd		65.3	45.5			
Sm		12.7	9.51			
Eu		2.30	2.28			
Tb		1.88	1.60			
Yb		6.28	5.86			
Lu		0.92	0.87			
Th		19.0	15.4			
U		1.9	1.9			
Ta		1.67	1.98			
Hf		11.7	9.06			
Isotopes						
$^{87}Sr/^{86}Sr_i$		0.71898				
$^{143}Nd/^{144}Nd_i$		0.51189				
delta O_{18}						

Name	*Lascano*	*Lascano*	*Lascano*	*Lascano*	*Lascano*	*Lascano*
Sample #	**93L109**	**93L122**	**93L121**	**93L112**	**93L99**	**92-U14**
SiO_2	73.48	74.60	74.93	75.57	76.30	76.54
TiO_2	0.43	0.45	0.48	0.32	0.33	0.31
Al_2O_3	12.50	11.69	11.78	12.02	11.63	11.58
Fe_2O_3	4.42	4.18	4.59	2.98	3.10	2.72
MnO	0.05	0.06	0.05	0.04	0.02	0.02
MgO	0.18	0.36	0.31	0.21	0.11	0.08
CaO	0.84	0.33	0.38	0.44	0.27	0.50
Na_2O	2.12	0.92	2.02	1.79	1.66	1.63
K_2O	5.85	7.27	5.33	6.57	6.51	6.56
P_2O_5	0.12	0.15	0.13	0.06	0.06	0.06
LOI	1.28	1.67	2.00	1.30	1.59	0.92
Total	100.31	99.49	99.95	100.33	100.54	99.50
XRF						
Rb	199.70	250.80	193.00	221.60	212.10	208.60
Sr	117.90	421.00	132.20	73.60	60.90	71.50
Y	63.20	76.00	61.10	56.20	54.90	62.40
Zr	389.00	349.00	417.00	303.00	327.00	304.00
Nb	22.80	20.60	22.40	20.30	20.00	21.30
Ba	1527.00	2004.00	1306.00	1536.00	1226.00	1270.00
Pb	28.00	24.00	24.00	29.00	27.00	31.00
Th	23.00	17.00	19.00	20.00	22.00	21.00
U	2.00	1.00	3.00	1.00	2.00	2.00
Sc	9.00	7.00	9.00	7.00	6.00	8.00
V	23.00	25.00	14.00	9.00	17.00	13.00
Cr	10.00	8.00	8.00	5.00	6.00	8.00
Co	5.00	4.00	1.00	2.00	3.00	5.00
Ni	6.00	5.00	5.00	6.00	4.00	7.00
Cu	8.00	8.00	10.00	7.00	7.00	7.00
Zn	75.00	51.00	93.00	62.00	52.00	57.00
Ga	16.00	13.00	15.00	15.00	15.00	15.00
Mo	1.00	1.00	1.00	0.00	0.00	
As	9.00	10.00	5.00	6.00	2.00	
S	100.00	249.00	227.00	87.00	49.00	
INAA						
La	71.7	61.3		67.7	66.20	65.70
Ce	154	131		139	132.00	138.00
Nd	68.8	65.4		61.0	57.60	60.60
Sm	12.9	13.6		11.7	10.90	11.60
Eu	2.30	2.57		1.71	1.64	1.60
Tb	1.89	2.08		1.72	1.54	1.65
Yb	5.79	6.92		5.60	5.38	5.77
Lu	0.83	1.03		0.80	0.79	0.82
Th	19.2	16.6		19.9	20.12	20.50
U	1.9	1.9		1.4	2.12	3.48
Ta	1.55	1.33		1.50	1.48	1.57
Hf	10.3	9.55		9.16	8.78	8.15
Isotopes						
$^{87}Sr/^{86}Sr_i$	0.72039	0.75454			0.72241	0.72262
$^{143}Nd/^{144}Nd_i$	0.51191	0.51199			0.51190	0.51197
delta O_{18}						10.80

Name	*Lascano*	*Lascano*	*Lascano*	*Lascano*	*Aigüa*	*Aigüa*
Sample #	**93L118**	**93L101**	**93L120B**	**93L126**	**93L86**	**93L83**
SiO_2	77.80	78.29	78.81	78.88	61.74	63.30
TiO_2	0.17	0.47	0.28	0.33	0.43	0.58
Al_2O_3	11.14	9.43	9.76	9.80	17.10	15.97
Fe_2O_3	1.76	3.72	2.68	3.10	7.15	6.61
MnO	0.03	0.05	0.03	0.06	0.21	0.11
MgO	0.03	0.21	0.03	0.29	0.29	0.48
CaO	0.34	0.12	0.07	0.22	0.74	1.58
Na_2O	1.61	0.39	0.04	0.70	5.79	5.42
K_2O	7.08	7.26	8.25	6.56	6.45	5.80
P_2O_5	0.03	0.06	0.06	0.05	0.10	0.14
LOI	0.78	1.26	0.72	1.75	1.06	1.11
Total	100.59	100.32	100.51	100.13	99.54	100.27
XRF						
Rb	253.30	179.00	160.20	163.60	188.10	143.70
Sr	32.60	86.80	47.50	35.40	15.50	39.10
Y	56.70	28.00	40.20	42.00	94.90	82.90
Zr	237.00	191.00	246.00	285.00	1008.00	954.00
Nb	20.60	12.70	13.50	17.00	191.30	114.10
Ba	387.00	588.00	505.00	776.00	162.00	327.00
Pb	28.00	25.00	12.00	23.00	17.00	12.00
Th	31.00	10.00	10.00	16.00	22.00	25.00
U	1.00	2.00	1.00	1.00	1.00	4.00
Sc	6.00	6.00	4.00	9.00	12.00	10.00
V	14.00	28.00	24.00	40.00	15.00	4.00
Cr	5.00	23.00	12.00	6.00	5.00	6.00
Co	2.00	2.00	3.00	2.00	2.00	2.00
Ni	3.00	11.00	4.00	4.00	4.00	5.00
Cu	9.00	9.00	5.00	7.00	9.00	8.00
Zn	41.00	51.00	27.00	62.00	162.00	154.00
Ga	16.00	11.00	11.00	10.00	32.00	31.00
Mo	0.00	0.00	0.00	1.00	8.00	12.00
As	11.00	6.00	6.00	4.00	4.00	0.00
S	38.00	51.00	34.00	67.00	43.00	54.00
INAA						
La	76.5	36.8		44.50	133.00	
Ce	163	61.8		91.90	245.00	
Nd	68.7	27.5		40.40	98.80	
Sm	12.6	5.03		7.90	17.20	
Eu	0.93	1.04		1.34	2.01	
Tb	1.77	0.77		1.17	2.59	
Yb	5.84	2.64		3.89	10.90	
Lu	0.81	0.41		0.57	1.59	
Th	26.7	8.08		13.55	17.50	
U	2.2	1.6		1.60	1.30	
Ta	1.67	0.92		1.17	11.40	
Hf	7.31	4.88		6.75	20.40	
Isotopes						
$^{87}Sr/^{86}Sr_i$				0.71650		
$^{143}Nd/^{144}Nd_i$				0.51196	0.5121	
delta O_{18}						

Name	*Aigüa*	*Aigüa*	*Aigüa*	*Aigüa*	*Aigüa*	*Aigüa*
Sample #	**93L71**	**93L85**	**93L18**	**93L70**	**93L48**	**93L81**
SiO_2	63.58	63.65	64.76	64.60	67.37	67.06
TiO_2	0.67	0.62	0.70	0.59	0.55	0.69
Al_2O_3	15.86	15.01	15.61	16.62	14.51	14.93
Fe_2O_3	6.29	9.02	5.70	5.90	6.46	6.02
MnO	0.15	0.16	0.13	0.10	0.08	0.07
MgO	0.55	0.25	0.63	0.26	0.32	0.51
CaO	2.35	0.80	2.16	0.44	1.54	1.70
Na_2O	4.87	4.60	3.93	5.42	3.04	3.05
K_2O	5.53	5.63	6.25	5.94	6.00	5.78
P_2O_5	0.16	0.24	0.13	0.12	0.14	0.19
LOI	2.38	1.59	6.41	1.48	1.39	1.91
Total	100.20	99.78	102.78	100.49	99.58	100.32
XRF						
Rb	148.50	185.40	163.80	130.20	144.50	123.50
Sr	144.80	100.80	263.70	29.80	196.60	242.80
Y	95.60	88.90	86.50	47.10	94.00	56.90
Zr	1168.00	1046.00	955.00	536.00	1047.00	1259.00
Nb	128.30	123.50	135.80	92.50	39.70	33.80
Ba	946.00	2237.00	935.00	387.00	2291.00	2867.00
Pb	26.00	19.00	26.00	13.00	23.00	22.00
Th	17.00	19.00	17.00	13.00	12.00	10.00
U	4.00	3.00	2.00	2.00	1.00	1.00
Sc	6.00	22.00	9.00	7.00	11.00	15.00
V	21.00	10.00	6.00	11.00	10.00	18.00
Cr	7.00	7.00	6.00	6.00	7.00	5.00
Co	6.00	3.00	2.00	3.00	3.00	3.00
Ni	5.00	5.00	3.00	3.00	5.00	4.00
Cu	10.00	13.00	6.00	11.00	11.00	12.00
Zn	149.00	147.00	142.00	90.00	120.00	118.00
Ga	27.00	27.00	27.00	27.00	20.00	20.00
Mo	4.00	7.00	7.00	4.00	3.00	3.00
As	0.00	1.00	3.00	4.00	2.00	2.00
S	49.00	520.00	68.00	129.00	58.00	63.00
INAA						
La		164.00	110.00	77.50	91.80	
Ce		236.00	214.00	127.00	170.00	
Nd		117.00	86.50	54.10	88.80	
Sm		19.80	15.23	9.06	16.50	
Eu		2.92	2.21	1.12	4.46	
Tb		2.63	2.29	1.31	2.34	
Yb		9.00	9.27	5.58	8.11	
Lu		1.28	1.34	0.81	1.25	
Th		16.50	14.09	11.70	10.90	
U		3.50	3.13	1.80	1.60	
Ta		7.28	7.80	5.72	2.14	
Hf		21.50	19.65	11.40	22.60	
Isotopes						
$^{87}Sr/^{86}Sr_i$		0.7076	0.7114	0.7054	0.70845	
$^{143}Nd/^{144}Nd_i$		0.5117	0.5118	0.5119	0.51181	
delta O_{18}						

Name	*Aigüa*	*Aigüa*	*Aigüa*	*Aigüa*	*Aigüa*	*Aigüa*
Sample #	**93L16**	**93L37**	**93L129**	**93L51**	**93L46**	**93L76**
SiO_2	69.82	70.82	72.46	72.88	73.00	73.74
TiO_2	0.51	0.18	0.69	0.33	0.30	0.48
Al_2O_3	14.10	13.24	12.03	12.88	13.05	12.66
Fe_2O_3	5.47	4.18	5.25	4.00	4.10	3.41
MnO	0.03	0.07	0.20	0.06	0.07	0.05
MgO	0.21	1.31	0.61	0.15	0.14	0.20
CaO	0.91	0.22	1.46	0.56	0.65	0.73
Na_2O	3.46	4.61	3.36	2.93	2.74	2.97
K_2O	5.40	5.34	3.76	6.17	5.88	5.65
P_2O_5	0.09	0.02	0.18	0.04	0.05	0.10
LOI	0.98	1.75	1.34	1.31	1.37	1.17
Total	99.85	100.02	99.76	100.62	100.12	99.92
XRF						
Rb	118.00	303.80	154.40	174.80	173.80	209.00
Sr	159.20	23.20	117.50	55.00	59.10	112.70
Y	77.60	162.30	109.00	77.60	57.80	53.40
Zr	749.00	1546.00	321.00	713.00	620.00	492.00
Nb	32.40	314.70	19.80	47.90	50.70	54.20
Ba	1788.00	84.00	885.00	748.00	705.00	805.00
Pb	20.00	44.00	17.00	30.00	34.00	22.00
Th	13.00	53.00	13.00	14.00	15.00	21.00
U	3.00	9.00	3.00	1.00	2.00	2.00
Sc	8.00	0.00	14.00	2.00	5.00	5.00
V	7.00	5.00	18.00	7.00	4.00	22.00
Cr	6.00	4.00	7.00	3.00	4.00	6.00
Co	3.00	2.00	5.00	1.00	2.00	3.00
Ni	3.00	2.00	4.00	4.00	3.00	4.00
Cu	11.00	5.00	11.00	10.00	10.00	13.00
Zn	136.00	255.00	107.00	127.00	118.00	75.00
Ga	27.00	37.00	18.00	21.00	21.00	19.00
Mo	4.00	2.00	0.00	2.00	2.00	3.00
As	3.00	3.00	9.00	2.00	0.00	2.00
S	100.00	66.00	73.00	49.00	60.00	61.00
INAA						
La		193.00			95.20	
Ce		375.00			196.00	
Nd		133.00			86.60	
Sm		24.20			13.60	
Eu		0.74			2.35	
Tb		3.95			1.64	
Yb		17.06			6.43	
Lu		2.22			0.94	
Th		49.20			14.70	
U		10.10			1.90	
Ta		19.10			2.83	
Hf		37.70			16.30	
Isotopes						
$^{87}Sr/^{86}Sr_i$						
$^{143}Nd/^{144}Nd_i$		0.51177				
delta O_{18}				9.70		

Name	*Aigüa*	*Aigüa*	*Aigüa*	*Aigüa*	*Aigüa*	*Aigüa*
Sample #	**93L60**	**93L55**	**93L29**	**93L41**	**93L44**	**93L22**
SiO_2	73.81	74.23	74.61	75.26	75.80	77.15
TiO_2	0.46	0.37	0.08	0.19	0.28	0.19
Al_2O_3	11.05	10.44	13.24	13.30	11.50	12.09
Fe_2O_3	5.08	5.97	2.31	1.89	3.65	1.56
MnO	0.07	0.10	0.03	0.01	0.03	0.01
MgO	0.36	0.33	0.03	0.09	0.14	0.05
CaO	0.40	1.17	0.04	0.33	0.73	0.34
Na_2O	3.83	2.13	4.52	3.65	2.24	3.05
K_2O	4.82	5.26	5.12	5.24	5.57	5.52
P_2O_5	0.11	0.01	0.03	0.03	0.05	0.04
LOI	0.60	2.28	0.40	1.35	1.23	0.82
Total	99.94	99.64	100.46	100.88	100.32	100.69
XRF						
Rb	226.50	233.30	478.90	210.50	163.10	164.00
Sr	24.80	23.70	2.60	27.70	82.90	24.90
Y	176.50	237.60	104.70	41.40	67.50	31.40
Zr	1628.00	1659.00	443.00	461.00	574.00	391.00
Nb	280.40	262.10	314.50	102.30	44.80	33.20
Ba	130.00	399.00	32.00	540.00	742.00	262.00
Pb	45.00	42.00	18.00	20.00	28.00	26.00
Th	35.00	41.00	49.00	32.00	13.00	15.00
U	6.00	8.00	9.00	5.00	4.00	1.00
Sc	1.00	0.00	1.00	0.00	5.00	0.00
V	36.00	0.00	5.00	5.00	4.00	5.00
Cr	15.00	5.00	3.00	3.00	5.00	3.00
Co	4.00	2.00	3.00	1.00	1.00	0.00
Ni	6.00	9.00	2.00	4.00	3.00	2.00
Cu	14.00	9.00	3.00	7.00	10.00	5.00
Zn	183.00	303.00	95.00	57.00	130.00	62.00
Ga	31.00	33.00	43.00	27.00	17.00	25.00
Mo	4.00	3.00	2.00	6.00	1.00	2.00
As	0.00	0.00	8.00	2.00	2.00	2.00
S	46.00	72.00	34.00	152.00	62.00	41.00
INAA						
La			52.80			48.50
Ce			128.00			92.20
Nd			50.80			43.50
Sm			15.40			7.74
Eu			0.36			0.70
Tb			2.91			0.93
Yb			14.20			4.42
Lu			1.84			0.64
Th			45.60			13.70
U			8.20			1.60
Ta			18.80			2.22
Hf			20.00			11.40
Isotopes						
$^{87}Sr/^{86}Sr_i$						0.70560
$^{143}Nd/^{144}Nd_i$						0.51166
delta O_{18}						

Name	*Aigüa*	*Aigüa*	*Aigüa*	*Aigüa*	*Aigüa*	*Aigüa*
Sample #	**93L39**	**93L36**	**93L40**	**93L19**	**93L45**	**93L21**
SiO_2	76.09	76.46	76.97	77.13	77.24	77.26
TiO_2	0.09	0.10	0.08	0.19	0.26	0.18
Al_2O_3	12.40	12.36	12.16	11.90	10.79	11.16
Fe_2O_3	2.40	2.04	2.07	2.37	3.54	2.64
MnO	0.02	0.02	0.05	0.03	0.05	0.02
MgO	0.33	0.05	0.08	0.03	0.12	0.10
CaO	0.15	0.10	0.54	0.07	0.44	0.55
Na_2O	2.90	3.44	3.34	2.80	1.29	2.58
K_2O	5.61	5.41	4.70	5.45	6.24	5.24
P_2O_5	0.01	0.03	0.01	0.02	0.03	0.27
LOI	1.41	0.71	1.34	0.73	0.96	1.45
Total	100.76	100.38	99.81	100.56	100.06	100.70
XRF						
Rb	326.50	323.60	361.30	233.70	178.50	154.50
Sr	8.00	3.60	20.20	5.50	46.00	38.80
Y	53.20	135.70	180.10	84.40	55.90	62.80
Zr	310.00	333.00	361.00	538.00	524.00	382.00
Nb	161.40	166.50	236.20	82.20	41.40	32.20
Ba	26.00	28.00	31.00	18.00	618.00	329.00
Pb	21.00	17.00	20.00	40.00	22.00	25.00
Th	37.00	40.00	43.00	22.00	14.00	14.00
U	5.00	5.00	8.00	4.00	2.00	2.00
Sc	0.00	1.00	2.00	0.00	4.00	1.00
V	8.00	10.00	6.00	8.00	15.00	7.00
Cr	4.00	3.00	4.00	5.00	6.00	4.00
Co	0.00	2.00	1.00	1.00	1.00	2.00
Ni	3.00	4.00	2.00	2.00	3.00	3.00
Cu	5.00	5.00	4.00	7.00	6.00	9.00
Zn	120.00	85.00	182.00	109.00	80.00	112.00
Ga	30.00	29.00	36.00	25.00	18.00	22.00
Mo	2.00	1.00	0.00	2.00	1.00	1.00
As	2.00	6.00	1.00	7.00	2.00	4.00
S	47.00	33.00	46.00	37.00	48.00	210.00
INAA						
La	14.00	79.60			95.20	52.30
Ce	25.90	172.00			181.00	176.00
Nd	11.20	60.65			90.78	47.30
Sm	2.65	14.42			15.39	9.27
Eu	0.10	0.24			2.17	0.64
Tb	0.79	3.24			1.80	1.71
Yb	9.90	12.76			5.23	7.16
Lu	1.41	1.73			0.76	1.01
Th	35.50	37.28			11.36	14.55
U	5.60	4.26			1.58	2.07
Ta	12.10	11.10			2.10	2.04
Hf	12.30	12.02			12.66	11.30
Isotopes						
$^{87}Sr/^{86}Sr_i$						0.70715
$^{143}Nd/^{144}Nd_i$		0.51171	0.51175			0.51157
delta O_{18}						

Name	*Aigüa*	*Aigüa*	*Aigüa*	*Aigüa*	*Aigüa*	*Aigüa*
Sample #	**93L87b**	**93L80**	**93L25**	**93L73**	**93L28**	**93L26**
SiO_2	77.56	79.35	79.62	79.83	80.47	81.15
TiO_2	0.10	0.18	0.17	0.18	0.09	0.17
Al_2O_3	11.48	10.09	10.29	10.16	9.30	9.50
Fe_2O_3	2.53	2.30	2.43	2.15	1.97	2.06
MnO	0.01	0.04	0.01	0.04	0.06	0.03
MgO	0.00	0.05	0.00	0.03	0.06	0.08
CaO	0.03	0.07	0.21	0.10	0.32	0.27
Na_2O	4.23	2.28	1.46	1.77	1.24	1.44
K_2O	4.04	5.62	5.75	5.68	6.30	5.28
P_2O_5	0.02	0.02	0.05	0.06	0.20	0.02
LOI	0.83	0.62	1.22	1.05	0.98	1.06
Total	100.78	100.29	99.95	99.84	100.01	100.14
XRF						
Rb	293.60	220.40	170.90	237.70	437.00	157.50
Sr	5.50	10.60	21.00	7.30	4.80	24.60
Y	149.90	57.00	53.70	61.60	116.00	41.80
Zr	1121.00	637.00	373.00	599.00	464.00	367.00
Nb	214.20	82.60	29.60	83.30	166.00	25.80
Ba	16.00	56.00	229.00	17.00	38.00	310.00
Pb	43.00	31.00	25.00	21.00	16.00	16.00
Th	53.00	19.00	15.00	20.00	38.00	12.00
U	9.00	3.00	2.00	2.00	5.00	0.00
Sc	0.00	0.00	2.00	0.00	0.00	0.00
V	3.00	23.00	11.00	14.00	8.00	11.00
Cr	16.00	7.00	8.00	5.00	7.00	12.00
Co	2.00	1.00	2.00	1.00	1.00	2.00
Ni	3.00	2.00	2.00	4.00	2.00	1.00
Cu	3.00	7.00	7.00	8.00	5.00	6.00
Zn	103.00	121.00	27.00	125.00	132.00	66.00
Ga	33.00	19.00	17.00	21.00	18.00	19.00
Mo	0.00	1.00	1.00	1.00	0.00	1.00
As	5.00	3.00	8.00	4.00	4.00	4.00
S	45.00	32.00	51.00	46.00	37.00	64.00
INAA						
La	19.70	89.60	99.70	103.00	54.20	
Ce	75.00	126.00	222.00	202.00	114.00	
Nd	31.60	74.10	84.50	87.80	47.20	
Sm	12.20	11.71	14.20	14.10	12.40	
Eu	0.25	0.26	0.65	0.31	0.24	
Tb	3.33	1.60	1.53	1.76	2.69	
Yb	16.90	7.09	4.82	6.84	11.80	
Lu	2.19	1.00	0.68	0.96	1.56	
Th	48.10	18.01	12.50	18.32	34.70	
U	9.80	2.78	1.70	3.00	5.40	
Ta	16.20	5.22	1.75	5.21	12.40	
Hf	34.70	15.52	10.30	15.31	16.20	
Isotopes						
$^{87}Sr/^{86}Sr_i$			0.70729			
$^{143}Nd/^{144}Nd_i$		0.51177	0.51157			
delta O_{18}					9.10	

Name	*Basement*	*Basement*	*Basement*	*Basement*	*Dykes*	*Dykes*
Sample #	**93L20**	**93L58**	**93L24**	**93L120A**	**93L12**	**93L11**
SiO_2	65.00	66.51	60.46	82.67	51.32	51.38
TiO_2		0.90	0.70	0.32	1.99	2.22
Al_2O_3		13.83	11.46	8.07	15.73	15.83
Fe_2O_3		4.14	4.19	2.56	11.94	12.19
MnO		0.05	0.06	0.04	0.19	0.20
MgO		2.15	8.40	0.22	5.31	3.93
CaO		2.92	10.64	0.12	7.24	7.12
Na_2O		3.55	0.11	0.48	3.50	3.61
K_2O		5.48	3.81	5.44	2.06	2.60
P_2O_5		0.46	0.18	0.08	0.72	0.92
LOI		1.56	15.48	1.08	1.51	0.92
Total		98.95	86.57	98.66	99.56	99.61
XRF						
Rb	110.00	117.00	88.40	118.30	38.90	47.20
Sr	309.00	1219.00	59.70	98.80	745.40	736.70
Y	0.90	20.60	18.80	46.90	41.00	44.80
Zr	91.00	325.00	151.00	218.00	280.00	367.00
Nb	3.70	14.40	13.20	12.10	18.40	25.90
Ba	830.00	2925.00	352.00	519.00	1363.00	1599.00
Pb	57.00	27.00	13.00	20.00	4.00	8.00
Th	18.00	13.00	8.00	12.00	4.00	4.00
U	1.00	2.00	1.00	2.00	0.00	3.00
Sc	4.00	8.00	13.00	5.00	23.00	22.00
V	21.00	63.00	59.00	25.00	179.00	211.00
Cr	23.00	57.00	63.00	12.00	91.00	24.00
Co	5.00	13.00	9.00	3.00	41.00	35.00
Ni	19.00	34.00	22.00	7.00	61.00	22.00
Cu	31.00	15.00	11.00	12.00	32.00	25.00
Zn	25.00	81.00	55.00	34.00	121.00	130.00
Ga	15.00	19.00	12.00	11.00	20.00	21.00
Mo	0.00	0.00	0.00	0.00	1.00	1.00
As	2.00	2.00	3.00	8.00	1.00	4.00
S	26.00	37.00	30.00	41.00	615.00	276.00
INAA						
La	15.00				48.20	72.09
Ce	21.40				103.00	145.00
Nd	7.40				52.50	66.58
Sm	0.99				10.10	11.95
Eu	0.61				2.93	3.36
Tb	0.13				1.33	1.39
Yb	0.14				3.61	3.67
Lu	0.02				0.55	0.54
Th	17.60				3.21	4.33
U	1.00				0.70	0.82
Ta	0.12				1.18	1.35
Hf	3.29				6.42	7.54
Isotopes						
$^{87}Sr/^{86}Sr_i$					0.70679	
$^{143}Nd/^{144}Nd_i$					0.51144	
delta O_{18}	10.00					

Name	*Dykes*	*Dykes*	*Dykes*	*Dykes*	*Dykes*	*Dykes*
Sample #	**93L9**	**93L2**	**93L10**	**93L14**	**93L13**	**93L56**
SiO_2	51.57	52.96	54.78	73.49	74.31	68.57
TiO_2	1.03	2.38	1.60	0.25	0.22	0.61
Al_2O_3	21.32	14.75	16.03	12.38	12.86	13.53
Fe_2O_3	6.65	11.63	9.48	3.50	2.51	7.54
MnO	0.11	0.19	0.15	0.10	0.08	0.02
MgO	3.75	3.58	4.16	0.03	0.10	0.02
CaO	10.06	6.66	6.88	0.46	0.73	0.04
Na_2O	3.47	3.60	3.41	4.87	4.19	3.89
K_2O	1.48	2.67	2.78	4.91	4.98	5.73
P_2O_5	0.40	1.24	0.73	0.02	0.03	0.05
LOI	1.60	1.27	1.80	0.32	0.85	1.12
Total	100.41	100.13	100.36	100.73	99.99	100.18
XRF						
Rb			57.90	171.10	145.10	181.90
Sr			777.00	4.90	28.20	11.00
Y			36.60	104.30	73.70	128.00
Zr			341.00	1353.00	585.00	1364.00
Nb			22.20	69.40	52.80	244.60
Ba			1538.00	11.00	154.00	73.00
Pb			6.00	36.00	21.00	28.00
Th			7.00	22.00	19.00	27.00
U			0.00	2.00	1.00	5.00
Sc			18.00	2.00	0.00	8.00
V			172.00	4.00	4.00	26.00
Cr			80.00	22.00	7.00	6.00
Co			28.00	2.00	3.00	1.00
Ni			33.00	2.00	3.00	4.00
Cu			17.00	3.00	3.00	10.00
Zn			112.00	168.00	100.00	109.00
Ga			18.00	28.00	24.00	34.00
Mo			1.00	7.00	3.00	2.00
As			2.00	1.00	1.00	4.00
S			361.00	37.00	45.00	54.00
INAA						
La			75.80			
Ce			156.00			
Nd			65.87			
Sm			11.13			
Eu			2.96			
Tb			1.25			
Yb			3.11			
Lu			0.46			
Th			5.95			
U			0.83			
Ta			1.14			
Hf			7.30			
Isotopes						
$^{87}Sr/^{86}Sr_i$						
$^{143}Nd/^{144}Nd_i$						
delta O_{18}						

Name	*Dykes*	*Mixed flows*	*Mixed flows*
Sample #	**93L57**	**93L82**	**93L49**
SiO_2	66.07	49.61	64.73
TiO_2	0.67	2.60	1.10
Al_2O_3	14.70	16.13	13.05
Fe_2O_3	7.16	13.90	8.33
MnO	0.08	0.21	0.11
MgO	0.15	2.64	1.99
CaO	0.30	6.68	3.21
Na_2O	4.13	4.39	3.06
K_2O	6.68	2.72	4.19
P_2O_5	0.07	1.12	0.24
LOI	1.18	2.76	1.29
Total	100.49	100.50	100.94
XRF			
Rb	139.10	48.10	96.30
Sr	84.70	714.70	123.60
Y	68.10	46.80	62.60
Zr	523.00	306.00	313.00
Nb	101.50	75.30	31.70
Ba	191.00	1711.00	462.00
Pb	14.00	7.00	20.00
Th	11.00	6.00	10.00
U	4.00	2.00	2.00
Sc	6.00	21.00	22.00
V	17.00	187.00	130.00
Cr	4.00	5.00	22.00
Co	0.00	35.00	27.00
Ni	2.00	15.00	49.00
Cu	9.00	38.00	50.00
Zn	137.00	122.00	123.00
Ga	25.00	18.00	20.00
Mo	4.00	2.00	0.00
As	0.00	2.00	1.00
S	49.00	170.00	62.00
INAA			
La		68.40	
Ce		129.00	
Nd		57.10	
Sm		10.50	
Eu		3.23	
Tb		1.39	
Yb		4.02	
Lu		0.58	
Th		5.61	
U		1.60	
Ta		4.30	
Hf		6.45	
Isotopes			
$^{87}Sr/^{86}Sr_i$			0.70806
$^{143}Nd/^{144}Nd_i$			0.51190
delta O_{18}			10.00

APPENDIX B

ANALYTICAL TECHNIQUES

B1. Sample Preparation

Samples were initially crudely broken using a hydraulic splitter. This resulted in the removal of surface weathering and alteration, and allowed the retrieval of fresh material, which where possible was devoid of amygdales. This material was then reduced in size to less than 5mm in a hardened steel jaw crusher. The resultant chips were sieved through to remove any possible sources of contamination by secondary mineralisation. A 100 g fraction was then placed in an agate tema for at least 15 mins in the case of the basalts, and 30-40 mins for the rhyolites. The resultant powder was less than 200 mesh size. Carefully cleaning of equipment was carried out at each stage to avoid possible outside contamination.

B2. X-Ray Fluorescence (XRF) Analysis

B2.1 Sample Preparation

Approximately 10-12 g of each sample was placed in a porcelain crucible and was dried over night in an oven set at 105 °C to eliminate atmospheric moisture. For major element analyses glass discs were made by mixing dried Flux 100B (lithium tetraborate-metaborate) with rock powder in a 5:1 ratio. ~0.35 g of flux was weighed into a platinum/5% gold crucible and 0.07 g of rock powder was mixed in using a polythene mixing rod, this was then placed in an oven at 1100 °C for 15 mins, swirling every 5 mins to ensure the dissolution of gas bubbles and complete mixing. The molten glass was then poured onto a heated brass mould and pressed to form a glass disc (elimates mineralogical and crystallinity defects in determination of the light majors), which was allowed to cool slowly and then labelled.

Loss On Ignition (LOI) values were calculated by weighing accurately 1-1.5 g of rock powder into a pre-ignited silica crucible. This was placed in an oven at 1000 °C for 45 mins, then allowed to cool for 10 mins before re-weighing. The percentage mass loss was then calculated which relates to the total volatile content of the rock.

For trace element analyses ~8 g of rock powder was weighed into small plastic bags. 6-7 drops of polyvinylpyrollidone (PVP) - methyl cellulose binder was then added and mixed vigorously into the powder. This was then made into a pellet by placing the mixture into a mould and exerting 10-15 ton per square inch of pressure using a hydraulic press. The pellets were then labelled and dried overnight in an oven at 105 °C.

B2.2 Element Analyses

All major and trace element analyses were carried out by Dr. J. Watson at the Open University on an ARL 8420+ goniometer wavelength dispersive XRF spectrometer. Two sets of standards to measure internal and external results these included BHVO-1, a USGS standard used as the external monitor. The techniques and running conditions for analysis are described in Potts *et al* (1984). Comparison between calculated and expected standard results provides accuracy and internal consistency of data. In all ten major elements and twenty trace elements were analysed, which are listed in Appendix A.

B3. Instrumental Neutron Activation Analysis (INAA).

Eight rare earth elements, as well as the abundance of Th, U, Ta, Hf, Cs, Rb, Zn, Co, Cr and Sc in selected samples were determined by Instrumental Neutron Activation Analysis (INAA) at the Open University. Potts *et al* (1981, 1985) contain full details of the analytical techniques employed.

B3.1 Sample Preparation

Dried rock powder (0.3 g) was weighed into polythene vials, these were then sealed using a soldering iron. Nine samples plus two standards AC-2 (Ailsa Craig microgranite) and WS (Whin Sill dolerite) were then placed in cylindrical polythene containers, each vial was separated from the next by an iron foil lacquered to a polythene disc. These iron foils are used to monitor the neutron flux along the cylinder during irradiation. Irradiation was carried out at the Imperial College Reactor Centre, near Ascot in a thermal neutron flux of $5x10^{12}$ n cm^{-2} sec^{-1} for 24-30 hrs. Short lived radio-nuclides were allowed to decay during a period of 'cooling' prior to counting at the Open University.

Two detectors were used in tandem to count the induced radioactivity: a coaxial Ge(Li) detector and a planar low energy photon spectrometer (LEPS). Two sets of counting were performed over a period of one month. The first 'short count' lasted for 800secs, and this was followed by a 6-10 hour 'long count' two to four weeks after irradiation. This second count ensures precision values for the longer lived isotopes.

B4. Radiogenic Isotope Analysis

All isotope analyses were carried out in the clean chemistry laboratories in the Earth Sciences Dept., Open University. The reagents used were either two-stage quartz distilled (QD) or teflon distilled (TD) to reduce contamination. All addition of acids to sample powders occurred within the laminar flow fume cupboards. All water for cleaning and dilution purposes was reverse osmosis purified (RO), using a Millipore system.

B4.1 Beaker Cleaning

15ml and 30ml teflon Savillex beakers were used for Strontium and Neodymium chemistry respectively. Prior to beginning any analysis the beakers were labelled and then rigorously cleaned. Initially rinsed with RO water, 5-10 mls of

1.5M QD HNO_3 was then added and left overnight on a hot plate to dissolve any remaining sample. The beaker was then rinsed with RO water, and placed in a large beaker full of hot, concentrated HNO_3. After 24 hrs on the hot plate, the beakers were removed, rinsed, and placed in a large beaker of hot RO water for another 24 hrs. The contents of both large beakers were changed frequently to avoid residue build up. The beakers were rinsed again using RO water and 10-15 ml of 6M QD HCl was added, this was then heated under lamps in the fume cupboard for 1hr. Following which the beakers were rinsed with RO water and placed upside down to dry.

B4.2 Strontium Chemistry

Approximately 150 g of rock powder was weighed into a cleaned beaker for each sample, to which a few drops of 15M TD HNO_3 was added, this wet the powder prior to addition of < 4 ml of TD HF (48%). ~4 ml of saturated boric acid was also added to the first few sets of samples dissolved, however, the acid was found to contain an excess of Sr and so the stage was eliminated. The sealed beaker was then allowed to stand on a hot plate overnight. The HF was then evaporated off slowly under evaporating hoods with a continuous compressed air supply. When the solution resembled wall paper paste, 2-3 mls of 15M TD HNO_3 was added to prevent the formation of fluorides. The solution was then evaporated down to dryness, 6 ml of 6M TD HCl was added to the residue and left to stand on a hotplate overnight before being evaporated to dryness for a final time. The sample was then dissolved in 2 ml of 2.5M QD HCl and transferred to centrifuge tubes that had been rinsed with 2.5M QD HCl, and centrifuged at 4000 rpm for 5 mins. The sample was then ready for loading onto the columns.

1ml of sample solution was loaded onto the resin bed of a preconditioned ion exchange column for Strontium separation. Once absorbed by the resin the sample was washed through by 2 x 1 ml 2.5M QD HCl. 36 ml of 2.5M QD HCl was eluted through the column to remove the Rb fraction before another 14mls was added from which the Sr fraction was collected into a rinsed beaker. This was then evaporated down to dryness and then loaded onto a single Ta filament for analysis.

B4.4 Neodymium Chemistry

The separation of the Nd fraction requires two stages, the first part continues directly after the collection of the Sr fraction. Once the Sr was collected, the resin was washed by 18 ml of 3M QD HNO_3 to remove the Sm fraction. Followed by 14ml of the same acid, to collect the Nd fraction, along with other MREE and Ba, into a cleaned 15ml beaker. This solution was evaporated down to dryness before being dissolved in 1 ml of 0.25M QD HCl and loaded onto a set of ion exchange reverse chromatography columns. The sample was washed through by 2 x 1 ml 0.25M QD HCl initially, followed by 14 ml of the same acid. Finally 8 ml of 0.25M QD HCl was eluted and collected in a clean beaker. This was then evaporated to dryness, and loaded onto a double Re filament for analysis. Both sets of columns were cleaned thoroughly using 6M QD HCl, 2.5M QD HCl and RO water for the Sr columns; and 0.25M QD HCl, RO water for Nd columns. Standards were run frequently including BHVO-1 and NBS 987 for Sr and the J&M standard for Nd.

B4.5 Sample Loading

Samples were loaded onto cleaned, outgassed filaments (single Ta for Sr; Re double for Nd) by pipette in a filtered loading cabinet. 2µl of H_3PO_4 was loaded onto the filament and evaporated off at a current of 1.4 A, meanwhile the sample was dissolved in 2µl of TD water. This was then placed on the filament and the current increased to ~2A, this allowed all excess to be removed, when the filament glowed red the current was returned to 0. Nd samples were loaded onto dry Re filaments, after being dissolved in 1µl of TD water, the current was increased to 0.8A and held there until the droplet had evaporated off.

B4.6 Mass Spectrometry

All samples were analysed on either a Finnegan MAT261 or MAT262 multi-collector mass spectrometer at the Open University. Blanks for Sr and Nd were in

general below 5ng and so considered not to interfere with the isotopic results. During a period of three months unacceptable blanks of > 30 ng and as high as 500 ng were found to be a result of the use of contaminated boric acid after rigorous testing of beakers, columns, acids and loading procedures. All samples analysed during this period were re-evaluated and a second set of samples run as analyses were found to vary in the fourth decimal place, with such errors deemed unacceptable.

Table B1. Internal standards measured during run time of samples for Sr & Nd. Official value is the machine number average to which individual analyses are compared and corrected before being used in sample corrections.

From	To		Standard	1δ
		Sr	**NBS987**	
25-10-94	3-11-94		0.710294	11
12-12-94	18-12-94		0.710247	10
4-2-95	11-2-95		0.710275	10
12-2-95	17-2-95		0.710236	10
31-8-95	12-9-95		0.71024	10
24-8-96	31-8-96		0.71025	7
8-3-97	15-3-97		0.710145	6
Official value			0.710223	16
		Nd	**J&M**	
4-2-95	15-2-95		0.511760	5
31-8-95	12-9-95		0.511773	5
11-10-95	17-10-95		0.511788	4
15-7-96	22-7-96		0.511788	4
24-8-96	31-8-96		0.511759	3
11-2-97	22-2-97		0.511762	7
Official value			0.511778	12

Repeat analyses of Sr standard NBS987, and the Nd J&M standard were used to standardise variations in machine running conditions. Table B1 contains the mean values used for corrections. All samples were age corrected to 130 Ma.

B5. Electron Microprobe

Mineral phase analyses were made using a wavelength dispersive electron microprobe, initially a Cambridge Instruments Microscan 9. Polished thin sections of certain samples were carbon coated, this was in order to reduce the build up of charge across the section whilst under the electron beam. Diffracting crystals used to calibrate elements were TAP, PET and LiF. The instrument was calibrated before each session using mineral standards: Wollastonite (Si, Ca), Rutile (Ti), metal (Cr, Mn, Ni), Jadeite (Al, Na), Fayalite (Fe) and Forsterite (Mg). The standard ABG (a basaltic glass from the rim of a pillow lava in the North Atlantic, Tindle (1982)) was used to check accuracy, and run before and during every sample, if the analysed ABG fell outside the 2σ range the element(s) were re calibration prior to continuation of analysis. Running conditions involved a 20kV, soft focused beam of 20nA, 15μm in diameter.

A new Cameca SX100 microprobe was installed late 1995 and so the majority of analyses were made on this. Analyses were undertaken using a 20 nA beam current, 20 kV accelerating potential, and a typical spot size of 20 μm. For iron oxide analyses, a reduced beam size of 1μm was used due to the small size of the crystals. The SX100 has four spectrometers, and major elements were analysed using the PET, LiF and TAP diffracting crystals, calibrated using the following standards:

Si, Al, K	fspr-In5	Fe	hematite-ast3
Ti	rutile-BM4	Mg	forsterite-BM4
Mn, Ca	bustamite-ast3	Na	jadeite-BM4
P	apatite-BM4	Cr	crocoite-ast3
Cl	sylvite-BM4	F	LiF-4

APPENDIX C

SAMPLE TEXTURES & MICROPROBE ANALYSES

A variety of textures are evident in the basalt - rhyolite suite of samples examined from southern Uruguay. In order to highlight some of this textural diversity a number of photomicrographs are including in this Appendix with a brief description of the textures. Rhyolite names are as described in the petrology section of Chapter 2.

The following pages also contain representative microprobe analyses for the samples analysed. All analyses are expressed as weight percent oxides and formulas with feldspars formulated for eight oxygens, pyroxene for six and iron oxides for twenty two. Fe is presented as Fe^{2+}. Running conditions for the microprobe are listed in Appendix B.

C1. Textural Details.

Plate 1. Sample 93L53. Santa Lucía magma type. Subophitic enclosure of lamellar twinned plagioclase by clinopyroxene and highly fractured olivine in porphyritic basalt. Crossed polarised light (XPL). Plan 2,5.

Plate 2. Sample 93L94. Treinte Y Trés magma type. Large porphyroblast of plagioclase feldspar which is being resorpted into the matrix, together with phenocrysts of clinopyroxene set in a microcrystalline matrix of similar composition. XPL. Plan 2,5.

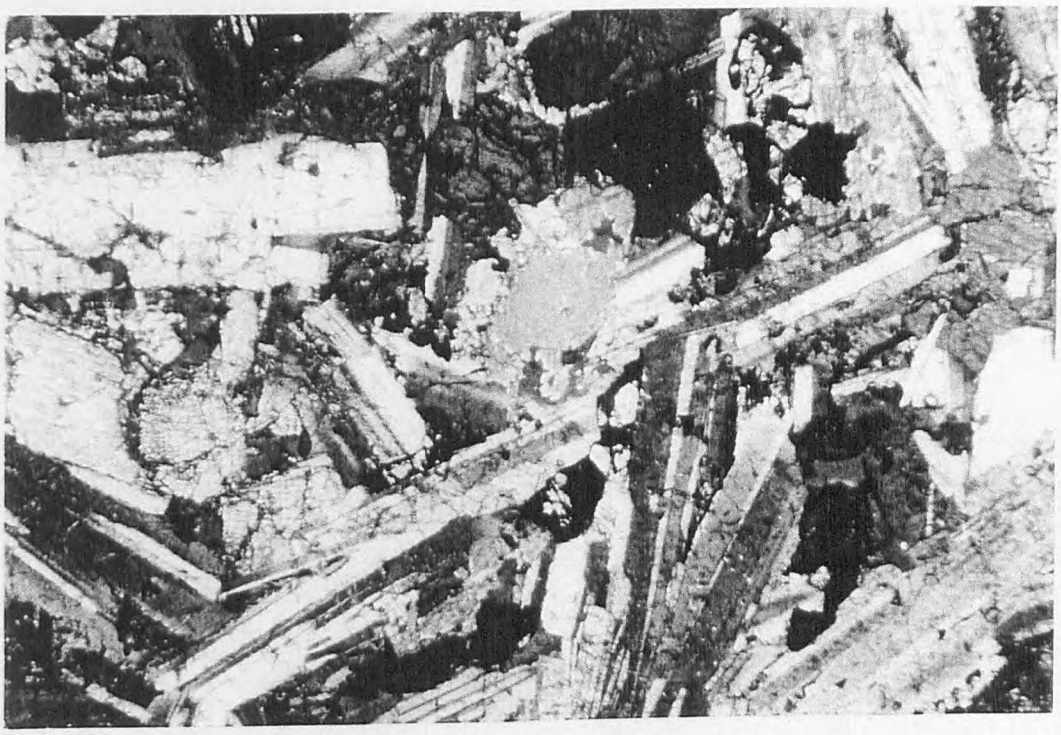

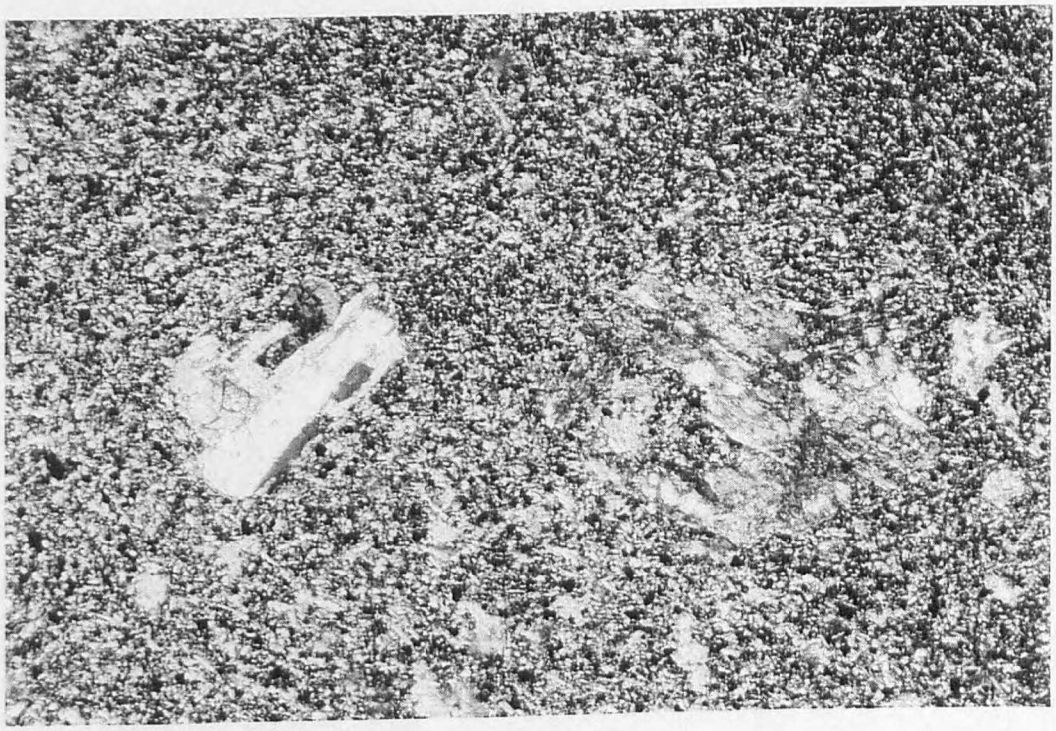

Plate 3. Sample 93L96. Treinte Y Trés. Glomerophyric intergrowths of plagioclase feldspar set in a microcrystalline matrix with secondary iron oxides. Plane polarised light (PPL). Plan 2,5.

Plate 4. Sample 93L96. Treinte Y Trés. Showing top left hand section of Plate 3 in XPL. Porphyroblasts of lamellar twinned plagioclase set in a matrix of plagioclase laths, anhedral clinopyroxene and both primary and secondary iron oxides. Plan 2,5.

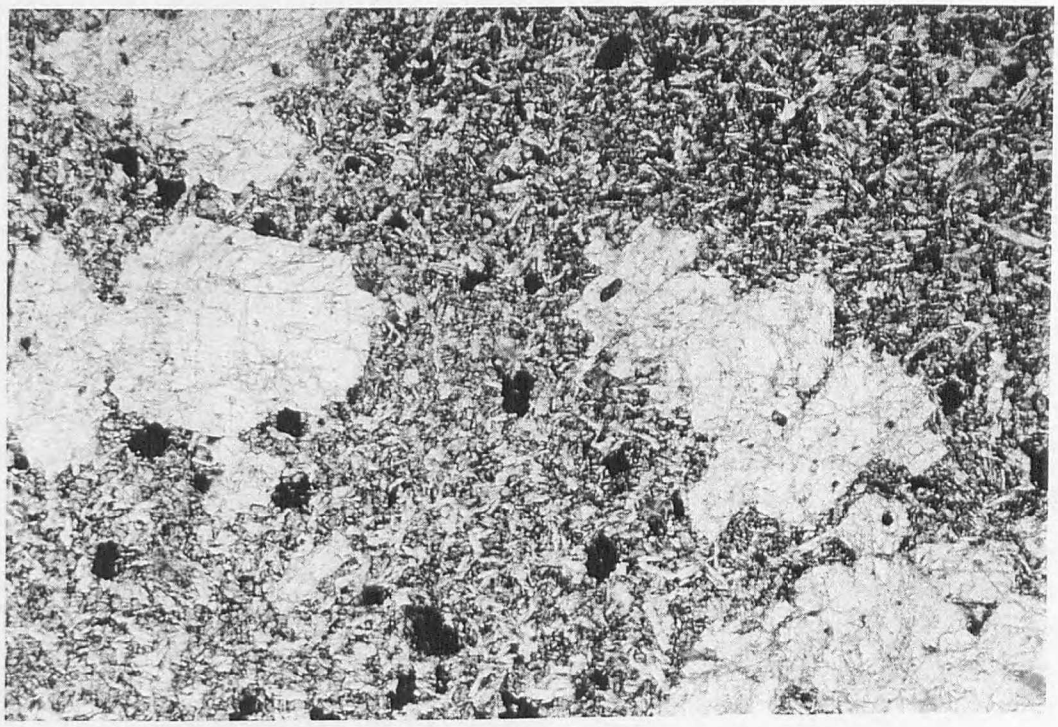

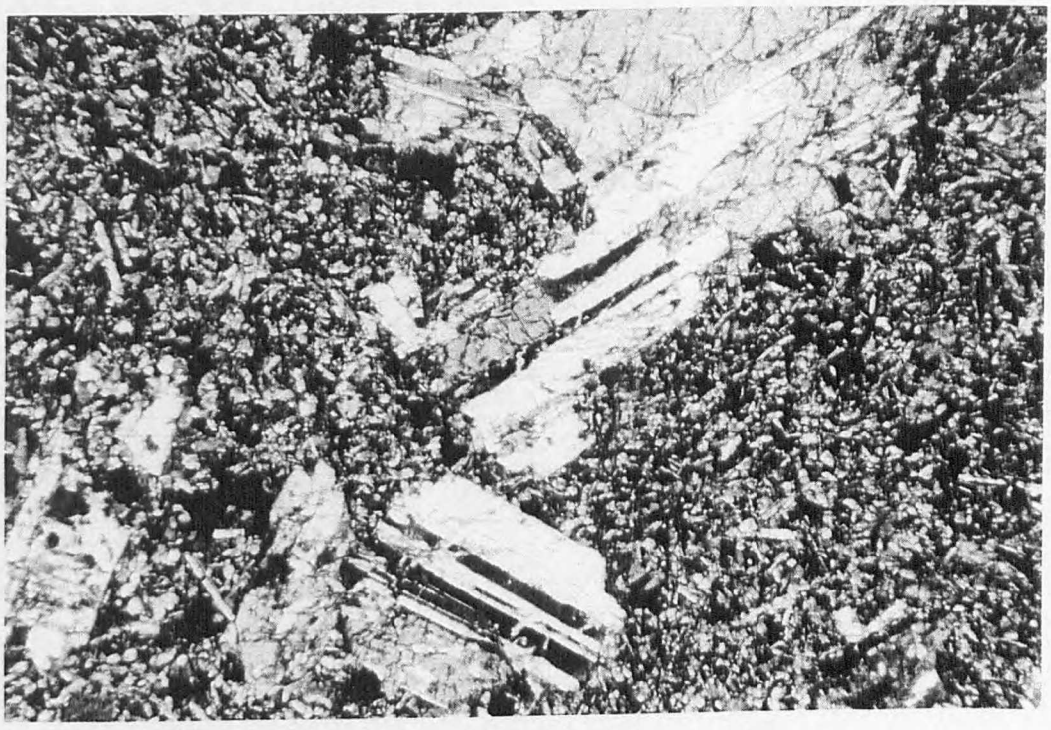

Plate 5. 93L83. Type 1 Rhyolite. Large phenocrysts of lamellar twinned plagioclase and alklai feldspar set in a microcrystalline matrix of feldspar primarily with < 10 % pyroxene. A reaction rim is evident around the edge of the alkali feldspar in the lower part of the photo suggesting disequilibrium at the time of cooling. Plan 2,5.

Plate 6. 93L81. Type 2 Rhyolite. Large skeletal alkali feldpar phenocryst (7 mm) set in a cryptocrystalline matrix. Sieve or skeletal textures are associated with resorption. Magnification x 10/0,22.

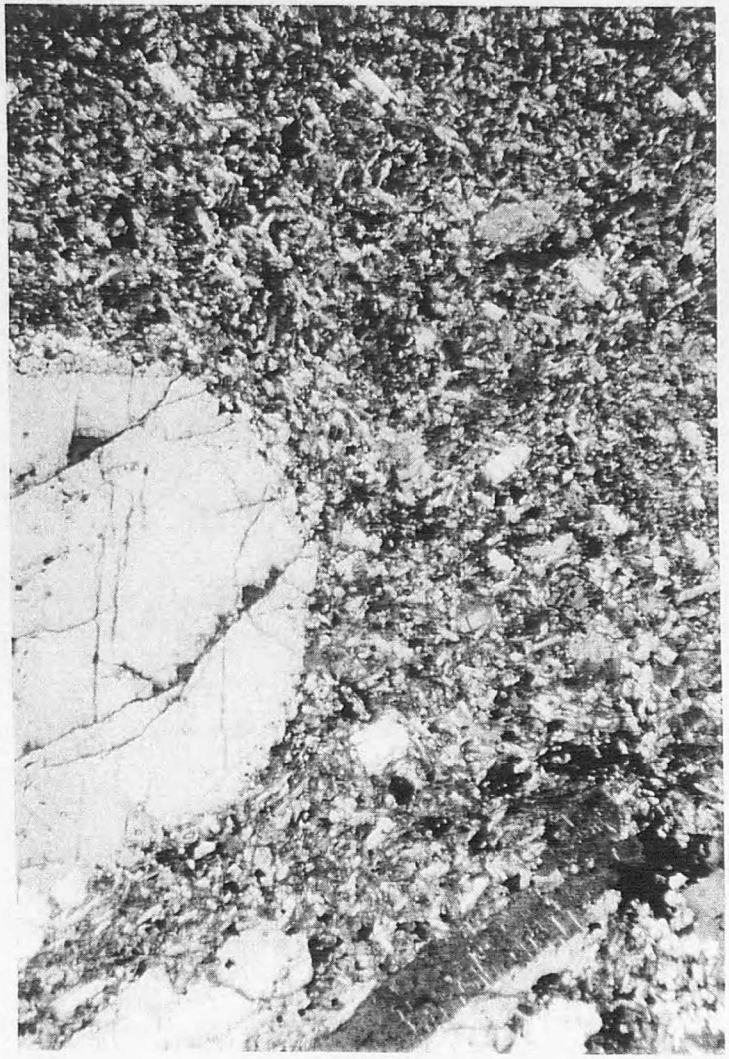

Plate 7. 93L22. Type 2 Rhyolite. Embayed quartz phenocryst indicating arrested development, with two smaller alkali feldspar phenocrysts set in a cryptocrystalline matrix. Plan 2,5.

Plate 8. 93L120. Interaction between lithic sandstone (right hand side) and rhyolite (left), which suggests that the rhyolites were erupted onto an unconsolidated sandy substrate.

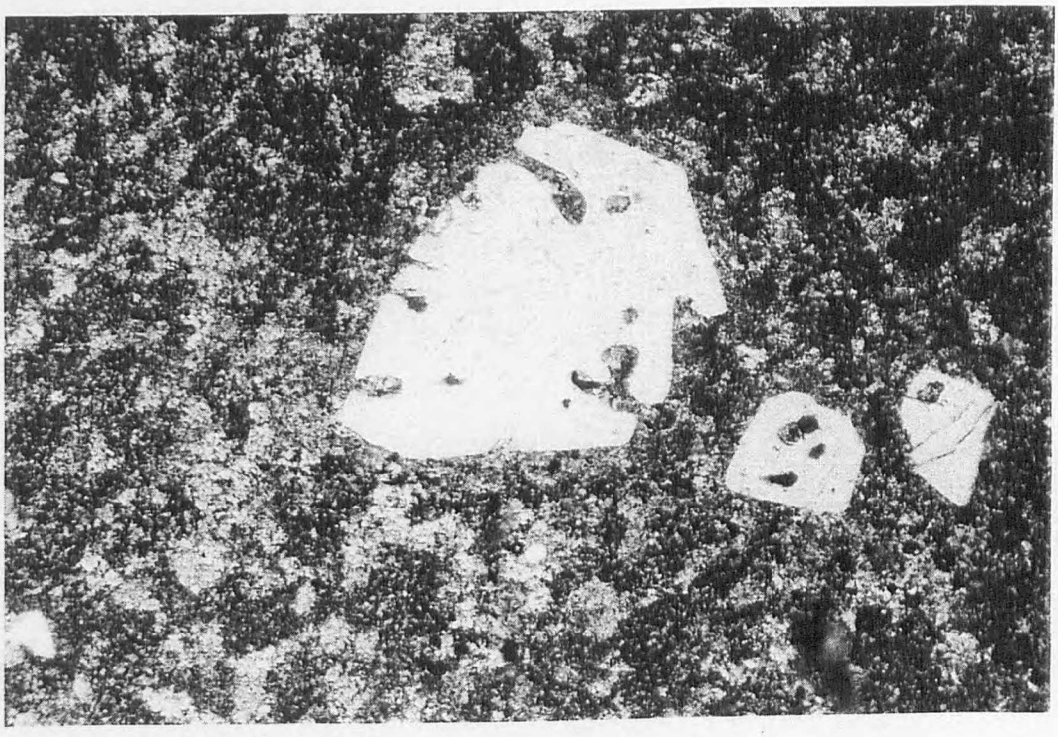

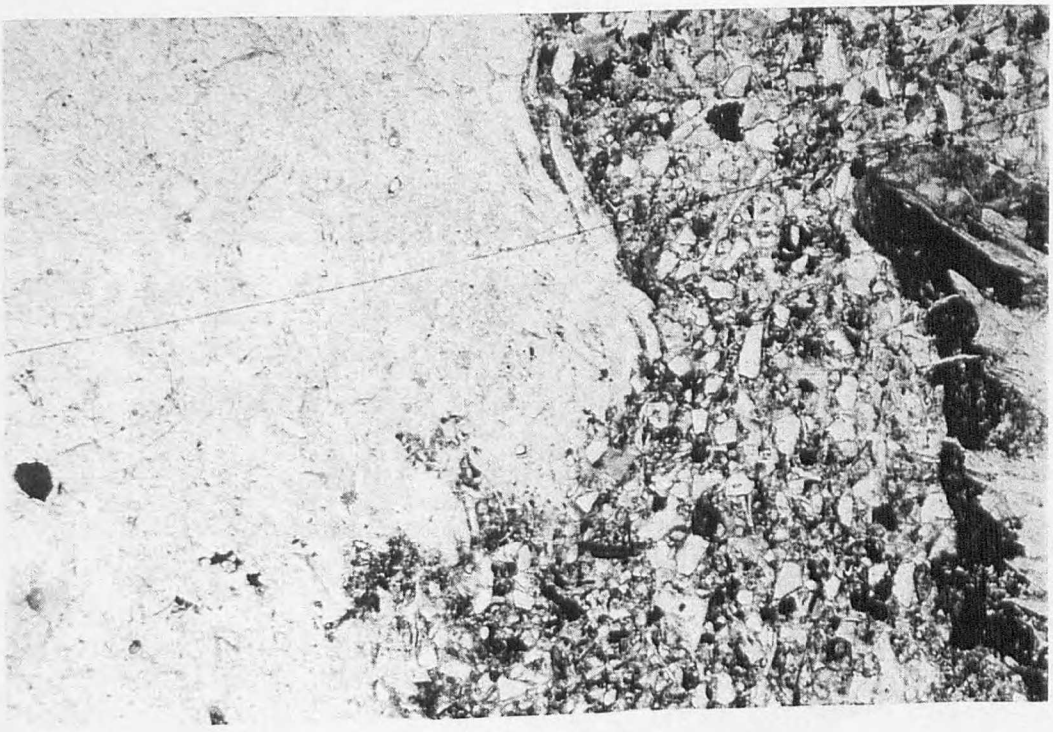

Plate 9. Type 1 93L87. XPL. Glomerophyric intergrowth (1cm) of feldspar set in a microcrystalline matrix of plagioclase, alkali feldspar and quartz. Note perthitic textures of feldspars. Magnification x 10/0,22.

Plate 10. Type 2 93L129. XPL. Graphic or granophyric intergrowth of quartz and alkali feldspar with some alteration to clay minerals evident. Texture such as this have been reported from old devitrified glassy rhyolite systems where quartz and alkali feldspar have intergrown either during slow cooling or devitrification. Magnification x 10/0,22.

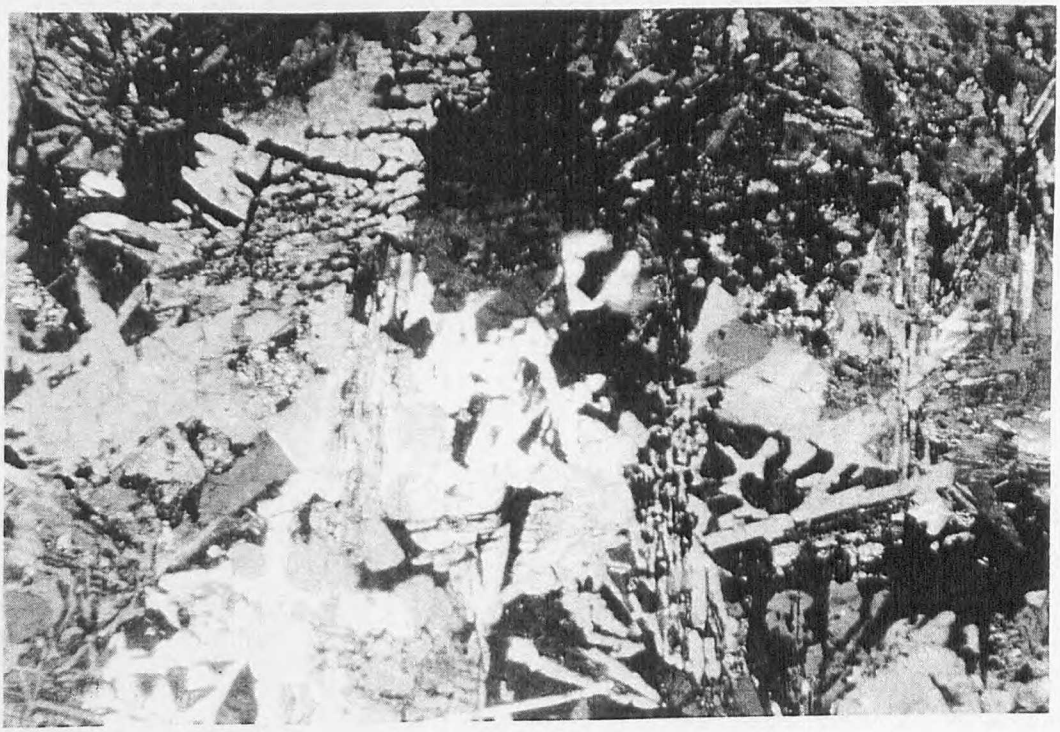

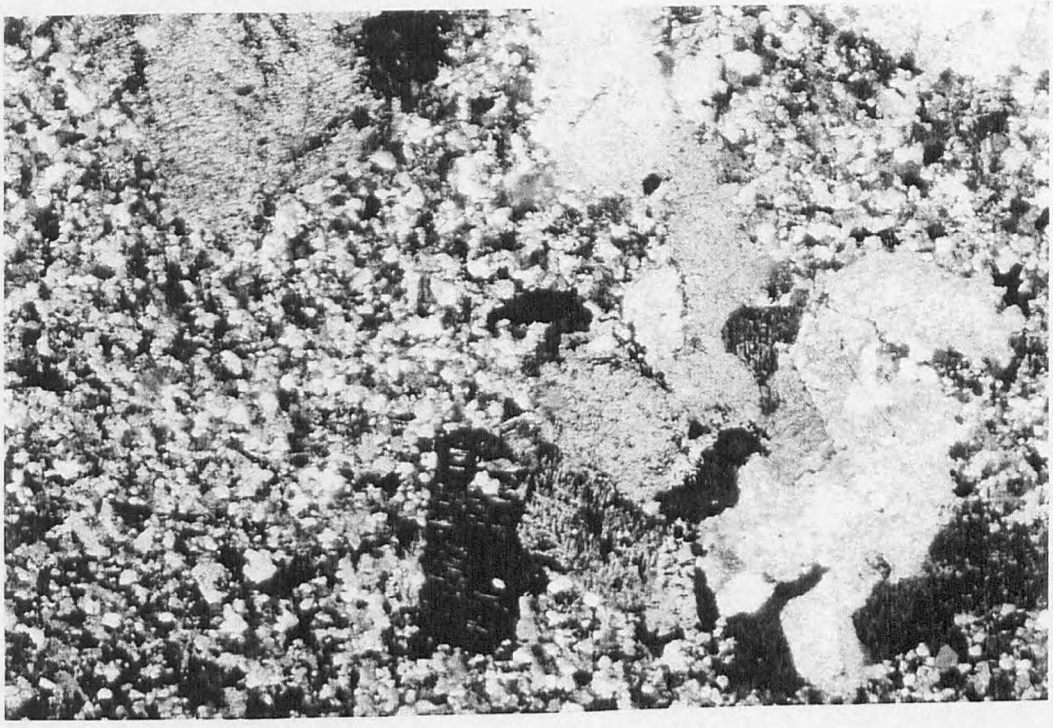

Plate 11. Type 2 93L57. Spherulitic devitrification of a glassy matrix in a fairly altered sample as indicated by the green tinge in this view in plane polarised light. Plan 1,6.

Plate 12. Type 1 93L126. Extensive secondary alteration to chlorite. Magnification x 10/0,22.

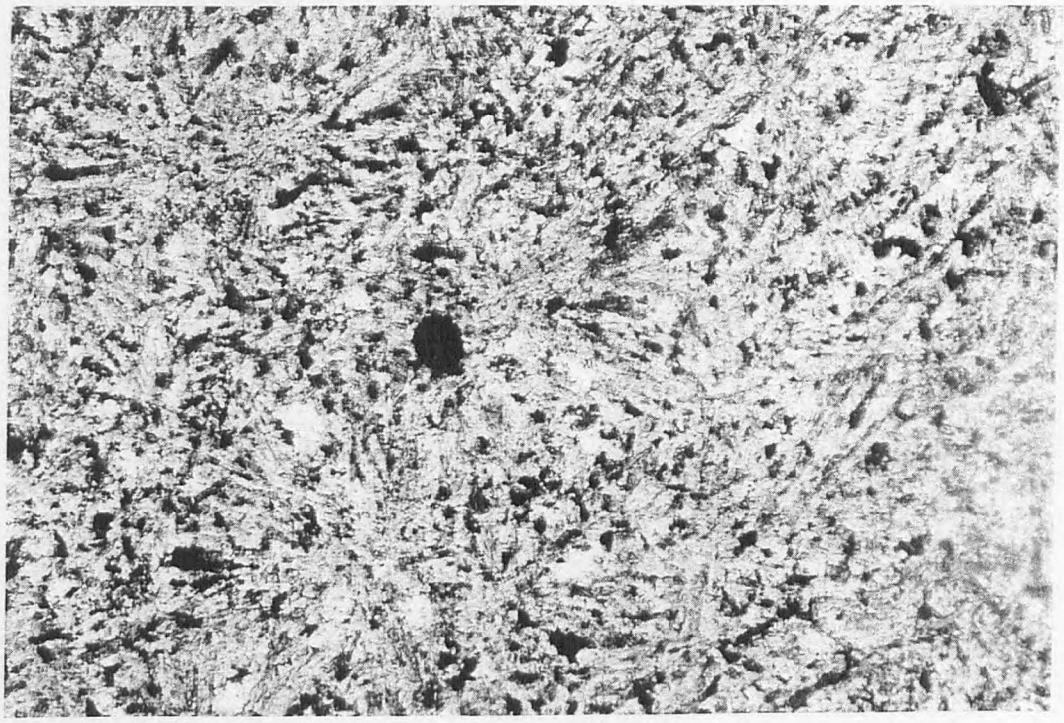

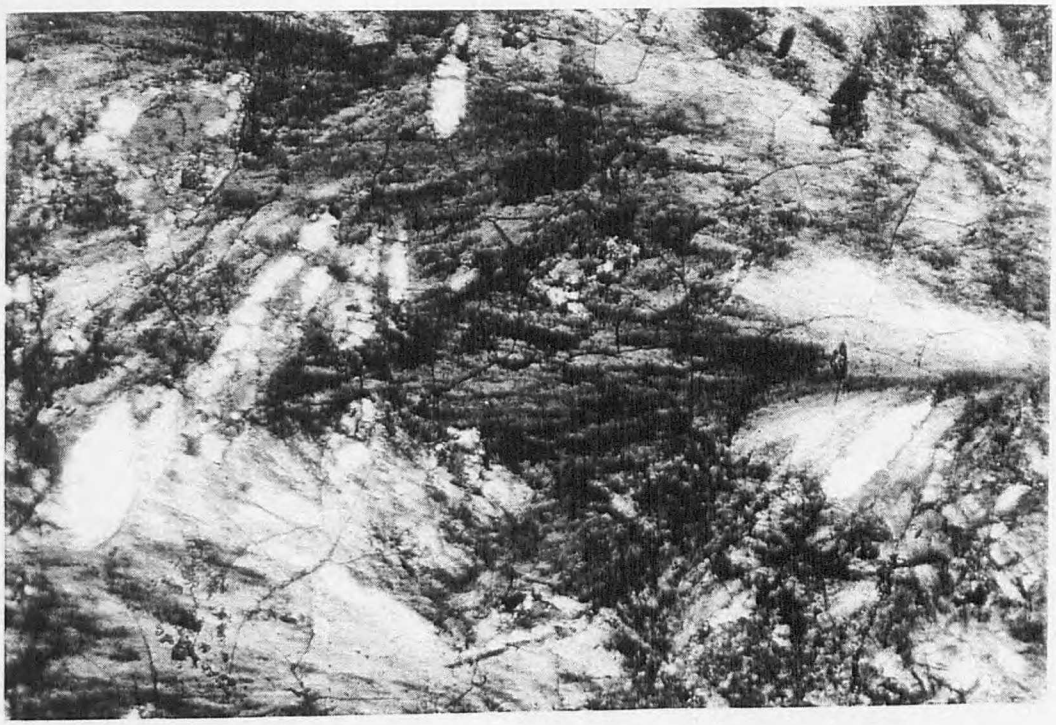

Plate 13. Type 2 93L28. Rhyolite. PPL view of ignimbritic texture rhyolite with β form quartz evident together with equant feldspar phenocrysts aligned parallel to the flow direction. Magnification x 10/0,22.

Plate 14. Type 2 93L99. Rhyolite. Flattened vesicle and alkali feldspar phenocrysts with flow evident around the phenocrysts. Magnification x 10/0,22.

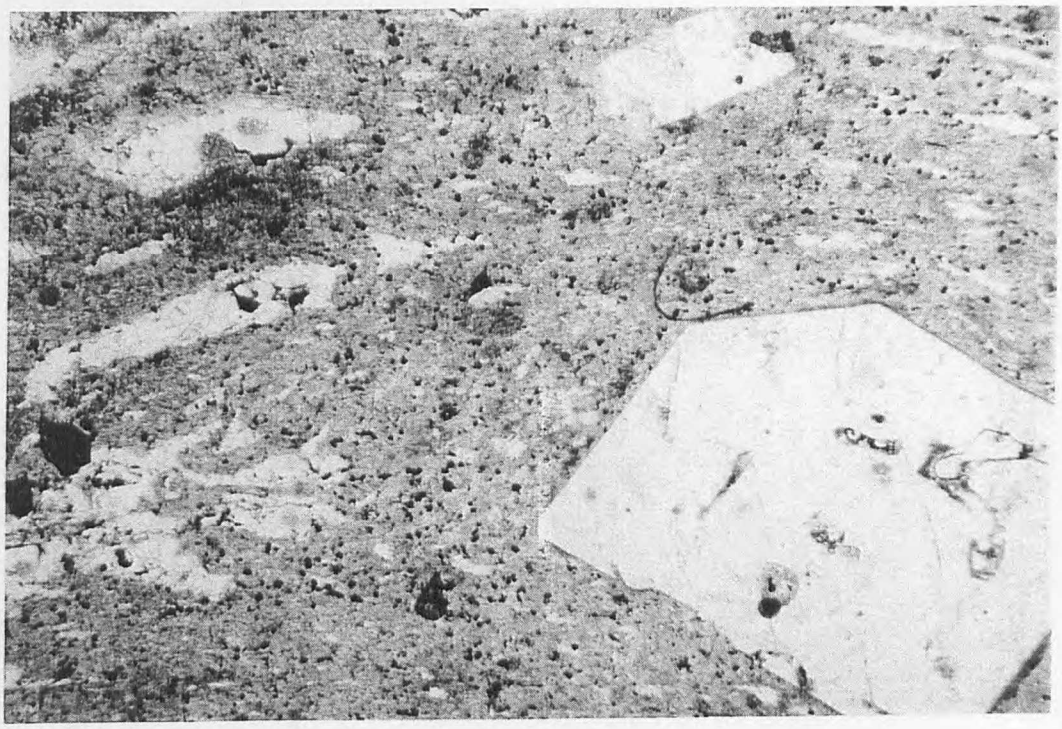

C2. Microprobe Data.

Name	92U12	92U12	92U12	92U12	92U12	92U12
Mineral	Plagioclase	Plagioclase	Plagioclase	Plagioclase	Plagioclase	Plagioclase
SiO_2	51.02	55.34	52.15	52.58	51.80	51.88
TiO_2	0.06	0.14	0.07	1.12	0.10	0.08
Al_2O_3	30.31	27.60	29.76	27.80	29.95	30.01
MgO	0.11	0.12	0.13	0.22	0.11	0.12
CaO	13.96	10.46	13.13	11.04	13.52	13.44
MnO	0.00	0.01	0.01	0.01	0.02	0.01
FeO	0.53	0.76	0.61	1.57	0.60	0.56
BaO	0.03	0.04	0.04	0.05	0.04	0.00
Na_2O	3.63	5.37	4.07	4.99	3.80	3.88
K_2O	0.20	0.50	0.24	0.40	0.20	0.22
Total	99.86	100.34	100.22	99.77	100.12	100.20
Formula Units	8	8	8	8	8	8
Si	2.33	2.50	2.37	2.41	2.36	2.36
Ti	0.00	0.01	0.00	0.04	0.00	0.00
Al	1.63	1.47	1.60	1.50	1.61	1.61
Mg	0.01	0.01	0.01	0.02	0.01	0.01
Ca	0.68	0.51	0.64	0.54	0.66	0.66
Mn	0.00	0.00	0.00	0.00	0.00	0.00
Fe	0.02	0.03	0.02	0.06	0.02	0.02
Ba	0.00	0.00	0.00	0.00	0.00	0.00
Na	0.32	0.47	0.36	0.44	0.34	0.34
K	0.01	0.03	0.01	0.02	0.01	0.01
Total	5.02	5.01	5.02	5.03	5.01	5.01

Name	92U12	92U12	93L125	93L105	93L105	93L105
Mineral	Plagioclase	Plagioclase	Plagioclase	Plagioclase	Plagioclase	Plagioclase
SiO_2	51.76	50.99	52.73	57.09	55.62	56.01
TiO_2	0.08	0.09		0.02	0.03	0.03
Al_2O_3	29.79	29.74	28.47	26.39	25.73	27.14
MgO	0.13	0.27		0.02	0.01	0.01
CaO	13.06	13.21	12.08	9.42	8.92	10.23
MnO	0.01	0.00		0.00	0.00	0.01
FeO	0.53	0.82	1.03	0.35	0.52	0.27
BaO	0.02	0.02	0.00	0.08	0.11	0.11
Na_2O	3.98	3.88	4.42	5.52	5.43	5.09
K_2O	0.33	0.22	0.34	0.95	0.90	0.80
Total	99.70	99.24	99.07	99.83	97.27	99.71
Formula Units	8	8	8	8	8	8
Si	2.37	2.35	2.42	2.58	2.58	2.54
Ti	0.00	0.00		0.00	0.00	0.00
Al	1.61	1.61	1.54	1.40	1.41	1.45
Mg	0.01	0.02		0.00	0.00	0.00
Ca	0.64	0.65	0.60	0.46	0.44	0.50
Mn	0.00	0.00	0.04	0.00	0.00	0.00
Fe	0.02	0.03	0.00	0.01	0.02	0.01
Ba	0.00	0.00		0.00	0.00	0.00
Na	0.35	0.35	0.39	0.48	0.49	0.45
K	0.02	0.01	0.02	0.06	0.05	0.05
Total	5.01	5.02	5.01	4.99	4.99	4.99

Name	93L104	93L104	93L104	93L104	93L104	93L104
Mineral	Plagioclase	Plagioclase	Plagioclase	Plagioclase	Plagioclase	Plagioclase
SiO_2	50.39	49.55	50.52	51.62	50.34	50.18
TiO_2	0.06	0.07	0.09	0.61	0.06	0.02
Al_2O_3	29.99	30.46	29.89	1.58	29.71	30.96
MgO	0.22	0.11	0.12	16.20	0.12	0.12
CaO	13.67	14.21	13.45	18.80	13.51	14.28
MnO	0.00	0.01	0.01	0.28	0.01	0.01
FeO	1.09	0.86	0.89	9.85	1.20	0.40
BaO	0.00	0.00	0.02	0.01	0.00	0.01
Na_2O	3.51	3.46	3.78	0.19	3.83	3.34
K_2O	0.38	0.27	0.30	0.00	0.31	0.20
Total	99.31	99.01	99.07	99.27	99.09	99.51
Formula Units	8	8	8	8	8	8
Si	2.32	2.30	2.33	2.58	2.33	2.30
Ti	0.00	0.00	0.00	0.02	0.00	0.00
Al	1.61	1.65	1.61	0.09	1.60	1.66
Mg	0.02	0.01	0.01	1.21	0.01	0.01
Ca	0.68	0.71	0.67	1.01	0.67	0.70
Mn	0.00	0.00	0.00	0.01	0.00	0.00
Fe	0.04	0.03	0.03	0.41	0.05	0.02
Ba	0.00	0.00	0.00	0.00	0.00	0.00
Na	0.31	0.31	0.34	0.02	0.34	0.30
K	0.02	0.02	0.02	0.00	0.02	0.01
Total	5.01	5.02	5.01	5.36	5.02	5.00

Name	93L47	93L47	93L47	93L47	93L78	93L78
Mineral	Plagioclase	Plagioclase	Plagioclase	Plagioclase	Plagioclase	Plagioclase
SiO_2	50.59	49.98	50.98	49.00	59.40	60.24
TiO_2	0.09	0.09	0.07	0.06	0.06	0.05
Al_2O_3	30.62	30.66	30.20	31.49	24.60	24.25
MgO	0.16	0.14	0.14	0.18	0.03	0.02
CaO	13.85	14.13	13.75	15.01	6.70	6.11
MnO	0.00	0.00	0.01	0.01	0.00	0.01
FeO	0.44	0.44	0.45	0.42	0.48	0.40
BaO	0.02	0.02	0.01	0.02	0.27	0.35
Na_2O	3.49	3.43	3.64	2.94	7.28	7.34
K_2O	0.21	0.21	0.23	0.16	0.71	1.13
Total	99.47	99.09	99.49	99.28	99.53	99.91
Formula Units	8	8	8	8	8	8
Si	2.32	2.30	2.34	2.26	2.68	2.70
Ti						
Al	1.64	1.65	1.62	1.70	1.29	1.27
Mg	0.01	0.01	0.01	0.01	0.00	0.00
Ca	0.68	0.70	0.68	0.74	0.32	0.29
Mn	0.00	0.00	0.00	0.00	0.00	0.00
Fe	0.02	0.02	0.02	0.02	0.02	0.01
Ba	0.00	0.00	0.00	0.00	0.00	0.01
Na	0.31	0.31	0.32	0.26	0.64	0.64
K	0.01	0.01	0.01	0.01	0.04	0.06
Total	4.99	5.00	5.00	5.00	4.99	4.99

Name	93L111	93L111	93L111	93L111	93L111	93L111
Mineral	Plagioclase	Plagioclase	Plagioclase	Plagioclase	Plagioclase	Plagioclase
SiO_2	57.37	56.45	57.84	57.87	56.84	56.26
TiO_2	0.01	0.05	0.02	0.03	0.03	0.01
Al_2O_3	26.44	26.57	26.06	25.93	26.92	27.00
MgO	0.03	0.03	0.01	0.01	0.01	0.03
CaO	9.20	9.85	8.90	8.71	9.73	10.11
MnO	0.00	0.01	0.00	0.00	0.00	0.02
FeO	0.41	0.44	0.44	0.48	0.48	0.41
BaO	0.15	0.16	0.11	0.11	0.11	0.10
Na_2O	5.54	5.22	5.87	5.98	5.72	5.31
K_2O	0.95	0.84	0.92	0.94	0.63	0.75
Total	100.10	99.63	100.17	100.06	100.46	99.99
Formula Units	8	8	8	8	8	8
Si	2.58	2.56	2.60	2.60	2.55	2.54
Ti	0.00	0.00	0.00	0.00	0.00	0.00
Al	1.40	1.42	1.38	1.38	1.43	1.44
Mg	0.00	0.00	0.00	0.00	0.00	0.00
Ca	0.44	0.48	0.43	0.42	0.47	0.49
Mn	0.00	0.00	0.00	0.00	0.00	0.00
Fe	0.02	0.02	0.02	0.02	0.02	0.02
Ba	0.00	0.00	0.00	0.00	0.00	0.00
Na	0.48	0.46	0.51	0.52	0.50	0.47
K	0.05	0.05	0.05	0.05	0.04	0.04
Total	4.99	4.99	4.99	5.00	5.00	5.00

Name	93L97	93L97	93L97	93L125	93L125	93L125
Mineral	Plagioclase	Plagioclase	Plagioclase	Plagioclase	Plagioclase	Plagioclase
SiO_2	48.65	47.71	49.05	63.05	52.22	53.88
TiO_2	0.03	0.03	0.04	0.11	0.05	0.10
Al_2O_3	31.66	32.28	30.81	22.41	28.71	27.84
MgO	0.24	0.23	0.21	0.05	0.13	0.02
CaO	15.89	16.41	15.21	7.29	12.75	11.18
MnO	0.00	0.00	0.00	0.00	0.01	0.00
FeO	0.46	0.42	0.44	0.95	0.73	0.92
BaO	0.00	0.02	0.00	0.08	0.00	0.04
Na_2O	2.50	2.15	2.82	5.74	4.13	5.11
K2O	0.15	0.12	0.19	0.66	0.32	0.40
Total	99.58	99.37	98.76	100.33	99.05	99.48
Formula units	8	8	8	8	8	8
Si	2.24	2.21	2.28	2.79	2.40	2.46
Ti	0.00	0.00	0.00	0.00	0.00	0.00
Al	1.70	1.74	1.67	1.16	1.54	1.48
Mg	0.02	0.02	0.01	0.00	0.01	0.00
Ca	0.78	0.81	0.76	0.35	0.63	0.55
Mn	0.00	0.00	0.00	0.00	0.00	0.00
Fe2+	0.02	0.02	0.02	0.04	0.03	0.04
Ba	0.00	0.00	0.00	0.00	0.00	0.00
Na	0.22	0.19	0.25	0.49	0.37	0.45
K	0.01	0.01	0.01	0.04	0.02	0.02
Total	5.00	4.99	5.00	4.87	5.00	5.01

Name	93L53	93L53	93L53	93L125	93L125	93L125
Mineral	Plagioclase	Plagioclase	Plagioclase	Plagioclase	Plagioclase	Plagioclase
SiO_2	51.42	55.08	51.31	52.51	52.98	51.71
TiO_2	0.06	0.15	0.07	0.07	0.05	0.03
Al_2O_3	30.41	27.78	29.86	28.64	28.53	29.17
MgO	0.13	0.08	0.13	0.11	0.11	0.13
CaO	13.89	10.65	13.49	12.67	12.62	13.59
MnO	0.01	0.01	0.00	0.01	0.00	0.01
FeO	0.50	0.64	0.48	0.81	0.80	0.84
BaO	0.02	0.05	0.00	0.02	0.03	0.00
Na_2O	3.56	5.33	3.87	4.25	4.24	3.79
K2O	0.23	0.52	0.29	0.34	0.31	0.28
Total	100.23	100.27	99.49	99.41	99.69	99.55
Formula units	8	8	8	8	8	8
Si	2.34	2.49	2.35	2.41	2.42	2.37
Ti	0.00	0.01	0.00	0.00	0.00	0.00
Al	1.62	1.46	1.60	1.53	1.52	1.56
Mg	0.01	0.01	0.01	0.01	0.01	0.01
Ca	0.68	0.52	0.66	0.62	0.62	0.67
Mn	0.00	0.00	0.00	0.00	0.00	0.00
Fe	0.02	0.02	0.02	0.03	0.03	0.03
Ba	0.00	0.00	0.00	0.00	0.00	0.00
Na	0.31	0.47	0.34	0.38	0.38	0.34
K	0.01	0.03	0.02	0.02	0.02	0.02
Total	4.99	5.00	5.00	5.00	4.99	5.00

Name	93L104	93L104	93L104	93L104	93L47	93L47
Mineral	Plagioclase	Plagioclase	Plagioclase	Plagioclase	Plagioclase	Plagioclase
SiO_2	50.39	49.55	50.52	50.34	50.18	50.59
TiO_2	0.06	0.07	0.09	0.06	0.02	0.09
Al_2O_3	29.99	30.46	29.89	29.71	30.96	30.62
MgO	0.22	0.11	0.12	0.12	0.12	0.16
CaO	13.67	14.21	13.45	13.51	14.28	13.85
MnO	0.00	0.01	0.01	0.01	0.01	0.00
FeO	1.09	0.86	0.89	1.20	0.40	0.44
BaO	0.00	0.00	0.02	0.00	0.01	0.02
Na_2O	3.51	3.46	3.78	3.83	3.34	3.49
K2O	0.38	0.27	0.30	0.31	0.20	0.21
Total	99.31	99.01	99.07	99.09	99.51	99.47
Formula units	8	8	8	8	8	8
Si	2.32	2.30	2.33	2.33	2.30	2.32
Ti						
Al	1.61	1.65	1.61	1.60	1.66	1.64
Mg	0.02	0.01	0.01	0.01	0.01	0.01
Ca	0.68	0.71	0.67	0.67	0.70	0.68
Mn	0.00	0.00	0.00	0.00	0.00	0.00
Fe	0.04	0.03	0.03	0.05	0.02	0.02
Ba						
Na	0.31	0.31	0.34	0.34	0.30	0.31
K	0.02	0.02	0.02	0.02	0.01	0.01
Total	5.01	5.02	5.01	5.02	5.00	4.99

Name	93L27	93L47	93L47	93L47	93L78	93L78
Mineral	Plagioclase	Plagioclase	Plagioclase	Plagioclase	Plagioclase	Plagioclase
SiO_2	49.65	49.98	50.98	49.00	60.24	59.40
TiO_2	0.27	0.09	0.07	0.06	0.05	0.06
Al_2O_3	24.66	30.66	30.20	31.49	24.25	24.60
MgO	3.95	0.14	0.14	0.18	0.02	0.03
CaO	14.83	14.13	13.75	15.01	6.11	6.70
MnO	0.06	0.00	0.01	0.01	0.01	0.00
FeO	3.42	0.44	0.45	0.42	0.40	0.48
BaO	0.02	0.02	0.01	0.02	0.35	0.27
Na_2O	2.67	3.43	3.64	2.94	7.34	7.28
K2O	0.13	0.21	0.23	0.16	1.13	0.71
Total	99.75	99.09	99.49	99.28	99.91	99.53
Formula units	8	8	8	8	8	8
Si	2.33	2.30	2.34	2.26	2.70	2.68
Ti	0.01	0.00	0.00	0.00	0.00	0.00
Al	1.35	1.65	1.62	1.70	1.27	1.29
Mg	0.28	0.01	0.01	0.01	0.00	0.00
Ca	0.74	0.70	0.68	0.74	0.29	0.32
Mn	0.00	0.00	0.00	0.00	0.00	0.00
Fe	0.13	0.02	0.02	0.02	0.01	0.02
Ba	0.00	0.00	0.00	0.00	0.01	0.00
Na	0.24	0.31	0.32	0.26	0.64	0.64
K	0.01	0.01	0.01	0.01	0.06	0.04
Total	5.09	5.00	5.00	5.00	4.99	4.99

Name	93L97	93L97	93L97	93L125	93L125	93L125
Mineral	Plagioclase	Plagioclase	Plagioclase	Plagioclase	Plagioclase	Plagioclase
SiO_2	48.65	47.71	49.05	52.22	53.88	63.05
TiO_2	0.03	0.03	0.04	0.05	0.10	0.11
Al_2O_3	31.66	32.28	30.81	28.71	27.84	22.41
MgO	0.24	0.23	0.21	0.13	0.02	0.05
CaO	15.89	16.41	15.21	12.75	11.18	7.29
MnO	0.00	0.00	0.00	0.01	0.00	0.00
FeO	0.46	0.42	0.44	0.73	0.92	0.95
BaO	0.00	0.02	0.00	0.00	0.04	0.08
Na_2O	2.50	2.15	2.82	4.13	5.11	5.74
K2O	0.15	0.12	0.19	0.32	0.40	0.66
Total	99.58	99.37	98.76	99.05	99.48	100.33
Formula units	8	8	8	8	8	8
Si	2.24	2.21	2.28	2.40	2.46	2.79
Ti	0.00	0.00	0.00	0.00	0.00	0.00
Al	1.70	1.74	1.67	1.54	1.48	1.16
Mg	0.02	0.02	0.01	0.01	0.00	0.00
Ca	0.78	0.81	0.76	0.63	0.55	0.35
Mn	0.00	0.00	0.00	0.00	0.00	0.00
Fe	0.02	0.02	0.02	0.03	0.04	0.04
Ba	0.00	0.00	0.00	0.00	0.00	0.00
Na	0.22	0.19	0.25	0.37	0.45	0.49
K	0.01	0.01	0.01	0.02	0.02	0.04
Total	5.00	4.99	5.00	5.00	5.01	4.87

Name	93L53	93L53	93L125	93L125	93L125	93L53
Mineral	Plagioclase	Plagioclase	Plagioclase	Plagioclase	Plagioclase	Plagioclase
SiO_2	51.42	55.08	52.51	52.98	51.71	51.31
TiO_2	0.06	0.15	0.07	0.05	0.03	0.07
Al_2O_3	30.41	27.78	28.64	28.53	29.17	29.86
MgO	0.13	0.08	0.11	0.11	0.13	0.13
CaO	13.89	10.65	12.67	12.62	13.59	13.49
MnO	0.01	0.01	0.01	0.00	0.01	0.00
FeO	0.50	0.64	0.81	0.80	0.84	0.48
BaO	0.02	0.05	0.02	0.03	0.00	0.00
Na_2O	3.56	5.33	4.25	4.24	3.79	3.87
K2O	0.23	0.52	0.34	0.31	0.28	0.29
Total	100.23	100.27	99.41	99.69	99.55	99.49
Formula units	8	8	8	8	8	8
Si	2.34	2.49	2.41	2.42	2.37	2.35
Ti	0.00	0.01	0.00	0.00	0.00	0.00
Al	1.62	1.46	1.53	1.52	1.56	1.60
Mg	0.01	0.01	0.01	0.01	0.01	0.01
Ca	0.68	0.52	0.62	0.62	0.67	0.66
Mn	0.00	0.00	0.00	0.00	0.00	0.00
Fe	0.02	0.02	0.03	0.03	0.03	0.02
Ba	0.00	0.00	0.00	0.00	0.00	0.00
Na	0.31	0.47	0.38	0.38	0.34	0.34
K	0.01	0.03	0.02	0.02	0.02	0.02
Total	4.99	5.00	5.00	4.99	5.00	5.00

Name	93L105	93L125	93L125	93L125	93L125	93L125
Mineral	Plagioclase	Plagioclase	Plagioclase	Plagioclase	Plagioclase	Plagioclase
SiO_2	56.45	53.63	53.55	53.08	52.25	52.47
TiO_2	0.01	0.07	0.10	0.07	0.06	0.05
Al_2O_3	27.04	28.73	28.57	28.65	29.11	28.12
MgO	0.02	0.12	0.12	0.11	0.10	0.10
CaO	10.17	12.49	12.47	12.62	12.99	12.04
MnO	0.00	0.02	0.02	0.00	0.01	0.02
FeO	0.34	0.84	1.08	0.80	0.86	0.79
Na_2O	5.16	4.38	4.47	4.35	4.09	4.41
K_2O	0.78					
Total	100.05	100.27	100.38	99.68	99.47	98.04
Formula Units	8	8	8	8	8	8
Si	2.54	2.43	2.43	2.42	2.39	2.43
Al	1.42	1.52	1.51	1.52	1.55	1.52
Mg	0.00	0.01	0.01	0.01	0.01	0.01
Ca	0.49	0.61	0.61	0.62	0.64	0.60
Fe	0.01	0.03	0.04	0.03	0.03	0.03
Ba	0.00	0.00	0.00	0.00	0.00	0.00
Na	0.45	0.38	0.39	0.38	0.36	0.40
K	0.04					
Total	4.97	4.98	4.99	4.99	4.99	4.98

Name	93L125	93L125	93L27	93L27	93L125
Mineral	Plagioclase	Plagioclase	Plagioclase	Plagioclase	Plagioclase
SiO_2	52.78	52.55	51.40	49.83	52.30
TiO_2	0.06	0.08	0.07	0.03	0.07
Al_2O_3	28.15	28.40	30.12	31.12	28.32
MgO	0.13	0.13	0.20	0.17	0.11
CaO	12.46	12.71	13.49	14.78	12.56
MnO	0.02	0.02	0.00	0.01	0.02
FeO	0.95	0.81	0.88	0.59	0.95
Na_2O	4.40	4.33	3.87	3.29	4.25
Total	98.93	99.02	100.12	99.82	98.84
Formula Units	8	8	8	8	8
Si	2.43	2.41	2.34	2.28	2.41
Al	1.51	1.52	1.60	1.67	1.53
Mg	0.01	0.01	0.01	0.01	0.01
Ca	0.61	0.63	0.66	0.73	0.62
Fe					
Ba	0.04	0.03	0.03	0.02	0.04
Na	0.39	0.39	0.34	0.29	0.38
Total	4.99	4.99	5.00	5.00	4.99

Name	93L27	93L105	93L83	93L83	93L83	93L83
Mineral	Plagioclase	Plagioclase	Alkali feld.	Alkali feld.	Alkali feld.	Alkali feld.
SiO_2	49.65	57.21	65.50	65.28	64.53	64.65
TiO_2	0.27	0.01	0.09	0.04	0.06	0.50
Al_2O_3	24.66	26.11	18.61	20.47	19.04	18.74
MgO	3.95	0.02	0.14	0.17	0.14	0.02
CaO	14.83	9.32	0.25	1.58	1.31	0.42
MnO	0.06	0.00	0.00	0.01	0.04	0.01
FeO	3.42	0.34	1.95	0.28	1.29	2.11
BaO	0.02	0.08	0.02	0.11	0.06	0.00
Na_2O	2.67	5.52	6.30	7.92	7.23	7.34
K_2O	0.13	0.95	7.22	4.31	6.03	6.34
Total	99.75	99.56	100.09	100.18	99.73	100.13
Formula Units	8	8	8	8	8	8
Si	2.33	2.59	2.96	2.91	2.93	2.93
Ti	0.01	0.00	0.00	0.00	0.00	0.02
Al	1.35	1.39	0.98	1.06	1.01	0.99
Mg	0.28	0.00	0.01	0.01	0.01	0.00
Ca	0.74	0.45	0.01	0.08	0.06	0.02
Mn	0.00	0.00	0.00	0.00	0.00	0.00
Fe	0.13	0.01	0.07	0.01	0.05	0.08
Ba	0.00	0.00	0.00	0.00	0.00	0.00
Na	0.24	0.48	0.55	0.68	0.64	0.64
K	0.01	0.06	0.42	0.25	0.35	0.37
Total	5.09	4.99	5.01	5.01	5.04	5.05

Name	93L83	93L44	93L44	93L44	93L44	93L44
Mineral	Alkali feld.	Alkali feld.	Alkali feld.	Alkali feld.	Alkali feld.	Alkali feld.
SiO_2	66.39	65.69	65.55	65.33	65.21	65.13
TiO_2	0.07	0.01	0.02	0.02	0.04	0.00
Al_2O_3	18.08	19.14	18.99	19.21	19.07	18.98
MgO	0.15	0.00	0.00	0.00	0.00	0.00
CaO	0.31	0.71	0.58	0.78	0.78	0.60
MnO	0.01	0.00	0.00	0.01	0.00	0.01
FeO	1.44	0.10	0.10	0.14	0.11	0.11
BaO	0.04	0.33	0.26	0.55	0.51	0.37
Na_2O	6.47	3.95	3.88	3.91	3.97	3.78
K_2O	6.44	10.62	10.70	10.34	10.38	10.63
Total	99.39	100.55	100.06	100.28	100.07	99.60
Formula Units	8	8	8	8	8	8
Si	3.00	2.97	2.98	2.97	2.97	2.98
Ti	0.00	0.00	0.00	0.00	0.00	0.00
Al	0.95	1.02	1.02	1.03	1.02	1.02
Mg	0.01	0.00	0.00	0.00	0.00	0.00
Ca	0.02	0.03	0.03	0.04	0.04	0.03
Mn	0.00	0.00	0.00	0.00	0.00	0.00
Fe	0.05	0.00	0.00	0.01	0.00	0.00
Ba	0.00	0.01	0.01	0.01	0.01	0.01
Na	0.57	0.35	0.34	0.34	0.35	0.34
K	0.37	0.61	0.62	0.60	0.60	0.62
Total	4.97	5.00	5.00	4.99	5.00	4.99

Name	93L44	93L44	93L44	93L44	93L44	93L44
Mineral	Alkali feld.	Alkali feld.	Alkali feld.	Alkali feld.	Alkali feld.	Alkali feld.
SiO_2	65.21	65.69	65.55	64.12	62.14	65.61
TiO_2	0.03	0.01	0.02	0.04	0.01	0.01
Al_2O_3	19.16	19.14	18.99	19.64	23.10	19.00
MgO	0.00	0.00	0.00	0.00	0.00	0.00
CaO	0.74	0.71	0.58	1.12	5.23	0.70
MnO	0.00	0.00	0.00	0.00	0.00	0.00
FeO	0.12	0.10	0.10	0.16	0.30	0.13
BaO	0.49	0.33	0.26	1.05	0.02	0.40
Na_2O	3.90	3.95	3.88	3.86	7.32	3.91
K_2O	10.38	10.62	10.70	9.96	2.07	10.45
Total	100.03	100.55	100.06	99.95	100.19	100.22
Formula Units	8	8	8	8	8	8
Si	2.97	2.97	2.98	2.93	2.77	2.98
Ti	0.00	0.00	0.00	0.00	0.00	0.00
Al	1.03	1.02	1.02	1.06	1.21	1.02
Mg	0.00	0.00	0.00	0.00	0.00	0.00
Ca	0.04	0.03	0.03	0.06	0.25	0.03
Mn	0.00	0.00	0.00	0.00	0.00	0.00
Fe	0.01	0.00	0.00	0.01	0.01	0.01
Ba	0.01	0.01	0.01	0.02	0.00	0.01
Na	0.34	0.35	0.34	0.34	0.63	0.34
K	0.60	0.61	0.62	0.58	0.12	0.61
Total	4.99	5.00	5.00	5.00	5.00	4.99

Name	93L44	93L44	93L44	93L112	93L112	93L112
Mineral	Alkali feld.	Alkali feld.	Alkali feld.	Alkali feld.	Alkali feld.	Alkali feld.
SiO_2	65.52	65.51	65.21	64.92	65.32	64.31
TiO_2	0.02	0.03	0.03	0.02	0.05	0.04
Al_2O_3	19.11	19.06	19.16	19.11	18.74	18.99
MgO	0.00	0.00	0.00	0.01	0.00	0.00
CaO	0.72	0.66	0.74	0.43	0.33	0.36
MnO	0.00	0.00	0.00	0.01	0.00	0.00
FeO	0.12	0.10	0.12	0.09	0.08	0.08
BaO	0.40	0.39	0.49	1.82	1.00	2.32
Na_2O	3.89	3.88	3.90	3.31	3.06	2.97
K_2O	10.47	10.56	10.38	11.02	11.71	11.20
Total	100.25	100.20	100.03	100.73	100.29	100.25
Formula Units	8	8	8	8	8	8
Si	2.97	2.97	2.97	2.97	2.98	2.96
Ti	0.00	0.00	0.00	0.00	0.00	0.00
Al	1.02	1.02	1.03	1.03	1.01	1.03
Mg	0.00	0.00	0.00	0.00	0.00	0.00
Ca	0.04	0.03	0.04	0.02	0.02	0.02
Mn	0.00	0.00	0.00	0.00	0.00	0.00
Fe	0.00	0.00	0.01	0.00	0.00	0.00
Ba	0.01	0.01	0.01	0.03	0.02	0.04
Na	0.34	0.34	0.34	0.29	0.27	0.27
K	0.61	0.61	0.60	0.64	0.68	0.66
Total	4.99	4.99	4.99	4.99	4.99	4.98

Name	93L112	93L112	93L112	93L112	93L112	93L83
Mineral	Alkali feld.	Alkali feld.	Alkali feld.	Alkali feld.	Alkali feld.	Alkali feld.
SiO_2	65.31	65.33	63.37	65.90	64.44	65.41
TiO_2	0.02	0.04	0.03	0.01	0.02	0.04
Al_2O_3	19.07	18.67	18.99	18.77	18.81	19.03
MgO	0.00	0.00	0.00	0.00	0.00	0.01
CaO	0.45	0.23	0.37	0.40	0.33	0.30
MnO	0.00	0.00	0.01	0.02	0.00	0.00
FeO	0.10	0.07	0.10	0.08	0.08	0.69
BaO	1.42	1.46	2.23	0.70	1.30	0.04
Na_2O	3.34	3.11	3.06	3.20	3.08	6.90
K_2O	11.04	11.38	11.26	11.45	11.51	7.06
Total	100.74	100.29	99.42	100.53	99.57	99.48
Formula Units	8	8	8	8	8	8
Si	2.97	2.99	2.95	2.99	2.97	2.96
Ti	0.00	0.00	0.00	0.00	0.00	0.00
Al	1.02	1.01	1.04	1.01	1.02	1.01
Mg	0.00	0.00	0.00	0.00	0.00	0.00
Ca	0.02	0.01	0.02	0.02	0.02	0.01
Mn	0.00	0.00	0.00	0.00	0.00	0.00
Fe	0.00	0.00	0.00	0.00	0.00	0.03
Ba	0.03	0.03	0.04	0.01	0.02	0.00
Na	0.30	0.28	0.28	0.28	0.28	0.61
K	0.64	0.66	0.67	0.66	0.68	0.41
Total	4.98	4.98	5.00	4.98	4.99	5.03

Name	93L83	93L83	93L83	93L83	93L83	93L83
Mineral	Alkali feld.	Alkali feld.	Alkali feld.	Alkali feld.	Alkali feld.	Alkali feld.
SiO_2	66.39	65.50	65.28	64.53	64.65	71.19
TiO_2	0.07	0.09	0.04	0.06	0.50	0.04
Al_2O_3	18.08	18.61	20.47	19.04	18.74	15.93
MgO	0.15	0.14	0.17	0.14	0.02	0.00
CaO	0.31	0.25	1.58	1.31	0.42	0.24
MnO	0.01	0.00	0.01	0.04	0.01	0.00
FeO	1.44	1.95	0.28	1.29	2.11	0.77
BaO	0.04	0.02	0.11	0.06	0.00	0.01
Na_2O	6.47	6.30	7.92	7.23	7.34	5.94
K2O	6.44	7.22	4.31	6.03	6.34	5.85
Total	99.39	100.09	100.18	99.73	100.13	99.96
Formula units	8	8	8	8	8	8
Si	3.00	2.96	2.91	2.93	2.93	3.15
Ti	0.00	0.00	0.00	0.00	0.02	0.00
Al	0.95	0.98	1.06	1.01	0.99	0.82
Mg	0.01	0.01	0.01	0.01	0.00	0.00
Ca	0.02	0.01	0.08	0.06	0.02	0.01
Mn	0.00	0.00	0.00	0.00	0.00	0.00
Fe	0.05	0.07	0.01	0.05	0.08	0.03
Ba	0.00	0.00	0.00	0.00	0.00	0.00
Na	0.57	0.55	0.68	0.64	0.64	0.51
K	0.37	0.42	0.25	0.35	0.37	0.33
Total	4.97	5.01	5.01	5.04	5.05	4.85

Name	93L78	93L78	93L78	93L78	93L39	93L39
Mineral	Alkali feld.	Alkali feld.	Alkali feld.	Alkali feld.	Alkali feld.	Alkali feld.
SiO_2	59.68	62.25	62.60	61.81	66.98	67.07
TiO_2						
Al_2O_3	24.47	22.81	22.61	23.40	19.00	19.13
MgO						
CaO	6.63	4.53	4.26	5.28	0.21	0.28
MnO						
FeO	0.46	0.32	0.34	0.53	0.15	0.14
BaO	0.32	0.57	0.73	0.29	0.00	0.04
Na_2O	7.24	7.22	7.76	7.07	5.84	6.00
K2O	1.09	2.76	2.22	2.35	8.57	8.28
Total	99.90	100.47	100.51	100.74	100.74	100.93
Formula units	8	8	8	8	8	8
Si	2.68	2.78	2.79	2.75	2.99	2.99
Al	1.30	1.20	1.19	1.23	1.00	1.01
Ca	0.32	0.22	0.20	0.25	0.01	0.01
Fe	0.02	0.01	0.01	0.02	0.01	0.01
Ba	0.01	0.01	0.01	0.01	0.00	0.00
Na	0.63	0.63	0.67	0.61	0.51	0.52
K	0.06	0.16	0.13	0.13	0.49	0.47
Total	5.02	5.01	5.01	5.01	5.00	5.00

Name	93L39	93L39	93L39	93L39	93L39	93L39
Mineral	Alkali feld.	Alkali feld.	Alkali feld.	Alkali feld.	Alkali feld.	Alkali feld.
SiO_2	66.51	66.37	66.39	66.12	65.97	66.73
TiO_2						
Al_2O_3	18.82	18.87	18.87	18.95	18.81	19.15
MgO						
CaO	0.24	0.22	0.26	0.23	0.28	0.31
MnO						
FeO	0.14	0.14	0.13	0.13	0.15	0.12
BaO	0.00	0.03	0.00	0.00	0.07	0.13
Na_2O	5.67	5.91	5.92	5.92	5.86	6.09
K2O	8.76	8.52	8.42	8.36	8.11	8.16
Total	100.13	100.06	99.98	99.71	99.24	100.69
Formula units	8	8	8	8	8	8
Si	2.99	2.99	2.99	2.99	2.99	2.98
Al	1.00	1.00	1.00	1.01	1.01	1.01
Ca	0.01	0.01	0.01	0.01	0.01	0.02
Fe	0.01	0.01	0.01	0.01	0.01	0.01
Ba	0.00	0.00	0.00	0.00	0.00	0.00
Na	0.49	0.52	0.52	0.52	0.52	0.53
K	0.50	0.49	0.48	0.48	0.47	0.47
Total	5.01	5.01	5.01	5.01	5.00	5.01

Name	93L39	93L39	93L39	93L39	93L39	93L39
Mineral	Alkali feld.	Alkali feld.	Alkali feld.	Alkali feld.	Alkali feld.	Alkali feld.
SiO_2	66.59	67.47	66.62	66.29	66.65	66.71
TiO_2						
Al_2O_3	19.05	19.23	19.03	18.79	18.88	18.88
MgO						
CaO	0.29	0.27	0.28	0.24	0.20	0.24
MnO						
FeO	0.15	0.15	0.12	0.14	0.15	0.13
BaO	0.00	0.00	0.00	0.00	0.00	0.06
Na_2O	6.12	6.01	6.01	5.91	5.83	5.84
K2O	7.98	8.30	8.21	8.34	8.60	8.45
Total	100.17	101.42	100.27	99.71	100.32	100.29
Formula units	8	8	8	8	8	8
Si	2.99	2.99	2.99	2.99	2.99	2.99
Al	1.01	1.01	1.01	1.00	1.00	1.00
Ca	0.01	0.01	0.01	0.01	0.01	0.01
Fe	0.01	0.01	0.01	0.01	0.01	0.01
Ba	0.00	0.00	0.00	0.00	0.00	0.00
Na	0.53	0.52	0.52	0.52	0.51	0.51
K	0.46	0.47	0.47	0.48	0.49	0.48
Total	5.00	5.00	5.01	5.01	5.01	5.00

Name	93L105	93L105	93L105	93L105	93L105	93L105
Mineral	Alkali feld.	Alkali feld.	Alkali feld.	Alkali feld.	Alkali feld.	Alkali feld.
SiO_2	63.40	64.36	65.33	63.45	64.25	65.49
TiO_2	0.03	0.03	0.04	0.02	0.02	0.04
Al_2O_3	18.89	18.98	18.31	19.08	18.72	18.45
MgO	0.01	0.00	0.00	0.00	0.00	0.00
CaO	0.42	0.35	0.23	0.36	0.36	0.34
MnO	0.01	0.01	0.00	0.00	0.00	0.00
FeO	0.07	0.11	0.10	0.08	0.10	0.09
BaO	3.09	1.99	1.45	2.76	1.99	0.95
Na_2O	2.75	2.78	2.62	2.86	2.61	2.71
K_2O	10.73	11.44	11.69	11.00	11.51	12.04
Total	99.40	100.03	99.76	99.60	99.54	100.09
Formula Units	8	8	8	8	8	8
Si	2.96	2.97	3.00	2.95	2.98	3.00
Ti	0.00	0.00	0.00	0.00	0.00	0.00
Al	1.04	1.03	0.99	1.05	1.02	1.00
Mg	0.00	0.00	0.00	0.00	0.00	0.00
Ca	0.02	0.02	0.01	0.02	0.02	0.02
Mn	0.00	0.00	0.00	0.00	0.00	0.00
Fe	0.00	0.00	0.00	0.00	0.00	0.00
Ba	0.06	0.04	0.03	0.05	0.04	0.02
Na	0.25	0.25	0.23	0.26	0.24	0.24
K	0.64	0.67	0.69	0.65	0.68	0.70
Total	4.96	4.98	4.96	4.98	4.97	4.97

Name	93L99	93L99	93L99	93L99	93L99	93L60
Mineral	Alkali feld.	Alkali feld.	Alkali feld.	Alkali feld.	Alkali feld.	Alkali feld.
SiO_2	64.92	65.71	64.84	64.73	63.37	69.39
TiO_2	0.06	0.02	0.05	0.04	0.08	0.01
Al_2O_3	18.82	18.44	18.66	18.76	19.28	19.46
MgO	0.00	0.00	0.00	0.00	0.00	0.01
CaO	0.40	0.30	0.26	0.33	0.45	0.01
MnO	0.01	0.01	0.00	0.00	0.00	0.00
FeO	0.08	0.10	0.09	0.10	0.09	0.03
BaO	2.03	1.08	1.64	1.71	3.43	0.00
Na_2O	2.68	2.72	2.43	2.38	2.77	11.78
K_2O	11.46	11.84	12.19	12.05	10.94	0.06
Total	100.45	100.21	100.16	100.10	100.41	100.75
Formula Units	8	8	8	8	8	8
Si	2.98	3.00	2.98	2.98	2.94	3.01
Ti	0.00	0.00	0.00	0.00	0.00	0.00
Al	1.02	0.99	1.01	1.02	1.05	0.99
Mg	0.00	0.00	0.00	0.00	0.00	0.00
Ca	0.02	0.02	0.01	0.02	0.02	0.00
Mn	0.00	0.00	0.00	0.00	0.00	0.00
Fe	0.00	0.00	0.00	0.00	0.00	0.00
Ba	0.04	0.02	0.03	0.03	0.06	0.00
Na	0.24	0.24	0.22	0.21	0.25	0.99
K	0.67	0.69	0.72	0.71	0.65	0.00
Total	4.97	4.97	4.98	4.97	4.98	4.99

Name	93L28	93L28	93L28	93L28	93L28	93L28
Mineral	Alkali feld.	Alkali feld.	Alkali feld.	Alkali feld.	Alkali feld.	Alkali feld.
SiO_2	66.91	67.30	67.00	66.79	66.53	66.74
TiO_2						
Al_2O_3	18.68	18.62	18.67	18.56	18.67	18.63
MgO						
CaO	0.07	0.05	0.04	0.06	0.08	0.07
MnO				0.01		0.01
FeO	0.17	0.14	0.15	0.19	0.19	0.17
BaO	0.03		0.02			
Na_2O	6.32	6.32	6.12	6.36	6.54	6.31
K_2O	7.80	7.97	8.15	7.70	7.44	7.91
Total	99.96	100.41	100.14	99.65	99.45	99.84
Formula Units	8	8	8	8	8	8
Si	3.00	3.01	3.01	3.01	3.00	3.00
Ti						
Al	0.99	0.98	0.99	0.99	0.99	0.99
Mg	0.00	0.00	0.00	0.00	0.00	0.00
Ca	0.00	0.00	0.00	0.00	0.00	0.00
Mn	0.00	0.00	0.00	0.00	0.00	0.00
Fe	0.01	0.01	0.01	0.01	0.01	0.01
Ba	0.00	0.00	0.00	0.00	0.00	0.00
Na	0.55	0.55	0.53	0.56	0.57	0.55
K	0.45	0.46	0.47	0.44	0.43	0.45
Total	5.00	5.00	5.00	5.00	5.00	5.01

Name	93L28	93L28	93L28	93L28	93L28	93L28
Mineral	Alkali feld.	Alkali feld.	Alkali feld.	Alkali feld.	Alkali feld.	Alkali feld.
SiO_2	66.83	66.70	66.40	66.98	66.89	67.30
TiO_2						
Al_2O_3	18.76	18.66	18.64	18.62	18.50	18.62
MgO	0.00	0.00	0.00	0.00	0.00	0.00
CaO	0.07	0.08	0.06	0.07	0.07	0.07
MnO	0.00	0.00	0.00	0.01	0.00	0.02
FeO	0.16	0.18	0.18	0.17	0.17	0.17
BaO	0.00	0.00	0.00	0.00	0.00	0.02
Na_2O	6.51	6.48	6.25	6.28	6.49	6.47
K_2O	7.64	7.75	7.77	7.89	7.63	7.67
Total	99.97	99.84	99.30	100.02	99.75	100.33
Formula Units	8	8	8	8	8	8
Si	3.00	3.00	3.00	3.01	3.01	3.01
Ti						
Al	0.99	0.99	0.99	0.99	0.98	0.98
Mg	0.00	0.00	0.00	0.00	0.00	0.00
Ca	0.00	0.00	0.00	0.00	0.00	0.00
Mn	0.00	0.00	0.00	0.00	0.00	0.00
Fe	0.01	0.01	0.01	0.01	0.01	0.01
Ba	0.00	0.00	0.00	0.00	0.00	0.00
Na	0.57	0.57	0.55	0.55	0.57	0.56
K	0.44	0.45	0.45	0.45	0.44	0.44
Total	5.01	5.01	5.00	5.00	5.00	5.00

Name	93L28	93L28	93L28	93L39	93L39	93L39
Mineral	Alkali feld.	Alkali feld.	Alkali feld.	Alkali feld.	Alkali feld.	Alkali feld.
SiO_2	66.89	67.04	66.86	66.25	66.62	66.30
TiO_2						
Al_2O_3	18.50	18.69	18.66	18.68	18.77	18.64
MgO						
CaO	0.07	0.06	0.06	0.22	0.23	0.25
MnO		0.01				
FeO	0.17	0.20	0.17	0.13	0.14	0.15
BaO			0.02	0.01		
Na_2O	6.49	6.16	6.26	5.76	5.64	5.88
K_2O	7.63	7.87	7.96	8.43	8.48	8.39
Total	99.75	100.02	99.99	99.47	99.86	99.62
Formula Units	8	8	8	8	8	8
Si	3.01	3.01	3.00	3.00	3.00	3.00
Ti						
Al	0.98	0.99	0.99	1.00	1.00	0.99
Mg	0.00	0.00	0.00	0.00	0.00	0.00
Ca	0.00	0.00	0.00	0.01	0.01	0.01
Mn	0.00	0.00	0.00	0.00	0.00	0.00
Fe	0.01	0.01	0.01	0.01	0.01	0.01
Ba	0.00	0.00	0.00	0.00	0.00	0.00
Na	0.57	0.54	0.55	0.51	0.49	0.52
K	0.44	0.45	0.46	0.49	0.49	0.48
Total	5.00	4.99	5.00	5.00	4.99	5.01

Name	93L39	93L39	93L39	93L39	93L39	93L39
Mineral	Alkali feld.	Alkali feld.	Alkali feld.	Alkali feld.	Alkali feld.	Alkali feld.
SiO_2	67.08	66.68	66.52	67.27	66.05	65.88
TiO_2	0.00	0.00	0.03	0.00	0.01	0.02
Al_2O_3	18.87	18.75	18.85	18.88	18.79	18.83
MgO	0.01	0.01	0.00	0.00	0.00	0.00
CaO	0.21	0.20	0.27	0.28	0.31	0.27
MnO	0.00	0.01	0.00	0.00	0.01	0.01
FeO	0.13	0.12	0.15	0.14	0.15	0.15
BaO	0.00	0.00	0.00	0.00	0.02	0.00
Na_2O	5.75	5.61	5.87	5.98	6.01	5.83
K_2O	8.50	8.70	8.33	8.05	8.26	8.45
Total	100.55	100.08	100.02	100.60	99.61	99.44
Formula Units	8	8	8	8	8	8
Si	3.00	3.00	2.99	3.00	2.99	2.99
Ti	0.00	0.00	0.00	0.00	0.00	0.00
Al	1.00	0.99	1.00	0.99	1.00	1.01
Mg						
Ca	0.01	0.01	0.01	0.01	0.02	0.01
Mn						
Fe	0.01	0.01	0.01	0.01	0.01	0.01
Ba						
Na	0.50	0.49	0.51	0.52	0.53	0.51
K	0.49	0.50	0.48	0.46	0.48	0.49
Total	4.99	5.00	5.00	4.99	5.01	5.01

Name	93L39	93L36	93L36	93L36	93L36	93L36
Mineral	Alkali feld.	Alkali feld.	Alkali feld.	Alkali feld.	Alkali feld.	Alkali feld.
SiO_2	67.23	66.72	66.57	66.11	66.01	66.90
TiO_2	0.02	0.01	0.00	0.01	0.00	0.00
Al_2O_3	18.83	18.68	18.68	18.74	18.81	18.99
MgO	0.00	0.00	0.00	0.00	0.00	0.00
CaO	0.24	0.16	0.25	0.29	0.32	0.40
MnO	0.00	0.00	0.01	0.00	0.00	0.00
FeO	0.14	0.13	0.12	0.10	0.14	0.13
BaO	0.02	0.00	0.00	0.02	0.00	0.01
Na_2O	5.84	5.26	5.69	5.95	6.15	6.29
K_2O	8.44	9.27	8.55	8.35	7.95	7.58
Total	100.75	100.24	99.88	99.57	99.38	100.29
Formula Units	8	8	8	8	8	8
Si	3.00	3.00	3.00	2.99	2.99	2.99
Ti	0.00	0.00	0.00	0.00	0.00	0.00
Al	0.99	0.99	0.99	1.00	1.00	1.00
Mg	0.00	0.00	0.00	0.00	0.00	0.00
Ca	0.01	0.01	0.01	0.01	0.02	0.02
Mn	0.00	0.00	0.00	0.00	0.00	0.00
Fe	0.01	0.01	0.01	0.00	0.01	0.01
Ba	0.00	0.00	0.00	0.00	0.00	0.00
Na	0.51	0.46	0.50	0.52	0.54	0.55
K	0.48	0.53	0.49	0.48	0.46	0.43
Total	5.00	5.00	5.00	5.01	5.01	5.00

Name	93L36	93L36	93L83	93L83	93L83	93L83
Mineral	Alkali feld.	Alkali feld.	Alkali feld.	Alkali feld.	Alkali feld.	Alkali feld.
SiO_2	66.38	66.38	65.31	64.87	65.60	65.50
TiO_2	0.01		0.05	0.04	0.05	0.04
Al_2O_3	18.91	18.52	20.48	20.26	20.45	20.21
MgO						
CaO	0.30	0.18	1.65	2.45	1.64	1.49
MnO						
FeO	0.12	0.15	0.19	0.14	0.17	0.16
BaO	0.00	0.02	0.12	0.14	0.10	0.12
Na_2O	5.93	5.57	7.60	7.30	7.29	7.72
K_2O	8.16	8.64	4.18	4.22	4.24	3.95
Total	99.80	99.46	99.59	99.41	99.54	99.18
Formula Units	8	8	8	8	8	8
Si	2.99	3.01	2.92	2.91	2.93	2.94
Ti						
Al	1.00	0.99	1.08	1.07	1.08	1.07
Mg						
Ca	0.01	0.01	0.08	0.12	0.08	0.07
Mn						
Fe	0.01	0.01	0.01	0.01	0.01	0.01
Ba						
Na	0.52	0.49	0.66	0.64	0.63	0.67
K	0.47	0.50	0.24	0.24	0.24	0.23
Total	5.00	5.00	4.99	4.99	4.97	4.98

Name	93L83	93L83	93L83	93L83	93L83	93L83
Mineral	Alkali feld.	Alkali feld.	Alkali feld.	Alkali feld.	Alkali feld.	Alkali feld.
SiO_2	65.23	65.95	71.19	65.41	66.20	65.78
TiO_2	0.01	0.04	0.04	0.04	0.05	0.03
Al_2O_3	20.19	20.13	15.93	19.03	20.16	19.85
MgO	0.01		0.00	0.01		
CaO	1.17	1.32	0.24	0.30	1.28	1.16
MnO	0.01		0.00	0.00		
FeO	0.19	0.19	0.77	0.69	0.17	0.15
BaO	0.08	0.11	0.01	0.04	0.14	0.06
Na_2O	7.54	7.22	5.94	6.90	7.10	6.55
K_2O	5.24	4.61	5.85	7.06	4.53	6.09
Total	99.69	99.57	99.96	99.48	99.62	99.66
Formula Units	8	8	8	8	8	8
Si	2.93	2.95	3.15	2.96	2.95	2.95
Ti	0.00	0.00	0.00	0.00	0.00	0.00
Al	1.06	1.06	0.82	1.01	1.06	1.05
Mg	0.00		0.00	0.00		
Ca	0.06	0.06	0.01	0.01	0.06	0.06
Mn	0.00		0.00	0.00		
Fe	0.01	0.01	0.03	0.03	0.01	0.01
Ba	0.00	0.00	0.00	0.00	0.00	0.00
Na	0.66	0.63	0.51	0.61	0.61	0.57
K	0.30	0.26	0.33	0.41	0.26	0.35
Total	5.01	4.97	4.85	5.03	4.95	4.98

Name	92U12	93L93	93L97	93L97	93L125	93L125
Mineral	Augite	Augite	Pigeonite	Pigeonite	Augite	Augite
SiO_2	49.92	52.34	54.76	53.79	48.99	48.45
TiO_2	0.83	0.48	0.19	0.17	1.14	0.72
Al_2O_3	5.92	1.56	1.62	1.77	3.70	1.15
Cr_2O_3			0.33	0.42	0.00	0.00
MgO	14.76	16.96	29.22	29.06	10.79	8.54
CaO	19.19	16.93	2.00	2.09	10.60	13.62
MnO	0.21	0.25	0.27	0.25	0.51	0.58
FeO*	8.40	11.03	11.97	11.50	23.74	26.10
Na_2O	0.60	0.18	0.02	0.03	0.53	0.13
K2O	0.00	0.01	0.01	0.00	0.09	0.04
Total	99.82	99.74	100.38	99.08	100.12	99.34
Formula units	6	6	6	6	6	6
Si	1.84	1.94	1.94	1.93	1.88	1.92
Ti	0.02	0.01	0.00	0.00	0.03	0.02
Al	0.26	0.07	0.07	0.07	0.17	0.05
Cr	0.00	0.00	0.01	0.01	0.00	0.00
Mg	0.81	0.94	1.54	1.55	0.62	0.50
Ca	0.76	0.67	0.08	0.08	0.44	0.58
Mn	0.01	0.01	0.01	0.01	0.02	0.02
Fe2+	0.22	0.29	0.30	0.29	0.65	0.74
Fe3+	0.04	0.05	0.05	0.05	0.11	0.13
Na	0.01	0.00	0.00	0.00	0.01	0.00
K	0.00	0.00	0.00	0.00	0.00	0.00
Total	3.97	3.98	3.99	4.00	3.93	3.96

Name	93L125	93L125	93L125	93L125	93L53	93L104
Mineral	Pigeonite	Augite	Augite	Augite	Augite	Augite
SiO_2	49.94	50.21	49.78	50.29	49.73	49.56
TiO_2	0.45	0.69	0.82	0.76	1.57	1.05
Al_2O_3	0.84	1.36	1.56	1.40	2.52	2.05
Cr_2O_3	0.02	0.02	0.00	0.00	0.04	0.05
MgO	16.46	12.76	13.19	12.31	12.77	15.38
CaO	5.29	16.23	13.18	17.28	20.38	17.35
MnO	0.58	0.43	0.52	0.40	0.28	0.30
FeO*	25.28	17.58	20.62	17.05	12.48	12.55
Na_2O	0.03	0.16	0.14	0.16	0.37	0.22
K2O	0.00	0.00	0.01	0.00	0.00	0.00
Total	98.90	99.46	99.81	99.65	100.15	98.50
Formula units	6	6	6	6	6	6
Si	1.93	1.92	1.91	1.92	1.88	1.89
Ti	0.01	0.02	0.02	0.02	0.04	0.03
Al	0.04	0.06	0.07	0.06	0.11	0.09
Cr	0.00	0.00	0.00	0.00	0.00	0.00
Mg	0.95	0.73	0.75	0.70	0.72	0.87
Ca	0.22	0.67	0.54	0.71	0.82	0.71
Mn	0.02	0.01	0.02	0.01	0.01	0.01
Fe2+	0.69	0.48	0.56	0.46	0.33	0.34
Fe3+	0.12	0.08	0.10	0.08	0.06	0.06
Na	0.00	0.00	0.00	0.00	0.01	0.00
K	0.00	0.00	0.00	0.00	0.00	0.00
Total	3.98	3.98	3.98	3.98	3.98	4.00

Name	93L104	93L104	93L104	93L104	93L104	93L27
Mineral	Augite	Augite	Augite	Augite	Augite	Augite
SiO_2	50.57	50.10	50.34	41.09	51.62	50.16
TiO_2	0.65	0.71	0.77	0.49	0.61	0.90
Al_2O_3	1.84	1.66	2.29	21.57	1.58	2.80
Cr_2O_3	0.04	0.05	0.21	0.00	0.12	0.41
MgO	16.28	15.98	16.11	2.77	16.20	16.36
CaO	16.33	17.80	18.67	8.05	18.80	17.64
MnO	0.31	0.31	0.25	0.10	0.28	0.27
FeO*	12.73	11.62	9.94	20.51	9.85	10.05
Na_2O	0.23	0.21	0.21	3.46	0.19	0.23
K2O	0.01	0.00	0.00	0.30	0.00	0.01
Total	99.00	98.43	98.78	98.38	99.27	98.84
Formula units	6	6	6	6	6	6
Si	1.91	1.90	1.89	1.58	1.93	1.88
Ti	0.02	0.02	0.02	0.01	0.02	0.03
Al	0.08	0.07	0.10	0.97	0.07	0.12
Cr	0.00	0.00	0.01	0.00	0.00	0.01
Mg	0.91	0.90	0.90	0.16	0.90	0.92
Ca	0.66	0.72	0.75	0.33	0.75	0.71
Mn	0.01	0.01	0.01	0.00	0.01	0.01
Fe2+	0.34	0.31	0.27	0.56	0.26	0.27
Fe3+	0.06	0.05	0.05	0.10	0.05	0.05
Na	0.00	0.00	0.00	0.06	0.00	0.00
K	0.00	0.00	0.00	0.00	0.00	0.00
Total	4.00	4.01	4.00	3.79	3.99	3.99

Name	93L104	93L125	93L125	93L125	93L125	93L125
Mineral	Augite	Augite	Augite	Augite	Augite	Augite
SiO_2	49.72	50.45	50.65	49.65	50.30	49.94
TiO_2	1.31	0.49	0.70	0.91	0.37	0.68
Al_2O_3	1.88	0.82	1.41	1.82	0.74	1.38
Cr_2O_3	0.00	0.00	0.02	0.00	0.17	0.12
MgO	14.88	16.67	13.89	12.40	15.95	12.54
CaO	16.03	5.15	15.49	16.61	5.08	16.70
MnO	0.38	0.58	0.42	0.42	0.62	0.42
FeO*	15.72	25.29	17.84	17.89	26.28	17.51
Na_2O		0.06	0.14	0.16	0.05	0.16
K2O						
Total	99.93	99.50	100.55	99.85	99.58	99.44
Formula units	6	6	6	6	6	6
Si	1.88	1.93	1.92	1.90	1.93	1.92
Ti	0.04	0.01	0.02	0.03	0.01	0.02
Al	0.08	0.04	0.06	0.08	0.03	0.06
Cr	0.00	0.00	0.00	0.00	0.01	0.00
Mg	0.84	0.95	0.78	0.71	0.91	0.72
Ca	0.65	0.21	0.63	0.68	0.21	0.69
Mn	0.01	0.02	0.01	0.01	0.02	0.01
Fe2+	0.42	0.69	0.48	0.49	0.72	0.48
Fe3+	0.07	0.12	0.08	0.09	0.13	0.08
Na	0.00	0.00	0.00	0.00	0.00	0.00
K	0.00	0.00	0.00	0.00	0.00	0.00
Total	4.00	3.97	3.99	3.98	3.97	3.98

Name	93L125	93L125	93L125	93L125	93L125	93L125
Mineral	Augite	Augite	Augite	Augite	Augite	Augite
SiO_2	48.75	48.31	49.69	49.69	51.27	48.02
TiO_2			0.85	0.85	0.33	
Al_2O_3	1.31	1.26	1.70	1.70	0.70	1.70
Cr_2O_3			0.17	0.17	0.00	
MgO	16.68		12.91	12.91	18.35	16.01
CaO	15.90	16.31	15.58	15.58	4.66	15.34
MnO			0.44	0.44	0.54	
FeO*	17.04	18.07	18.65	18.65	23.84	18.67
Na_2O	0.16	0.17	0.16	0.16	0.07	0.16
K2O	0.16	0.18				0.09
Total	83.32	84.28	100.15	100.15	99.74	83.99
Formula units	6	6	6	6	6	6
Si	1.86	2.18	1.90	1.90	1.94	1.84
Ti	0.00	0.00	0.02	0.02	0.01	0.00
Al	0.06	0.07	0.08	0.08	0.03	0.08
Cr	0.00	0.00	0.01	0.01	0.00	0.00
Mg	0.95	0.00	0.73	0.73	1.03	0.92
Ca	0.65	0.79	0.64	0.64	0.19	0.63
Mn	0.00	0.00	0.01	0.01	0.02	0.00
Fe2+	0.46	0.58	0.51	0.51	0.64	0.51
Fe3+	0.08	0.10	0.09	0.09	0.11	0.09
Na						
K						
Total	4.06	3.73	3.99	3.99	3.98	4.07

Name	93L125	93L125	93L125	93L125	93L125
Mineral	Augite	Augite	Augite	Augite	Augite
SiO_2	48.50	48.46	48.13	49.16	48.39
TiO_2					
Al_2O_3	1.63	0.93	1.24	7.11	0.75
Cr_2O_3					
MgO	14.92	17.78	16.46	11.32	20.13
CaO	16.65	9.87	16.23	9.59	5.40
MnO					
FeO*	18.02	22.85	17.60	21.16	25.28
Na_2O	0.18	0.11	0.14	1.36	0.06
K2O	0.11	0.00	0.19	0.18	0.00
Total	85.08	82.22	83.54	88.68	79.87
Formula units	6	6	6	6	6
Si	1.86	1.86	1.85	1.86	1.85
Ti	0.00	0.00	0.00	0.00	0.00
Al	0.07	0.04	0.06	0.31	0.03
Cr	0.00	0.00	0.00	0.00	0.00
Mg	0.85	1.02	0.94	0.64	1.15
Ca	0.68	0.41	0.67	0.39	0.22
Mn	0.00	0.00	0.00	0.00	0.00
Fe2+	0.49	0.62	0.48	0.57	0.69
Fe3+	0.09	0.11	0.08	0.10	0.12
Na	0.00	0.00	0.00	0.00	0.00
K	0.00	0.00	0.00	0.02	0.00
Total	4.05	4.06	4.08	3.90	4.07

Name	93L83	93L83	93L83	93L83	93L83	93L83
Mineral	Ti-Mag.	Ti-Mag.	Ti-Mag.	Ti-Mag.	Ti-Mag.	Ti-Mag.
SiO_2	0.29	0.22	1.30	0.48	1.75	0.74
TiO_2	16.15	20.34	19.55	18.96	17.39	17.94
Al_2O_3	0.12	0.15	0.30	0.16	0.30	0.21
V_2O_3						
Cr_2O_3	0.00	0.00	0.01	0.01	0.09	0.00
MgO	0.10	0.05	0.24	0.12	0.21	0.14
CaO	0.00	0.05	0.10	0.56	0.05	4.83
MnO	0.57	0.63	1.49	0.86	0.63	1.06
FeO	73.82	68.32	68.30	68.34	70.09	61.67
Na_2O	0.01	0.02	0.00	0.03	0.03	0.05
K_2O	0.08	0.03	0.04	0.03	0.01	0.07
Total	91.27	90.02	91.55	89.75	90.70	86.86
Formula Units	32	32	32	32	32	32
Si	0.11	0.08	0.47	0.17	0.64	0.27
Ti	4.45	5.60	5.38	5.22	4.79	4.94
Al	0.05	0.06	0.13	0.07	0.13	0.09
Cr	0.00	0.00	0.00	0.00	0.03	0.00
Mg	0.05	0.03	0.13	0.06	0.11	0.08
Ca	0.00	0.02	0.04	0.22	0.02	1.89
Mn	0.14	0.16	0.38	0.22	0.16	0.27
Fe	22.60	20.92	20.91	20.92	21.46	18.88
Na	0.01	0.01	0.00	0.02	0.02	0.04
K	0.04	0.02	0.02	0.01	0.00	0.03
Total	27.45	26.90	27.47	26.93	27.36	26.49

Name	93L83	93L83	93L83	93L83	93L83	93L125
Mineral						
SiO_2	0.65	0.28	0.22	0.32	0.47	1.24
TiO_2	19.10	20.47	20.73	20.70	19.07	27.63
Al_2O_3	0.25	0.15	0.10	0.11	0.24	2.42
V_2O_3						
Cr_2O_3	0.00	0.02	0.01	0.00	0.00	0.29
MgO	0.20	0.15	0.07	0.07	0.11	0.08
CaO	0.03	0.04	0.29	0.03	0.06	0.10
MnO	1.21	1.79	0.68	0.85	0.95	0.89
FeO	69.07	68.31	68.16	69.20	69.90	57.32
Na_2O	0.03	0.01	0.01	0.01	0.01	0.03
K_2O	0.02	0.00	0.01	0.01	0.05	0.03
Total	90.73	91.43	90.47	91.49	91.05	90.32
Formula Units	32	32	32	32	32	32
Si	0.24	0.10	0.08	0.12	0.17	0.45
Ti	5.26	5.64	5.71	5.70	5.25	7.61
Al	0.11	0.07	0.04	0.04	0.10	1.03
Cr	0.00	0.01	0.00	0.00	0.00	0.08
Mg	0.11	0.08	0.04	0.04	0.06	0.04
Ca	0.01	0.02	0.11	0.01	0.02	0.04
Mn	0.31	0.45	0.17	0.21	0.24	0.23
Fe	21.14	20.91	20.87	21.18	21.40	17.55
Na	0.02	0.01	0.01	0.01	0.01	0.02
K	0.01	0.00	0.01	0.01	0.02	0.01
Total	27.20	27.28	27.04	27.32	27.27	27.07

Name	93L125	93L125	93L125	93L125	93L125	93L125
Mineral	Ti-Mag.	Ti-Mag.	Ti-Mag.	Ti-Mag.	Ti-Mag.	Ti-Mag.
SiO_2	0.98	2.57	0.71	1.23	1.85	0.80
TiO_2	27.42	26.06	27.23	28.61	29.76	28.84
Al_2O_3	2.40	2.46	2.33	2.24	2.20	2.15
V_2O_3						
Cr_2O_3	0.25	0.28	0.28	0.20	0.19	0.20
MgO	0.06	0.10	0.05	0.07	0.06	0.07
CaO	0.05	0.10	0.06	0.11	0.27	0.14
MnO	0.91	0.72	0.89	0.86	0.98	0.91
FeO	58.40	56.91	59.08	57.50	55.32	57.37
Na_2O	0.06	0.02	0.00	0.03	0.08	0.08
K_2O	0.03	0.21	0.02	0.06	0.05	0.01
Total	90.89	89.67	90.95	91.20	91.14	90.88
Formula Units	32	32	32	32	32	32
Si	0.36	0.94	0.26	0.45	0.68	0.29
Ti	7.55	7.17	7.50	7.88	8.19	7.94
Al	1.03	1.05	1.00	0.96	0.94	0.92
Cr	0.07	0.08	0.08	0.06	0.05	0.06
Mg	0.03	0.05	0.03	0.04	0.03	0.04
Ca	0.02	0.04	0.02	0.04	0.11	0.05
Mn	0.23	0.18	0.23	0.22	0.25	0.23
Fe	17.88	17.42	18.09	17.60	16.94	17.56
Na	0.04	0.01	0.00	0.02	0.05	0.05
K	0.02	0.10	0.01	0.03	0.03	0.00
Total	27.23	27.05	27.21	27.29	27.27	27.15

Name	93L125	93L125	93L125	93L125	93L125	93L53
Mineral	Ti-Mag.	Ti-Mag.	Ti-Mag.	Ti-Mag.	Ti-Mag.	Ti-Mag.
SiO_2	1.67	0.66	0.94	1.81	1.17	0.57
TiO_2	29.24	26.02	28.94	29.22	29.00	20.64
Al_2O_3	2.13	2.73	2.30	2.15	2.22	0.82
V_2O_3						
Cr_2O_3	0.19	0.18	0.16	0.21	0.21	0.08
MgO	0.07	0.06	0.07	0.07	0.05	0.43
CaO	0.29	0.10	0.12	0.29	0.20	0.29
MnO	0.90	0.79	0.89	1.01	0.95	0.58
FeO	55.54	60.52	57.11	55.37	56.88	67.96
Na_2O	0.09	0.03	0.04	0.11	0.08	0.00
K_2O	0.05	0.02	0.04	0.07	0.02	0.00
Total	90.48	91.39	90.88	90.66	91.11	91.56
Formula Units	32	32	32	32	32	32
Si	0.61	0.24	0.34	0.66	0.43	0.21
Ti	8.05	7.16	7.97	8.04	7.98	5.68
Al	0.91	1.16	0.98	0.92	0.95	0.35
Cr	0.05	0.05	0.05	0.06	0.06	0.02
Mg	0.04	0.03	0.04	0.04	0.02	0.24
Ca	0.11	0.04	0.05	0.11	0.08	0.11
Mn	0.23	0.20	0.22	0.25	0.24	0.15
Fe	17.00	18.53	17.49	16.95	17.41	20.81
Na	0.07	0.02	0.03	0.08	0.06	0.00
K	0.02	0.01	0.02	0.03	0.01	0.00
Total	27.10	27.44	27.17	27.15	27.24	27.56

Name	93L53	93L53	93L53	93L53	93L53	92U12
Mineral	Ti-Mag.	Ti-Mag.	Ilmenite	Ti-Mag.	Ilmenite	Ti-Mag.
SiO_2	0.93	0.44	1.06	0.15	0.12	1.75
TiO_2	15.23	15.48	34.41	6.90	44.00	24.32
Al_2O_3	1.04	0.82	0.59	1.40	0.06	2.04
V_2O_3						
Cr_2O_3	0.11	0.10	0.06	0.10	0.00	0.64
MgO	0.28	0.27	0.39	0.21	0.70	1.56
CaO	0.56	0.04	0.76	0.00	0.03	0.15
MnO	0.58	0.66	1.87	0.11	0.80	0.68
FeO	72.76	72.94	53.60	83.66	48.32	63.56
Na_2O		0.03			0.01	0.09
K_2O		0.01				
Total	91.63	90.90	93.10	92.61	94.47	94.82
Formula Units	32	32	32	32	32	32
Si	0.34	0.16	0.39	0.05	0.05	0.64
Ti	4.19	4.26	9.47	1.90	12.11	6.70
Al	0.44	0.35	0.25	0.60	0.02	0.87
Cr	0.03	0.03	0.02	0.03	0.00	0.18
Mg	0.15	0.15	0.21	0.11	0.38	0.85
Ca	0.22	0.02	0.30	0.00	0.01	0.06
Mn	0.15	0.17	0.47	0.03	0.20	0.17
Fe	22.27	22.33	16.41	25.61	14.79	19.46
Na		0.02				0.07
K						
Total	27.80	27.48	27.53	28.33	27.58	28.99

Name	92U12	92U12	92U12	92U12	92U12	92U12
Mineral	Ti-Mag.	Ti-Mag.	Ti-Mag.	Ti-Mag.	Ti-Mag.	Ti-Mag.
SiO_2	0.17	0.16	0.16	0.18	0.17	0.17
TiO_2	26.79	27.50	27.26	26.48	27.33	26.04
Al_2O_3	1.48	1.03	1.44	1.40	1.44	1.64
V_2O_3	0.12	0.08	0.12	0.10	0.07	0.14
Cr_2O_3	0.11	0.05	0.29	0.34	0.48	1.93
MgO	0.05	0.24	0.06	1.04	0.06	0.05
CaO	0.12	0.15	0.07	0.19	0.24	0.18
MnO	1.20	0.70	1.21	0.69	1.04	0.99
FeO	64.30	64.79	64.18	65.30	63.35	63.34
Na_2O	0.04	0.02	0.01	0.00	0.01	0.00
K_2O	0.03	0.03	0.02	0.01	0.02	0.01
Total	94.39	94.74	94.83	95.73	94.22	94.48
Formula Units	32	32	32	32	32	32
Si	0.06	0.06	0.06	0.06	0.06	0.06
Ti	7.37	7.57	7.51	7.29	7.52	7.17
Al	0.63	0.44	0.62	0.60	0.62	0.70
V	0.08	0.06	0.08	0.07	0.05	0.10
Cr	0.03	0.01	0.08	0.10	0.14	0.55
Mg	0.02	0.13	0.03	0.57	0.03	0.03
Ca	0.05	0.06	0.03	0.08	0.09	0.07
Mn	0.30	0.18	0.31	0.17	0.26	0.25
Fe	19.69	19.83	19.65	19.99	19.39	19.39
Na	0.02	0.01	0.01	0.00	0.01	0.00
Total	28.26	28.35	28.37	28.93	28.18	28.33

Name	92U12	92U12	92U12	92U12	92U12	93L44
Mineral	Ti-Mag.	Ti-Mag.	Ti-Mag.	Ti-Mag.	Ti-Mag.	Ilmenite
SiO_2	1.42	0.18	0.17	0.17	0.17	0.07
TiO_2	26.46	26.42	26.96	26.19	26.97	60.58
Al_2O_3	1.70	1.45	1.55	1.65	1.27	0.04
V_2O_3						0.31
Cr_2O_3	0.14	1.57	0.15	0.59	0.32	0.01
MgO	0.67	0.04	0.06	0.06	0.06	0.03
CaO	0.10	0.13	0.12	0.15	0.16	0.00
MnO	1.23	1.21	1.18	0.95	1.27	0.41
FeO	62.18	63.38	64.36	64.18	63.36	35.16
Na_2O	0.11	0.11	0.10	0.12	0.11	0.07
Total	94.01	94.53	94.67	94.09	93.71	96.70
Formula Units	32	32	32	32	32	32
Si	0.52	0.07	0.06	0.06	0.06	0.03
Ti	7.29	7.27	7.42	7.21	7.42	16.68
Al	0.72	0.62	0.66	0.70	0.54	0.02
Cr	0.04	0.45	0.04	0.17	0.09	0.00
Mg	0.36	0.02	0.03	0.03	0.03	0.01
Ca	0.04	0.05	0.05	0.06	0.06	0.00
Mn	0.31	0.31	0.30	0.24	0.32	0.10
Fe	19.04	19.40	19.70	19.65	19.40	10.76
Na	0.08	0.08	0.07	0.08	0.08	0.05
Total	28.40	28.28	28.34	28.22	28.01	27.65

Name	93L44	93L44	93L44	93L44	93L112	93L112
Mineral	Ilmenite	Ti-Mag.	Ilmenite	Ilmenite	Ti-Mag.	Ti-Mag.
SiO_2	0.07	0.19	0.14	0.42	0.25	0.17
TiO_2	58.23	28.79	51.88	58.36	11.69	19.36
Al_2O_3	0.04	1.95	0.05	0.06	2.96	0.93
V_2O_3	0.31	0.17	0.23	0.20	0.05	0.12
Cr_2O_3	0.00	0.01	0.00	0.00	0.00	0.04
MgO	0.04	0.07	0.04	0.08	0.07	0.13
CaO	0.00	0.02	0.00	0.06	0.10	0.05
MnO	0.58	0.24	0.20	0.22	0.33	0.26
FeO	37.84	62.39	42.19	34.29	73.68	70.59
Na_2O	0.01	0.01	0.01	0.01	0.01	0.01
NiO	0.07	0.24	0.03	0.06	0.25	0.29
Total	97.19	94.11	94.78	93.78	89.49	91.95
Formula Units	32	32	32	32	32	32
Si	0.03	0.07	0.05	0.15	0.09	0.06
Ti	16.03	7.93	14.28	16.07	3.22	5.33
Al	0.02	0.83	0.02	0.03	1.26	0.40
Cr	0.00	0.00	0.00	0.00	0.00	0.01
Mg	0.02	0.04	0.02	0.05	0.04	0.07
Ca	0.00	0.01	0.00	0.02	0.04	0.02
Mn	0.15	0.06	0.05	0.06	0.08	0.07
Fe	11.59	19.10	12.92	10.50	22.56	21.61
Ni	0.05	0.17	0.02	0.04	0.18	0.21
Na	0.00	0.00	0.01	0.00	0.00	0.01
Total	27.88	28.21	27.37	26.92	27.47	27.78

Name	93L112	93L112	93L112	93L107	93L107	93L107
Mineral	Ilmenite	Ti-Mag.	Ilmenite	Ti-Mag.	Ilmenite	Ilmenite
SiO_2	0.04	0.21	0.08	1.41	0.09	0.06
TiO_2	50.31	23.14	49.62	17.20	55.71	56.06
Al_2O_3	0.08	1.62	0.08	1.12	0.38	0.24
V_2O_3	0.24	0.12	0.28	0.32	0.26	0.28
Cr_2O_3	0.01	0.00	0.00	0.47	0.02	0.00
MgO	0.13	0.09	0.16	0.14	0.12	0.11
CaO	0.05	0.00	0.00	0.04	0.00	0.00
MnO	0.91	0.63	0.71	0.25	0.23	0.67
FeO	48.01	66.52	48.81	68.52	38.01	38.75
NiO	0.05	0.12	0.08	0.11	0.00	0.02
Na_2O	0.00	0.06	0.00	0.03	0.00	0.00
Total	99.84	92.52	99.84	89.63	94.82	96.19
Formula Units	32	32	32	32	32	32
Si	0.02	0.08	0.03	0.52	0.03	0.02
Ti	13.85	6.37	13.66	4.73	15.34	15.43
Al	0.04	0.69	0.04	0.48	0.16	0.10
Cr	0.00	0.00	0.00	0.13	0.01	0.00
Mg	0.07	0.05	0.09	0.08	0.07	0.06
Ca	0.02	0.00	0.00	0.02	0.00	0.00
Mn	0.23	0.16	0.18	0.06	0.06	0.17
Fe	14.70	20.37	14.94	20.98	11.64	11.86
Ni	0.04	0.09	0.06	0.08	0.00	0.01
Na	0.00	0.03	0.00	0.01	0.00	0.00
Total	28.96	27.83	29.00	27.09	27.30	27.66

Name	93L107	93L107	93L107	93L107	93L107	93L107
Mineral	Ilmenite	Ti-mag.	Ti-mag.	Ti-mag.	Ilmenite	Ilmenite
SiO_2	0.07	1.93	0.30	0.36	0.07	0.05
TiO_2	58.51	4.51	19.70	7.52	52.02	59.94
Al_2O_3	0.16	3.27	0.66	0.52	0.11	0.11
V_2O_3	0.33	0.10	0.40	0.43	0.21	0.30
Cr_2O_3	0.01	0.02	0.16	0.18	0.00	0.00
MgO	0.12	0.21	0.07	0.11	0.10	0.09
CaO	0.00	0.09	0.03	0.00	0.00	0.00
MnO	0.86	0.20	0.28	0.18	0.85	0.48
FeO	36.27	82.65	73.00	82.25	43.63	36.03
NiO	0.04	0.04	0.04	0.00	0.00	0.00
Na_2O	0.00	0.02	0.00	0.02	0.00	0.03
Total	96.38	93.10	94.65	91.58	97.00	97.04
Formula Units	32	32	32	32	32	32
Si	0.03	0.71	0.11	0.13	0.03	0.02
Ti	16.11	1.24	5.42	2.07	14.32	16.50
Al	0.07	1.40	0.28	0.22	0.04	0.05
Cr	0.00	0.01	0.05	0.05	0.00	0.00
Mg	0.06	0.11	0.04	0.06	0.05	0.05
Ca	0.00	0.04	0.01	0.00	0.00	0.00
Mn	0.22	0.05	0.07	0.04	0.22	0.12
Fe	11.10	25.30	22.35	25.18	13.36	11.03
Ni	0.03	0.03	0.03	0.00	0.00	0.00
Na	0.00	0.01	0.00	0.01	0.00	0.01
Total	27.62	28.90	28.36	27.78	28.02	27.79

Name	93L107	93L105	93L105	93L105	93L99	93L99
Mineral	Ilmenite	Ilmenite	Ilmenite	Ilmenite	Ilmenite	Ti-mag.
SiO_2	7.56	0.06	0.09	0.05	0.07	0.66
TiO_2	37.90	53.16	53.65	49.33	44.73	3.69
Al_2O_3	4.63	0.05	0.15	0.15	0.01	0.21
V_2O_3	0.16	0.28	0.29	0.38	0.26	0.22
Cr_2O_3	0.02	0.01	0.00	0.02	0.01	0.22
MgO	0.96	0.06	0.12	0.20	0.05	0.13
CaO	0.19	0.00	0.00	0.00	0.00	0.02
MnO	0.53	0.81	4.66	1.36	0.68	0.12
FeO	43.59	44.26	35.84	44.90	50.79	84.48
NiO	0.07	0.05	0.21	0.14	0.07	0.02
Na_2O	0.59	0.00	0.02	0.01	0.00	0.00
K_2O	0.22	0.00	0.01	0.00	0.00	0.04
Total	96.41	98.76	95.03	96.55	96.68	89.82
Formula Units	32	32	32	32	32	32
Si	2.77	0.02	0.03	0.02	0.03	0.24
Ti	10.43	14.63	14.77	13.58	12.32	1.02
Al	1.98	0.02	0.06	0.07	0.00	0.09
Cr	0.01	0.00	0.00	0.01	0.00	0.06
Mg	0.52	0.03	0.06	0.11	0.03	0.07
Ca	0.07	0.00	0.00	0.00	0.00	0.01
Mn	0.13	0.20	1.18	0.34	0.17	0.03
Fe	13.34	13.55	10.97	13.75	15.55	25.86
Na	0.05	0.04	0.15	0.10	0.05	0.02
K	0.27	0.00	0.01	0.01	0.00	0.00
Total	29.58	28.51	27.24	27.97	28.14	27.40

Name	93L99	93L99	93L99	93L99	93L99	93L60
Mineral	Ti-Mag.	Ilmenite	Ilmenite	Ilmenite	Ti-Mag.	Ilmenite
SiO_2	1.38	0.05	0.07	0.05	0.30	1.66
TiO_2	17.33	59.63	69.54	58.57	8.75	76.97
Al_2O_3	0.53	0.04	0.00	0.02	1.75	0.11
V_2O_3	0.50	0.37	0.36	0.38	0.20	0.44
Cr_2O_3	0.11	0.03	0.00	0.02	0.11	0.02
MgO	0.10	0.01	0.00	0.02	0.11	0.02
CaO	0.02	0.00	0.00	0.00	0.01	0.07
MnO	0.13	0.27	0.24	0.81	0.28	0.00
FeO	69.96	35.78	25.69	36.35	79.62	6.23
Na_2O	0.20	0.00	0.01	0.00	0.01	0.22
K_2O	0.06	0.00	0.00	0.00	0.00	0.11
Total	90.41	96.18	95.94	96.27	91.17	85.87
Formula Units	32	32	32	32	32	32
Si	0.51	0.02	0.03	0.02	0.11	0.61
Ti	4.77	16.42	19.14	16.12	2.41	21.19
Al	0.22	0.01	0.00	0.01	0.75	0.05
Cr	0.03	0.01	0.00	0.01	0.03	0.01
Mg	0.05	0.00	0.00	0.01	0.06	0.01
Ca	0.01	0.00	0.00	0.00	0.00	0.03
Mn	0.03	0.07	0.06	0.21	0.07	0.00
Fe	21.42	10.95	7.86	11.13	24.38	1.91
Na	0.07	0.01	0.02	0.02	0.01	0.00
K	0.10	0.00	0.00	0.00	0.00	0.10
Total	27.21	27.49	27.12	27.52	27.83	23.90

Name	93L111	93L111	93L111	93L111	93L111	93L111
Mineral	Ilmenite	Ti-Mag.	Ti-Mag.	Ti-Mag.	Ti-Mag.	Ti-Mag.
SiO_2	0.59	0.32	0.22	0.14	0.26	0.60
TiO_2	42.30	22.79	23.80	18.72	25.80	19.90
Al_2O_3	0.35	1.22	1.23	1.20	1.25	1.14
V_2O_3	0.27	0.32	0.27	0.38	0.32	0.34
Cr_2O_3	0.02	0.05	0.01	0.07	0.06	0.09
MgO	0.27	0.19	0.21	0.17	0.23	0.20
CaO	0.03	0.08	0.06	0.01	0.05	0.07
MnO	1.45	0.84	0.92	0.52	0.60	1.02
FeO	47.05	63.73	62.79	71.98	64.70	68.12
NiO	0.04	0.26	0.32	0.17	0.14	0.45
Na_2O	0.01	0.03	0.00	0.04	0.01	0.06
K_2O	0.01	0.07	0.08	0.00	0.01	0.00
Total	92.39	89.90	89.90	93.40	93.43	92.01
Formula Units	32	32	32	32	32	32
Si	0.22	0.12	0.08	0.05	0.10	0.22
Ti	11.65	6.27	6.55	5.15	7.10	5.48
Al	0.15	0.52	0.52	0.51	0.53	0.49
Cr	0.01	0.01	0.00	0.02	0.02	0.02
Mg	0.15	0.10	0.11	0.09	0.12	0.11
Ca	0.01	0.03	0.02	0.00	0.02	0.03
Mn	0.37	0.21	0.23	0.13	0.15	0.26
Fe	14.40	19.51	19.22	22.04	19.81	20.85
Ni	0.03	0.18	0.23	0.12	0.10	0.32
Na	0.00	0.01	0.00	0.02	0.00	0.03
Total	26.98	26.98	26.98	28.14	27.95	27.80

Name	93L111	93L104	93L104	93L104	93L104	93L104
Mineral	Ti-Mag.	Ti-Mag.	Ti-Mag.	Ti-Mag.	Ti-Mag.	Ti-Mag.
SiO_2	0.15	0.67	0.60	0.44	0.50	0.11
TiO_2	16.17	4.46	19.91	26.62	19.96	34.07
Al_2O_3	1.87	0.82	0.69	0.37	0.86	0.70
V_2O_3	0.36	0.16	0.15	0.14	0.12	0.07
Cr_2O_3	0.07	0.26	0.39	0.50	0.40	0.84
MgO	0.14	0.11	0.11	0.11	0.12	0.15
CaO	0.00	0.08	0.39	0.51	0.35	0.16
MnO	0.41					
FeO	70.65	82.65	67.93	61.91	74.37	56.33
NiO	0.19					
K_2O	0.03					
Total	90.04	89.21	90.16	90.60	96.68	92.41
Formula Units	32	32	32	32	32	32
Si	0.06	0.25	0.22	0.16	0.18	0.04
Ti	4.45	1.23	5.48	7.33	5.50	9.38
Al	0.80	0.35	0.29	0.16	0.37	0.30
Cr	0.02	0.07	0.11	0.14	0.11	0.24
Mg	0.08	0.06	0.06	0.06	0.07	0.08
Ca	0.00	0.03	0.15	0.20	0.14	0.06
Mn	0.10	0.00	0.00	0.00	0.00	0.00
Fe	21.63	25.30	20.80	18.95	22.77	17.24
Na	0.13	0.00	0.00	0.00	0.00	0.00
Total	27.27	27.29	27.11	27.00	29.13	27.34

Name	93L104	93L104	93L104	93L104	93L104	93L47
Mineral	Ilmenite	Ilmenite	Ti-Mag.	Ilmenite	Ti-Mag.	Ti-Mag.
SiO_2	0.12	0.09	0.70	0.10	0.78	0.67
TiO_2	48.47	43.03	21.51	49.24	18.10	17.01
Al_2O_3	0.14	0.13	0.80	0.17	2.10	1.04
V_2O_3	0.04	0.01	0.14	0.05	0.10	0.43
Cr_2O_3	2.52	1.98	0.58	1.97	0.95	0.37
MgO	0.24	0.20	0.10	0.18	0.17	0.26
CaO	0.54	0.51	0.45	0.52	0.34	0.22
MnO						
FeO	43.15	46.76	66.07	43.28	69.19	70.87
Total	95.20	92.70	90.34	95.52	91.73	90.86
Formula Units	32	32	32	32	32	32
Si	0.04	0.03	0.26	0.04	0.29	0.24
Ti	13.34	11.85	5.92	13.55	4.98	4.68
Al	0.06	0.05	0.34	0.07	0.90	0.44
Cr	0.72	0.57	0.17	0.57	0.27	0.10
Mg	0.13	0.11	0.05	0.10	0.09	0.14
Ca	0.21	0.20	0.17	0.21	0.13	0.09
Mn	0.00	0.00	0.00	0.00	0.00	0.00
Fe	13.21	14.31	20.23	13.25	21.18	21.70
Total	27.72	27.12	27.14	27.79	27.85	27.40

Name	93L47	93L47	93L78	93L78	93L78	93L78
Mineral	Ti-Mag.	Ti-Mag.	Ti-Mag.	Ti-Mag.	Ti-Mag.	Ti-Mag.
SiO_2	1.20	0.46	0.74	0.12	0.38	0.41
TiO_2	26.87	18.60	20.55	18.33	22.36	23.39
Al_2O_3	1.07	2.49	1.48	1.35	1.73	1.61
V_2O_3	0.27	0.47	0.01	0.01	0.01	0.02
Cr_2O_3	0.97	0.48	0.12	0.21	0.06	0.22
MgO	0.29	0.20	0.09	0.00	0.03	0.08
CaO	0.90	0.41	5.78	0.67	6.80	2.26
MnO						
FeO*	58.30	67.15	62.66	69.06	60.23	63.81
Total	89.86	90.25	91.42	89.75	91.61	91.81
Formula Units	32	32	32	32	32	32
Si	0.44	0.17	0.27	0.05	0.14	0.15
Ti	7.40	5.12	5.66	5.05	6.16	6.44
Al	0.46	1.06	0.63	0.58	0.74	0.69
Cr	0.28	0.14	0.03	0.06	0.02	0.06
Mg	0.16	0.11	0.05	0.00	0.02	0.04
Ca	0.35	0.16	2.27	0.26	2.67	0.89
Mn						
Fe	17.85	20.56	19.18	21.14	18.44	19.54
Total	26.93	27.31	28.09	27.13	28.18	27.81

Name	93L78	93L78	93L78	93L78	93L28	93L36
Mineral	Ti-mag.	Ti-mag.	Ilmenite	Ilmenite	Ilmenite	Ti-mag.
SiO_2	0.92	0.54	0.44	1.11	0.13	0.77
TiO_2	23.36	21.62	57.00	48.26	54.35	16.81
Al_2O_3	1.70	1.87	0.09	0.28	0.05	0.67
V_2O_3	0.02	0.00	0.00	0.02	0.00	0.00
Cr_2O_3	0.14	0.11	0.13	0.24	0.01	0.07
MgO	0.10	0.07	0.06	0.06	0.00	0.04
CaO	3.22	6.78	3.23	1.62	4.18	0.45
MnO						
FeO*	60.51	61.50	34.61	40.99	31.44	70.99
Na_2O					0.01	0.00
K_2O					0.46	0.18
Total	89.98	92.48	95.55	92.58	90.63	89.98
Formula Units	32	32	32	32	32	32
Si	0.34	0.20	0.16	0.41	0.05	0.28
Ti	6.43	5.95	15.69	13.29	14.96	4.63
Al	0.73	0.80	0.04	0.12	0.02	0.29
Cr	0.04	0.03	0.04	0.07	0.00	0.02
Mg	0.06	0.04	0.03	0.03	0.00	0.02
Ca	1.26	2.66	1.27	0.63	1.64	0.18
Mn	0.00	0.00	0.00	0.00	0.00	0.00
Fe	18.52	18.83	10.59	12.55	9.62	21.73
Na					0.32	0.13
Total	27.38	28.50	27.82	27.10	26.63	27.27

Name	93L36	93L93	93L93	93L93	93L93	93L93
Mineral	Ilmenite	Ti-mag.	Ti-mag.	Ilmenite	Ti-mag.	Ti-mag.
SiO_2	0.20	0.28	0.92	0.92	2.60	0.19
TiO_2	50.60	20.87	20.74	55.56	20.17	19.06
Al_2O_3	0.07	2.19	2.34	0.18	2.16	2.52
V_2O_3	0.00	0.20	0.20	0.01	0.25	0.32
Cr_2O_3	0.07	0.18	0.15	0.31	0.20	0.88
MgO	0.01	0.06	0.08	0.11	0.14	0.06
CaO	4.46	1.14	1.06	1.67	1.00	0.26
MnO						
FeO*	34.67	67.05	66.97	35.19	65.65	68.06
Na_2O	0.00	0.06	0.07	0.03	0.08	0.09
K_2O	0.07	0.13	0.15	0.00	0.12	0.10
Total	90.14	92.16	92.70	93.97	92.37	91.53
Formula Units	32	32	32	32	32	32
Si	0.07	0.10	0.34	0.34	0.95	0.07
Ti	13.93	5.74	5.71	15.30	5.55	5.25
Al	0.03	0.93	1.00	0.08	0.92	1.08
Cr	0.02	0.05	0.04	0.09	0.06	0.25
Mg	0.01	0.03	0.04	0.06	0.08	0.03
Ca	1.75	0.45	0.41	0.65	0.39	0.10
Mn						
Fe	10.61	20.53	20.50	10.77	20.10	20.83
Na	0.00	0.01	0.01	0.00	0.01	0.01
K	0.05	0.09	0.11	0.00	0.09	0.07
Total	26.47	27.94	28.17	27.29	28.15	27.70

APPENDIX D

ARGON DATING, TECHNIQUE & RESULTS

D1. Introduction.

The Ar-Ar dating technique first developed by Turner in 1966 depends upon the decay of a naturally occurring isotope of potassium, ^{40}K, to the argon isotope, ^{40}Ar. In Ar-Ar dating, potassium is measured by the transmutation of another naturally occurring isotope, ^{39}K to ^{39}Ar by neutron bombardment. In this present work, laser step heating was performed on both single and multiple grains of either plagioclase or potassium feldspar, except in the case of 93L59 where biotite separates were analysed.

D2. Sample Preparation.

Samples were chosen according to a number of criteria, including their microscopic appearance, phenocryst assemblage, the size and degree of freshness of phenocrysts, and the absence of amygdaloidal fragments. Only samples that appeared to be fresh and unaltered were crushed using a pneumatic jaw crusher and disc grinder and then sieved into three fractions: > 1 mm; > 250 μm & < 250 μm. The > 250 μm fractions were examined under a Leica Wild M8 microscope with Intralux® lighting and fresh, single phenocrysts were hand picked. On average 100 grains were placed in 50% acetic acid solution in an ultrasonic bath for 20 mins. to remove any clay minerals. The samples were washed with RO water, centrifuged at 1000 rpm for 3 mins., drained and then dried under an evaporating hood. The samples were finally washed in methanol, and then de ionised water in an ultrasonic bath for 15 mins. The samples were wrapped in Al foil and placed in pure quartz tubes together with ages standards of either 410.3Ma Tinto biotite (Rex & Guise, 1995) or 27.9 Ma 85G003 sanidine spaced every 0.5 - 1cm. Ca and K salts were also included in the package to measure and calculate the relevant (39/37) Ca, (36/37) Ca, and (40/39) K correction factors due to neutron induced interferences. The

quartz tubes were vacuum sealed to prevent absorption of atmospheric argon during irradiation. The tubes were placed in a pure quartz glass bucket for irradiation at either the Ford reactor, Michigan or Oregon State University (O.S.U).

D3. Radiation Procedure.

All samples of Table D3 apart from 93L36; 93L19; 93L107 & 93L125 were irradiated at the Ford reactor, Michigan, all others at O.S.U. At the Ford reactor one of two positions is used, H5 at the core and L67 at the outer edges, the latter being preferential as the thermal neutron dose received is lower. At O.S.U. the CLICIT sample system was used with the result that different correction factors apply. The duration of irradiations is variable, for the samples analysed -18hrs at O.S.U. and 60hrs at Ford. Samples at the Ford reactor received approx. 10^{18} fast neutrons per cm at position L67. The quantity of $^{39}Ar_K$ produced during neutron irradiation is dependent on the neutron flux density $\phi(\varepsilon)$ at energy ε and the length of the irradiation 'ΔT' :

$$^{39}Ar_K = {}^{39}K \Delta T \int \phi(\varepsilon)\sigma(\varepsilon)d\varepsilon$$

where $\sigma(\varepsilon)$ is the capture cross section for neutron having energy in the ^{39}K (nap) ^{39}Ar reaction. However, it is not always possible to make direct measurements of the flux density or the neutron capture cross section, therefore, monitoring is achieved using age standards with accurately determined K-Ar ages. This defines the dimensionless parameter J, which is substituted into the age equation. Following a period of cooling in the order of a month the samples are returned and loaded into an infra-red laser port for analysis.

D4. Analysis of Samples.

The samples were loaded into individual holes in a laser tray. The five major isotopes analysed using a Mass Analyser Products 215 noble gas mass spectrometer fitted with an electron multiplier detector. ^{36}Ar is measured to correct for atmospheric ^{40}Ar using the measured present day atmospheric $^{40}Ar/^{36}Ar$ ratio (295.5; Steiger & Jäger, 1977). However, mass spectrometers in general do not yield absolute abundance ratios of the isotopes analysed therefore the machine has to be calibrated and appropriate

corrections applied to the measured ratios. Calibration for argon is achieved by analysing atmospheric argon (here, by melting pieces of glass containing argon of the $^{40}Ar/^{36}Ar$ atmospheric ratio 295.5). The departure from the absolute value, the mass discrimination $^{40}Ar/^{36}Ar$ measurement in this case is either 283 or 285. ^{36}Ar, however, can be affected by chlorine and hydrocarbons.

The three stable isotopes of Ar (^{36}Ar; ^{38}Ar and ^{40}Ar) in addition to the reactor produced isotopes (^{39}Ar and ^{37}Ar) are measured by the mass spectrometer. The myriad of reactions including $^{44,43,42,40}Ca$, $^{41,40,39}K$, $^{40,38,36}Ar$, and $^{35,37}Cl$ all going to produce $^{36\text{-}40}Ar$ are corrected for using the Ca and K salts included in each irradiation. ^{41}Ar and ^{35}Ar are additionally measured to monitor the build up of hydrocarbons and chlorine respectively in the extraction line. Table D1 contains information on the main five isotopes of argon and their uses.

Table D1. Isotopes of argon.

Isotope	Indicator of:
^{40}Ar	Radiogenic ^{40}Ar (once atmospheric component is removed).
^{39}Ar	^{39}K
^{38}Ar	Amount of chlorine in sample
^{37}Ar	Amount of Ca in sample
^{36}Ar	Atmospheric argon

Argon was extracted in stages from individual grains by laser step heating using a Nd-doped yttrium aluminium garnet (Nd-YAG) continuous wave (CW) laser. Initially samples were analysed using a laser without apertures (Multimode) which produces a wide beam of high power and so required less current to melt the samples. A TEM_{00} system was also used, which includes a small aperture to restrict the transverse modes and so focus the beam, one of the results is that a larger current is required to melt the sample. For example, using the Multimode system the lowest step required a current of ~ 8A to begin melting plagioclase, however using TEM_{00} a current of 15.7A is required.

The resulting analyses were corrected for blanks, ^{37}Ar decay and neutron interferences (see Table D2). J values were calculated using the standard minerals (Tinto

biotite & 85G003 sanidine) to monitor the neutron flux for each sample (see Table D3). Ages were calculated using the equation:

$$t = \frac{1}{\lambda} \ln(1 + J\frac{^{40}Ar^*}{^{39}Ar})$$

where $\lambda = 5.543 \times 10^{-10}$ years.

Table D2. Correction factors for the the interfering reactions produced during neutron irradiation.

	Correction factor: Ford, Michigan (L67)	Correction factor: Oregon State University
(36/37)Ca	0.000205	0.000264
(39/37)Ca	0.000781	0.000673
(40/39)K	0.031	0.00086

The samples analysed from Uruguay are included in Table D4 along with rock type and location, while the volcanics of the African margin are included in Table D5.

Table D3. J values for all samples calculated from standards irradiated at the same time.

Sample-Uruguay	J-value	Sample-Etendeka	J-value	Sample-Etendeka	J-value
93L19	0.004465	CP3	0.004223	SM60	0.004475
93L28/22/42	0.00925	LB1	0.004216	SM172	0.004495
93L36	0.004445	KK-119	0.004231	KU-66	0.004239
93L47	0.00936	KLS230	0.0045	KU-82	0.004247
93L53/59/93/97	0.0094	KLS327	0.00449	DRL507	0.00448
93L107	0.00447	KLS348	0.004485	DRL508	0.004515
93L125	0.00451	KLS488	0.004505	TK1-47	0.004254

Table D4. Uruguayan samples for argon analysis.

Sample name	Rock type	Location	Reactor
93L97	Basalt	Treinte Y Trés	Ford, Michigan
93L47	Basalt	Paso de los Talas	Ford, Michigan
93L53	Basalt	Cerro Partido	Ford, Michigan
93L93	Basalt	Piraraja	Ford, Michigan
93L125	Andesite	Lascano	Oregon State Uni.
93L42	Dacite	Paso de los Talas	Ford, Michigan
93L22	Rhyolite	Minas	Ford, Michigan
93L28	Rhyolite	Aigua	Ford, Michigan
93L107	Rhyolite	Lascano	Oregon State Uni.
93L36	Rhyolite	Aigua	Oregon State Uni.
93L19	Rhyolite	Cerro Partido	Oregon State Uni.

Table D5. Etendeka volcanics and associated dykes.

Sample	Rock type	Location	Reactor
DRL507/508	Qtz. tholeiite	Mehlberg dyke	Oregon State Uni.
KLS488	Basalt	Huab	Oregon State Uni.
KLS230	Basalt	Horingbaai	Oregon State Uni.
SM172	Latite	Springbok	Oregon State Uni.
KLS327	Latite	Sechomib	Oregon State Uni.
KLS348	Mafic volcanic		Oregon State Uni.
SM60	Latite	Tafelberg	Oregon State Uni.
LB1	Basalt	Cape Town	Oregon State Uni.
CP3	Andesite	Cape Town	Oregon State Uni.
KK-119	Dolerite	Kuiseb	Oregon State Uni.
KU-66		Ugab River	Oregon State Uni.
KU-82		Ugab River	Oregon State Uni.
TK1-47	Basalt	Suurberg	Oregon State Uni.

D5. Argon Results & Discussion.

Correlation plots of $^{36}Ar/^{40}Ar$ vs $^{39}Ar/^{40}Ar$ were used to distinguish excess argon and also to yield precise intercept ages. Atmospheric argon on the y-axis plots at 0.003384. A straight line from the point AIR through a cluster of data points intercepts the y-axis resulting in an intercept age, if the argon is pure and uncontaminated. Excess argon plots at the origin of such a diagram, thus the addition of ^{40}Ar to the sample results in a lower $^{36}Ar/^{40}Ar$ ratio than expected and hence an older intercept age. Plateau ages are described from plots of age vs cumulative ^{39}Ar and are defined by as the flattest trend defined by the majority of data. Total gas ages are averaged from all collected $^{40}Ar/^{39}Ar^*$.

93L19: Large variations in $^{37}Ar/^{39}Ar$ ratios (0.098 & 3.33), indicate contamination of phenocrysts with the result that data yielded wildly varying ages of 112.7 ± 5.8 Ma* (* indicates 2σ errors quoted on age) to 50.2 ± 115.0 Ma* respectively.

93L28 (a) & (b): Two separate experiments were performed on single sanidine grains. The first sanidine was analysed in 22 steps, using a initial current of 9.1A and a final fusion current of 22.0A (Fig. 4.6b). This yielded an intercept age of 126.3 ± 0.6Ma* at $^{36}Ar/^{40}Ar = 0.00335$. The second analysis using 19 steps resulted in a slightly older plateau age of 127.1 ± 0.6 Ma* (Fig. 4.6b). Similar experiments were performed on single sanidine phenocrysts from samples 93L22 (Fig. D1) and 93L36.

93L93: Plagioclase separate from porphyritic basalt. Age range variable from 141 ± 8 to 123 ± 6 Ma. Initial step-heating of the grains yielded older ages in all the analyses probably due to the presence of remnant clay minerals. The hydrocarbon contents (as indicated by ^{41}Ar peak) reached very high levels resulting in large errors on the ages. The apparent age obtained from the total gas is 133.1 ± 1.2 Ma*. A similar basalt (93L97) from the Piraraja/Treinte Y Trés region was separated for plagioclase also, however, age determination was again difficult with large age corrections on a seemingly very young sample of 118.0 ± 6 Ma.

93L107: Uruguayan rhyolite K-feldspar multi grain separate yielded an age of 127.7 ± 1.6 Ma*. Some mixing with atmospheric argon evident in the first three steps,

remaining six steps display a very tight array and are considered to reflect a true age (Fig. 4.6a).

Fig. D1. **Plateau age calculated on duplicate sanidine separates for sample 93L22. Arrow indicates the number of steps used to calculate final age (Ma) of (i) 130.9±0.7 (dashed line) and (ii) 131.9 ± 0.5 (solid line).**

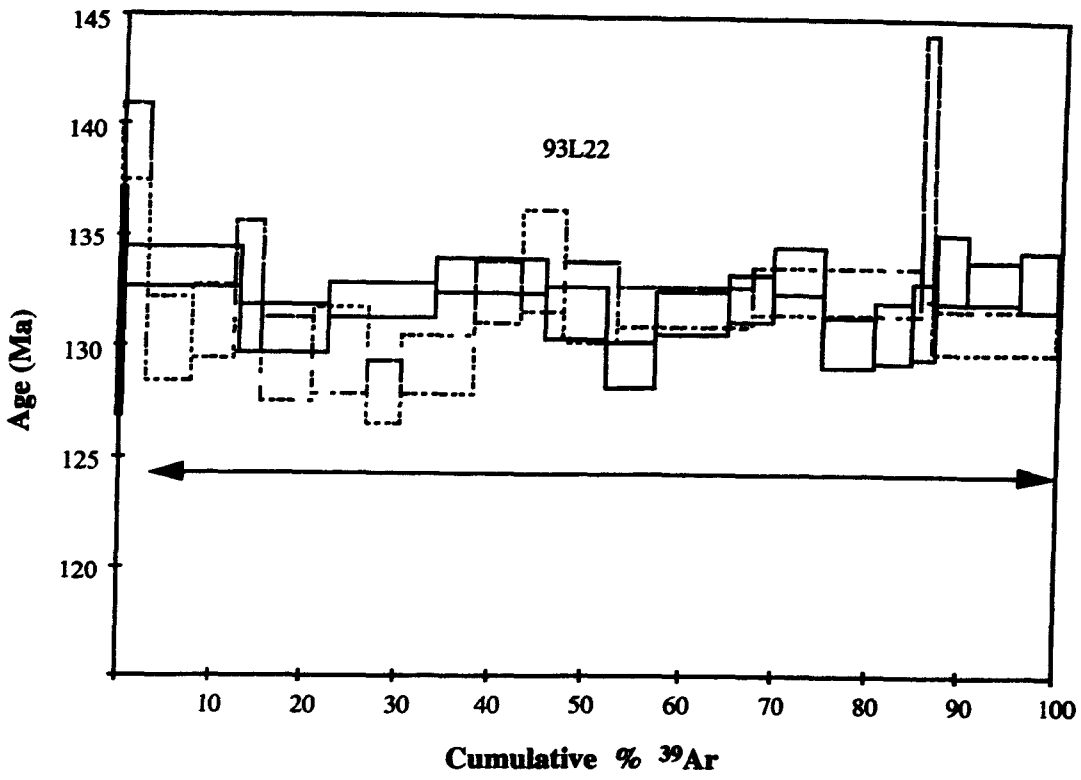

93L125: Plagioclase separated from this Uruguayan andesite yielded widely varying ages due to a problem with excess argon as indicated by the ^{36}Ar contents which vary from 0.000204 to 0.006077 from the start to end of the analysis. The best result obtained is an approximate Cretaceous age for the sample.

CP3: Chapman's Peak Drive, Cape Town. Only four heating steps were carried out on separated plagioclase multi grains with little gas being realised. A large spread in the $^{36}Ar/^{40}Ar$ and $^{39}Ar/^{40}Ar$ data indicates a problem of excess argon. As seen in Fig. D2 a line drawn to intersect through air (0.00335) and the majority of data yields an intercept age of 140.8 Ma. However, the intercept when averaged on the entire data set intersected the y axis at 0.00120, and resulted in a much younger age of 101.6 Ma.

Table D6. Results of samples analysed.

Sample	Intercept Ages	MSWD	Plateau Ages	Phase
93L19		0.358	111.7 ± 4.2	Multi, K-spar
93L22a 93L22b	129.7 ± 2.1	0.878	130.9 ± 0.7 131.9 ± 0.5	Single, K-spar
93L28a 93L28b	126.4 ± 1.2	1.059	124.3 ± 0.7 123.9 ± 0.4	Single, K-spar
93L36	123.9 ± 1.4	1.083	123.9 ± 0.4	Multi, K-spar
93L42	132.9 ± 0.9	1.020	131.8 ± 0.9	Multi, K-spar
93L47	125.8 ± 5.1	0.101	128.0 ± 3	Multi, Plag.
93L53		0.913	134.0 ± 5	Multi, Plag.
93L59	132.3 ± 1.2	0.195	132.0 ± 3	Multi, Biotite
93L93	136.1 ± 3.2	1.183	130.0 ± 2	Multi, Plag.
93L97	109.6 ± 32.8	0.353	118.0 ± 6	Multi, Plag.
93L107	127.8 ± 1.6	0.857	127.6 ± 0.6	Multi, K-spar
93L125		0.237	124.5 ± 12	Multi, Plag.
CP3	141.7 ± 10		141.9 ± 10.2	Multi Plag.
LB1	125.4 ± 3.4	1.282	125.4 ± 6.8	Multi, Plag.
KK-119			1623.2 ± 7.4	Multi, Plag.
KLS230	236.3± 2.8	6.458	272.3 ± 2.2	Multi, Plag.
KLS327	129.1± 1.0	1.165	128.6 ± 1.4	Multi, Plag.
KLS348	132.5 ± 2.4	1.265	132.4 ± 2.3	Multi, Plag.
KLS488	131.0 ± 1.9	0.617	130.5 ± 0.8	Multi, Plag.
SM60	129.1 ± 1.1	0.923	129.1 ± 1.8	Multi, Plag.
SM172	128.1 ± 1.1	1.307	128.2 ± 2.2	Multi, Plag.
KU-66			1780.6 ± 11.6	Multi, Plag.
KU-82	128.9 ± 4.4	0.524	129.5 ± 1.5	Multi, Plag.
DRL507	147.0 ± 7.5	1.758	214.9 ± 2.2	Multi, Plag.
DRL508	117.1 ± 0.9	0.784	117.2 ± 1.4	Multi, Plag.
TK1-47			194.4 ± 11.9	Multi, Plag.

Fig. D2. **Proposed intercept age for Cape Town dyke sample CP3 although excess argon is considered to contribute to a slightly old age.**

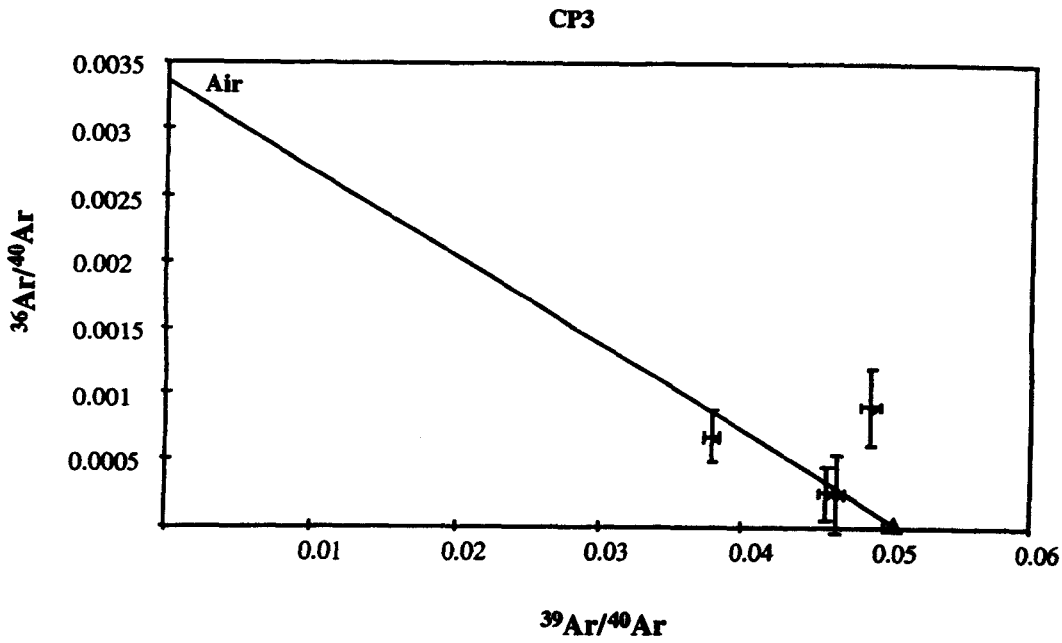

Fig. D3. **Intercept diagram for Cape Town dyke LB1. Mixing array is not well contrained therefore there is a relatively large error on the age quoted.**

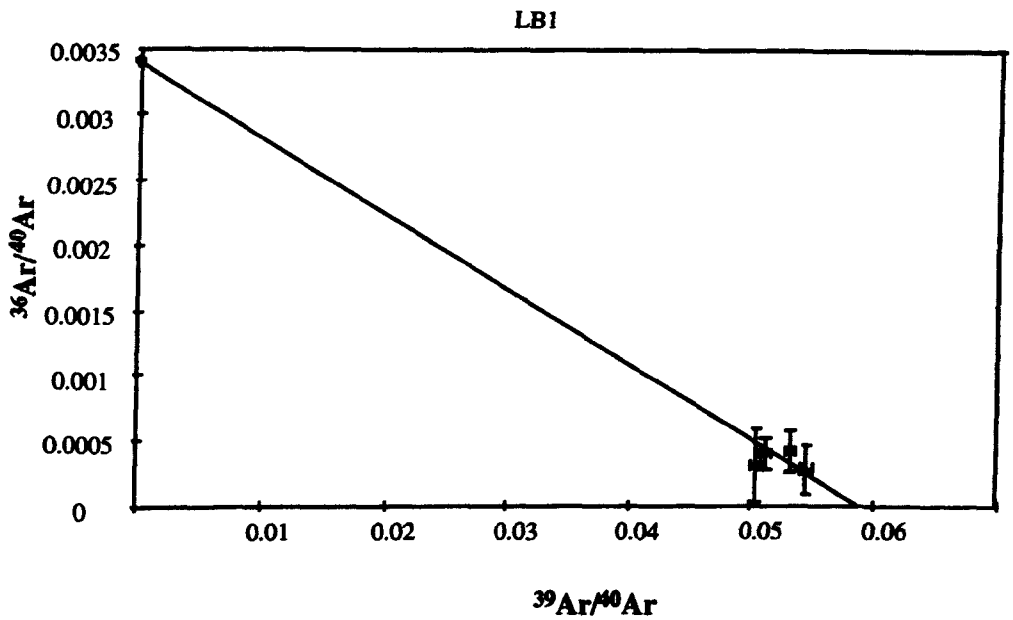

LB1: Cape Town dyke plagioclase separate. Multi grains analysed in six steps but with little emission of gas. Most of the gas was realised in the first two steps and is

principally excess argon. The high temperature stage although more reliable yielded 40% of the cumulative % ^{39}Ar and therefore an average total age was calculated. A large variation in Ca/K ratio (9.976-69.545) proves unreliable also. The intercept age was 108 Ma, while a line from Air through the high temperature ages yielded a 125.4 ± 8 Ma*. The total gas age is 135.2 Ma. With the result that a Lower Cretaceous age is inferred (Fig. D3).

KK-119: Plagioclase separate from an Etendeka dolerite dyke that gave a range of Archaean/Precambrian ages of 2.2 ± 0.2 Ga*. A plot of apparent age versus cumulative % ^{39}Ar gave what can only be described as a 'Step-machine' array. A correlation diagram shows a wide scatter along the x axis, implying either : (a) the sample is old and there has been argon loss or (b) it is a young sample that has been influenced by varying degrees of excess argon and/or contamination by host rock feldspar. The latter option is favoured as the dyke is observed intruding the ~600 Ma Damara granite and on an age versus $^{37}Ar/^{39}Ar$ plot shows a mixing array between younger and older components (Fig. D4).

Fig. D4. Mixing of feldspars of different ages due to the use of multiple phenocrysts in analyses giving rise to the old ages.

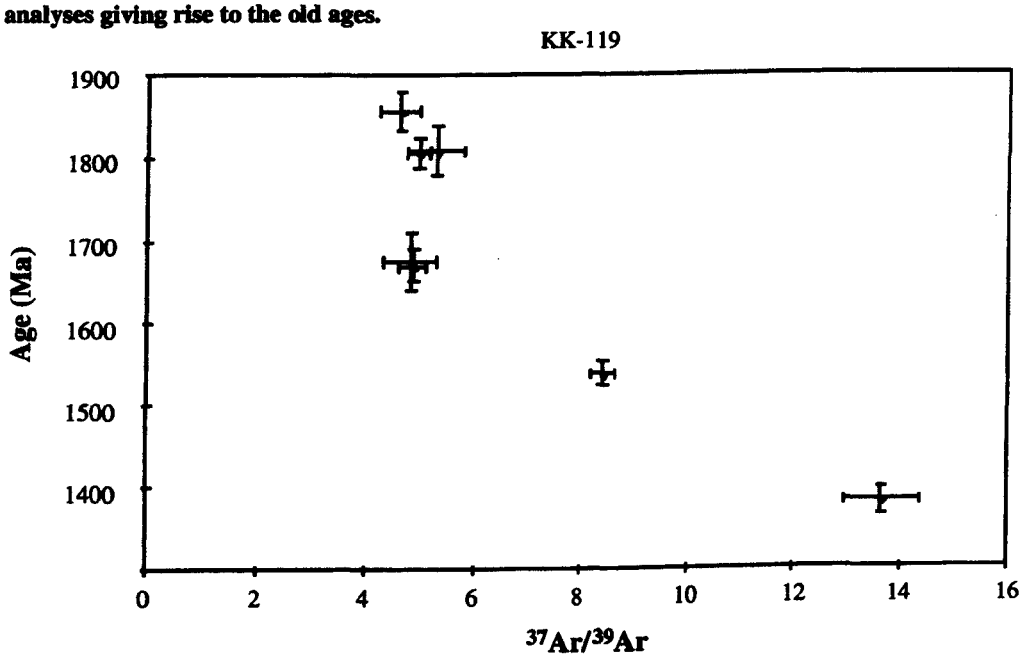

KLS230: Multiple grain, plagioclase separate. As with sample KK-119, this sample experiences a similar problem in that there appears to be mixing between feldspar

phenocrysts of different age and composition. A $^{37}Ar/^{39}Ar$ versus Age (Ma) plot illustrates this point with older ages corresponding to higher Ca/K ratios (Fig. 4.6d). A 'saddle' shape age spectrum highlights a problem with excess argon in both the low and high temperature steps (Fig. D5).

KLS348: Multiple grains of plagioclase were separated from this Etendeka mafic volcanic. Data yields an intercept age of 132.5 ± 4.76 Ma*, the error is large due to the interference of atmospheric argon in the initial stages of analysis. This resulted in exclusion of the first data point.

SM172: These multiple grains of plagioclase from the Etendeka region were analysed in 8 steps and yielded varying quantities of gas. Removing spurious points due to very low argon gas contents, resulted in an intercept age of 128.2 ± 2.2 Ma*.

Fig. D5. Classic saddle shaped profile of sample KLS 230 from the Etendeka indicating a problem with excess argon in the analyses.

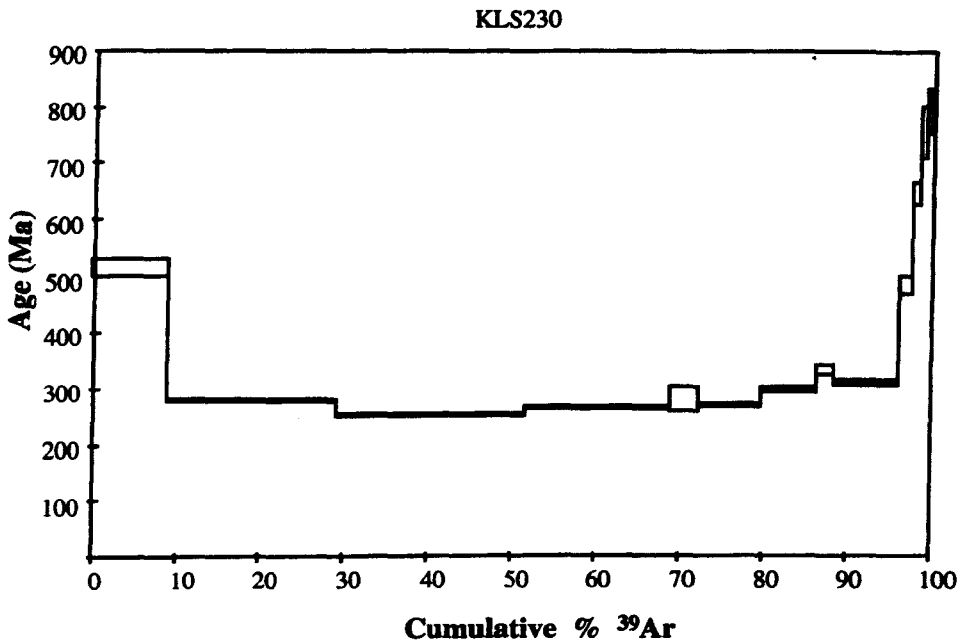

KU-66: Multi grain, plagioclase separate. This sample duplicates the behaviour of KK-119, although it results in a slightly younger Precambrian age. Again a mixing line is evident on an age vs $^{37}Ar/^{39}Ar$ plot with the older material having a low Ca/K ratio while the younger feldspars have higher Ca/K ratios (Fig. D6).

KU-82: Dolerite from the Ugab River region. First step heat of the multiple plagioclase grains gave an old age of 183.1 ± 8.8 Ma*, however, a plateau age of 129.5 ± 2Ma* appears more consistent. Low Ca/K ratios possibly indicate a mixture of plagioclase and K-feldspar in the separation process.

Fig. D6. Problem with mixing of older components highlighted in Etendeka samples.

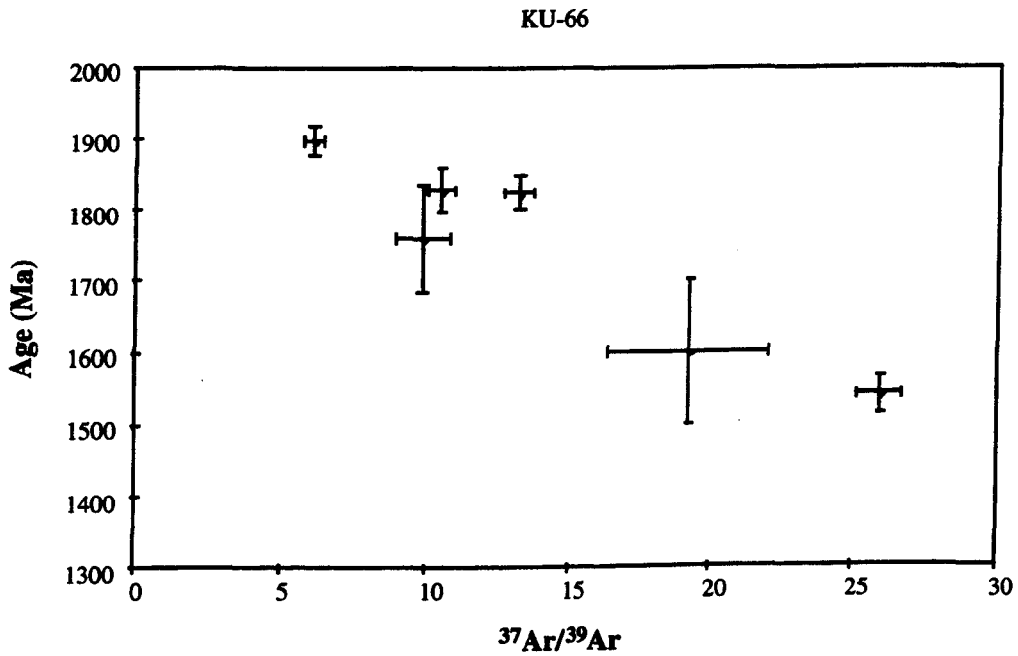

DRL507 & DRL508: Due to the difficulties of excess argon encountered by Reid & Rex (1994b) these samples were re-analysed as plagioclase separates. The samples originate from the Mehlberg dyke, a NNW trending 16 km long, 10-13 m wide dyke that intrudes both Precambrian sediments and granite in an en echelon manner. The two samples are from different sections along its length, DRL508 intruded massive quartzites while DRL507 intruded foliated granitoids.

An age spectrum for DRL507 reveals a 'saddle' shape spectrum indicative of excess argon (Fig. D7), also implied by the correlation diagram. Results indicate a much older, unreliable age of 220 ± 22 Ma* for this sample. Over 60% of the ^{39}Ar released from DRL508 occurred in the first three steps, the best estimate of a plateau age is 117 ± 1.1 Ma* although the error is underestimated (Fig. D8).

Fig. D7. Saddle shaped spectrum indicative of excess argon in the analysis of sample DRL 507.

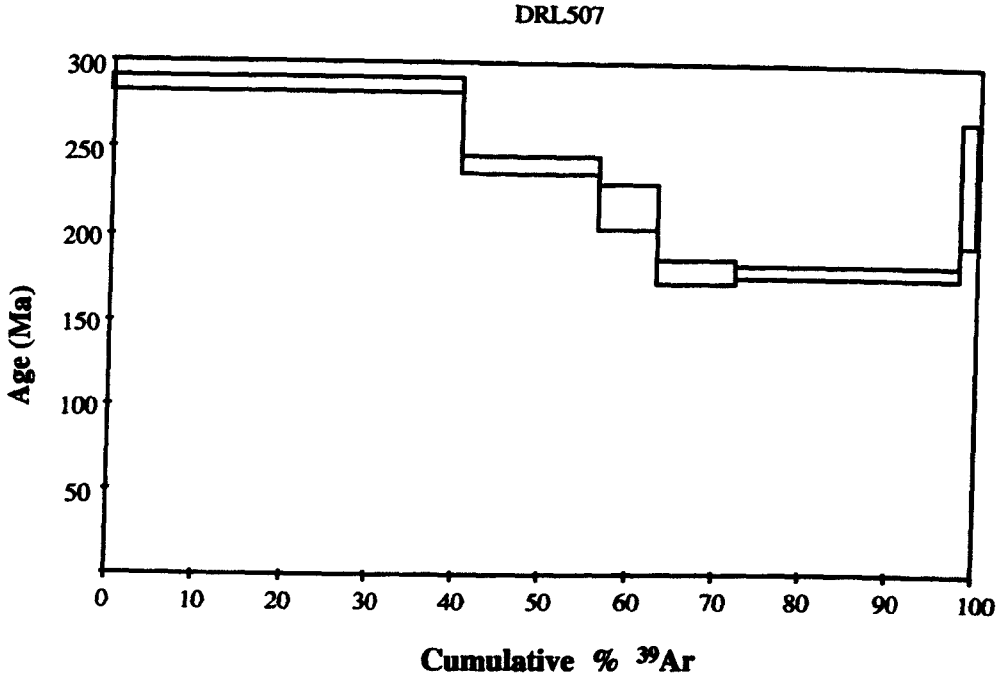

TK1-47: Suurberg basalt plagioclase separate. The multiple grains of separate yielded very little gas but consistently gave Jurassic Karoo ages of 194 ± 28 Ma*. This sample is thus unlikely to be associated with the rifting of the South Atlantic, and may instead be related to the rifting of Africa from India & Australia.

Fig. D8. Mehlberg dyke sample DRL 508 giving a very different age to that of DRL 507. The young age obtained is considered to be a function of loss of radiogenic argon.

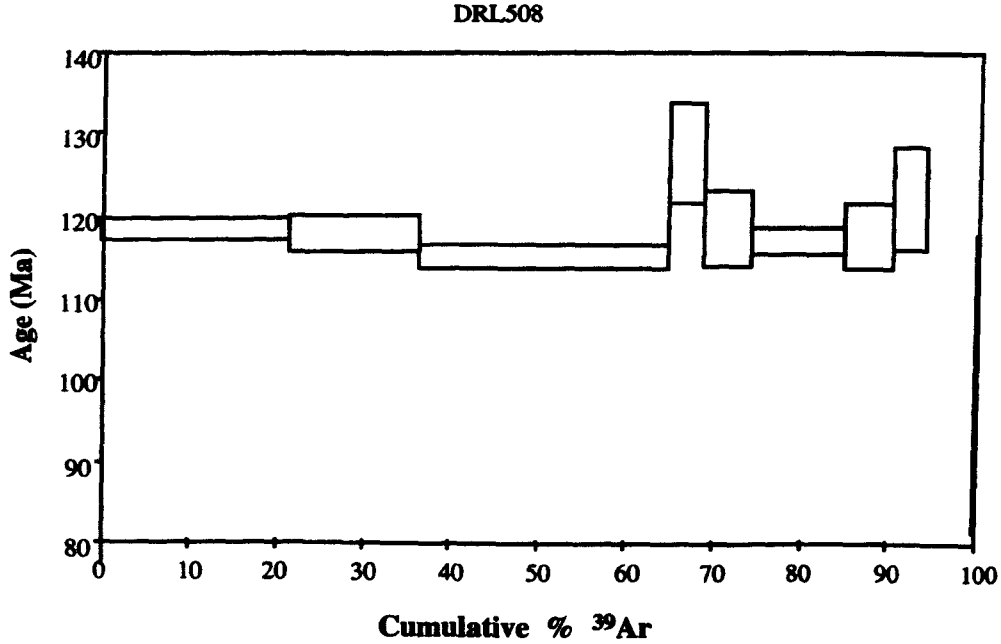

Table D7. Argon data on which ages were calculated.

Sample	40/39 Ar	±	40*/39 Ar	±	38/39 Ar	±	37/39 Ar	±	36/39 Ar	±	^{39}Ar (cm^{-3})
93L97	8.88	0.00151	7.87	0.54506	0.02	0.00021	44.58	0.37834	0.00	0.00022	1.31E-09
93L97	8.37	0.00121	6.72	0.52770	0.02	0.00020	56.93	0.46126	0.01	0.00022	1.35E-09
93L97	8.48	0.00113	6.79	0.87598	0.02	0.00015	61.98	0.64447	0.01	0.00016	7.4E-10
93L97b	9.14	0.00154	6.98	0.64486	0.02	0.00018	39.48	0.37907	0.01	0.00020	1.05E-09
93L97b	8.41	0.00150	6.82	0.41732	0.02	0.00025	56.26	0.48280	0.01	0.00027	1.72E-09
93L97b	9.16	0.00121	6.40	1.20455	0.03	0.00019	57.49	0.90628	0.01	0.00020	5.91E-10
93L97b	8.57	0.00132	6.62	0.68444	0.02	0.00022	60.81	0.68033	0.01	0.00023	1.04E-09
93L47a	9.05	0.00111	8.04	0.69503	0.02	0.00012	41.53	0.22558	0.00	0.00013	1.02E-09
93L47a	8.39	0.00216	6.52	0.42736	0.02	0.00022	57.43	0.30560	0.01	0.00023	2.03E-09
93L47c	12.29	0.00446	8.03	0.79464	0.03	0.00035	17.64	0.53894	0.01	0.00036	9.14E-10
93L47c	8.90	0.00907	7.84	0.31179	0.02	0.00079	30.42	0.55560	0.00	0.00078	3.47E-09
93L47c	8.63	0.00131	7.86	1.26881	0.02	0.00015	18.00	0.26752	0.00	0.00016	5.33E-10
93L47c	8.53	0.00175	7.73	0.33974	0.02	0.00026	21.53	0.16150	0.00	0.00028	2.12E-09
93L47c	8.45	0.00130	7.76	0.32966	0.02	0.00013	22.72	0.11829	0.00	0.00014	2.16E-09
93L47d	9.43	0.00207	7.99	0.28895	0.02	0.00023	26.62	0.14509	0.00	0.00023	2.64E-09
93L47d	8.54	0.00145	7.69	0.49611	0.02	0.00024	33.07	0.27547	0.00	0.00024	1.44E-09
93L47d	8.48	0.00152	7.75	0.36778	0.02	0.00023	32.18	0.20416	0.00	0.00025	2.07E-09
93L53a	9.28	0.00129	10.19	0.99430	0.02	0.00017	10.61	0.17185	0.00	0.00018	6.83E-10
93L53a	9.38	0.00137	8.41	0.93129	0.02	0.00021	14.13	0.21957	0.00	0.00021	7.29E-10
93L53a	9.13	0.00109	8.56	2.54846	0.02	0.00009	17.95	0.30934	0.00	0.00011	2.96E-10
93L53b	8.89	0.00171	9.22	1.03261	0.02	0.00020	15.06	0.31890	0.00	0.00022	6.96E-10
93L53b	8.30	0.00199	7.57	0.41927	0.02	0.00026	19.30	0.13300	0.00	0.00029	2.21E-09
93L59a	9.65	0.00152	9.91	0.71965	0.48	0.00026	0.20	0.06337	0.00	0.00023	1.06E-09
93L59aa	8.07	0.00121	8.36	0.97096	0.18	0.00015	0.48	0.07919	0.00	0.00015	6.96E-10
93L59aa	8.15	0.00273	7.95	0.28057	0.28	0.00034	3.98	0.04321	0.00	0.00034	2.49E-09
93L59aa	1.20	0.00094	100.66	111.60098	0.94	0.00006	0.82	7.91373	-0.34	0.00008	6.93E-12
93L59b	11.53	0.00371	9.30	0.34186	0.64	0.00072	0.46	0.01919	0.01	0.00042	2.98E-09
93L59b	8.08	0.00309	8.11	0.20710	0.25	0.00042	1.99	0.02304	0.00	0.00035	3.4E-09

Sample	40/39 Ar	±	40*/39 Ar	±	38/39 Ar	±	37/39 Ar	±	36/39 Ar	±	^{39} Ar (cm^3)
93L93a	9.24	0.00317	8.36	0.27775	0.02	0.00041	15.34	0.17600	0.00	0.00042	3.01E-09
93L93a	8.90	0.00234	7.66	0.39079	0.02	0.00036	33.37	0.28881	0.00	0.00039	2.39E-09
93L93a	8.73	0.00316	7.51	0.21284	0.02	0.00034	36.76	0.44705	0.00	0.00033	3.46E-09
93L93b	9.20	0.01271	8.63	0.23715	0.02	0.00133	13.89	0.33948	0.00	0.00131	4.95E-09
93L93b	8.61	0.00176	7.81	0.27584	0.02	0.00038	30.94	0.25907	0.00	0.00038	2.51E-09
93L93b	8.74	0.00223	7.65	0.17582	0.02	0.00039	36.90	0.23989	0.00	0.00039	3.72E-09
93L93c	9.36	0.00489	8.42	0.22664	0.02	0.00031	8.91	0.10940	0.00	0.00032	3.23E-09
93128b	7.77	0.00673	7.63	0.05755	0.01	0.00096	0.00	0.00319	0.00	0.00095	1.24E-08
93128b	7.86	0.00988	7.84	0.08160	0.01	0.00151	0.00	0.00291	0.00	0.00150	1.23E-08
93128b	7.99	0.00682	7.94	0.06402	0.01	0.00064	0.01	0.00348	0.00	0.00061	1.03E-08
93128b	7.88	0.01068	7.80	0.04700	0.01	0.00067	0.01	0.00213	0.00	0.00065	1.77E-08
93128b	7.93	0.00439	7.90	0.08157	0.01	0.00045	0.01	0.00491	0.00	0.00045	7.02E-09
93128b	7.87	0.00540	7.76	0.08145	0.01	0.00078	0.00	0.00449	0.00	0.00077	8.41E-09
93128b	7.92	0.00699	7.86	0.04538	0.01	0.00048	0.00	0.00252	0.00	0.00047	1.43E-08
93128b	7.98	0.01065	7.92	0.09451	0.01	0.00106	0.00	0.00351	0.00	0.00105	9.84E-09
93128b	7.97	0.00503	7.97	0.07012	0.01	0.00054	0.00	0.00422	0.00	0.00053	8.54E-09
93128b	7.96	0.00509	7.92	0.06230	0.01	0.00040	0.00	0.00385	0.00	0.00039	9.36E-09
93128b	7.91	0.00522	7.88	0.06291	0.01	0.00081	0.00	0.00319	0.00	0.00076	1.08E-08
93128b	7.99	0.00862	7.86	0.05689	0.01	0.00073	0.00	0.00285	0.00	0.00070	1.42E-08
93128b	7.85	0.02449	7.81	0.18656	0.01	0.00299	0.00	-0.00351	0.00	0.00296	9.95E-09
93128b	7.92	0.00612	7.81	0.06665	0.01	0.00058	0.21	0.26263	0.00	0.00057	1.15E-08
93128b	7.97	0.00443	7.93	0.06164	0.01	0.00051	0.00	0.00309	0.00	0.00051	1.18E-08
Sample no.											
93128b	7.90	0.01142	7.81	0.08528	0.01	0.00171	0.00	0.00313	0.00	0.00168	1.23E-08
93128b	8.04	0.00436	7.91	0.07368	0.01	0.00044	0.01	0.00487	0.00	0.00044	8.31E-09
93128b	8.07	0.00663	7.99	0.04603	0.01	0.00078	0.01	0.00247	0.00	0.00076	1.48E-08
93128b	14.44	0.00351	6.90	2.67411	0.02	0.00014	0.22	0.17273	0.03	0.00015	2.35E-10

Sample	40/39 Ar	±	40*/39 Ar	±	38/39 Ar	±	37/39 Ar	±	36/39 Ar	±	39 Ar (cm^3)
93L28a	13.45	0.00093	26.84	23.83095	0.08	0.00013	-0.19	-0.16265	-0.05	0.00014	2.62E-11
93L28a	7.68	0.00118	7.70	0.49016	0.01	0.00021	0.00	-0.00331	0.00	0.00021	1.13E-09
93L28a	7.77	0.00239	7.69	0.23308	0.01	0.00026	0.00	0.00141	0.00	0.00025	2.92E-09
93L28a	7.93	0.04630	7.86	0.18278	0.01	0.00573	0.00	0.00021	0.00	0.00569	1.91E-08
93L28a	7.83	0.01119	7.79	0.08288	0.01	0.00124	0.00	0.00035	0.00	0.00120	1.22E-08
93L28a	7.61	0.01787	7.60	0.06392	0.01	0.00166	0.00	0.00022	0.00	0.00163	2.04E-08
93L28a	7.77	0.01653	7.76	0.12348	0.01	0.00155	0.00	0.00042	0.00	0.00155	1.03E-08
93L28a	7.79	0.00873	7.70	0.06768	0.01	0.00079	0.00	0.00036	0.00	0.00077	1.15E-08
93L28a	7.76	0.00905	7.68	0.07822	0.01	0.00104	0.00	0.00035	0.00	0.00103	1.12E-08
93L28a	7.75	0.00859	7.71	0.07731	0.01	0.00098	0.00	0.00039	0.00	0.00096	1.02E-08
93L28a	7.78	0.00462	7.69	0.07410	0.01	0.00053	0.00	0.00059	0.00	0.00050	6.74E-09
93L28a	7.86	0.00505	7.83	0.07465	0.01	0.00059	0.00	0.00041	0.00	0.00057	9.14E-09
93L28a	7.72	0.00298	7.66	0.09039	0.01	0.00045	0.00	0.00079	0.00	0.00043	5.56E-09
93L28a	7.83	0.00697	7.77	0.11187	0.01	0.00076	0.00	0.00053	0.00	0.00077	6.3E-09
93L28a	7.69	0.00406	7.52	0.10265	0.01	0.00054	0.00	0.00071	0.00	0.00053	5.23E-09
93L28a	7.86	0.00379	7.82	0.13969	0.02	0.00028	0.00	0.00087	0.00	0.00027	3.6E-09
93L28a	7.77	0.00543	7.70	0.09638	0.01	0.00053	0.00	0.00046	0.00	0.00052	6.48E-09
93L28a	7.68	0.00422	7.71	0.11496	0.01	0.00055	0.00	0.00066	0.00	0.00054	4.73E-09
93L28a	7.94	0.00297	7.95	0.24153	0.01	0.00028	0.00	0.00164	0.00	0.00029	2.27E-09
93L28a	7.86	0.00256	7.78	0.27969	0.01	0.00029	0.00	0.00193	0.00	0.00028	1.72E-09
93L28a	7.89	0.00269	8.05	0.40875	0.02	0.00029	0.00	-0.00265	0.00	0.00028	1.18E-09
93L28a	7.79	0.00307	7.69	0.12629	0.01	0.00034	0.00	0.00076	0.00	0.00034	4.91E-09
93L28a	7.63	0.00140	7.78	0.29440	0.01	0.00023	0.00	0.00185	0.00	0.00024	1.79E-09
93I22b	8.42	0.00357	8.20	0.32978	0.01	0.00018	0.02	0.02423	0.00	0.00018	1.51E-09
93I22b	8.32	0.01572	8.29	0.03964	0.01	0.00120	0.03	0.00152	0.00	0.00113	2.83E-08
93I22b	8.14	0.01908	8.11	0.05764	0.01	0.00111	0.02	0.00183	0.00	0.00108	2.22E-08
93I22b	8.22	0.00946	8.20	0.03137	0.01	0.00076	0.02	0.00178	0.00	0.00073	2.57E-08
93I22b	8.31	0.01271	8.27	0.03511	0.01	0.00094	0.03	0.00143	0.00	0.00085	2.7E-08
93I22b	8.20	0.01338	8.17	0.06520	0.01	0.00081	0.02	0.00255	0.00	0.00079	1.53E-08
93I22b	8.04	0.00617	8.02	0.05502	0.01	0.00066	0.01	0.00331	0.00	0.00064	1.18E-08
93I22b	8.21	0.00742	8.17	0.04476	0.01	0.00094	0.02	0.00227	0.00	0.00089	1.72E-08

93122b	8.31	0.00502	8.22	0.05812	0.01	0.00049	0.02	0.00328	0.00	0.00047	1.09E-08
Sample	40/39 Ar	±	40*/39 Ar	±	38/39 Ar	±	37/39 Ar	±	36/39 Ar	±	39 Ar (cm^3)
93122b	8.38	0.00712	8.29	0.05783	0.01	0.00063	0.03	0.00274	0.00	0.00061	1.38E-08
93122b	8.16	0.00606	8.09	0.05644	0.01	0.00084	0.02	0.00308	0.00	0.00083	1.21E-08
93122b	8.16	0.00556	8.11	0.07066	0.01	0.00078	0.02	0.00404	0.00	0.00074	9.22E-09
93122b	8.26	0.00500	8.15	0.10526	0.01	0.00042	0.02	0.00628	0.00	0.00042	5.95E-09
93122b	8.39	0.00458	8.30	0.09569	0.01	0.00051	0.02	0.00528	0.00	0.00050	7.07E-09
93122b	8.39	0.00476	8.26	0.04821	0.01	0.00048	0.04	0.00302	0.00	0.00046	1.38E-08
93122b	8.45	0.00560	8.27	0.07413	0.01	0.00046	0.03	0.00400	0.00	0.00044	9.34E-09
931.22a	8.80	0.00327	8.66	0.10753	0.01	0.00051	0.01	0.00089	0.00	0.00049	3.2E-09
931.22a	8.10	0.00231	8.09	0.11507	0.01	0.00047	0.01	0.00049	0.00	0.00045	5.03E-09
931.22a	8.27	0.00336	8.14	0.09821	0.01	0.00044	0.01	0.00075	0.00	0.00043	4.64E-09
931.22a	8.32	0.00292	8.24	0.19095	0.01	0.00045	0.01	0.00122	0.00	0.00044	3.07E-09
931.22a	8.23	0.00441	8.03	0.11185	0.01	0.00060	0.01	0.00044	0.00	0.00060	5.66E-09
931.22a	8.17	0.00529	8.05	0.11776	0.01	0.00067	0.01	0.00057	0.00	0.00067	6.2E-09
931.22a	8.08	0.00228	7.93	0.08503	0.01	0.00028	0.01	0.00102	0.00	0.00026	3.42E-09
931.22a	8.12	0.00664	8.01	0.07529	0.01	0.00082	0.01	0.00055	0.00	0.00077	8.11E-09
931.22a	8.26	0.00357	8.23	0.08118	0.01	0.00046	0.01	0.00070	0.00	0.00043	5E-09
931.22a	8.27	0.00401	8.32	0.14096	0.01	0.00043	0.01	0.00083	0.00	0.00042	4.78E-09
931.22a	8.22	0.00466	8.20	0.10410	0.01	0.00055	0.01	0.00054	0.00	0.00055	6.07E-09
931.22a	8.24	0.00857	8.19	0.04277	0.01	0.00059	0.01	0.00032	0.00	0.00055	1.42E-08
931.22a	8.21	0.01455	8.23	0.05569	0.01	0.00122	0.01	0.00023	0.00	0.00117	1.86E-08
931.22a	8.42	0.00150	8.60	0.39178	0.01	0.00025	0.01	0.00217	0.00	0.00026	1.41E-09
931.22a	8.13	0.00672	8.12	0.04648	0.01	0.00089	0.01	0.00029	0.00	0.00084	1.36E-08
931.42d	9.57	0.01731	8.18	0.11026	0.01	0.00110	0.01	0.00044	0.00	0.00107	1.18E-08
931.42d	8.17	0.00335	8.04	0.10913	0.01	0.00060	0.01	0.00085	0.00	0.00058	5.51E-09
931.42d	8.28	0.01857	8.23	0.06875	0.01	0.00159	0.01	0.00032	0.00	0.00155	1.91E-08
931.42d	8.34	0.03154	8.29	0.07999	0.01	0.00265	0.01	0.00029	0.00	0.00264	2.66E-08
931.42d	8.33	0.00991	8.28	0.07316	0.01	0.00085	0.01	0.00044	0.00	0.00082	1.13E-08
931.42d	8.20	0.01017	8.21	0.10368	0.01	0.00104	0.01	0.00066	0.00	0.00103	8.16E-09
931.42d	8.12	0.01416	8.09	0.06212	0.01	0.00124	0.01	0.00054	0.00	0.00123	1.81E-08
931.42d	8.36	0.00948	8.24	0.18051	0.01	0.00045	0.01	0.00079	0.00	0.00042	4.98E-09
931.42d	8.31	0.00211	7.92	0.31735	0.01	0.00024	0.01	0.00254	0.00	0.00022	1.55E-09

Table D7. Cont.

93L42d	8.29	0.00435	8.18	0.21075	0.01	0.00036	0.01	0.00154	0.00	0.00036	3.05E-09
Sample	40/39 Ar	±	40*/39 Ar	±	38/39 Ar	±	37/39 Ar	±	36/39 Ar	±	39 Ar (cm^3)
93L42d	8.26	0.06560	8.21	0.45854	0.01	0.00645	0.01	0.00084	0.00	0.00639	9.87E-09
93L42d	8.21	0.00408	8.10	0.19057	0.01	0.00046	0.01	0.00151	0.00	0.00046	4.03E-09
93L42d	8.16	0.00137	7.92	0.51648	0.01	0.00022	0.01	0.00360	0.00	0.00022	1.14E-09
93L42d	8.33	0.00304	8.18	0.13303	0.01	0.00041	0.01	0.00119	0.00	0.00040	3.95E-09
93L42d	8.37	0.01270	8.28	0.10942	0.01	0.00086	0.01	0.00044	0.00	0.00086	8.59E-09
93L42d	8.31	0.02147	8.20	0.06877	0.01	0.00239	0.01	0.00017	0.00	0.00233	2.36E-08
93I42Be	301.12	0.00362	47.85	10.52796	0.18	0.00014	0.50	0.55920	0.86	0.00014	6.55E-11
93I42Be	249.87	0.00939	15.41	3.50352	0.19	0.00020	0.97	0.14655	0.79	0.00021	3.1E-10
93I42Be	91.67	0.00431	-1.59	-7.10251	0.15	0.00015	2.13	0.53518	0.32	0.00015	8.31E-11
93I42Be	68.89	0.00358	-6.17	-8.36439	0.08	0.00014	1.59	0.57632	0.25	0.00014	7.52E-11
93I42f	67.91	0.01235	9.38	0.59871	0.06	0.00039	0.28	0.01919	0.20	0.00045	3.13E-09
93I42f	11.61	0.00394	8.09	0.18160	0.02	0.00026	0.11	0.01389	0.01	0.00026	3.85E-09
93I42f	9.57	0.00682	8.29	0.07237	0.01	0.00076	0.05	0.00401	0.00	0.00075	9.54E-09
93I42f	9.01	0.01074	8.34	0.06825	0.01	0.00081	0.05	0.00346	0.00	0.00081	1.23E-08
93I42f	8.94	0.00625	8.30	0.07415	0.01	0.00082	0.05	0.00321	0.00	0.00082	1.25E-08
93I42f	9.46	0.00433	7.97	0.18605	0.01	0.00049	0.08	0.01127	0.01	0.00048	3.1E-09
93I42f	9.79	0.00453	8.39	0.24115	0.01	0.00032	0.07	0.01433	0.00	0.00033	2.96E-09
93I42f	13.64	0.00369	7.88	0.30756	0.02	0.00017	0.14	0.02338	0.02	0.00016	1.74E-09
93I42f	11.04	0.00418	8.23	0.14175	0.01	0.00032	0.07	0.00749	0.01	0.00033	5.43E-09
93I42f	12.08	0.00480	8.35	0.10875	0.01	0.00035	0.07	0.00703	0.01	0.00034	6.11E-09
93I42f	31.18	0.00577	8.88	0.38157	0.03	0.00019	0.18	0.01783	0.08	0.00019	2.09E-09
93I42f	17.85	0.01064	8.33	0.19600	0.02	0.00030	0.07	0.00674	0.03	0.00032	6.04E-09
93I42f	68.29	0.00406	9.32	1.82742	0.06	0.00014	0.25	0.08294	0.20	0.00017	4.91E-10
93I42f	187.99	0.00429	7.08	4.78044	0.20	0.00016	0.71	0.29518	0.61	0.00016	1.47E-10
93I42f	111.27	0.00355	12.16	15.47454	0.14	0.00014	0.90	1.04834	0.34	0.00014	3.74E-11
DRL 508	16.75	0.00413	15.01	0.16555	0.01	0.00023	2.44	0.01352	0.01	0.00024	3.68E-09
DRL508	16.10	0.00644	14.92	0.28346	0.01	0.00050	4.38	0.06160	0.00	0.00050	2.5E-09
DRL508	15.70	0.00910	14.57	0.18293	0.01	0.00063	3.54	0.03876	0.00	0.00064	4.82E-09
DRL508	15.69	0.00049	16.19	0.77994	0.01	0.00008	4.80	0.03000	0.00	0.00010	6.97E-10
DRL508	15.90	0.00053	15.02	0.58431	0.02	0.00016	4.95	0.04235	0.00	0.00016	9.31E-10
DRL508	15.67	0.00182	14.83	0.19744	0.01	0.00023	4.59	0.03539	0.00	0.00022	1.82E-09

Sample	40/39 Ar	±	40*/39 Ar	±	38/39 Ar	±	37/39 Ar	±	36/39 Ar	±	39 Ar (cm^3)
DRL508	15.92	0.00170	14.90	0.51612	0.01	0.00014	6.08	0.04952	0.00	0.00014	9.59E-10
DRL 508	16.43	0.00960	15.49	0.80217	0.01	0.00012	9.29	0.10238	0.00	0.00013	6.06E-10
DRL 508	16.74	0.00946	16.45	0.71856	0.01	0.00007	14.54	0.08820	0.00	0.00007	6.35E-10
DRL 508	17.50	0.00038	18.62	1.07174	0.02	0.00007	26.60	0.24928	0.00	0.00007	3.56E-10
931125	30.93	0.00075	23.21	2.69222	0.02	0.00005	12.78	0.18914	0.03	0.00007	2.22E-10
931125	45.32	0.00432	16.49	1.66353	0.04	0.00020	16.93	0.42539	0.10	0.00024	5.5E-10
931125	31.57	0.00050	14.23	1.64860	0.02	0.00006	17.93	0.12741	0.06	0.00009	4E-10
931125	47.79	0.00024	9.04	5.28395	0.06	0.00005	18.35	0.43625	0.13	0.00006	8.59E-11
931125	73.18	0.00057	-10.49	-16.25951	0.11	0.00005	16.36	0.68227	0.28	0.00007	4.46E-11
931125	300.75	0.00182	-101.16	-35.17811	0.25	0.00005	6.11	0.54496	1.36	0.00009	2.74E-11
931125	217.11	0.00208	-305.53	-82.75112	0.22	0.00007	4.33	0.93711	1.77	0.00024	3.91E-11
931125	318.65	0.00434	-175.93	-38.30303	0.24	0.00012	2.74	0.51836	1.67	0.00032	1.04E-10
kls488	19.14	0.00603	16.68	0.17340	0.02	0.00040	7.72	0.05336	0.01	0.00041	4.4E-09
kls488	18.10	0.00369	16.65	0.21183	0.01	0.00023	5.59	0.02672	0.00	0.00024	3.66E-09
kls488	17.54	0.00107	16.93	0.28189	0.01	0.00020	8.67	0.04847	0.00	0.00022	2.03E-09
kls488	17.23	0.00110	16.49	0.45104	0.02	0.00014	12.86	0.06750	0.00	0.00016	1.35E-09
kls488	17.31	0.00095	16.59	0.35961	0.02	0.00012	13.08	0.06781	0.00	0.00012	1.36E-09
kls488	17.80	0.00080	16.61	0.49647	0.02	0.00010	12.39	0.08079	0.00	0.00011	9.77E-10
kls488	17.92	0.00022	15.48	1.21294	0.02	0.00007	13.57	0.14391	0.01	0.00007	3.13E-10
kls488	19.12	0.00559	16.54	0.20274	0.01	0.00029	9.91	0.06523	0.01	0.00031	3.87E-09
kls488 ii	17.48	0.00130	16.18	0.27955	0.01	0.00017	5.66	0.03307	0.00	0.00018	1.84E-09
kls488 ii	17.36	0.00076	16.18	0.36965	0.01	0.00015	6.22	0.03898	0.00	0.00015	1.37E-09
kls488 ii	17.04	0.00108	16.40	0.23313	0.01	0.00012	12.72	0.04941	0.00	0.00012	1.86E-09
kls488 ii	17.20	0.00215	16.40	0.20582	0.01	0.00024	14.00	0.07467	0.00	0.00024	2.63E-09
93136	16.28	0.00219	15.64	0.14831	0.01	0.00025	0.02	0.00194	0.00	0.00025	4.1E-09
93136	16.09	0.01271	15.92	0.09646	0.01	0.00087	0.04	0.00887	0.00	0.00085	1.16E-08
93136	16.05	0.00442	16.01	0.09371	0.01	0.00034	0.07	0.00135	0.00	0.00033	5.45E-09
93136	16.20	0.00546	16.07	0.11221	0.01	0.00072	0.06	0.00121	0.00	0.00071	7.48E-09

Sample	40/39 Ar	±	40*/39 Ar	±	38/39 Ar	±	37/39 Ar	±	36/39 Ar	±	39 Ar (cm^3)
93136	16.16	0.00934	15.96	0.05635	0.01	0.00073	0.02	0.00341	0.00	0.00070	1.54E-08
93136	16.09	0.00773	15.95	0.07131	0.01	0.00044	0.06	0.00083	0.00	0.00043	9.79E-09
93136	16.01	0.00551	16.01	0.09281	0.01	0.00041	0.03	0.00081	0.00	0.00041	7.11E-09
93136	16.05	0.00574	16.18	0.12620	0.01	0.00048	0.05	0.00147	0.00	0.00049	6.25E-09
93136	16.20	0.00454	15.92	0.18226	0.01	0.00032	0.01	0.00203	0.00	0.00031	3.26E-09
93136	16.11	0.00685	15.97	0.13035	0.01	0.00068	0.03	0.00091	0.00	0.00067	6.98E-09
93136	16.16	0.00340	15.81	0.10193	0.01	0.00038	0.07	0.00153	0.00	0.00036	4.9E-09
93136	16.34	0.00906	15.98	0.27181	0.01	0.00076	0.05	0.00197	0.00	0.00076	3.74E-09
93136	15.60	0.02947	14.79	0.76809	0.01	0.00417	0.07	0.00465	0.00	0.00422	5.71E-09
93136	16.40	0.00223	16.16	0.17211	0.01	0.00023	0.03	0.00182	0.00	0.00024	3.39E-09
93136	16.25	0.00508	16.00	0.07772	0.01	0.00049	0.27	0.00216	0.00	0.00049	8.4E-09
93136	16.38	0.00282	15.85	0.12825	0.01	0.00022	0.02	0.00208	0.00	0.00022	3.97E-09
93136	16.54	0.00308	16.24	0.11061	0.01	0.00025	0.02	0.00122	0.00	0.00026	5.43E-09
93136	16.21	0.00538	15.98	0.08572	0.01	0.00041	0.06	0.00095	0.00	0.00044	8.82E-09
93136	16.08	0.01691	15.82	0.09323	0.01	0.00099	0.05	0.00078	0.00	0.00098	1.51E-08
93136	16.30	0.00372	15.91	0.13941	0.01	0.00017	0.02	0.00139	0.00	0.00018	4.69E-09
93136	16.27	0.01531	16.07	0.08461	0.01	0.00109	0.02	0.00142	0.00	0.00106	1.58E-08
93136	16.73	0.00072	15.66	0.55818	0.01	0.00012	0.02	0.00607	0.00	0.00012	1.02E-09
93136	16.29	0.01244	16.12	0.08292	0.01	0.00085	0.02	0.00154	0.00	0.00082	1.33E-08
93136	18.00	0.00054	15.38	0.98016	0.01	0.00009	0.00	0.00772	0.01	0.00010	6.11E-10
sm172	31.53	0.00336	13.59	0.64045	0.03	0.00019	4.83	0.04593	0.06	0.00020	1.25E-09
sm172	16.80	0.00105	15.28	0.41932	0.01	0.00019	7.72	0.04702	0.01	0.00021	1.75E-09
sm172	17.07	0.00102	16.44	0.80993	0.01	0.00012	10.32	0.07959	0.00	0.00013	7.61E-10
sm172	16.99	0.00028	18.22	2.67656	0.01	0.00003	10.70	0.09655	0.00	0.00006	2.11E-10
sm172	17.53	0.00028	22.16	3.78136	0.01	0.00005	11.11	0.21169	-0.02	0.00006	1.12E-10
sm172	16.89	0.00094	16.57	0.68059	0.01	0.00016	11.23	0.10372	0.00	0.00018	9.16E-10
SM172	16.74	0.00557	16.59	0.19923	0.01	0.00026	11.39	0.05373	0.00	0.00028	3.9E-09
sm172	16.78	0.00222	16.38	0.14980	0.01	0.00011	11.73	0.03639	0.00	0.00011	3.33E-09

Sample	40/39 Ar	±	40*/39 Ar	±	38/39 Ar	±	37/39 Ar	±	36/39 Ar	±	^{39} Ar (cm^{-3})
kls327	100.68	0.01456	15.87	0.78130	0.07	0.00022	3.76	0.02846	0.29	0.00025	2.011E-09
kls327	39.26	0.00512	15.32	0.69521	0.03	0.00017	4.57	0.03074	0.08	0.00023	2.166E-09
kls327	26.99	0.00646	16.56	0.32117	0.02	0.00021	4.38	0.02824	0.04	0.00023	3.051E-09
kls327	19.46	0.00517	16.85	0.30436	0.01	0.00030	3.14	0.03310	0.01	0.00032	2.191E-09
kls327	19.69	0.00103	17.85	0.60902	0.01	0.00014	4.81	0.04248	0.01	0.00016	9.148E-10
kls327	19.97	0.00641	16.42	0.23700	0.02	0.00050	4.84	0.04177	0.01	0.00052	3.498E-09
kls327	20.51	0.00148	16.39	0.37600	0.02	0.00012	4.97	0.05372	0.01	0.00013	1.938E-09
kls327	21.59	0.00094	16.59	0.24764	0.02	0.00021	5.40	0.03548	0.02	0.00021	1.858E-09
kls327	29.58	0.00220	16.42	0.32496	0.02	0.00015	5.31	0.02636	0.04	0.00017	2.048E-09
kls327	20.37	0.00145	16.30	0.14424	0.02	0.00016	5.98	0.01905	0.01	0.00016	3.088E-09
kls327	20.35	0.00150	16.01	0.30364	0.02	0.00020	5.91	0.03702	0.01	0.00020	1.728E-09
kls327	19.83	0.00043	12.93	1.05724	0.01	0.00011	5.95	0.06897	0.02	0.00012	5.148E-10
kls327	27.25	0.00071	8.33	4.02699	0.02	0.00009	6.35	0.23164	0.06	0.00010	1.348E-10
kls348	19.03	0.00057	17.49	1.06995	0.02	0.00008	12.48	0.09530	0.01	0.00010	5.718E-10
kls348	16.87	0.00036	15.75	0.98680	0.01	0.00008	15.13	0.09466	0.00	0.00009	5.498E-10
kls348	16.99	0.00033	15.49	1.14907	0.02	0.00008	15.85	0.14999	0.01	0.00008	3.698E-10
kls348	17.21	0.00114	16.88	0.53689	0.01	0.00012	17.07	0.13663	0.00	0.00013	8.128E-10
kls348	17.16	0.00134	17.50	0.43304	0.01	0.00013	17.87	0.09855	0.00	0.00013	1.288E-09
drl507	57.75	0.01509	38.32	0.65095	0.03	0.00035	7.89	0.07120	0.07	0.00037	2.268E-09
drl507	41.30	0.00094	31.62	0.71500	0.02	0.00009	12.52	0.06112	0.03	0.00010	8.698E-10
drl507	35.48	0.00050	28.34	1.90894	0.02	0.00007	14.65	0.11768	0.02	0.00008	3.768E-10
drl507	31.07	0.00032	23.20	0.86776	0.02	0.00009	18.70	0.17729	0.03	0.00009	5.068E-10
drl507	27.23	0.00163	23.22	0.44118	0.02	0.00016	31.22	0.18262	0.01	0.00017	1.428E-09
drl507	23.78	0.00038	30.32	5.13389	-0.01	0.00006	-43.00	0.94427	-0.02	0.00007	1.068E-10
sm60	22.12	0.00426	18.27	0.27342	0.02	0.00025	9.89	0.06104	0.01	0.00025	2.318E-09
sm60	18.51	0.00089	16.92	0.46905	0.02	0.00010	14.88	0.08836	0.01	0.00011	9.218E-10
sm60	20.06	0.00059	16.72	0.63732	0.02	0.00008	18.79	0.08916	0.01	0.00009	8.528E-10
sm60	19.04	0.00063	16.60	0.20289	0.02	0.00016	16.68	0.09860	0.01	0.00015	1.338E-09
sm60	19.19	0.00120	16.09	0.26331	0.02	0.00020	17.26	0.11349	0.01	0.00019	1.578E-09

Table D7. Cont.

Sample	40/39 Ar	±	40*/39 Ar	±	38/39 Ar	±	37/39 Ar	±	36/39 Ar	±	39 Ar (cm^3)
sm60	18.69	0.00388	16.60	0.35442	0.01	0.00025	16.51	0.14114	0.01	0.00026	1.8E-09
sm60	18.58	0.00101	16.52	0.55020	0.02	0.00021	16.69	0.15261	0.01	0.00022	1.15E-09
#sm60	19.52	0.00130	15.72	0.46504	0.02	0.00019	16.54	0.12204	0.01	0.00020	1.35E-09
#sm60	19.64	0.00095	15.60	0.68158	0.02	0.00012	16.64	0.11866	0.01	0.00013	8.41E-10
sm60	18.75	0.00106	16.61	0.72750	0.01	0.00010	16.47	0.08640	0.01	0.00012	1.07E-09
931107	23.25	0.00129	16.54	0.75742	0.02	0.00013	4.15	0.03025	0.02	0.00015	9.7E-10
931107	18.49	0.00389	15.95	0.47606	0.02	0.00024	4.75	0.06107	0.01	0.00025	1.39E-09
931107	17.48	0.00129	16.22	0.46513	0.01	0.00017	4.71	0.03296	0.00	0.00018	1.45E-09
931107	16.92	0.00178	16.43	0.21822	0.01	0.00020	4.43	0.01731	0.00	0.00022	3.14E-09
931107	16.83	0.00198	16.50	0.22484	0.01	0.00022	4.97	0.02522	0.00	0.00023	2.57E-09
931107	16.66	0.00476	16.50	0.16608	0.01	0.00039	3.35	0.02179	0.00	0.00040	4.39E-09
931107	16.63	0.00627	16.49	0.11033	0.01	0.00055	1.94	0.01154	0.00	0.00053	6.85E-09
931107	16.68	0.00143	16.45	0.20184	0.01	0.00023	2.57	0.01156	0.00	0.00025	3.87E-09
931107	16.42	0.00656	16.13	0.16034	0.01	0.00059	1.98	0.02079	0.00	0.00059	5.1E-09
93119	17.38	0.00114	14.44	0.38729	0.02	0.00019	0.11	0.00582	0.01	0.00017	1.31E-09
93119	16.96	0.00059	14.22	0.36865	0.02	0.00014	0.10	0.00653	0.01	0.00012	1.16E-09
93119	36.89	0.00017	6.32	6.71150	0.02	0.00005	3.35	0.13818	0.10	0.00006	7.1E-11
93119	67.18	0.00019	-17.16	-19.22527	0.03	0.00005	0.51	0.38254	0.29	0.00005	2.2E-11
LBI	22.12	0.00192	19.50	0.57371	0.01	0.00009	9.98	0.42024	0.01	0.00009	5.2E-10
LBI	20.41	0.00255	19.14	0.32778	0.01	0.00040	10.52	0.41610	0.00	0.00040	1.61E-09
LBI	18.29	0.00039	16.89	1.04145	0.02	0.00005	15.38	0.46478	0.00	0.00006	2.59E-10
LBI	18.73	0.00036	16.53	0.90396	0.01	0.00005	16.31	0.50636	0.01	0.00006	3.4E-10
LBI	19.48	0.00024	17.31	0.73117	0.02	0.00007	38.65	1.22107	0.01	0.00007	4.22E-10
LBI	19.76	0.00020	18.06	1.61256	0.02	0.00004	69.55	1.92497	0.01	0.00004	1.89E-10
CP3	26.29	0.00050	21.21	1.59442	0.02	0.00006	34.62	1.30805	0.02	0.00007	1.95E-10
CP3	21.39	0.00029	19.98	1.82657	0.02	0.00004	40.34	1.50559	0.00	0.00005	1.48E-10
CP3	21.68	0.00047	20.22	1.30960	0.02	0.00006	45.14	1.35990	0.00	0.00007	2.37E-10
CP3	20.35	0.00026	15.00	1.75560	0.02	0.00005	51.28	2.07376	0.02	0.00006	1.53E-10

Sample	40/39 Ar	±	40*/39 Ar	±	38/39 Ar	±	37/39 Ar	±	36/39 Ar	±	^{39}Ar (cm^{3})
kk119	281.54	0.01096	271.29	4.29641	0.03	0.00006	13.71	0.70141	0.03	0.00007	2.45E-10
kk119	374.61	0.00108	361.42	11.38850	0.02	0.00003	4.85	0.48066	0.04	0.00004	4.34E-11
kk119	415.25	0.00161	406.44	9.89953	0.02	0.00003	5.31	0.52419	0.03	0.00004	5.48E-11
kk119	427.46	0.00328	423.67	8.45638	0.02	0.00004	4.64	0.35603	0.01	0.00004	8.11E-11
kk119	319.48	0.00438	317.22	4.15514	0.02	0.00004	8.44	0.23796	0.01	0.00004	1.44E-10
kk119	409.65	0.01073	406.00	5.93062	0.01	0.00005	4.99	0.20208	0.01	0.00006	2.08E-10
kk119	362.70	0.00748	359.62	6.32713	0.02	0.00006	4.90	0.25912	0.01	0.00007	1.95E-10
kk119	486.14	0.00042	528.83	52.88745	-0.08	0.00001	-8.23	2.83966	-0.14	0.00002	5.83E-12
kk119	404.80	0.00029	427.85	40.48388	-0.10	0.00001	-1.55	2.25512	-0.08	0.00002	7.27E-12
TK1-47	31.06	0.00045	26.82	2.14865	0.01	0.00004	5.13	0.32965	0.01	0.00005	1.27E-10
TK1-47	25.98	0.00011	26.91	7.86290	0.00	0.00002	11.95	0.74784	0.00	0.00003	3.39E-11
TK1-47	27.42	0.00018	26.55	3.16853	0.02	0.00003	11.41	0.65285	0.00	0.00004	8.46E-11
KU-82	35.05	0.00363	25.16	0.62359	0.03	0.00021	6.10	0.21959	0.03	0.00022	8.69E-10
KU-82	19.09	0.00369	17.48	0.35478	0.01	0.00045	4.39	0.14204	0.01	0.00045	1.57E-09
KU-82	18.05	0.00174	17.44	0.38399	0.01	0.00015	1.33	0.06105	0.00	0.00016	8.18E-10
KU-82	18.92	0.00079	18.36	0.96291	0.01	0.00010	2.55	0.15204	0.00	0.00010	3.31E-10
KU-82	19.30	0.00210	17.53	0.34050	0.02	0.00038	3.28	0.12225	0.01	0.00039	1.54E-09
KU-82	17.46	0.00240	16.29	0.28605	0.01	0.00022	0.82	0.02777	0.00	0.00022	1.22E-09
KU-82	19.45	0.00013	-7.28	-8.91607	0.05	0.00002	5.93	0.62021	0.09	0.00003	3.41E-11
KU-66	343.27	0.00034	335.31	31.91673	-0.02	0.00001	19.30	2.86877	0.03	0.00002	8.9E-12
KU-66	418.61	0.00178	412.65	11.07897	0.01	0.00003	10.51	0.48396	0.02	0.00004	4.97E-11
KU-66	324.29	0.00115	316.66	7.36928	0.01	0.00002	26.01	0.76393	0.03	0.00003	5.23E-11
KU-66	442.79	0.00396	437.78	6.72842	0.02	0.00004	6.10	0.38090	0.02	0.00005	1.23E-10
KU-66	417.61	0.00296	411.33	8.44870	0.02	0.00003	13.22	0.51892	0.02	0.00004	8.06E-11
KU-66	382.00	0.00061	388.59	26.09268	-0.01	0.00002	9.88	0.96032	-0.02	0.00003	1.45E-11

Sample	40/39 Ar	±	40*/39 Ar	±	38/39 Ar	±	37/39 Ar	±	36/39 Ar	±	39 Ar (cm^3)
KLS230	96.82	0.02065	74.49	2.44285	0.04	0.00044	11.27	0.23886	0.08	0.00050	1.23E-09
KLS230	45.78	0.01048	37.16	0.33593	0.02	0.00028	8.34	0.06818	0.03	0.00027	2.78E-09
KLS230	35.61	0.00647	33.47	0.22649	0.02	0.00027	6.69	0.05009	0.01	0.00026	3.03E-09
KLS230	36.90	0.00712	35.51	0.32046	0.01	0.00023	5.73	0.04013	0.00	0.00024	2.34E-09
KLS230	38.50	0.02320	37.56	3.19442	0.01	0.00020	7.08	0.99460	0.00	0.00020	4.52E-10
KLS230	36.77	0.00432	35.97	0.53562	0.01	0.00022	5.17	0.06454	0.00	0.00022	1.05E-09
KLS230	41.86	0.00194	40.37	0.66022	0.01	0.00008	9.94	0.05273	0.01	0.00009	8.93E-10
KLS230	50.02	0.00083	45.41	1.19969	0.01	0.00006	17.39	0.19604	0.02	0.00006	3.11E-10
KLS230	43.32	0.00406	42.01	0.51221	0.01	0.00011	15.06	0.11922	0.00	0.00011	1.02E-09
KLS230	72.18	0.00214	69.16	2.34620	0.01	0.00008	43.19	0.80373	0.01	0.00008	1.98E-10
KLS230	99.70	0.00073	96.99	3.32538	0.01	0.00007	86.89	1.88764	0.01	0.00007	1.42E-10
KLS230	137.26	0.00186	117.68	8.80664	0.04	0.00004	110.79	3.13328	0.07	0.00005	5.67E-11
KLS230	199.48	0.00102	124.46	7.65108	0.06	0.00006	104.69	3.12010	0.25	0.00008	9.11E-11